

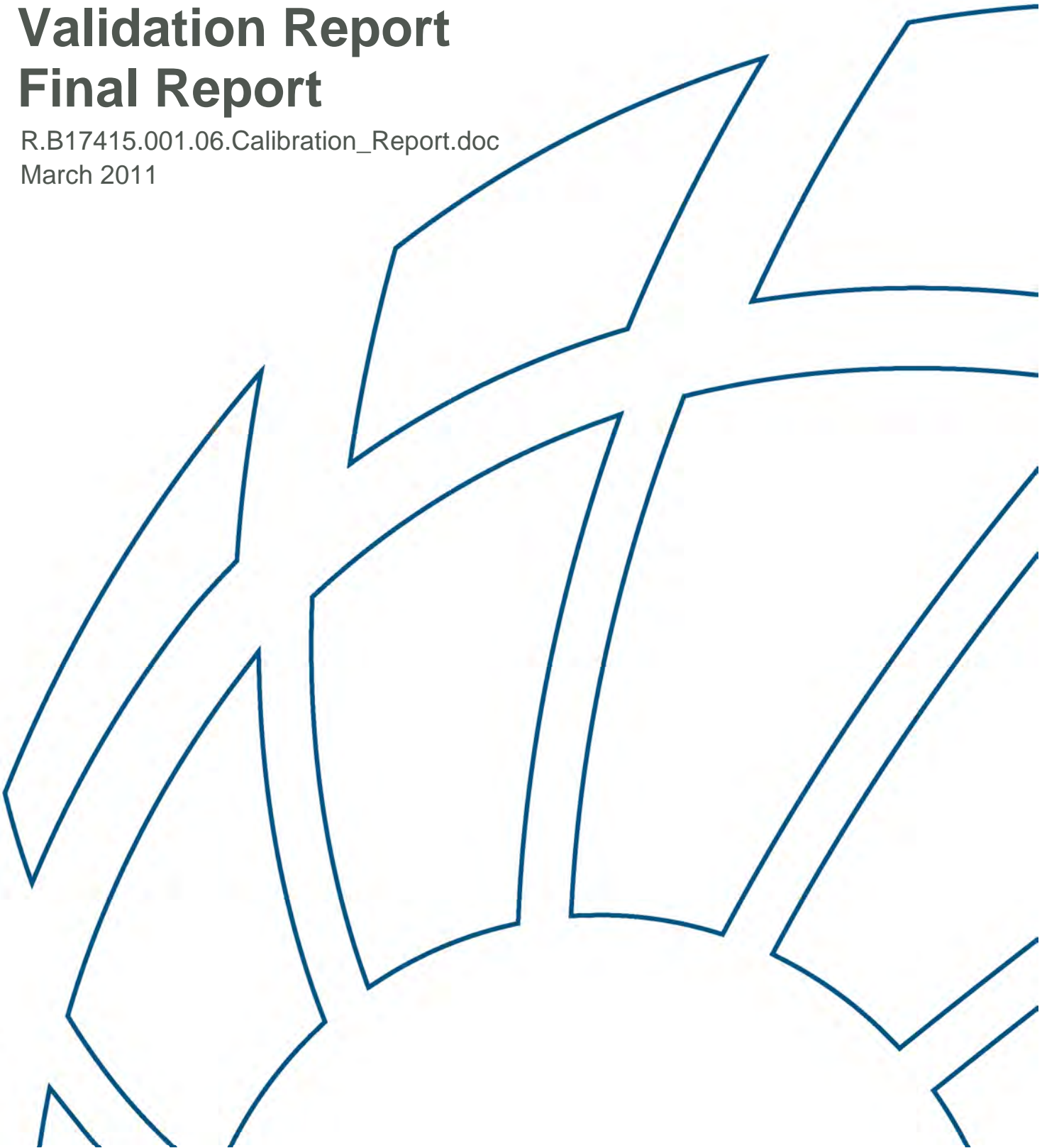


APPENDIX H5.2

## **Spencer Gulf model validation report**

# Hydrodynamic and Water Quality Modelling of Spencer Gulf: Model Validation Report Final Report

R.B17415.001.06.Calibration\_Report.doc  
March 2011



# Hydrodynamic and Water Quality Modelling of Spencer Gulf: Model Validation Report Final Report

Prepared For: BHP Billiton

Prepared By: BMT WBM Pty Ltd (Member of the BMT group of companies)

## **Offices**

*Brisbane  
Denver  
Mackay  
Melbourne  
Newcastle  
Perth  
Sydney  
Vancouver*

## DOCUMENT CONTROL SHEET

<p><b>BMT WBM Pty Ltd</b>                  BMT WBM Pty Ltd                  Level 11, 490 Upper Edward Street                  Brisbane 4000                  Queensland Australia                  PO Box 203 Spring Hill 4004</p> <p>Tel: +61 7 3831 6744                  Fax: + 61 7 3832 3627</p> <p>ABN 54 010 830 421</p> <p><a href="http://www.wbmpl.com.au">www.wbmpl.com.au</a></p>	<table style="width: 100%; border-collapse: collapse;"> <tr> <td style="width: 30%;"><b>Document :</b></td> <td>R.B17415.001.06.Calibration_Report.doc</td> </tr> <tr> <td><b>Project Manager :</b></td> <td>Tony McAlister</td> </tr> </table> <hr/> <table style="width: 100%; border-collapse: collapse;"> <tr> <td style="width: 30%;"><b>Client :</b></td> <td>BHP Billiton</td> </tr> <tr> <td><b>Client Contact:</b></td> <td>David Wiltshire</td> </tr> <tr> <td><b>Client Reference</b></td> <td></td> </tr> </table>	<b>Document :</b>	R.B17415.001.06.Calibration_Report.doc	<b>Project Manager :</b>	Tony McAlister	<b>Client :</b>	BHP Billiton	<b>Client Contact:</b>	David Wiltshire	<b>Client Reference</b>	
<b>Document :</b>	R.B17415.001.06.Calibration_Report.doc										
<b>Project Manager :</b>	Tony McAlister										
<b>Client :</b>	BHP Billiton										
<b>Client Contact:</b>	David Wiltshire										
<b>Client Reference</b>											

<b>Title :</b>	Hydrodynamic and Water Quality Modelling of Spencer Gulf: Model Validation Report. Final Report
<b>Author :</b>	Daniel Botelho
<b>Synopsis :</b>	This report presents the set-up and validation of an upgraded model of Spencer Gulf to assist with the design and impact assessment of a proposed desalination plant brine outfall at Port Bonython.

### REVISION/CHECKING HISTORY

REVISION NUMBER	DATE OF ISSUE	CHECKED BY	ISSUED BY
0	15 <sup>th</sup> October 2009	MEB	DAB
1	29 <sup>th</sup> October 2009	MEB	DAB
2	17 <sup>th</sup> March 2010	MEB	DAB
3	17 <sup>th</sup> May 2010	MEB	DAB
4	8 <sup>th</sup> October 2010	MEB	DAB
5	11 <sup>th</sup> March 2011	MEB	DAB
6	15 March 2011	MEB	DAB

### DISTRIBUTION

DESTINATION	REVISION						
	0	1	2	3	4	5	6
BHP Billiton	PDF	PDF	PDF	PDF	PDF	PDF	PDF
BMT WBM File	PDF	PDF	PDF	PDF	PDF	PDF	PDF
BMT WBM Library	PDF	PDF	PDF	PDF	PDF	PDF	PDF

## CONTENTS

<b>Contents</b>	<b>i</b>
<b>Acronym Glossary</b>	<b>i</b>
<b>1 INTRODUCTION</b>	<b>1-1</b>
<b>2 SITE DESCRIPTION</b>	<b>2-1</b>
2.1 Spencer Gulf	2-1
2.2 Point Lowly	2-2
<b>3 FIELD MEASUREMENTS</b>	<b>3-1</b>
3.1 Meteorological Measurements	3-5
3.2 Measurements of Vertical Profiles of Velocity	3-8
3.3 CTD Measurements	3-11
3.4 Hand-Sample Salinity Measurements	3-13
3.5 CTD Salinity Corrections	3-13
3.6 ADCP Cross-Sectional Velocity Measurements	3-19
<b>4 NUMERICAL MODEL SET UP</b>	<b>4-1</b>
4.1 Model Bathymetry and Grid	4-1
4.2 Surface Boundary Conditions	4-4
4.3 Open Boundary Conditions	4-4
4.4 Other Boundary Conditions	4-12
4.5 Model Time Step and Stability Condition	4-12
4.6 Drag Distribution	4-12
<b>5 MODEL VALIDATION</b>	<b>5-1</b>
5.1 Seasonal Validation Period	5-1
5.1.1 Initial Conditions	5-1
5.1.2 Tidal Amplification and Modulation	5-2
5.1.3 Seasonal Evolution	5-4
5.1.4 Water Age Analysis	5-5
5.2 Forty-Days Validation Period (Targeted Deployment)	5-32
5.2.1 Initial Conditions	5-32
5.2.2 Tidal Elevations	5-32

---

5.2.3	Temperature and Salinity	5-39
5.2.4	Moored ADCP Velocities	5-44
5.2.5	Tidal Eddies	5-67
5.2.6	Boat-Mounted ADCP Velocity Transects	5-67
<b>5.3</b>	<b>Three-Month Validation Period</b>	<b>5-73</b>
5.3.1	Initial Conditions	5-73
5.3.2	Velocity Comparisons	5-73
<b>6</b>	<b>REFERENCES</b>	<b>6-1</b>
<b>APPENDIX A:</b>	<b>MOORED ADCP MEASUREMENTS</b>	<b>A-1</b>
<b>APPENDIX B:</b>	<b>CTD MEASUREMENTS</b>	<b>B-1</b>
<b>APPENDIX C:</b>	<b>ADCP TRANSECTS</b>	<b>C-1</b>
<b>APPENDIX D:</b>	<b>SEASONAL VALIDATION PERIOD TIDAL-ELEVATION COMPARISONS – (TOP – RAW SIGNALS, BOTTOM – SIGNAL RECONSTRUCTED FROM HARMONIC ANALYSIS)</b>	<b>D-1</b>
<b>APPENDIX E:</b>	<b>FORTY DAYS VALIDATION PERIOD MOORED-ADCP COMPARISONS</b>	<b>E-1</b>
<b>APPENDIX F:</b>	<b>FORTY-DAYS VALIDATION PERIOD ADCP TRANSECTS COMPARISONS</b>	<b>F-1</b>
<b>APPENDIX G:</b>	<b>THREE-MONTH VALIDATION PERIOD ADCP COMPARISONS</b>	<b>G-1</b>
<b>APPENDIX H:</b>	<b>ADDITIONAL FACTORY CTD CALIBRATION</b>	<b>H-1</b>
<b>APPENDIX I:</b>	<b>THREE-MONTH VALIDATION PERIOD – LOW AND HIGH FREQUENCY ANALYSIS</b>	<b>I-1</b>

---

## ACRONYM GLOSSARY

ADCP – Acoustic Doppler Current Profiler

BoM – Bureau of Meteorology

CDF – Cumulative Distribution Function

CFL – Courant-Friedrich-Lévy numerical stability condition

CTD – Conductivity, Temperature and Depth probe

CWR – Centre for Water Research

Draft EIS - Olympic Dam Expansion Draft Environmental Impact Statement

ELCOM – Estuary, Lake, and Coastal Ocean Model

FPC – Flinders Ports Corporation

GFS – Global Forecast System

HYCOM – HYbrid Coordinate Ocean Model

MAE – Mean Absolute Error

NCAR - National Center for Atmospheric Research

NCEP – NOAA's National Center for Environmental Prediction

NCEP-GSF – NCEP Global Forecasting System

NOAA – National Oceanic and Atmospheric Administration

PDF – Probability Distribution Function

$R^2$  – Correlation Coefficient

RMSE – Root Mean Square Error

SAR – Synthetic Aperture Radar

TKE – Turbulent Kinetic Energy

UNESCO – United Nations Educational, Scientific, and Cultural Organization

WRF – Weather Research and Forecast Model

# 1 INTRODUCTION

BHP Billiton is proposing to expand its mining operations at Olympic Dam, South Australia. Part of this proposal includes construction and operation of a desalination plant at Point Lowly on the coastline of Upper Spencer Gulf (Figure 1-1). This plant would provide water to the proposed mine if it is approved.

BHP Billiton (2009) released the Olympic Dam Expansion Draft Environmental Impact Statement (hereafter Draft EIS) document with respect to the proposed expansion and desalination plant in May 2009. Part of this Draft EIS described numerical modelling undertaken to better understand any potential impacts that brine discharged from the proposed desalination plant may have on receiving waters and biota. BMT WBM and The Centre for Water Research (CWR) of The University of Western Australia undertook this numerical modelling on behalf of BHP Billiton, and details have been provided in a series of peer reviewed reports contained in the Draft EIS (see Appendices O11.2, O11.3, O11.4). Similar studies have been undertaken in the Australian context, and the reader is referred to these contextually relevant studies for further information (Okely et al. 2007a, 2007b; SA Water 2008, 2009; DSE 2008)

This Draft EIS modelling work deployed a three-tiered framework to assist with impact assessment. These models captured different spatial and temporal scales and were referred to as 'near field', 'mid field' and 'far field' models. The near field model was used to predict the brine plume behaviour at short spatial and time scales (i.e. orders of hours and up to a few hundred meters), whereas the far-field model was used to provide information for long-term assessments (i.e. seasonal and inter-annual) at the Spencer Gulf scale. The mid-field model was used to predict the plume behaviour on intermediate time scales (i.e. over a few days to a couple of months) and over the Upper Spencer Gulf.

This report presents an upgraded three dimensional modelling framework that supersedes the mid-field and far-field models adopted in the previous work. In line with current best-practice standards, the modelling upgrade includes incorporation of (see Section 4 for details):

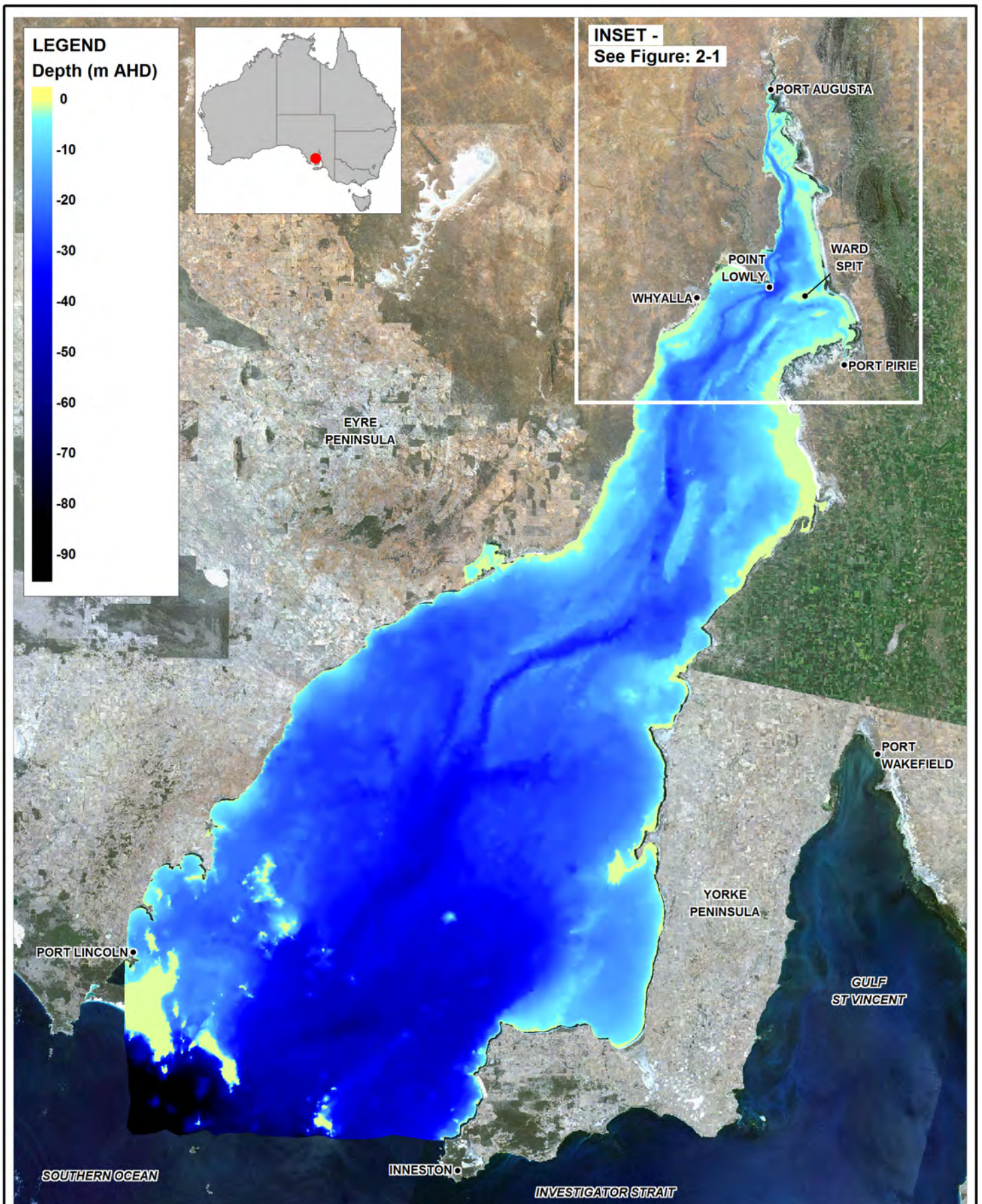
- Upgraded site specific (Point Lowly) local bathymetry from a variety of sources;
- High spatial and temporal resolution meteorological forcing data (i.e. local forcing data is at approximately 0.1 degree resolution at 1 hour resolution for all variables);
- High spatial and temporal resolution two-dimensional tidal boundary forcing data (i.e. tidal elevations at 8 locations and 1 hour resolution, and temperature and salinity at same locations as depth profiles from surface to 40 m depth and daily resolution);
- Improved spatial and temporal model resolution in the key areas of interest (i.e. up to 40 m resolution in the location of the proposed diffuser and 24 s time step); and
- Validation of the model to an expanded suite (compared to the Draft EIS) of targeted, relevant, and quality controlled field data collected over separate deployments. For example, four ADCPs (Acoustic Doppler Current Profiler), six CTDs (Conductivity-Temperature-Depth) and a weather station were deployed for 6 weeks over a May dodge tide period in 2009, in an effort to deliver the highest standard of data to the study. Boat mounted ADCP transects were also collected.



Importantly, the upgraded model is a single model that encapsulates the processes, temporal and spatial scales of both the previous 'far field' and 'mid field' models. Model validation (in the context of this report) refers to the model's ability to reproduce both hydrodynamic details as well as broad scale processes in Spencer Gulf. Development of this single model provides a significant improvement to the modelling study over previous work, and was only feasible due to the increased computational power that was not available at the time of production of the Draft EIS.

This report specifically describes the set up and validation of this upgraded model, as well as a targeted data collection program executed to support this model development. Linkage of this model with upgraded near field models is described elsewhere. Specifically, this report presents:

- Contextually relevant background material and a site description;
- Targeted, relevant, and quality-controlled field measurements;
- Numerical model set-up; and
- Numerical model validation.

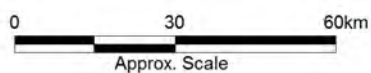


Title:  
**Spencer Gulf  
Location and Bathymetry**

Figure:  
**1-1**

Rev:  
**A**

BMT WBM endeavours to ensure that the information provided in this map is correct at the time of publication. BMT WBM does not warrant, guarantee or make representations regarding the currency and accuracy of information contained in this map.



Filepath :

## 2 SITE DESCRIPTION

### 2.1 Spencer Gulf

Spencer Gulf is a large (length approximately 300km, mean width approximately 60km), relatively shallow (mean depth approx 22m) semi-enclosed sea, adjacent to the South Australian coast (Figure 1-1). Flow in the Gulf is largely tidally driven, with tidal ranges reaching up to 2.7 m in the northern reaches of the Gulf. Smaller tidal ranges associated with neap tides, sometimes referred to as 'dodge' tides, also occur in the South Australian gulfs (Easton 1978), and these correspond to periods in which the amplitude of the dominant semi-diurnal M2 and S2 tidal components are phase cancelling, or about every 14.77 days (Easton 1978; Nunes-Vaz, pers. comm.). The other dominant harmonics include O1 and K1, which are coincidentally of similar amplitude to each other, and are also phase-cancelling on a fortnightly basis or about 13.66 days in this case (Nunes-Vaz, pers. comm.) The slightly differing periods of these fortnightly signals means that each pair of constituents reinforce and cancel each other on a 6 monthly basis, producing exaggerated "dodge" tides that occur mid-late May and mid-late November every year (i.e. when the phases of both O1-K1 and M2-S2 harmonics nullify their amplitudes), further reducing the tidal excursions (Nunes-Vaz, pers. comm.). Another feature of the Spencer Gulf tidal regime is its longitudinal modulation of tidal elevations. In particular, the regime demonstrates predominantly diurnal elevation changes near the centre of the Gulf (Wallaroo), and a semi-diurnal character of elevation at both the mouth and northern ends (Easton 1978).

Local meteorology governs hydrodynamic temperature and salinity responses in the region, rather than the interaction with the continental shelf (Nunes and Lennon 1986). North-south water temperature differences are up to 2°C from Port Bonython to the head of the Gulf, with the mean water temperature at Port Augusta ranging between 12 and 24°C over the annual cycle. Corresponding salinities at this location range from ~43 to 48 g/L. This range decreases to ~38 to 39 g/L 160km south of Port Augusta (Nunes and Lennon 1986). Strong evaporation north of Point Lowly drives these high salinities at the head of the Gulf and results in development of a broadscale north-south salinity gradient during summer. This gradient is relaxed during autumn and winter due to the combined effects of reduced evaporation and a large scale ejection of salt from the Gulf (Nunes et al. 1990).

In the Upper Gulf, isohalines run approximately east-west. To the south of Whyalla, isohalines are generally oriented north-south (or more accurately, NNW-SSE), consistent with a large-scale cyclonic (clockwise) gyre (Nunes and Lennon 1986). A scaling based on the non-dimensional Rossby number ( $R$ ), which reflects a ratio between inertia and the Earth's rotation (Kundu 1990), can be used to infer the importance of the Earth's rotation in the water motion (in this case, the gyre) in Spencer Gulf.

$$R = \frac{U}{Lf}$$

where  $U$  is a velocity scale,  $L$  is a structure length scale, and  $f$  is the Coriolis parameter or inertial frequency.

Using data from Nunes and Lennon (1986) or mean current speeds presented herein (Section 5), gives a velocity scale  $U = 0.02-0.2$  m/s,  $f = 7.92e^{-5}$  rad/s, and a conservative  $L = 10$ km (i.e. Gulf width). These scales provide  $R = O(0.01-0.1)$  and thus indicate that the Earth's rotation plays a significant role in the dynamics of the flow. In the southern hemisphere, flows affected by the earth's rotation move with the coastline to the left. This is consistent with the observed behaviour of the saline discharge from the Gulf along the eastern shoreline being balanced with the fresher inflow along the western shore leading to the cyclonic (clockwise) gyre (Nunes-Vaz et al. 1990).

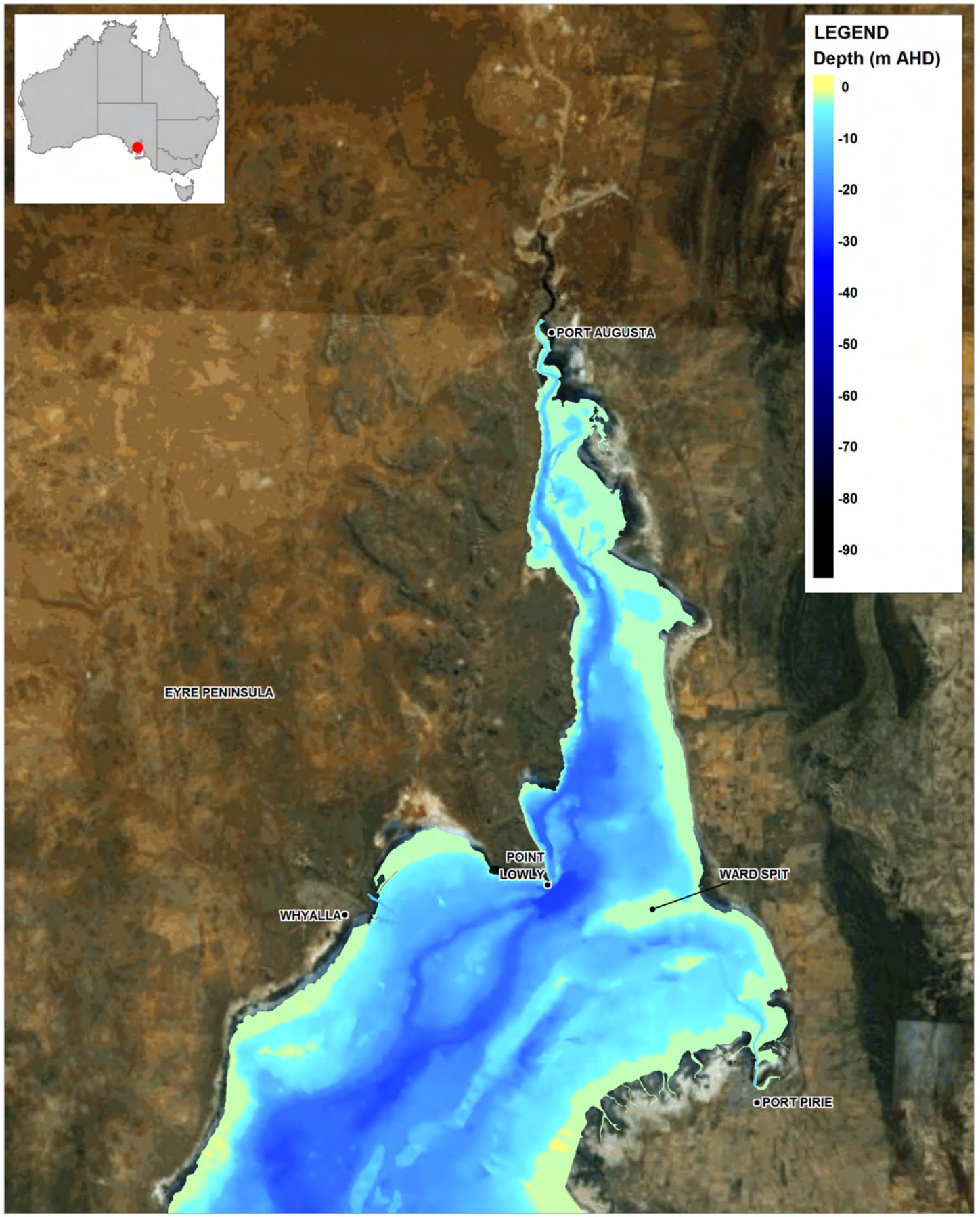
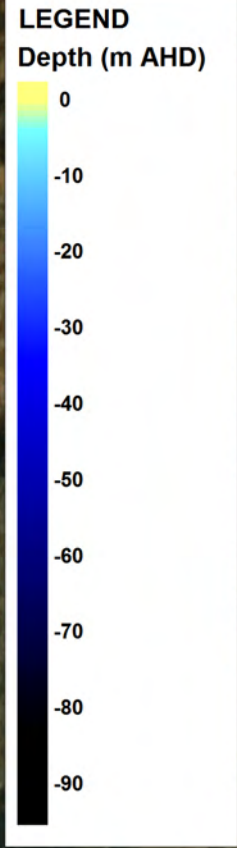
A second mechanism for salt removal observed in the Gulf relates to the fortnightly stratification of Upper Gulf waters due to the weak neap tides (Nunes-Vaz et al. 1990). This stratification results in the periodic formation of high salinity fluid packets that flow southwards, initially close to the coast, but move increasingly westward as it leaves the Upper Gulf (Nunes-Vaz et al. 1990).

## 2.2 Point Lowly

The key area of interest to this study is within Spencer Gulf north of approximately latitude 34 degrees South, which can broadly be referred to as Upper Spencer Gulf (Figure 2-1). This section of the Gulf has a mean depth of approximately 13m, with the mean depth decreasing to approximately 7m north of Point Lowly. Two features of the hydrodynamic circulation in Upper Spencer Gulf, particularly in the vicinity of Point Lowly, are as follows.

First, as Spencer Gulf is a semi-enclosed water body, tides behave as standing waves co-oscillating with the beat imposed at the ocean boundary. As a result, tidal flows converge periodically (i.e. according to the dominant tidal periods), imposing a relatively large discharge through "the Rip", which is a very narrow passage adjacent to Point Lowly (Easton 1978). Targeted BMT WBM field measurements indicate that velocities through this narrow passage can reach over 1.5 m/s (see Section 3.2 below).

Second, it is well known that tidal eddies occur in the lee sides of Point Lowly (Lewis and Noye 1998, Draft EIS – Appendix O11.2). During both ebb and flood tides, a recirculation cell forms to the south and north (respectively) of Point Lowly, controlling the flux through the main channel and the inshore area. Measurements and modelling results clearly show the eddy formation during ebb tides with a clockwise flow producing an easterly along-shore transport. In contrast, a counter clockwise eddy forms north of Point Lowly during flood tides. These observed velocities, although not negligible, correspond to only a small fraction ( $\leq 10\%$ ) of the tidal flow through "the Rip" (Draft EIS – Appendix O11.2).



Title:  
**Upper Spencer Gulf  
Location and Bathymetry**

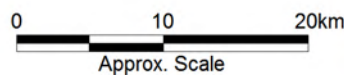
Figure:

**2-1**

Rev:

**A**

BMT WBM endeavours to ensure that the information provided in this map is correct at the time of publication. BMT WBM does not warrant, guarantee or make representations regarding the currency and accuracy of information contained in this map.



Filepath :

### 3 FIELD MEASUREMENTS

A targeted field measurement program was devised and executed specifically for model validation purposes. In particular, these data were used to:

- 1 Verify the model's ability to reproduce overall hydrodynamic conditions around Point Lowly in winter, particularly during well known late autumn 'dodge' tide periods (Nunes-Vaz, pers. comm.);
- 2 Verify the model's ability to capture the details of the spatial variability of hydrodynamic processes in the vicinity of Point Lowly;
- 3 Support and complement the meteorological forcing data adopted in the model framework (see section 4.2).

A description of the measurements undertaken is given below and a summary is provided in Table 3-1. The deployment locations are presented in Figure 3-1 and Figure 3-2.

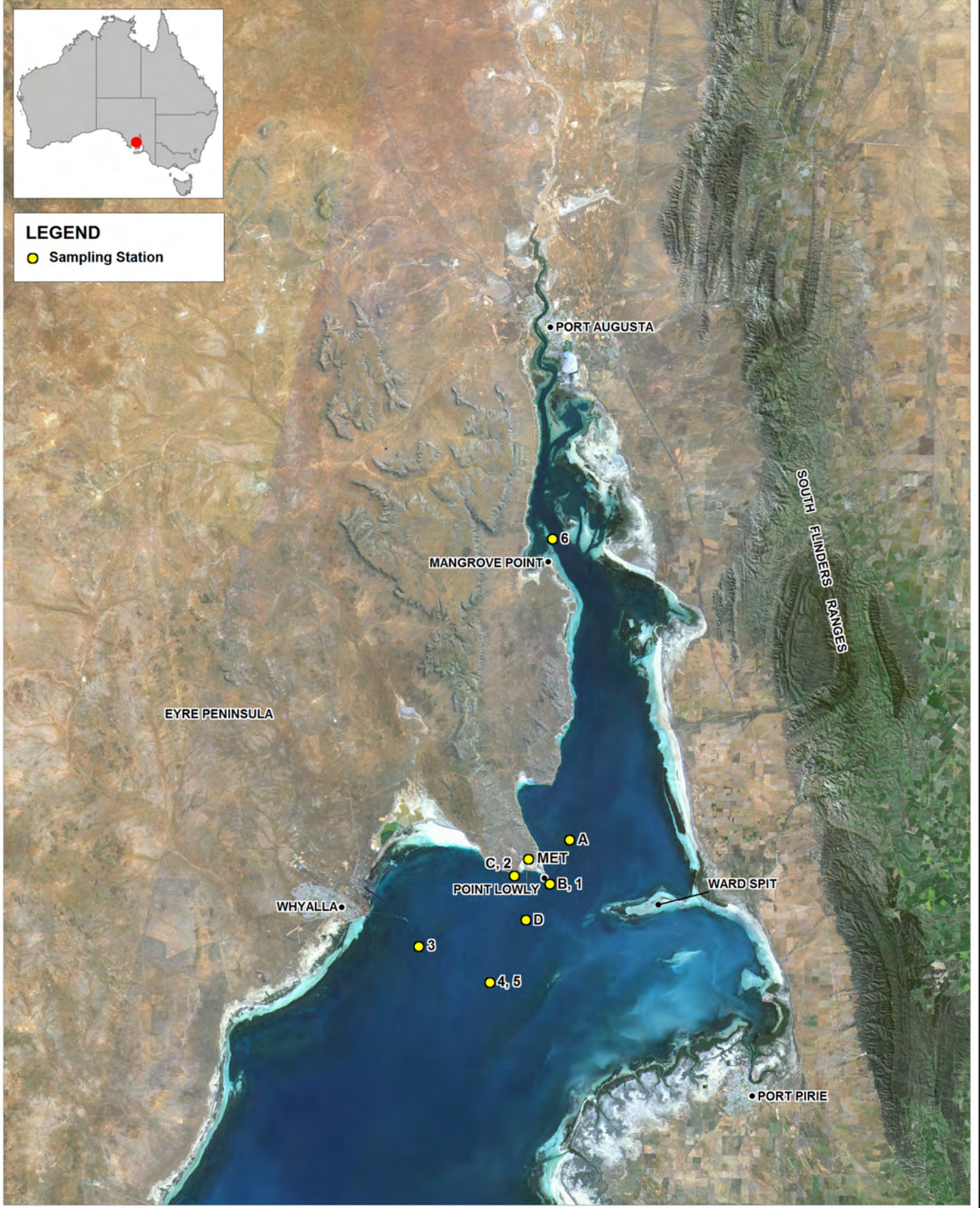
Table 3-1 Summary of measurements specifically undertaken for model development

Measurement Type	Station	Location		Measurement Interval	Measured Variables
		Longitude	Latitude		
Meteorological Data	Met	137° 46' E	32° 59' S	26/04/2009 to 09/06/2009	Air temperature, relative humidity, solar radiation, wind speed, and wind direction
Vertical Velocity Profile (ADCP)	A (~17 m depth)	137° 48.64' E	32° 57.87' S	25/04/2009 to 05/06/2009	Current speed and direction (and backup water depth)
	B (~26 m depth)	137° 47.44' E	33° 00.31' S	27/04/2009 to 02/06/2009	
	C (~10 m depth)	137° 45.09' E	32° 59.94' S	27/04/2009 to 05/06/2009	
	D (~24 m depth)	137° 45.93' E	33° 02.33' S	27/04/2009 to 03/06/2009	
Conductivity Temperature and Depth (CTD)	1 (as B) (~12 m depth)	137° 47.44' E	33° 00.31' S	27/04/2009 to 02/06/2009	Temperature, conductivity (salinity and density), and pressure (depth)
	2 (as C) (~9 m depth)	137° 45.09' E	32° 59.94' S	27/04/2009 to 05/06/2009	
	3 (~12 m depth)	137° 39.03' E	33° 03.96' S	28/04/2009 to 07/06/2009	
	4 (~9 m depth)	137° 43.72' E	33° 05.82' S	28/04/2009 to 07/06/2009	
	5 (~21 m depth)	137° 43.72' E	33° 05.82' S	28/04/2009 to 07/06/2009	
	6 (~7 m depth)	137° 46.92' E	32° 41.40' S	25/04/2009 to 02/06/2009	
Cross-sectional velocity	N/A	See Figure 3-2		19:00 to 02:00 08-09/06/2009	Current speed and direction



**LEGEND**

● Sampling Station

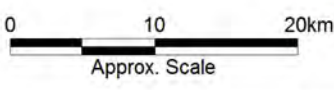


Title: **Location of Sampling Stations (40-Day Deployment 2009)**

Figure: **3-1**

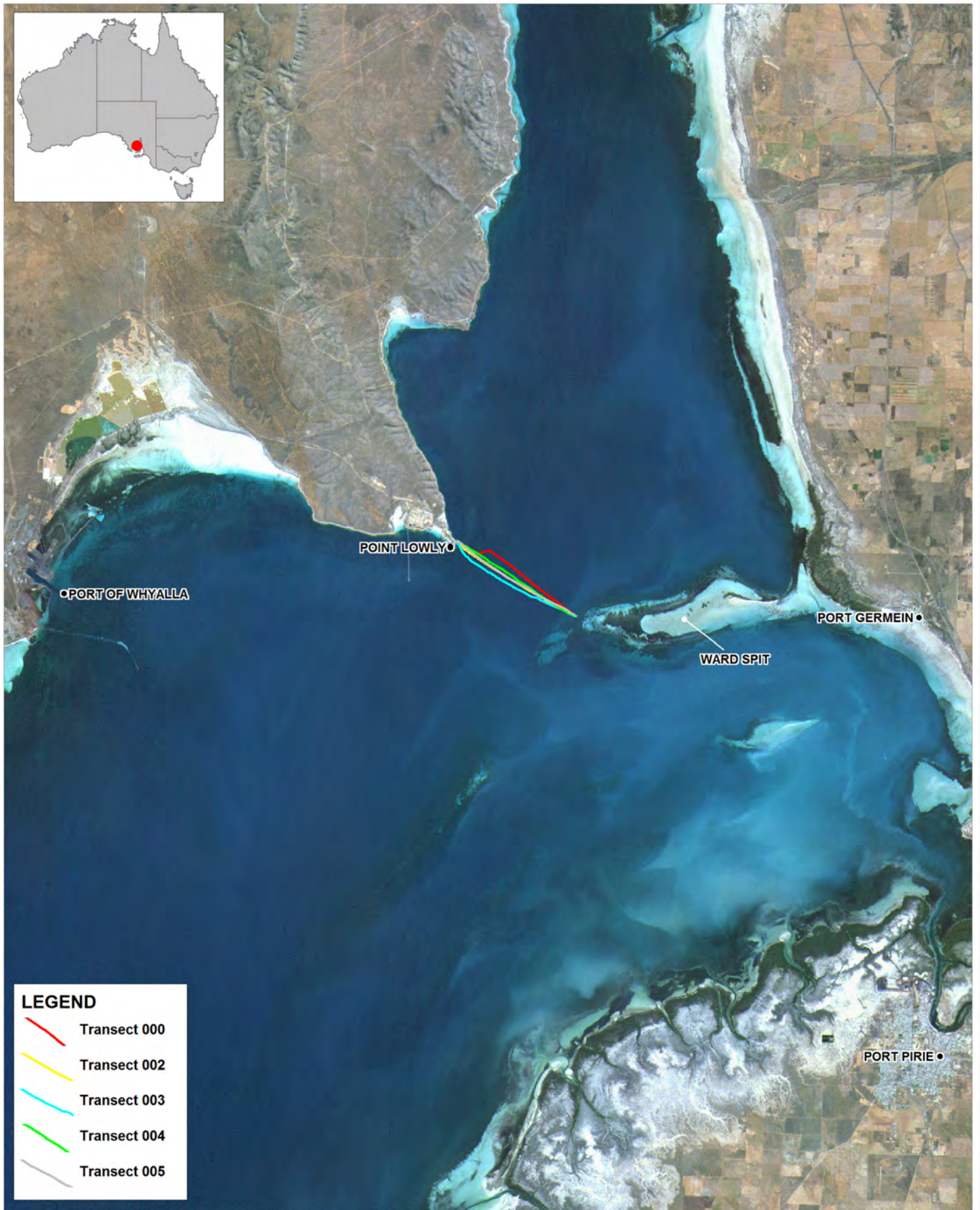
Rev: **A**

BMT WBM endeavours to ensure that the information provided in this map is correct at the time of publication. BMT WBM does not warrant, guarantee or make representations regarding the currency and accuracy of information contained in this map.








Filepath :





**LEGEND**

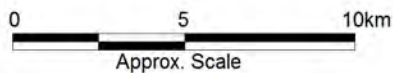
-  Transect 000
-  Transect 002
-  Transect 003
-  Transect 004
-  Transect 005

Title:  
**Locations of Cross-sectional Velocity Transects  
(Short Term 2009)**

Figure:  
**3-2**

Rev:  
**A**

BMT WBM endeavours to ensure that the information provided in this map is correct at the time of publication. BMT WBM does not warrant, guarantee or make representations regarding the currency and accuracy of information contained in this map.



Filepath :

### 3.1 Meteorological Measurements

A weather station was set up to collect a range of meteorological parameters that were used for both the hydrodynamic model forcing and verification of outsourced numerical forcing data (see Section 4.2). The weather station was located near Port Bonython in the Clean Seas Tuna Ltd. yard (137° 46' E, 32° 59' S) performing measurements at a 6-minute sampling interval. The measured data consisted of:

- Air temperature;
- Relative humidity;
- Solar radiation;
- Wind speed; and
- Wind direction.

Table 3-2 presents the weather-station sensor characteristics and the measured meteorological data is presented in Figure 3-3.

Table 3-2 Weather-Station Sensors' Characteristics

Measured Variable	Sensor Model	Accuracy	Resolution
Air temperature	Vaisala Temperature and Relative Humidity Sensor Model HMP50	Under measurement range 0-30 °C, typical accuracy is ±0.6 °C	0.1 °C
Relative humidity	Vaisala Temperature and Relative Humidity Sensor Model HMP50	Accuracy: ±3% (0-90% RH); ±5% (90-98% RH)	1% RH
Solar radiation	Li-Cor Model Li- 200	Under natural daylight conditions, typical accuracy is ±5%	Typically 90 µA per 1000 W m <sup>-2</sup>
Wind Speed	RM Young Mechanical Wind Sensor Model 05106 Marine Model	Wind speed: ±0.3 m/s (1 km/h) or 1% of reading	0.1 m/s
Wind Direction	RM Young Mechanical Wind Sensor Model 05106 Marine Model	Wind direction: ±3 degrees	0.5 degrees

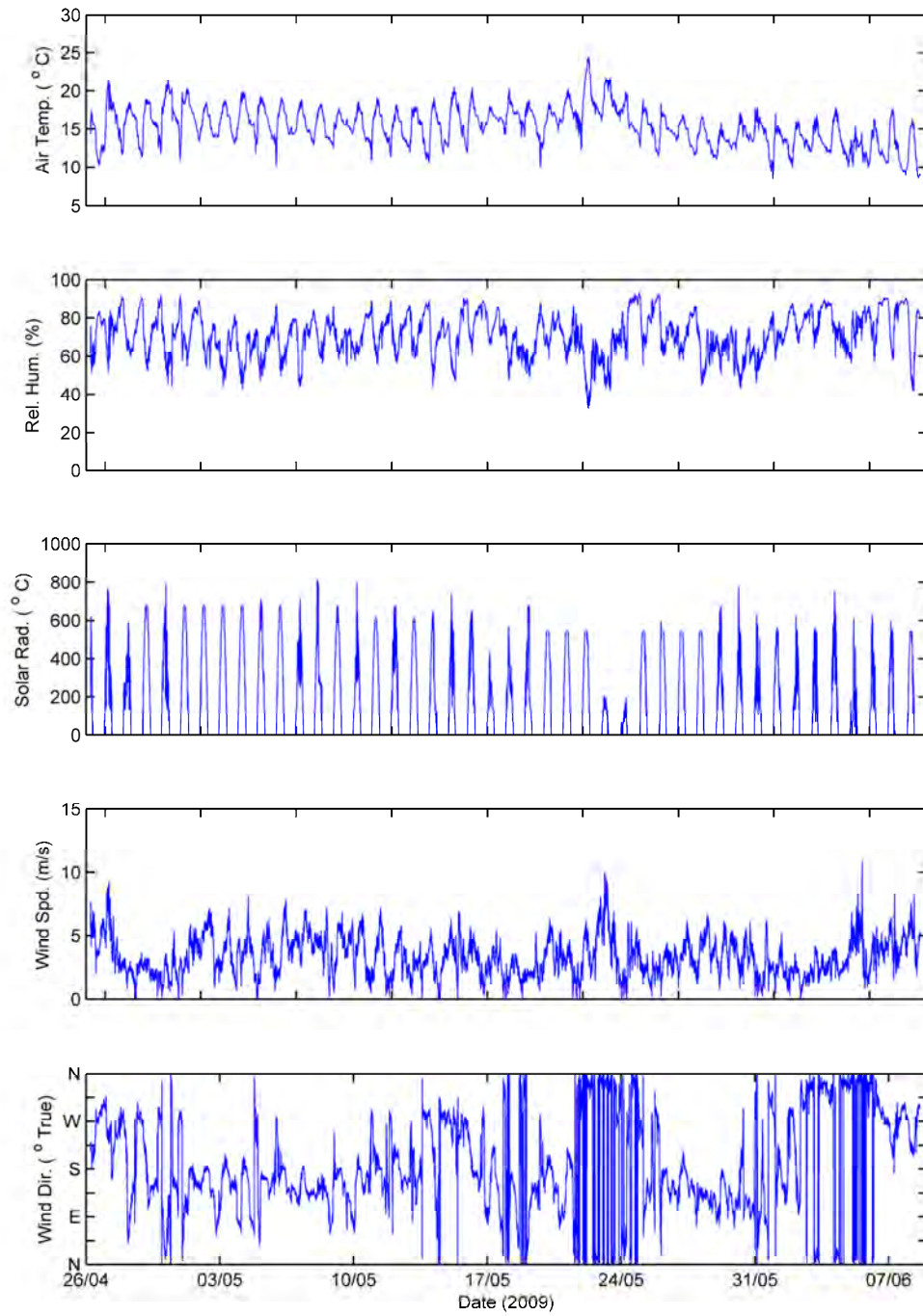


Figure 3-3 Meteorological Data Collected at the Clean Seas Tuna Ltd. Yard

## 3.2 Measurements of Vertical Profiles of Velocity

Vertical profiles of water currents were measured at four locations in the vicinity of Point Lowly using Acoustic Doppler Current Profiler (ADCP) instruments mounted on the seafloor (Figure 3-1). Workhorse Sentinel ADCPs manufactured by RD Instruments (<http://www.rdinstruments.com/>) were mounted within specialised gimbaled frames and positioned by a professional diving team from Whyalla Diving Services. The gimbaled frames were used to ensure the instrument was levelled regardless of the bottom slope. Additionally, the frame skirts were sufficiently wide to provide physical protection against ambient current tilting effects. Ballasting resulting from the relatively heavy ADCP batteries further ensured each instrument remained levelled throughout the deployment.

The ADCPs measured and recorded water currents for an approximate 6 week deployment period. For optimal performance 1200kHz ADCPs were deployed in the shallower locations (stations A and C) and 600kHz ADCPs were deployed in the deeper locations (stations B and D).

In the bed-mounted configuration, each ADCP was programmed to measure currents through the water column at regular intervals (0.5 metres) above the instrument. This provided 'binned' data sets, with each bin corresponding to a height in the water column. Samples were collected at 6-minute intervals through the deployment period, and each measurement consisted of an ensemble of 100 'pings', which were averaged to provide a single representative current speed and direction within each vertical bin at each time. Each ADCP was equipped with an on-board battery and had sufficient internal memory capacity for a deployment in excess of 90 days. An example of the ADCP vertical velocity profiles measured at station B is given in Figure 3-4. The remaining data is shown with the model validation results in Section 5 and in Appendix A.

Measurement statistics are also presented in Figure 3-4, indicating a mean velocity magnitude of 0.45 m/s, despite the occurrence of two 'dodge' tide periods within the deployment period. The magnitude of bottom currents during these 'dodge' tide periods is of particular interest. As can be seen in Figure 3-5, the mean velocities between 2.6 and 3.6 m (representative of the discharge level) are 0.15 m/s, approximately one third of the mean for the whole water column, when considering the entire measurement period. When compared to measurements at Port Stanvac in the Gulf of Saint Vincent, South Australia (Figure 3-5 bottom panel), the Spencer Gulf measurements during 'dodge' tides present larger velocity magnitudes at all percentiles, even though the percentile distributions at Port Stanvac included several spring tide periods. This comparison indicates that vigorous flow through "the Rip" sustains turbulence throughout the water column even during the expected worst cases during the 'dodge' tides at Point Lowly.

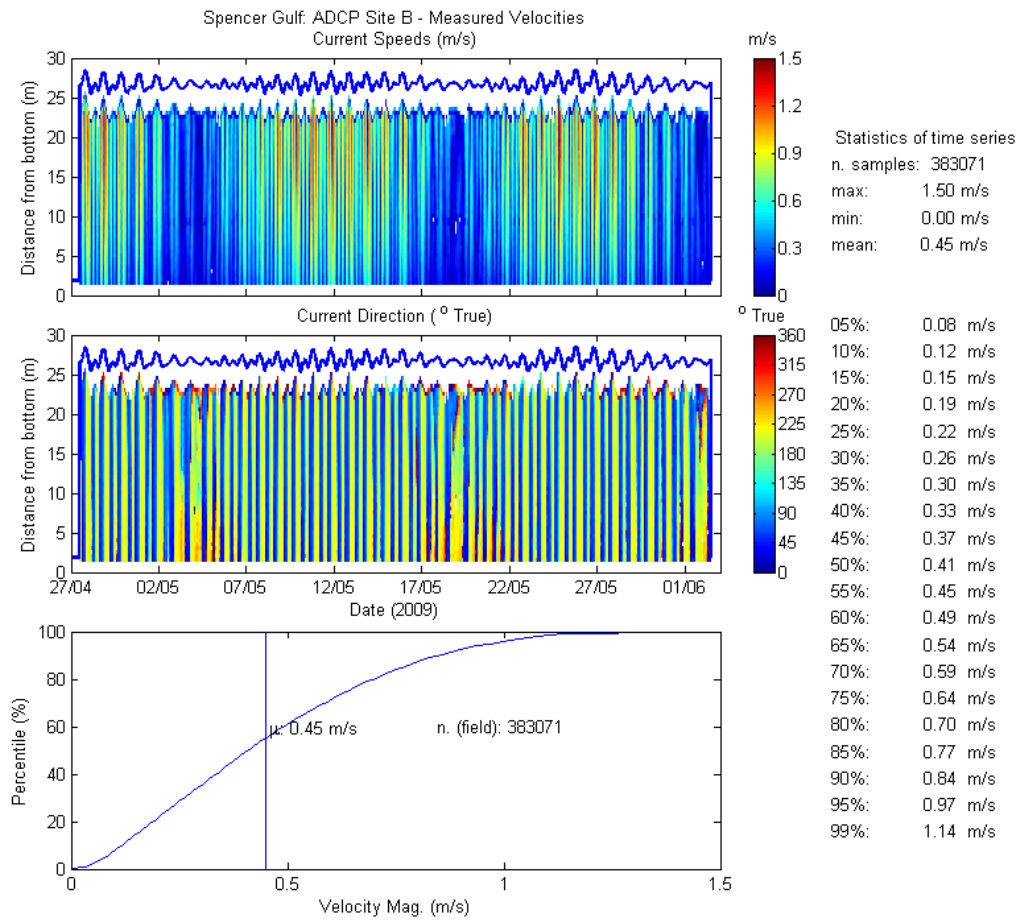


**Figure 3-4 Vertical ADCP Current Profile Measurements at Station B**

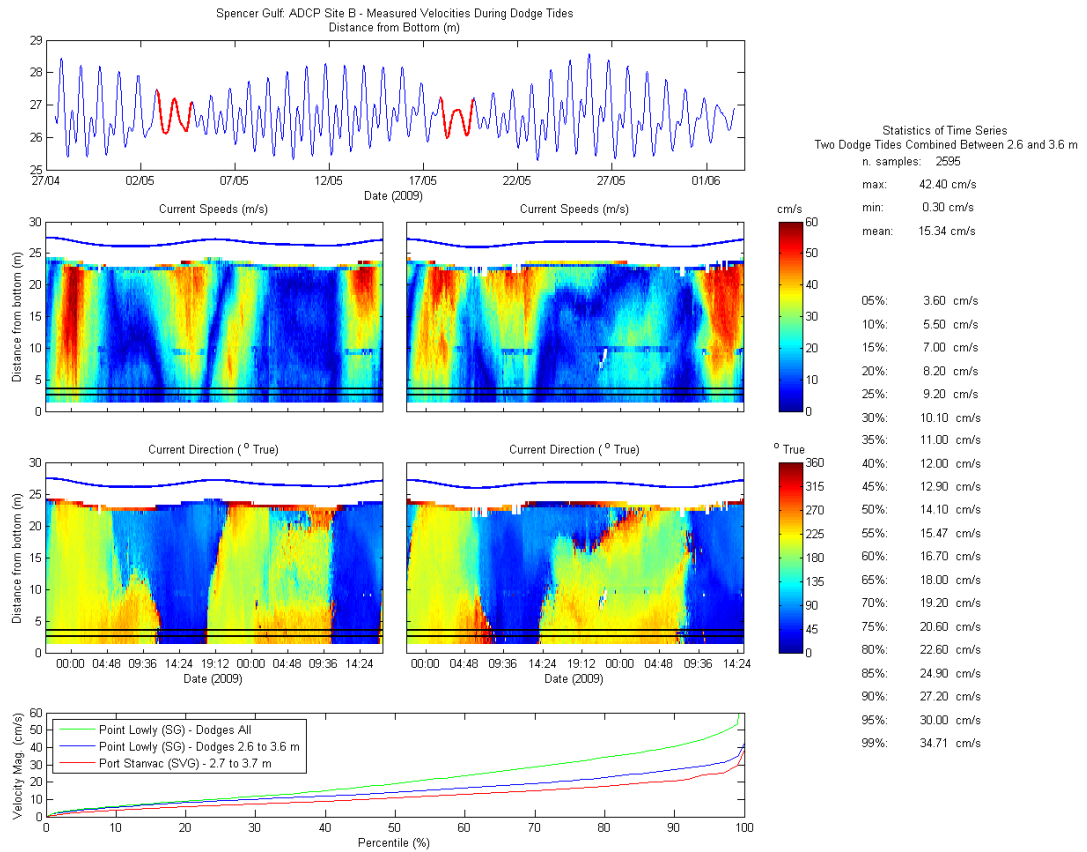


**Figure 3-5 Vertical ADCP Current Profile Measurements at Station B during 'Dodge' Tides. The Top Panel Illustrates the Tidal Elevations, with Red Lines Indicating Water Elevations for Current Magnitude and Direction Depicted in the Centre Panels. The Lower Panel Shows the Cumulative Distribution of Velocity Magnitudes, Including the Distribution of Measurements at Port Stanvac, in the Gulf of Saint Vincent (SA Water 2009).**

### 3.3 CTD Measurements

CTD (conductivity, temperature and depth (pressure)) measurements were designed to capture the salinity and temperature variation across the Point Lowly area and surrounds. Each CTD was a Greenspan CTD3100 probe mounted on an ADCP frame (where possible) or under several navigation-aid buoys. Due to the importance of this data set, the CTD manufacturer was instructed to provide additional factory calibration on all conductivity sensors and report on accuracies achieved as a result. Accuracy of all instruments was superior to 1000  $\mu\text{S}/\text{cm}$  (see Appendix H).

Measurements were performed at the bottom in each location, with the exception of measurements in Station 4 and 5 (same coordinates), in which both mid-depth (~10.0 m average depth) and bottom (~20.0 m average depth) measurements were made (Figure 3-1). Salinity values reported herein have no units, as they were calculated as a function of electrical conductivity (UNESCO 1985). In cases where units have been assumed for calculations, the assumption will be explicitly stated.

The pressure measurements were converted to depth assuming atmospheric pressure given by the WRF model (see Section 4.2), and densities computed from UNESCO (1981) using the local CTD measurements of salinity and temperature. Accuracies of depth calculations were estimated to be the order of 5 cm, or about 3% of the observed tidal amplitude. An example of the CTD measurements at station 5 is given in Figure 3-6. The remaining data is shown with the model validation results in Section 5 and in Appendix B.

A maintenance program in which instruments were attended to by professional divers was adopted to clean all sensor heads and to minimise the effects of drift through biofouling on the measurements. On these occasions hand samples of salinity were collected for laboratory examination (see below) and these were used to improve the salinity measurements (see Section 3.5).



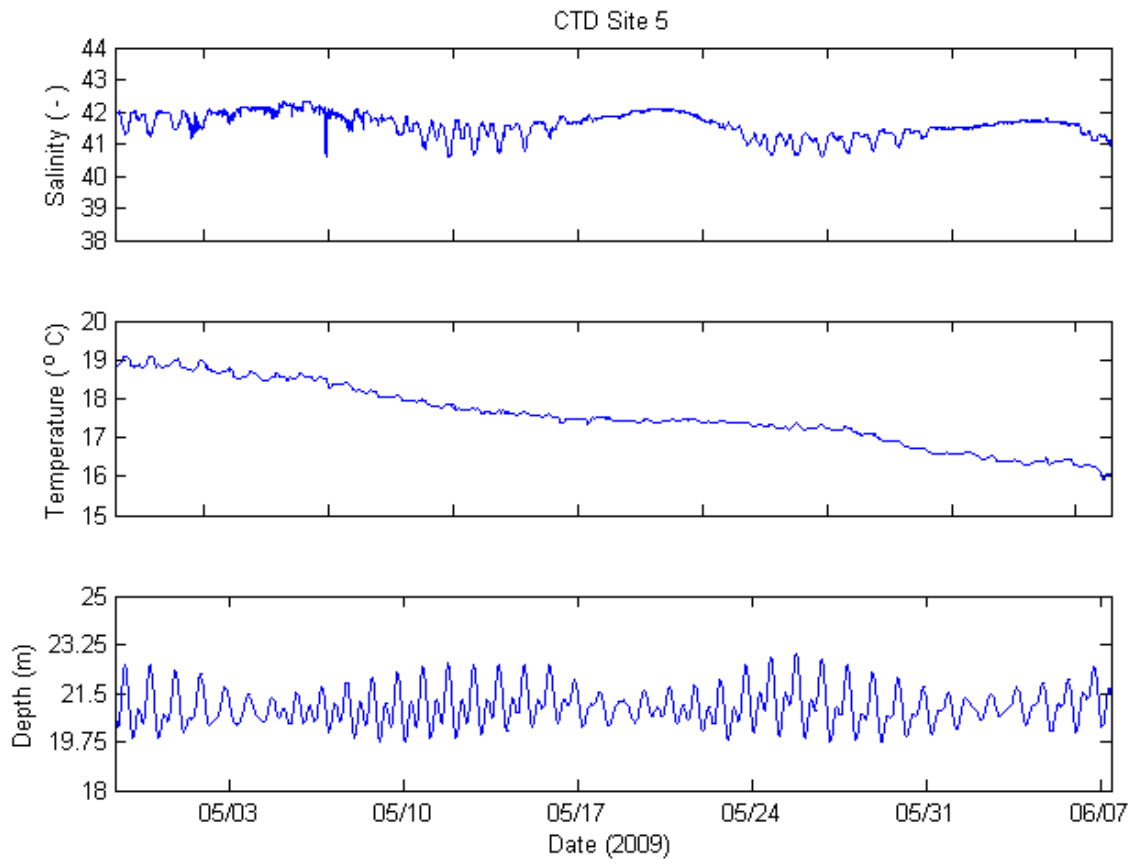


Figure 3-6 Example CTD Measurements at Station 5

### 3.4 Hand-Sample Salinity Measurements

A known feature of moored salinity measurements in Spencer Gulf is the noticeable biofouling and sensor drift (e.g. Nunes and Lennon 1986). As such, for this study hand samples of salinity at the location and depth of the measurements were collected to estimate and correct the potential drift in the CTD salinity measurements. Duplicate samples were collected by Whyalla Diving Services professional divers during deployment, maintenance, and recovery of the instruments. The samples were analysed by Dr. Rick Nunes-Vaz using a Yeo-Kal Autolab Bench Salinometer (Model 601 Mk III) at Flinders University of South Australia. Salinity results were then compared to the CTD measurements to estimate the CTD salinity drift. Table 3-3 presents the salinity data from the respective measurements.

From Figure 3-7 it is apparent that CTD salinity measurements at Site 3 and Site 6 cannot be characterised as accurate due to measurement character and excessive sensor drifting, respectively. Here, measurement character is defined as the spiked and erratic nature of the measurements with jumps of the order of measurement range between two consecutive samples. The stepped character of the measurements at Site 6 after 17 May 2009 shown in Figure 3-7 is questionable. As such, for model verification salinity results at Site 3 have been discarded. For other sites (and Site 6 before 17 May 2009), corrections for sensor drifting were performed as described below and used for model validation.

### 3.5 CTD Salinity Corrections

Corrections to the measurements presented in Section 3.3 were performed to compensate for instrument drift, particularly that introduced as a result of bio-fouling. Bio-fouling was deemed significant only at Site 6, where the CTD measurements after cleaning recovered to the same levels indicated by the hand samples (Figure 3-7). Assuming the hand samples were a true representation of the field salinity, the following procedure was applied for the correction of the CTD measurements.

- 1 Hand samples salinities were converted to electrical conductivities according to UNESCO (1983), assuming the depth and pressure measured by the CTD;
- 2 An average of the replicate hand samples conductivities was calculated;
- 3 It was assumed the first CTD reading was not affected by bio-fouling and therefore correct; then
- 4 Looping through each hand sample measurement:
  - (a) an offset was computed between the hand sample electrical conductivity and the CTD electrical conductivity measurement in the time the hand sample was taken;
  - (b) an offset rate was calculated as a linear variation between 0 and the offset over the time between the time in which the CTD sensor was cleaned and the previous hand sample time (or from the first CTD measurement if the first hand sample);
  - (c) the offset rate was then used to calculate electrical conductivity offsets for all CTD samples on times between the time in which the CTD sensor was cleaned and the previous hand sample time (or from the first CTD measurement if the first hand sample);
  - (d) the offsets were then added to the CTD samples;

- 5 The CTD salinities were then computed using UNESCO (1983), using the corrected CTD electrical conductivities and the same CTD pressure and temperature.

This correction assumes a linear effect of bio-fouling on electrical conductivity. The resulting corrected time series are presented in Figure 3-8 below and associated distributions are illustrated in Figure 3-9 and Table 3-4. Figure 3-8 shows that only very minimal sensor drift occurred at Sites 1, 2, 4, and 5, thus supporting the use of these sensors (and the additional factory calibration) to this study.

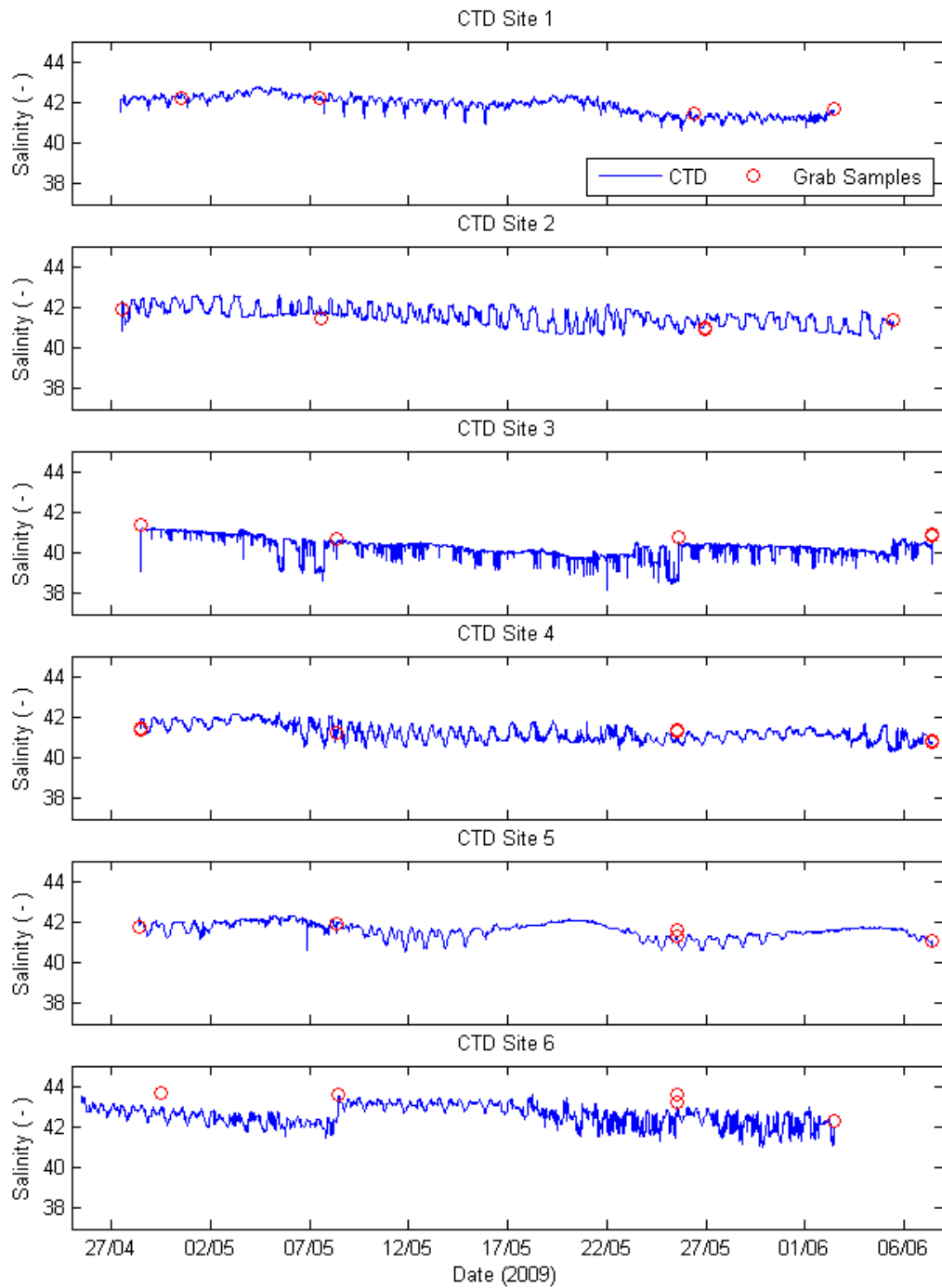


**Figure 3-7 Comparison between CTD and Hand-Sampled Salinity Measurements**

**Table 3-3 Salinity Measurements Verification**

Site	Date	Salinity		
		CTD	Hand Sample A	Hand Sample B
1	30-Apr-2009 12:30	42.37	42.23	42.24
	07-May-2009 11:28	42.18	42.24	42.24
	26-May-2009 09:50	41.19	41.43	41.43
	02-Jun-2009 10:45	41.57	41.72	-
2	27-Apr-2009 13:10	41.51	41.92	41.89
	07-May-2009 14:20	41.67	41.42	41.42
	26-May-2009 22:25	41.10	40.94	41.01
	05-Jun-2009 11:20	41.33	41.37	41.38
3	28-Apr-2009 12:30	40.61	41.35	41.35
	08-May-2009 08:40	40.25	40.72	40.72
	25-May-2009 14:47	38.70	40.80	40.79
	07-Jun-2009 10:36	40.04	40.87	40.89
4	28-Apr-2009 10:55	41.71	41.43	41.38
	08-May-2009 09:35	41.33	41.26	41.26
	25-May-2009 14:00	40.84	41.28	41.38
	07-Jun-2009 09:42	40.71	40.76	40.81
5	28-Apr-2009 10:45	41.85	41.80	41.75
	08-May-2009 09:40	41.81	41.95	41.95
	25-May-2009 14:00	41.18	41.62	41.34
	07-Jun-2009 09:36	40.82	41.05	41.04
6	29-Apr-2009 12:30	42.93	43.70	43.69
	08-May-2009 11:10	43.13	43.57	43.56
	25-May-2009 12:30	42.64	43.58	43.22
	02-Jun-2009 11:45	41.89	42.28	42.27

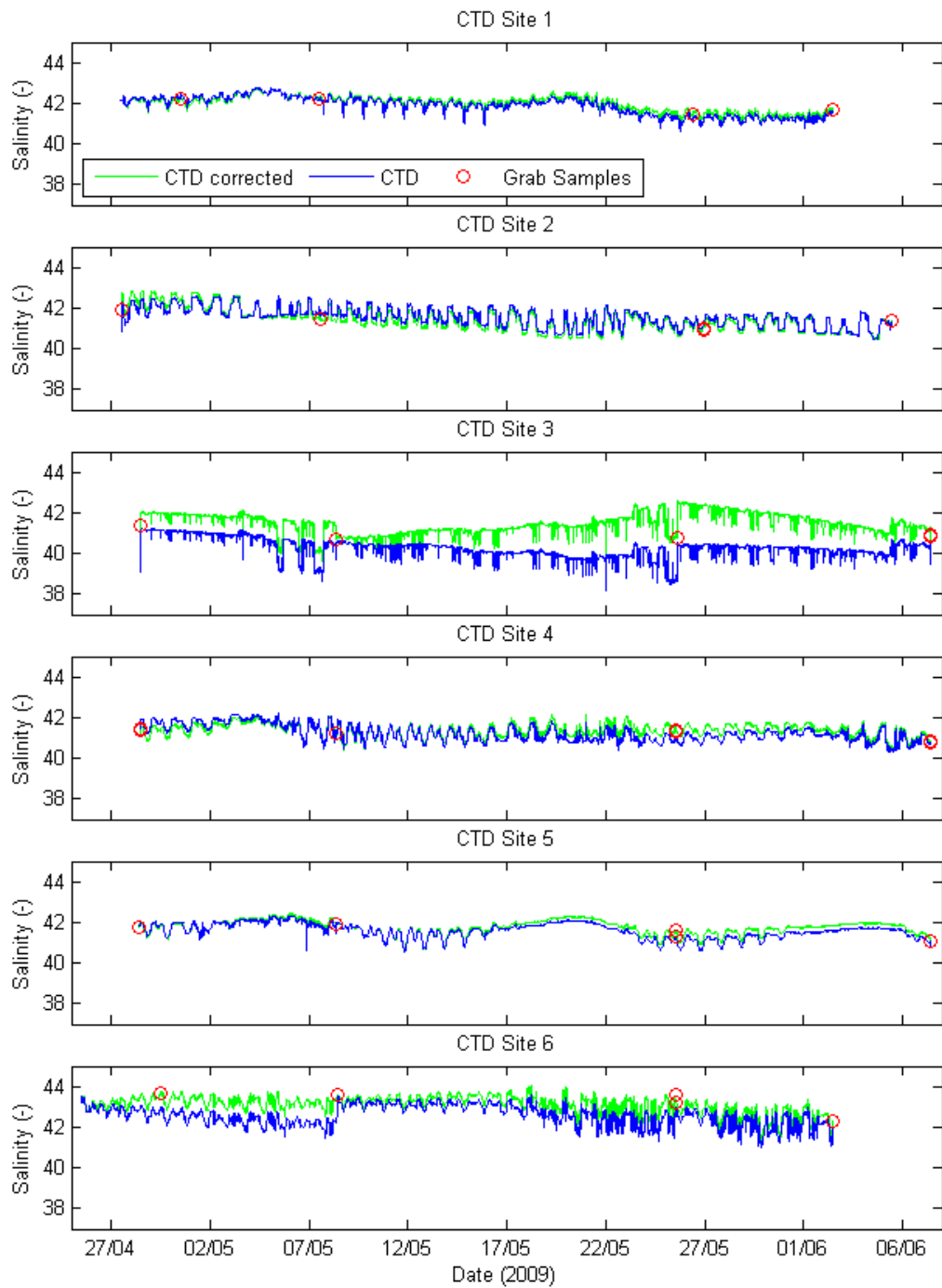
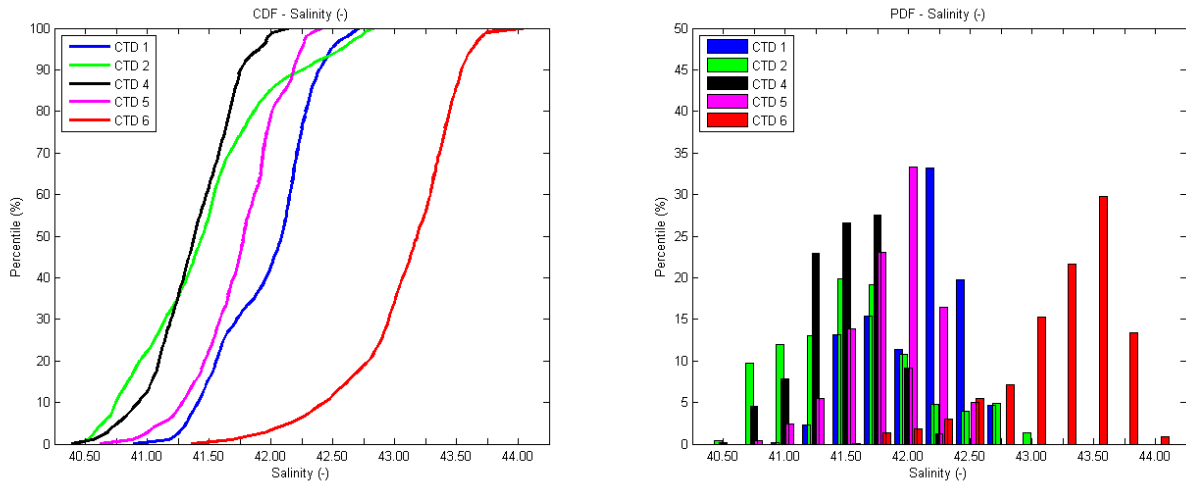


Figure 3-8 Raw and Corrected CTD Salinities



**Figure 3-9 Corrected CTD Salinity Distributions. CDF – Cumulative Distribution Function, PDF – Probability Distribution Function.**

**Table 3-4 Corrected CTD Salinity Percentile Distributions**

Site	CTD Site 1	CTD Site 2	CTD Site 4	CTD Site 5	CTD Site 6
<b>n. samples:</b>	8631	9345	9589	9592	9114
<b>max:</b>	42.72	42.84	42.16	42.43	44.08
<b>min:</b>	40.89	40.46	40.39	40.62	41.36
<b>mean:</b>	41.97	41.46	41.37	41.75	43.08
<b>1%:</b>	41.18	40.52	40.56	40.87	41.69
<b>5%:</b>	41.32	40.65	40.76	41.12	42.16
<b>10%:</b>	41.41	40.75	40.93	41.28	42.43
<b>15%:</b>	41.49	40.84	41.04	41.39	42.62
<b>20%:</b>	41.56	40.94	41.10	41.47	42.79
<b>25%:</b>	41.62	41.06	41.14	41.53	42.89
<b>30%:</b>	41.73	41.15	41.19	41.59	42.95
<b>35%:</b>	41.86	41.25	41.25	41.65	43.01
<b>40%:</b>	41.96	41.32	41.29	41.70	43.07
<b>45%:</b>	42.03	41.38	41.34	41.75	43.13
<b>50%:</b>	42.09	41.45	41.38	41.78	43.18
<b>55%:</b>	42.12	41.50	41.43	41.82	43.24
<b>60%:</b>	42.15	41.54	41.48	41.87	43.29
<b>65%:</b>	42.18	41.60	41.53	41.92	43.32
<b>70%:</b>	42.21	41.67	41.58	41.94	43.36
<b>75%:</b>	42.25	41.76	41.62	41.97	43.40
<b>80%:</b>	42.28	41.87	41.67	42.01	43.44
<b>85%:</b>	42.33	42.00	41.71	42.11	43.49
<b>90%:</b>	42.40	42.26	41.76	42.18	43.54
<b>95%:</b>	42.49	42.58	41.91	42.25	43.63
<b>99%:</b>	42.66	42.76	42.02	42.35	43.74

### 3.6 ADCP Cross-Sectional Velocity Measurements

A vessel-mounted ADCP was used to perform velocity (flux) measurements between Point Lowly and Ward Spit on transects of about 6 km in length and an approximately NW-SE orientation (Figure 3-2). To this end, a RDI 1200 kHz Workhorse Sentinel ADCP connected to a differential GPS (TRIMBLE ProXRS) and to a navigation data collector (TRIMBLE TSC1) was mounted on a survey vessel supplied by Whyalla Diving Services.

Five profile measurements were undertaken over a full ebbing tide period during a weak neap cycle, from approximately 19:00 on 08 June 2009 to 02:00 on 09 June 2009 (Figure 3-10). The vessel was driven at about 6 km/h along each transect, with each requiring about 1 hour to be completed. Velocity measurements were then converted to earth-coordinates for comparison with model results. This technique has been successfully applied by BMT WBM and others to collect data to assist with numerical model validation in a range of settings from rivers and estuaries to canal estates and semi-enclosed coastal embayments such as Moreton Bay. One specific example where these measurements were successfully used was in the validation of a numerical model of Pumicestone Passage, QLD. In this case, the boat mounted ADCP measurements and model were used to identify a subtle net northerly transport in the Passage, which had been proposed earlier (by others) through theoretical arguments (BMT WBM 2005).

An example of the ADCP cross-sectional velocity measurements (transect Section 003) is given in Figure 3-11. The Section 001 transect was discarded due to failure in the boat navigation signal (not shown). The remaining data is shown with the model validation results in Section 5 and in Appendix C.



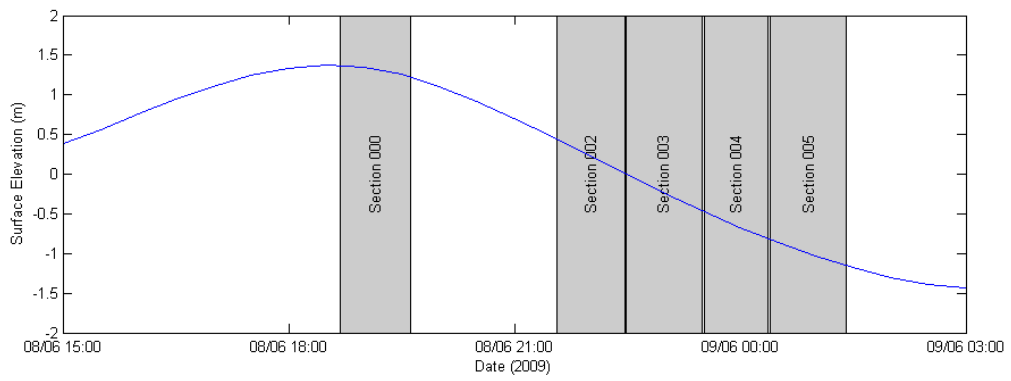


**Figure 3-10 Time of the ADCP Cross-Sectional Velocity Measurements in Relation to the Phase of the Tide**

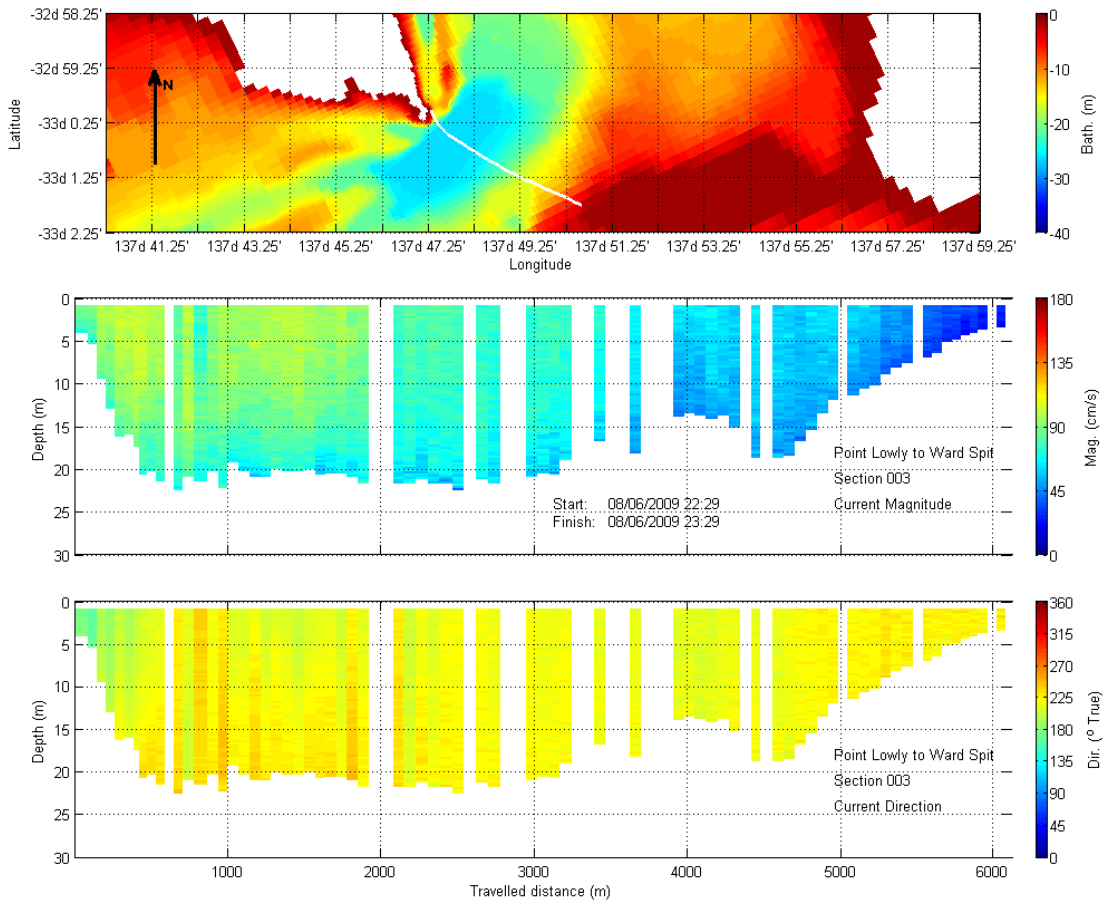


**Figure 3-11 ADCP Cross-Sectional Velocity Measurements (Section 003)**

## 4 NUMERICAL MODEL SET UP

The modelling adopted in the present study forms an “upgrade” of the model adopted in the Draft EIS (Appendices O11.2, O11.3, and O11.4). The three-dimensional modelling package ELCOM (Estuary, Lake, and Coastal Ocean Model) was used in this study (Figure 4-1). Details of the model characteristics and numerical scheme have been described previously and the reader is referred to previous reports for details and an explanation of the ‘fit-for-purpose’ nature of the modelling platform (Draft EIS – Appendix O11.2). The following sections describe the components of the model set up specific to this study.

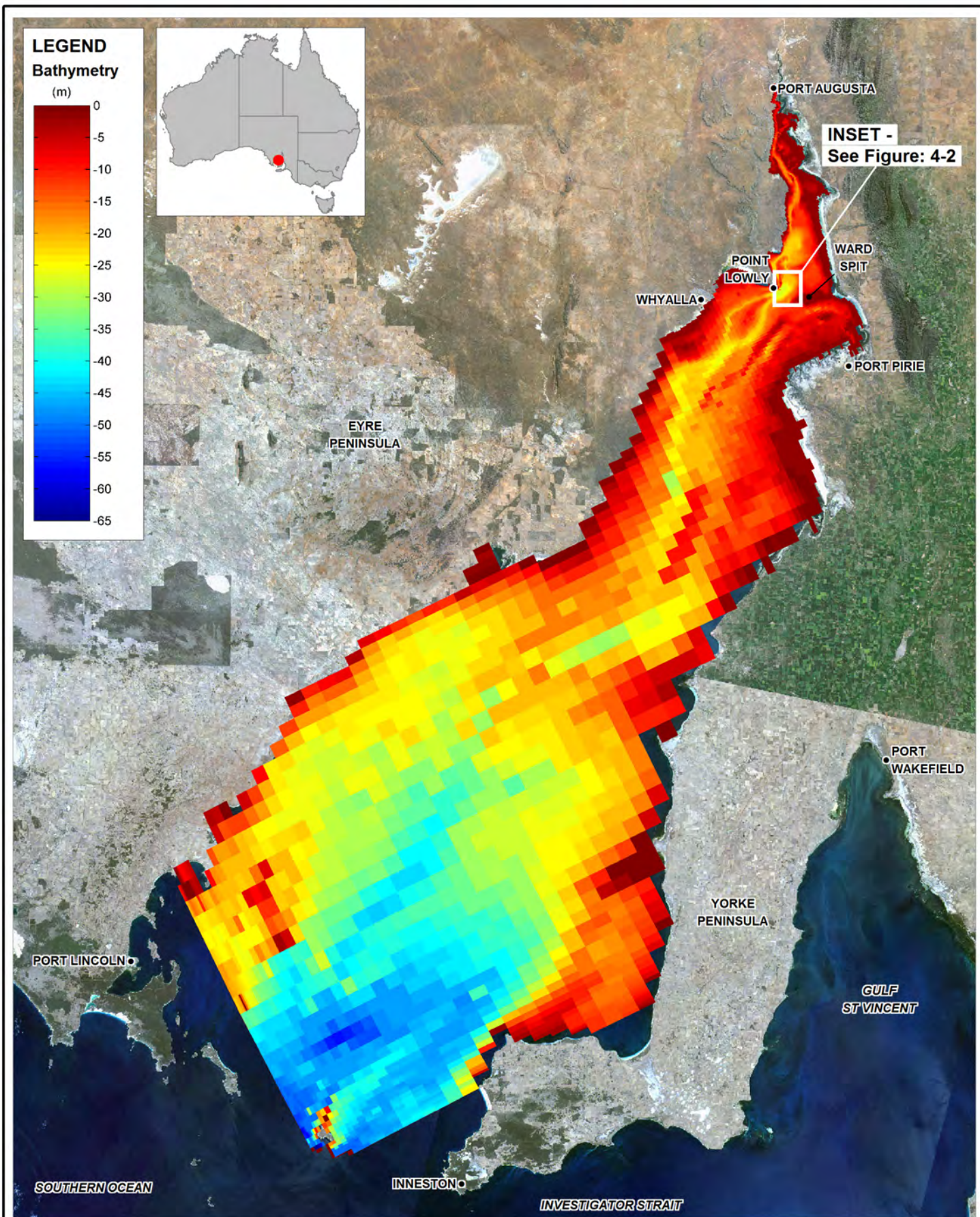
### 4.1 Model Bathymetry and Grid

The bathymetry data was obtained from a Digital Elevation Model (DEM) of Spencer Gulf produced from a combination of local navigation charts (AUS 136, AUS 776 to 778) and targeted echosoundings performed in the region of Point Lowly (see Figure 4.2 in the Draft EIS - Appendix O11.2). This DEM was then referenced to AHD (Australian Height Datum) to provide for a consistent vertical datum over the entire domain. The addition of the echo soundings forms an upgrade on the model presented in the Draft EIS (Appendix O11.2), which was solely based on the navigation charts.

A 228 (azimuthal) x 293 (longitudinal) x 31 (vertical) cell orthogonal grid was constructed. It was oriented to have cell faces approximately aligned with the currently proposed diffuser alignment centreline, as provided by BHP Billiton. This resulted in the model being rotated by an angle of approximately 64 degrees anti-clockwise to the N-S orientation (Figure 4-1). The grid contained a total of 244,755 possible wet cells and 21,018 surface cells.

In the horizontal, a 40-m grid size was used along and across the centreline alignment of the proposed diffuser (Figure 4-2). This size was progressively increased away from the proposed diffuser location in the direction of Port Augusta and Port Lincoln. Ultimate cell sizes at these locations were approximately 500 m and 5 km, respectively. The rate of grid size increase was always maintained below 10%.

In the vertical, the grid incorporated 31 layers designed to span -69.72 m (deepest bathymetry) to +3.98 m, such that spring tides and wind set-up of the free-surface could be accommodated (Figure 4-3). The vertical grid size was 2.00 m down to -4.02 m, then it was progressively decreased to 1.00 m at -13.97 m and kept at 1.00 m down to -22.97 m, where it was progressively increased to 1.65 m at -35.10 m. The rate of cell size decrease/increase was again maintained below 10%. In order to provide full coverage of the model bathymetry, five grid cells of 3.60, 5.00, 8.00, 10.00, and 12.00 m then formed the remainder of the vertical grid towards the bottom. It is noted that ELCOM has variable cell thicknesses at the bottom during grid construction and at the free-surface during simulation, so that shallow areas are sufficiently resolved as needed. No minimum water depths are imposed and wetting and drying process are included without a need for simplifying assumptions.

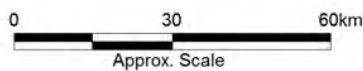


Title:  
**Model Grid and Bathymetry**

Figure:  
**4-1**

Rev:  
**A**

BMT WBM endeavours to ensure that the information provided in this map is correct at the time of publication. BMT WBM does not warrant, guarantee or make representations regarding the currency and accuracy of information contained in this map.



Filepath :

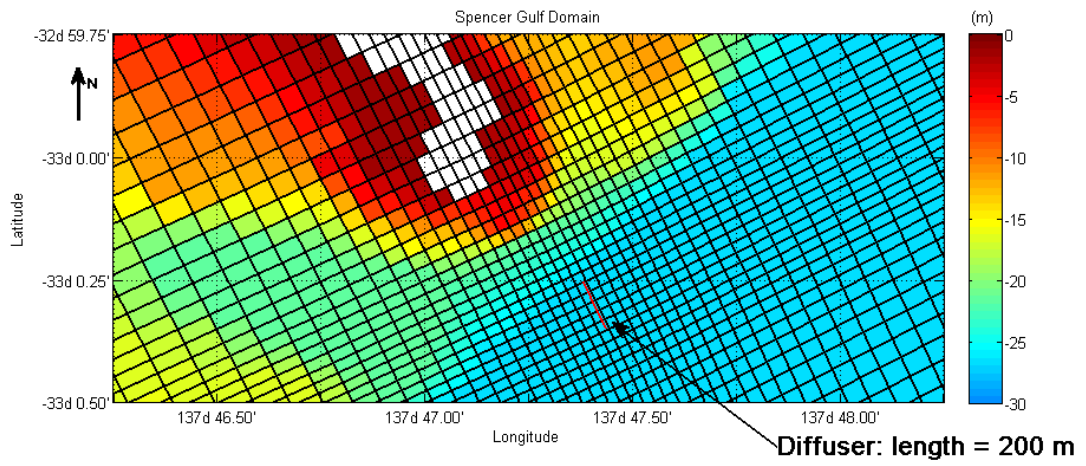


Figure 4-2 Detail of the High-Resolution Region of the Model Grid

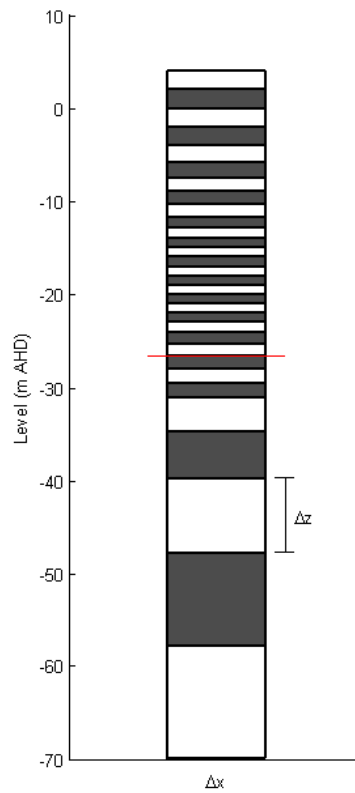


Figure 4-3 Vertical Grid. Red Line Indicates Bottom Level at the Location of the Proposed Diffuser

## 4.2 Surface Boundary Conditions

ELCOM requires air temperature, relative humidity, longwave radiation, solar radiation, wind speed, and wind direction data to compute the surface heat exchange. Wind speed is also used to calculate the surface wind stress as

$$\tau_w = \rho_a C_w |U_w| U_w$$

where  $\rho_a$  is the air density,  $C_w$  is the wind drag coefficient, and  $U_w$  is the wind speed at 10 m from the surface in a given direction.  $C_w$  is computed according to Imberger and Patterson (1990) to account for the effects of atmospheric stability and surface roughness. The atmospheric data were sourced from the Weather Research and Forecasting (WRF) global atmospheric model. This model is developed and actively maintained by several renowned institutes such as NCEP (National Center for Environmental Prediction – National Oceanic and Atmospheric Administration), NCAR (National Center for Atmospheric Research) and the United States Air Force.

The WRF model employed for this study was set up on a grid of 16-20 kilometres resolution in the horizontal by 27 pressure levels. Each variable was computed at a 1-hour time interval and output was recorded at 10 m height from mean sea level. This high resolution WRF model was forced with global NCEP-GFS (Global Forecast System) atmospheric forecast data at resolutions of 1 degree, both over land and the oceans. The high resolution data used for this modelling study was compared to wind fields extracted from satellite observations (scatterometer, SAR) and data obtained from the deployed meteorological station. These comparisons are presented in Figure 4-4 and show agreement and adequacy of the data.

The data was output from WRF at 1-hour intervals and was spatially interpolated to the ELCOM grid assuming a nearest neighbour interpolation. A total of 108 surface boundary condition data sets were employed in ELCOM to provide a smoothly spatially varying atmospheric forcing. The spatial distribution of the atmospheric forcing is presented in Figure 4-5. This spatial distribution is important, as it ensures that key north-south gradients in meteorological forcing are appropriately captured and their impacts on the hydrodynamics included. An example of this variation is illustrated below (Figure 4-6).

Six rainfall gauges sourced from the Bureau of Meteorology (BoM) were used to produce the rainfall field over the model surface (Figure 4-7). To complement data in the eastern side of the Gulf, data from coordinates -33.00 S, 138.00 E from the BoM Data Drill SILO (BoM Internet Database for Climate Data, no existing acronym specification) database was sourced (Figure 4-7). Daily rainfall data was interpolated over the same spatial distribution illustrated in Figure 4-5 using an inverse squared distance method. Rainfall data is presented in Figure 4-8.

## 4.3 Open Boundary Conditions

Open boundary conditions were imposed in the South and South Eastern ends of the rotated domain (Figure 4-1).

The tidal elevation dataset was sourced from a global tidal model which is validated with reference to approximately 5000 tidal stations and 15 years of satellite radar altimeter (BMT ARGOSS, pers.

comm.). This model has been developed by BMT ARGOSS and provides astronomical tidal elevations relative to Mean Sea Level at specified locations.

Salinity and temperature data for the boundaries was sourced from the global HYCOM 1/12 degree model database. HYCOM (HYbrid Coordinate Ocean Model, <http://www.hycom.org/>) is an operational global ocean model which assimilates all available satellite altimeter and Argo profiling float data (Argo is a global array of 3,000 free-drifting profiling floats that measures the temperature and salinity of the upper 2000 m of the ocean). In this way, HYCOM can achieve adequate initial conditions for its operational runs, and represent major oceanic processes. A total of eight points across the mouth of the Gulf were used to define depth and time varying temperature and salinity boundary conditions in ELCOM.

The HYCOM surface elevation data characterises low frequency features associated with major oceanic features (sea surface slopes, eddies, etc.), and was used to supplement the tidal data described previously.

The above tidal, salinity and temperature data was then imposed as boundary conditions for ELCOM. Tidal elevations were imposed at hourly intervals, whilst temperature and salinity were sourced directly from HYCOM outputs at 24-hour intervals. Open boundary condition data for simulations presented in Section 5 are illustrated in Figure 4-9 (i.e. the medium-term forty-days simulation) and Figure 4-10 (i.e. the long-term 1-year simulation). Only the eastern and western most points and temperature and salinity data at different depths are shown for each location.

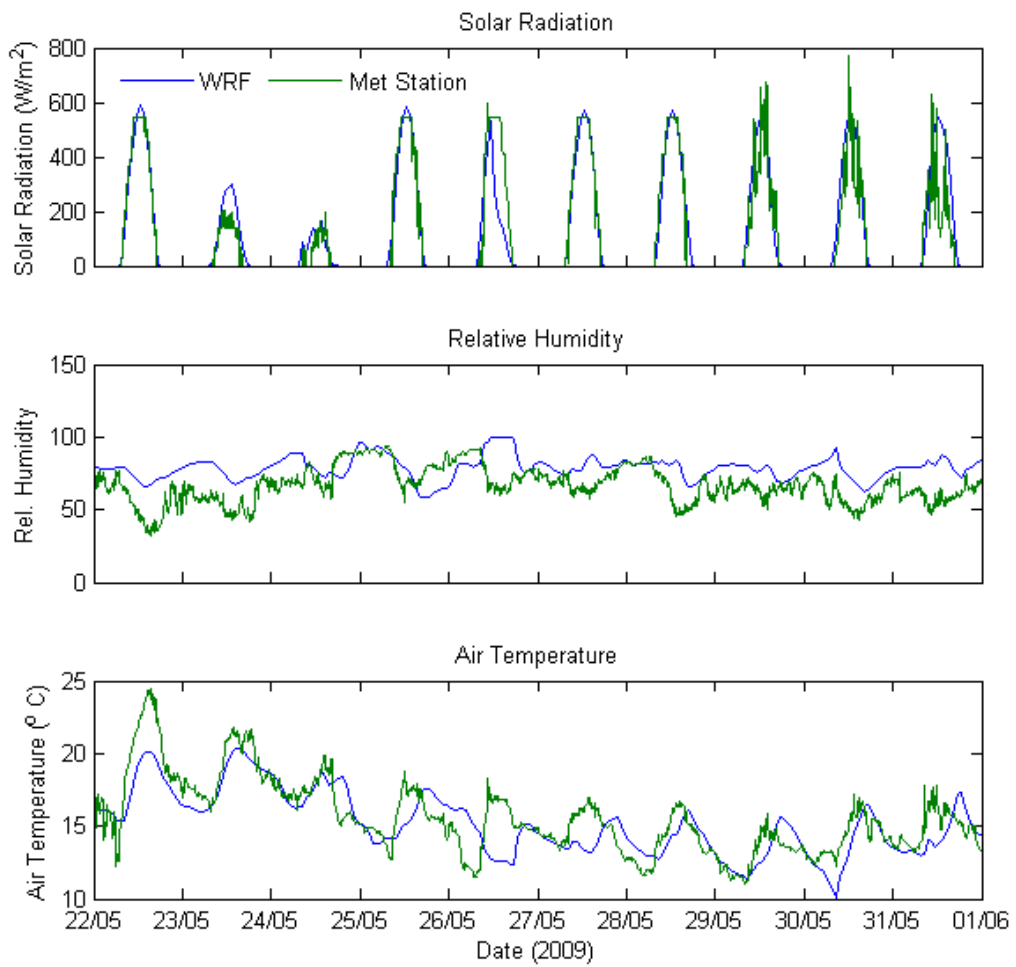
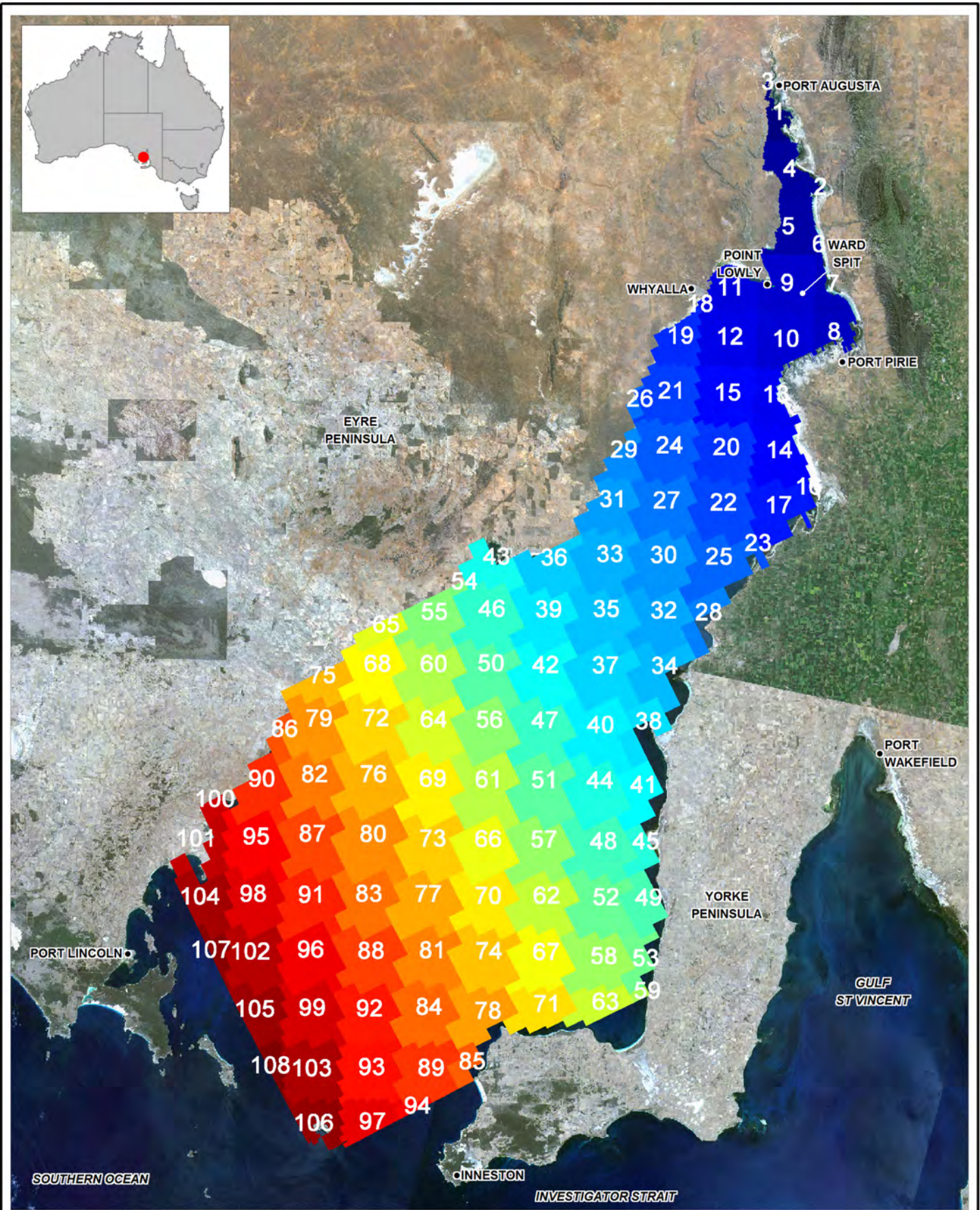


**Figure 4-4 Comparison of Meteorological Data between WRF-Extracted Boundary Conditions and the Port Bonython Met Station**



Title: **Spatial Distribution of the Surface Boundary Forcing**

Colour code indicates area of influence of each boundary condition and has no implicit quantitative meaning.

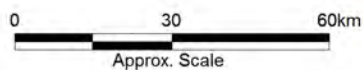
Figure:

4-5

Rev:

A

BMT WBM endeavours to ensure that the information provided in this map is correct at the time of publication. BMT WBM does not warrant, guarantee or make representations regarding the currency and accuracy of information contained in this map.



Filepath :



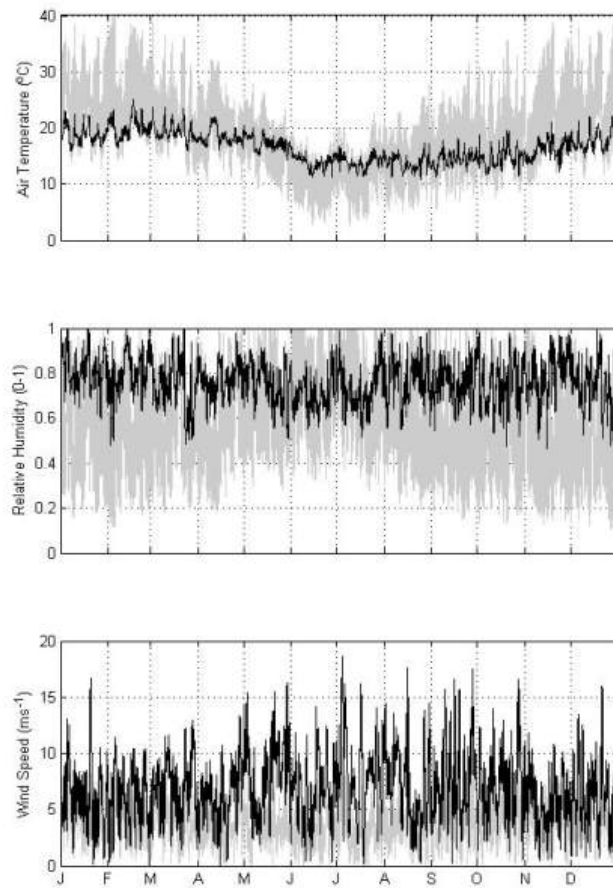
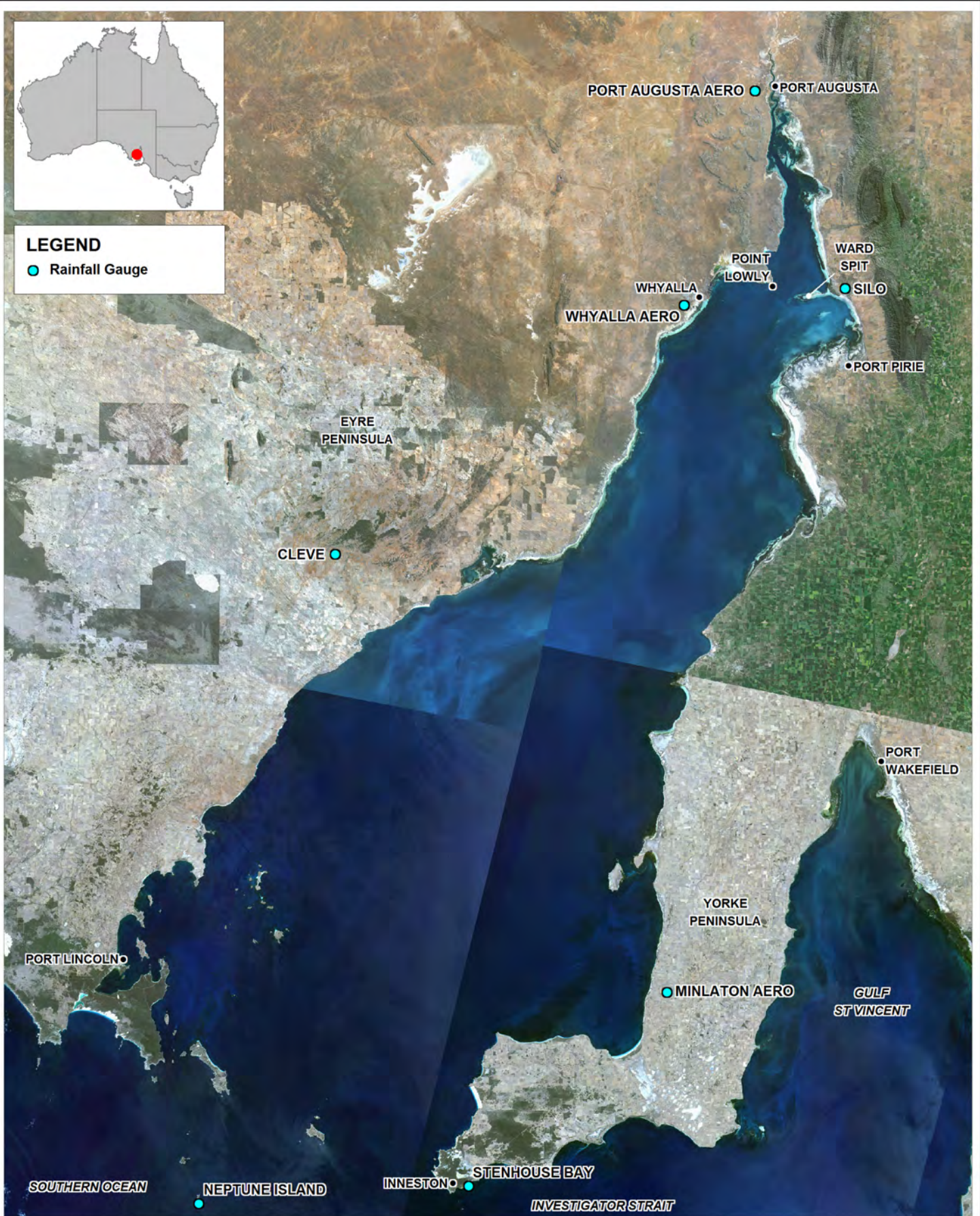


**Figure 4-6** A comparison of high temporal and spatial resolution air temperature (upper panel), relative humidity (middle panel) and wind speed (bottom panel) data from WRF over Spencer Gulf. The black and grey lines present data at Wedge Island (the mouth of Spencer Gulf) and Port Augusta, respectively.



**LEGEND**

● Rainfall Gauge

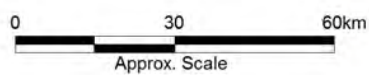


Title:  
**Location of Rainfall Gauges**

Figure:  
**4-7**

Rev:  
**A**

BMT WBM endeavours to ensure that the information provided in this map is correct at the time of publication. BMT WBM does not warrant, guarantee or make representations regarding the currency and accuracy of information contained in this map.



Filepath :

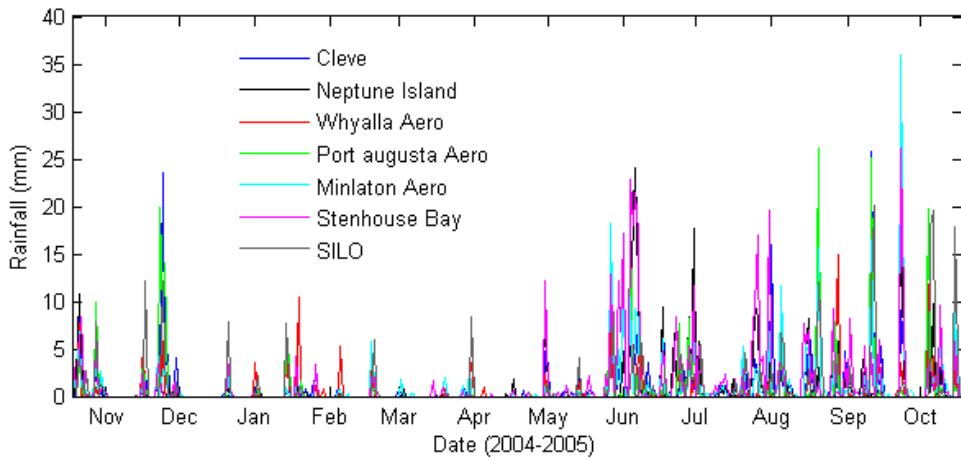


Figure 4-8 Rainfall Data

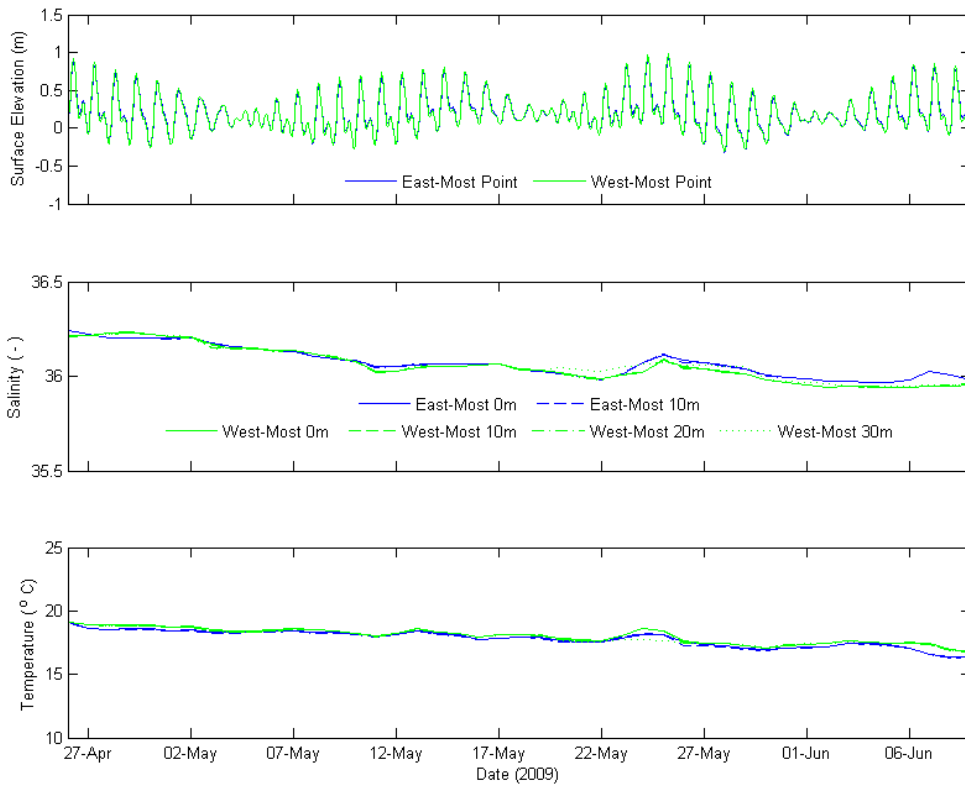
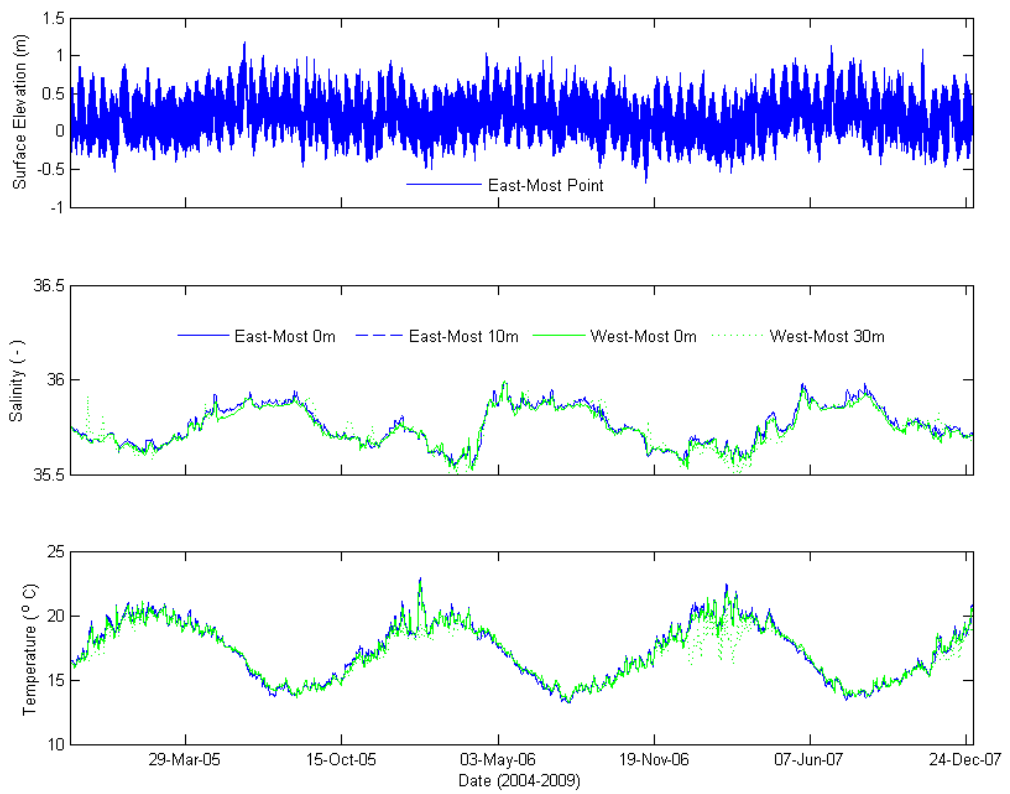


Figure 4-9 Open Boundary Condition Data (Forty-Days Simulation)



**Figure 4-10 Open Boundary Condition Data (2004-2007) for the Eastern-Most Point (Elevations) and Eastern-Most and Western-Most Point (Salinity and Temperature).**

## 4.4 Other Boundary Conditions

A power station outfall at Port Augusta and salt lake inflow from north of Port Augusta were both included in the simulations. The salt lake discharge was set to  $0.15 \text{ m}^3/\text{s}$  at a salinity of 70 (Bye and Harbison 1991) and introduced at a constant rate over the duration of the simulations. The power station discharge was included at  $22 \text{ m}^3/\text{s}$  (BHP Billiton, pers. comm.). The same salinity (i.e. ambient salinity) and temperature (i.e. ambient  $+2^\circ\text{C}$ ) boundary conditions as used in the Draft EIS (Appendix O11.2) were employed for the outfall and salt lake discharges in the current model.

## 4.5 Model Time Step and Stability Condition

Time steps for the simulations were designed for the large velocities experienced at Port Bonython ( $1.5 \text{ m/s}$ ) and associated smallest grid sizes ( $40 \text{ m}$ ). The hybrid Euler-Lagrange momentum advection scheme adopted in ELCOM can operate on a CFL (Courant-Friederich-Lévy) above unity but at the expense of losing numerical accuracy (Hodges 2000). For stratified flow, in general, the CFL condition is more restrictive as it requires an internal wave CFL below approximately 0.7 (Hodges 2000). Vertical density stratification in Spencer Gulf is generally small, so the order of magnitude of internal wave speeds in Spencer Gulf can be given by  $C=(g'D)^{1/2}$  where  $g'$  is the reduced acceleration due to gravity ( $g$ ),  $\rho_o$  is the reference density ( $1000 \text{ kg/m}^3$ ),  $\Delta\rho$  is the density difference between surface and bottom, and  $D$  is the total depth. A conservative assumption of  $\Delta\rho = 2 \text{ kg/m}^3$ ,  $g = 9.8 \text{ m/s}^2$ , and  $D = 25 \text{ m}$  gives  $C = 0.70$ . In this light, time steps required for flow velocity and internal wave speed are therefore below 27 s and 40 s, respectively. A time step of  $\Delta t = 24 \text{ s}$  was adopted in the simulations presented herein.

## 4.6 Drag Distribution

To compute the bottom shear stress ELCOM adopts a quadratic friction law, in which a drag coefficient ( $C_d$ ) provides the scaling for the shear velocity. In addition to the effects on the momentum balance, the drag coefficient in ELCOM is also used to estimate the bottom generation of turbulent kinetic energy (TKE – see Draft EIS, Appendix O11.2) by providing the turbulent velocity scale. Values for drag coefficients observed for sandy bottoms in the field are in the order of 0.0015-0.0040 (Soulsby 1997). However, larger drag values are generally adopted in numerical models (see e.g. [http://faq.dhigroup.com/images/FAQ164/Bottom\\_roughness\\_parameter\\_study.pdf](http://faq.dhigroup.com/images/FAQ164/Bottom_roughness_parameter_study.pdf) 01-Oct-2009).

In 3D structured mesh models such as ELCOM, drag is also imposed by the stair-stepped nature of the bottom configuration, which has been shown to be grid-size dependent (Adcroft and Marshall 1998). As such, the drag distribution adopted in the domain was assumed using the following rules (Figure 4-11):

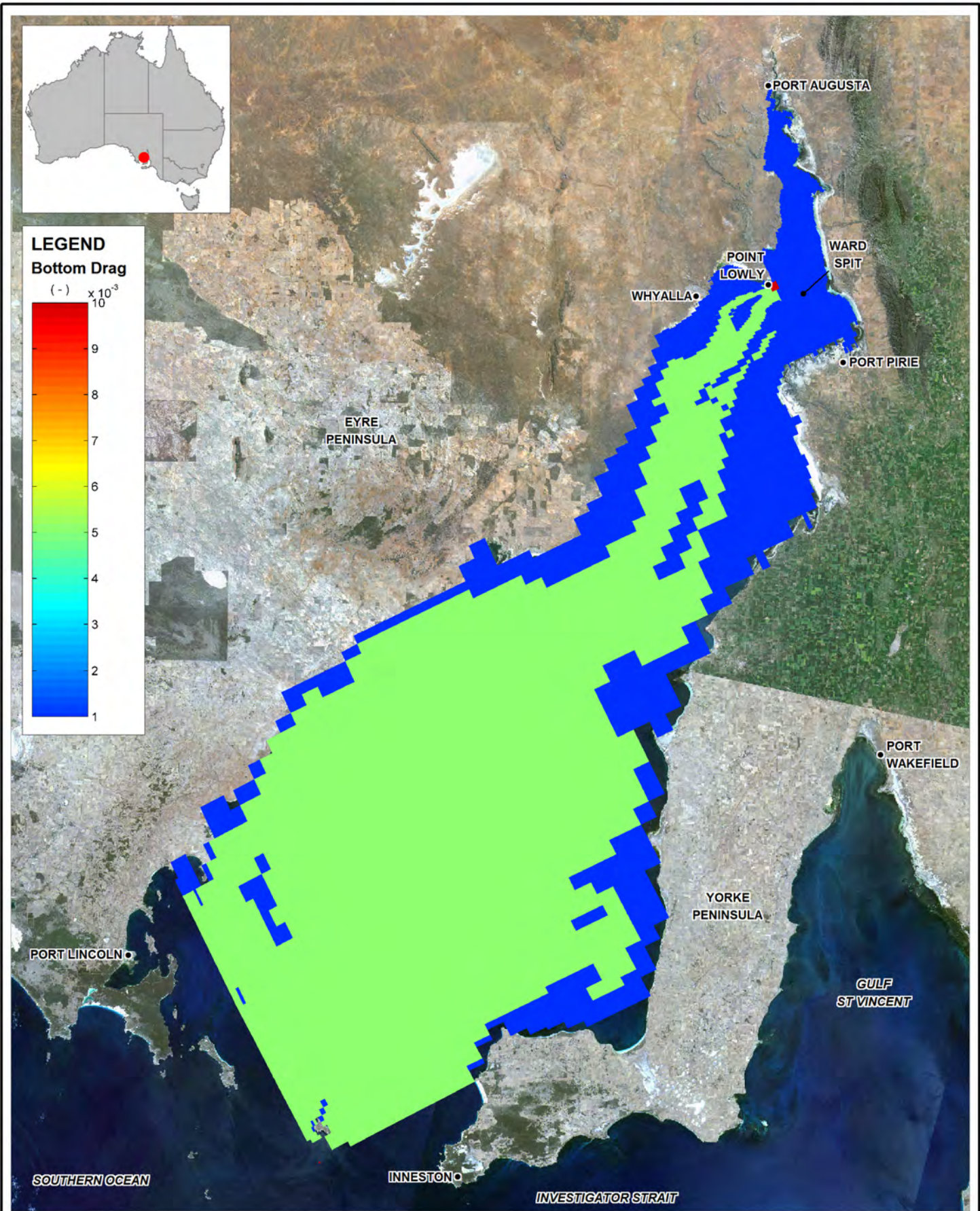
- $C_d = 0.010$  where grid size  $< 100 \text{ m}$ ;
- $C_d = 0.005$  elsewhere where  $H < -15.0 \text{ m}$  ( $H$  is the local bathymetry); and
- $C_d = 0.001$  elsewhere and North of Point Lowly, (including locations where  $H > -15.0 \text{ m}$ ).

The rationale for adopting such a distribution was the following:

- 1 For the larger  $C_d$ , where grid sizes were small, there is less “numerical” (stair-step) drag and as such, drag coefficients were required to be larger;

- 2 The seabed in this high-resolution region (Point Lowly) is known to be populated by sponge beds, which are assumed to exert more drag than a conventional sand bed;
- 3 For the intermediate  $C_d$ , a “neutral” value within the (modelling) literature range was assumed to be adequate; and
- 4 For the smaller  $C_d$ , representing shallower regions, the bathymetry slopes tended to be more abrupt and the stair-step effects more pronounced.

Model results adopting this drag coefficient distribution philosophy approach are presented in Section 5.



Title:  
**Spatial Distribution of Drag Coefficients**

Figure:  
**4-11**

Rev:  
**A**

BMT WBM endeavours to ensure that the information provided in this map is correct at the time of publication. BMT WBM does not warrant, guarantee or make representations regarding the currency and accuracy of information contained in this map.



0 30 60km  
Approx. Scale



Filepath :

## 5 MODEL VALIDATION

The model was validated using data collected over three periods as follows:

- 5 Nov 2004 to Nov 2005 (seasonal validation period):
  - (a) Seasonal CTD data sourced from Dr. Rick Nunes-Vaz collected between November 1983 and October 1984 (data shifted as per previous reports – Draft EIS Appendix O11.2);
  - (b) Tidal elevations sourced from Dr. Rick Nunes-Vaz collected from tide gauges along the Gulf between November 1983 and January 1984 (data also shifted)
- 6 April to June 2009 (forty-days validation period described in Section 3):
  - (a) Bottom-mounted ADCP current measurements;
  - (b) Boat mounted ADCP transect measurements;
  - (c) Moored CTD measurements.
- 7 December 2007 to March 2008 (three-month validation period)
  - (a) Bottom-mounted ADCP current measurements;

The Period 1) simulation was performed to benchmark the results against data (not temporally coincident) collected in the 1980's by Nunes-Vaz (Nunes 1985) and tide measurements of Flinders Ports Corporation (FPC) at three different locations: Port Lincoln, Wallaroo, and Whyalla (Figure 5-3). The Port Augusta tidal gauge location is also shown in Figure 5-3, however its data was not used for Period 1) comparisons, as the data was not coincident in time with the simulation period and data available for model boundary conditions. It is noted that Port Lincoln, Wallaroo, and Whyalla data are coincident in time. Synthetic tidal data (i.e. generated from harmonic constituents, see further details in Section 5.2.2) at Port Augusta was however used for Period 3) comparisons. Although not temporally coincident with Nunes (1985) data, Period 1) comparisons were nonetheless undertaken in order to provide confidence that the model was reproducing the annual pattern of cyclic temperature and salinity variation over the whole Gulf as per previous reports (Draft EIS – Appendix O11.2).

The Period 2) simulation was performed to validate the model against the recent targeted data collection program described in earlier sections of the report, which contrasts in hydrodynamic character to Period 3). Period 2) was deliberately selected to encompass what is a well known time of year when the smallest-amplitude 'dodge' tides occur in Spencer Gulf (Nunes-Vaz, pers. comm.).

Period 3) simulations were performed to validate the model against a period in which a BMT WBM ADCP deployment was carried out, and was characterised by large tides and current velocities.

### 5.1 Seasonal Validation Period

#### 5.1.1 Initial Conditions

For the seasonal validation period, salinity and temperature data collected on 1-2 November 1983 by Dr. Rick Nunes-Vaz (Nunes 1985) and BMT ARGOSS data at the open boundary were used to provide model initial conditions. The initial conditions were distributed internally by the model



executable using a linear interpolation method in the vertical and an inverse squared-distance interpolation method in the horizontal within each vertical level. A cold start was adopted for the momentum initialisation. BMT ARGOSS data was used in the interpolation to complement the Nunes (1985) data, which covered only the Upper Spencer Gulf region. BMT ARGOSS data was available at different levels, while Nunes (1985) was depth averaged and therefore was assumed constant over the water column at a particular point. As the salinity reduces further south towards the mouth, a more realistic initialisation was obtained with the BMT ARGOSS data, which also avoided large salinity gradients close to the boundary. The initial salinity and temperature fields at the surface are given in Figure 5-1 and Figure 5-2.

### 5.1.2 Tidal Amplification and Modulation

Modelled water surface elevations were compared to three data sets provided by FPC: Port Lincoln, Wallaroo, and Whyalla. Additionally, further harmonic analyses were conducted, following the method described in Pawlowicz et al. (2002). For the harmonic analyses, the measured signal was re-sampled at the same model output resolution (3 hours) prior to the tidal decomposition. A seven-month period was used for Port Lincoln and a ten month period for Wallaroo and Whyalla analyses. For illustrative purposes, only a selected period is presented in Figure 5-4, while comparisons for the entire simulation period are presented in Appendix D. Comparison for the amplitude and phase of the main diurnal and semi-diurnal harmonics are presented in Table 5-1 and Table 5-2, with an illustration of the reconstructed signal in Figure 5-5. Note that although the model did not extend into the local embayment at Port Lincoln, the closest model point to Port Lincoln was selected to produce the comparisons. It is also noted that Port Lincoln was not used strictly to indicate model performance but instead to verify the validity of the tidal elevations used in the model boundary conditions and the model's ability to transform "deep ocean" boundary conditions to surface elevations representative of nearshore conditions.

Three major features of the tides are present in the results shown in Figure 5-4, Figure 5-5, Table 5-1 and Table 5-2:

- The tidal amplification of both diurnal and semi diurnal harmonics between Port Lincoln and Whyalla;
- The phasing of these harmonics between Port Lincoln and Whyalla; and
- The relatively small semi-diurnal component associated with the (semi-diurnal) nodal point near Wallaroo.

It is noted that the model did not include the surface elevation effects due to atmospheric pressure gradients, which are obviously present in the real tidal water level measurements. This is the primary reason for the differences observed between model and measured amplitudes, as presented in Figure 5-4. Notwithstanding this, the model occasionally underpredicts amplitudes, being conservative from a tidal flow and mixing perspective. The phase comparisons, which are relatively unaffected by atmospheric variations, were satisfactory.

Table 5-1 Amplitude (m) of Tide Constituents Obtained from Harmonic Analysis

Tidal Constituent	Port Lincoln (March to October 2005)*		Wallaroo		Whyalla	
	Field	Model	Field	Model	Field	Model
<b>S2</b>	0.245	0.214	0.162	0.157	0.450	0.380
<b>M2</b>	0.228	0.175	0.164	0.139	0.425	0.341
<b>K2</b>	0.070	0.063	0.052	0.042	0.137	0.119
<b>K1</b>	0.234	0.196	0.338	0.318	0.433	0.438
<b>O1</b>	0.163	0.160	0.215	0.237	0.265	0.312
<b>P1</b>	0.075	0.056	0.099	0.085	0.123	0.112

\* Not spatially coincident

Table 5-2 Phase (degrees) of Tide Constituents Obtained from Harmonic Analysis

Tidal Constituent	Port Lincoln* (March to October 2005)		Wallaroo		Whyalla	
	Field	Model	Field	Model	Field	Model
<b>S2</b>	83.5	80.3	186.1	172.3	243.4	251.9
<b>M2</b>	32.4	23.0	132.9	117.8	183.9	189.0
<b>K2</b>	83.0	78.5	184.1	167.1	239.3	248.9
<b>K1</b>	29.6	29.3	62.2	65.8	70.9	77.5
<b>O1</b>	1.0	0.8	32.7	34.5	41.4	45.8
<b>P1</b>	32.6	24.6	64.6	61.6	76.4	77.7

\* Not spatially coincident

### 5.1.3 Seasonal Evolution

Model results were contrasted to data from both instantaneous and long-term measurements (Figure 5-6 and Figure 5-7) to illustrate the model's ability in reproducing seasonal evolution of water salinity and temperature across Spencer Gulf. Similar to the information presented in the Draft EIS (Appendix O11.2), temperature and salinity data at four different locations in the Spencer Gulf were plotted for comparison (Figure 5-8 and Figure 5-10). Additional comparisons were also made with the data collected by Dr. Rick Nunes-Vaz (Nunes-Vaz pers. comm.), which comprised moored instruments deployed at near-bed and near-surface locations as presented in Appendix B within Appendix O11.2 of the Draft EIS (Figure 5-9 and Figure 5-11). These data indicate that the model was able to reproduce the spatial (i.e. data range variation between stations) and seasonal variation revealed in the measured data set.

It is noted that the figures presenting comparison of model predictions with the Nunes-Vaz moored data do not present data from the same (absolute) time. The model data is over the period November 2004 to November 2005 and the Nunes (1985) data is from the 1980s. As such, direct comparison of the salinity and temperature absolute values is difficult. However, these figures are presented to demonstrate the model's ability to capture seasonality and cyclic variations.

Further appreciation of the seasonal and spatial data-range variation can be seen in the depth-averaged model snapshots (taken approximately at 11:30 AM every day) shown in Figure 5-12 to Figure 5-15 (temperature) and Figure 5-16 to Figure 5-19 (salinity). In the warmer months (i.e. December) the model simulated considerable warming at the head of the Gulf, whilst the colder months presented a somewhat more homogeneous distribution of temperature. In contrast, salinity presented a marked gradient in Upper Spencer Gulf all year round, with more noticeable development between December and April (see also Nunes and Lennon 1986). The development of the salinity gradient is due to salt build-up as a result of increased evaporation rates at the head of the Gulf over the summer months, pointing to the need to ensure application of spatially variable meteorological forcing data in such studies. Subsequent reduction of salinity observed in June and October indicates the model reproduces the salt ejection dynamics of Upper Spencer Gulf.

Salt ejection was estimated by computing the time series of total salt mass in the model domain, which is analogous to computing the salt flux at the model boundaries. In order to reveal the seasonal trends, a moving average window of approximately 4 complete tidal cycles (i.e. two neaps and two spring cycles or about 59 days) was applied to the salt flux time series (as per Draft EIS - Appendix O11.4). Another moving average window of approximately 4.5 days was applied to the resulting series to further remove high-frequency residual in the signal. One (1) salinity unit was assumed to be equivalent to 1 g/L of salt and the resulting flux, expressed in "equivalent" tons per second, is presented in Figure 5-20. The results reveal that salt fluxes are on average positive between November and May (summer months) and salt therefore accumulates in the Gulf. In the remaining months fluxes become negative on average and salt is effectively ejected from the Gulf.

Results of the far-field model presented in the Draft EIS (Appendix O11.2) are also shown in Figure 5-20 for comparative purposes, demonstrating similar trends. The current model trend however, demonstrates more high-frequency fluctuations than the Draft EIS (Appendix O11.2) predictions. These temporal fluctuations are most likely due to a combination of the following:

- The more resolved open ocean boundary condition formulation adopted in the current model (i.e. daily prescription of salinity and temperature in the current model against the monthly prescription in the Draft EIS - Appendix O11.2 - model);
- The higher spatial and temporal resolution surface (meteorological) boundary conditions that were applied in the current model allowing increased spatial variability in the latent heat flux calculations and associated evaporation and salt accumulation; and
- The smaller time step used in the current computations (i.e. 24 s in the current model against 50 minutes in the Draft EIS - Appendix O11.2 - model).

It is encouraging that even though the current study has seen a complete reconfiguration and reparameterisation of the original Draft EIS (Appendix O11.2) ELCOM model, it was able to reproduce the trends and absolute values of the Draft EIS (Appendix O11.2) salt fluxes. The total net flux over the year was approximately null, which is consistent with a water body that does not accumulate salt in the very long term. Both the original and upgraded models predicted in- and out-fluxes of approximately 253 Gt over a year. Agreement between the two models is within 0.5% in this regard.

Salt build-up at the head of the Gulf and subsequent ejection are inherent aspects of the dynamics of the large-scale gyre in the Gulf and are particularly noticeable in the winter months (Nunes-Vaz et al. 1990). The gyre motion forms as a result of reduced turbulence (and mixing) intensity during neap tides, allowing formation of a well-defined vertical density structure with the tide modulation. A horizontal density gradient at the head of the Gulf develops and the resulting baroclinic motion undergoes geostrophic adjustment to set the gyre into motion (Nunes-Vaz et al. 1990). The current model was able to reproduce both these features. Figure 5-21 shows that a density stratification of up to  $1.5 \text{ kg/m}^3$  was a recurrent pattern during modelled neap tide periods and Figure 5-22 shows increased bottom salinity along the eastern shore of the Upper Gulf. The increased salinity along the eastern shore does not originate locally (i.e. from local evaporation processes) but rather is advected from the northern parts of the gulf (not shown but verified from inspection of subsequent contour plots), therefore indicating the existence of a density current flowing along the eastern shore in Upper Spencer Gulf. The large scale gyre is further illustrated by the winter residual currents at the bottom of the Gulf (Figure 5-23).

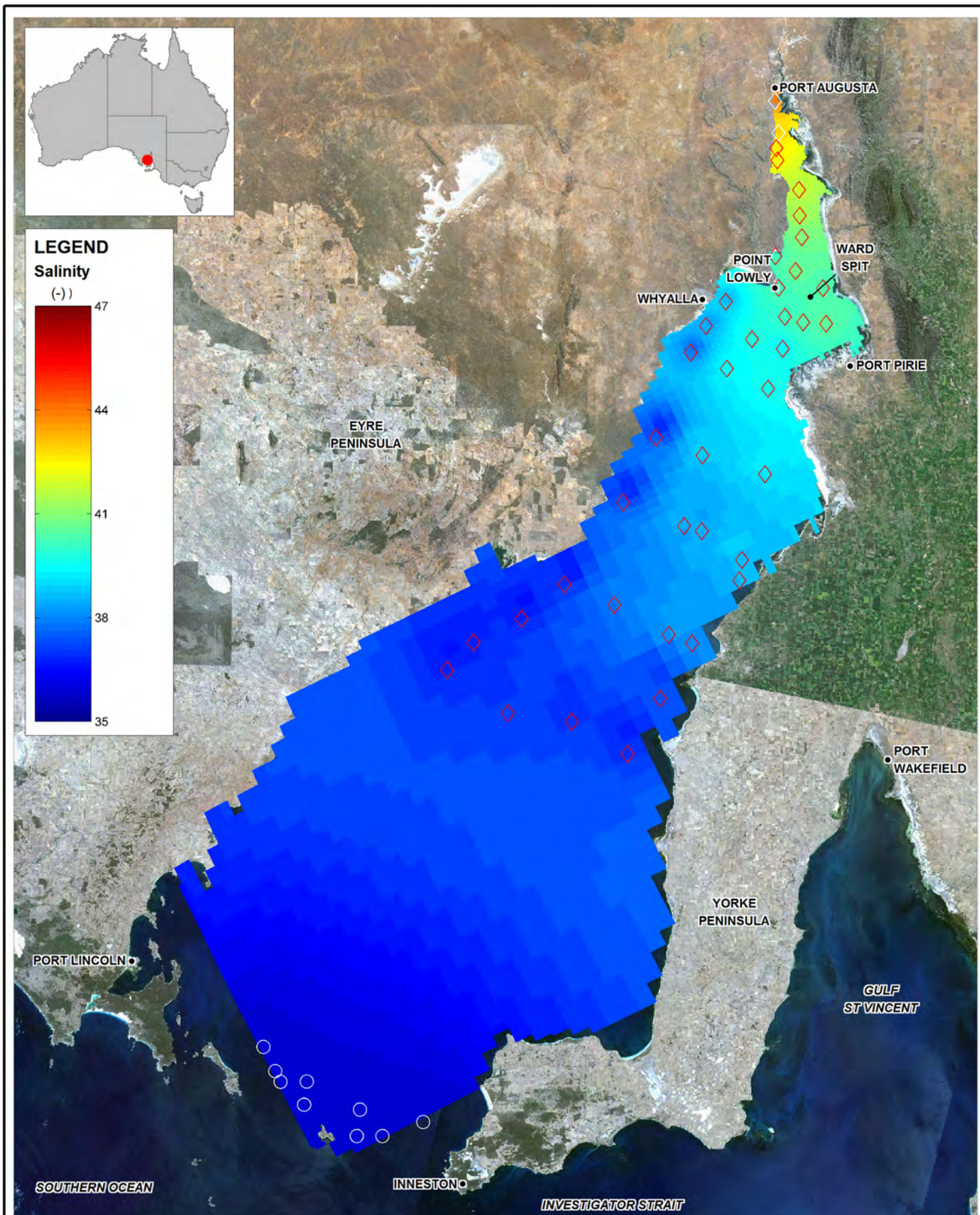
#### 5.1.4 Water Age Analysis

Water age analysis was used to infer the time scale in which internal Gulf waters interact with the boundary, and allows for an estimate of the flushing time scale within the gulf (Draft EIS – Appendix O11.4). The analysis consisted of determining the water age in each cell of the computational domain, in a process described as follows:

- At the simulation start, each cell in the domain is assigned a water age equals 0;
- At each time step, the water age is incremented by the time step, while water entering the domain through the boundaries is assigned a water age equals zero;
- The water age is then transported in the same fashion as a passive tracer (i.e. undergoes advection and turbulent mixing).

At the end of the model simulation, if all computational cells present a water age inferior to the simulation time, it implies that all water originally within the computational domain has felt the influence of water originating from the model boundaries and has, at least partially, flushed from the system.

Despite being produced by different models, results of the water age analysis were consistent with results presented in the Draft EIS (Appendix O11.4). The Upper Gulf presented the oldest waters, and more efficient renewal of water in the western coast of the Gulf as result of the cyclonic gyre dynamics (Figure 5-24 and Figure 5-25), in which new shelf water enters the domain along the western shore (Nunes-Vaz et al. 1990). Conversely, waters in the eastern coast presented the highest water ages, as these were waters being slowly removed from the domain via the salt ejection mechanism, and exiting southward as a submerged flow at the Gulf mouth via the deeper central channel (Figure 5-24 and Figure 5-25, Nunes-Vaz et al. 1990). Highest water ages occurred a few kilometres South of Port Augusta and varied between 306 and 331 days at the bottom and surface of the Gulf. At Port Augusta, the water age was low due to the influence of the salt lake inflows. Water age in “the Rip” (Site B), where the diffuser is proposed, was lower and differed less between surface and bottom (300 and 301 days, respectively). Results presented herein not only indicate that the model suitably reproduced details of the large-scale “gyre” circulation of Spencer Gulf, but also the flow path of the submerged flow that controls the salt water exchange with the shelf.

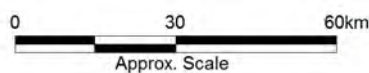


Title:  
**Initial Salinity Conditions: November 2004**  
 Nunes (1985) data (diamonds), BMT ARGOSS data (circles)

Figure:  
**5-1**

Rev:  
**A**

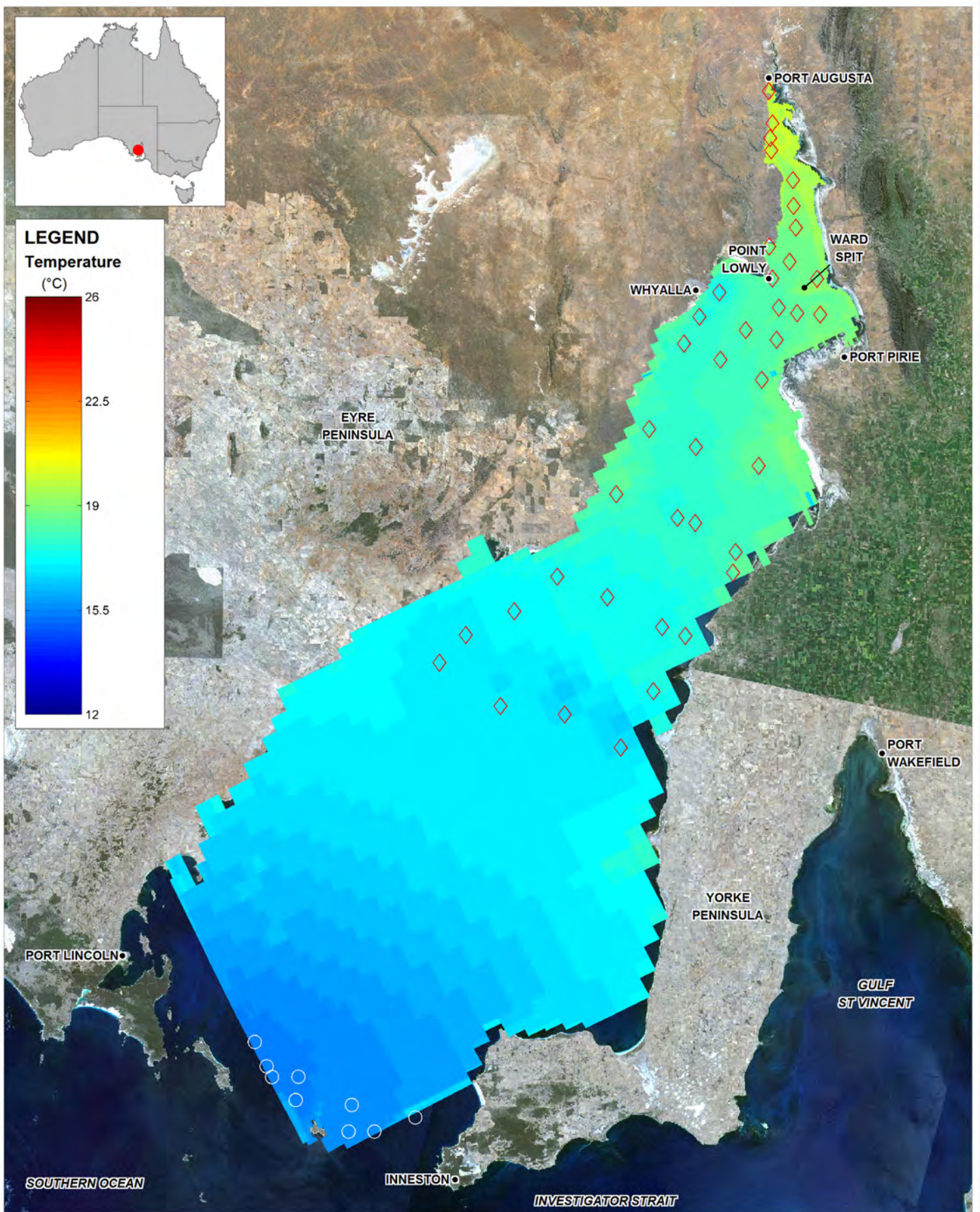
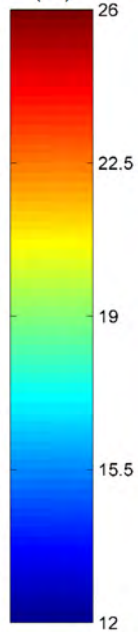
BMT WBM endeavours to ensure that the information provided in this map is correct at the time of publication. BMT WBM does not warrant, guarantee or make representations regarding the currency and accuracy of information contained in this map.



Filepath :



**LEGEND**  
Temperature  
(°C)

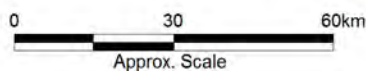


Title:  
**Initial Temperature Conditions: November 2004**  
Nunes (1985) data (diamonds), BMT ARGOSS data (circles)

Figure:  
**5-2**

Rev:  
**A**

BMT WBM endeavours to ensure that the information provided in this map is correct at the time of publication. BMT WBM does not warrant, guarantee or make representations regarding the currency and accuracy of information contained in this map.



Filepath :



**LEGEND**

● FPC Tide Gauge

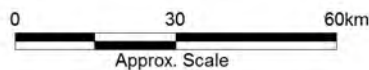


Title:  
**Location of FPC Tide Gauges**

Figure:  
**5-3**

Rev:  
**A**

BMT WBM endeavours to ensure that the information provided in this map is correct at the time of publication. BMT WBM does not warrant, guarantee or make representations regarding the currency and accuracy of information contained in this map.



Filepath :



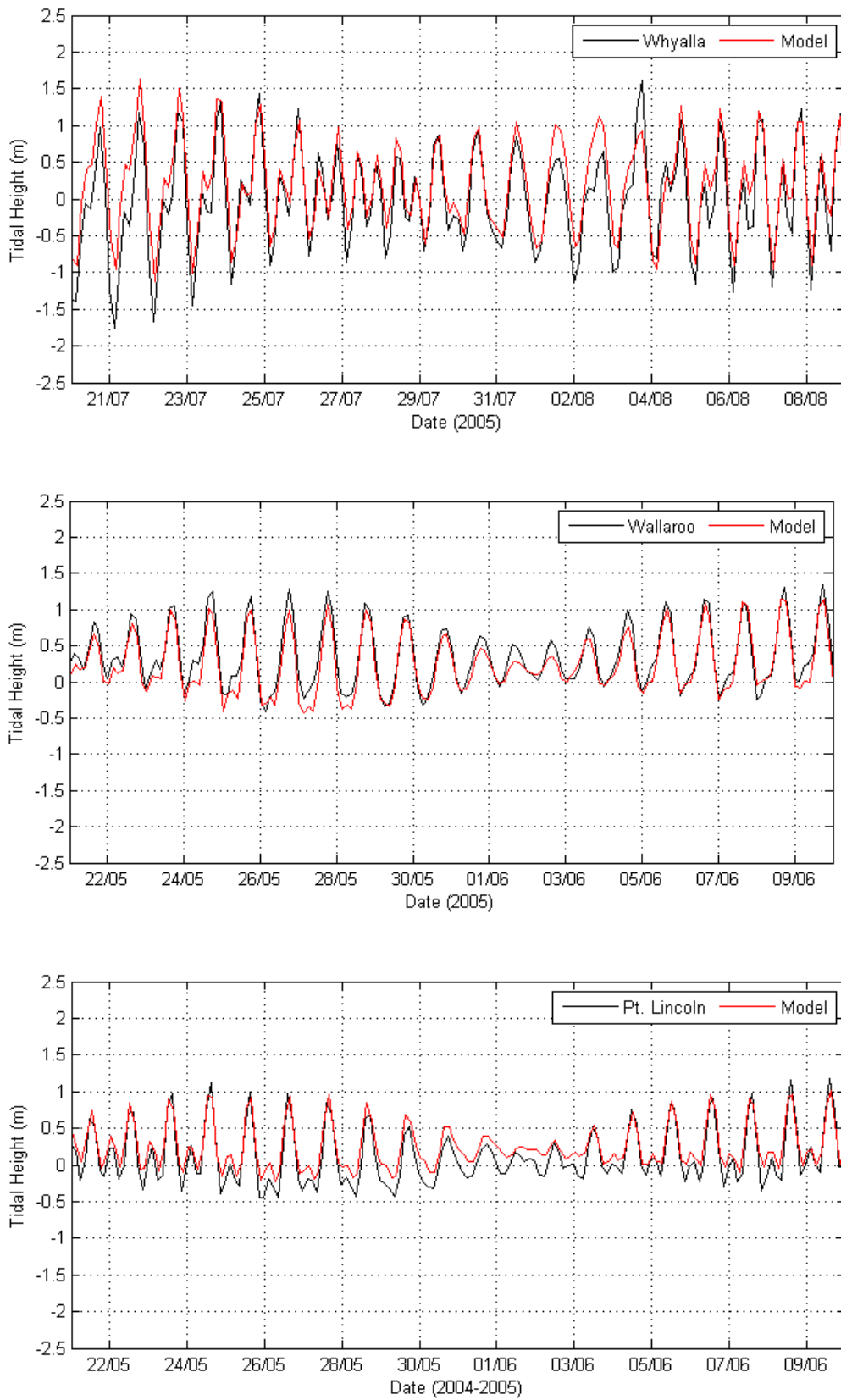
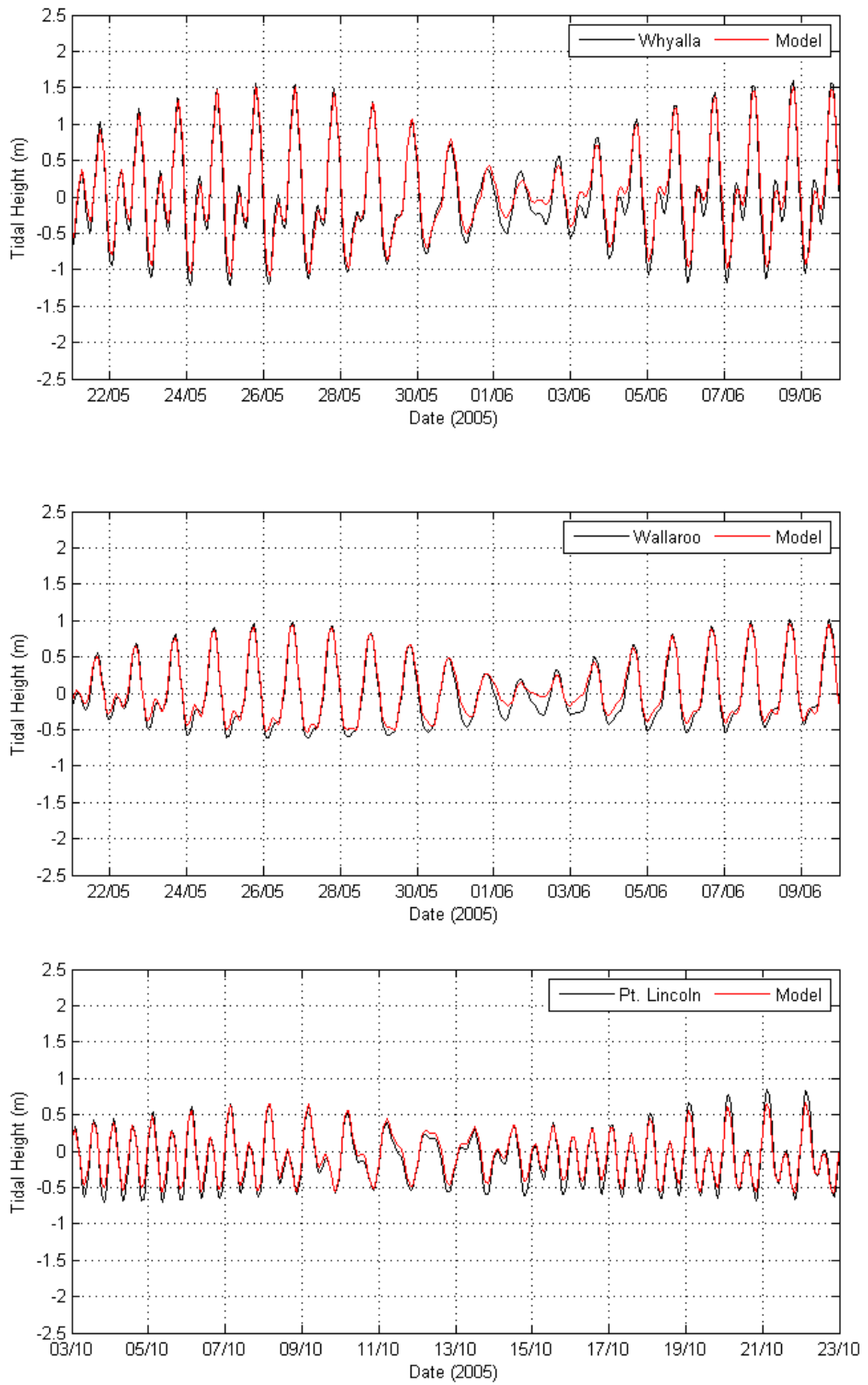


Figure 5-4 Comparison between Modelled and Observed Tidal Elevations

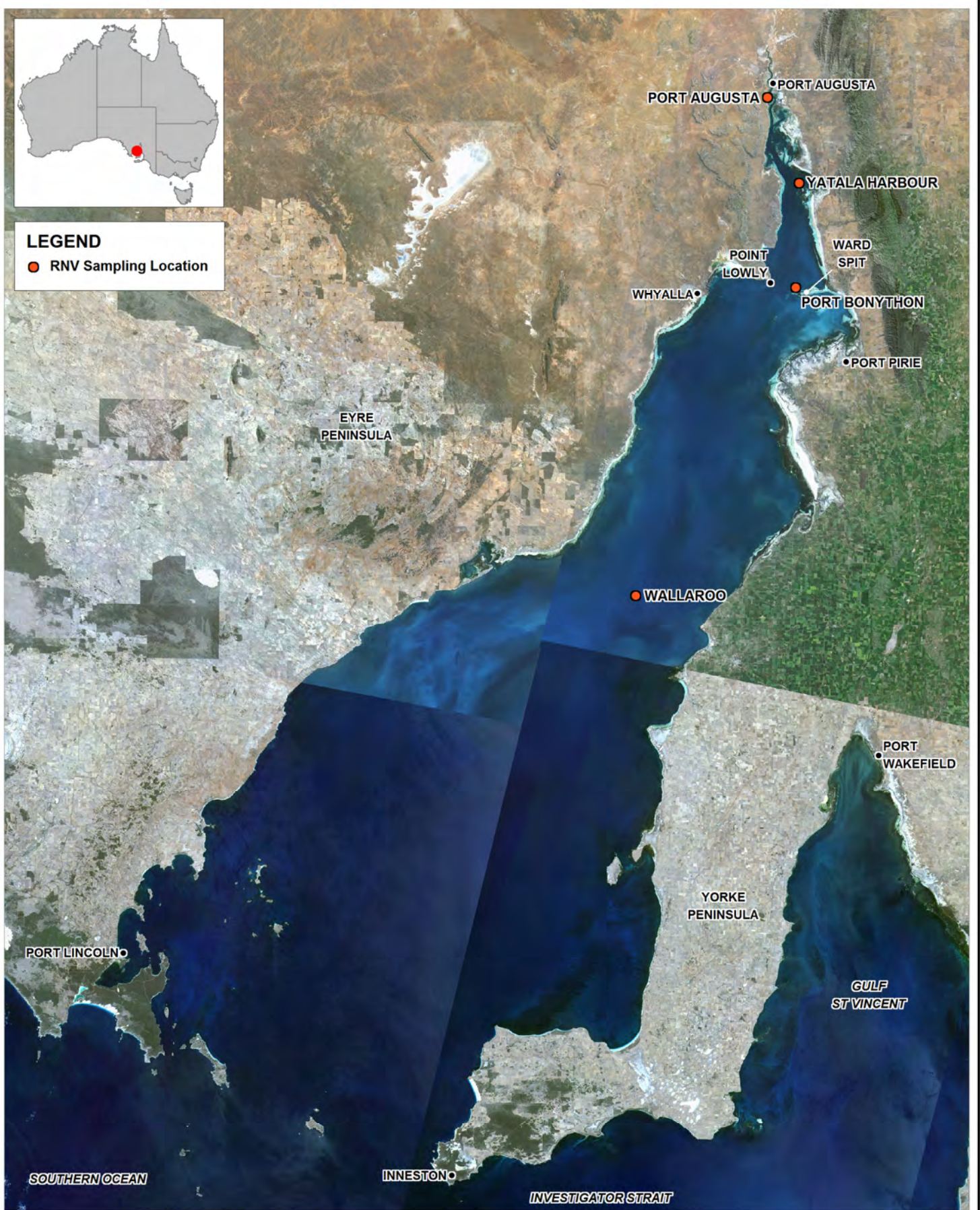


**Figure 5-5 Comparison between Modelled and Observed Tidal Elevations after Harmonic Analysis and Signal Reconstruction**



**LEGEND**

● RNV Sampling Location

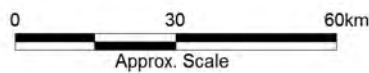


Title:  
**Location of Nunes-Vaz CTD Data  
 Used for Model Comparisons**

Figure:  
**5-6**

Rev:  
**A**

BMT WBM endeavours to ensure that the information provided in this map is correct at the time of publication. BMT WBM does not warrant, guarantee or make representations regarding the currency and accuracy of information contained in this map.

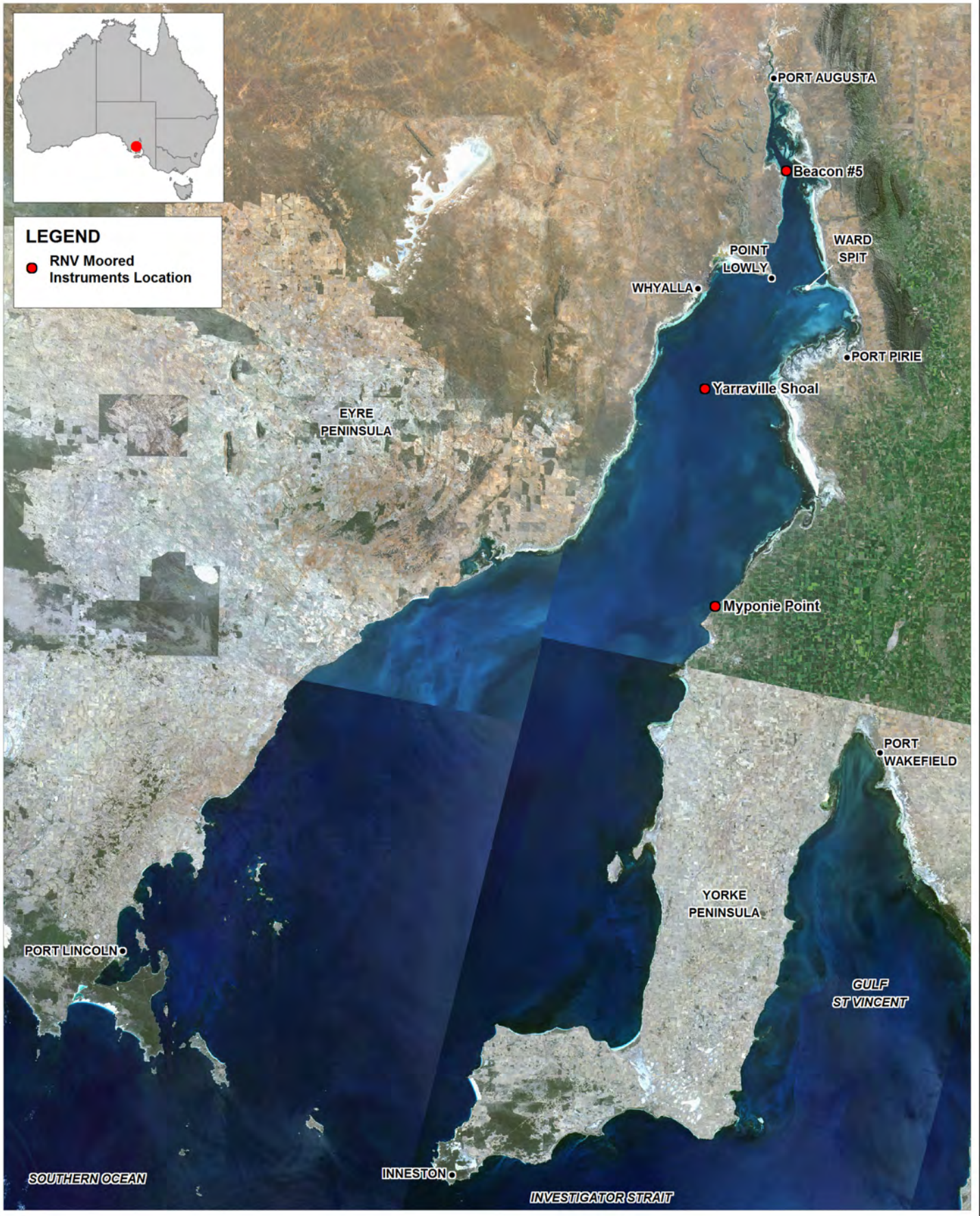


Filepath :



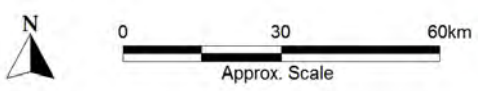
**LEGEND**

- RNV Moored Instruments Location



<p>Title: <b>Location of Nunes-Vaz Moored Instrument Data Used for Model Comparisons</b></p>	<p>Figure: <b>5-7</b></p>	<p>Rev: <b>A</b></p>
--------------------------------------------------------------------------------------------------	-------------------------------	--------------------------

BMT WBM endeavours to ensure that the information provided in this map is correct at the time of publication. BMT WBM does not warrant, guarantee or make representations regarding the currency and accuracy of information contained in this map.



Filepath :

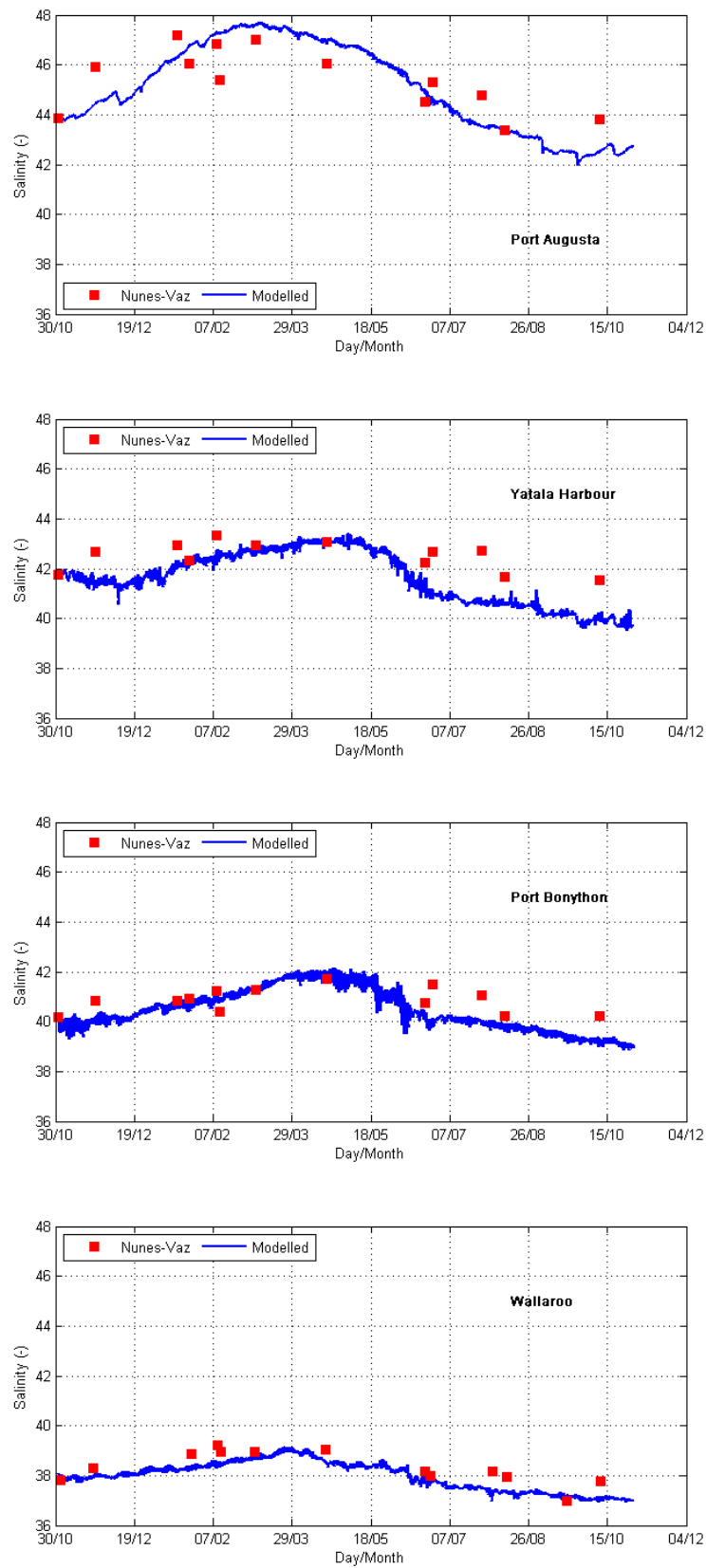
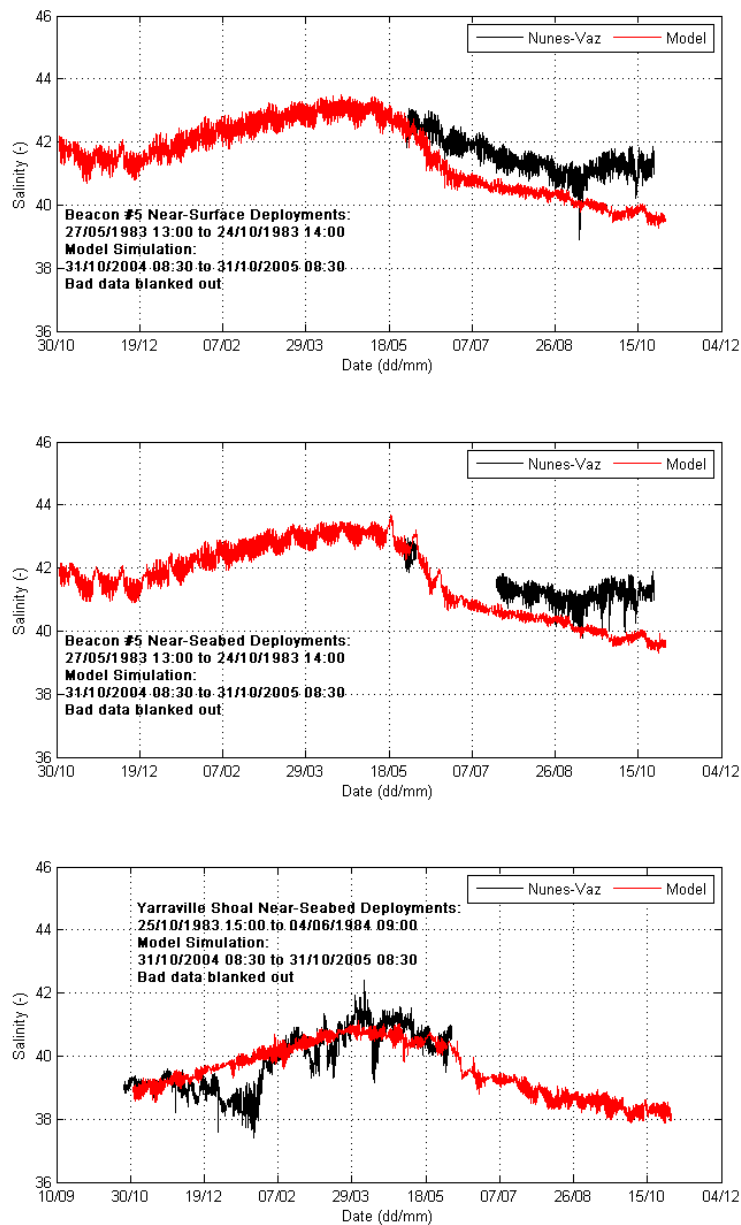


Figure 5-8 Comparison of Modelled and Observed Salinity (Long-Term 2005 Data - CTD).  
Data not temporally coincident



**Figure 5-9 Comparison of Modelled and Observed Salinity (Long-Term 2005 Data – Moored Instruments). “Blanked-out” data refers to salinities above 50 recorded in the data files. Data not temporally coincident.**

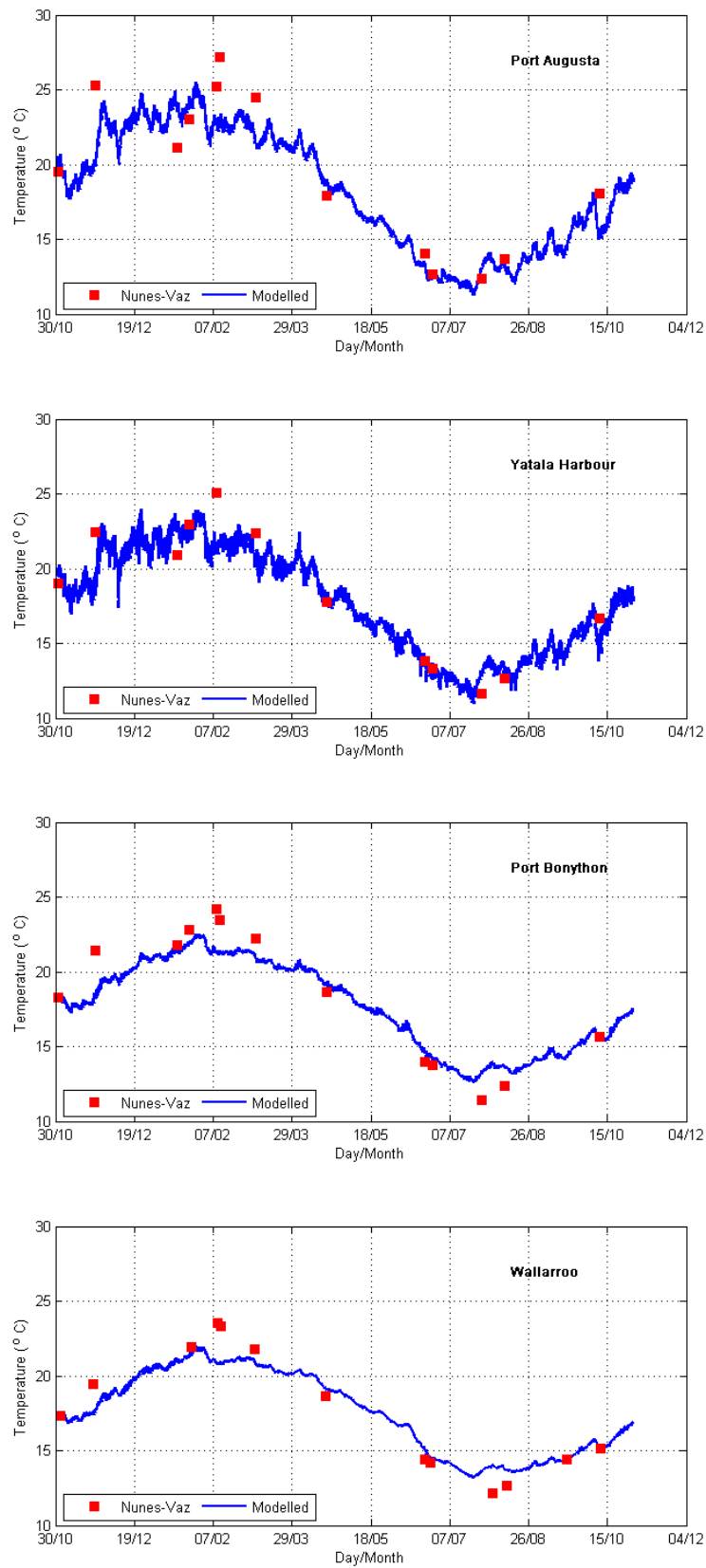
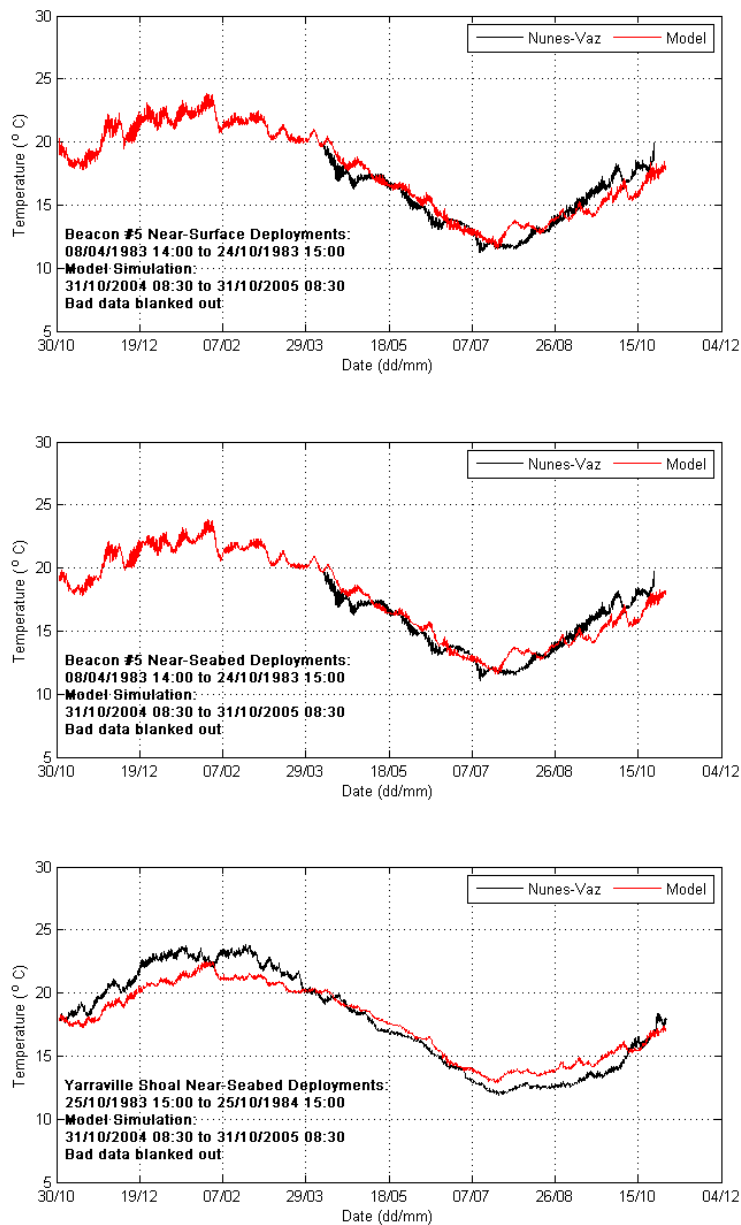
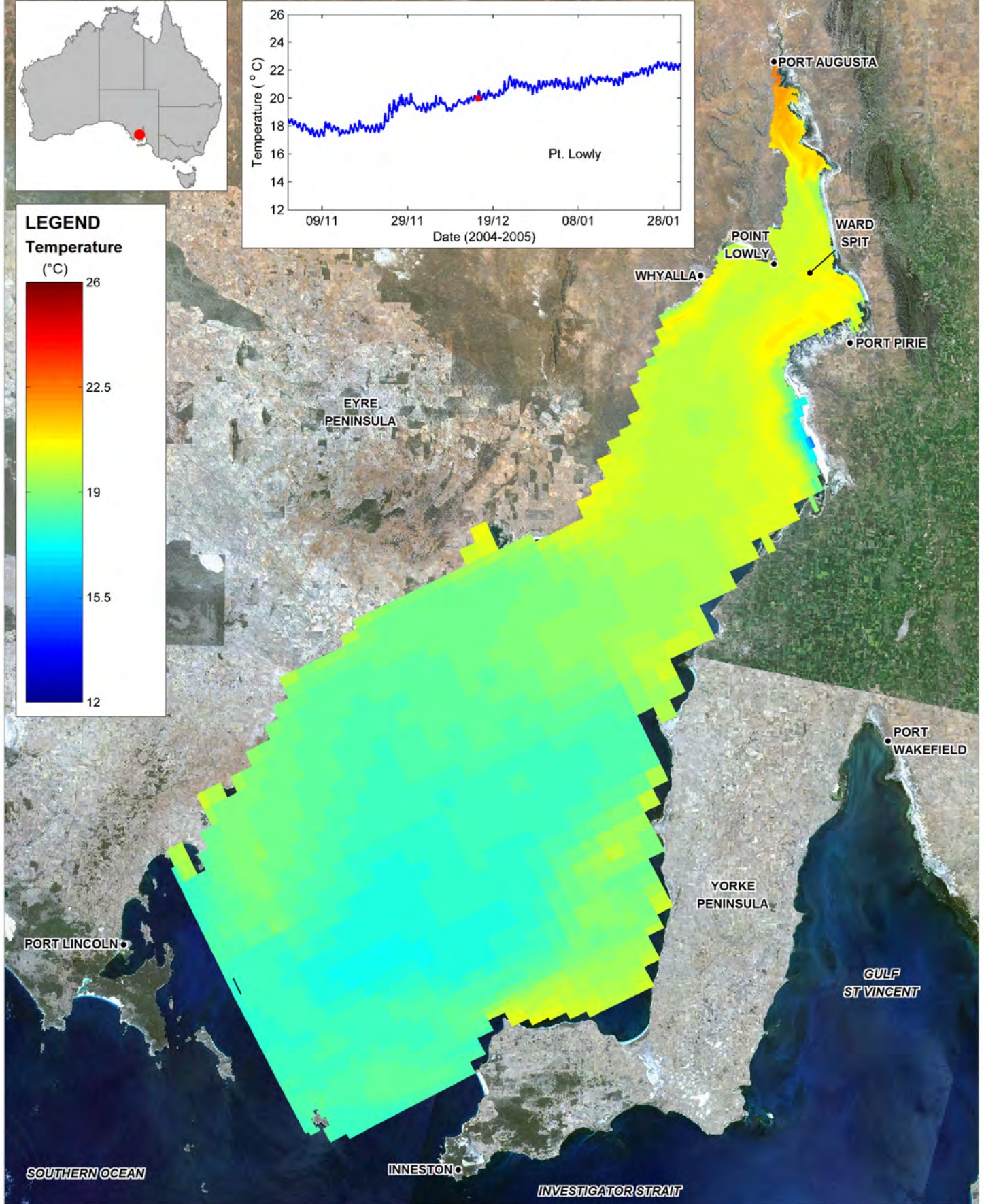
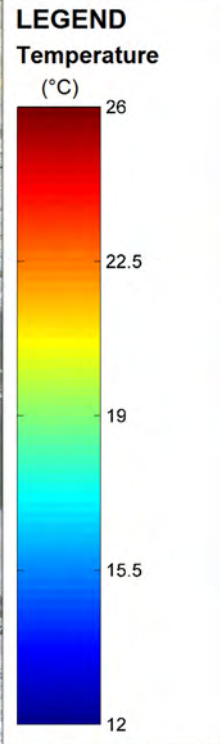
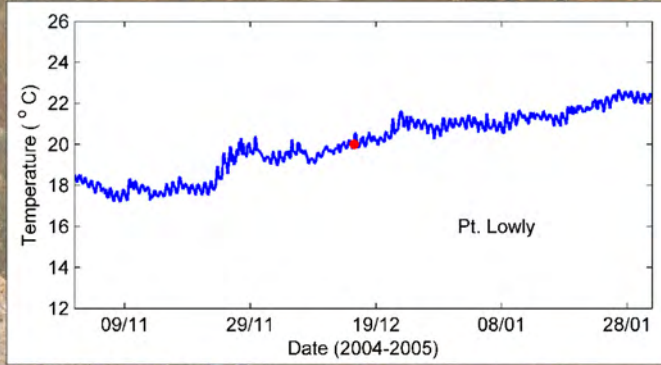


Figure 5-10 Comparison of Modelled and Observed Temperature (Long-Term 2005 Data - CTD). Data not temporally coincident.



**Figure 5-11 Comparison of Modelled and Observed Temperature (Long-Term 2005 Data – Moored Instruments). “Blanked-out” data refers to temperatures above 50°C recorded in the data files. Data not temporally coincident.**





Title:  
**Spatial Distribution of Modelled Temperature:  
 December 2004**

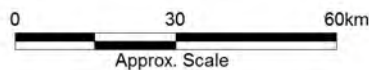
Figure:

**5-12**

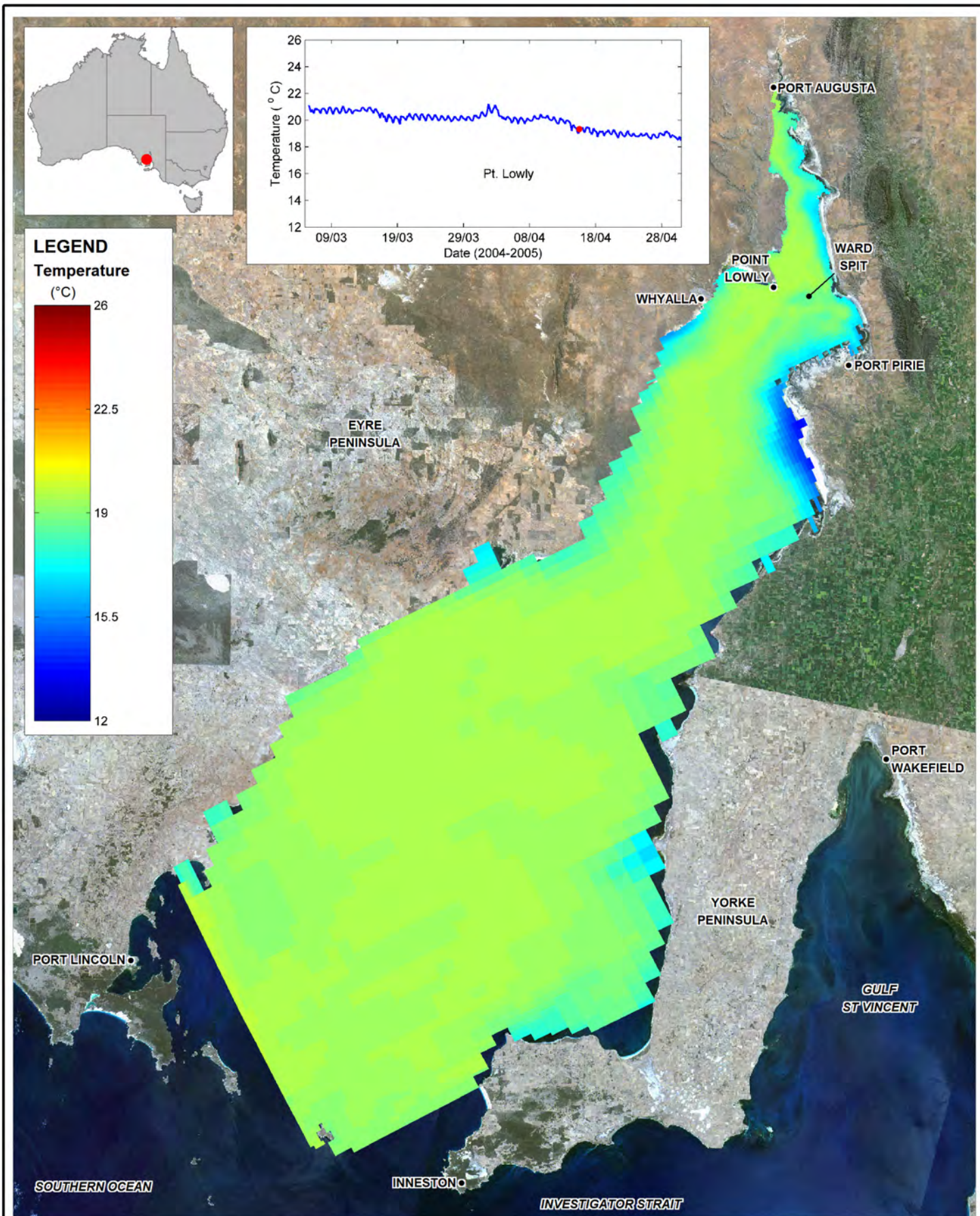
Rev:

**A**

BMT WBM endeavours to ensure that the information provided in this map is correct at the time of publication. BMT WBM does not warrant, guarantee or make representations regarding the currency and accuracy of information contained in this map.



Filepath :

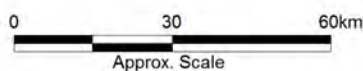


Title:  
**Spatial Distribution of Modelled Temperature:  
April 2005**

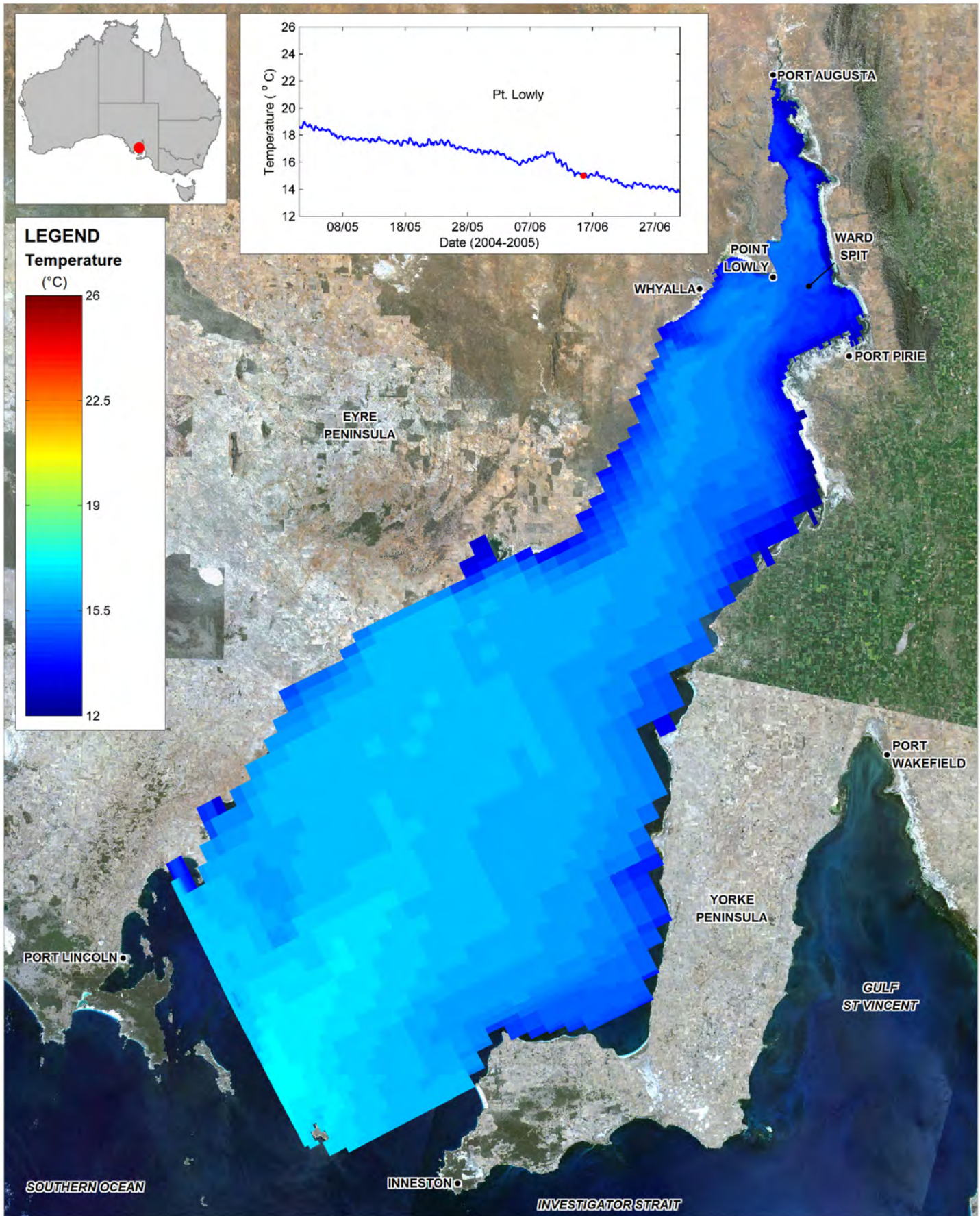
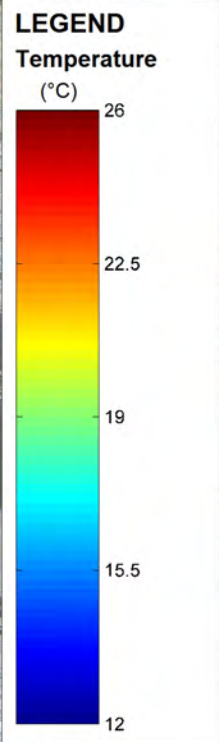
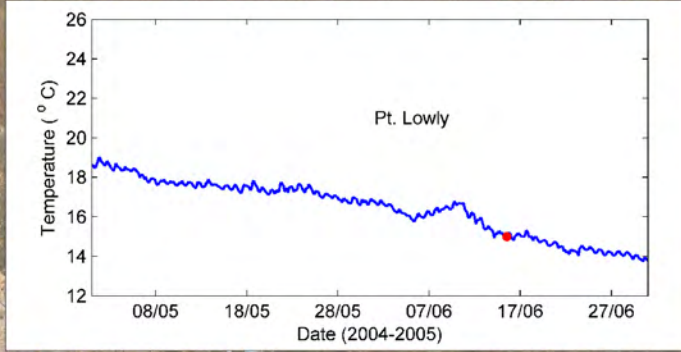
Figure:  
**5-13**

Rev:  
**A**

BMT WBM endeavours to ensure that the information provided in this map is correct at the time of publication. BMT WBM does not warrant, guarantee or make representations regarding the currency and accuracy of information contained in this map.



Filepath :



Title: **Spatial Distribution of Modelled Temperature: June 2005**

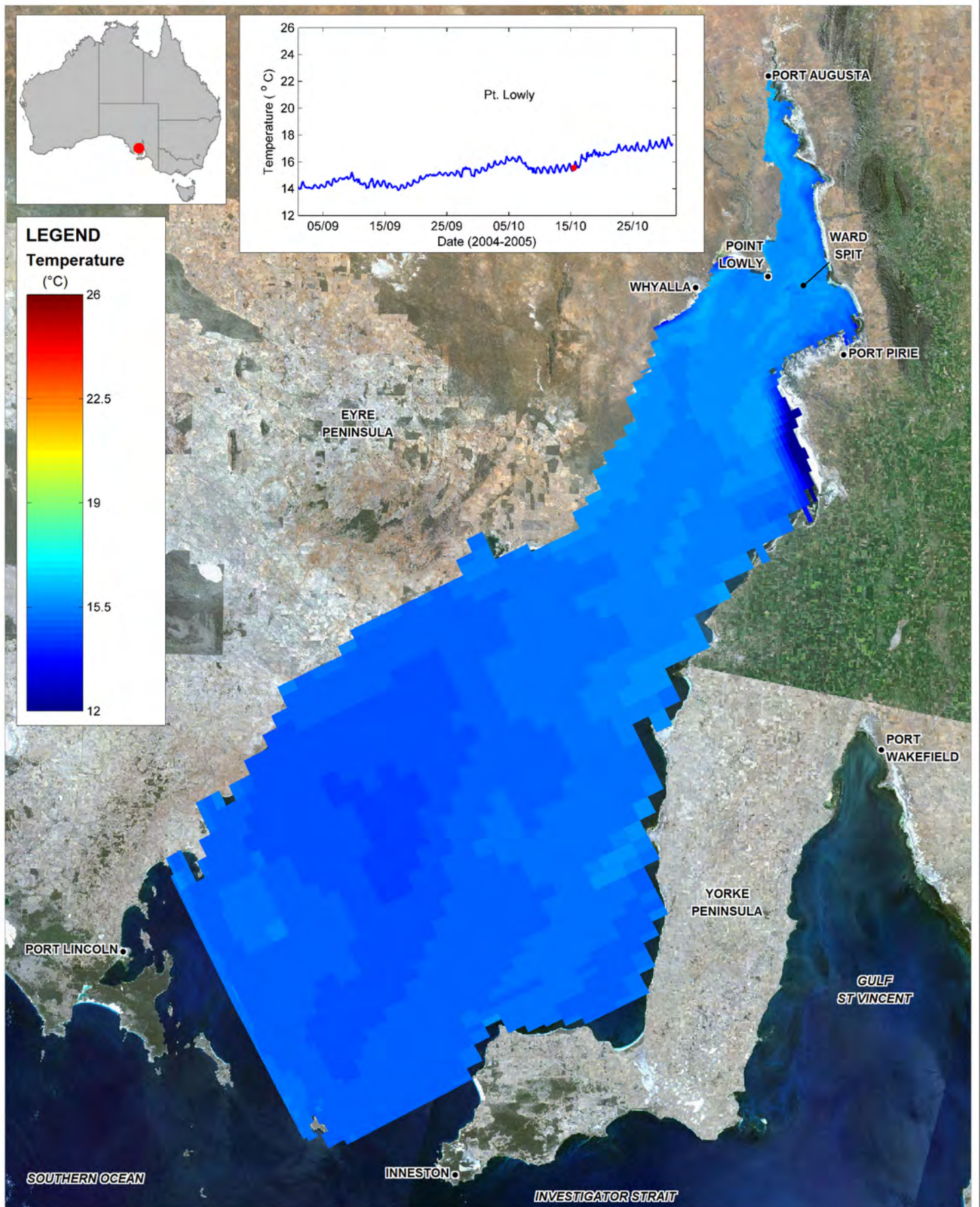
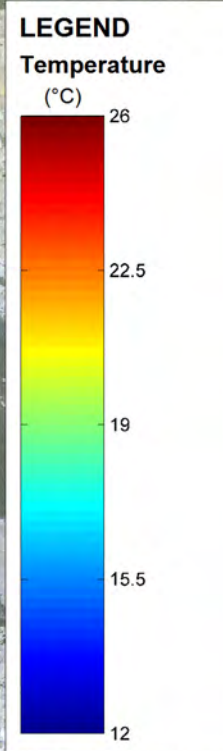
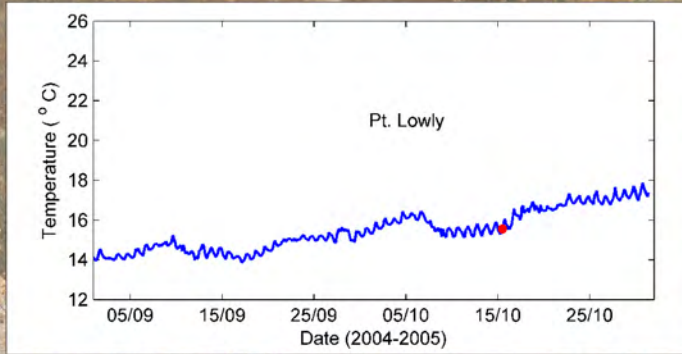
Figure: **5-14**

Rev: **A**

BMT WBM endeavours to ensure that the information provided in this map is correct at the time of publication. BMT WBM does not warrant, guarantee or make representations regarding the currency and accuracy of information contained in this map.



Filepath :

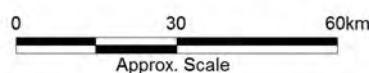


Title:  
**Spatial Distribution of Modelled Temperature:  
 October 2005**

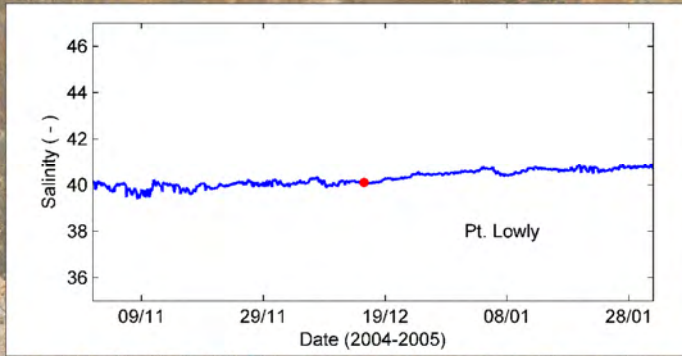
Figure:  
**5-15**

Rev:  
**A**

BMT WBM endeavours to ensure that the information provided in this map is correct at the time of publication. BMT WBM does not warrant, guarantee or make representations regarding the currency and accuracy of information contained in this map.



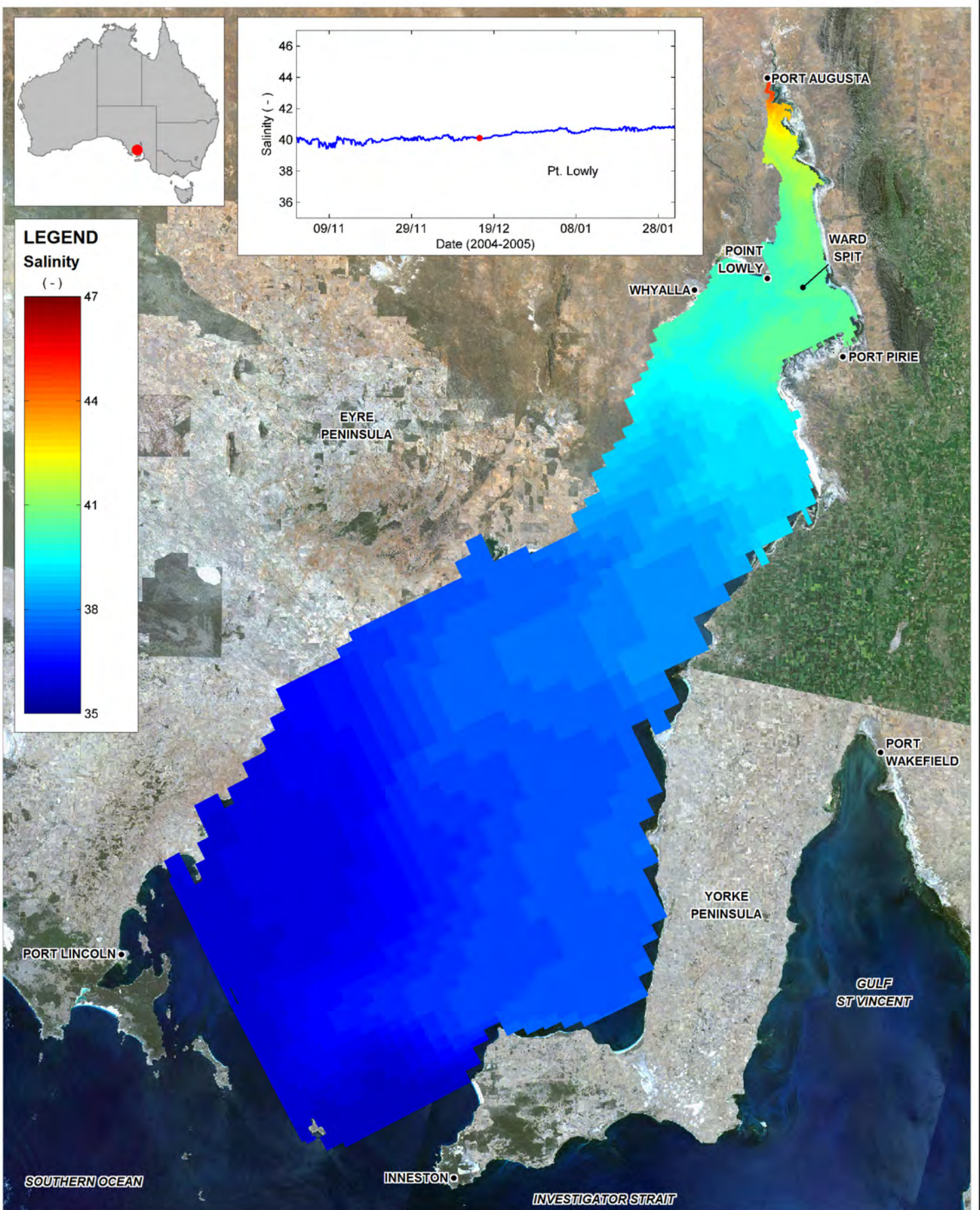
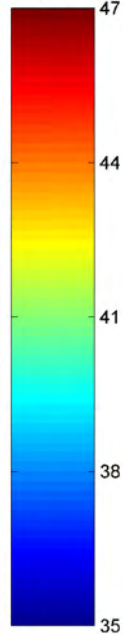
Filepath :



**LEGEND**

Salinity

(-)

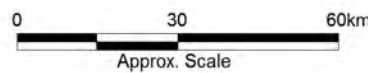


Title:  
**Spatial Distribution of Modelled Salinity:  
 December 2004**

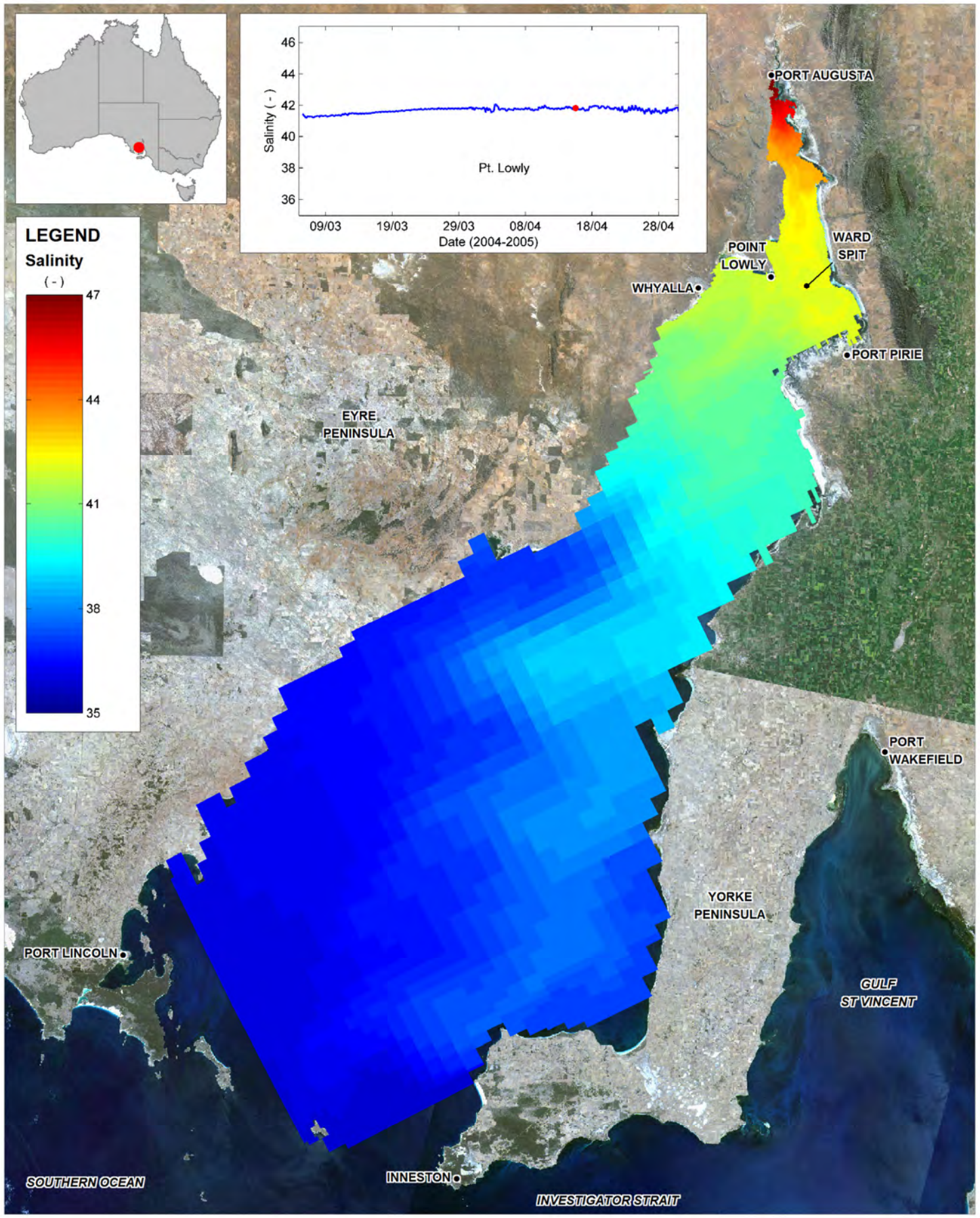
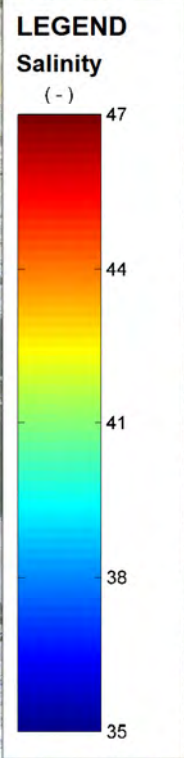
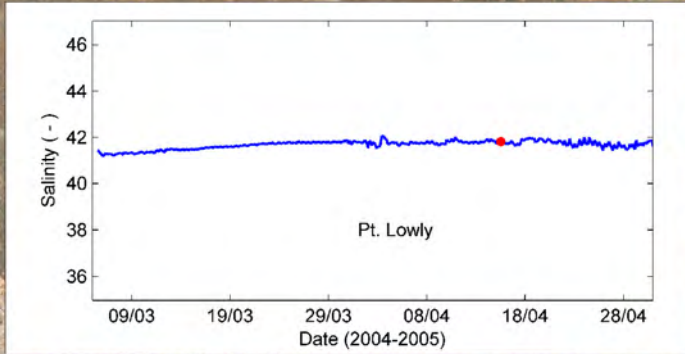
Figure:  
**5-16**

Rev:  
**A**

BMT WBM endeavours to ensure that the information provided in this map is correct at the time of publication. BMT WBM does not warrant, guarantee or make representations regarding the currency and accuracy of information contained in this map.



Filepath :

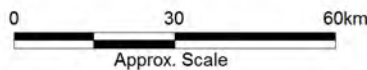


Title:  
**Spatial Distribution of Modelled Salinity:  
 April 2005**

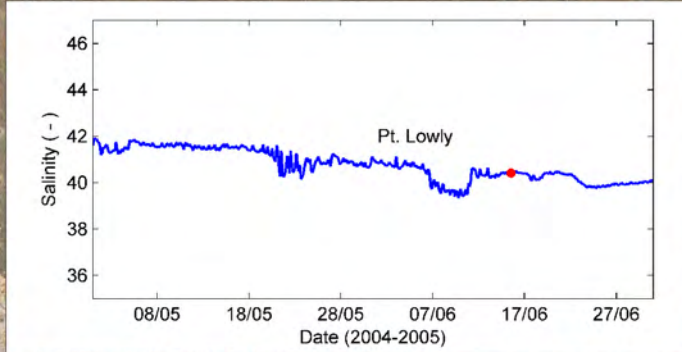
Figure:  
**5-17**

Rev:  
**A**

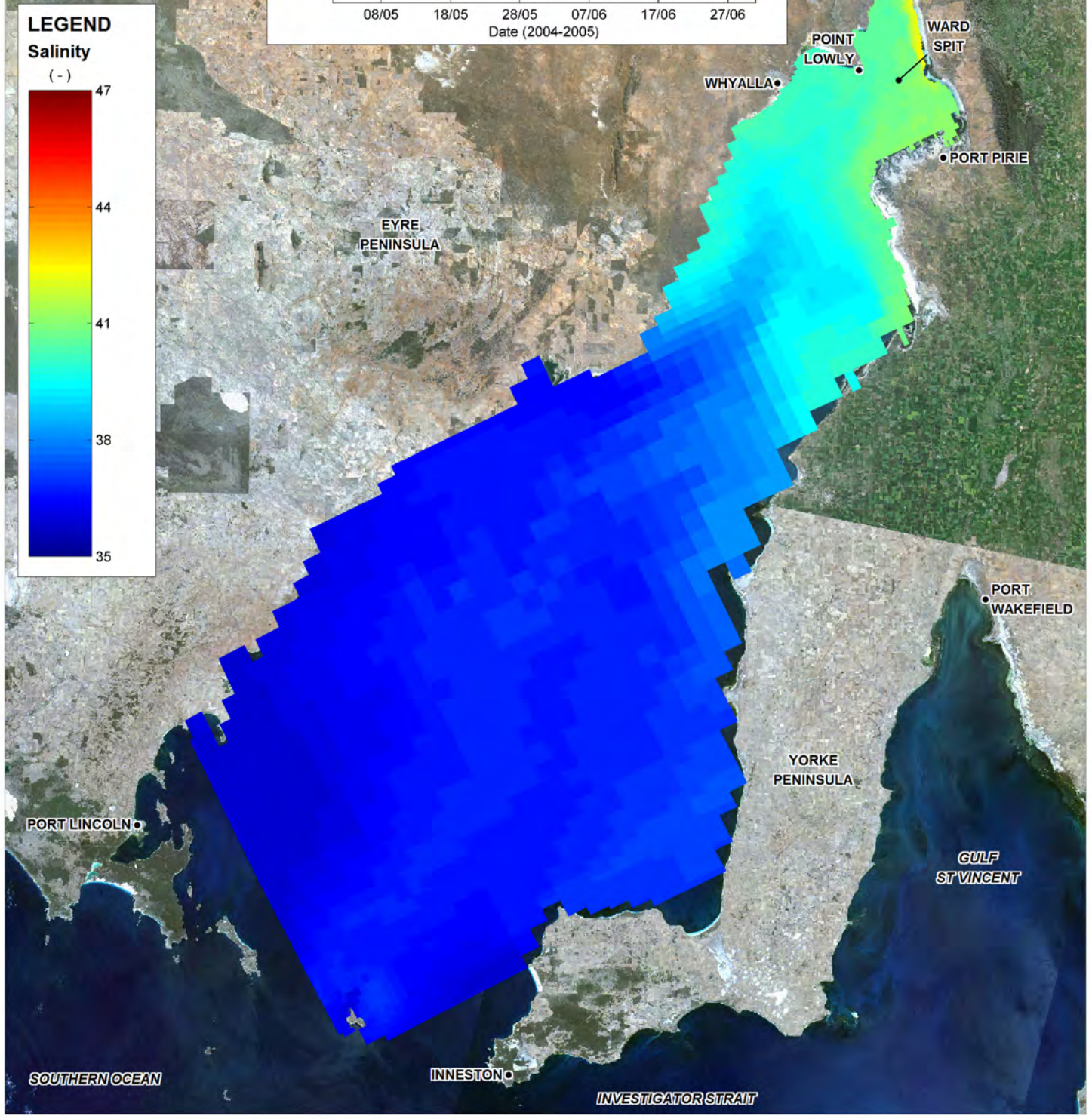
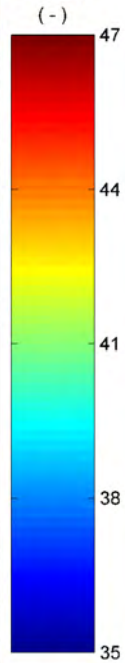
BMT WBM endeavours to ensure that the information provided in this map is correct at the time of publication. BMT WBM does not warrant, guarantee or make representations regarding the currency and accuracy of information contained in this map.



Filepath :



**LEGEND**  
Salinity (-)

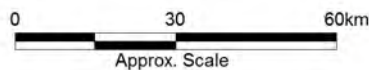


Title:  
**Spatial Distribution of Modelled Salinity:  
June 2005**

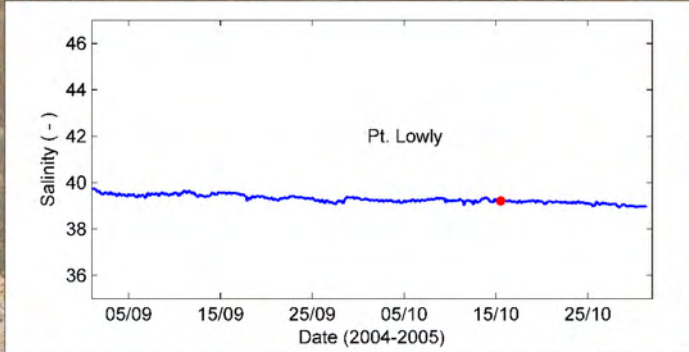
Figure:  
**5-18**

Rev:  
**A**

BMT WBM endeavours to ensure that the information provided in this map is correct at the time of publication. BMT WBM does not warrant, guarantee or make representations regarding the currency and accuracy of information contained in this map.

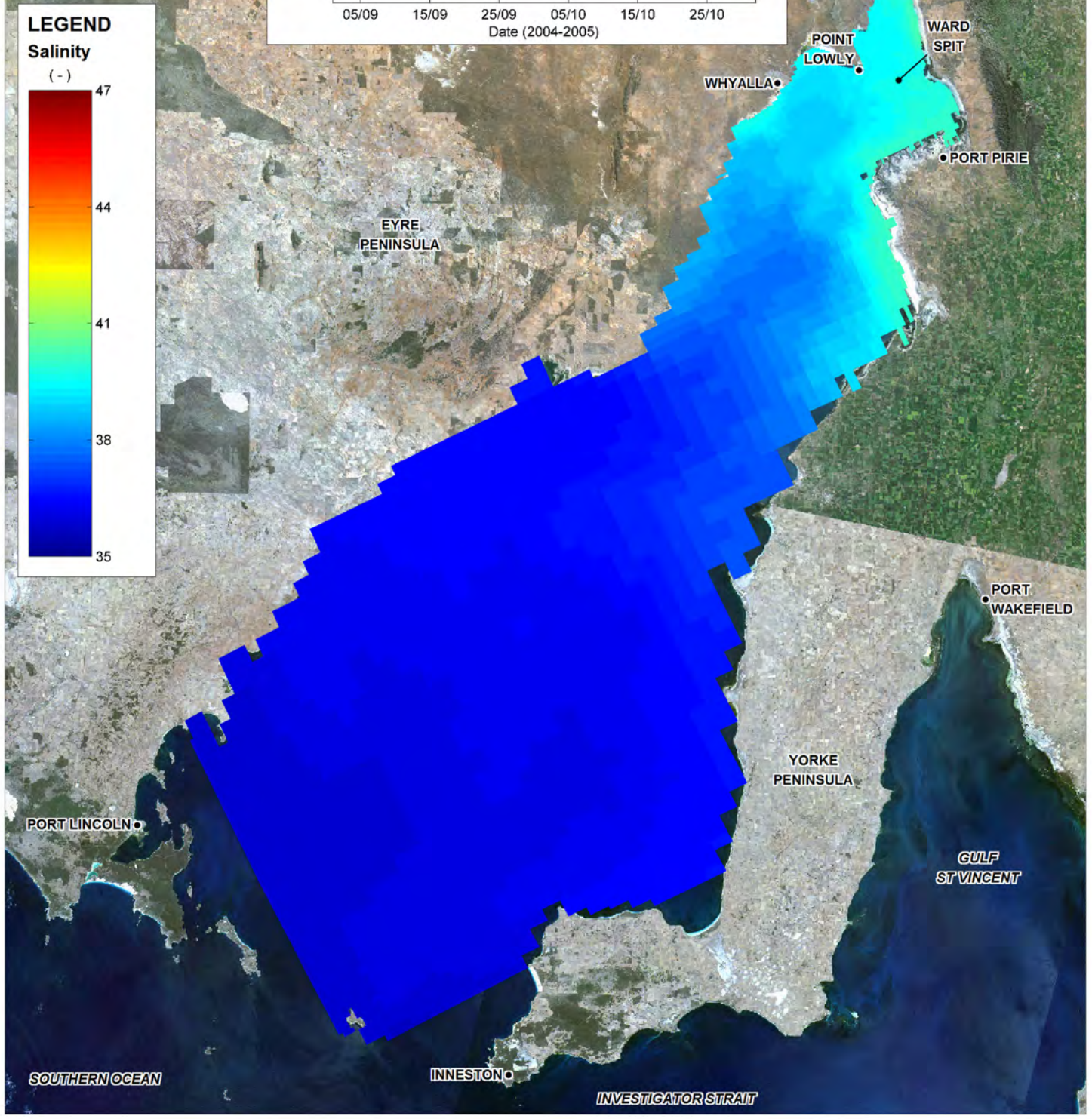
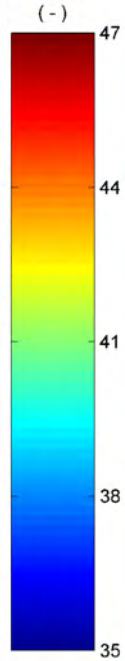


Filepath :



**LEGEND**

**Salinity**

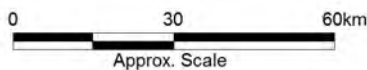


Title:  
**Spatial Distribution of Modelled Salinity:  
 October 2005**

Figure:  
**5-19**

Rev:  
**A**

BMT WBM endeavours to ensure that the information provided in this map is correct at the time of publication. BMT WBM does not warrant, guarantee or make representations regarding the currency and accuracy of information contained in this map.



Filepath :



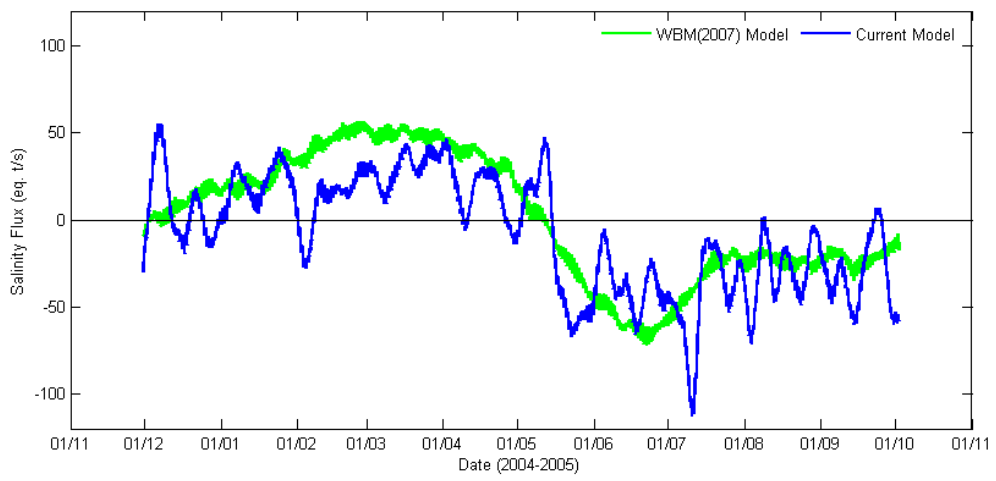


**Figure 5-20 Seasonal Salt Flux across the Model Open Boundaries**

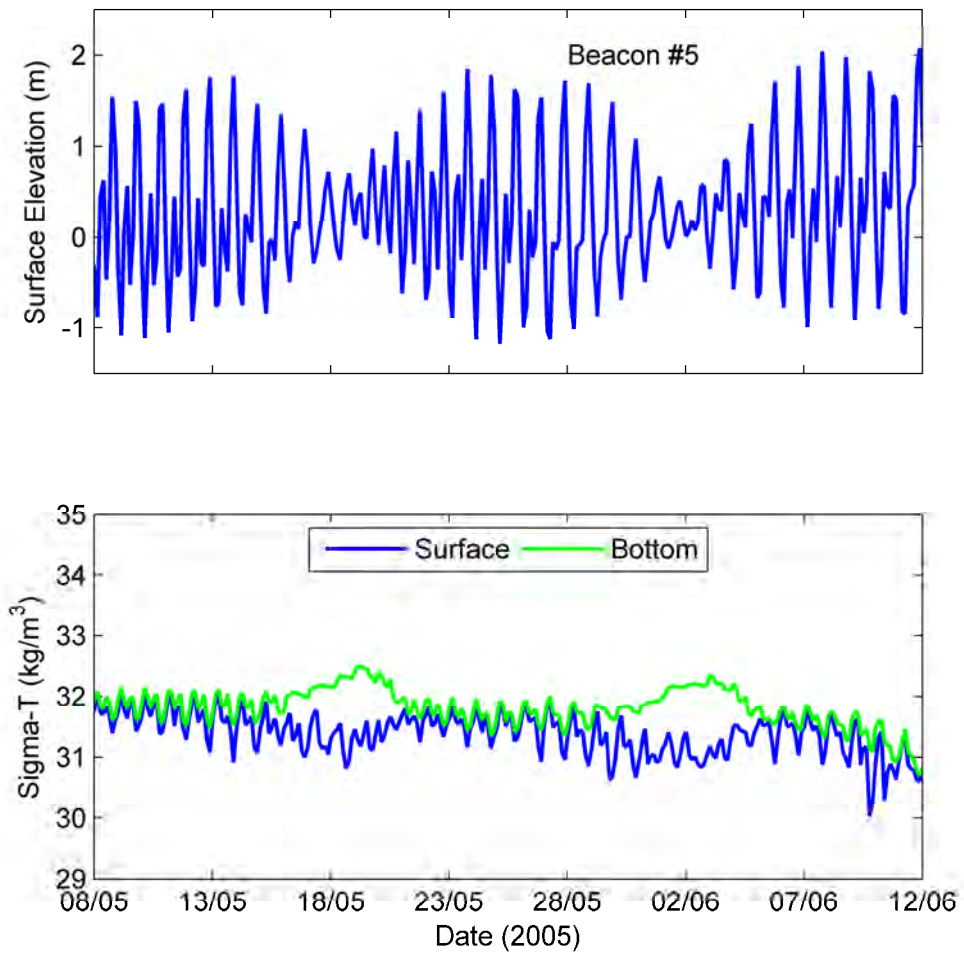
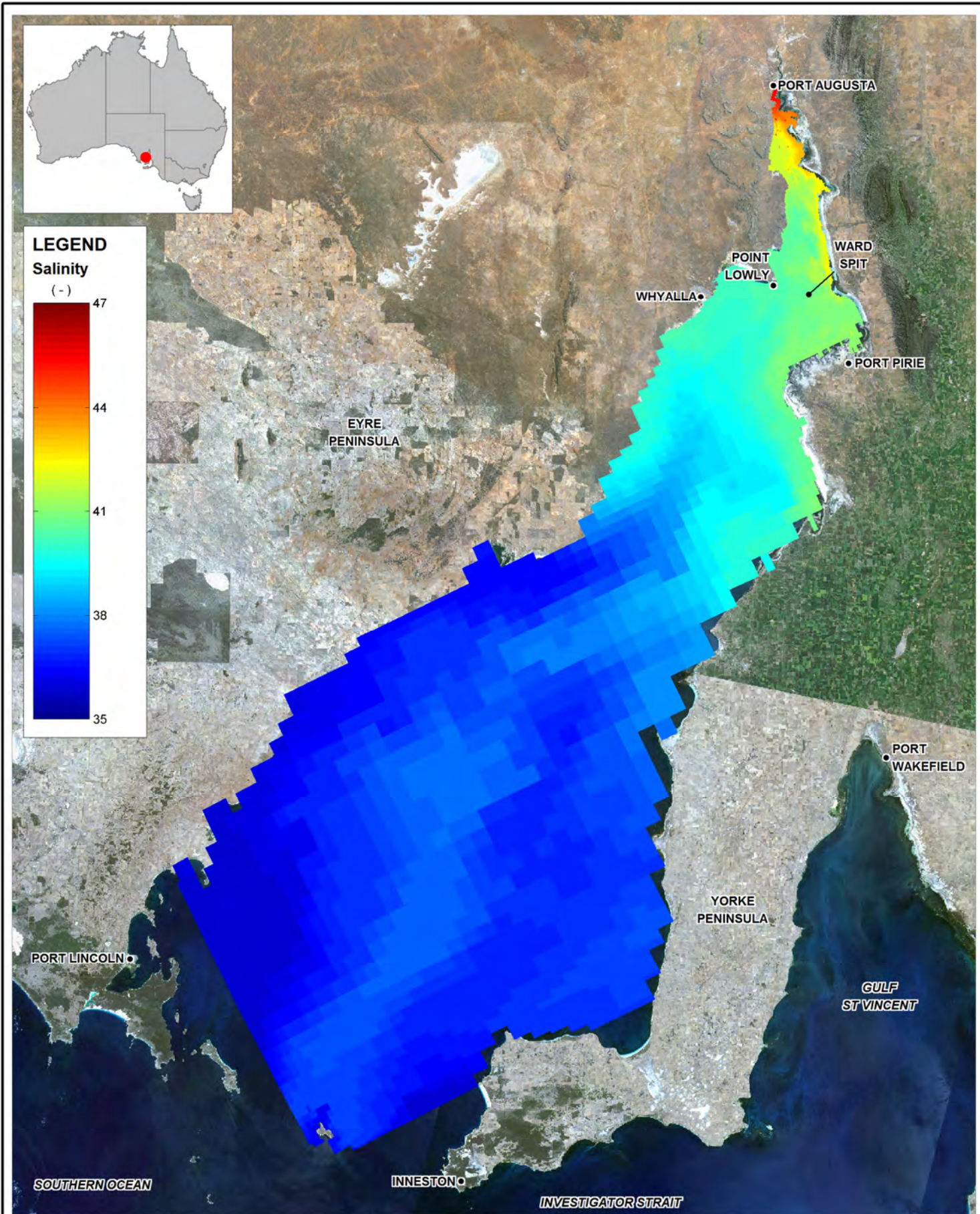


Figure 5-21 Modelled Stratification Development as a Result of Tide Modulation

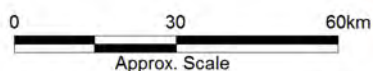


Title:  
**Modelled Bottom Salinity Indicating an Eastern Shore Density Current (June 2005)**

Figure:  
**5-22**

Rev:  
**A**

BMT WBM endeavours to ensure that the information provided in this map is correct at the time of publication. BMT WBM does not warrant, guarantee or make representations regarding the currency and accuracy of information contained in this map.



Filepath :

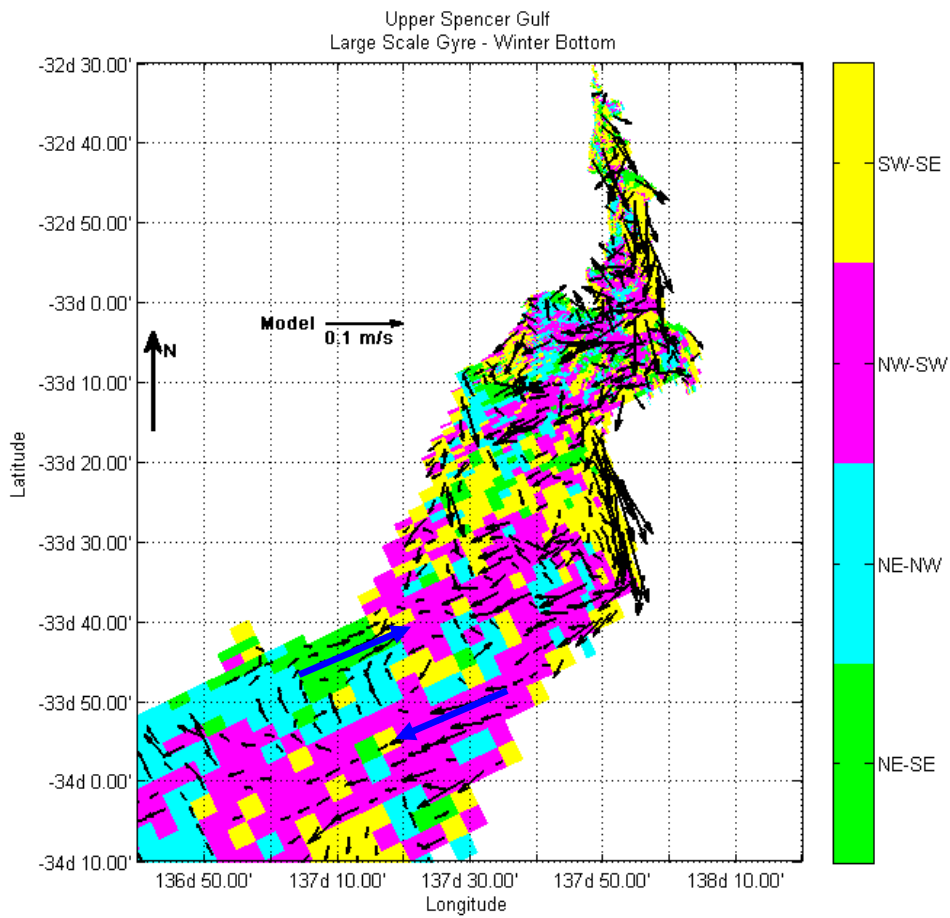
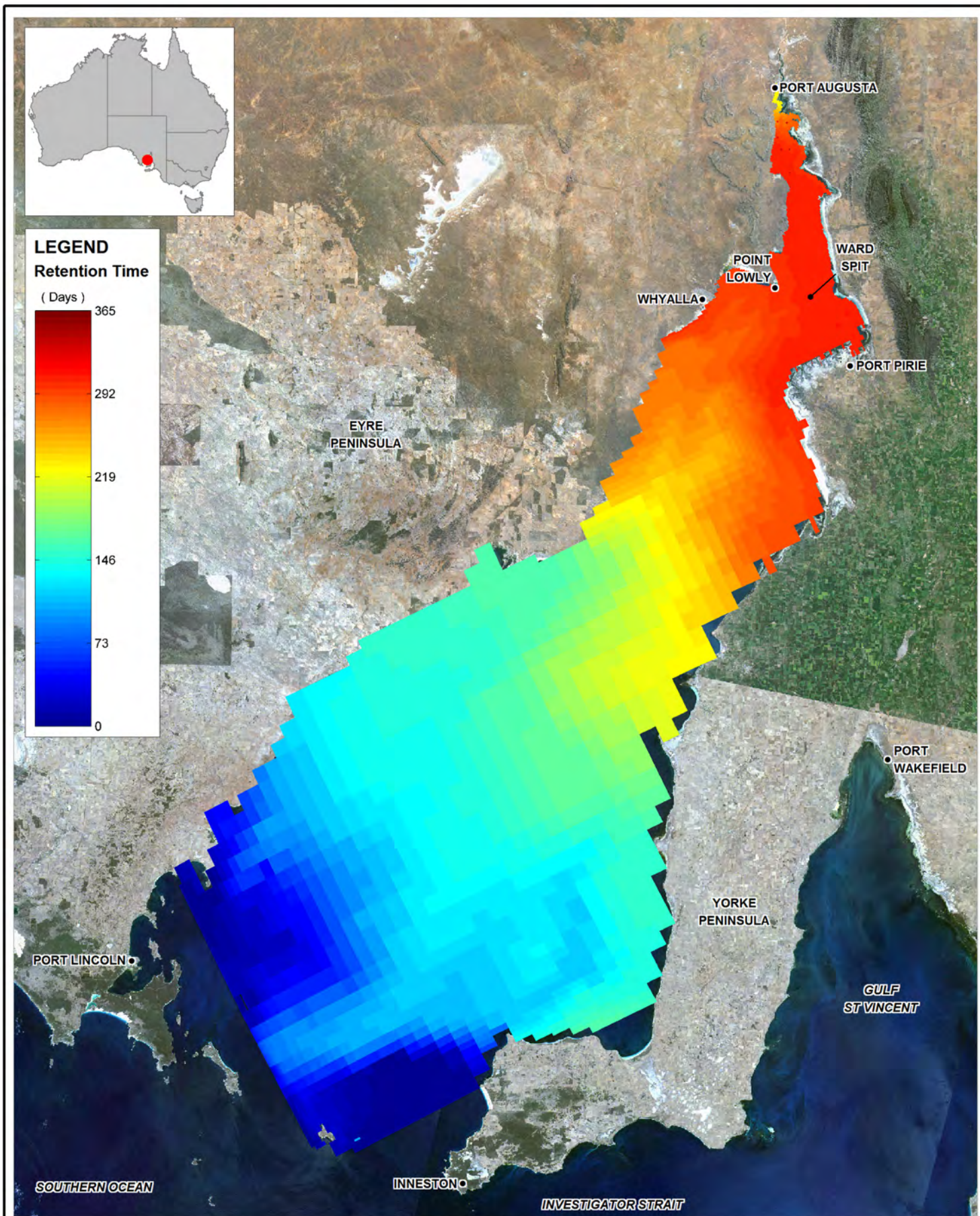


**Figure 5-23 Winter Residual Circulation at the Bottom. Change in Direction Given by the Change in Colour from Magenta to Cyan to Green Illustrates the Clockwise Gyre. Large blue arrows emphasize the distinct gyre circulation.**



Title:  
**Retention Time after 1 Year - 31 October 2005**  
**Bottom Layer**

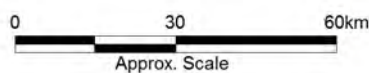
Figure:

**5-24**

Rev:

**A**

BMT WBM endeavours to ensure that the information provided in this map is correct at the time of publication. BMT WBM does not warrant, guarantee or make representations regarding the currency and accuracy of information contained in this map.

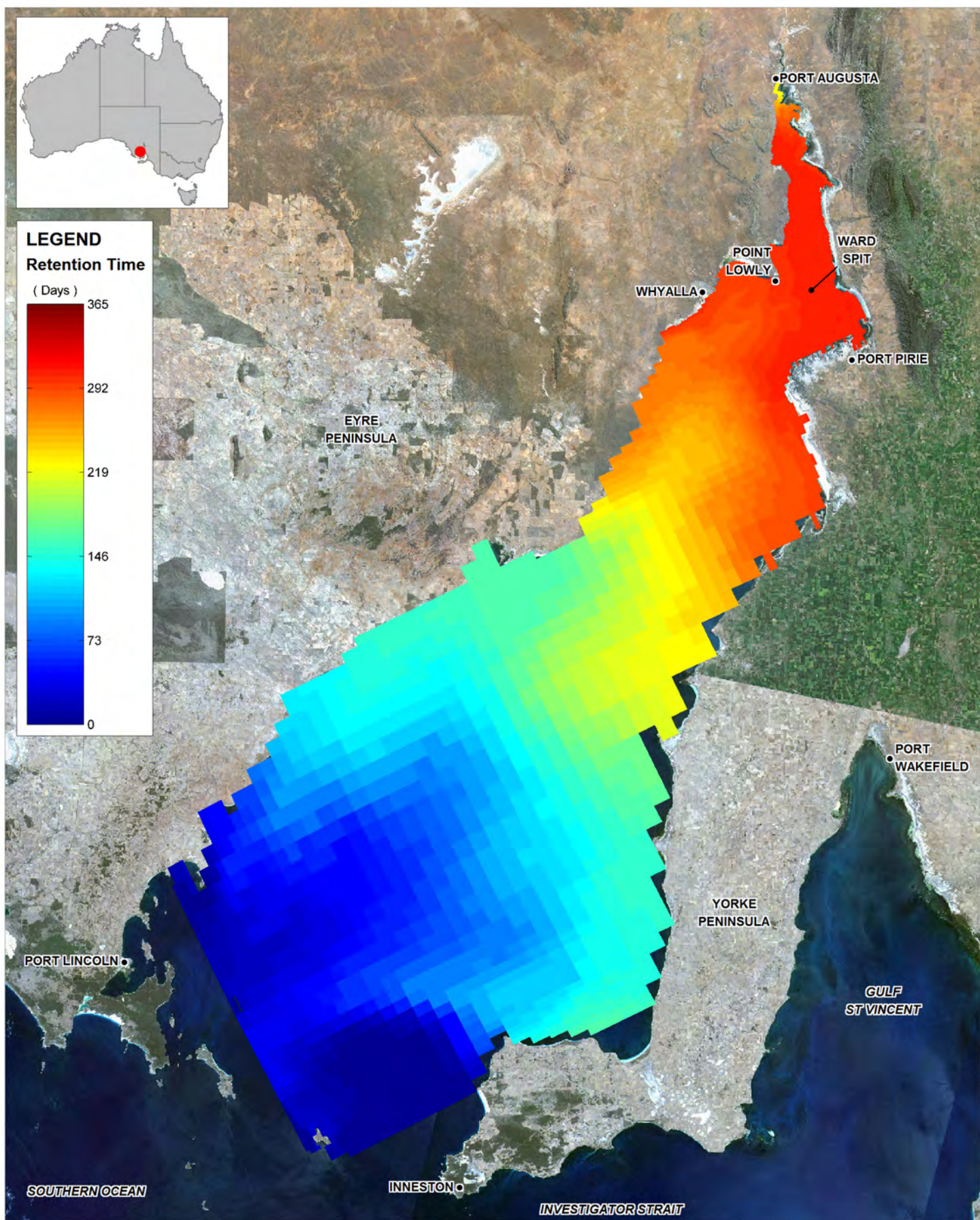
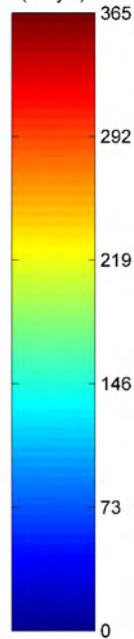


Filepath :



**LEGEND**  
Retention Time

( Days )



Title:  
**Retention Time after 1 Year - 31 October 2005**  
**Surface Layer**

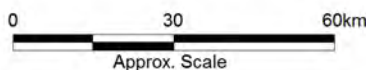
Figure:

**5-25**

Rev:

**A**

BMT WBM endeavours to ensure that the information provided in this map is correct at the time of publication. BMT WBM does not warrant, guarantee or make representations regarding the currency and accuracy of information contained in this map.



Filepath :

## 5.2 Forty-Days Validation Period (Targeted Deployment)

### 5.2.1 Initial Conditions

Moored ADCP measurements of currents were performed at stations shown in Figure 3-1 from 25 April to 06 June 2009. Simulations were started on 23 April 2009 using the salinity and temperature measured at the stations shown in Figure 3-1 and BMT ARGOSS data at the open boundary conditions. Similarly to the other simulations the initial conditions were distributed internally by the model executable using a linear interpolation method in the vertical and an inverse squared-distance interpolation method in the horizontal in each vertical level. A cold start was also adopted for the momentum initialisation.

### 5.2.2 Tidal Elevations

The depths measured from the CTDs were averaged in time to provide a mean sea level, which was assumed to be approximately the model reference level (0.0 m AHD). Tidal records at Port Augusta were not available but were synthesised utilising 22 tidal constituents sourced from Seafarer into the IOS tides software. Figure 5-26 shows the agreement between measured (and synthesised) and modelled tide phases and amplitudes for Sites 3, Site 6, and Port Augusta. The model was able to reproduce amplification of the tides from South to North of the Gulf, which was particularly noticeable for the semi-diurnal inequality (see e.g. Easton 1978, Table 5-3 and Table 5-4). Note that similarly to the comparisons shown in Section 5.1.2 the model did not take into consideration the effects of atmospheric pressure on the water level, apart from the tidal propagation across the open boundaries. The model however, did take into consideration effects of wind set-up (not considered in the synthesised tides), which can be as large as 1.0 m in Port Augusta for the predominant west to south-westerly winds observed in the period (i.e. AHS Chart AUS 778, see also wind records at Figure 3-3).

The spatial distribution of the tides followed the patterns documented in the literature (Easton 1978). First, the model reproduced the tide amplification and phase difference of about 180° between mouth and head of the Gulf (Figure 5-27 to Figure 5-30, and Table 5-3 and Table 5-4); that is, when the tide receded at the mouth it rose at the head, and vice-versa. Second, the model reproduced a partial nodal point for the semi-diurnal tidal components south of Wallaroo, where the semi-diurnal tidal components had small amplitude, and the remaining diurnal tidal constituents presented only relatively small phase differences with the Southern areas of the Gulf, as illustrated in Figure 5-27 to Figure 5-29. When the semi-diurnal tidal components cancelled each other, the effects of the diurnal components were more evident and tidal elevation gradients south of Wallaroo became more noticeable (Figure 5-30). These characteristics are further illustrated in Table 5-3 and Table 5-4 by comparisons between modelled and synthesised tides at Port Lincoln (near mouth), Wallaroo, Site 2, and Site 6 (near head). In these cases, the FPC records (available for other years) were used to obtain harmonic components (Pawlowicz et al. 2002), and these were then used to generate the elevations at the different locations at the same times in which the model was run. This procedure was performed to ensure comparable modelled and synthesised time series were used for subsequent harmonic analysis presented in Table 5-3 and Table 5-4.

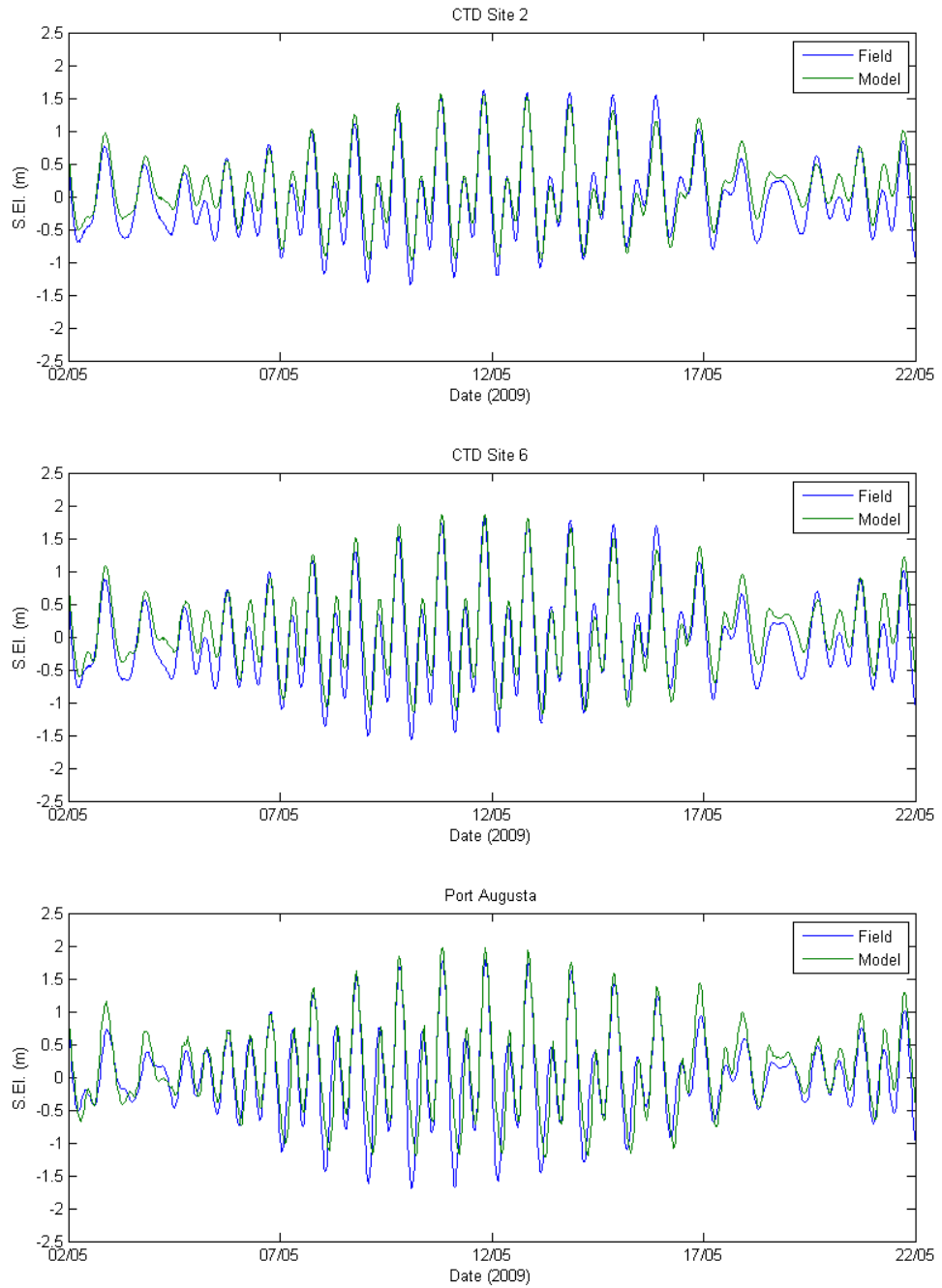


**Figure 5-26 Comparison of Modelled and Observed (CTD Site 2 and CTD Site 6) or Synthesised (Port Augusta) Tide Levels (Medium Term 2009 Data)**

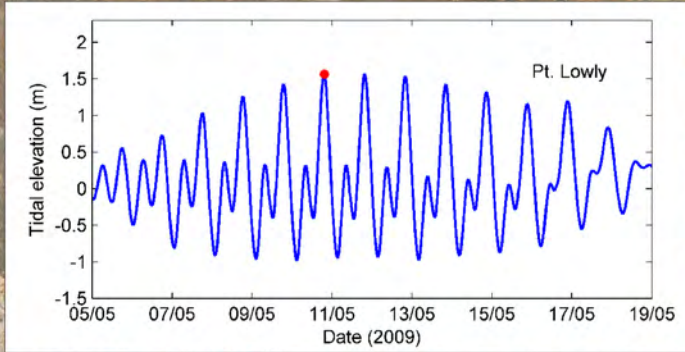


**Table 5-3 Amplitude (m) of Tide Constituents Obtained from Harmonic Analysis**

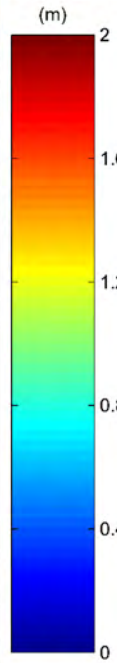
Tidal Constituent	Port Lincoln		Wallaroo		Site 2		Site 6	
	Field	Model	Field	Model	Field	Model	Field	Model
<b>S2</b>	0.208	0.172	0.135	0.123	0.399	0.347	0.510	0.463
<b>M2</b>	0.233	0.170	0.156	0.128	0.474	0.378	0.581	0.484
<b>N2</b>	0.023	0.022	0.013	0.010	0.029	0.045	0.045	0.062
<b>K1</b>	0.277	0.220	0.397	0.356	0.562	0.498	0.591	0.543
<b>O1</b>	0.155	0.155	0.195	0.223	0.242	0.286	0.236	0.301
<b>Q1</b>	0.037	0.034	0.051	0.044	0.048	0.055	0.043	0.058

**Table 5-4 Phase (degrees) of Tide Constituents Obtained from Harmonic Analysis**

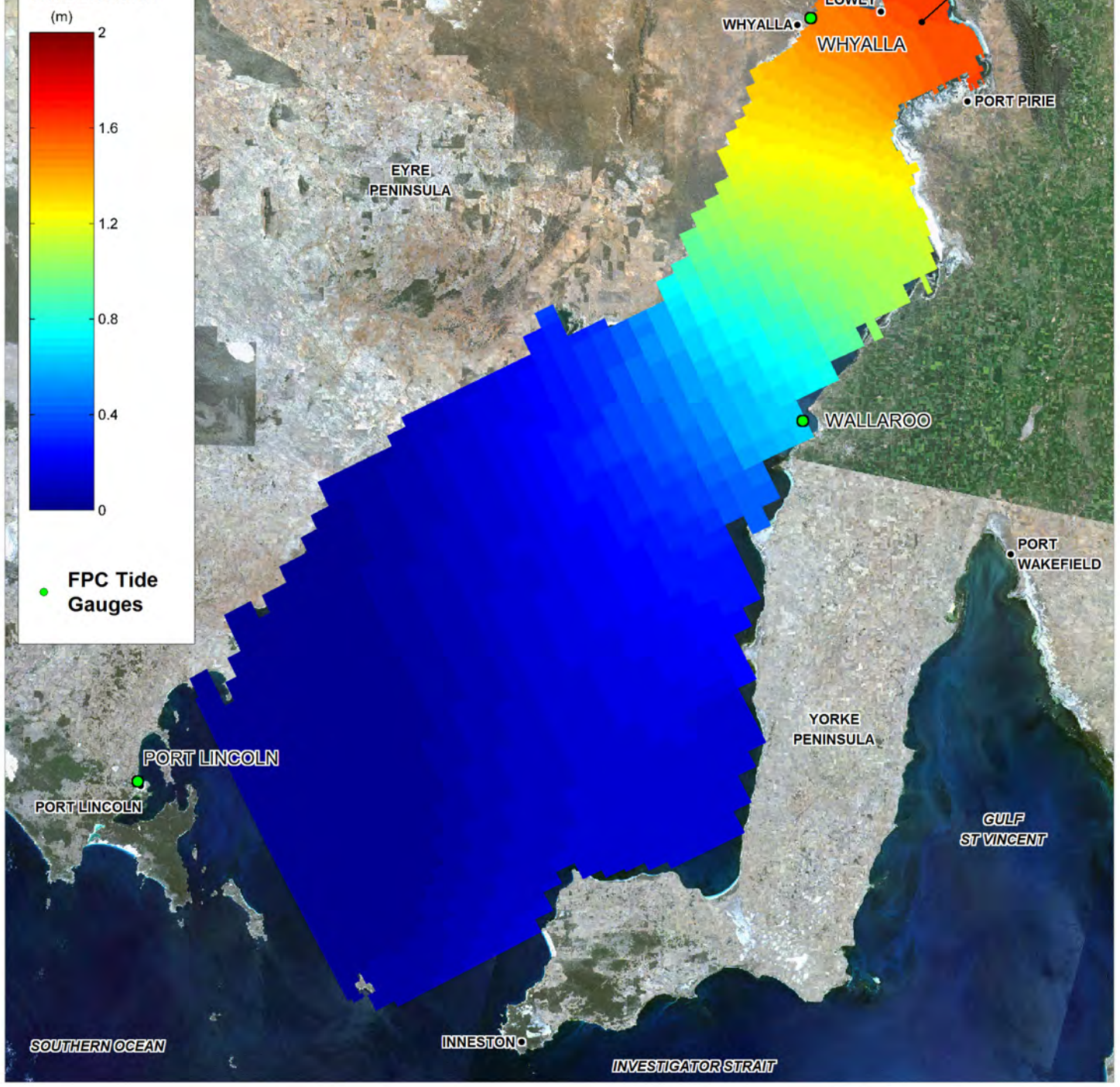
Tidal Constituent	Port Lincoln		Wallaroo		Site 2		Site 6	
	Field	Model	Field	Model	Field	Model	Field	Model
<b>S2</b>	67.6	66.7	168.6	161.7	228.6	238.7	238.9	254.7
<b>M2</b>	30.9	21.5	131.2	117.1	183.8	192.7	194.7	209.5
<b>N2</b>	122.5	105.9	224.1	221.9	268.3	285.0	264.1	268.7
<b>K1</b>	18.8	17.8	53.3	53.5	62.2	66.1	67.2	72.6
<b>O1</b>	5.8	2.2	36.3	35.8	47.3	49.4	52.0	56.2
<b>Q1</b>	354.7	356.1	18.8	19.0	14.9	37.9	22.1	46.1



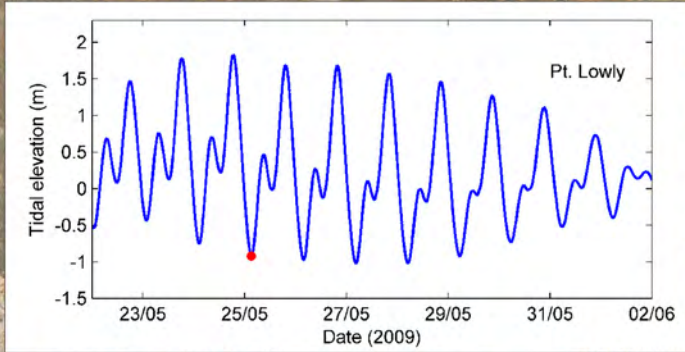
**LEGEND**  
Tidal Elevation



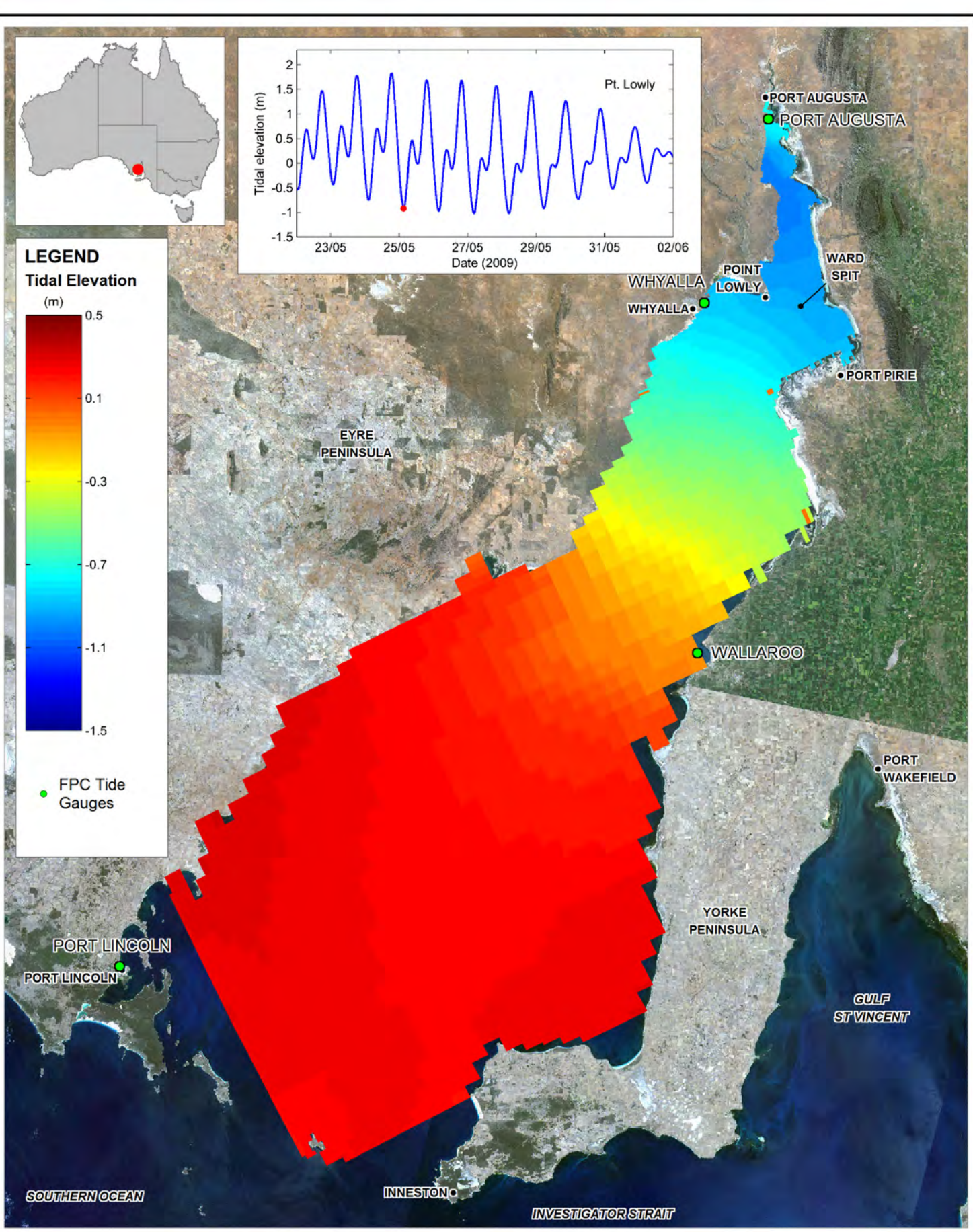
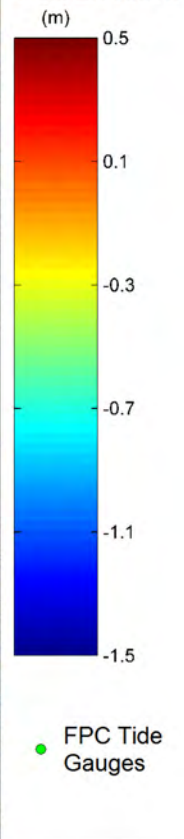
● FPC Tide Gauges



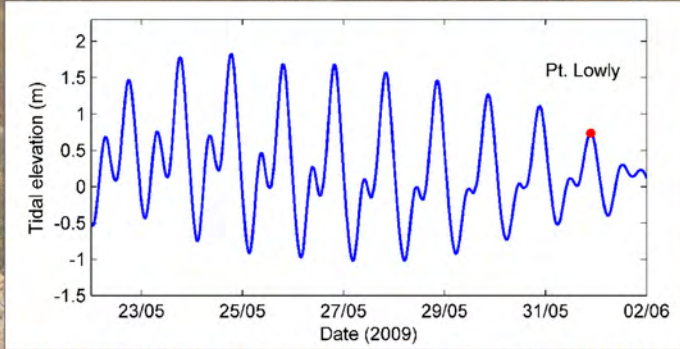
<p>Title: <b>Spatial Distribution of Tidal Elevations: Spring Tide High Water at Point Lowly</b></p>		<p>Figure: <b>5-27</b></p>	<p>Rev: <b>A</b></p>
<p>BMT WBM endeavours to ensure that the information provided in this map is correct at the time of publication. BMT WBM does not warrant, guarantee or make representations regarding the currency and accuracy of information contained in this map.</p>			
<p>Filepath :</p>			



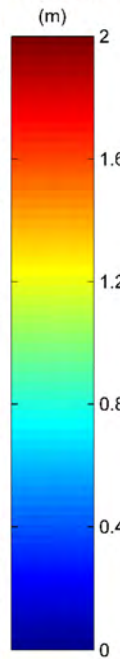
**LEGEND**  
Tidal Elevation



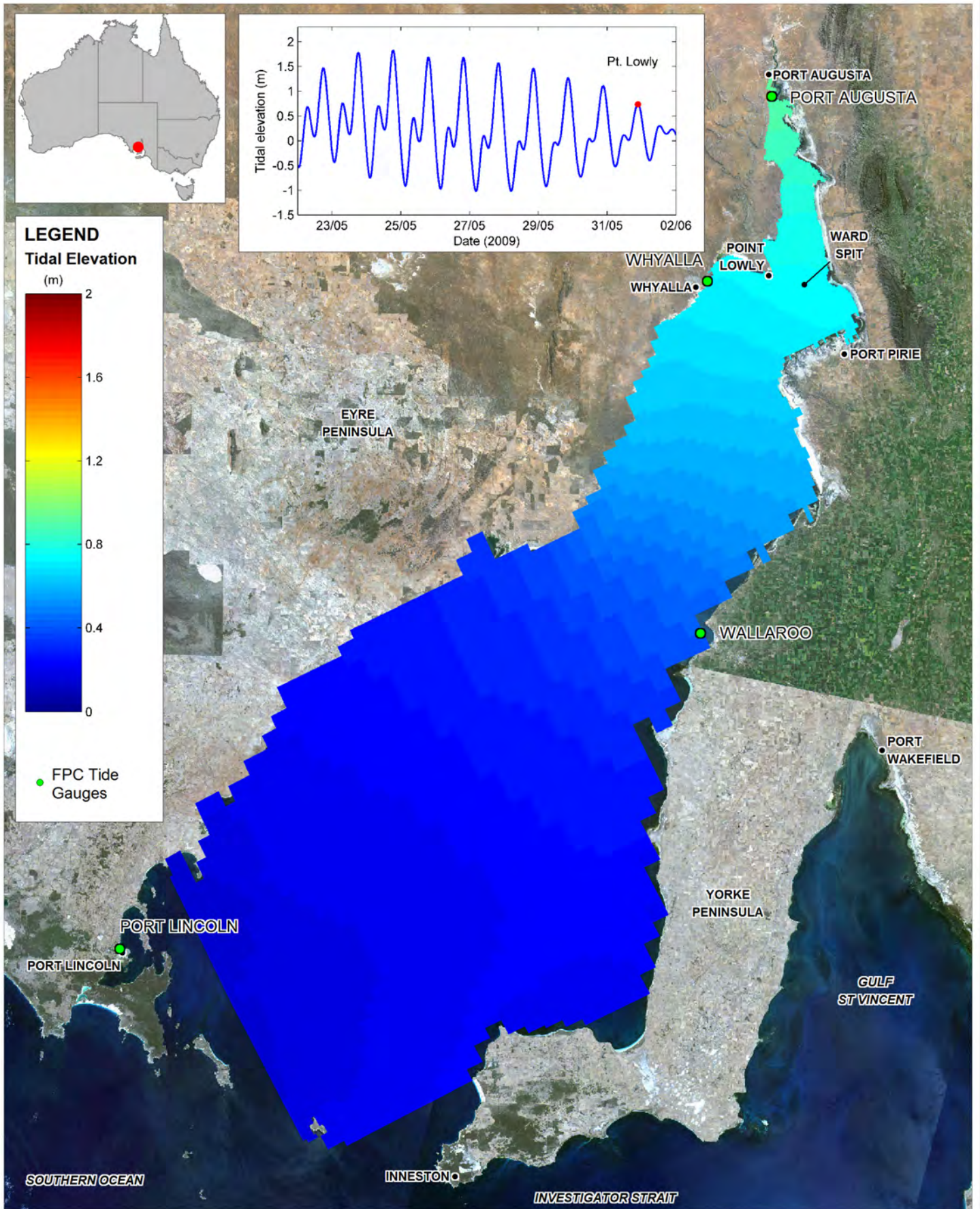
<p>Title:</p> <p><b>Spatial Distribution of Tidal Elevations: Spring Tide Low Water at Point Lowly</b></p>	<p>Figure:</p> <p><b>5-28</b></p>	<p>Rev:</p> <p><b>A</b></p>
<p>BMT WBM endeavours to ensure that the information provided in this map is correct at the time of publication. BMT WBM does not warrant, guarantee or make representations regarding the currency and accuracy of information contained in this map.</p>	<p>Approx. Scale</p>	<p><b>BMT WBM</b> www.wbmpl.com.au</p>
<p>Filepath :</p>		



**LEGEND**  
Tidal Elevation



● FPC Tide Gauges

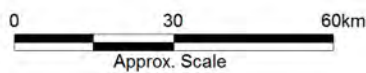


Title:  
**Spatial Distribution of Tidal Elevations:  
Neap Tide High Water at Point Lowly**

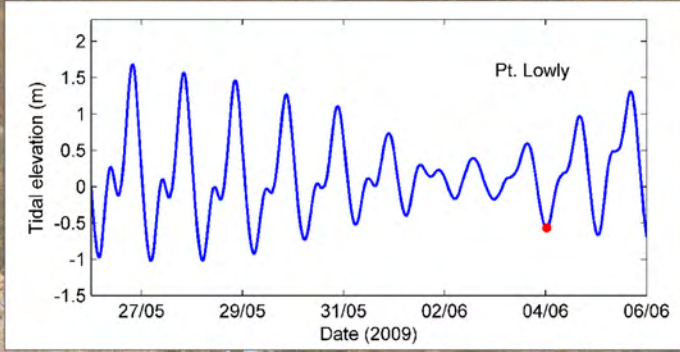
Figure:  
**5-29**

Rev:  
**A**

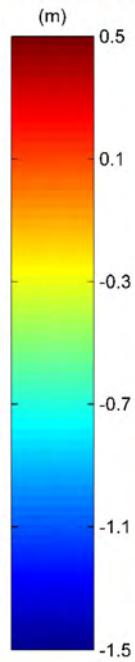
BMT WBM endeavours to ensure that the information provided in this map is correct at the time of publication. BMT WBM does not warrant, guarantee or make representations regarding the currency and accuracy of information contained in this map.



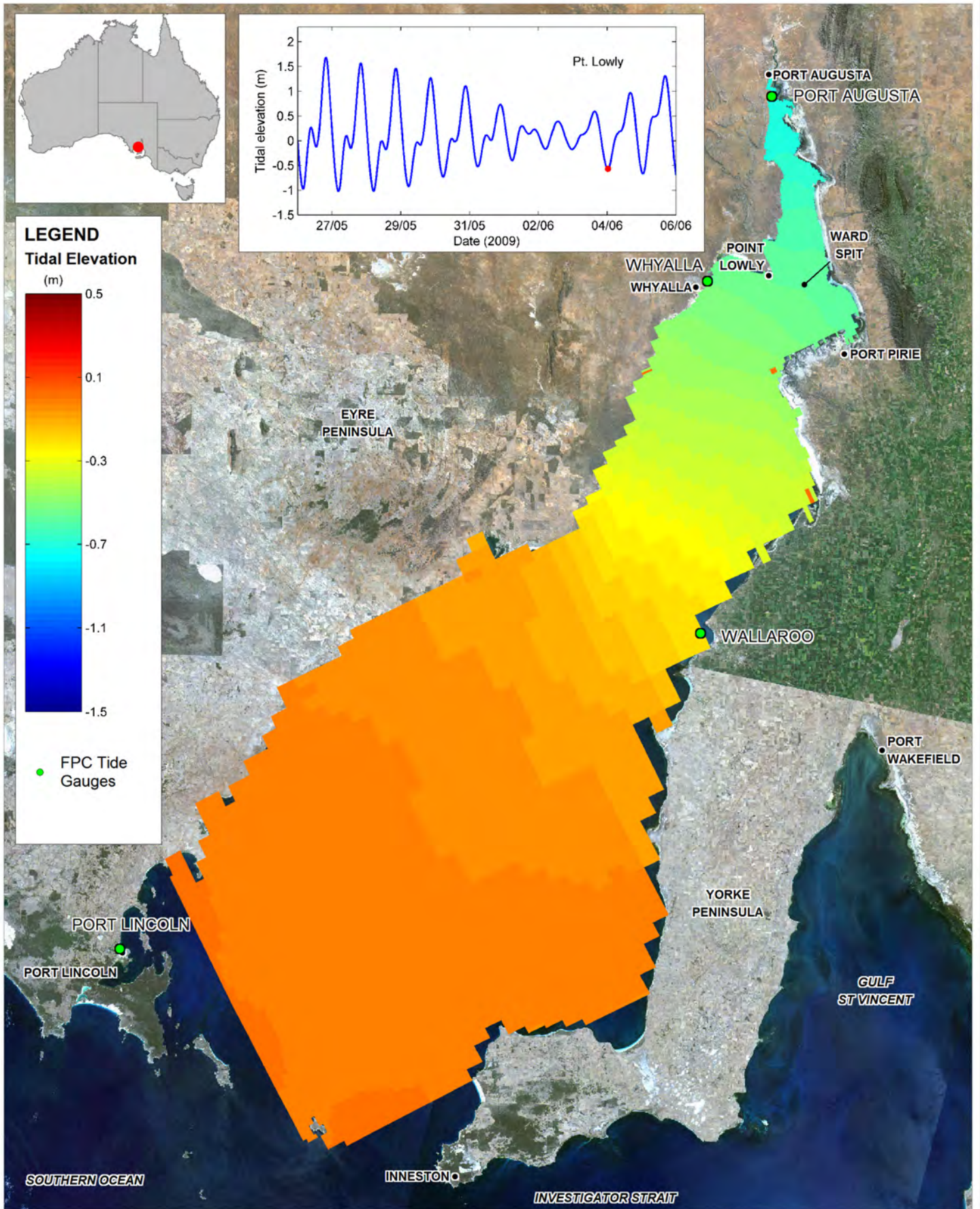
Filepath :



**LEGEND**  
Tidal Elevation



● FPC Tide Gauges

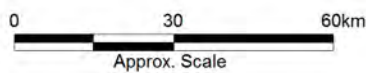


Title:  
**Spatial Distribution of Tidal Elevations:  
Neap Tide Low Water at Point Lowly**

Figure:  
**5-30**

Rev:  
**A**

BMT WBM endeavours to ensure that the information provided in this map is correct at the time of publication. BMT WBM does not warrant, guarantee or make representations regarding the currency and accuracy of information contained in this map.



Filepath :

### 5.2.3 Temperature and Salinity

Comparisons between temperature and salinity CTD measurements are presented in Figure 5-31 and Figure 5-32, respectively. It is noted that the modelled ranges were not reproduced as well for the salinity. This effect is due to the initialisation of the respective fields, which were given by a global averaging interpolation method therefore, smoothing out some natural gradients (see e.g. Botelho and Imberger 2009), particularly where there was a high concentration of initial profiles in an area of relatively large spatial gradients. The high-frequency of the measured signals was clearly a result of tidal motion that advected back and forth water of distinct temperature and salinity signatures. Because temperature is more strongly affected by the surface boundary condition impinging directly over the whole model surface, the modelled temperature field adjusted more quickly and both long term and high frequency variations are better modelled (see e.g. Site 6). Salinity however, requires the development of the gradients (smoothed out by the initialisation) to produce the seasonal trends of salinity decrease.

To demonstrate that the model is able to reproduce the low and high-frequency content, a simulation was initialised in 1 November 2008 with the same initial conditions presented in Section 5.1. All forcing data was coincident over this period, including the atmospheric and boundary conditions, which were derived as for the previously described simulations. Further details of this simulation are provided in Appendix I. Even though the spin-up time was approximately six months (i.e. less than the approximate 1-year Gulf residence time, see Draft EIS - Appendix O11.3), not only the high-frequency variation became clearly noticeable, but the low-frequency variation with tidal modulation evident at Site 5 were also reproduced (Figure 5-33 and Figure 5-34).

In addition to the figures and analysis below, further interrogation of the model was undertaken in frequency space. Specifically, spectral comparison of low and high pass filtered timeseries (i.e. tidal and sub-tidal frequencies) for both measured and modelled data over the spun up 40 day period in 2009 was considered. The corresponding results are described and presented in Appendix I and these further support the model's skill in reproducing the tidal motion, and indicate that the model reproduces the dispersive characteristics of the scalar fields.

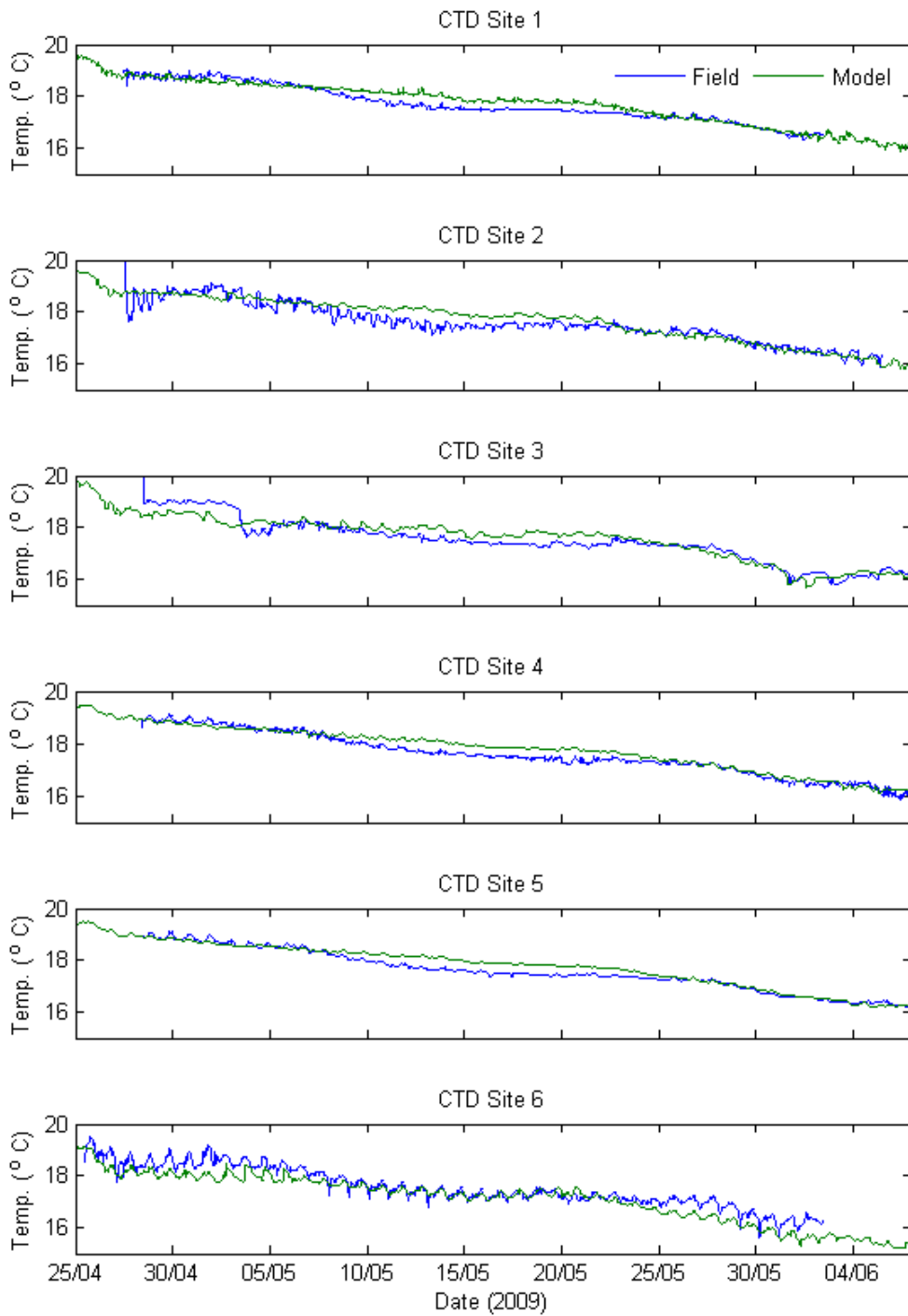


**Figure 5-31 Comparison of Modelled and Observed Temperature (Medium Term 2009 Data). Initial Conditions in April 2009.**

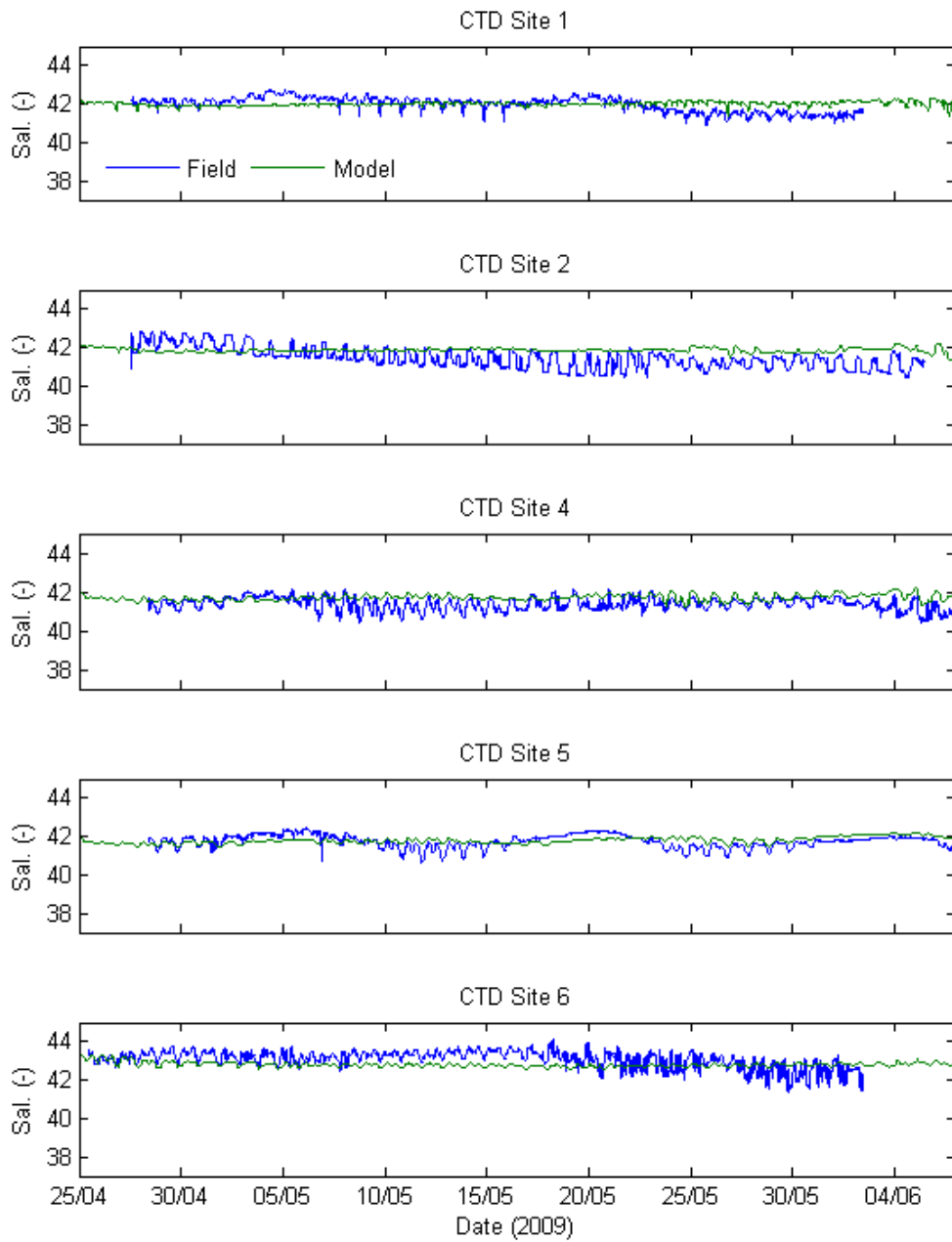


**Figure 5-32 Comparison of Modelled and Observed Salinity (MediumTerm 2009 Data). Initial Conditions in April 2009.**



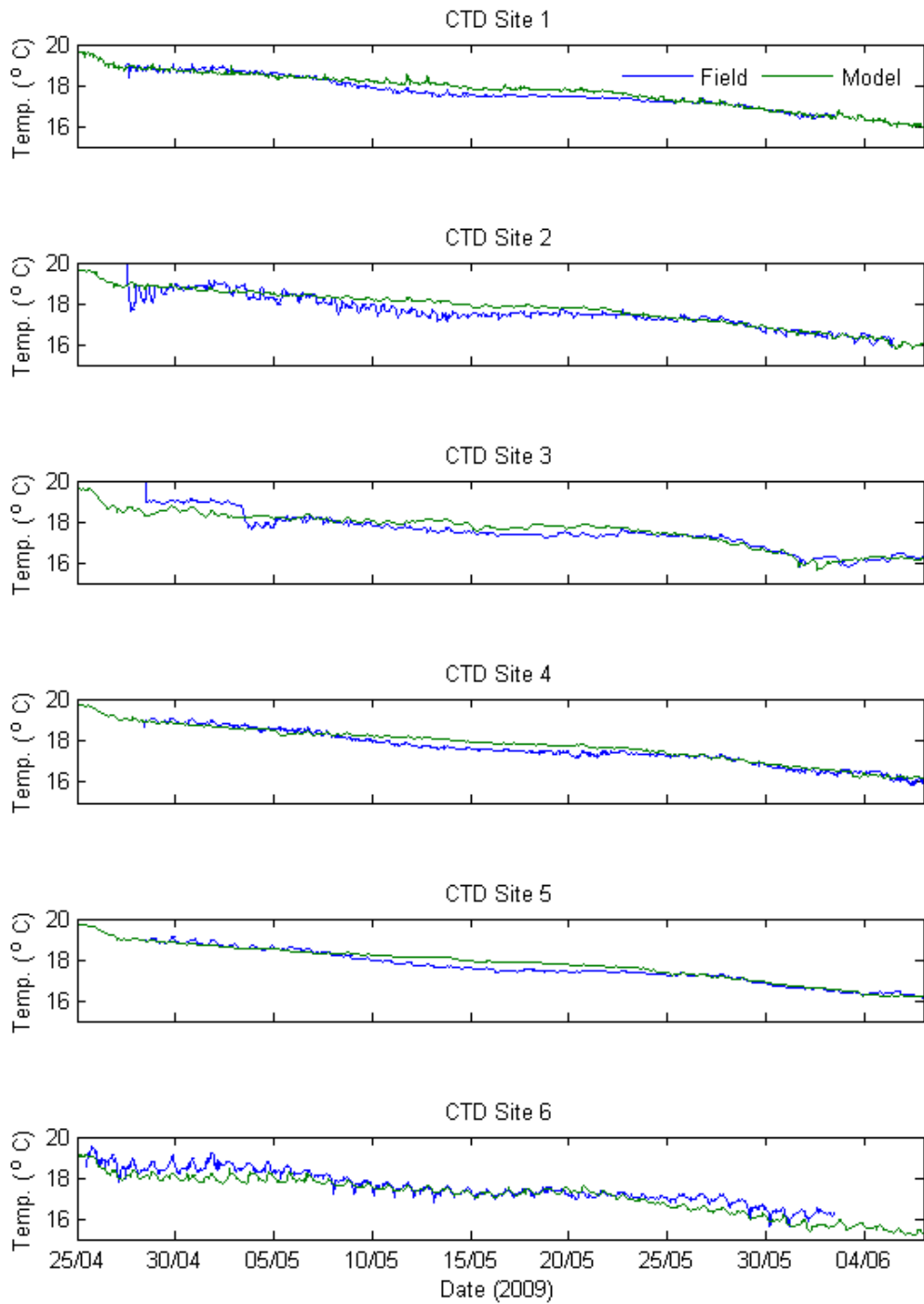


**Figure 5-33 Comparison of “Spun-Up” Modelled and Observed Temperature. Initial Conditions in Nov 2008. All Forcing Data Temporally Coincident.**

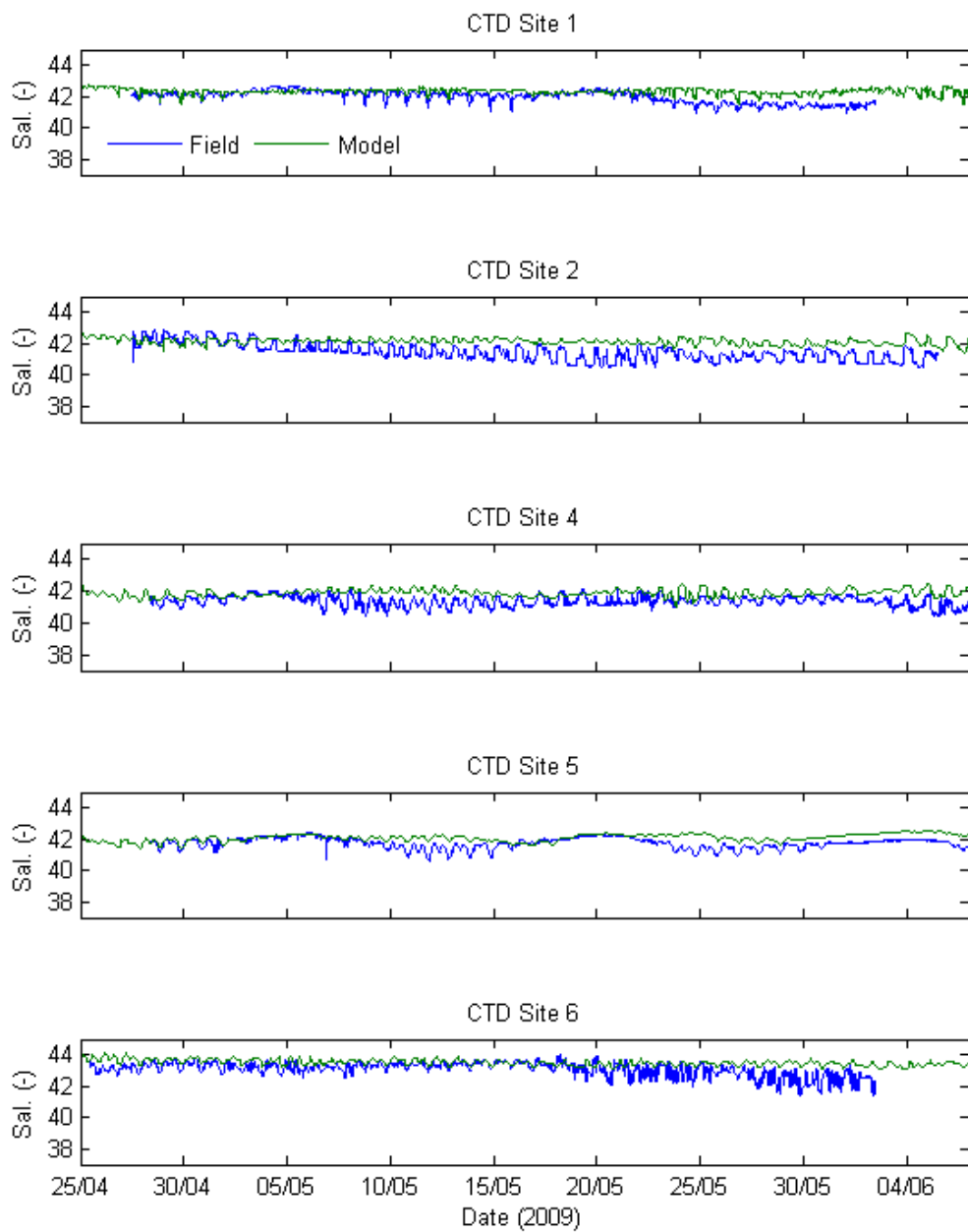


**Figure 5-34 Comparison of “Spun-Up” Modelled and Observed Salinity. Initial Conditions in Nov 2008. All Forcing Data Temporally Coincident.**

## 5.2.4 Moored ADCP Velocities

Time series at different depths and locations for periods in both spring and neap ('dodge') tidal cycles are shown in Figure 5-35 to Figure 5-42. Comparisons for the whole record are presented in Appendix E. As can be seen from these figures, the model is able to capture the tidal modulation of the currents during both spring and neap tides, particularly during 'dodge' tides observed between 04-06 May and 19-20 May. Another feature that can be seen is that the model captured the increased flow intensity observed at Station B, in comparison to the other stations.

Distribution of current magnitudes and scatter plots for all other sites are presented in Figure 5-43 to Figure 5-50, and associated error measures in Table 5-5 to Table 5-8. For Station B, modelled velocity magnitudes and directions were reproduced satisfactorily. Distributions of measured and modelled current speeds at 5.00 and 15.00 m from the bottom were similar, with distribution of modelled currents skewed to lower values (Figure 5-43), which is conservative in terms of mixing and dispersion. The scatter plots of different components clustered near the 1:1 line and indicate good correlation at all distances from the bottom (Figure 5-44 -  $R^2 > 0.93$  and  $p < 0.001$ , always). Associated model errors (see e.g. Hammel and Smith, 2007) are presented in Table 5-5. These measures are strongly influenced by slight phase differences between measured and modelled time series and are not necessarily indicative of the model's ability to capture physical processes (Hammel and Smith, 2007). This is particularly pronounced on strong (and rapidly changing) tidal flows in which phase errors dominate irrespective of adequate physical representation. The model was however able to reproduce the features of the measured flow (i.e. current magnitude, tidal reversals, maximum velocities, and flow direction), with these being critical to the intent of the current study.

The model performance for Station D was reflected in the similar observed and modelled distributions (Figure 5-45), clustering over the 1:1 line associated with high correlation coefficients (Figure 5-46 -  $R^2 > 0.94$  and  $p < 0.001$ , always), and relatively lower error measures (Table 5-6).

Distributions of current magnitudes at Station C showed a match between observed and modelled currents in both parts of the water column (Figure 5-47), which reflected in the data being clustered around the 1:1 line and good correlation coefficient for the E-W velocities (Figure 5-48). The correlation for the N-S velocities is immaterial, given the low current magnitude and high noise to signal ratio in the measured data (Figure 5-41).

At Station D, agreement was obtained between current magnitude distributions at the top of the water column, whilst under-estimation was sometimes observed in the lower water column (Figure 5-49). The scatter plots reflect this tendency in the lower water column with a tilted clustering in relation to the 1:1 line in both velocity components (Figure 5-50). Inspection of the time series indicates the errors are more relevant in the neap tides, and are further magnified by phase differences during spring tides (Figure 5-42). The model's occasional under prediction of the observed data is, however, conservative in terms of brine advection and dispersion, which is the focus of this study.

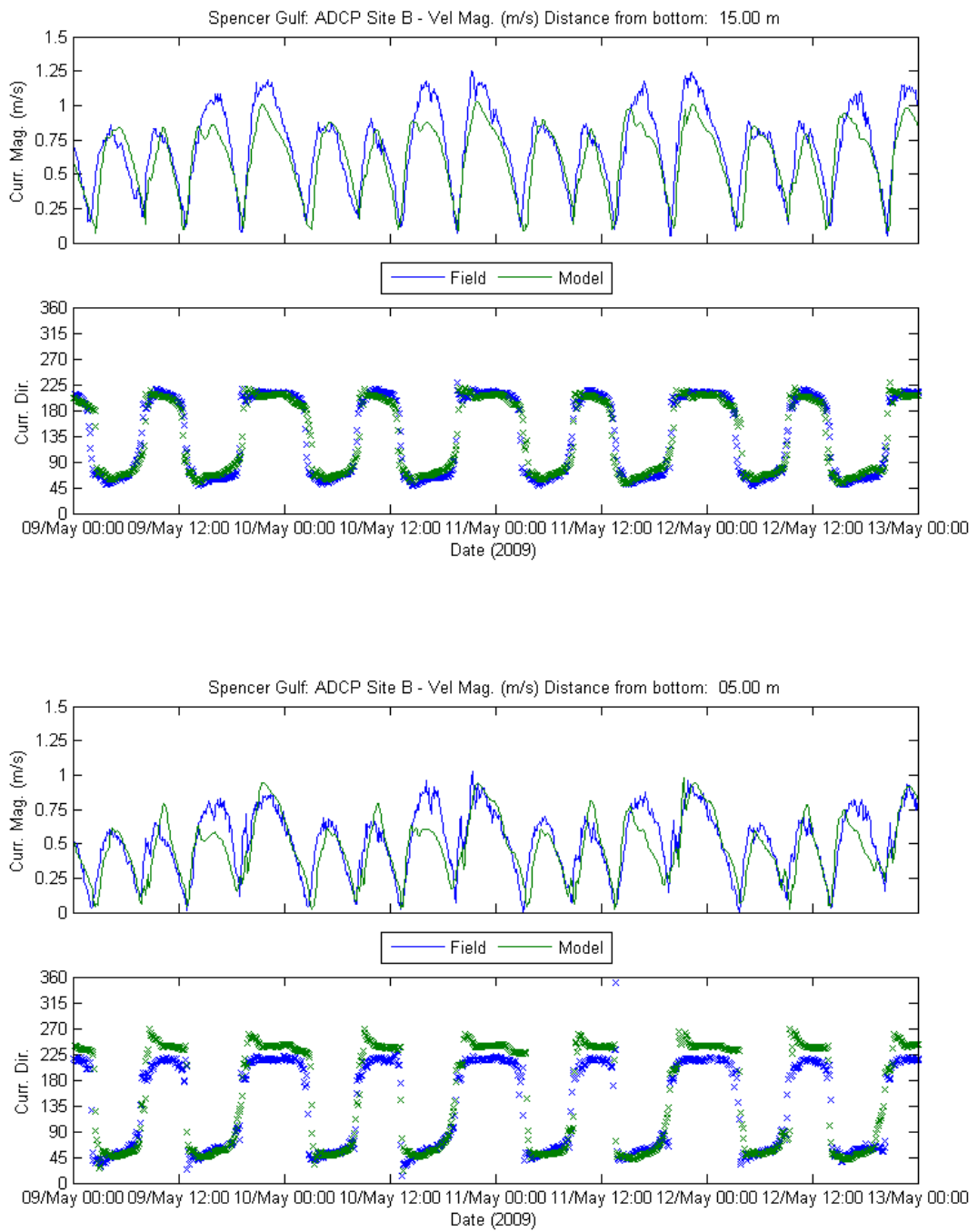
In addition to the distribution of current magnitudes, current roses were used to summarise the statistics of the measurements and model results. Figure 5-51 provides an illustrative rose for interpretation guidance. Also, in the computation of the statistics, velocities below 0.15 m/s were removed to facilitate the comparison for the other velocity magnitude bands, and as can be seen in

Figure 5-35 to Figure 5-42, these were reproduced by the model. Roses for observed and modelled velocities for two different depths at each ADCP location are shown in Figure 5-52 to Figure 5-55.

At Stations B and D (Figure 5-52 and Figure 5-53) the statistics indicate the model predicted the intensity of the velocities and also the frequency in which the velocities maintained a given direction. It also indicates the model captured the change in flow intensity and direction with depth, which is an important indicator for model skill in predicting shear-induced vertical mixing. It was noted however, that the very highest velocities bands (3% of the distribution) were slightly under predicted by the model.

At Station C, the statistics indicated the model simulated the predominance of the observed easterly flow (Figure 5-54). As shown in the Draft EIS (Appendix O11.2), Station C is within the lee side of an eddy that forms downstream of Point Lowly during ebbing tides, and as such was a good indicator of the model's ability to predict the returning longshore transport resulting from the eddy mass flux. Similarly to Stations B and D, the model predicted the increased flow intensity in the upper part of the water column, and therefore was able to reproduce the vertical shear.

At Station A, the model reproduced the main flow directions; however it occasionally slightly under predicted velocity magnitude at the bottom and in the upper water column during ebbing tides (Figure 5-55), which is generally conservative in terms of mixing and dispersion. Modelled flow at spring tides was reproduced (see below).



**Figure 5-35 Comparison of Observed and Modelled Velocities Magnitude and Direction at Two Different Levels at Site B (Spring Tide)**

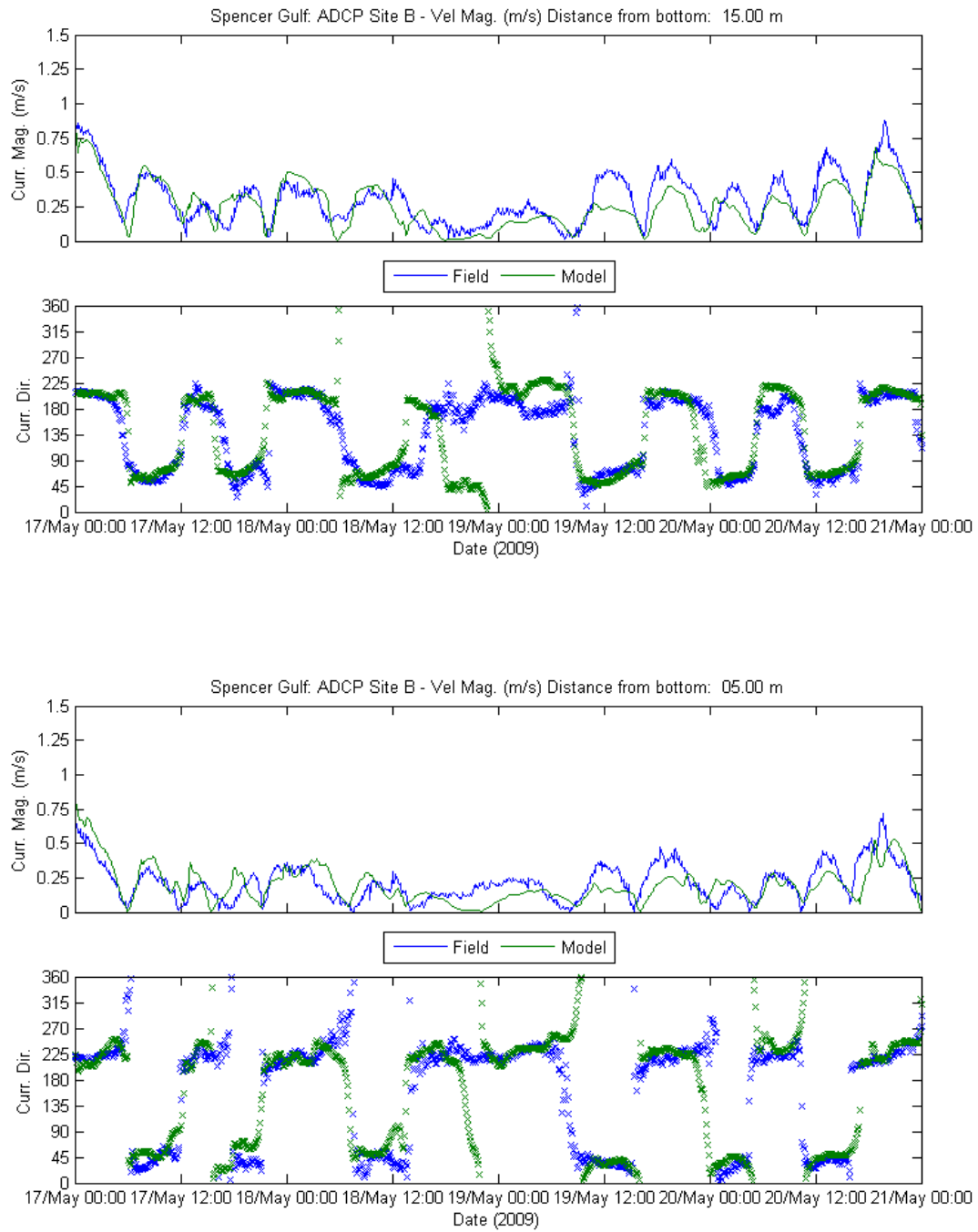


**Figure 5-36 Comparison of Observed and Modelled Velocities Magnitude and Direction at Two Different Levels at Site B (Neap Tide)**

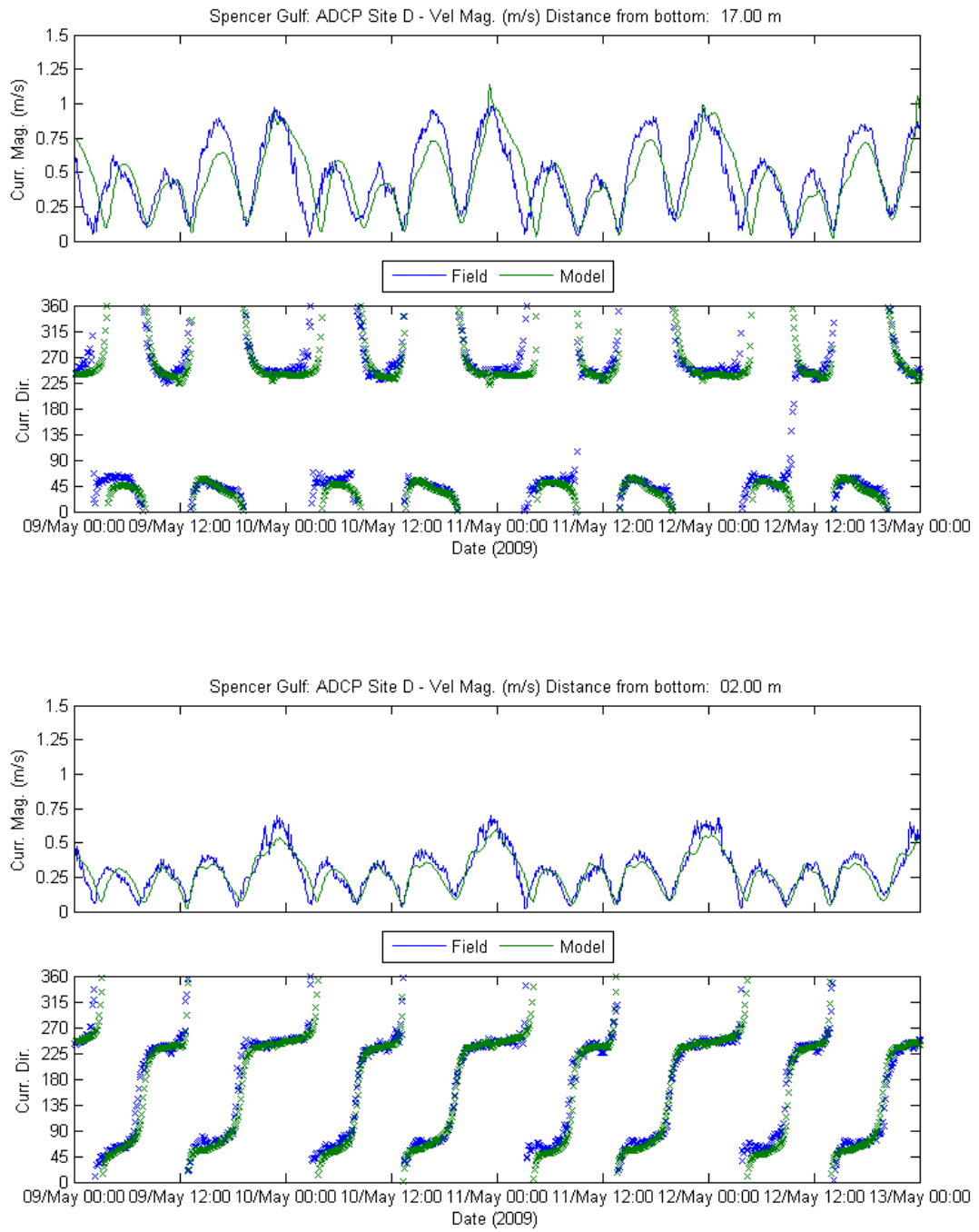


**Figure 5-37 Comparison of Observed and Modelled Velocities Magnitude and Direction at Two Different Levels at Site D (Spring Tide)**

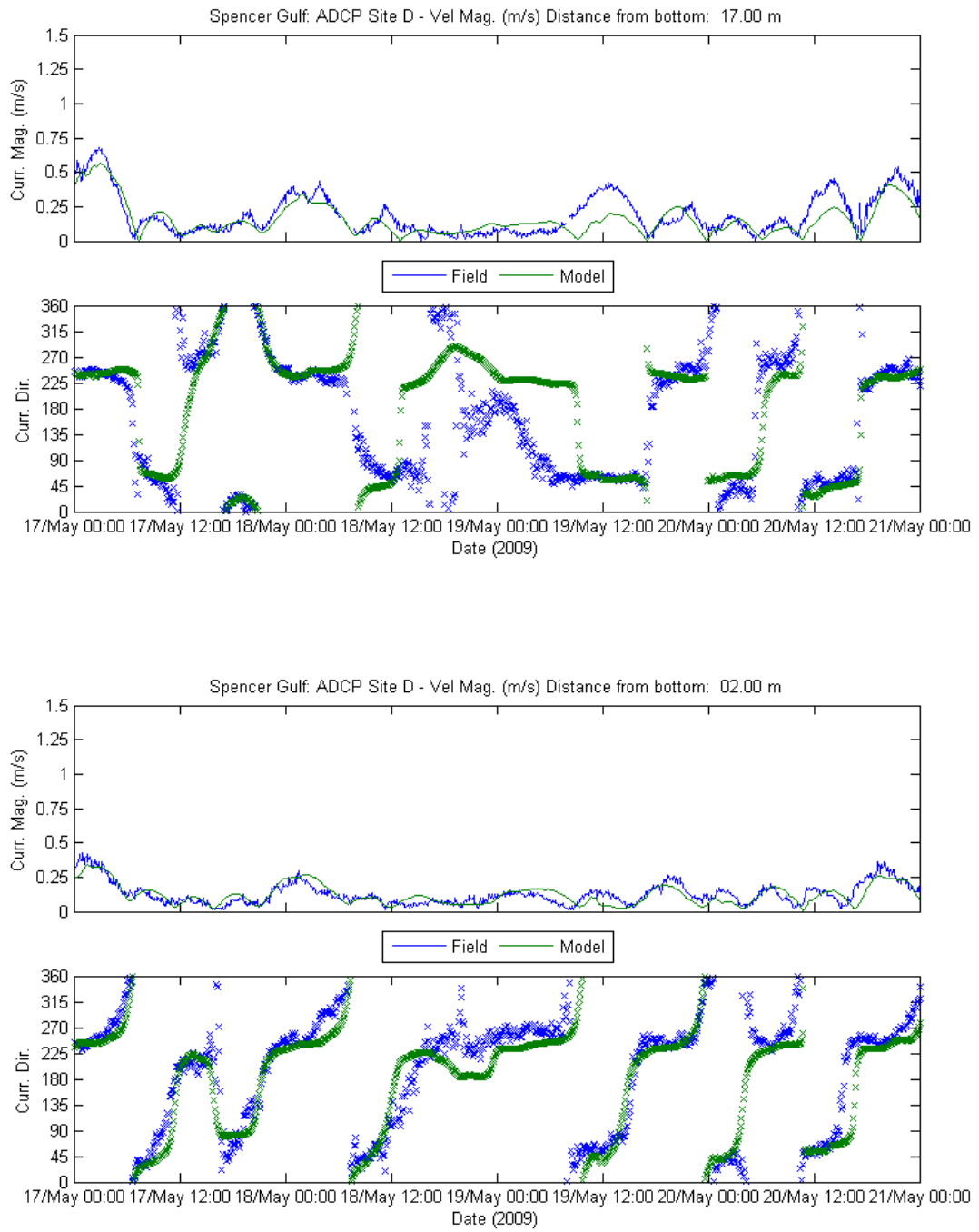


**Figure 5-38 Comparison of Observed and Modelled Velocities Magnitude and Direction at Two Different Levels at Site D (Neap Tide)**



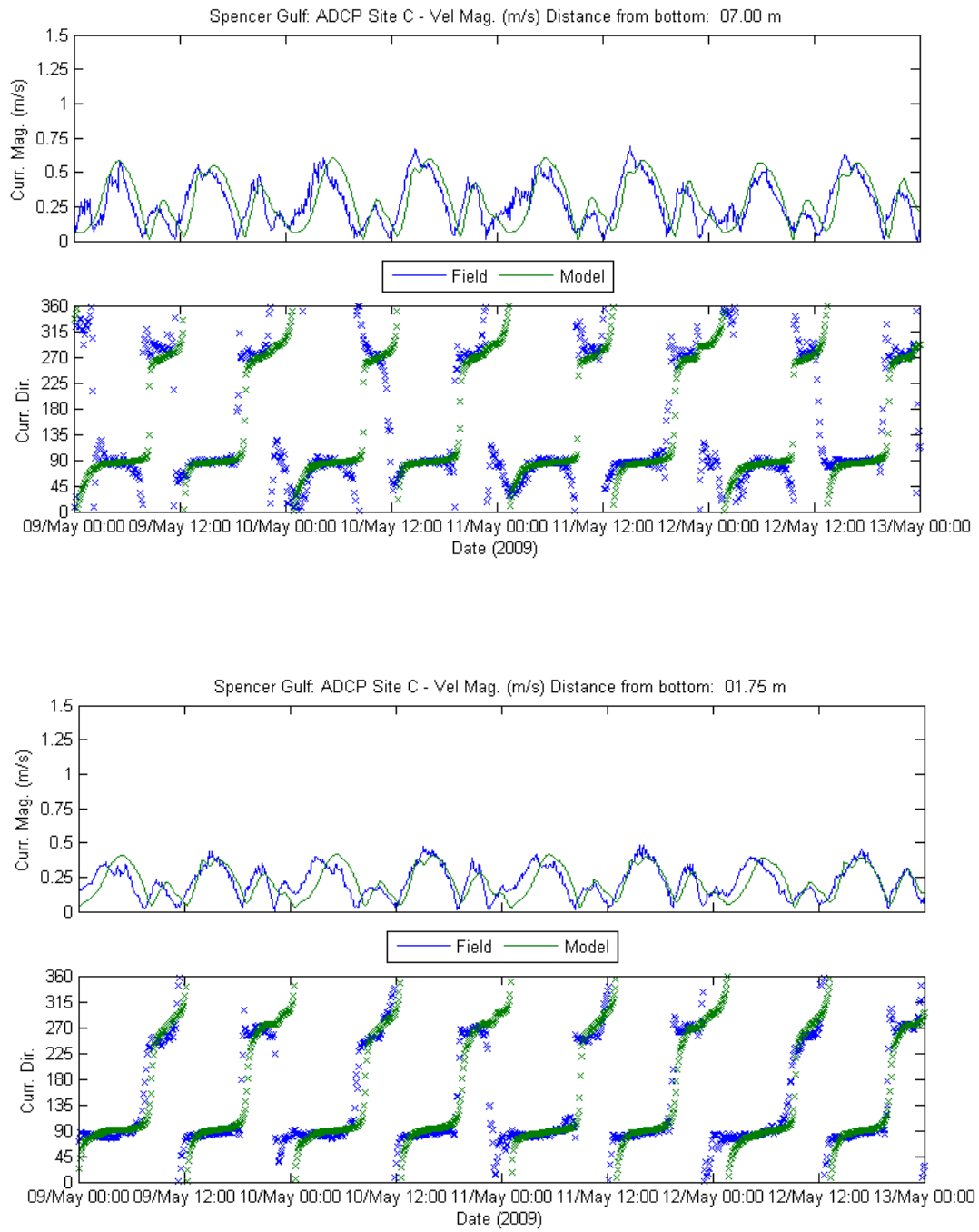


**Figure 5-39 Comparison of Observed and Modelled Velocities Magnitude and Direction at Two Different Levels at Site C (Spring Tide)**

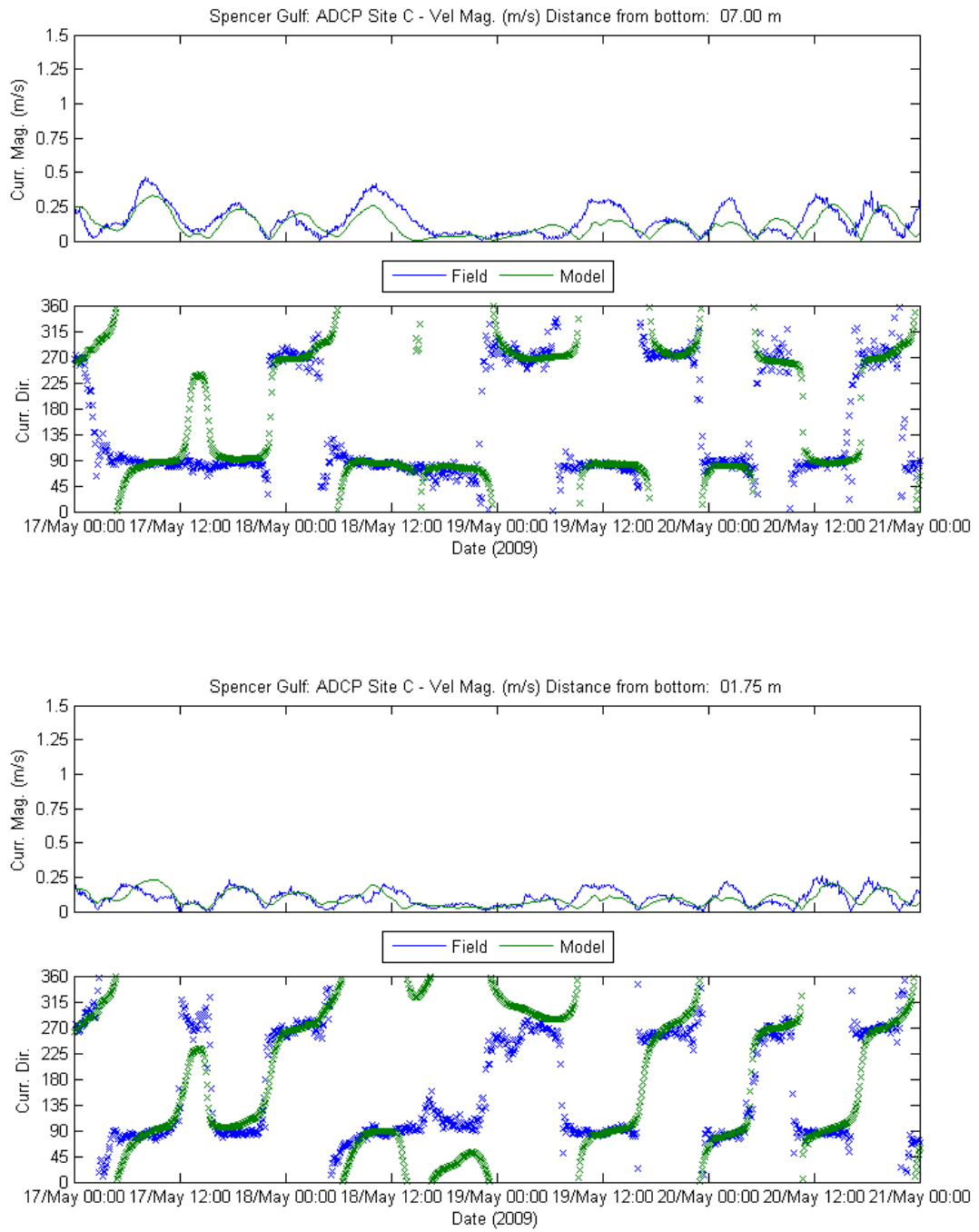


**Figure 5-40 Comparison of Observed and Modelled Velocities Magnitude and Direction at Two Different Levels at Site C (Neap Tide)**

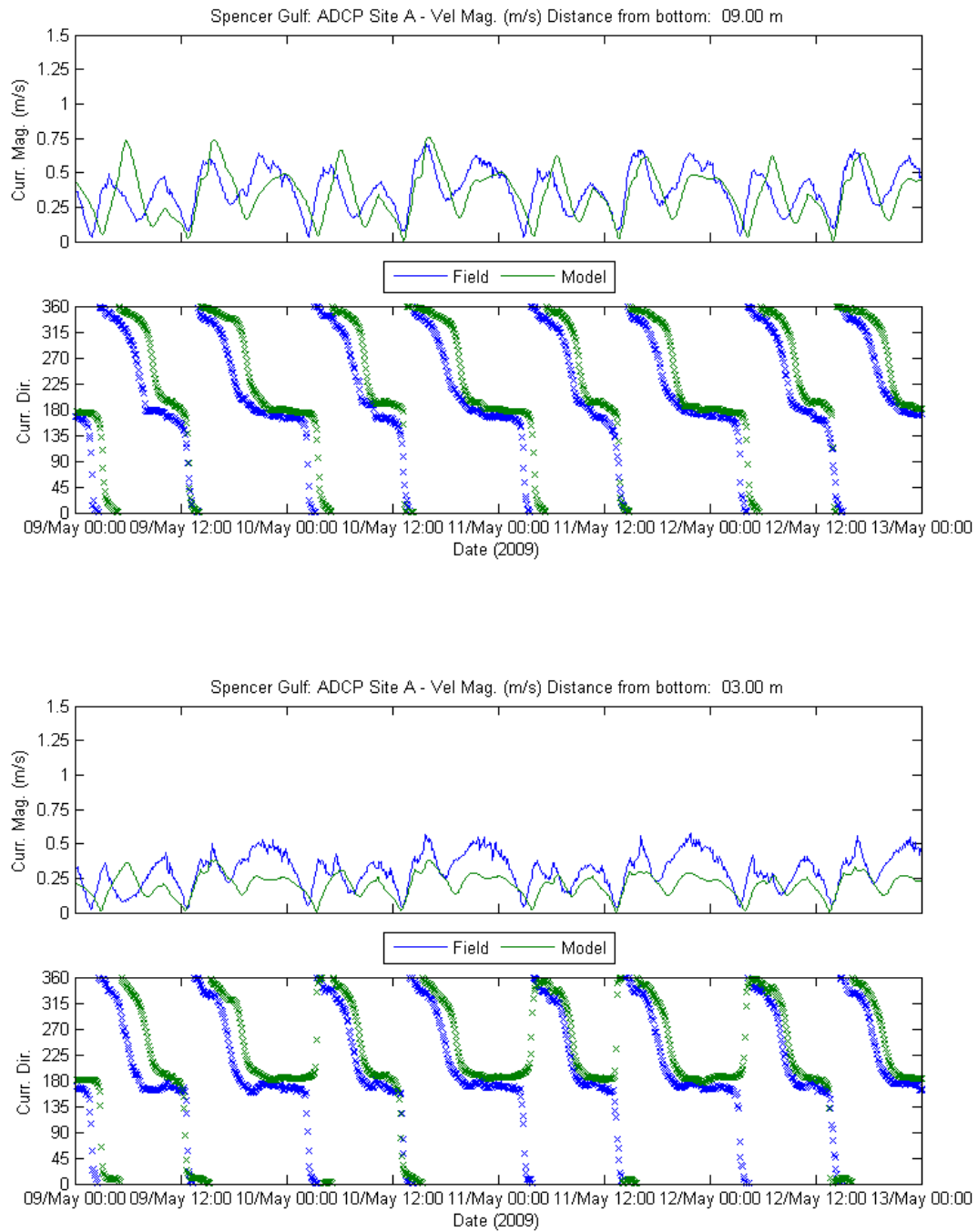


**Figure 5-41 Comparisons of Observed and Modelled Velocities Magnitude and Direction at Two Different Levels at Site A (Spring Tide)**

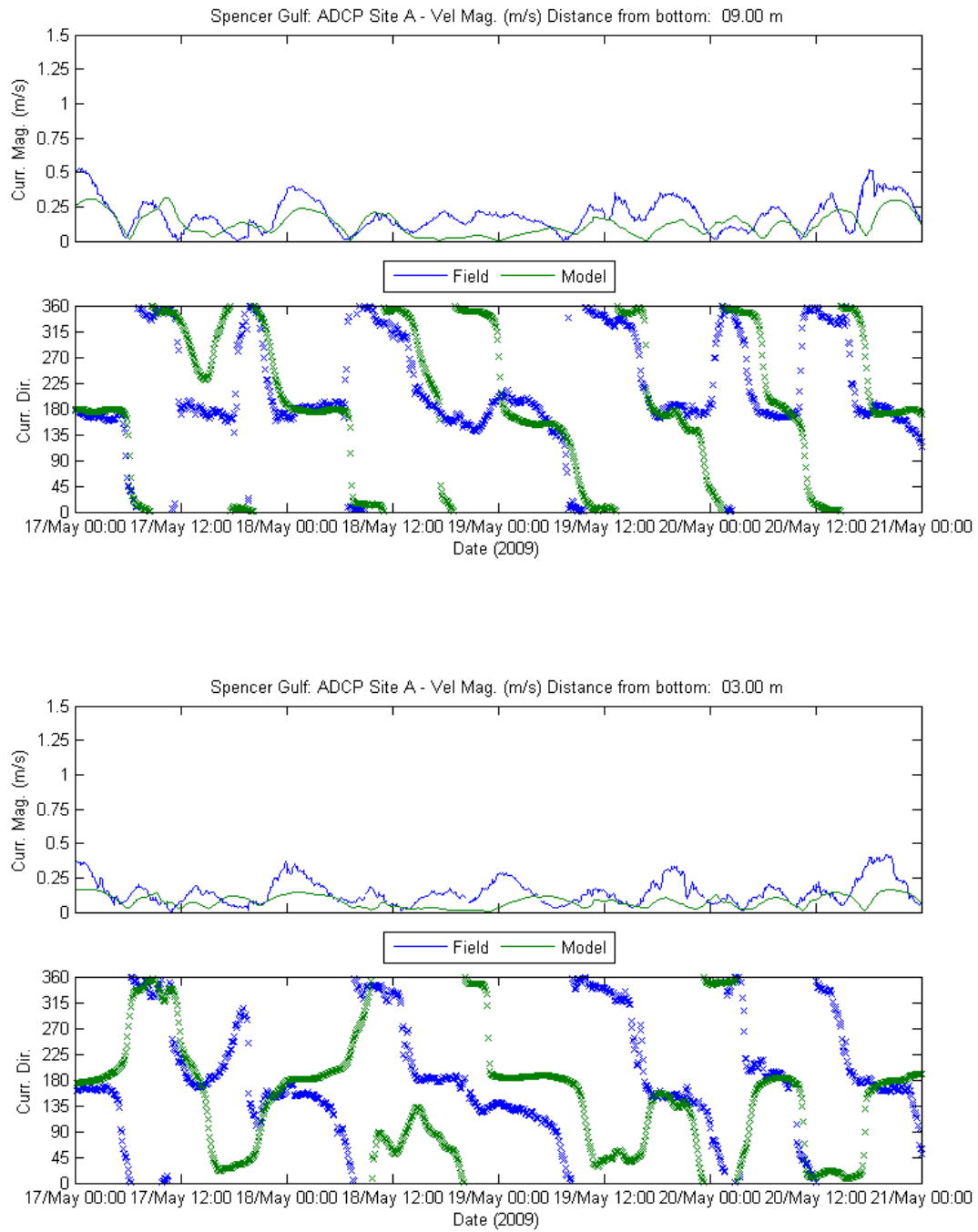


**Figure 5-42 Comparisons of Observed and Modelled Velocities Magnitude and Direction at Two Different Levels at Site A (Neap Tide)**

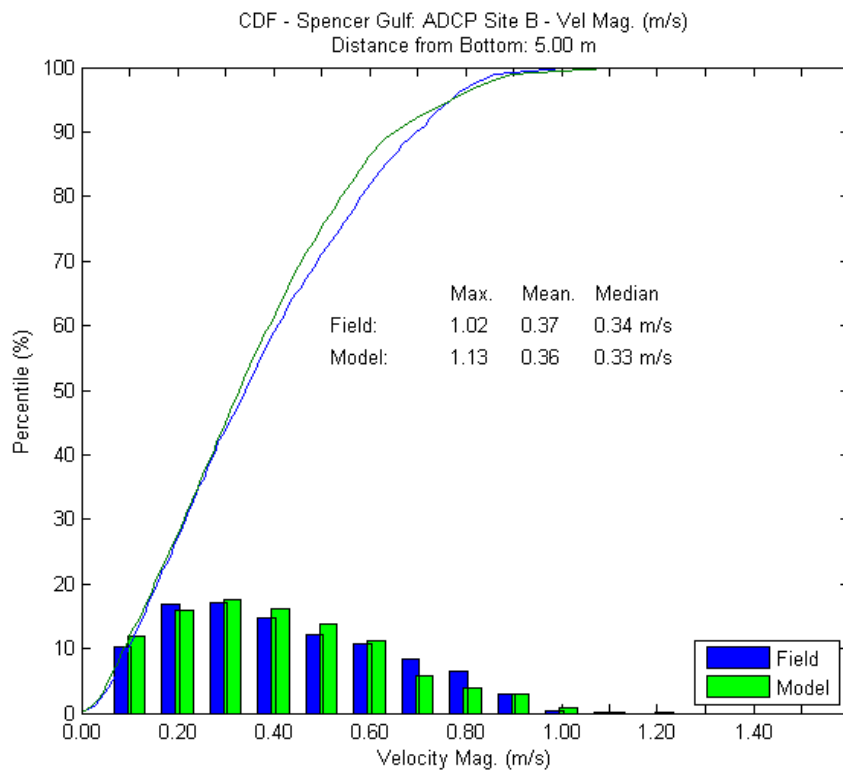
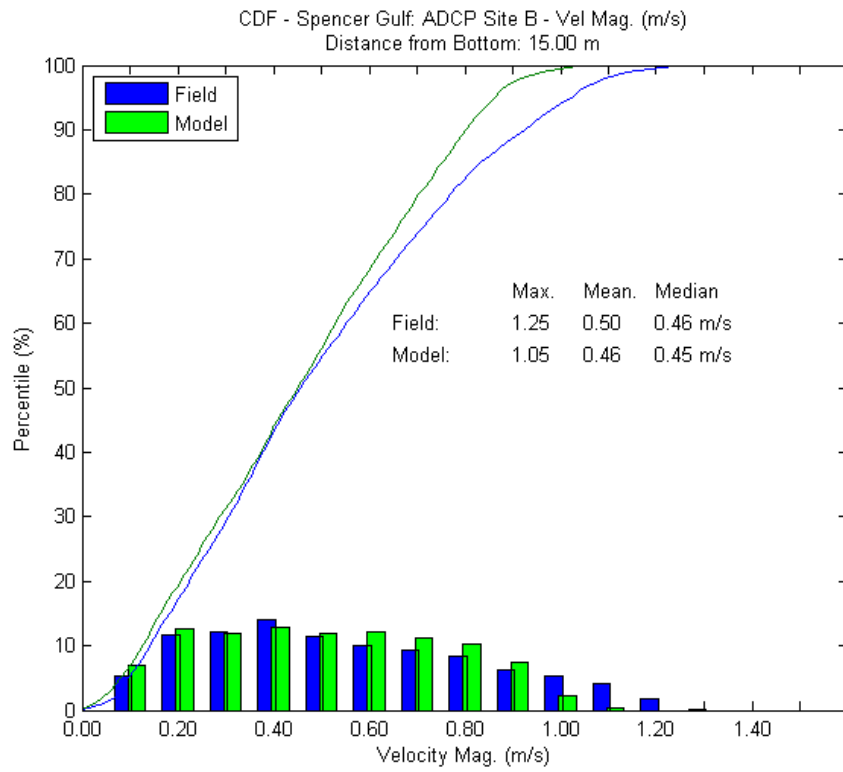


**Figure 5-43 Distribution of Measured and Modelled Currents at 5.00 and 15.00 m from Bottom at Site B for the April-June 2009 Measurement Period**

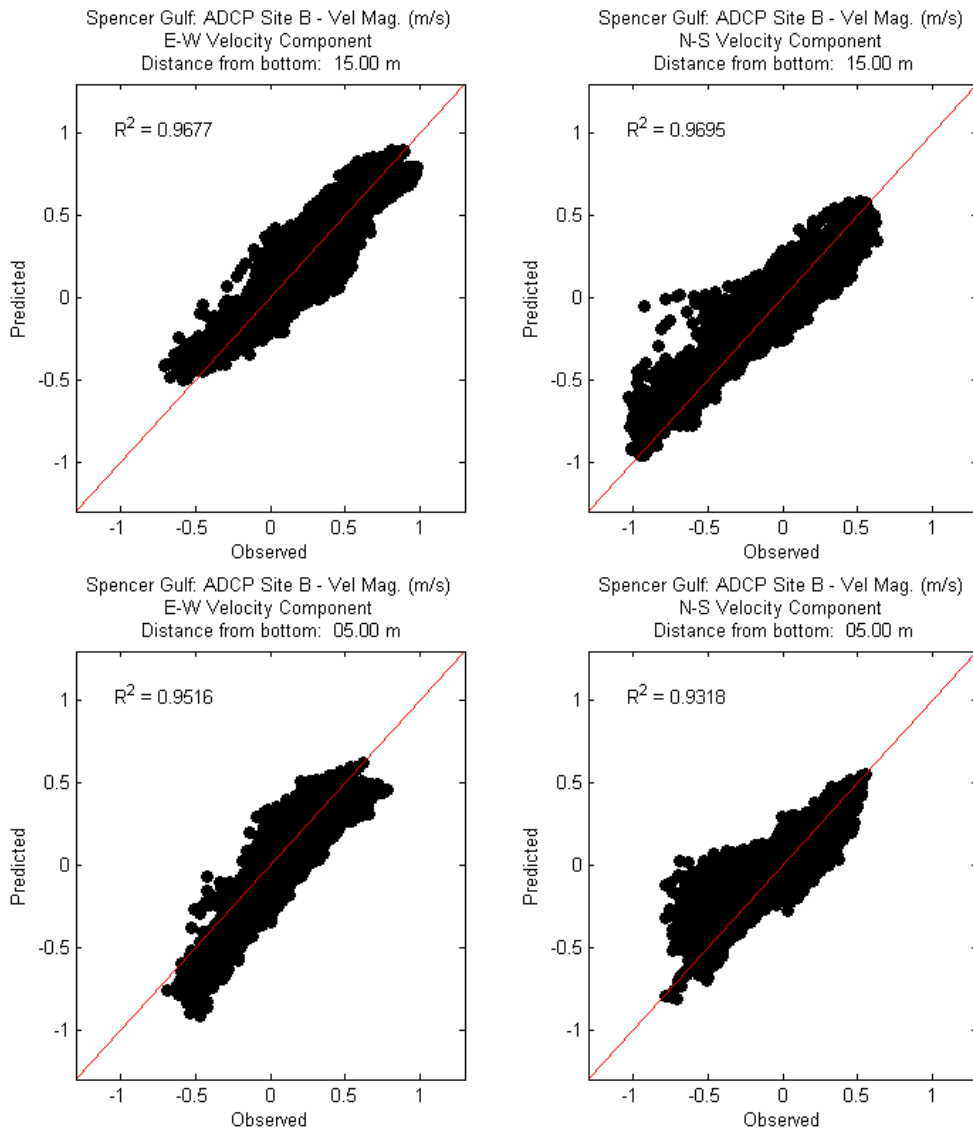


**Figure 5-44 Scatter Plots of Measured and Modelled Currents at 5.00 and 15.00 m from Bottom at Site B for the April-June 2009 Measurement Period**

**Table 5-5 Model Error at 5.00 and 15.00 m from the Bottom for the April-June 2009 Measurement Period**

Distance from Bottom	N-S current			E-W current		
	RMSE (m/s)	MAE (m/s)	R <sup>2</sup> (p<0.001)	RMSE (m/s)	MAE (m/s)	R <sup>2</sup> (p<0.001)
15.00 m	0.097	0.061	0.97	0.096	0.068	0.97
05.00 m	0.119	0.074	0.93	0.123	0.090	0.95

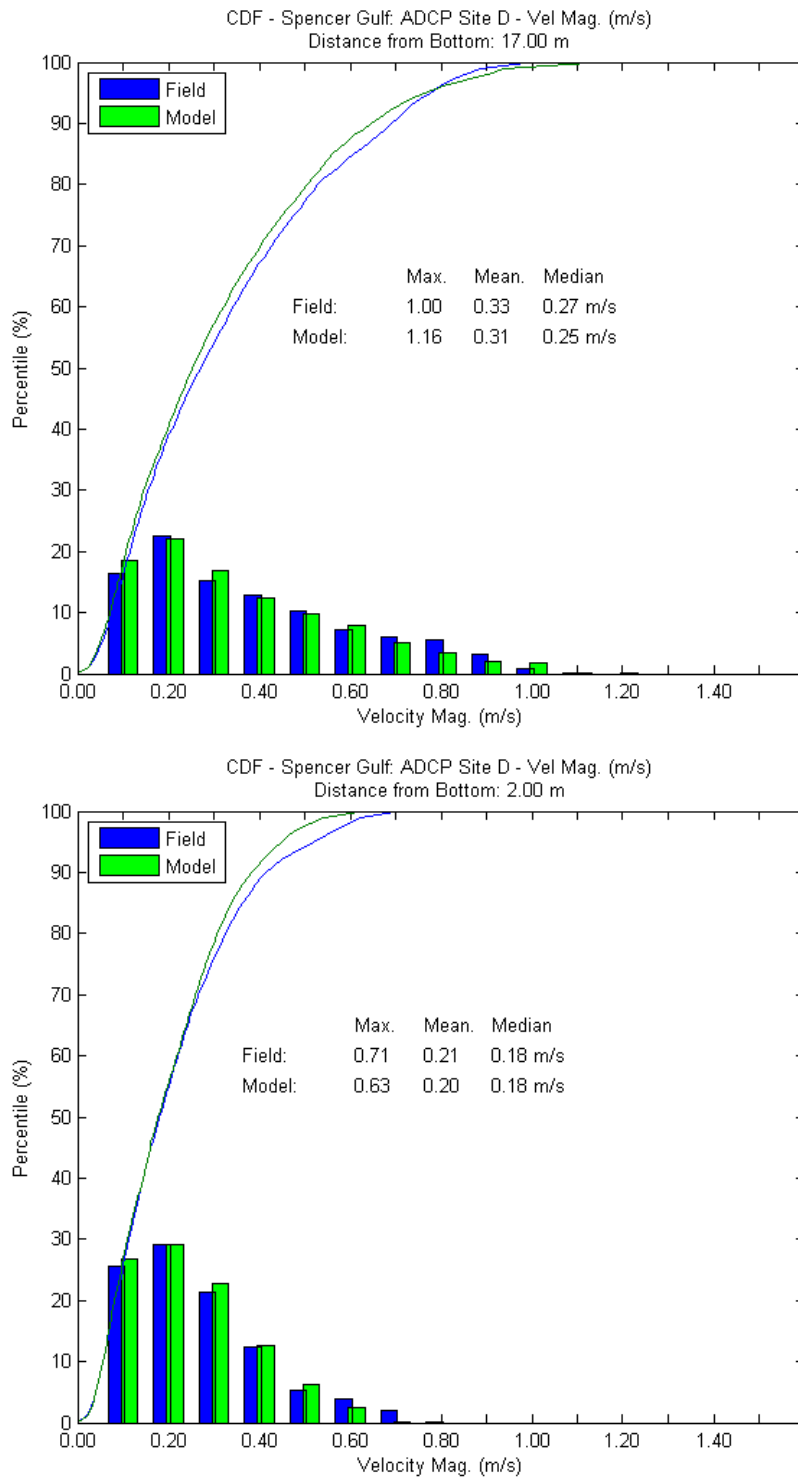


**Figure 5-45 Distribution of Measured and Modelled Currents at 2.00 and 17.00 m from Bottom at Site D for the April-June 2009 Measurement Period**

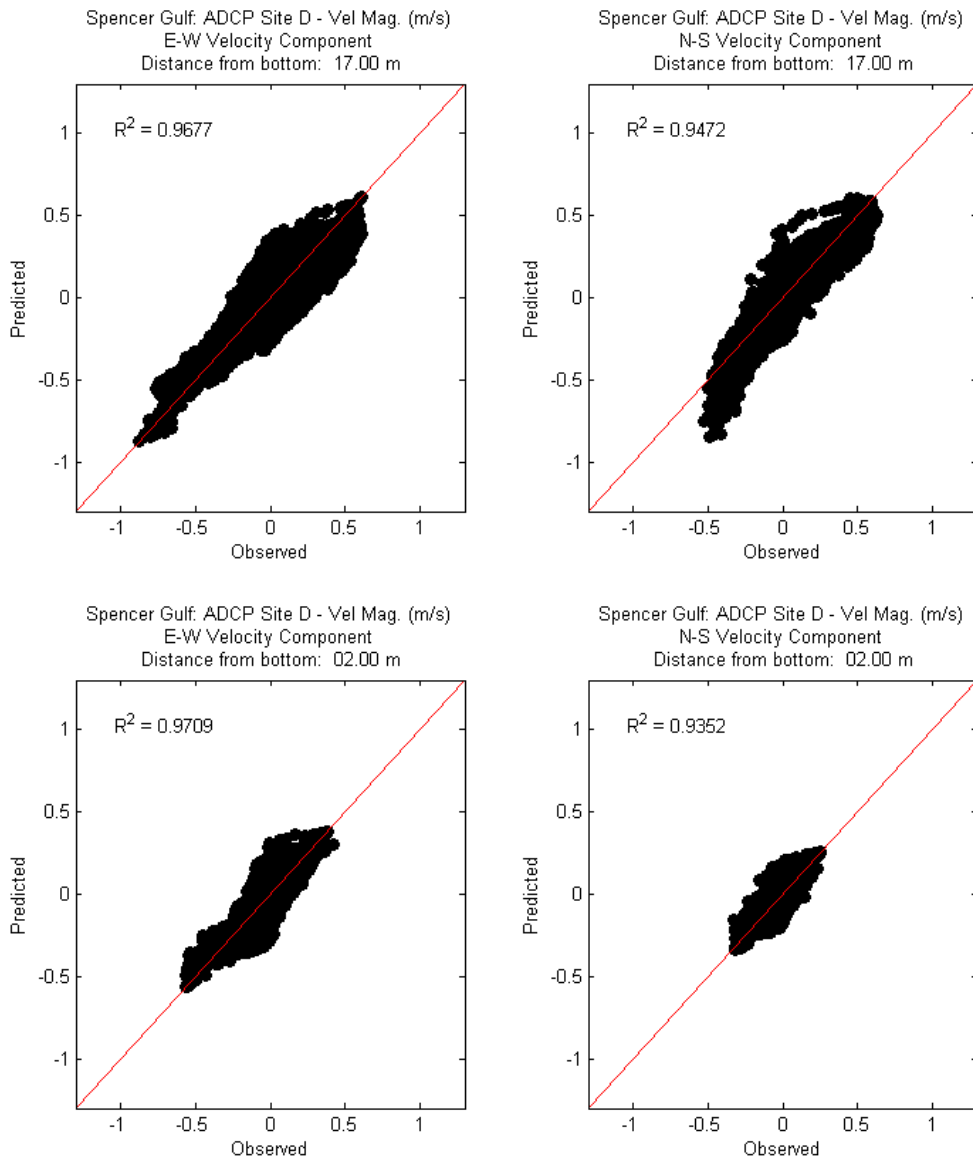


**Figure 5-46 Scatter Plots of Measured and Modelled Currents at 2.00 and 17.00 m from Bottom at Site D for the April-June 2009 Measurement Period**

**Table 5-6 Model Error at 2.00 and 17.00 m from the Bottom at Site D for the April-June 2009 Measurement Period**

Distance from Bottom	N-S current			E-W current		
	RMSE (m/s)	MAE (m/s)	R <sup>2</sup> (p<0.001)	RMSE (m/s)	MAE (m/s)	R <sup>2</sup> (p<0.001)
17.00 m	0.084	0.048	0.94	0.080	0.043	0.97
02.00 m	0.031	0.015	0.96	0.040	0.017	0.98



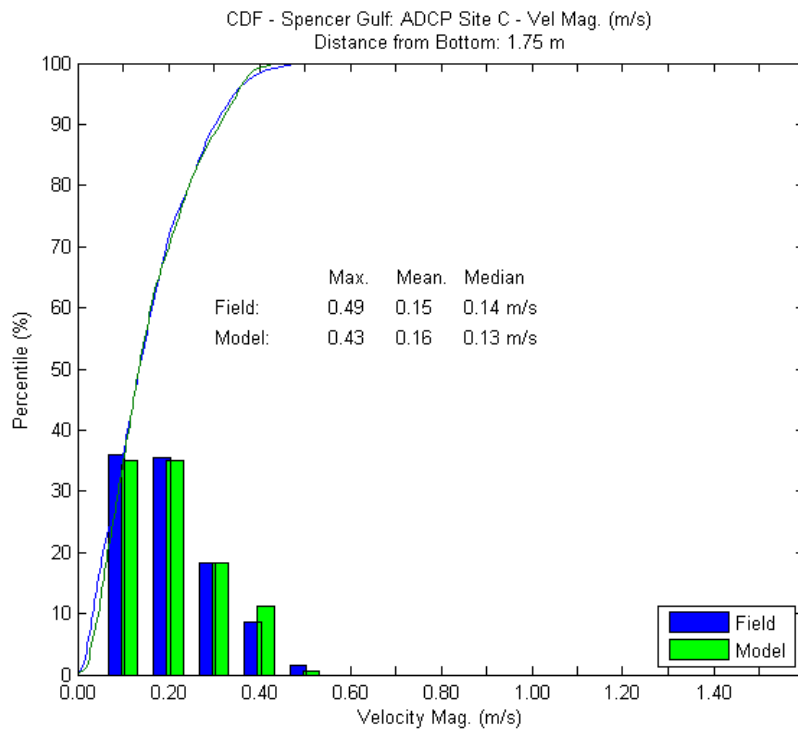
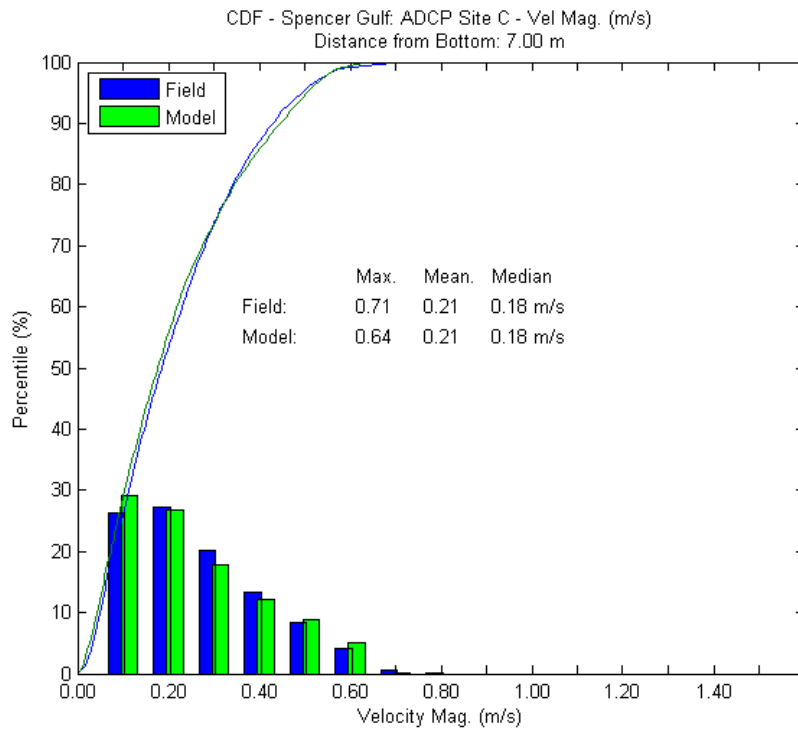


**Figure 5-47 Distribution of Measured and Modelled Currents at 1.75 and 7.00 m from Bottom at Site C for the April-June 2009 Measurement Period**

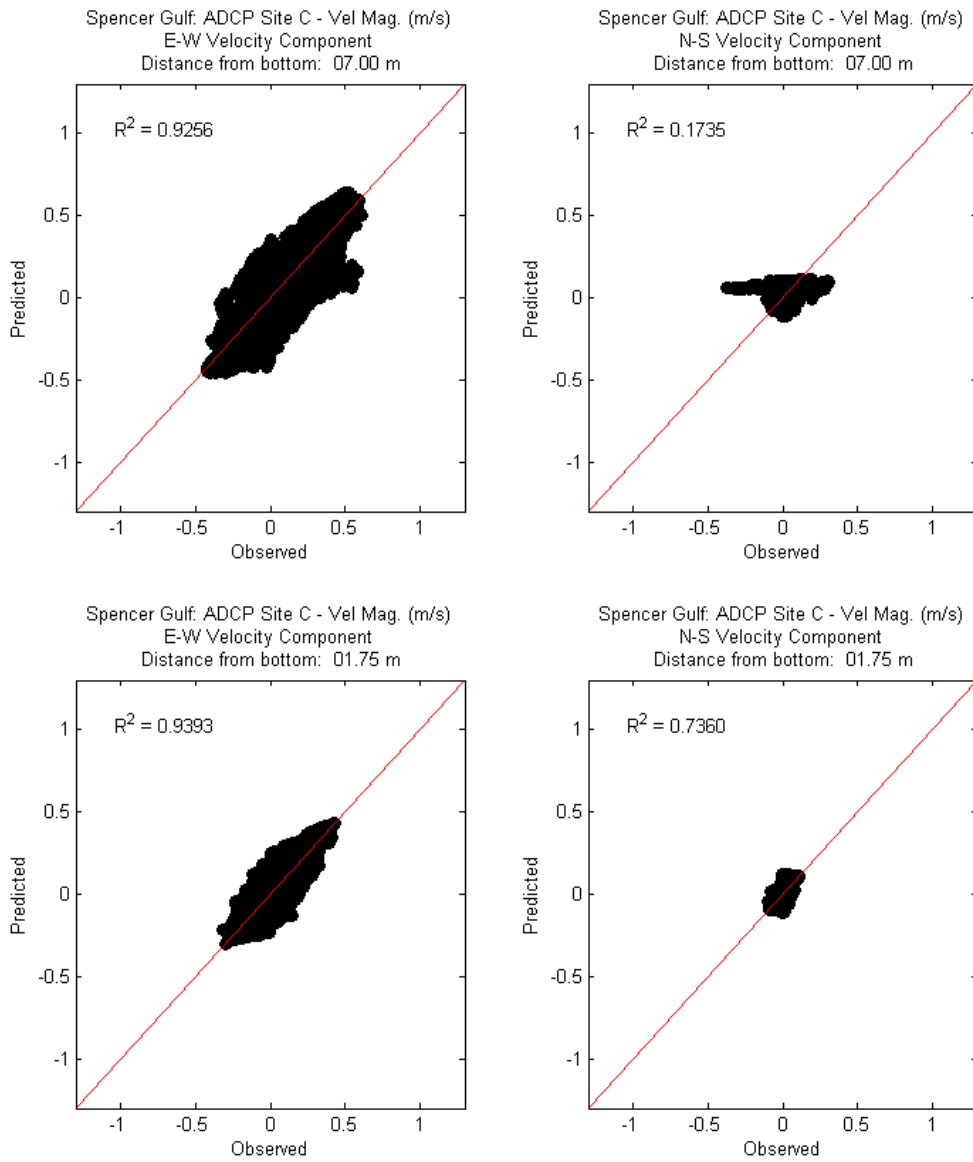


**Figure 5-48 Scatter Plots of Measured and Modelled Currents at 1.75 and 7.00 m from Bottom at Site C for the April-June 2009 Measurement Period**

**Table 5-7 Model Error at 1.75 and 7.00 m from the Bottom at Site C for the April-June 2009 Measurement Period**

Distance from Bottom	N-S current			E-W current		
	RMSE (m/s)	MAE (m/s)	R <sup>2</sup> (p<0.001)	RMSE (m/s)	MAE (m/s)	R <sup>2</sup> (p<0.001)
07.00 m	0.046	0.027	0.21	0.094	0.059	0.93
01.75 m	0.045	0.026	0.74	0.060	0.034	0.94

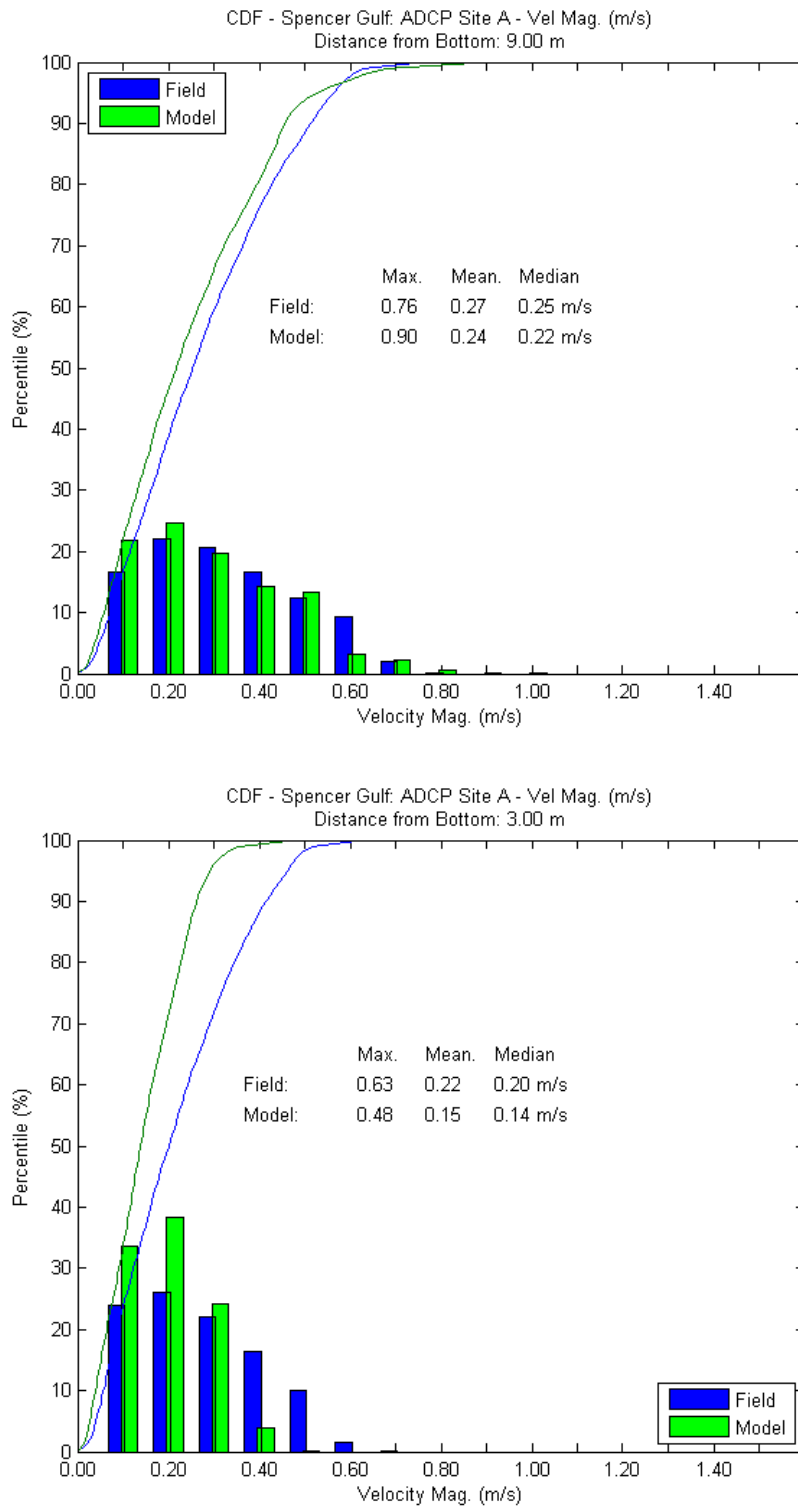


**Figure 5-49 Distribution of Measured and Modelled Currents at 3.00 and 9.00 m from Bottom at Site A for the April-June 2009 Measurement Period**

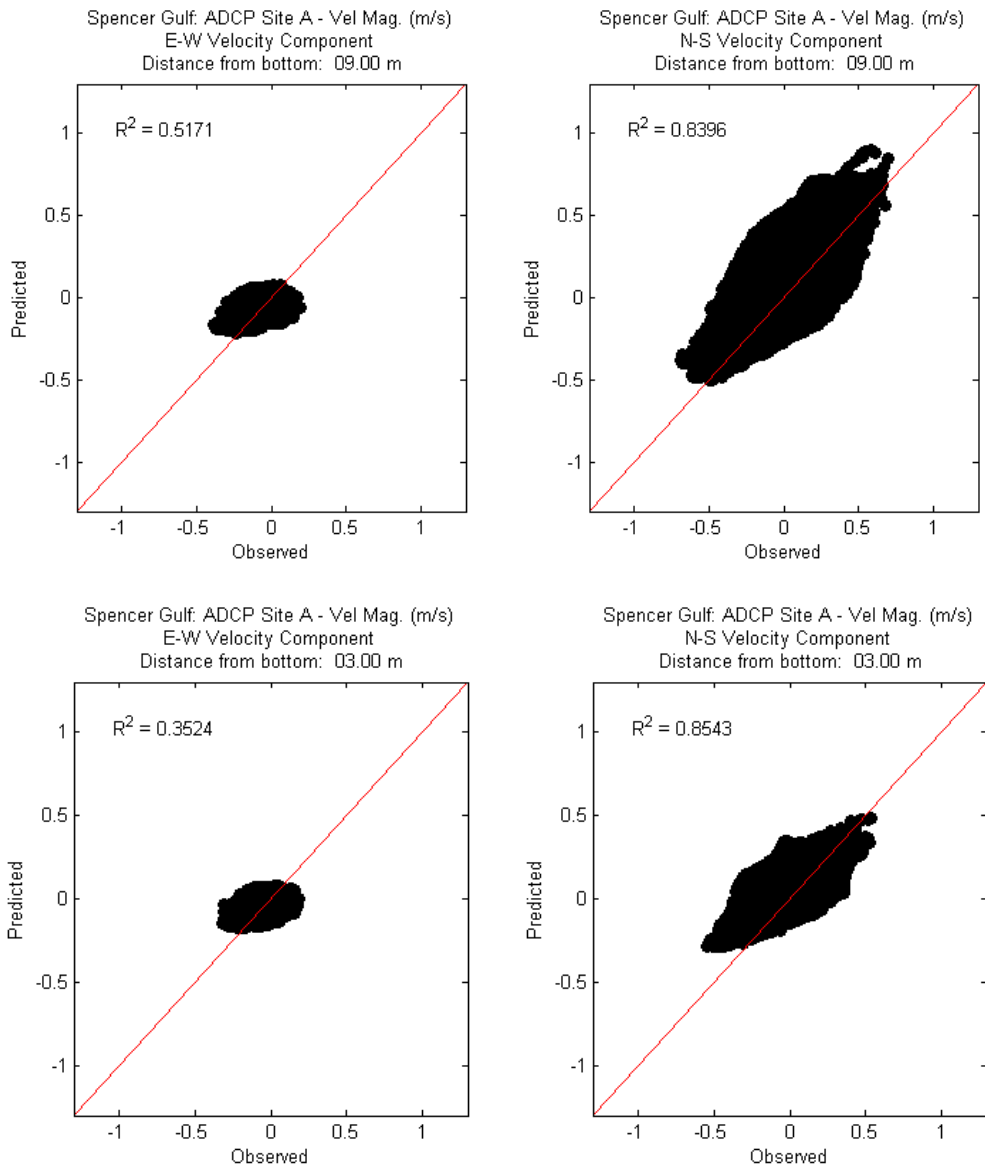


**Figure 5-50 Scatter Plots of Measured and Modelled Currents at 3.00 and 9.00 m from Bottom at Site A for the April-June 2009 Measurement Period**

**Table 5-8 Model Error at 3.00 and 9.00 m from the Bottom at Site A for the April-June 2009 Measurement Period**

Distance from Bottom	N-S current			E-W current		
	RMSE (m/s)	MAE (m/s)	$R^2$ ( $p < 0.001$ )	RMSE (m/s)	MAE (m/s)	$R^2$ ( $p < 0.001$ )
09.00 m	0.180	0.135	0.84	0.077	0.062	0.35
03.00 m	0.131	0.102	0.85	0.064	0.051	0.59

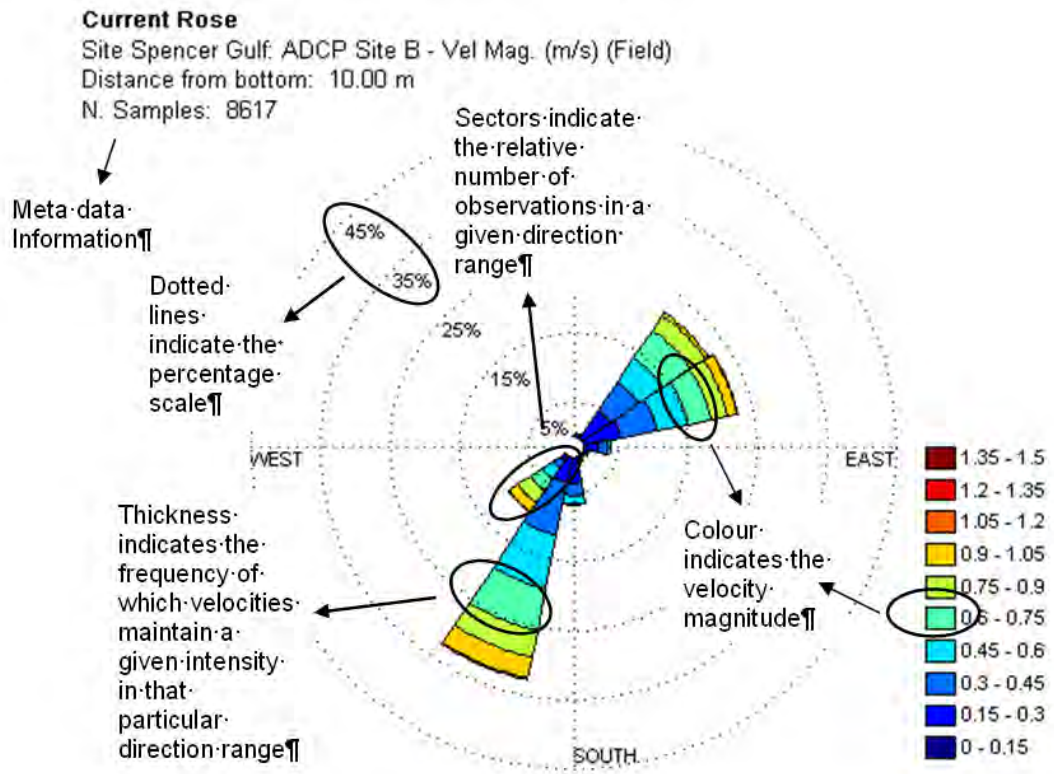


Figure 5-51 Interpretation of Rose Information

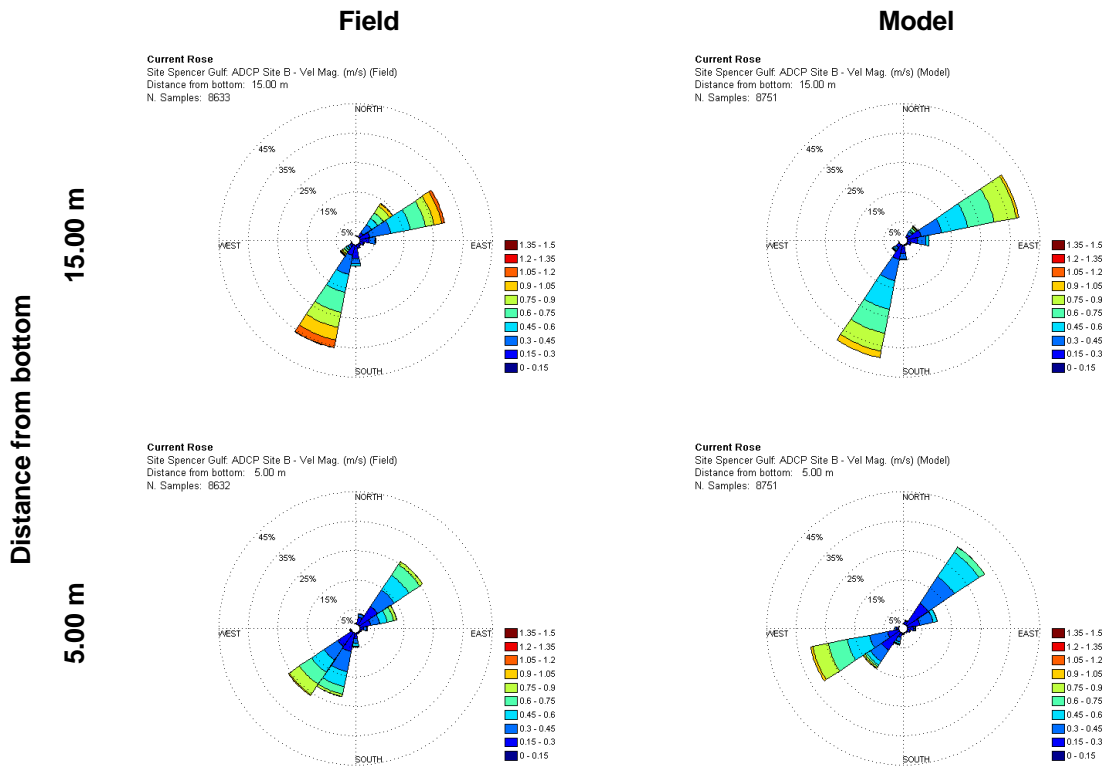


Figure 5-52 Current Roses of Modelled and Measured Velocities at Two Different Levels at Site B

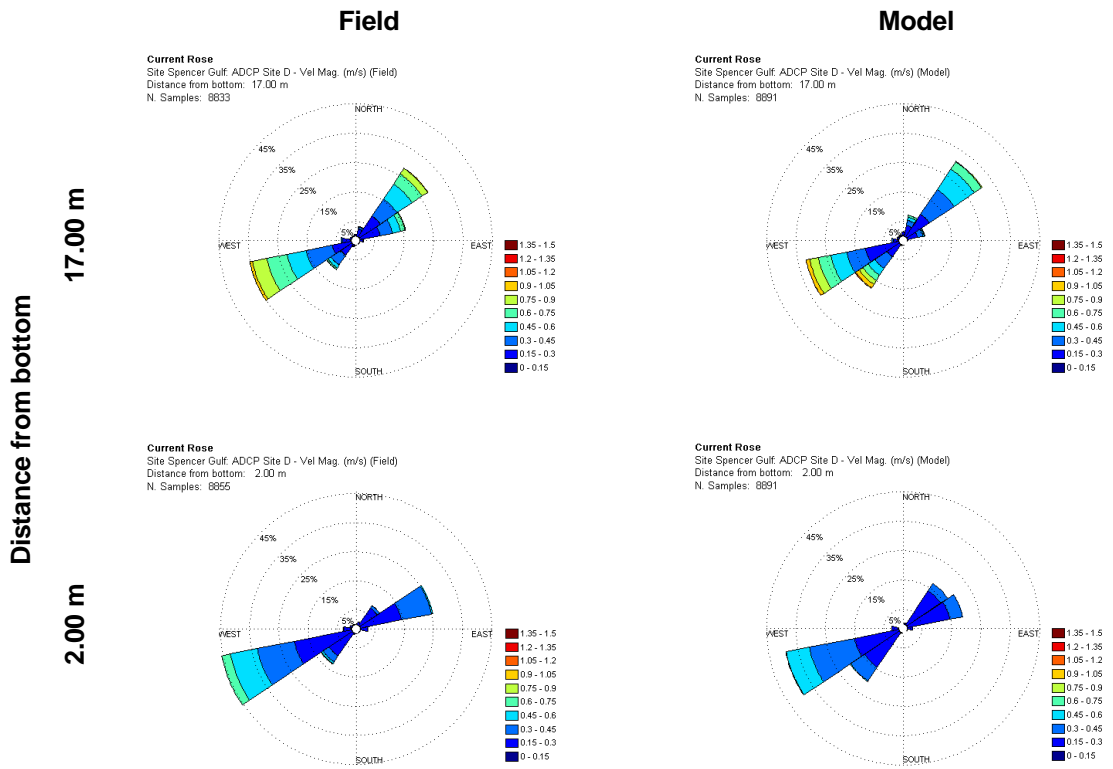


Figure 5-53 Current Roses of Modelled and Measured Velocities at Two Different Levels at Site D

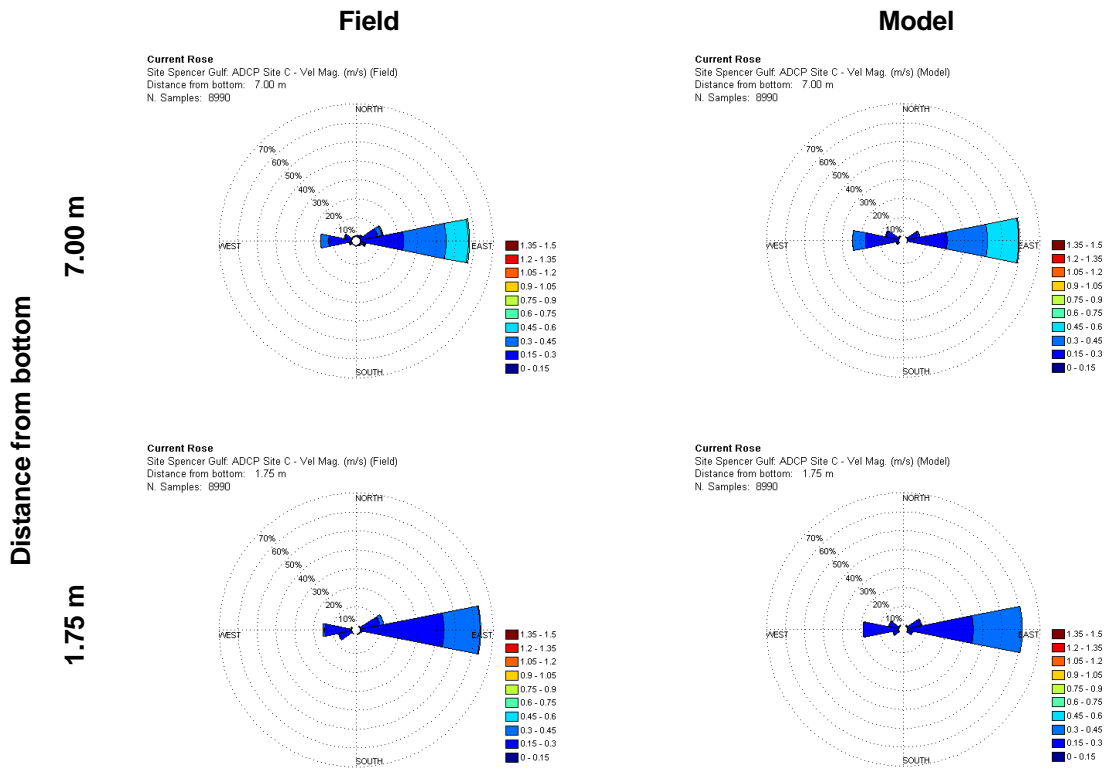


Figure 5-54 Current Roses of Modelled and Measured Velocities at Two Different Levels at Site C



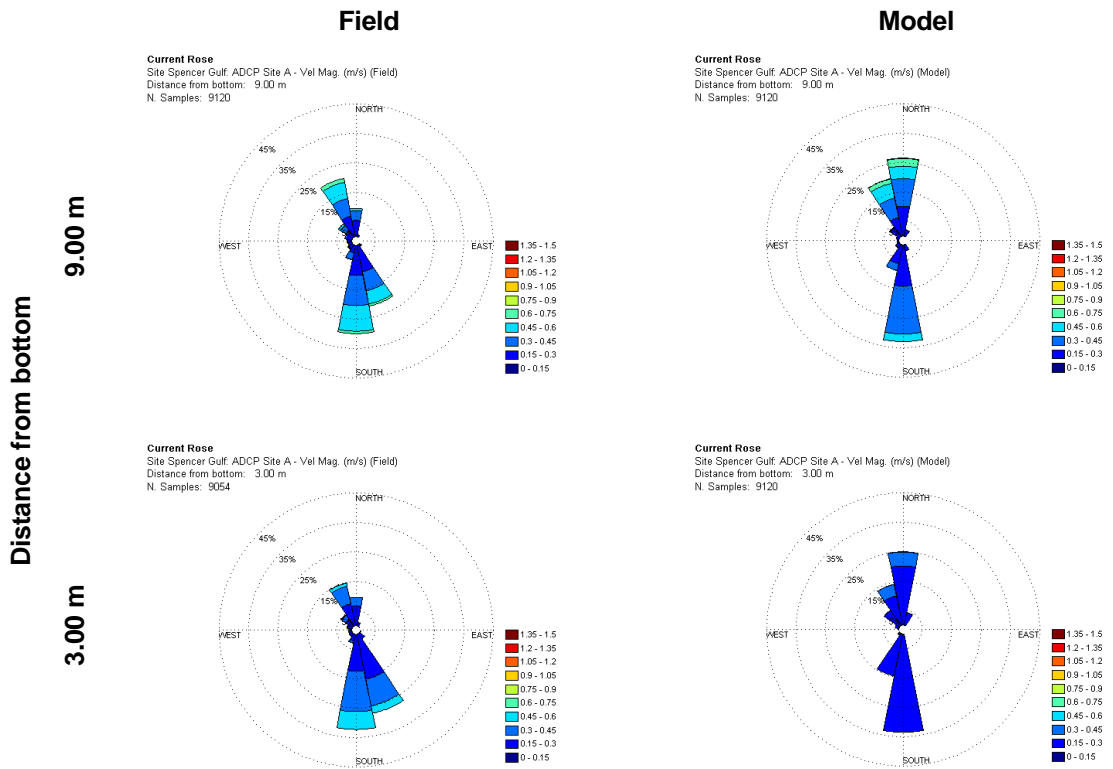


Figure 5-55 Current Roses of Modelled and Measured Velocities at Two Different Levels at Site A

### 5.2.5 Tidal Eddies

A prominent feature of the circulation in Upper Spencer Gulf is the presence of tidal eddies in the lee sides of Point Lowly in both flood and ebb tides (Lewis and Noye 1998, Draft EIS - Appendix O11.2). Similarly to what has been previously shown in the Draft EIS (Appendix O11.2), model results reproduced the appearance of eddies on both lee sides of Point Lowly during neaps and spring cycles. In this case, the size and position (and vorticity) of these eddies are clearly dependent on the magnitude and direction of the currents through “the Rip”. Figure 5-56 and Figure 5-57 illustrate these eddies in spring tides.

### 5.2.6 Boat-Mounted ADCP Velocity Transects

A comparison between modelled and measured surface currents for Section 002 is illustrated in Figure 5-58. Field measurements were averaged over every 60 ensembles (vertical profiles) in order to provide a similar resolution to the model (~ 50 m). It should be noted that:

- The model snapshots were taken every 30 minutes and the closest-in-time snapshot to the time mid-way through the collection time was chosen for the comparisons (shown by the red-dot in the tidal elevation plot);
- Model results were extracted from the closest grid locations and output along the transect path.

The model results captured the field measurements. In particular, the model captured:

- The veering motion along the western shore around Point Lowly;
- The velocity overshooting through “The Rip”, mid channel; and
- Progressive velocity reduction at the shallower depths next to Ward Spit.

Measurements at Section 005 are contrasted to a vertical curtain showing model results in Figure 5-59 and Figure 5-60. It should be noted that:

- The measurements did not extend to the bottom in the deeper parts of the transect, as measurements were performed with a 1200 kHz ADCP;
- Model bathymetry is based on navigation charts and details may not be representative of current conditions towards Ward Spit (i.e. from approximately 4000 m);
- Bad ensembles were obtained as a result of the swell (~1.0m) and wind-sea (~0.5m) straight against the ebbing tide, such that averages involving a large number of bad ensembles were removed by the ADCP post-processing software; and
- Model and field transect paths do not coincide exactly as shown in the top panel of the plots. This is because the model results were located on the model’s grid cells’ centre.

Model results reproduced both magnitude and direction measurements along transect paths and over the vertical direction. The measurements across channel in “The Rip” were reproduced by the model, showing a transition from S to SW flows across the channel in the upper water column and a nearly constant SW flow direction in the bottom part of the water column. This is evidence that the model reproduces vertical shear in the water column (i.e. water flowing in different direction at different

levels in the water column). Figures similar to Figure 5-58 to Figure 5-60 for all measured sections are presented in Appendix F.

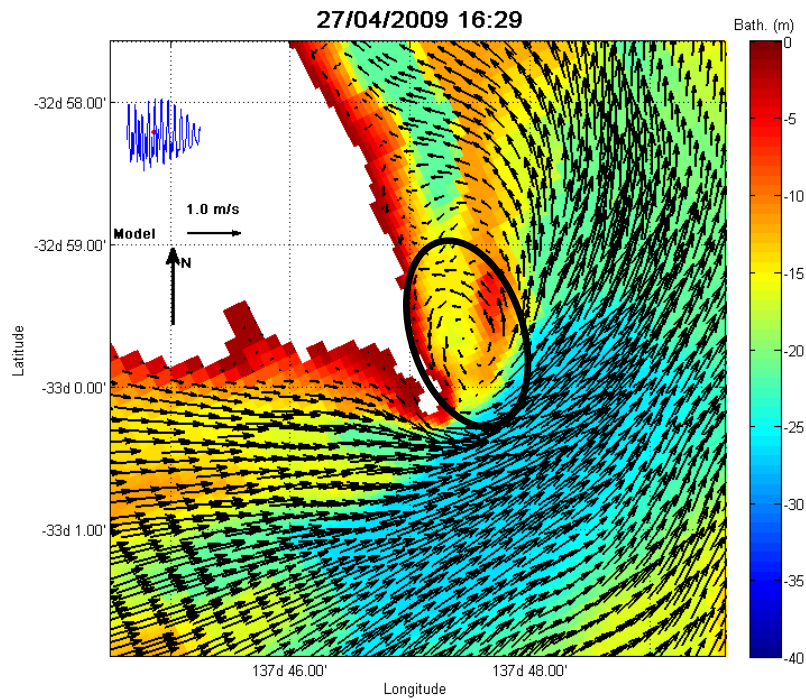


**Figure 5-56 Modelled Tidal Eddies during Flood of a Spring Tides. Location of the Eddies Indicated Inside the Ellipsis. Surface Elevation Indicated by the Blue Line on the Top Left Hand Side of the Figures. Red Dot Shows the Time in Which the Snapshot was Taken.**

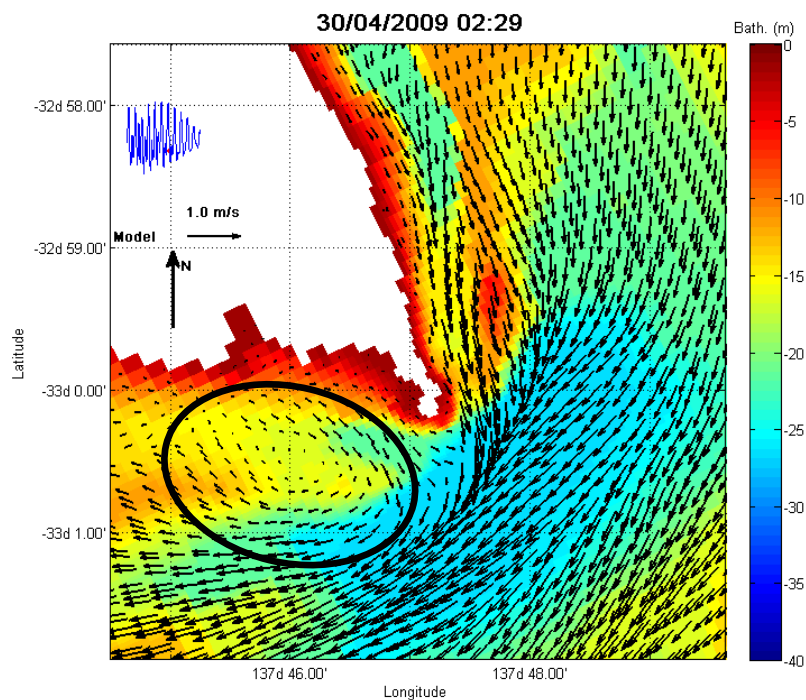


**Figure 5-57 Modelled Tidal Eddies during Ebb of a Spring Tide. Caption Details as Figure 5-56.**

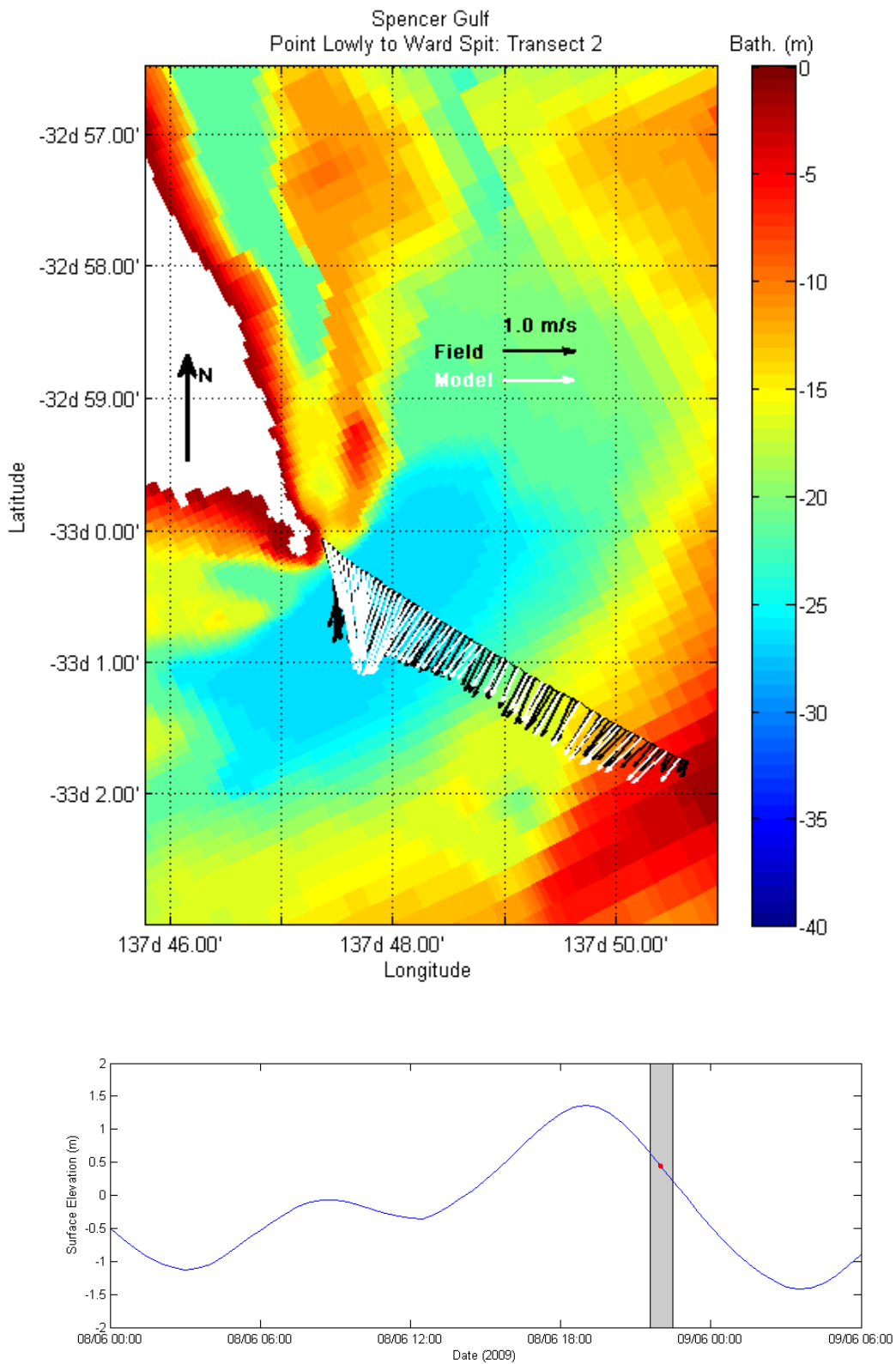


**Figure 5-58 Comparison of Observed and Modelled Surface Velocities along Section 002 Transect**

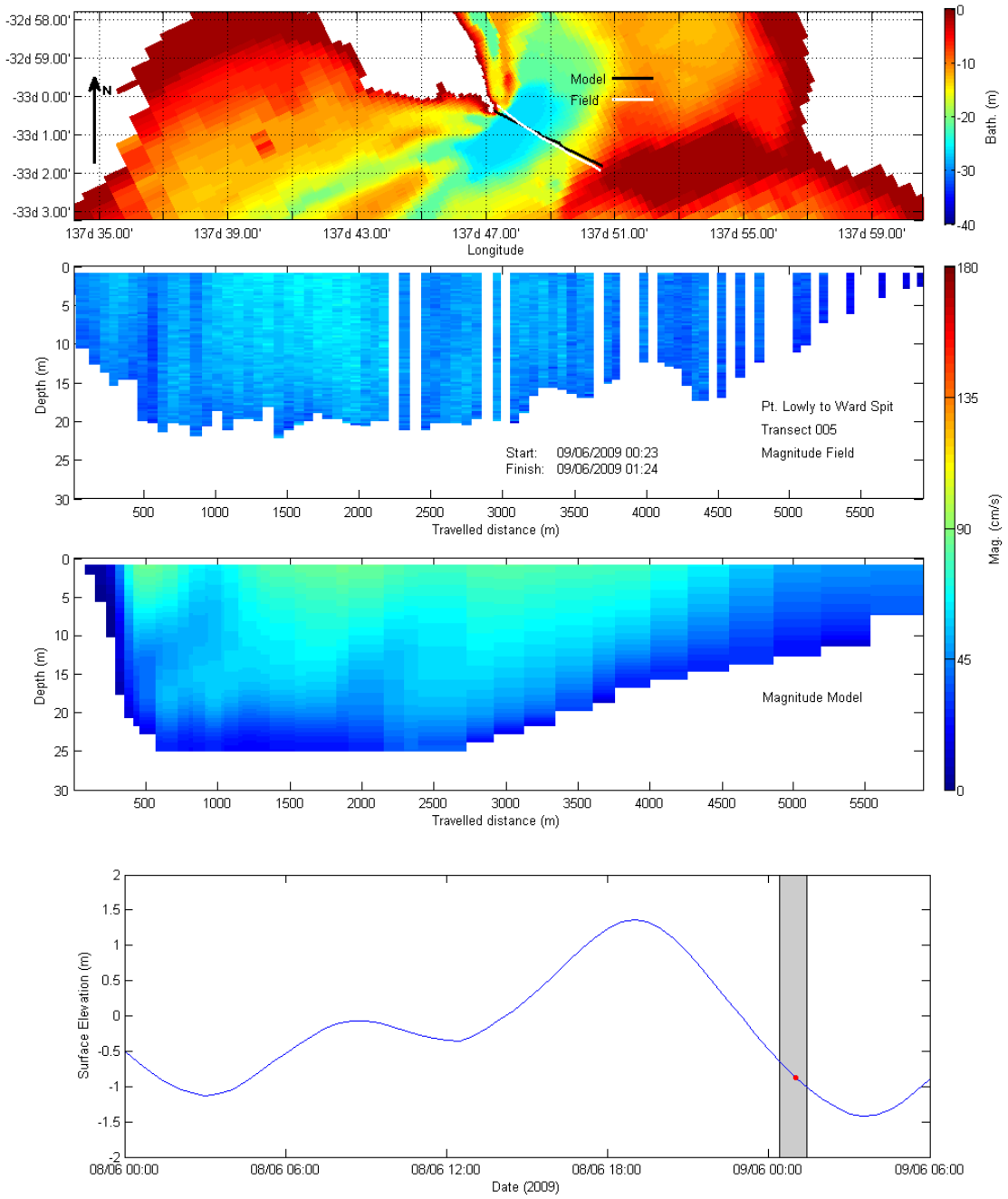


**Figure 5-59 Comparison of Observed and Modelled Velocity Magnitude across Section 005 Transect**

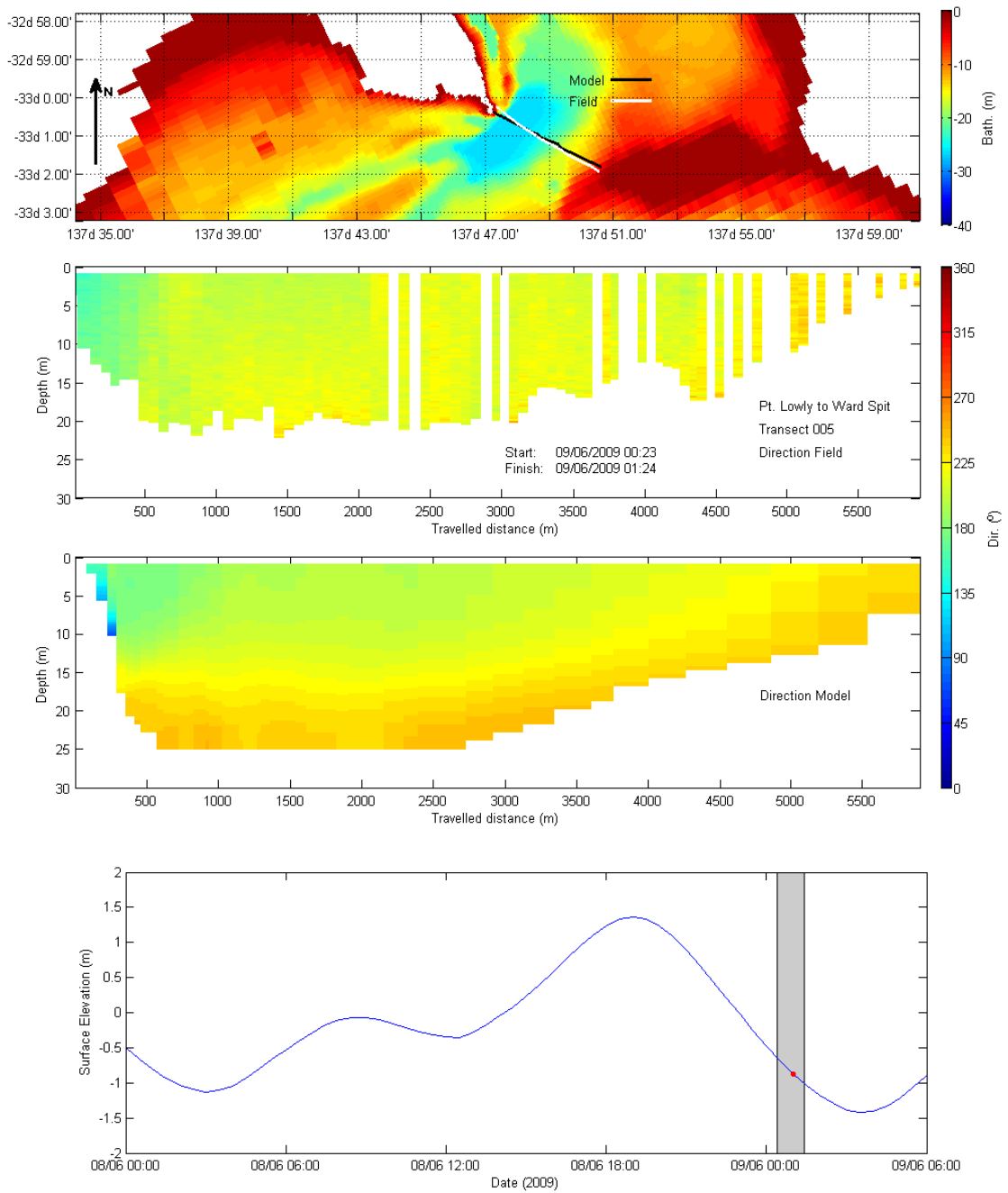


**Figure 5-60 Comparison of Observed and Modelled Velocity Direction across Section 005 Transect**

## 5.3 Three-Month Validation Period

### 5.3.1 Initial Conditions

Moored ADCP measurements of currents were performed at station B (Figure 3-1) in the period between 19 December 2007 and 3 March 2008. As such, simulations were started on 1 November 2007 and were initialised with the same salinity and temperature fields used for the seasonal simulations (Section 5.1.1). A cold start was also adopted for the momentum initialisation.

### 5.3.2 Velocity Comparisons

The velocity measurements for the whole 2007-2008 data set presented in Figure 5-61 to Figure 5-63 encompassed approximately 5 neap-spring cycles that were quite discernible and replicated by the model. The distribution of current magnitudes (Figure 5-64) provided a similar result to the 40-days validation period between April and June 2009, with similar observed and modelled distributions. These similarities are also reflected in the scatter plots (Figure 5-65) and error measures (Table 5-9), indicating that the model performance is consistent for both data sets, despite the less energetic environment reflected in the 40-day validation period (i.e. dodge tides).

Currents during neap tidal cycles peaked frequently above 0.50 m/s over the entire water column (Figure 5-62). The model was able to capture both magnitude peaks and stagnation periods. The semi-diurnal tidal reversals were also reproduced with agreement in both magnitudes and directions. It is noted that current directions during stagnation periods were not represented at times, which however do not hamper model skill given the large noise to signal ratio under such circumstances. The longest periods of relative stagnation (assumed to be currents continuously measured below 0.25 m/s) were of approximately 6 hours and occurred once on average at every measured neap cycle (see Appendix G for complete data set). The 0.25 m/s threshold that defines the period of relative stagnation, which is approximately the 30<sup>th</sup> percentile of velocities measured 5.00 m from the bottom at Site B (Figure 5-43), is conservative as this magnitude is comparable to the 85<sup>th</sup> percentile of near bed velocity measurements at Port Stanvac (Figure 3-5). If a lower threshold were chosen, the longest periods of relative stagnation would be further reduced.

During spring tidal cycles, currents frequently peaked above 1.0 m/s over the entire water column and no stagnation periods (as defined above) occurred (Figure 5-63). Modelled velocities magnitude and directions were reproduced, particularly for the levels between 5.0 and 15.0 m from the bottom. For the measurements at 20.0 m from the bottom the velocities magnitudes at all times and direction during flood tides were reproduced, whilst velocity direction during ebbing tides were more frequently oriented south than the south-south-westerly measured currents.



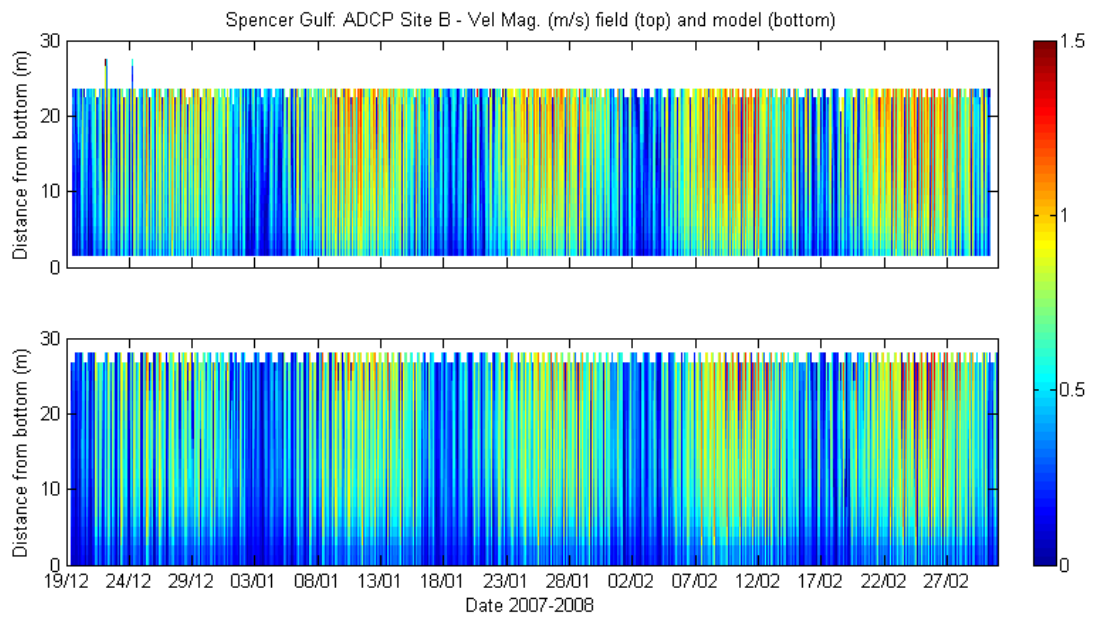


**Figure 5-61 2007-2008 ADCP Measurements of Currents: Field Data and Model Results**

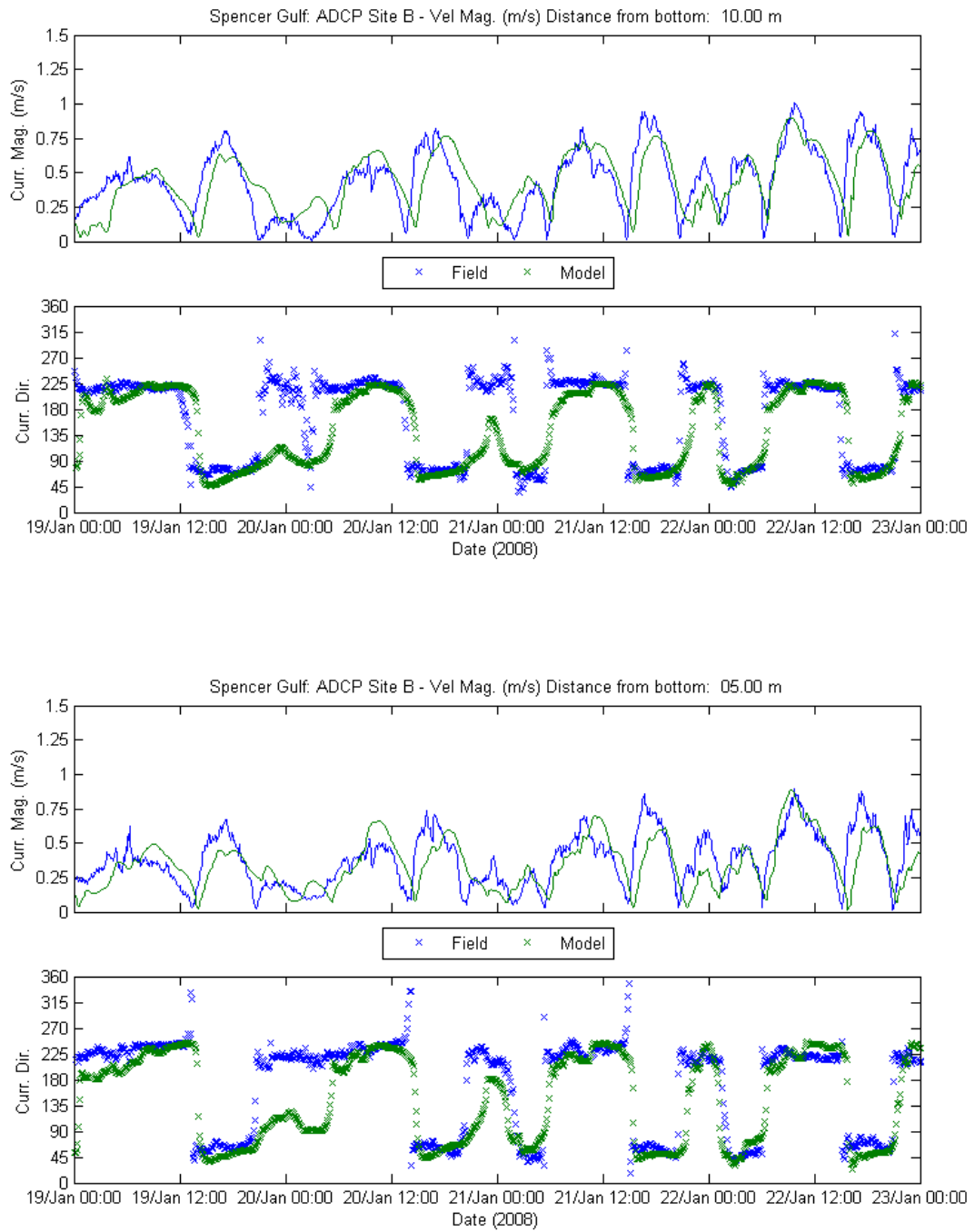
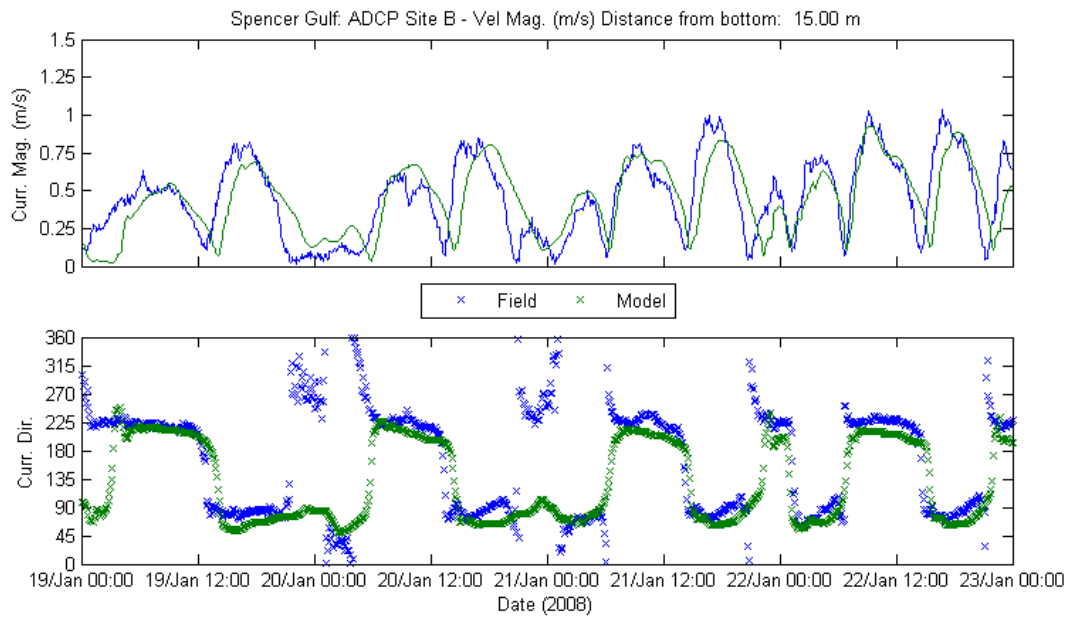
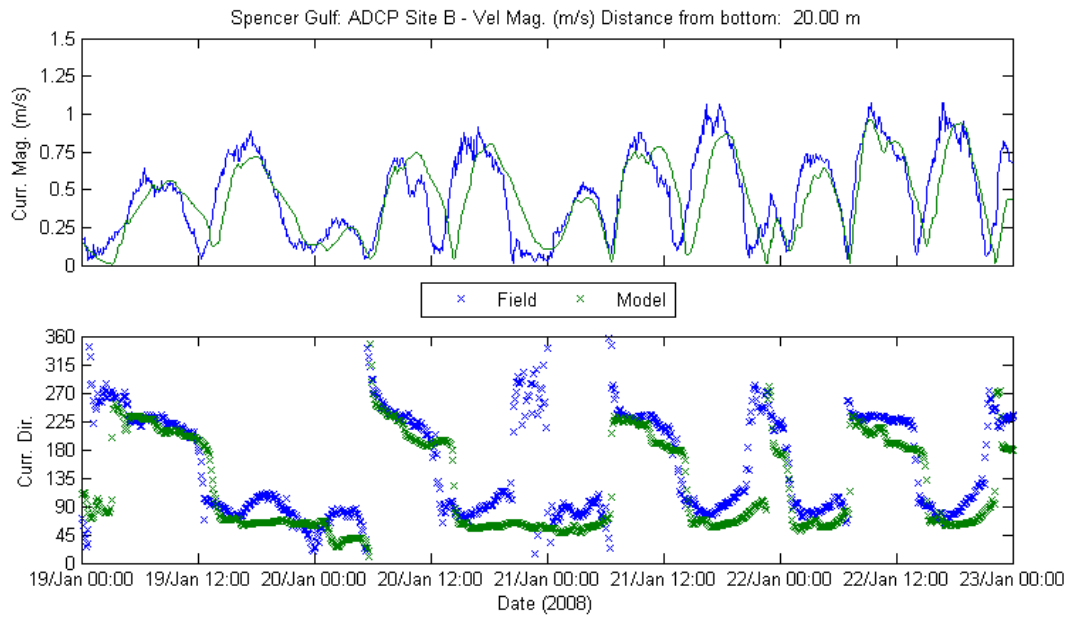


**Figure 5-62 Comparisons Between Model and Field Results at Different Levels in the Water Column: Neap Tides (January 2008)**



Continued

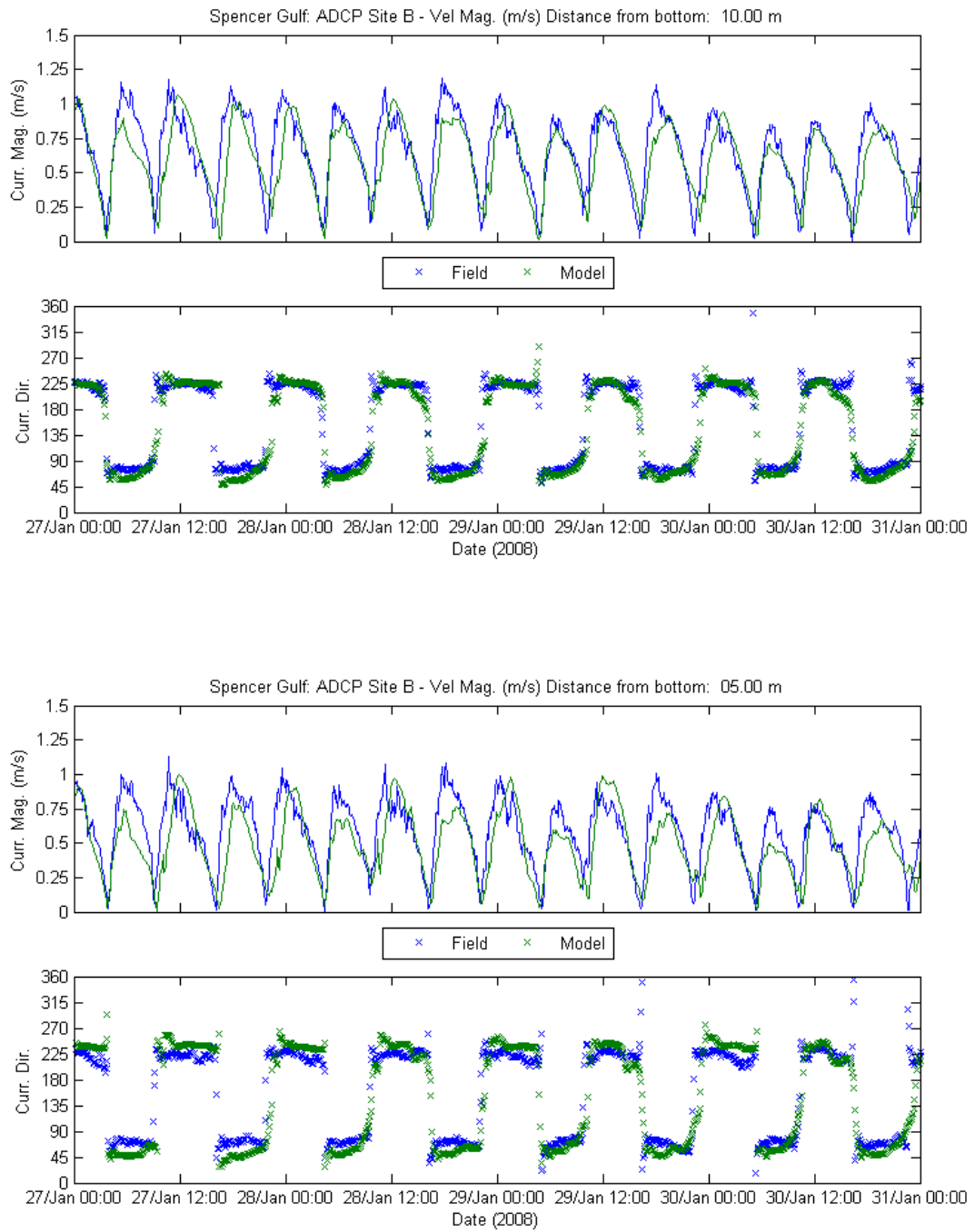
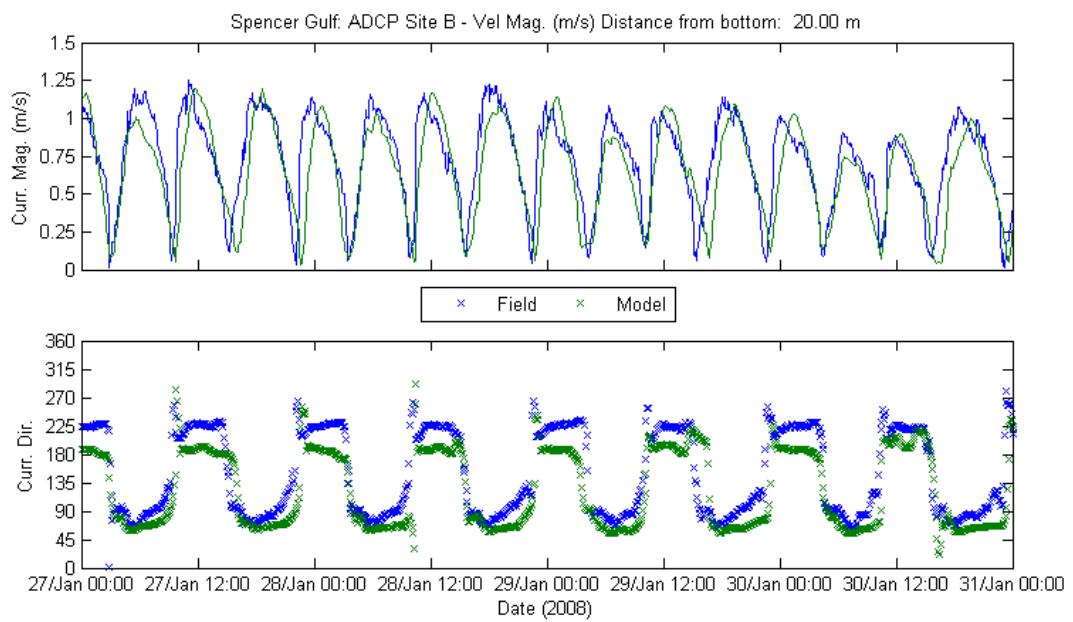
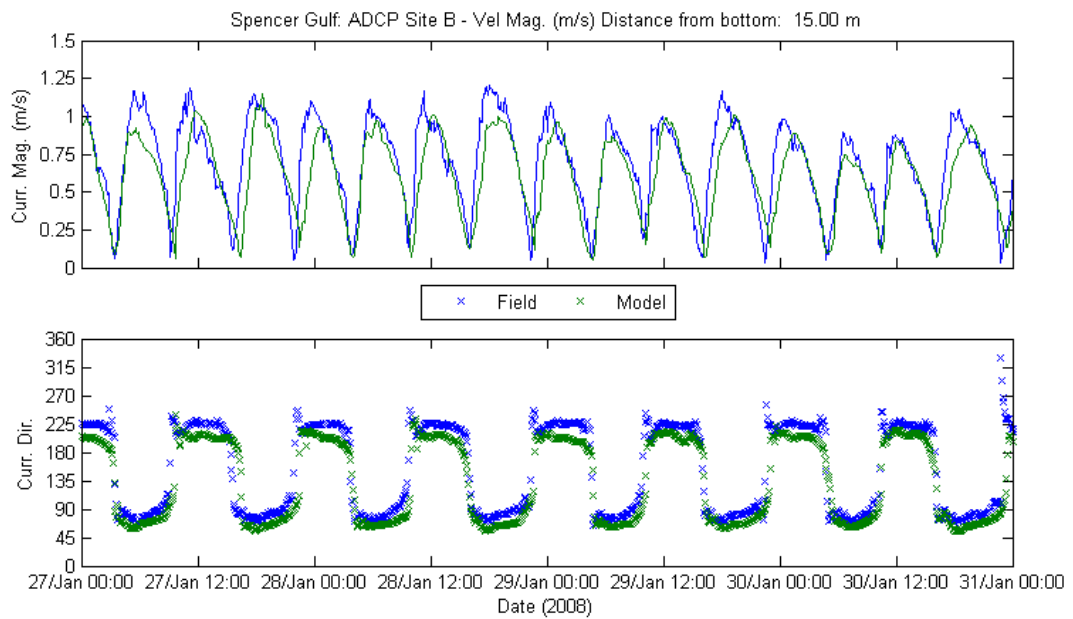


**Figure 5-63 Comparisons between Model and Field Results at Different Levels in the Water Column: Spring Tides (January 2008)**



Continued

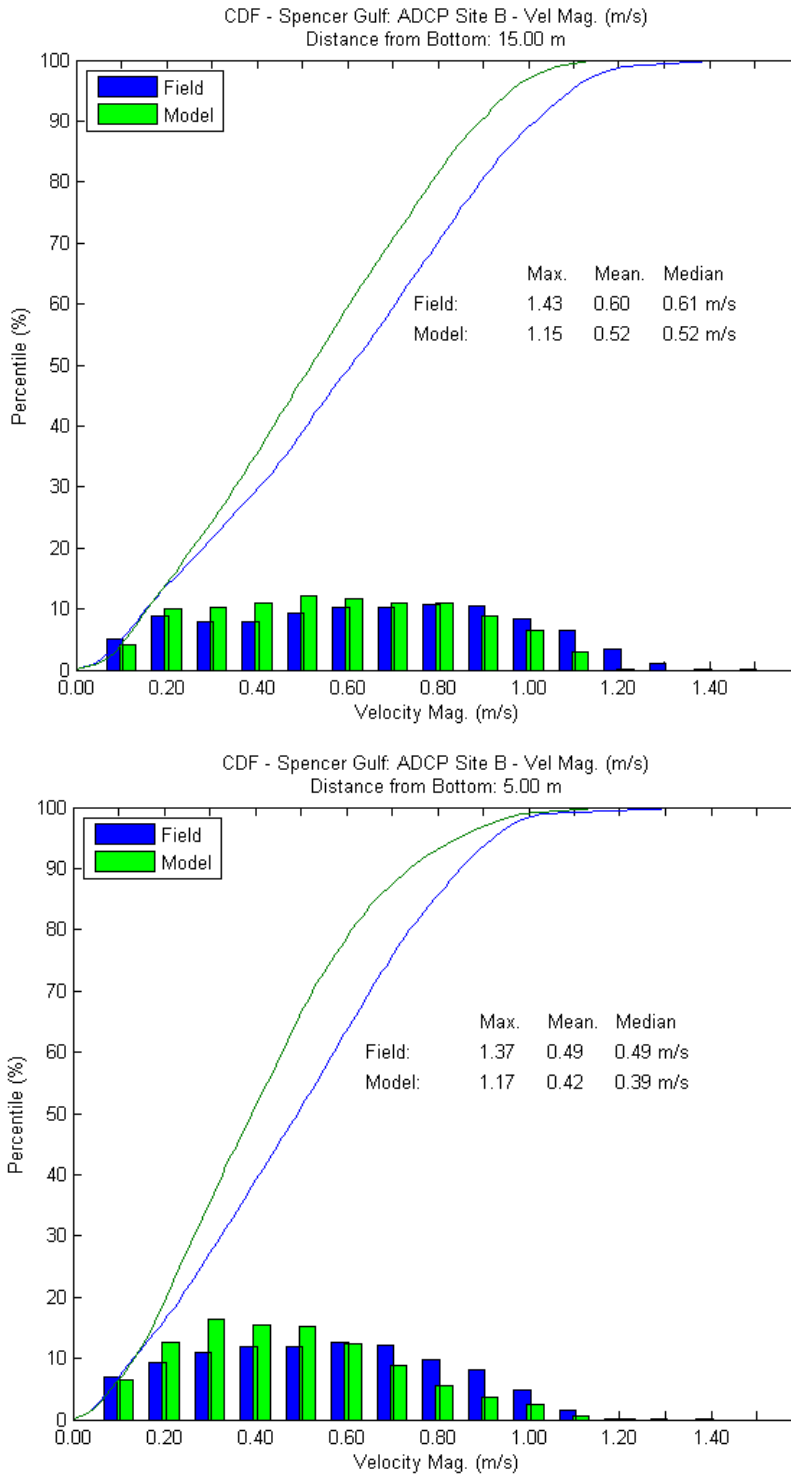


**Figure 5-64 Distribution of Measured and Modelled Currents at 5.00 and 15.00 m from Bottom for the 2007-2008 Measurement Period**

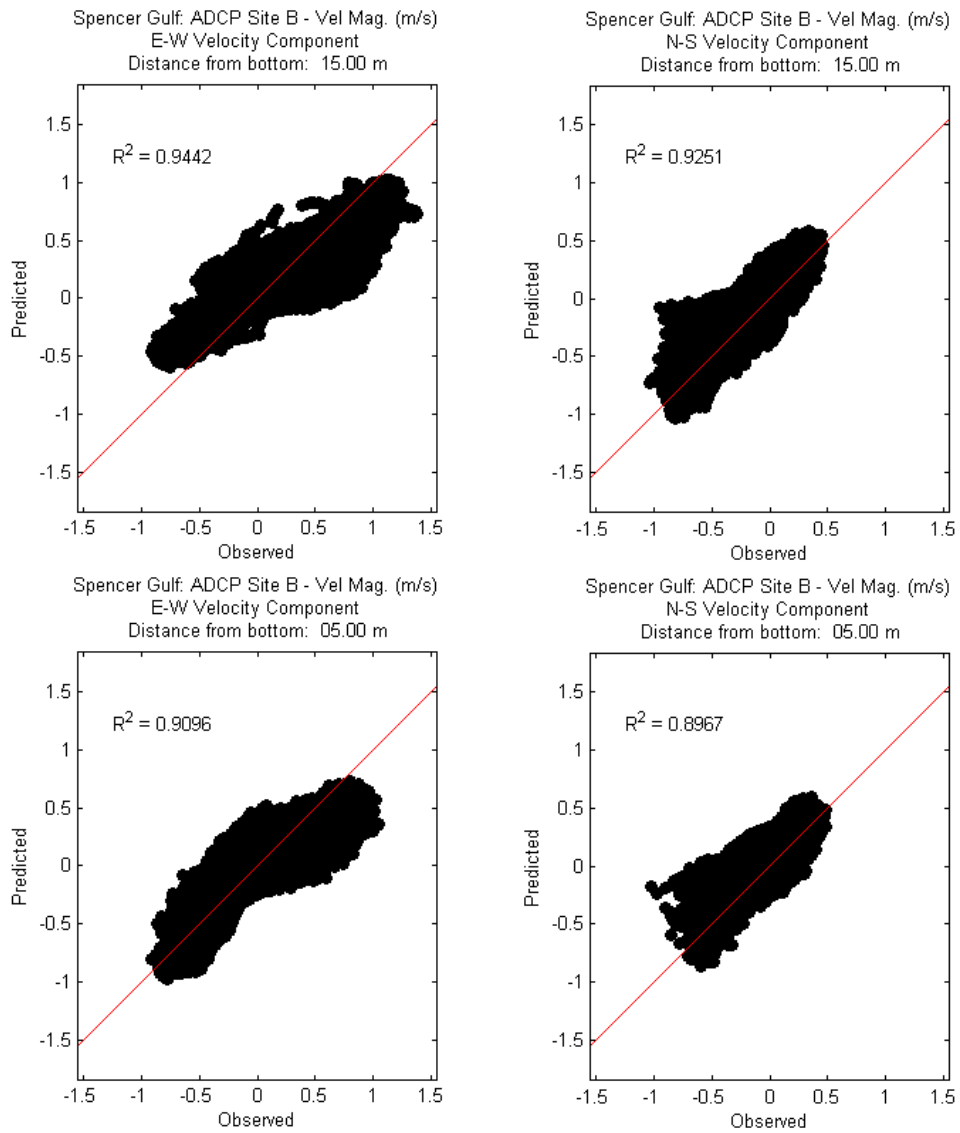


**Figure 5-65 Scatter Plots of Measured and Modelled Currents at 5.00 and 15.00 m from Bottom for the 2007-2008 Measurement Period**

**Table 5-9 Model Error at 5.00 and 15.00 m from the Bottom for the 2007-2008 Measurement Period. RMSE: Root Mean Square Error, MAE: Mean Absolute Error,  $R^2$ : Correlation Coefficient**

Distance from Bottom	N-S current			E-W current		
	RMSE (m/s)	MAE (m/s)	$R^2$ (p<0.001)	RMSE (m/s)	MAE (m/s)	$R^2$ (p<0.001)
15.00 m	0.155	0.117	0.92	0.205	0.159	0.94
05.00 m	0.140	0.098	0.90	0.187	0.139	0.91

## 6 REFERENCES

- Adcroft, A. and D. Marshall (1998) How slippery are piecewise-constant coastlines in numerical models? *Tellus*, **50A**(1):95–108.
- BMT WBM (2005) *Pumicestone Passage water quality modelling. Final report*. Technical Report R.B14024.004 prepared for Moreton Bay Waterways and Catchment Partnership.
- Bye, J.A.T., and I.P. Harbison (1991). Transfer of inland salts to the marine environment at the head of Spencer Gulf, South Australia. *Palaeogeogr. Palaeocl.* **84**: 357-368.
- BHP Billiton (2009). *Olympic Dam Expansion: Draft environmental impact statement 2009*.
- Botelho, D., J. Imberger, C. Dallimore, and B.R. Hodges (2009). A hydrostatic/non-hydrostatic grid-switching strategy for computing high-frequency, high wave number motions embedded in geophysical flows. *Environ. Modell. Softw.* **24**(4): 473-488
- DSE (2008) *Victorian Desalination Project Environment Effects Statements, Volume 2*.
- Easton, A.K. (1978) A reappraisal of the tides in Spencer Gulf, South Australia. *Aust. J. Mar. Freshwater Res.*, **29**: 467-477.
- Hodges, B.R. (2000). *Numerical techniques in CWR-ELCOM*. CWR manuscript WP 1422 BH. Centre for Water Research, The University of Western Australia.
- Imberger, J. and Patterson, J. C. 1990. Physical limnology. *Adv. Appl. Mech.*, **27**:303-455.
- Lewis, G., and J. Noye (1998) Analysis and prediction of tide heights over tidal flats and currents involving eddies. In: Noye, J. (ed.) *Modelling coastal sea processes*. World Scientific Publishing Co.
- Nunes, R.A. (1985) *Catalogue of data from a systematic programme of oceanographic measurements in Northern Spencer Gulf from 1982 to 1985*. Cruise Report No. 9. School of Earth Sciences, Flinders University of South Australia.
- Nunes, R.A., and G.W. Lennon (1986) Physical properties distributions and seasonal trends in Spencer Gulf, South Australia: an inverse estuary. *Aust. J. Mar. Freshwater Res.*, **37**: 39-53.
- Nunes-Vaz, R.A., G.W. Lennon, and D.G. Bowers (1990) Physical behaviour of a large, negative or inverse estuary. *Cont. Shelf Res.*, **10**(3): 277-304.
- Okely, P., J.P. Antenucci, P.S. Yeates, C.L. Marti and J. Imberger (2007a) *Summary of investigations into the impact of the Perth seawater desalination plant discharge on Cockburn Sound*. Centre for Water Research document WP2160PO.
- Okely, P., J.P. Antenucci, J. Imberger and C.L. Marti (2007b) *Field investigations into the impact of the Perth seawater desalination plant discharge on Cockburn Sound.*, Centre for Water Research document WP2150PO.
- SA Water (2008) *Proposed Adelaide Desalination Plant Environmental Impact Statement, Chapter 7*.



SA Water (2009) *Proposed Adelaide Desalination Plant – Environmental Impact Statement. Response Document January 2009.*

Soulsby, R. (1997). *Dynamics of marine sands.* Thomas Telford Ltd.

UNESCO (1981). *The practical salinity scale 1978 and the international equation of state of seawater 1980.* Technical papers in marine science no. 36.

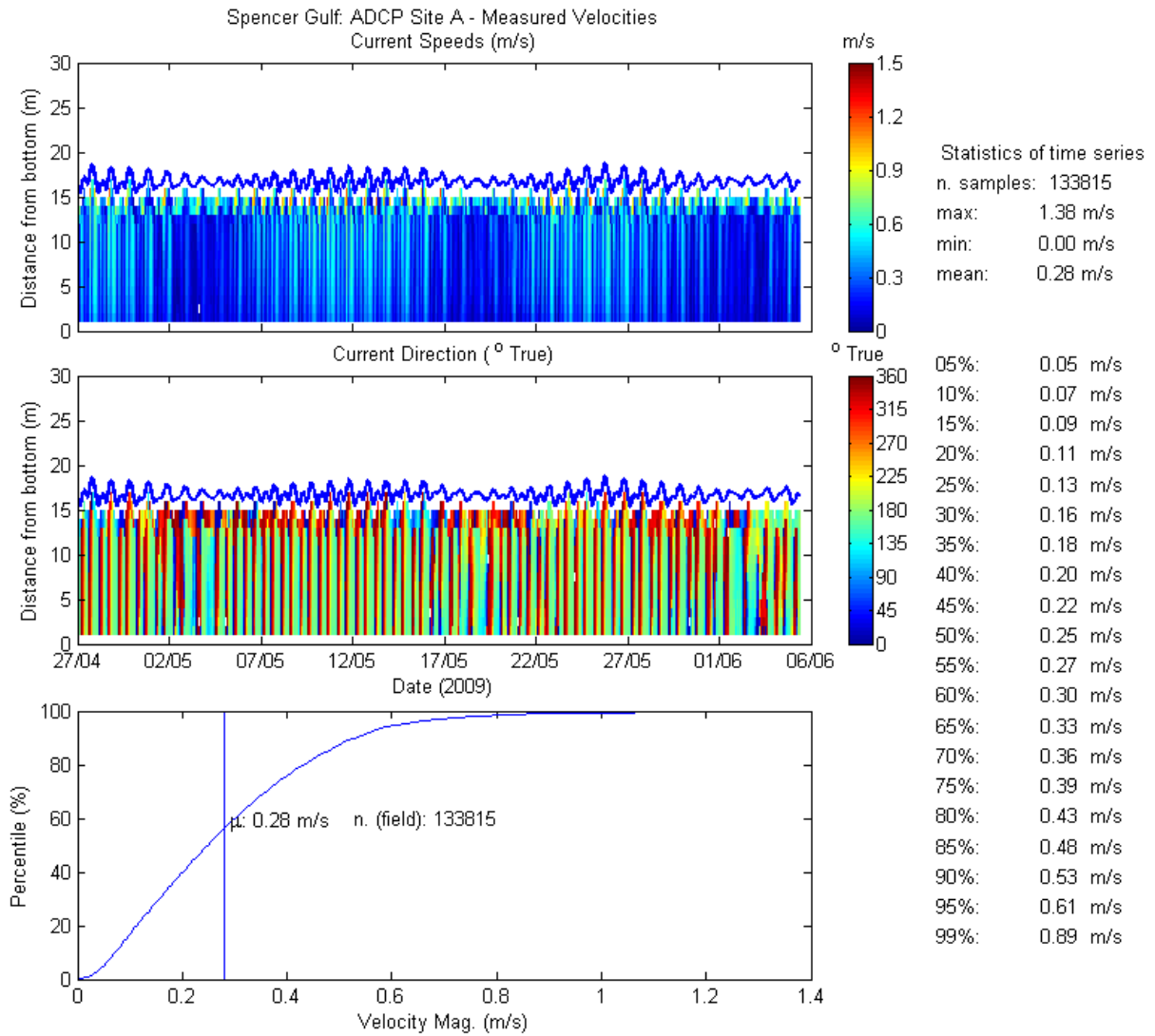
The references below form, respectively Appendices O11.2, O11.3, and O11.4 of the Draft EIS.

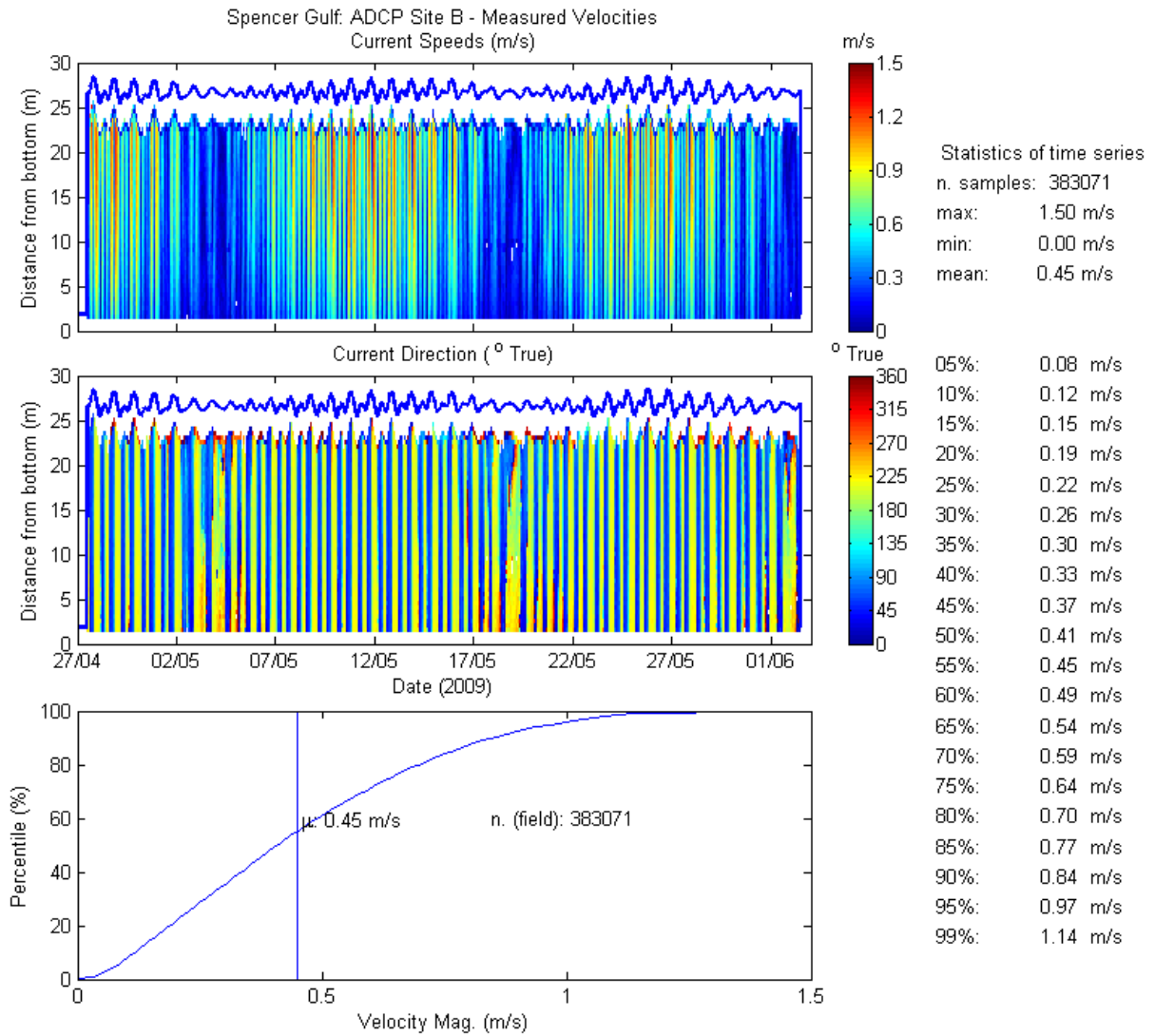
BMT WBM (2007) *Hydrodynamic and water quality modelling at Port Bonython: modelling assessments.* Technical report R.B15583.005. Prepared for BHP Billiton/Arup.

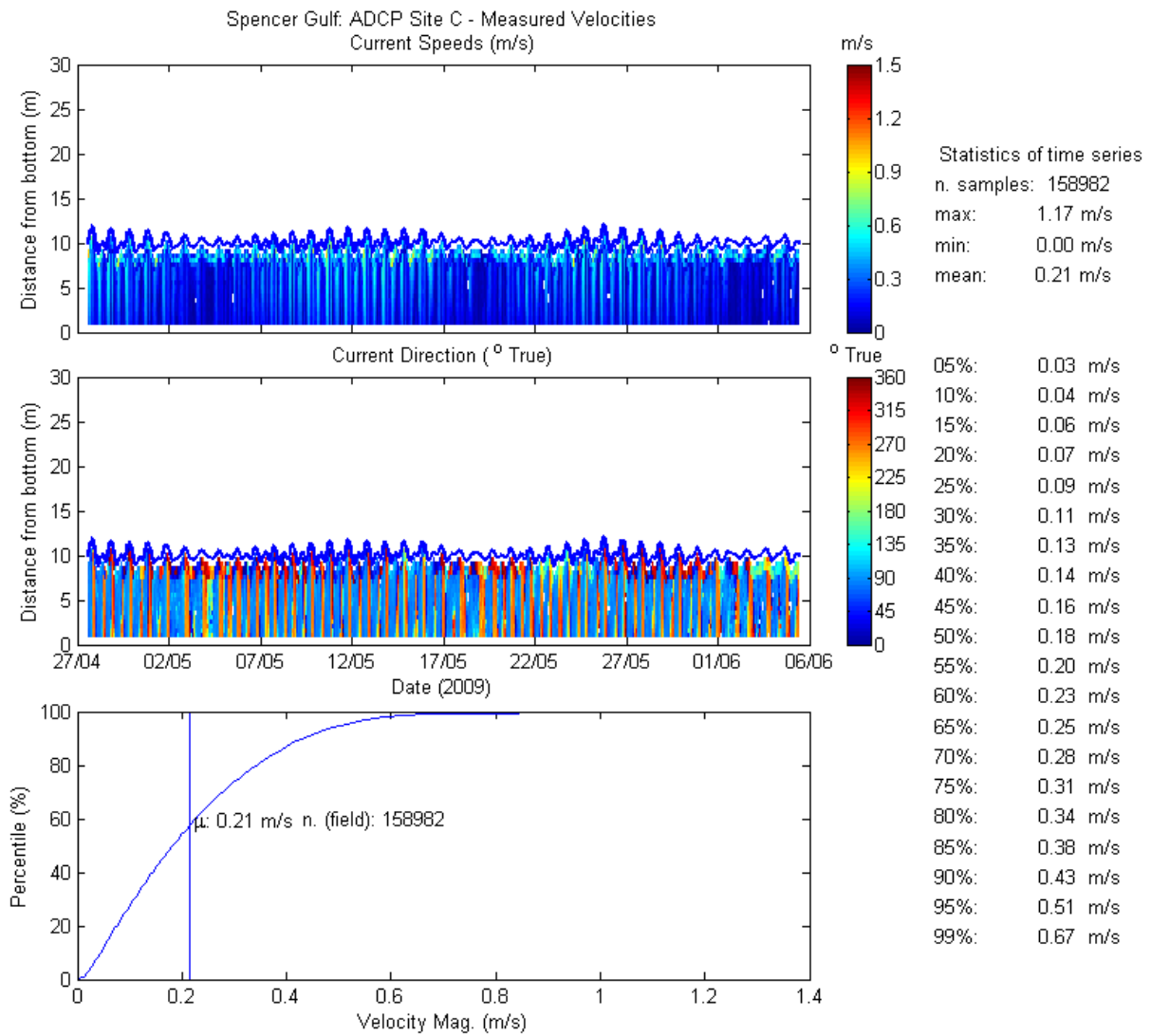
BMT WBM (2008a) *Hydrodynamic and water quality modelling in Spencer Gulf: calibration report.* Technical report R.B15583.004. Prepared for BHP Billiton/Arup.

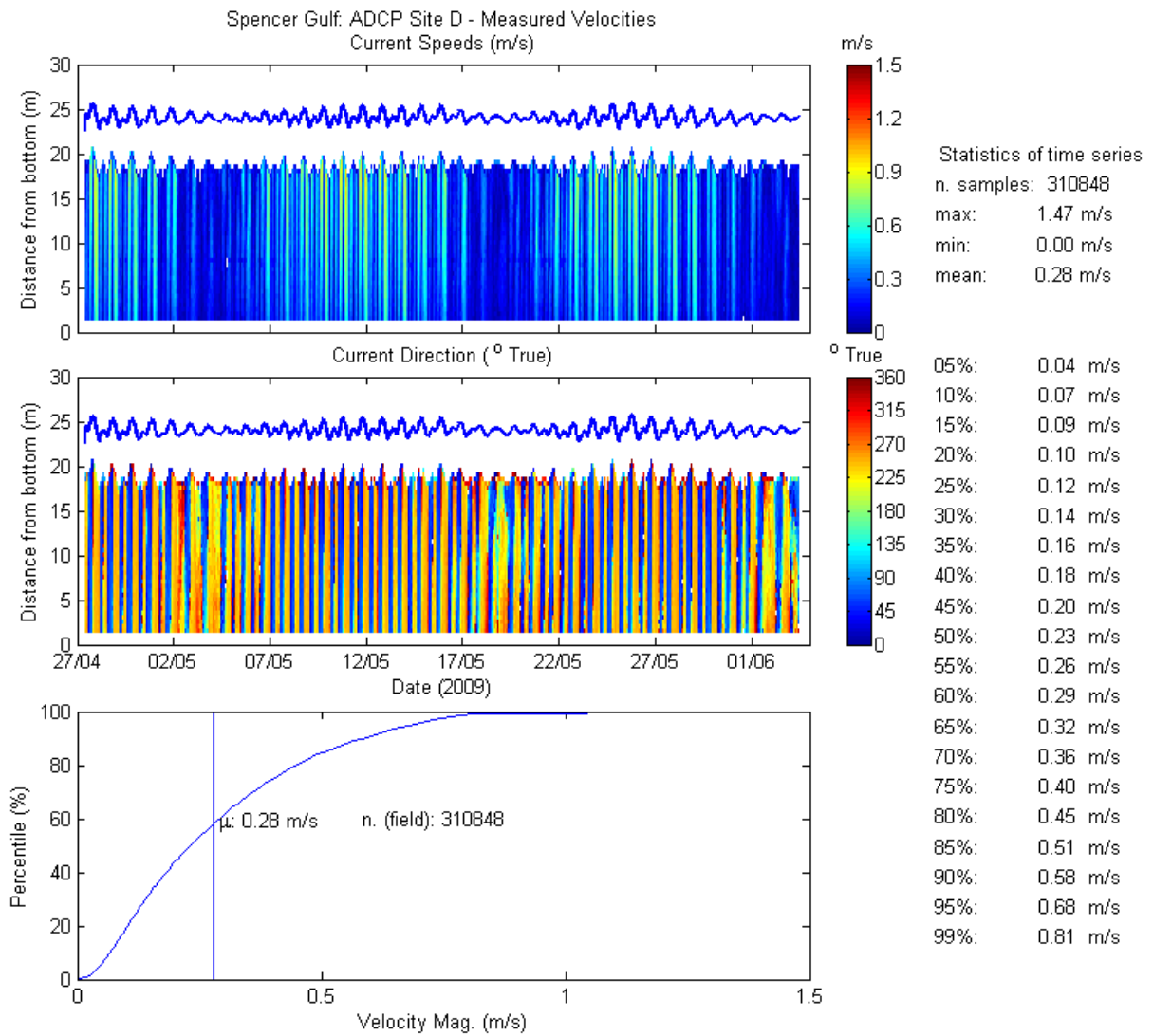
BMT WBM (2008b) *Additional hydrodynamic model runs – ODX and SA government.* Technical report R.B16750.001. Prepared for Arup HLA/BHP Billiton.

# APPENDIX A: MOORED ADCP MEASUREMENTS

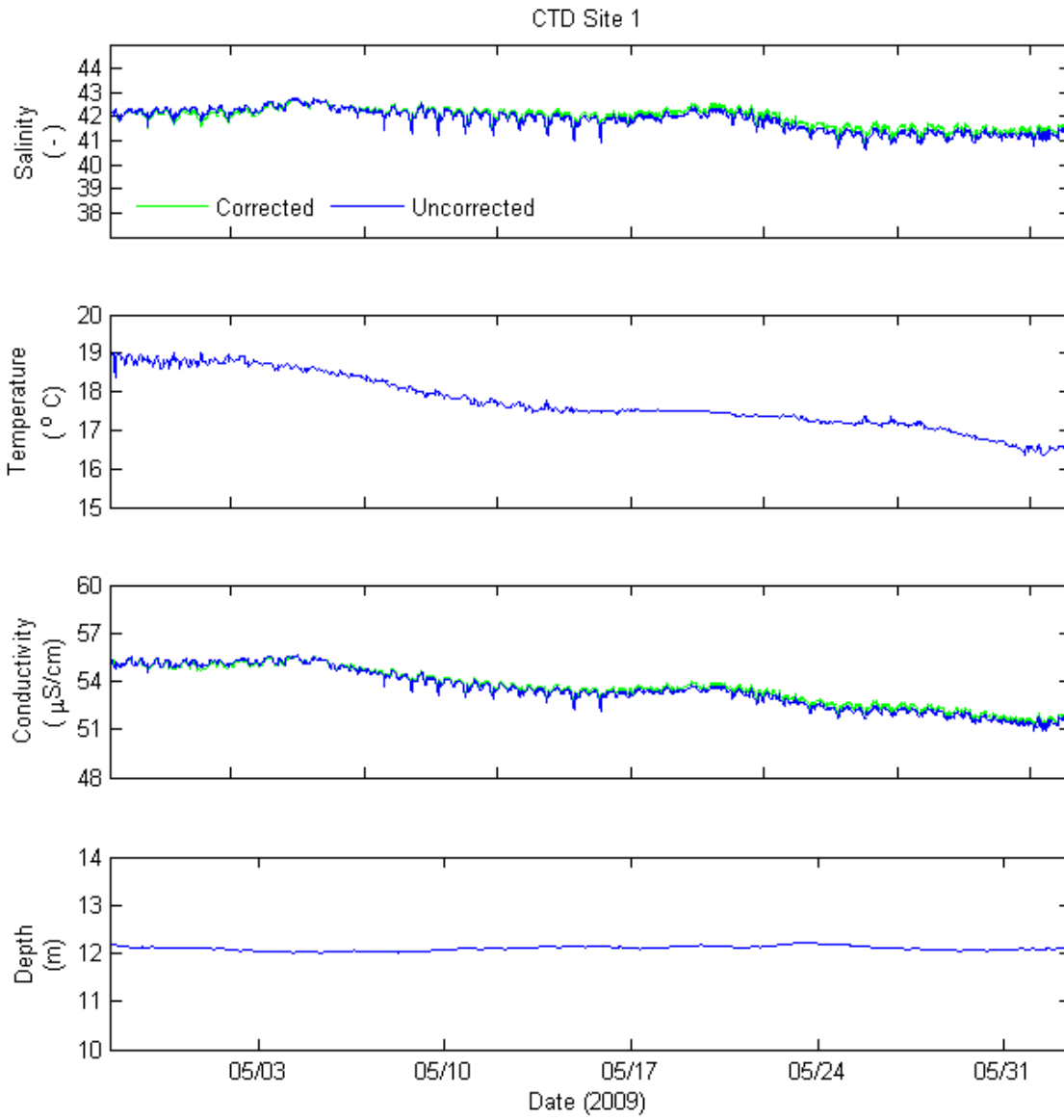


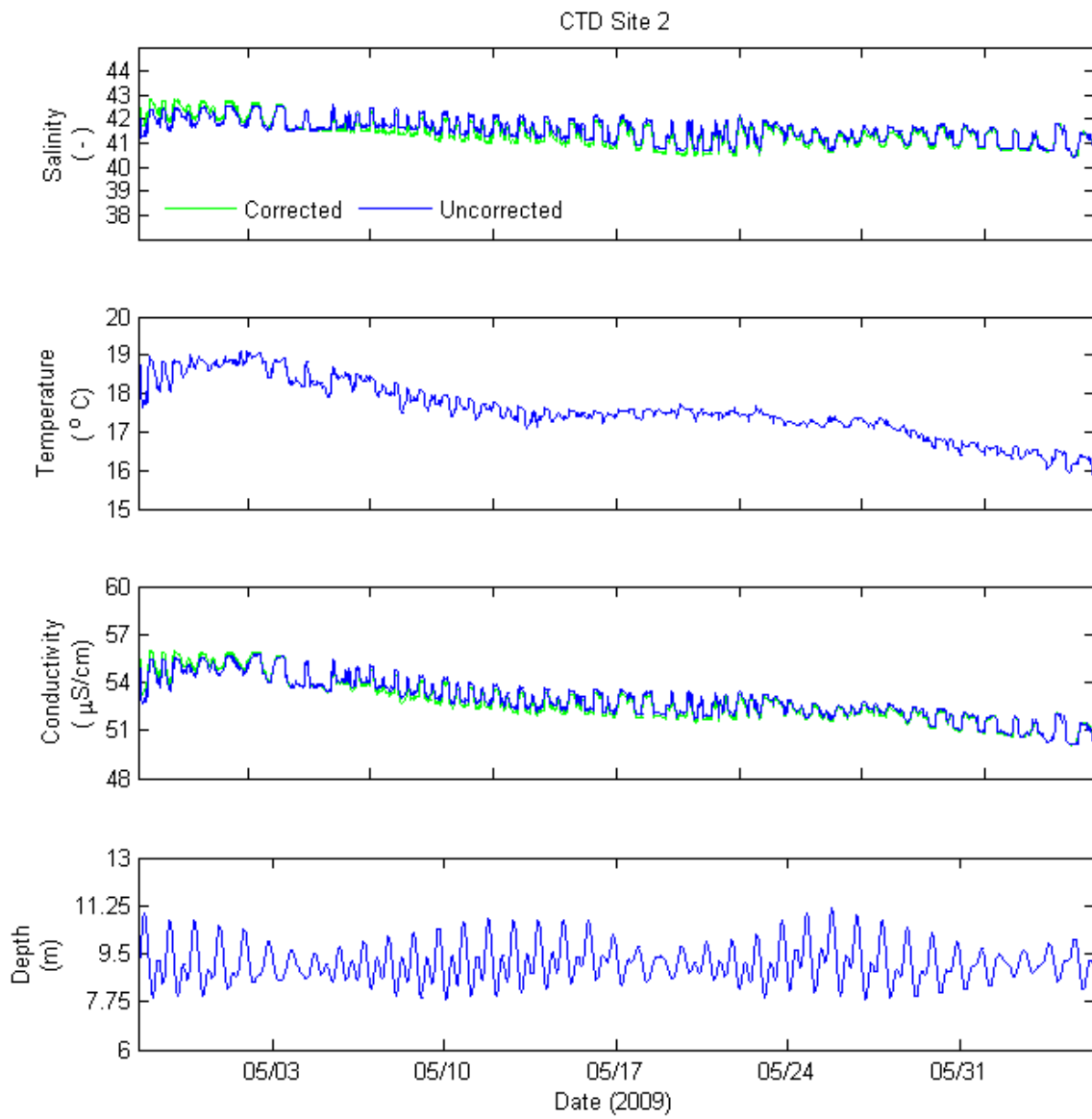


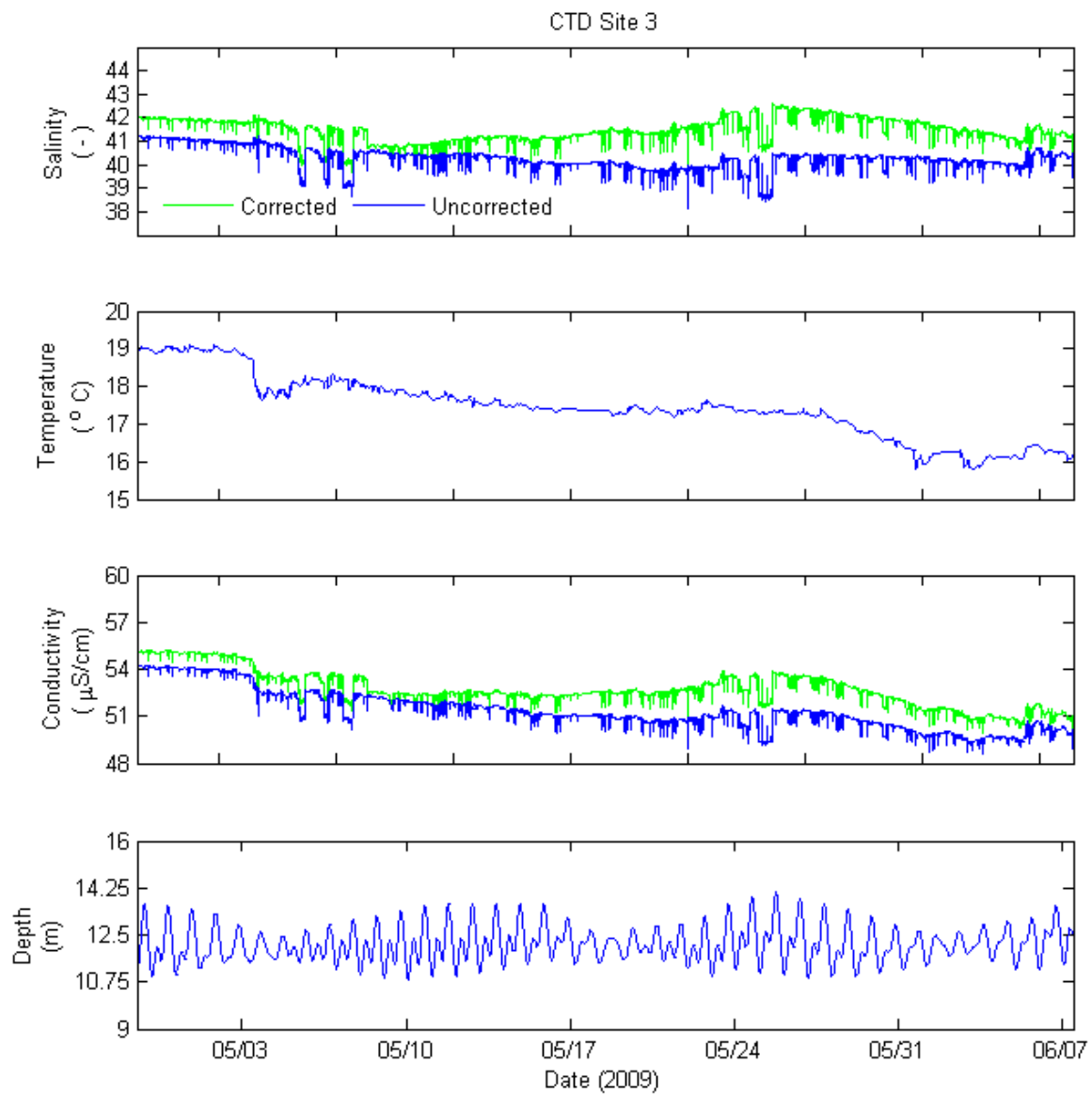




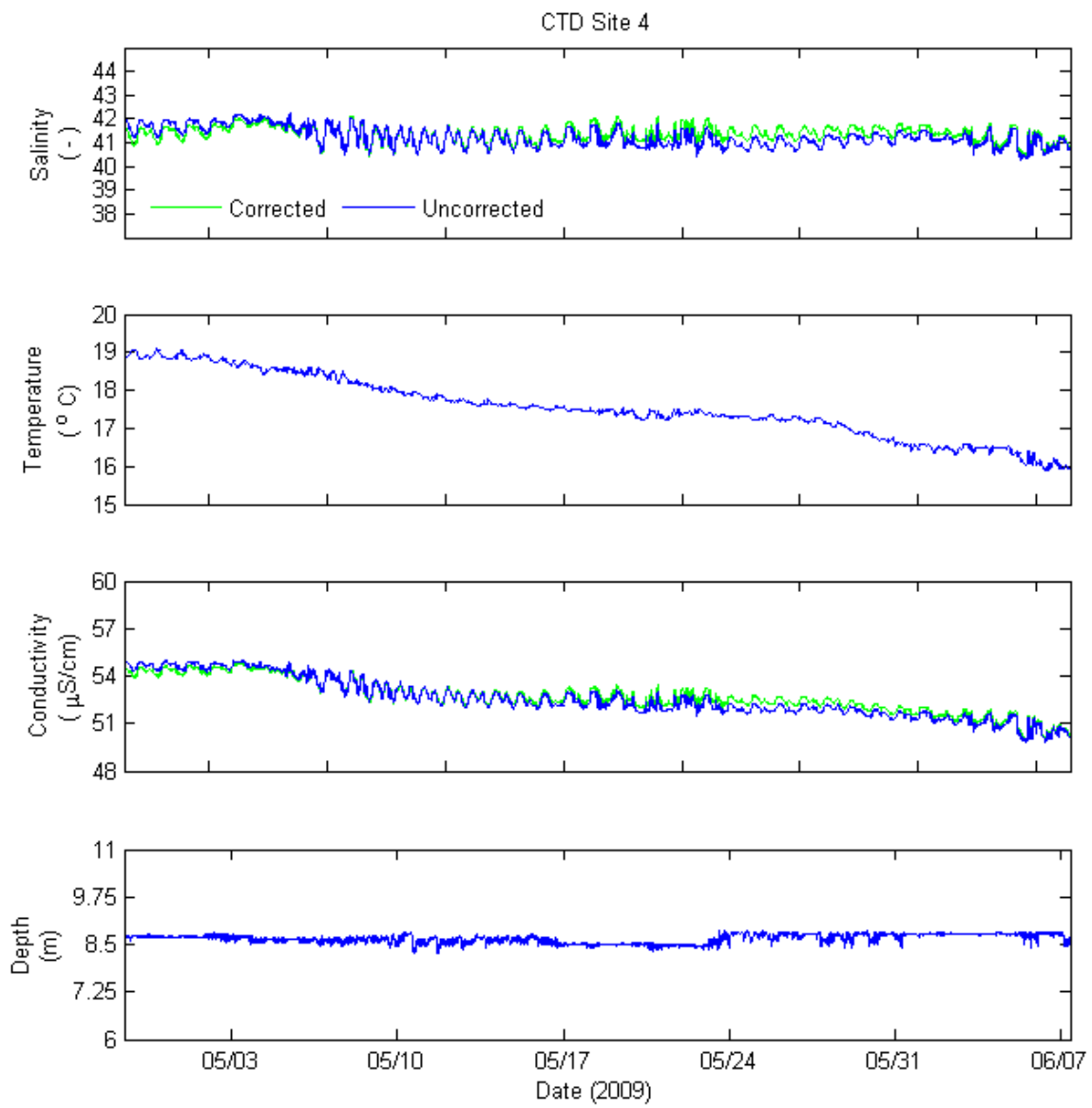
# APPENDIX B: CTD MEASUREMENTS

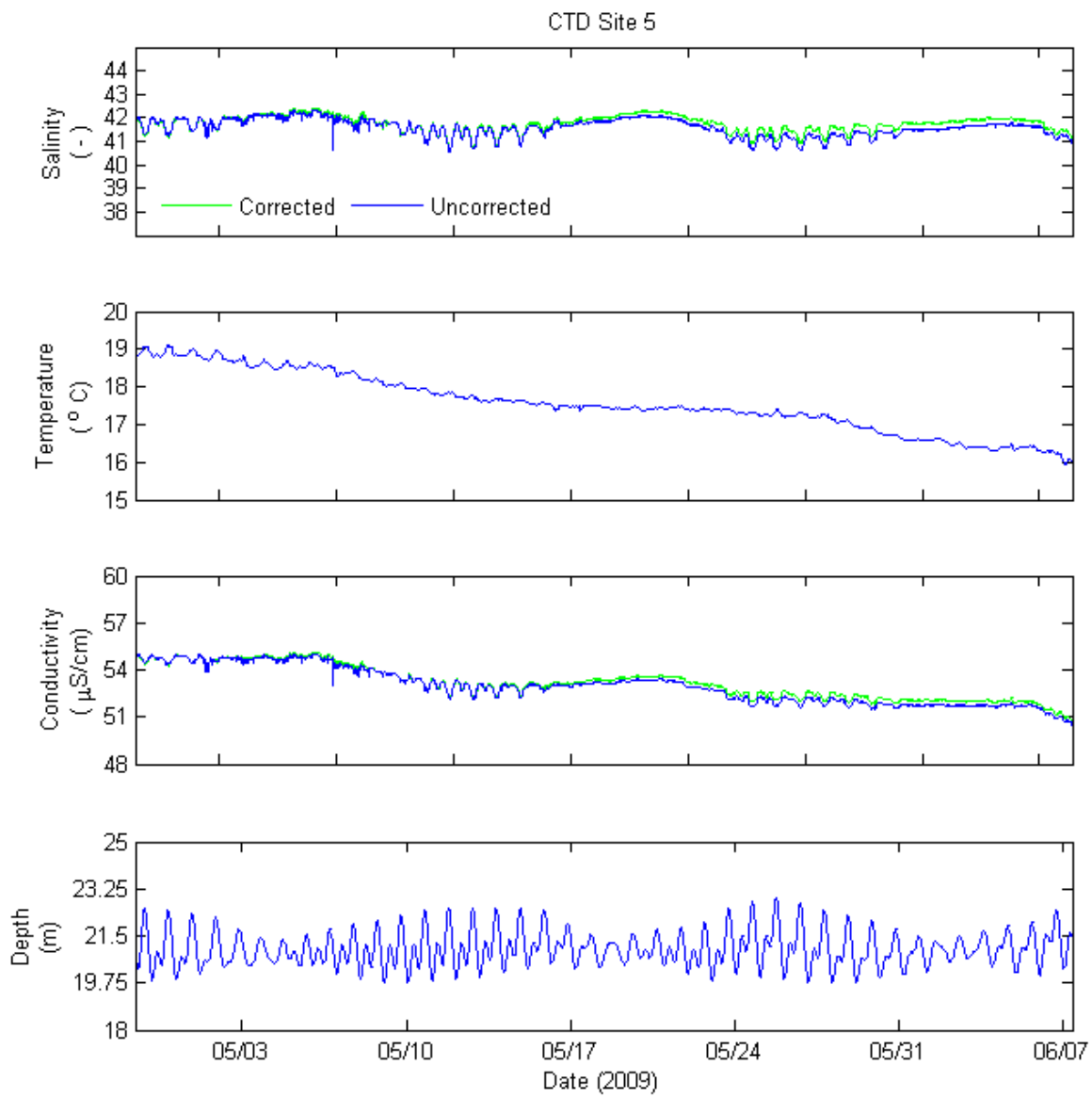


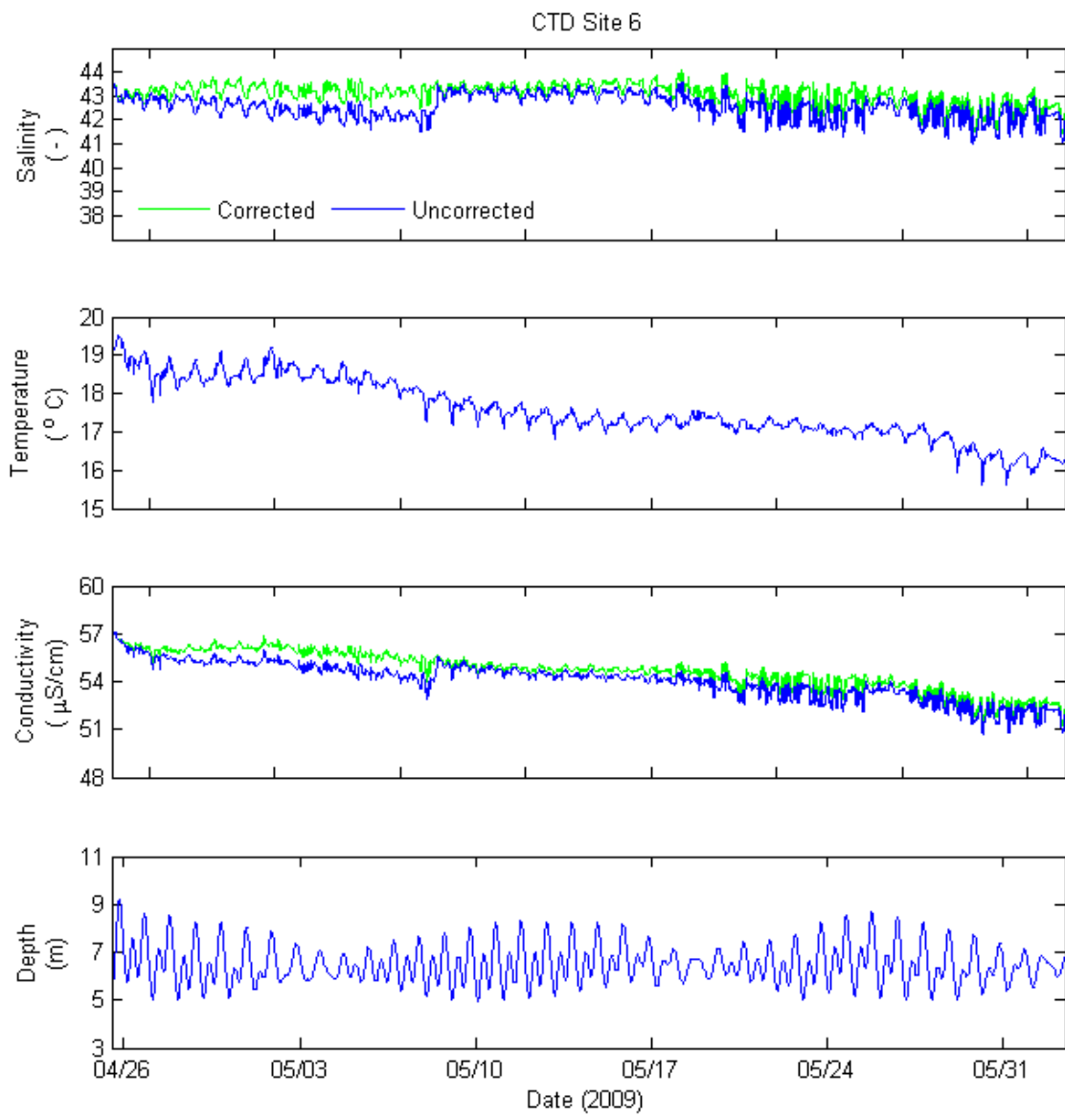




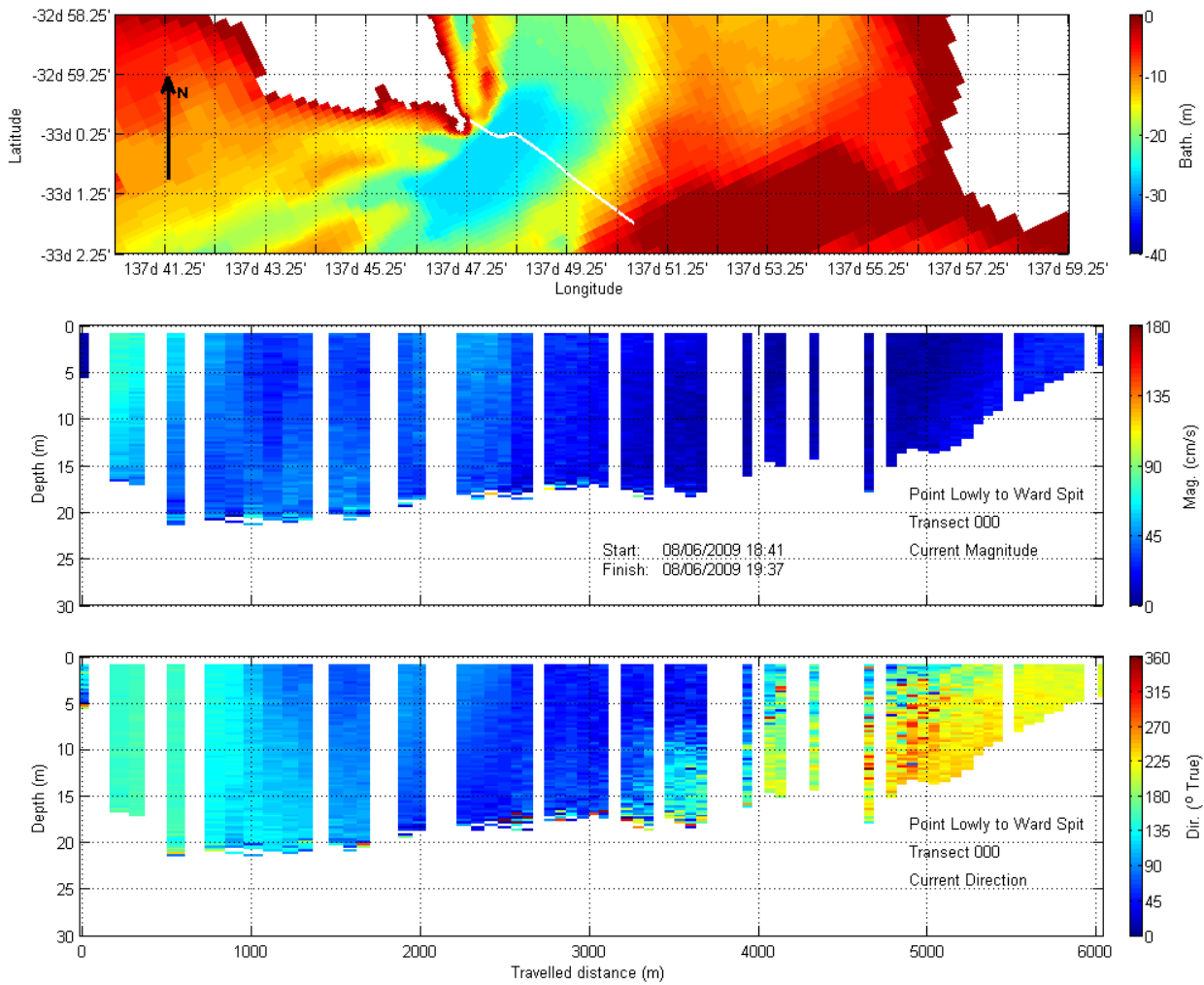


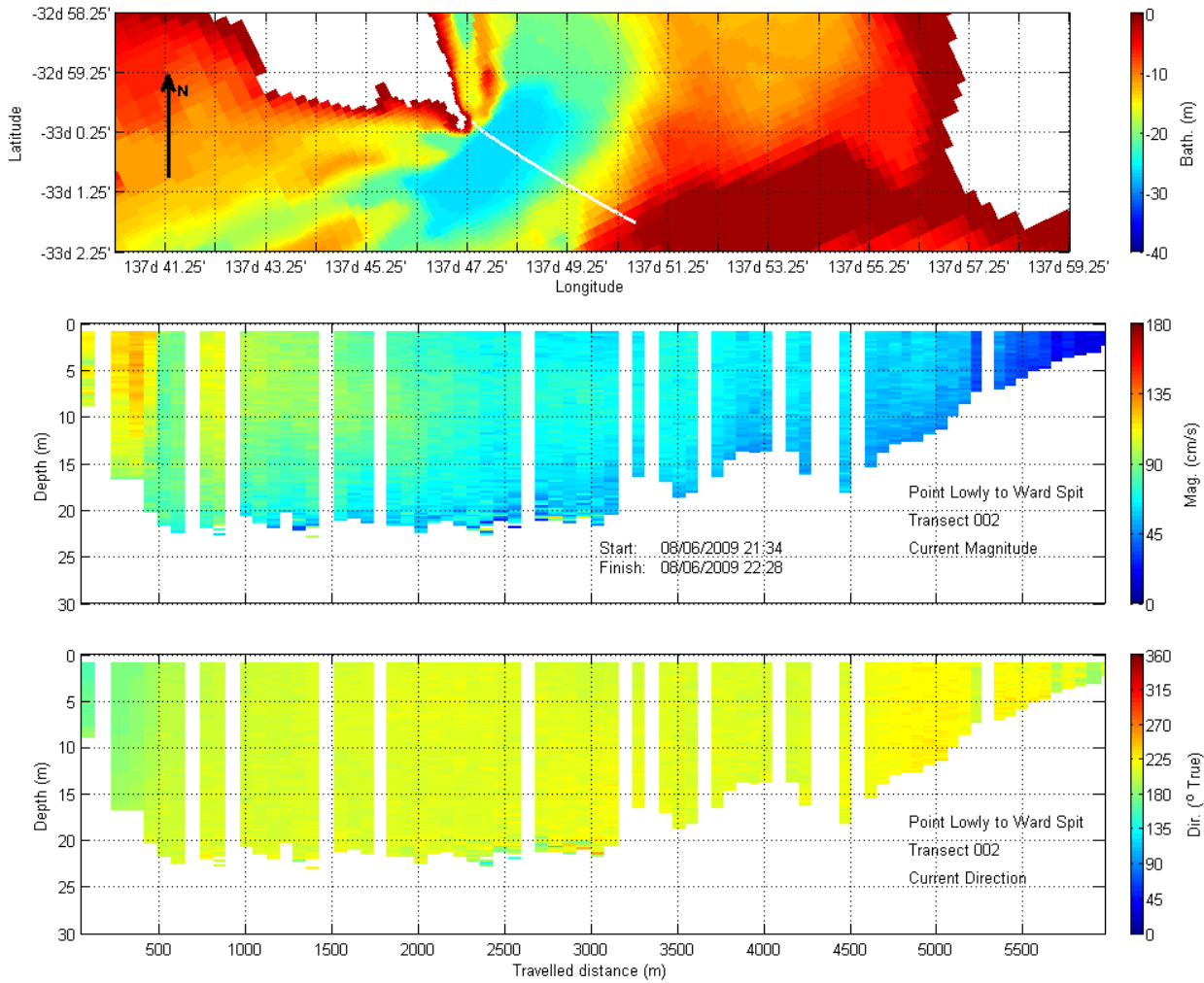


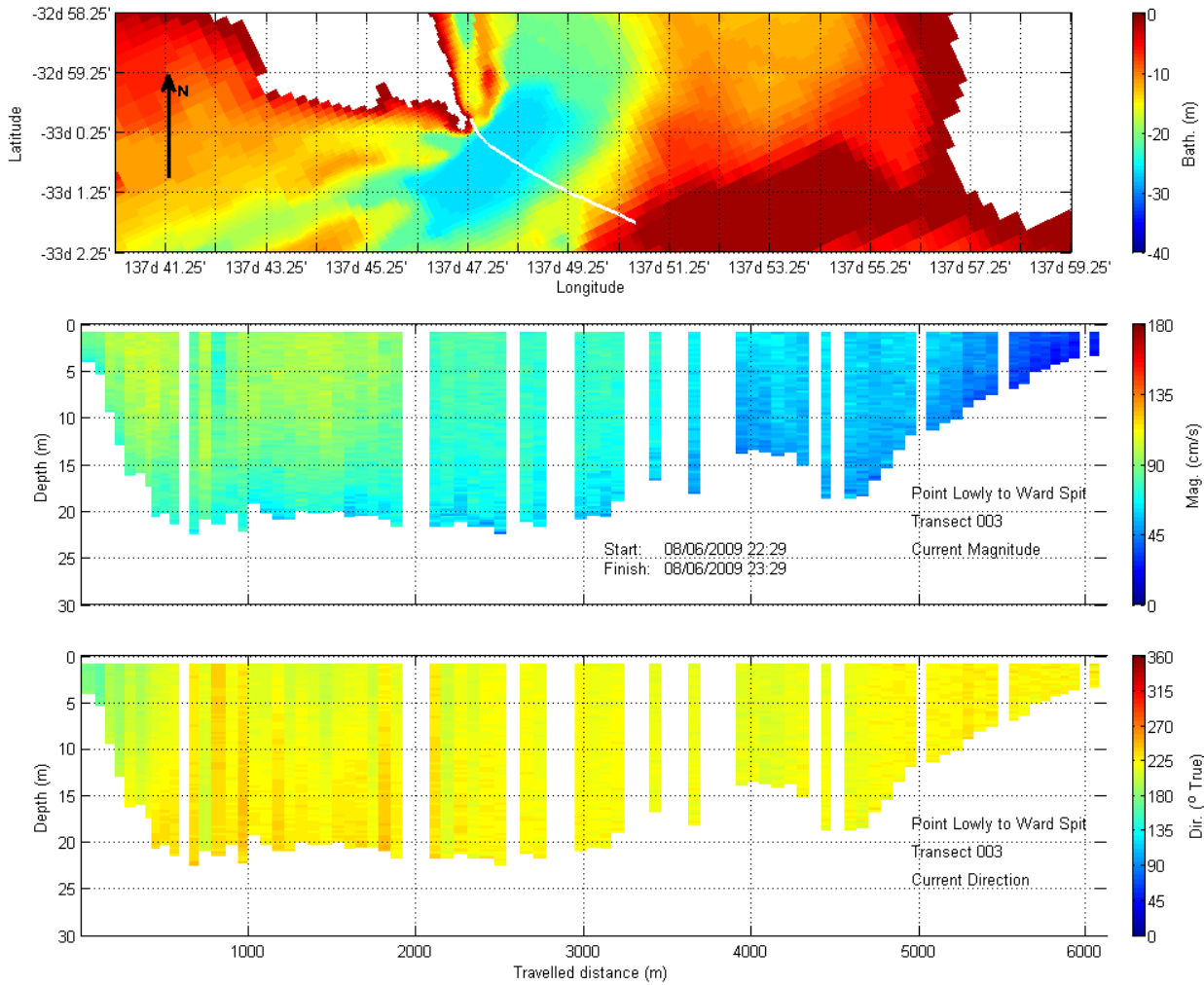


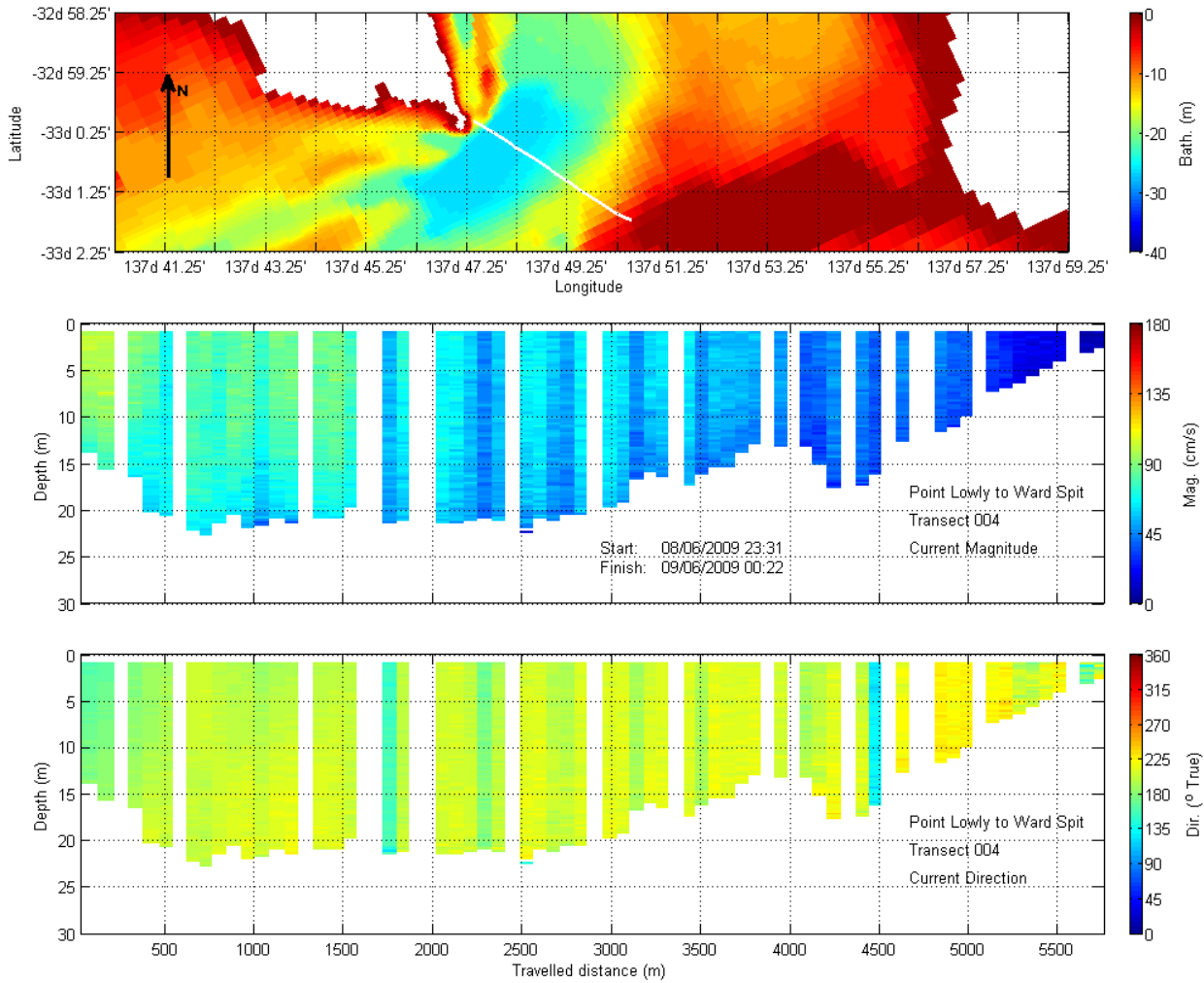


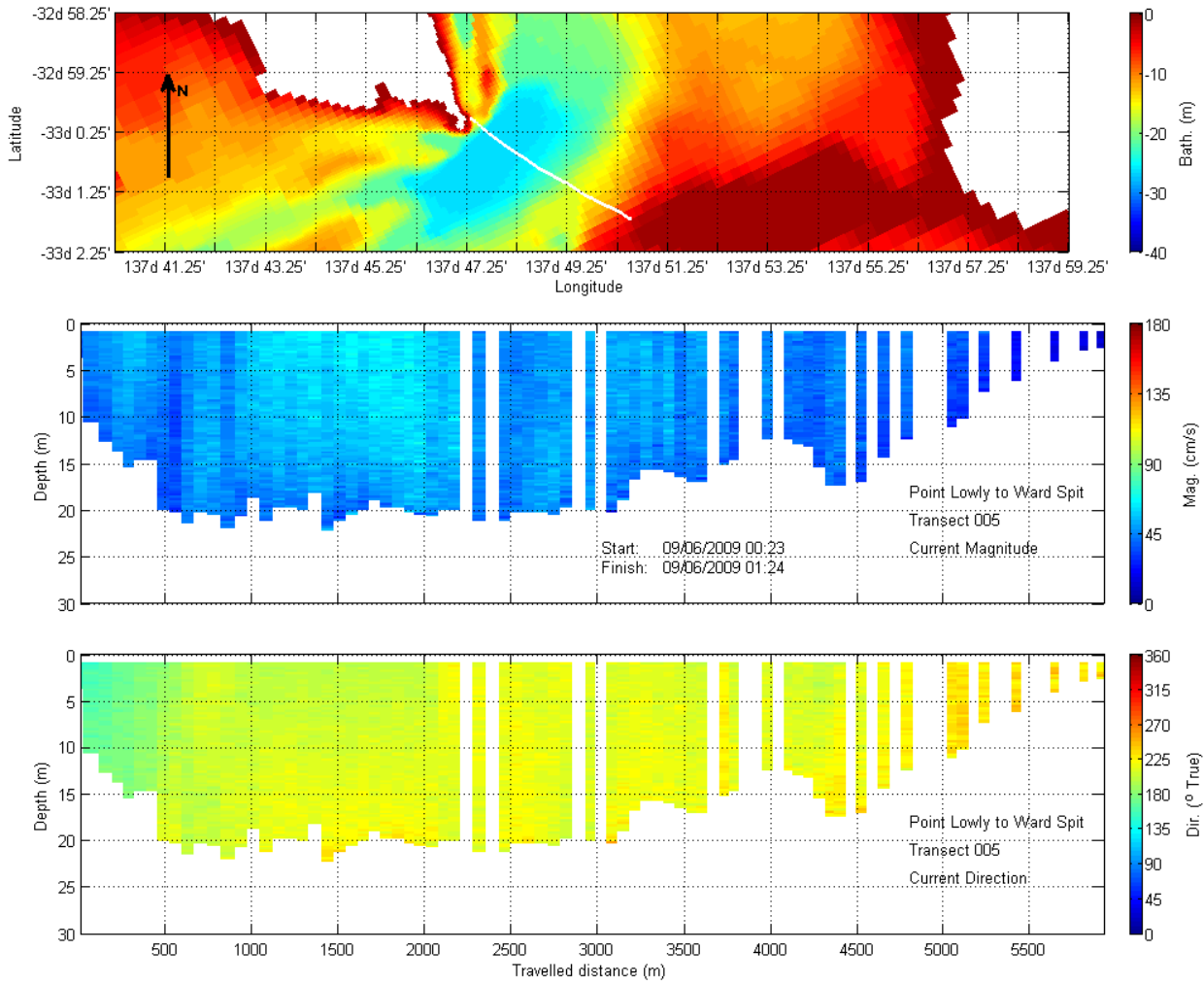
# APPENDIX C: ADCP TRANSECTS







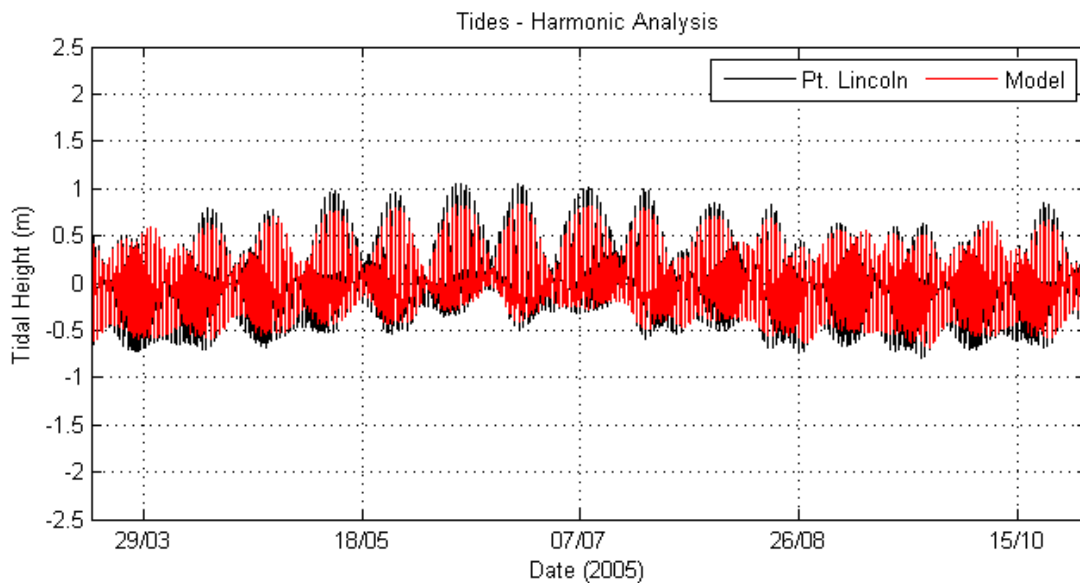
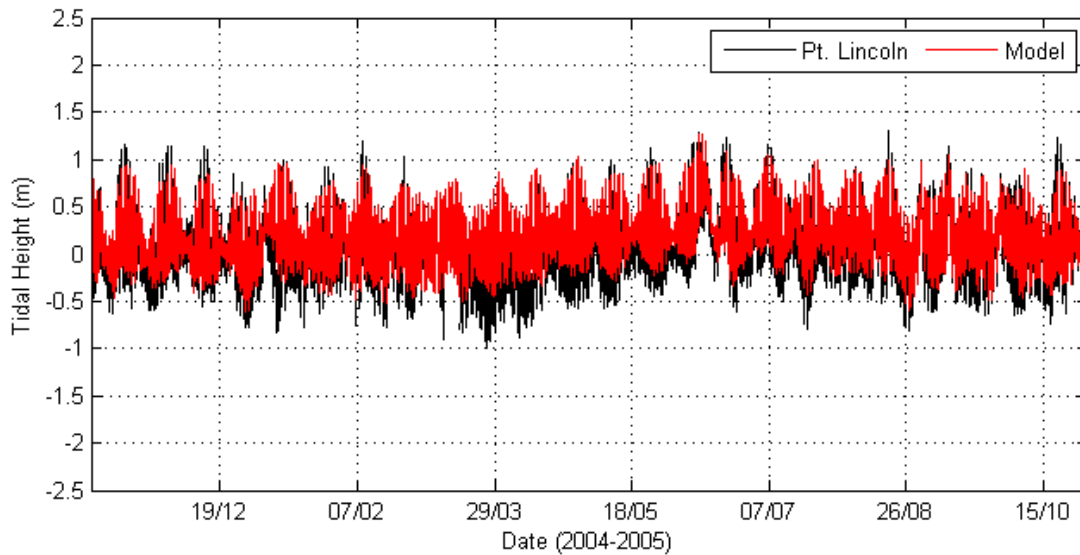


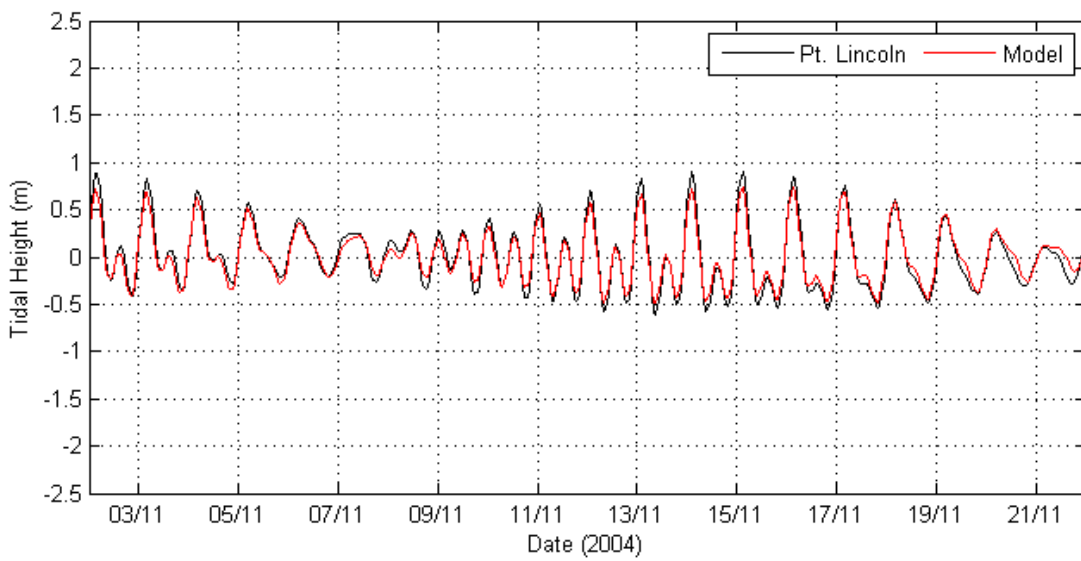
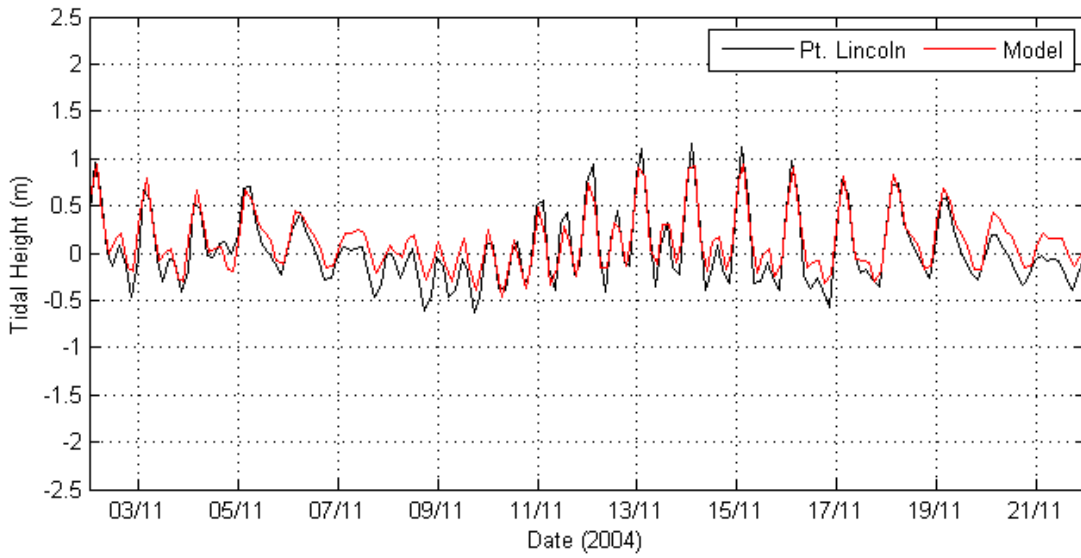


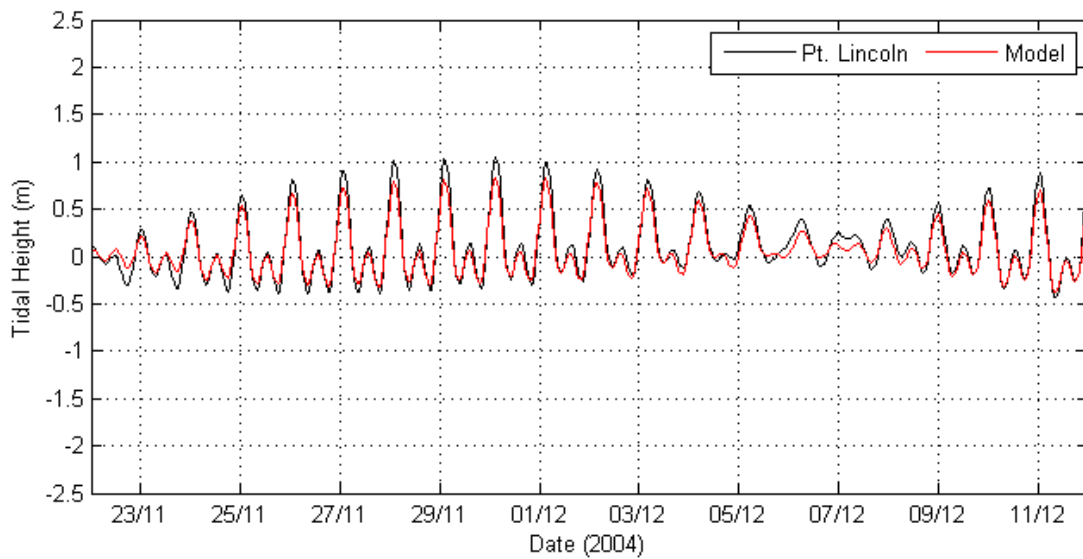
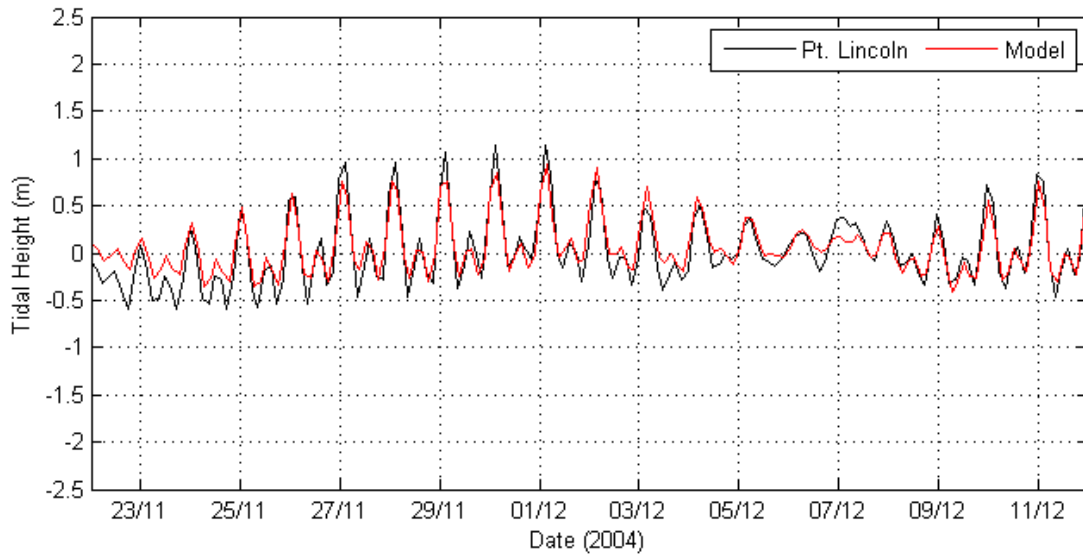


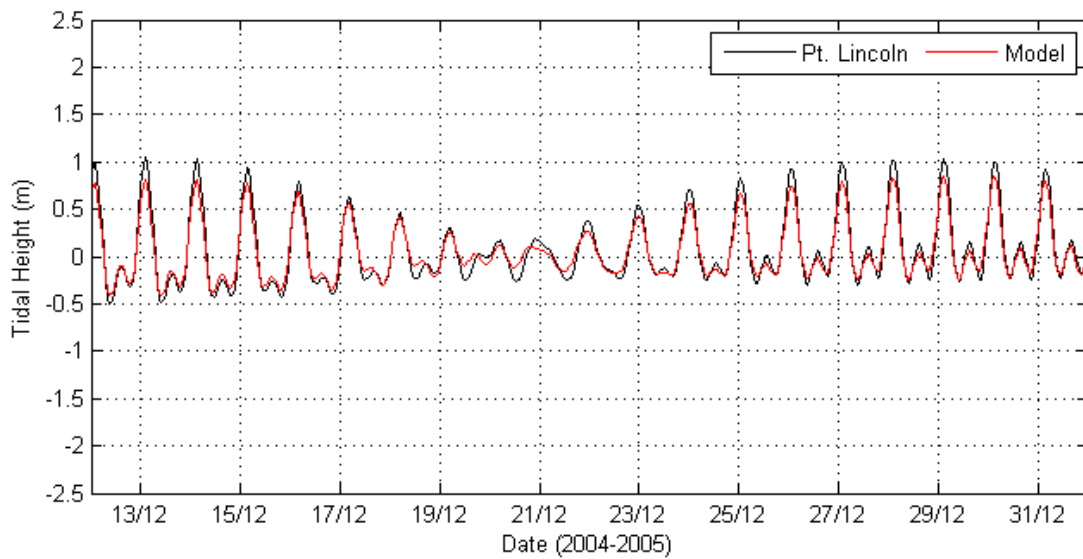
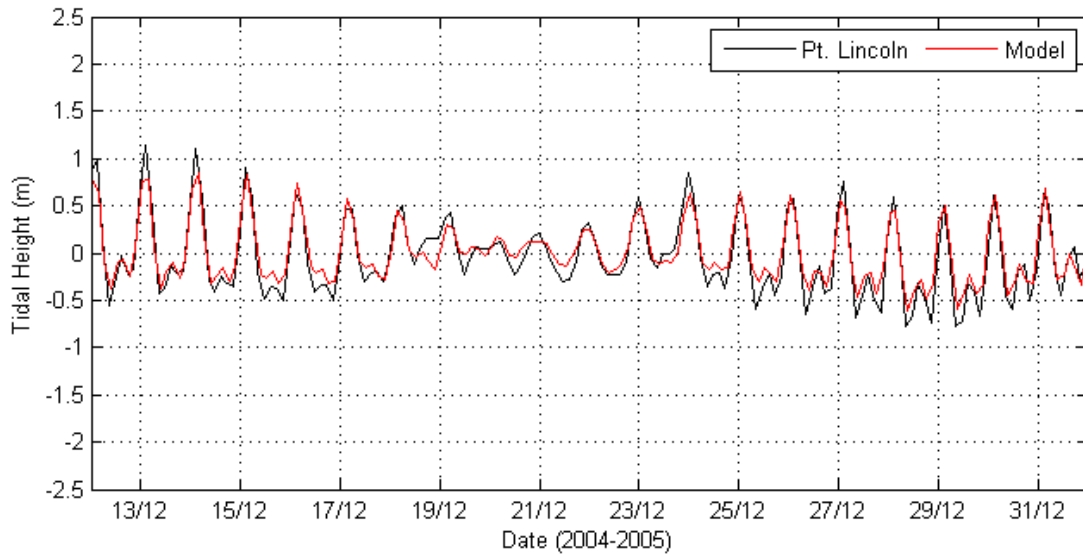
## APPENDIX D: SEASONAL VALIDATION PERIOD TIDAL-ELEVATION COMPARISONS – (TOP – RAW SIGNALS, BOTTOM – SIGNAL RECONSTRUCTED FROM HARMONIC ANALYSIS)

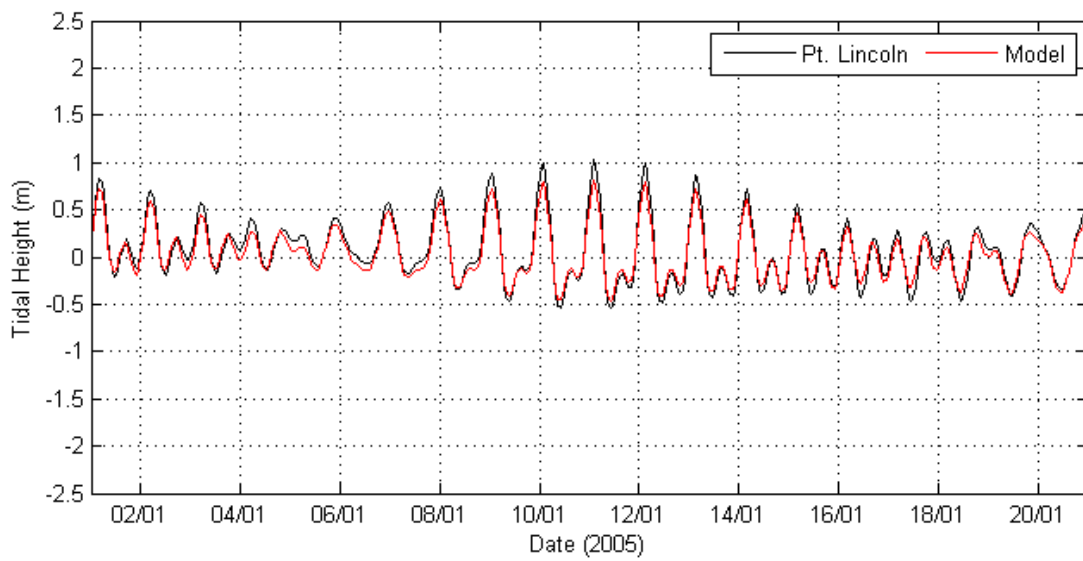
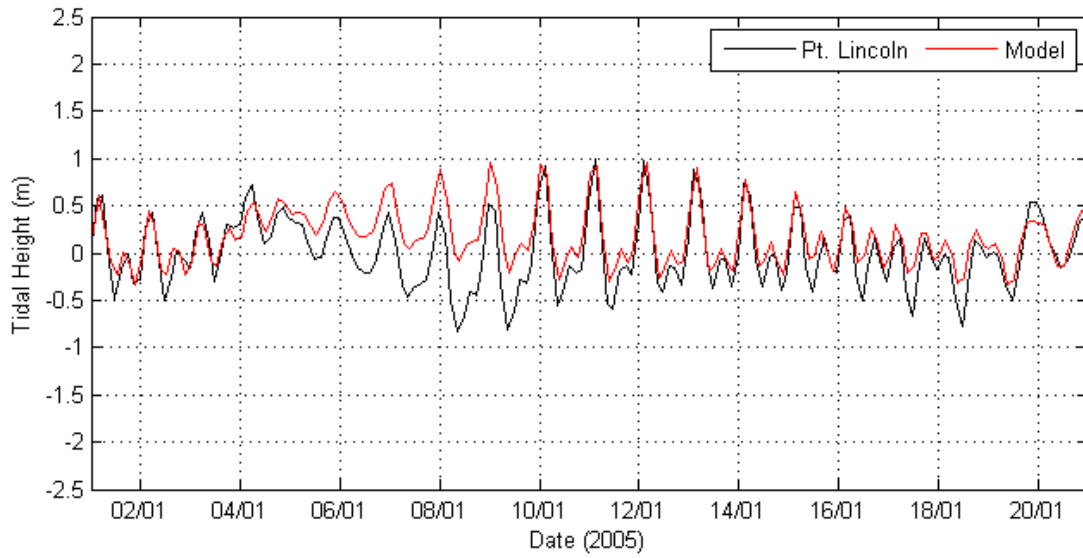
### Port Lincoln

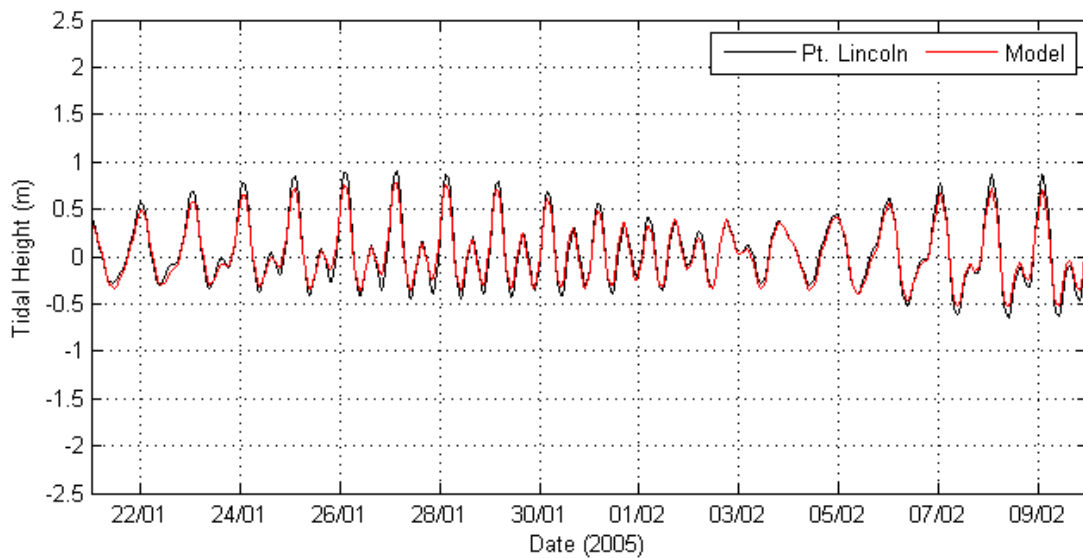
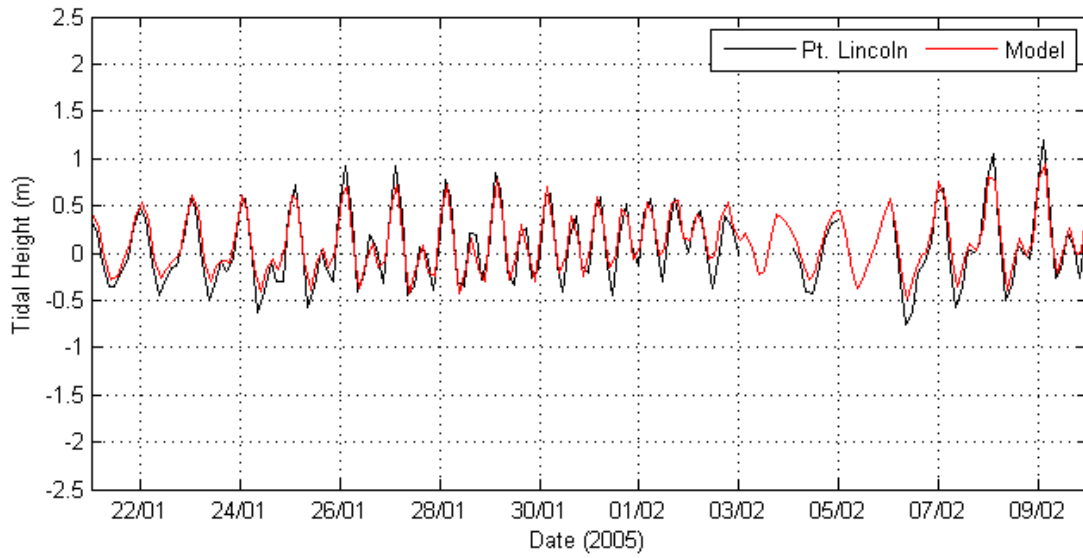


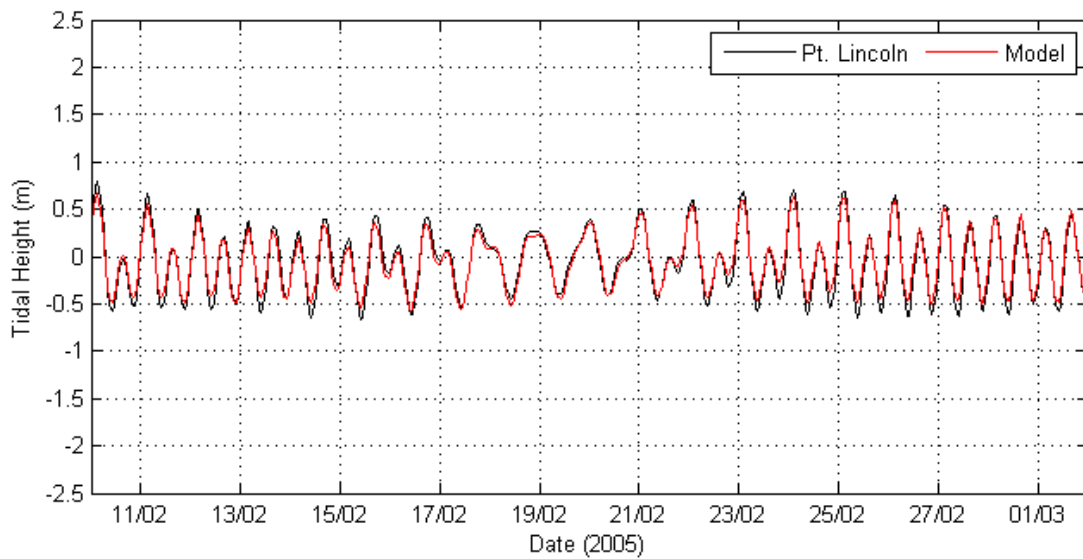
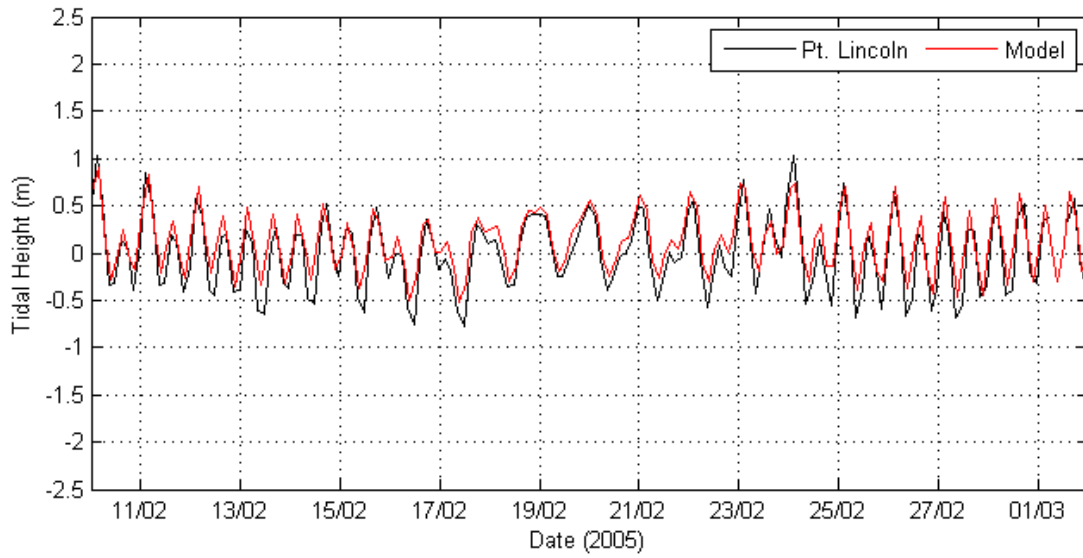


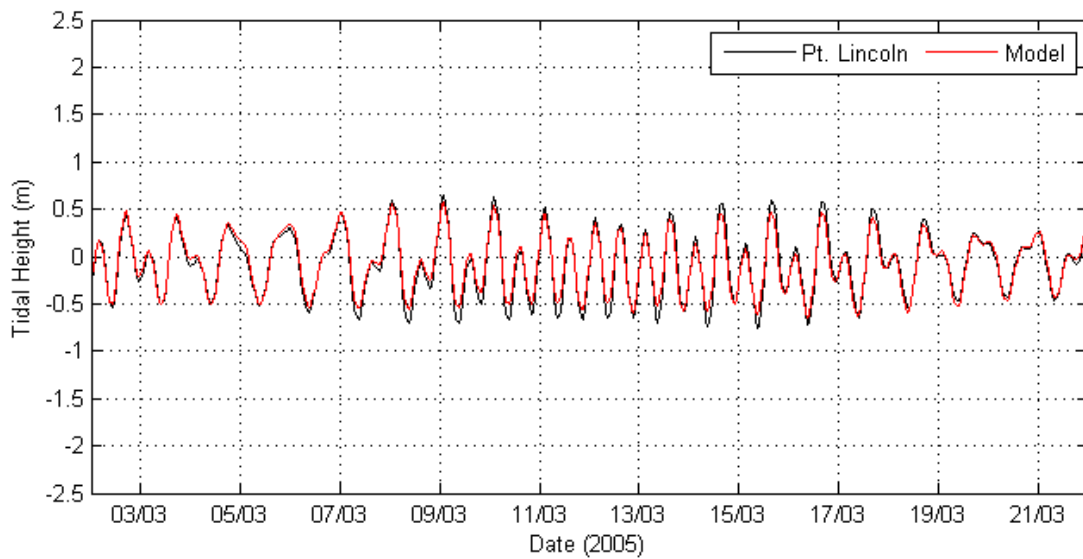
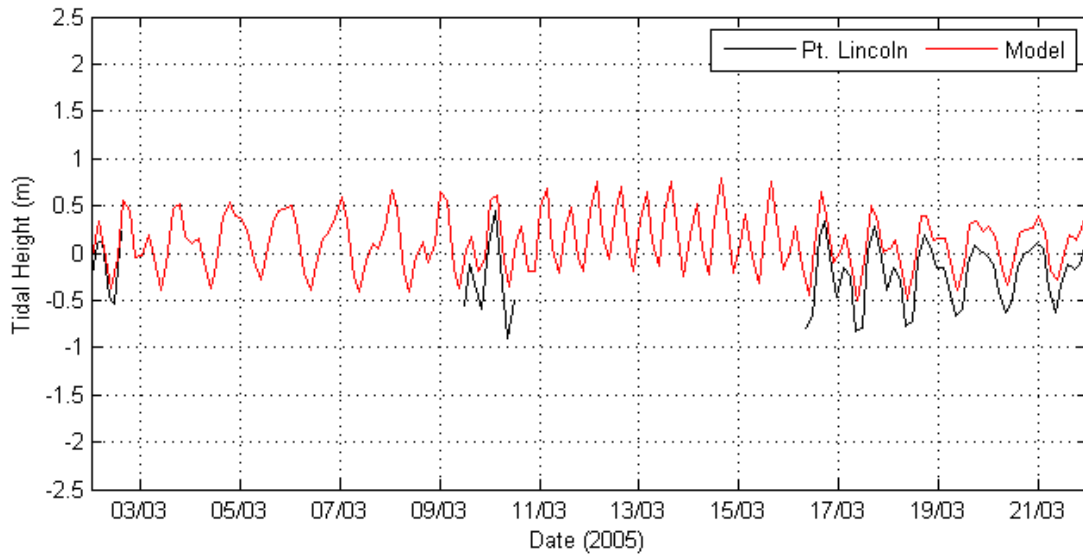




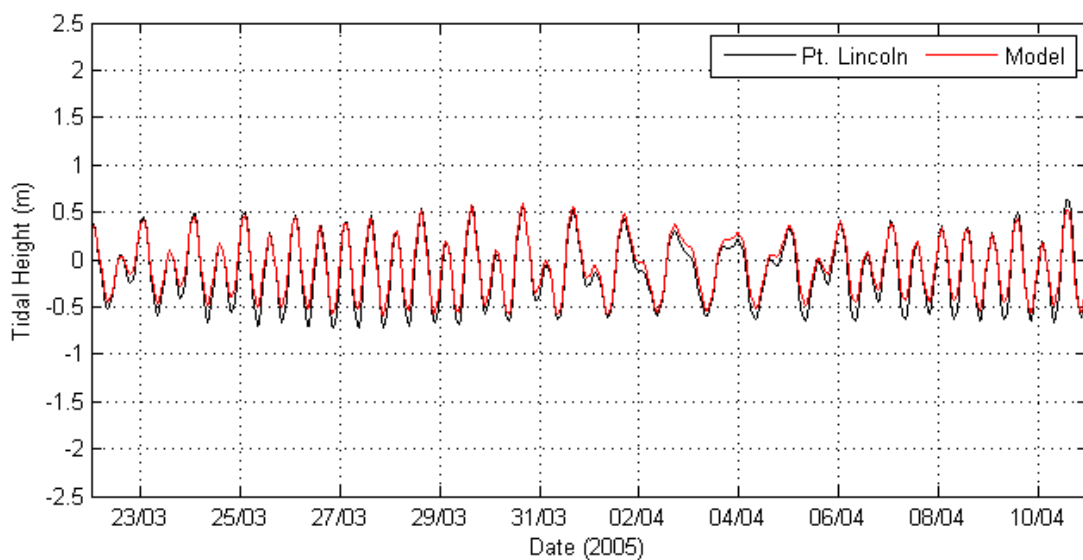
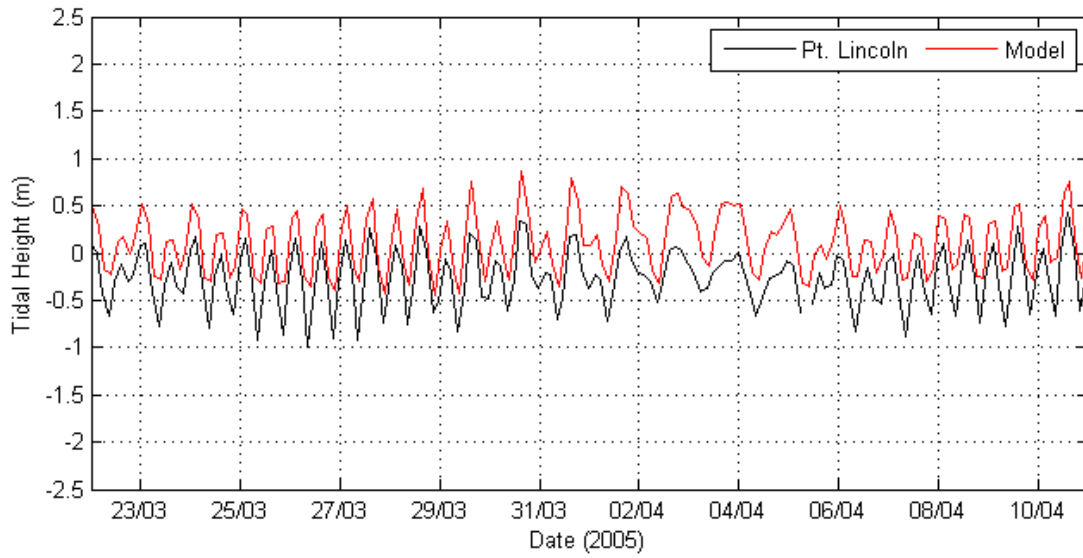


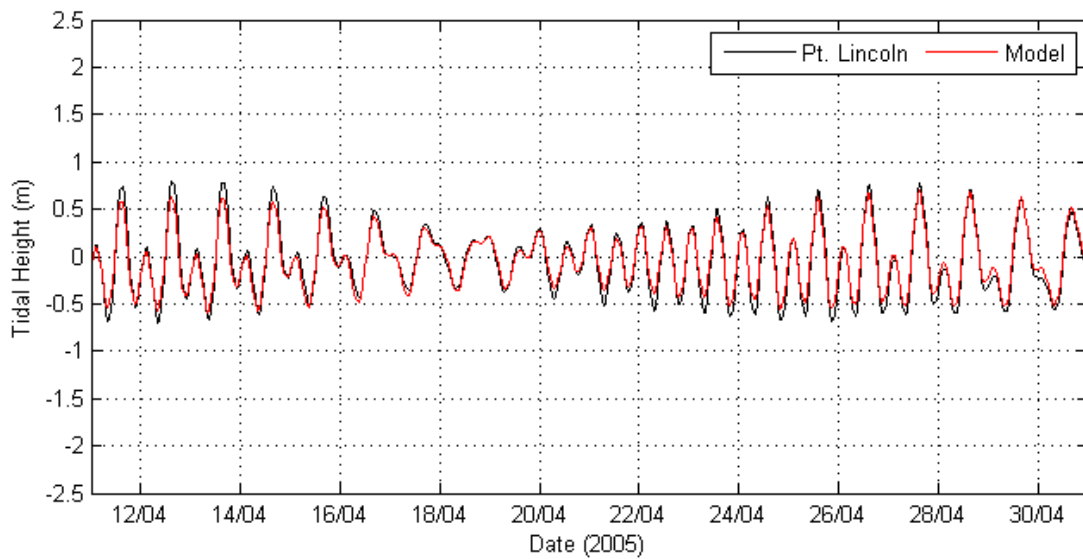
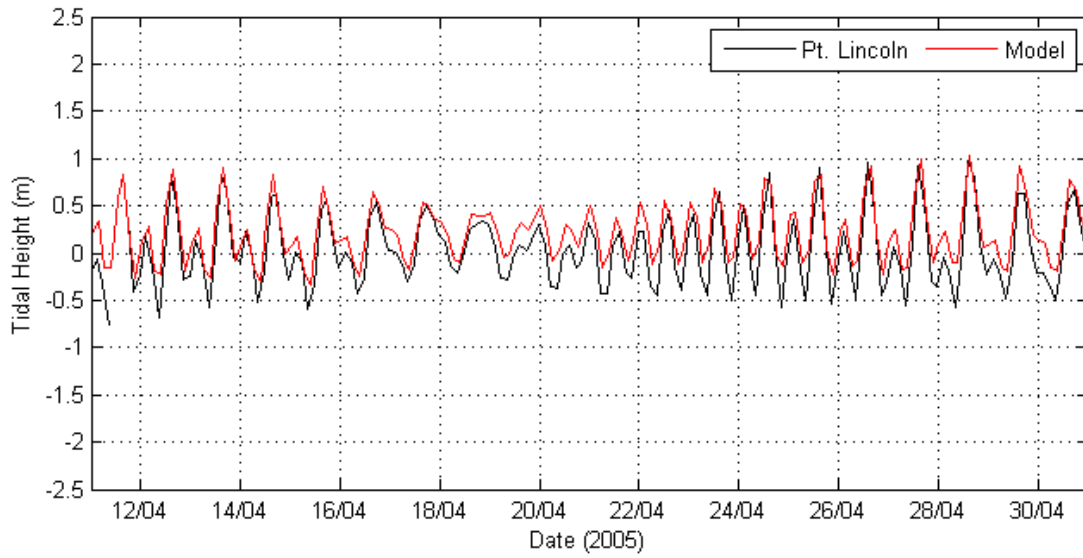


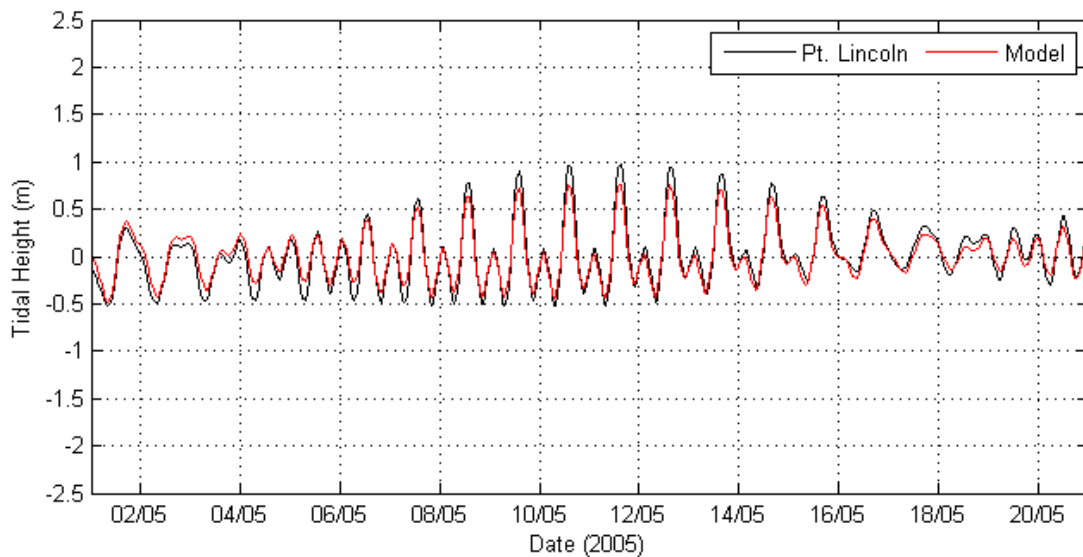
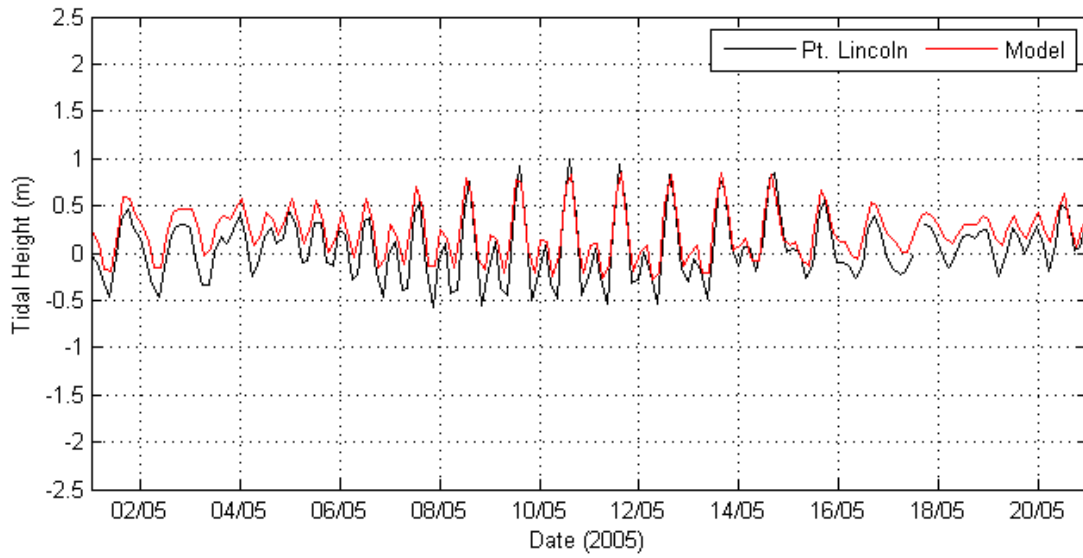


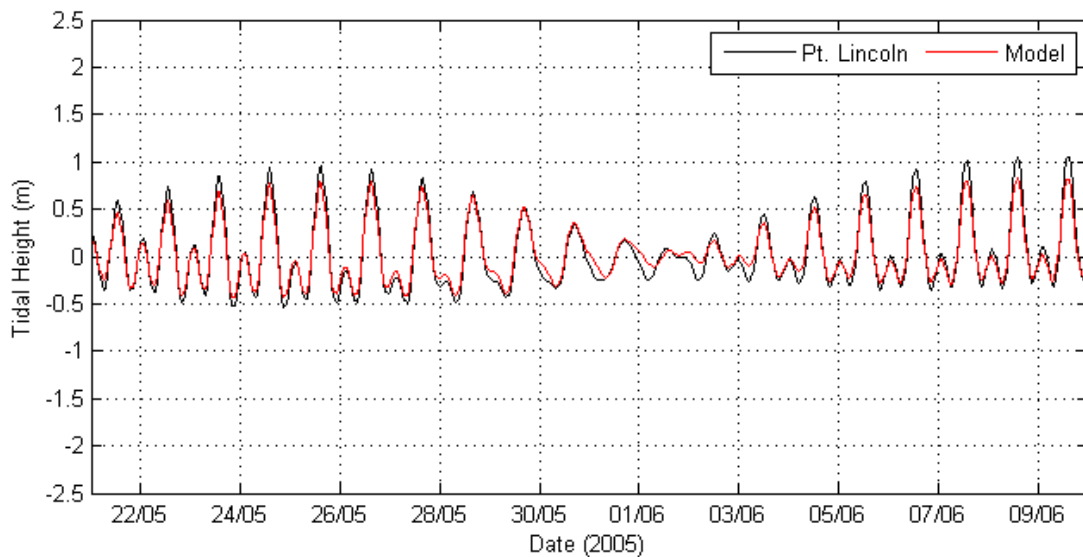
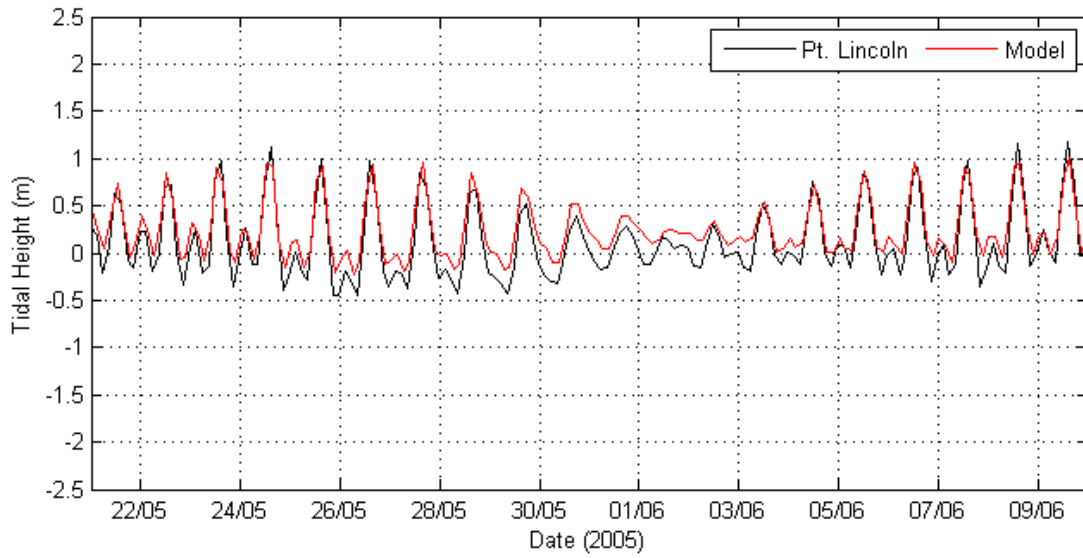


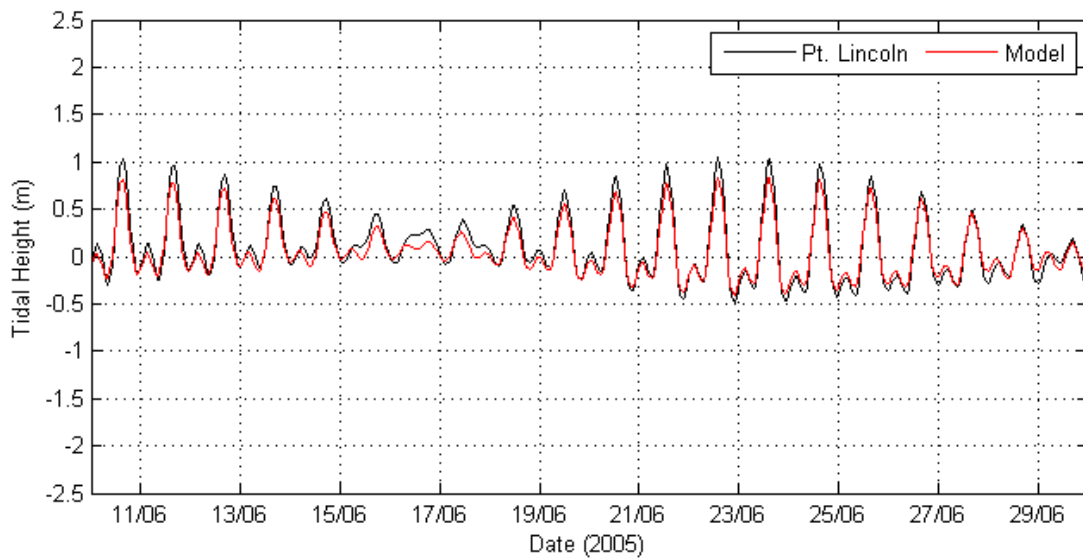
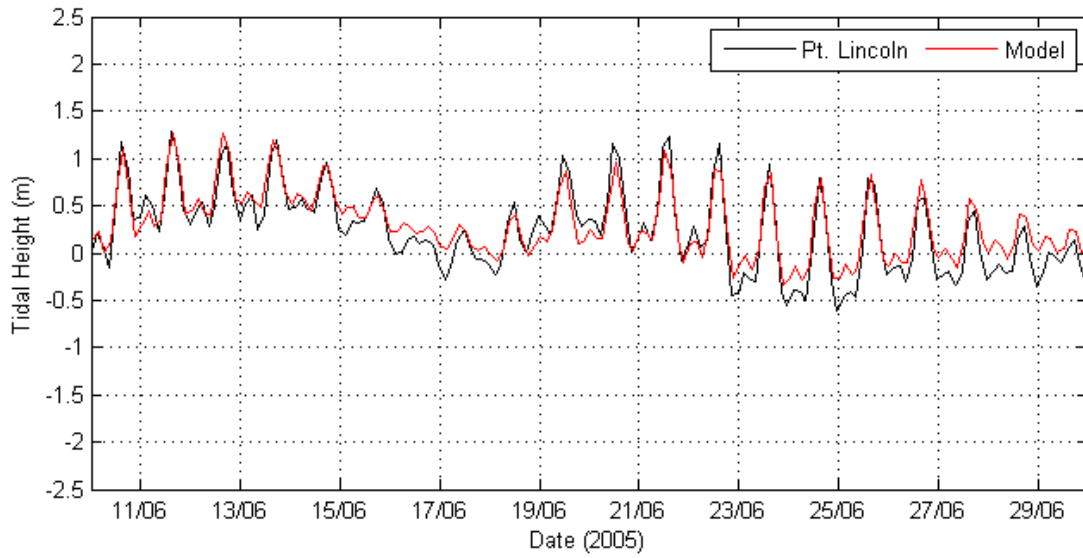


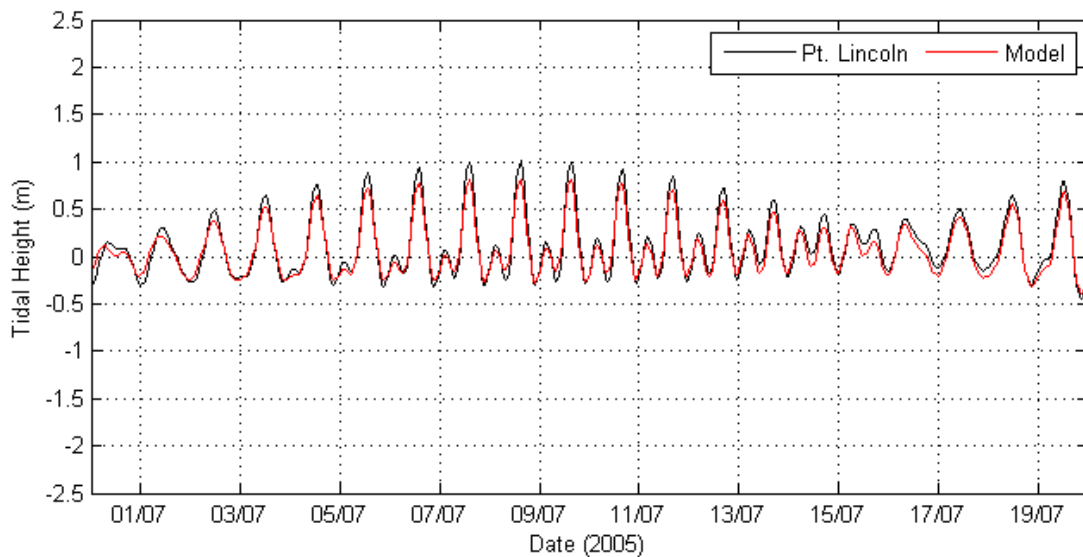
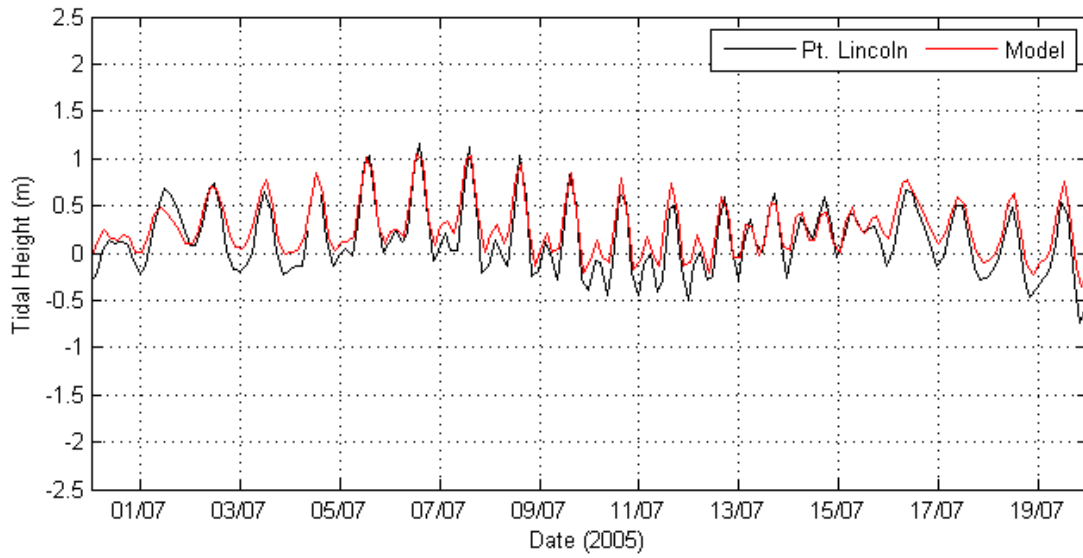


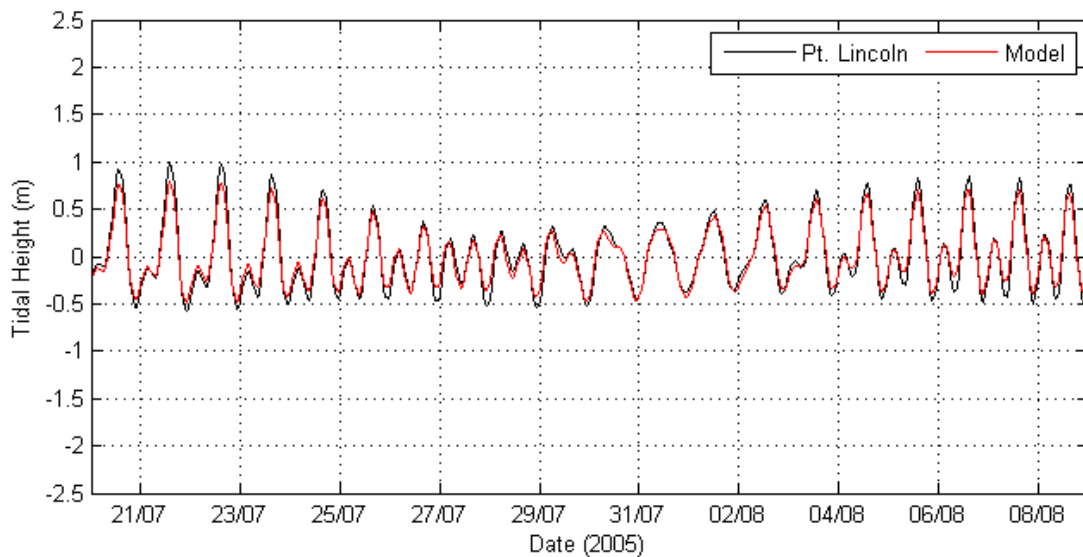
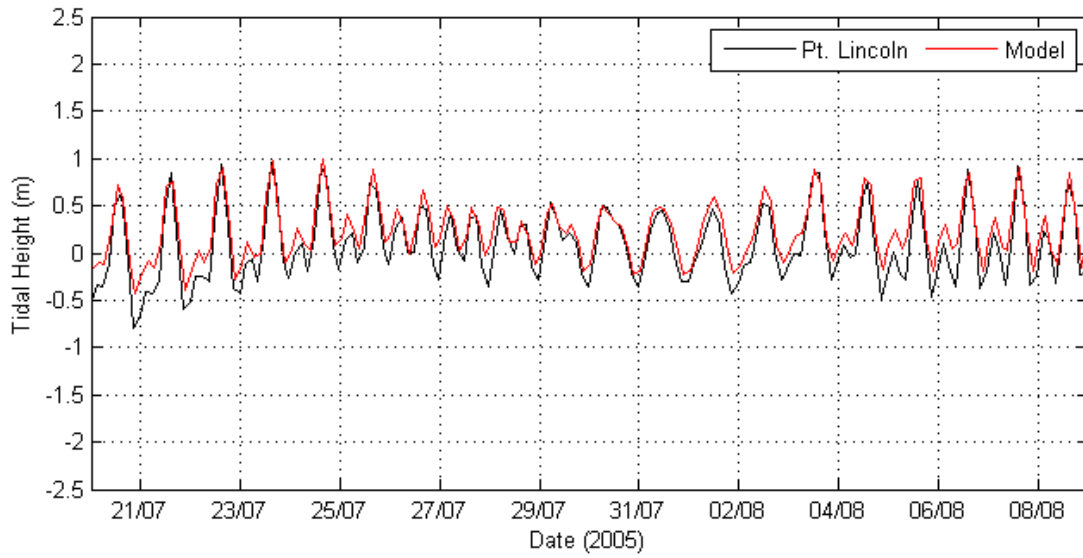


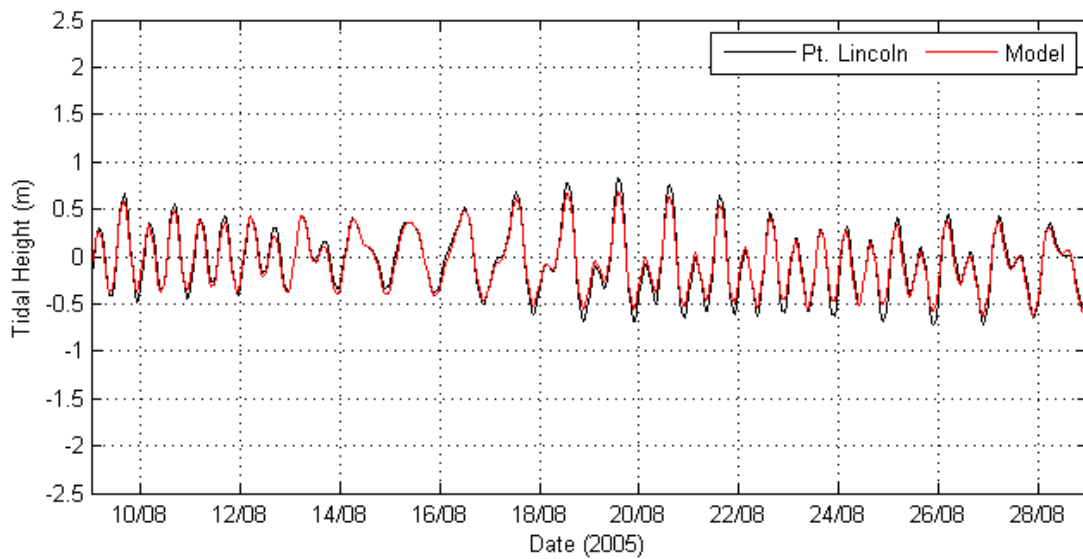
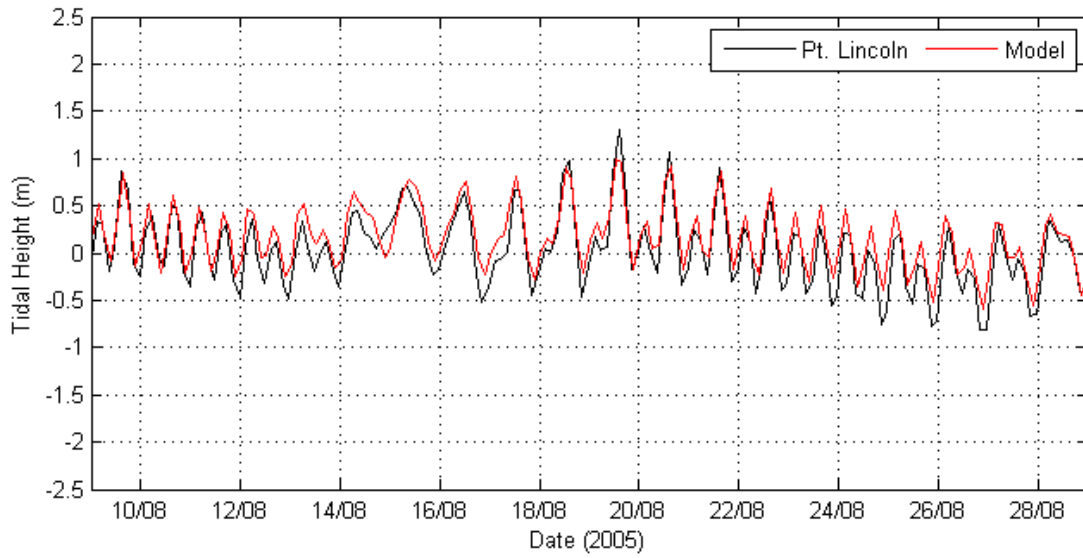




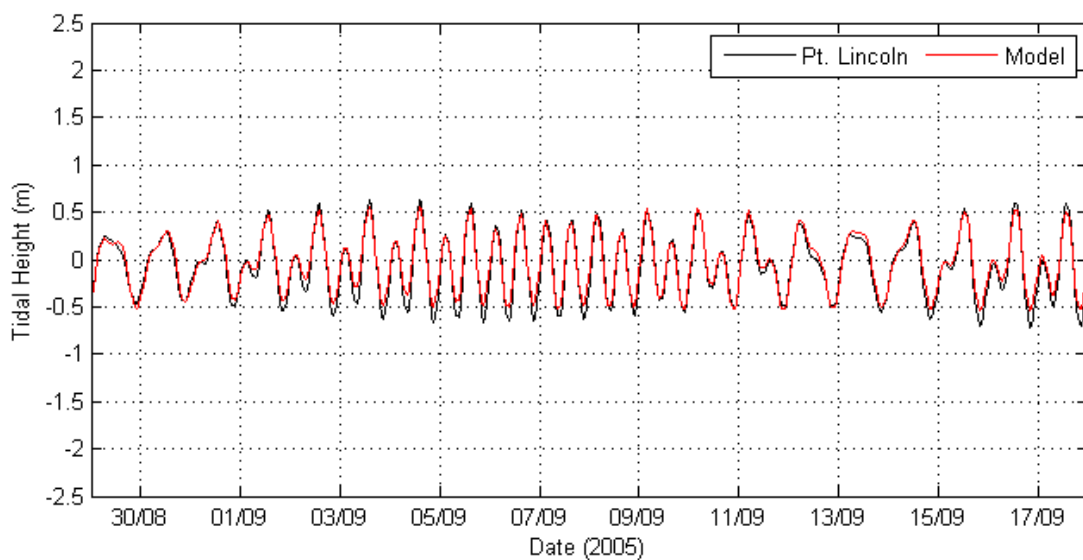
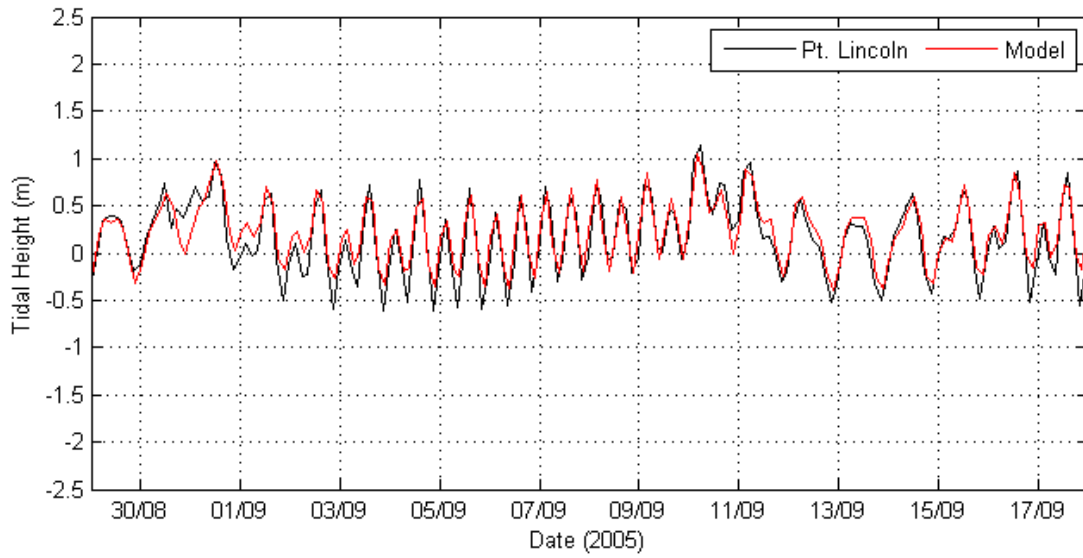


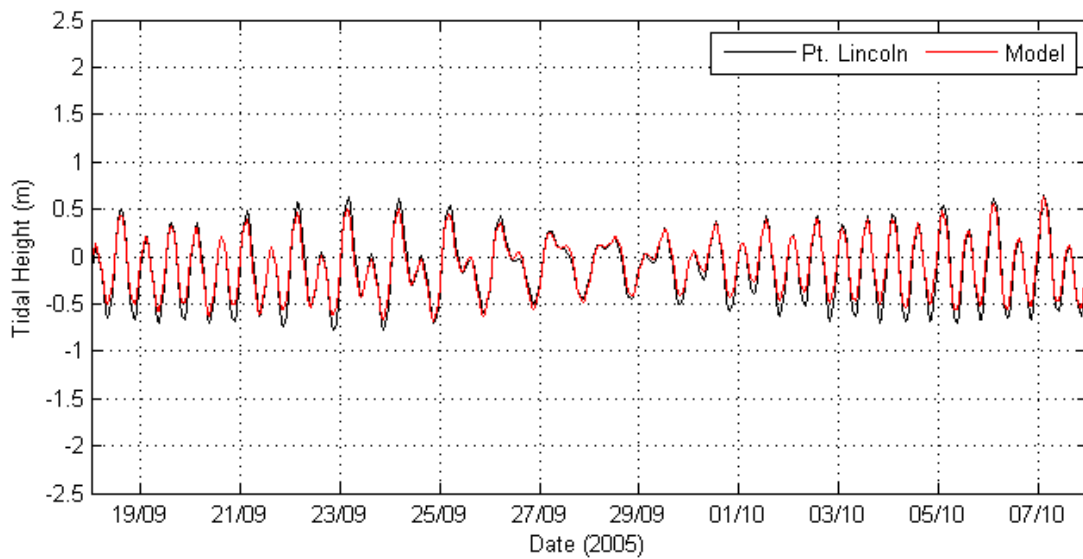
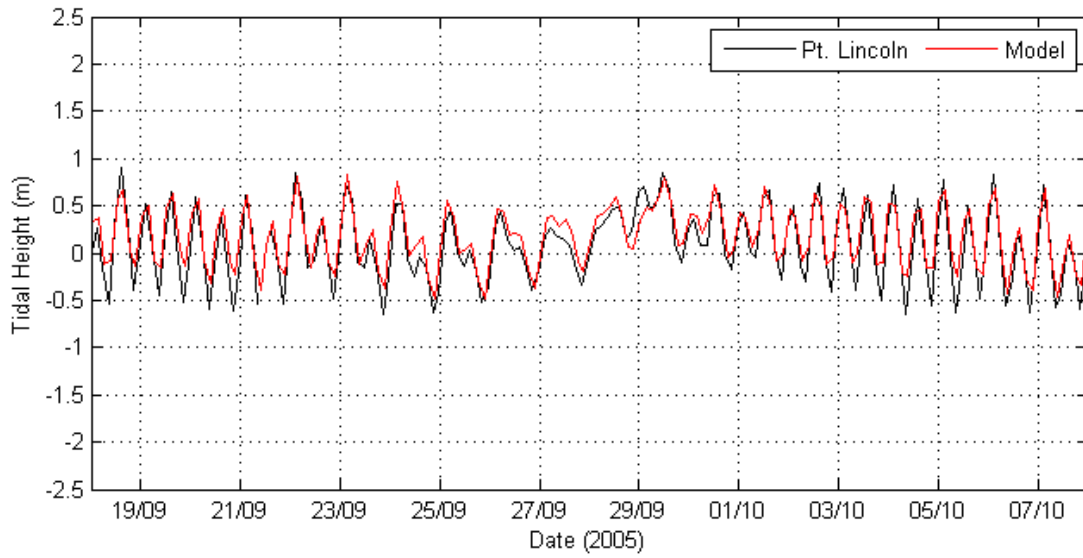


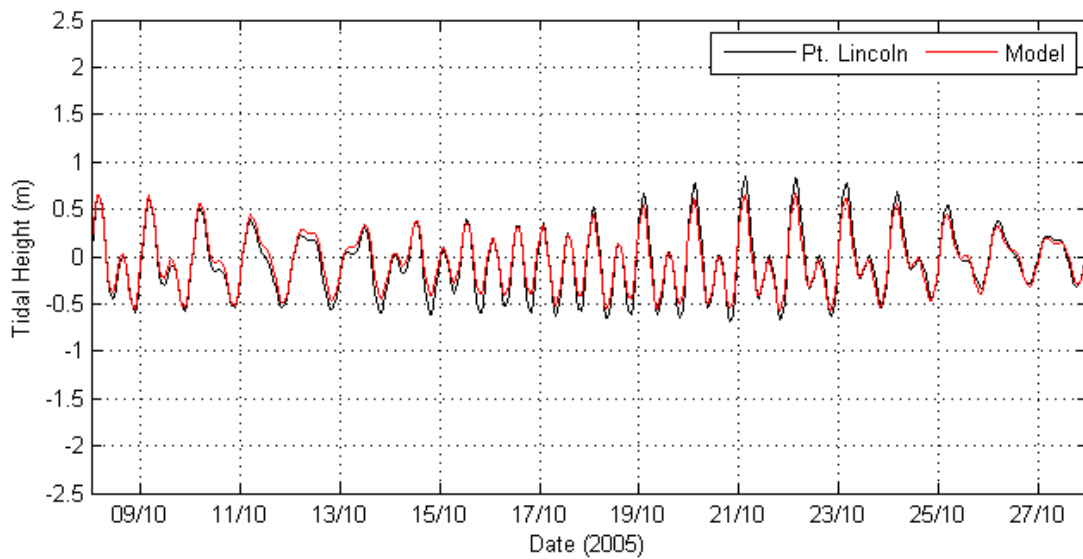
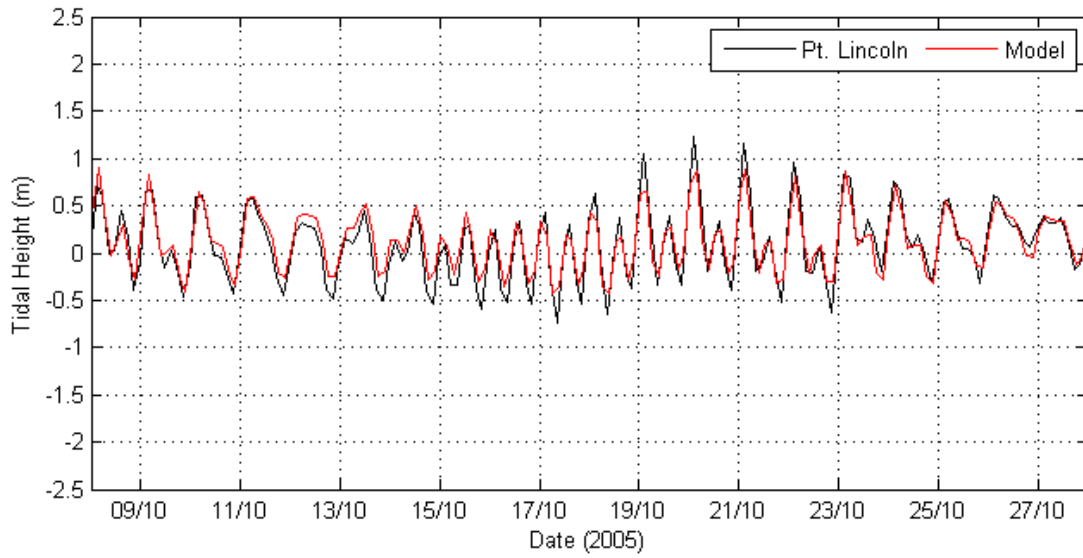


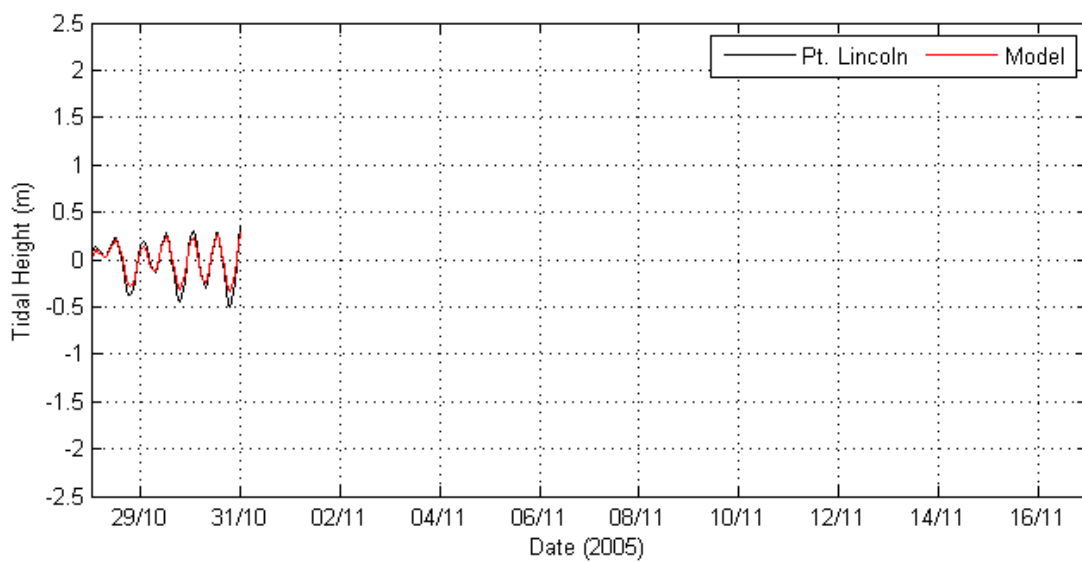
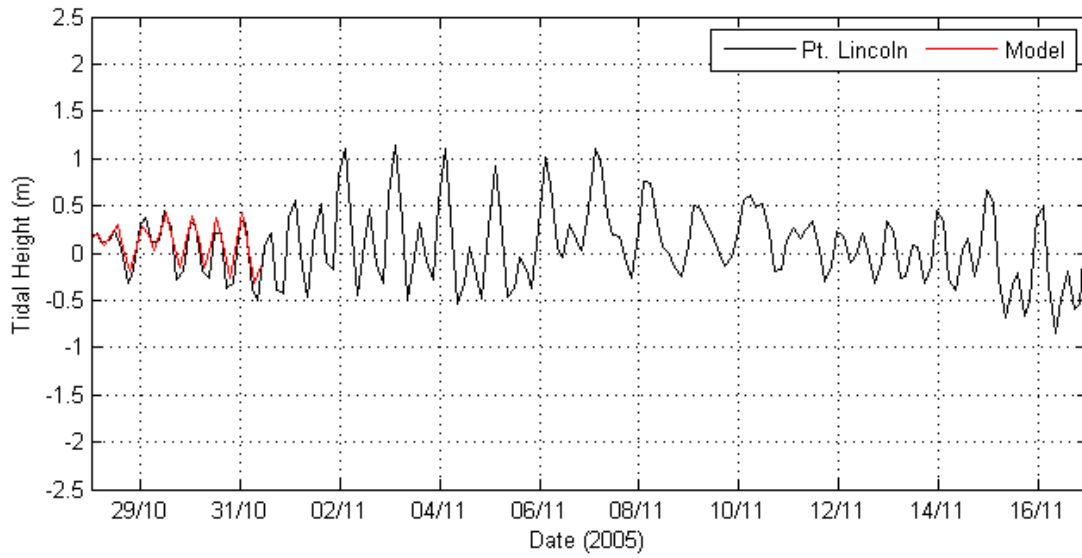




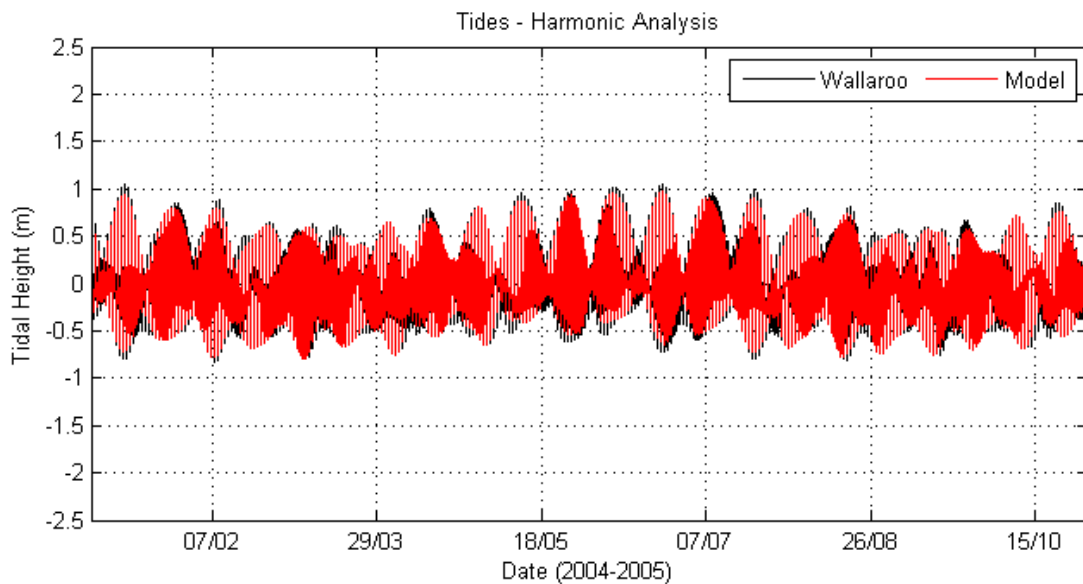
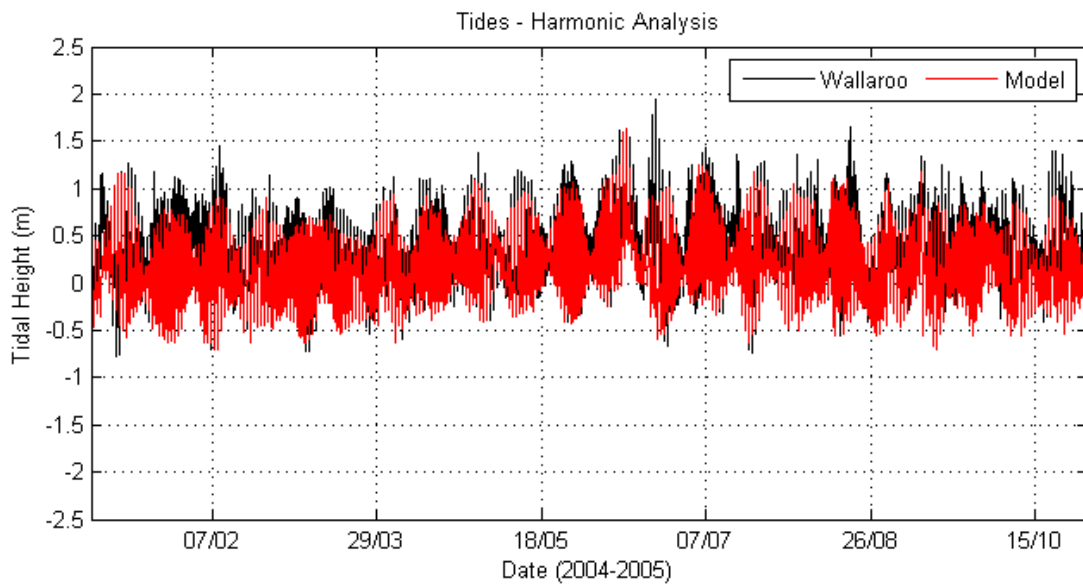


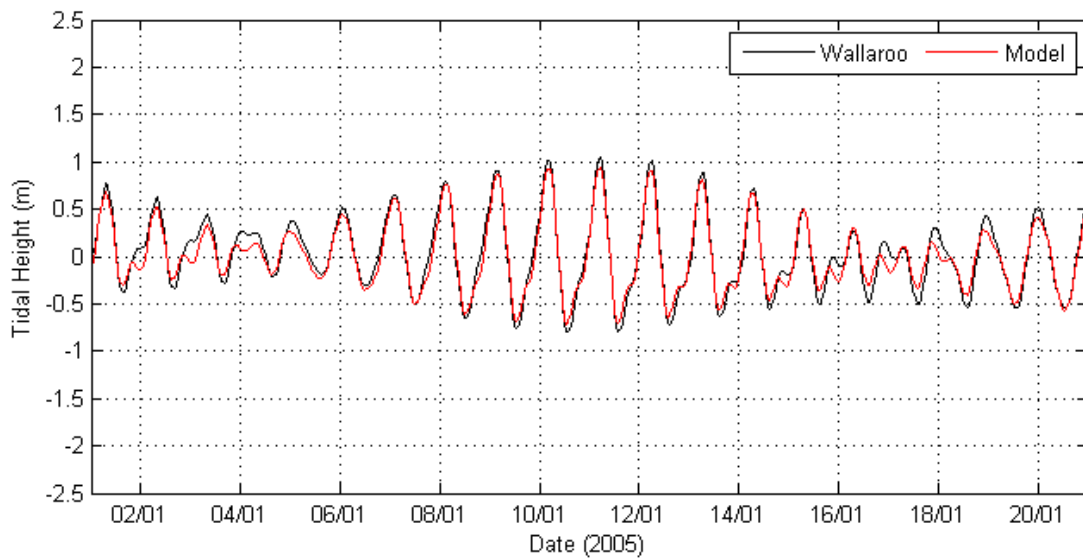
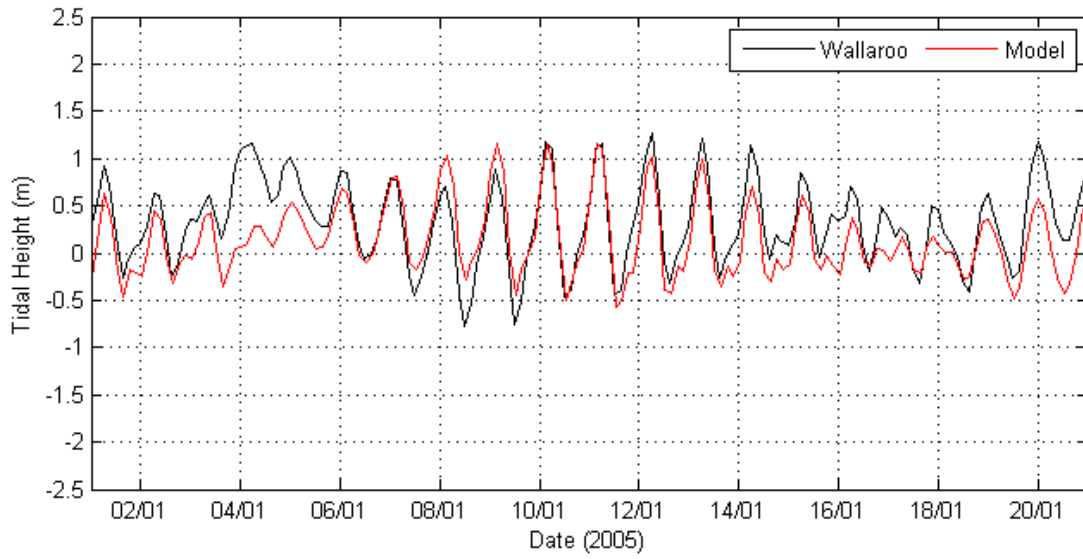


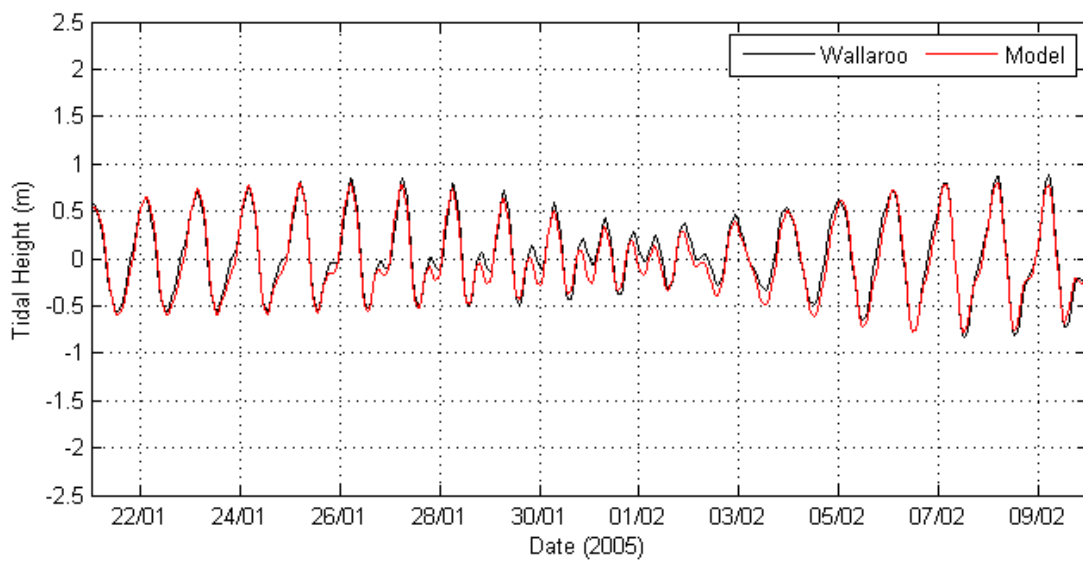
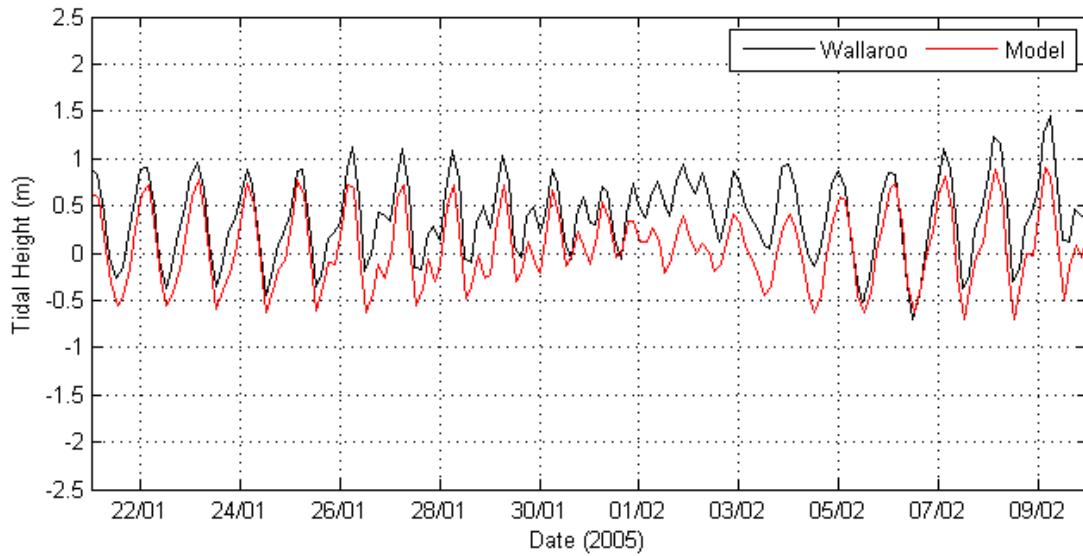


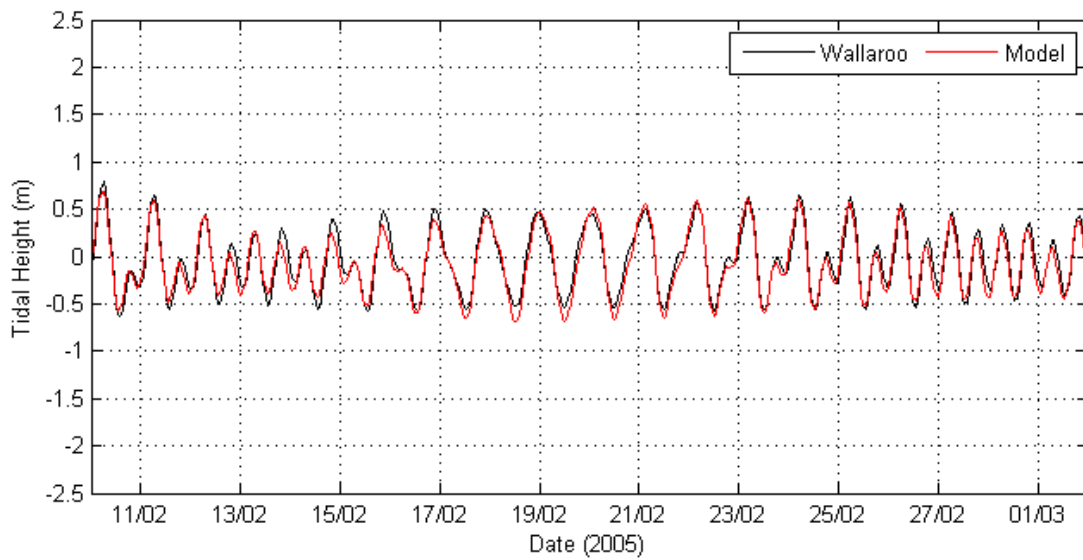
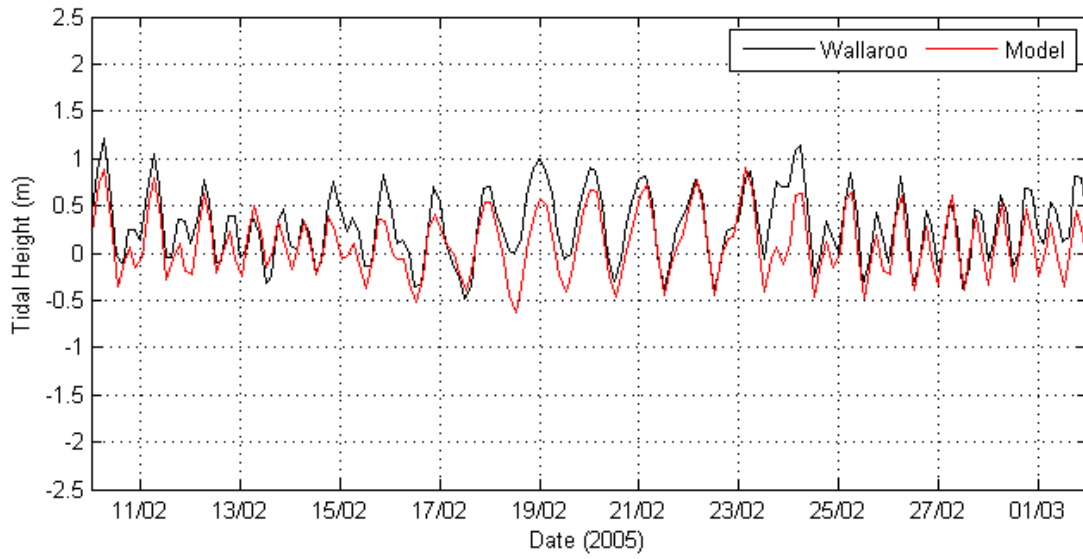


**Wallaroo**

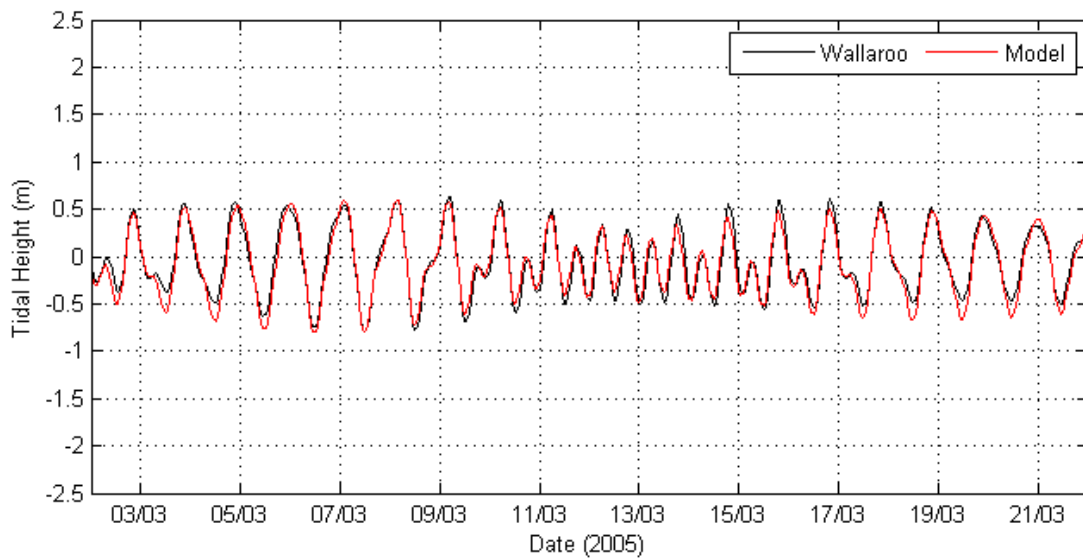
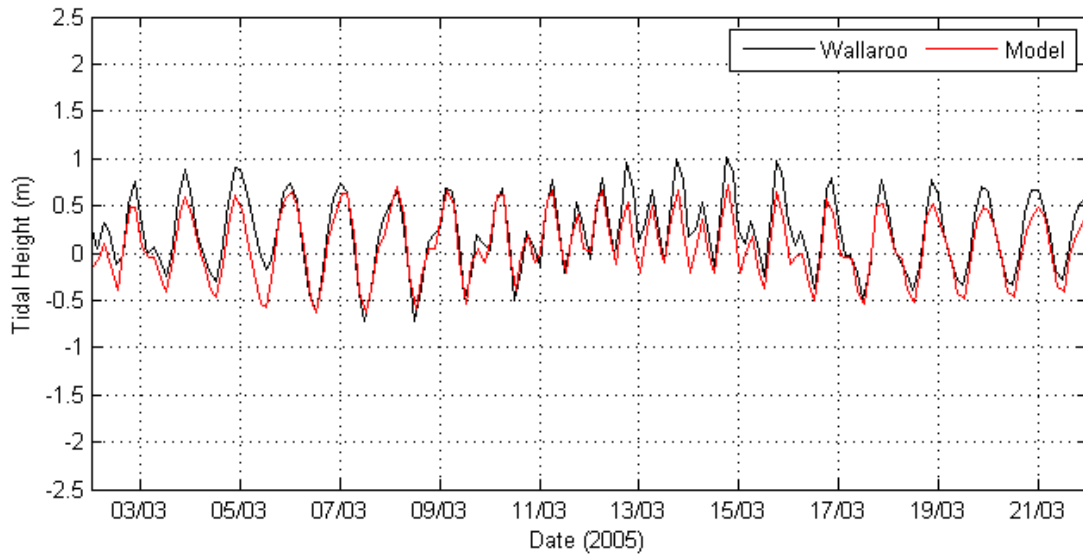


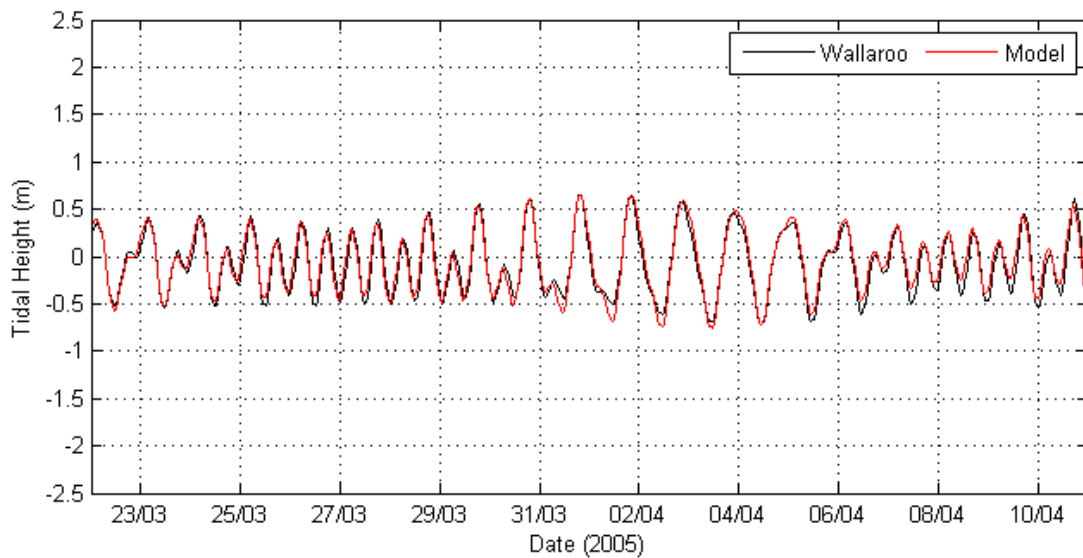
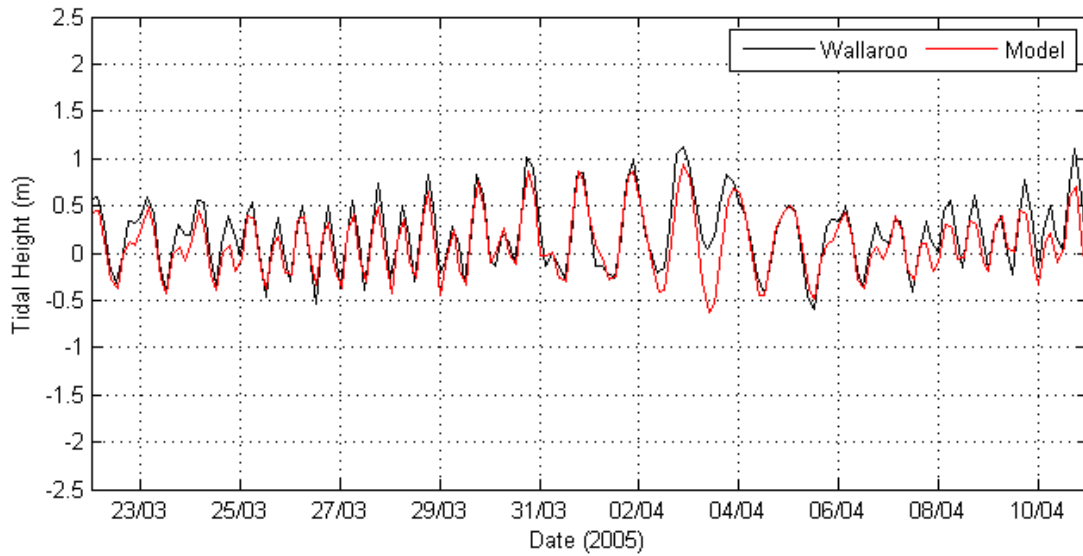


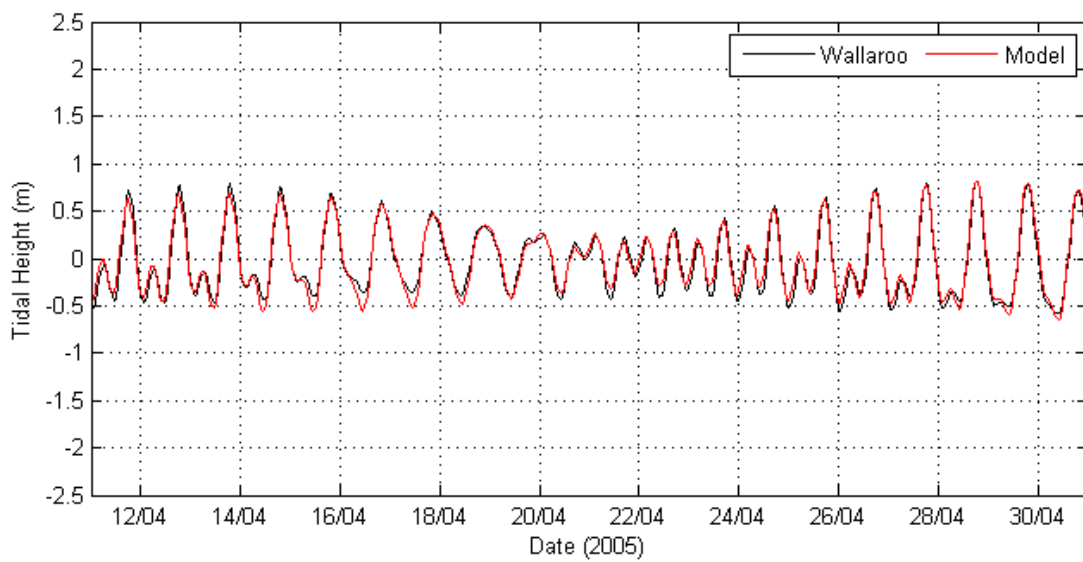
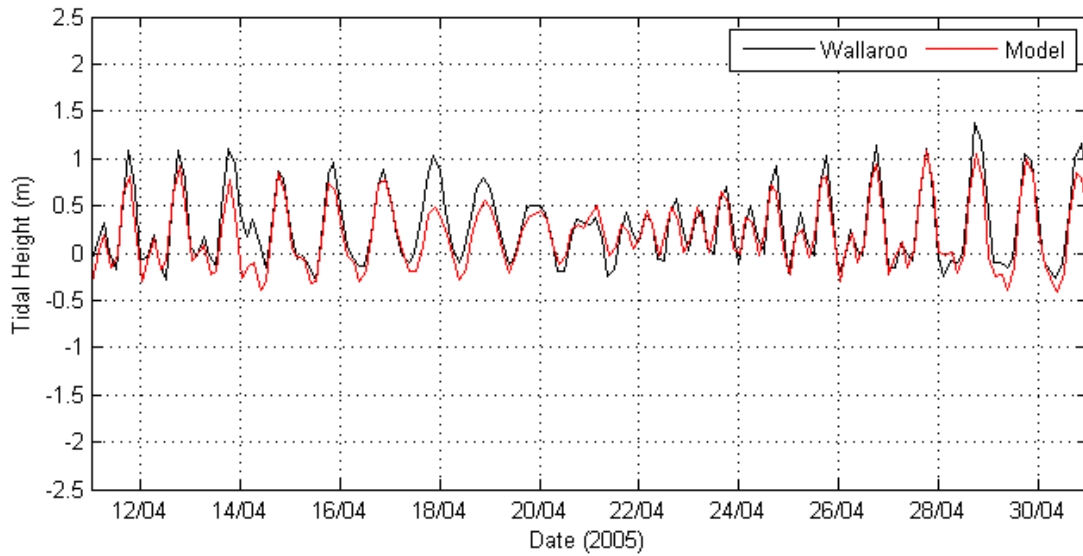


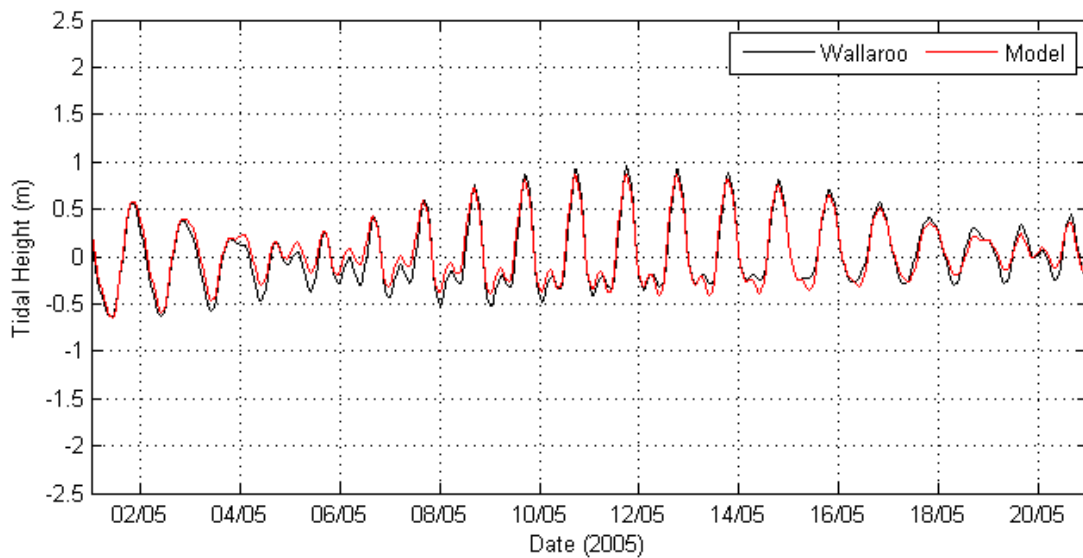
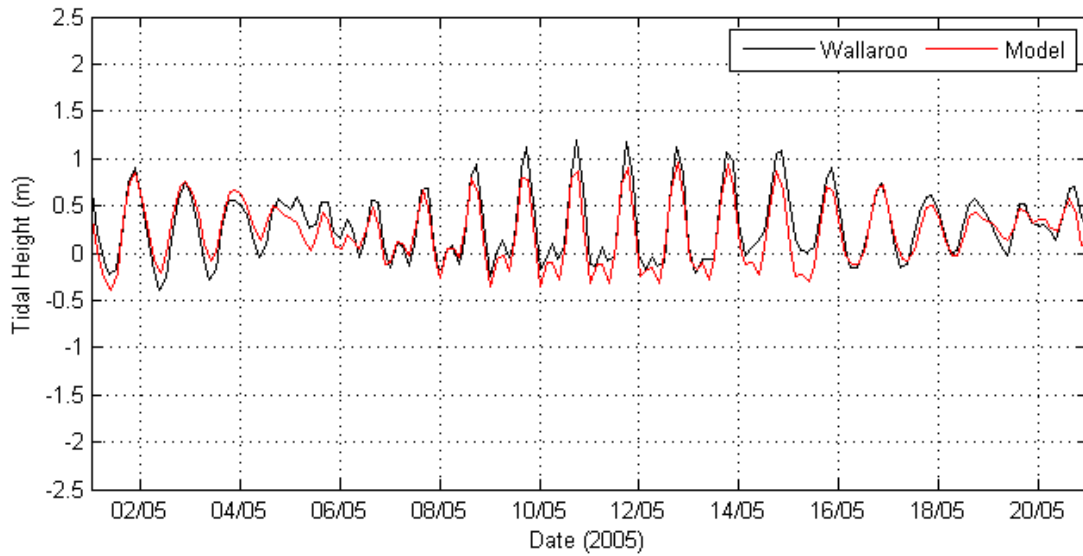


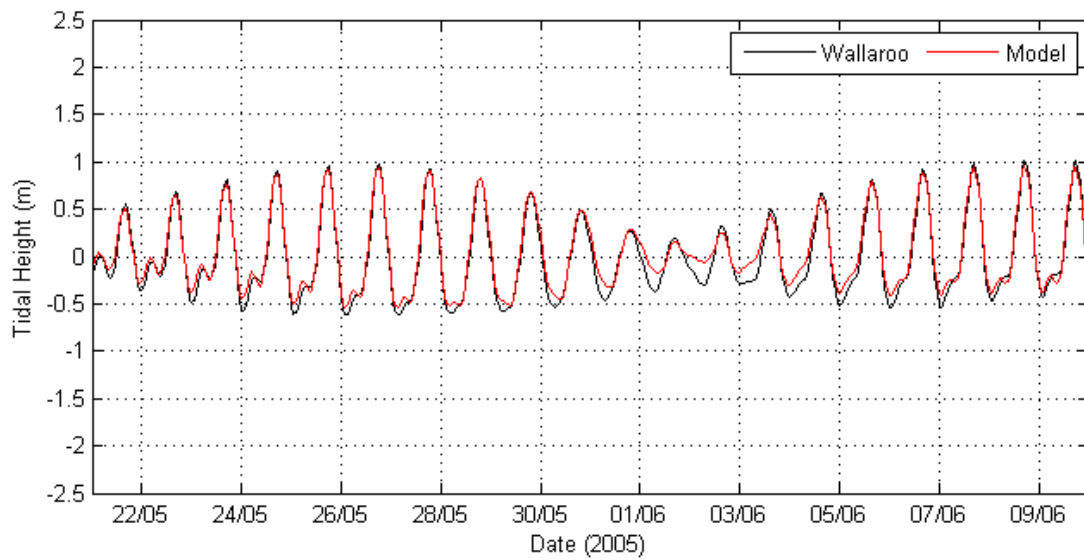
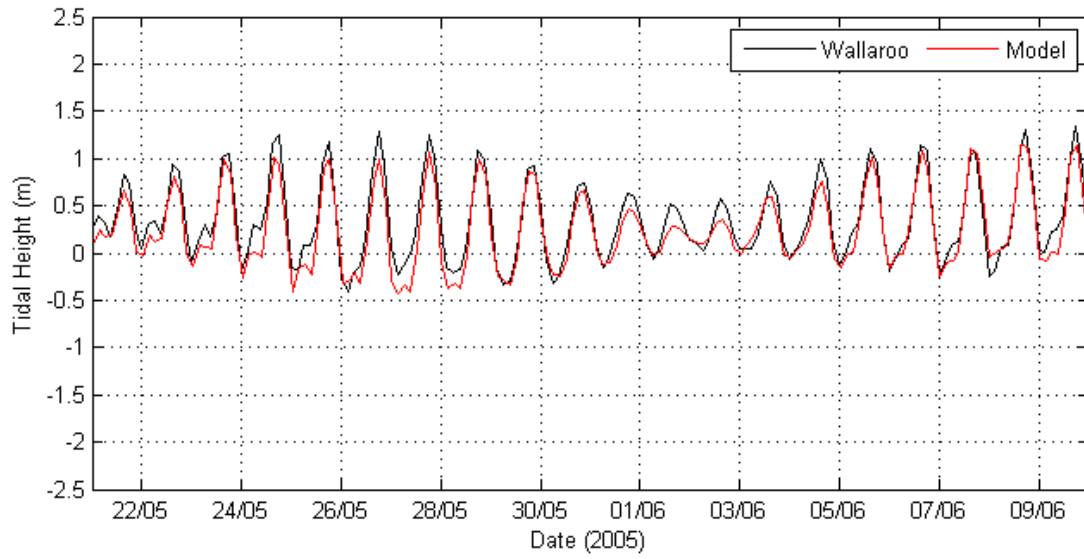


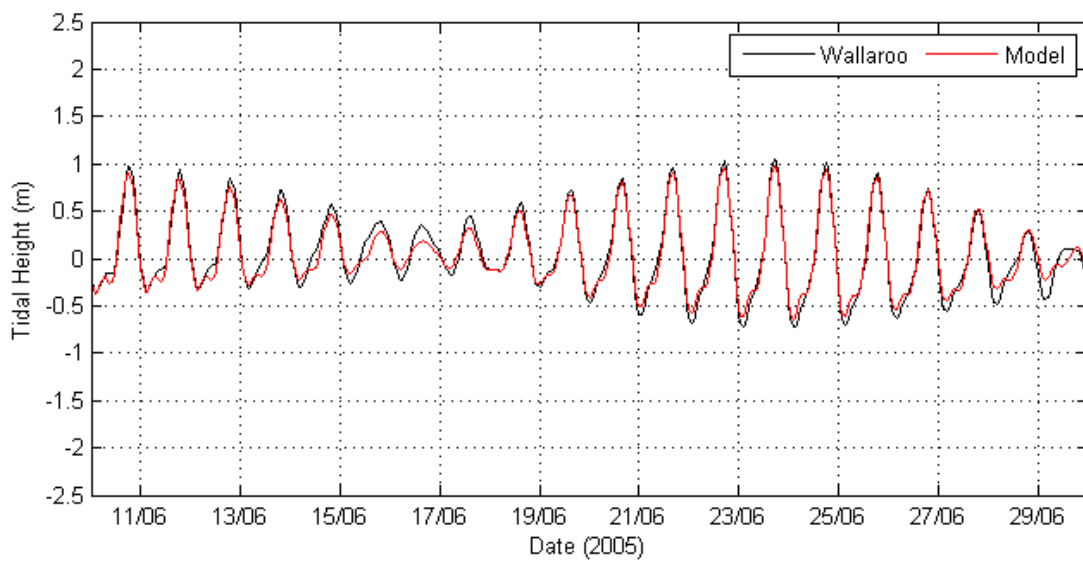
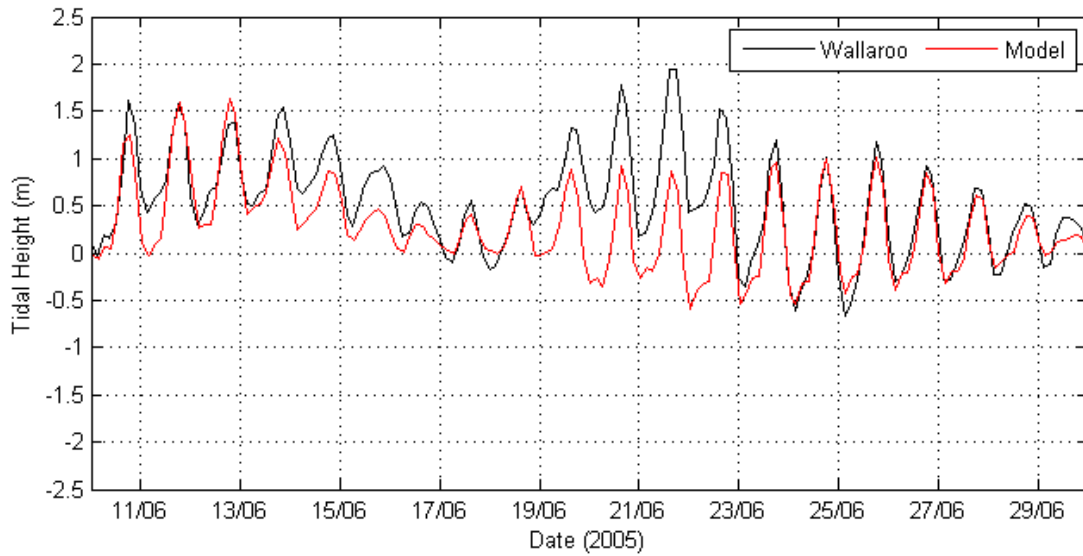


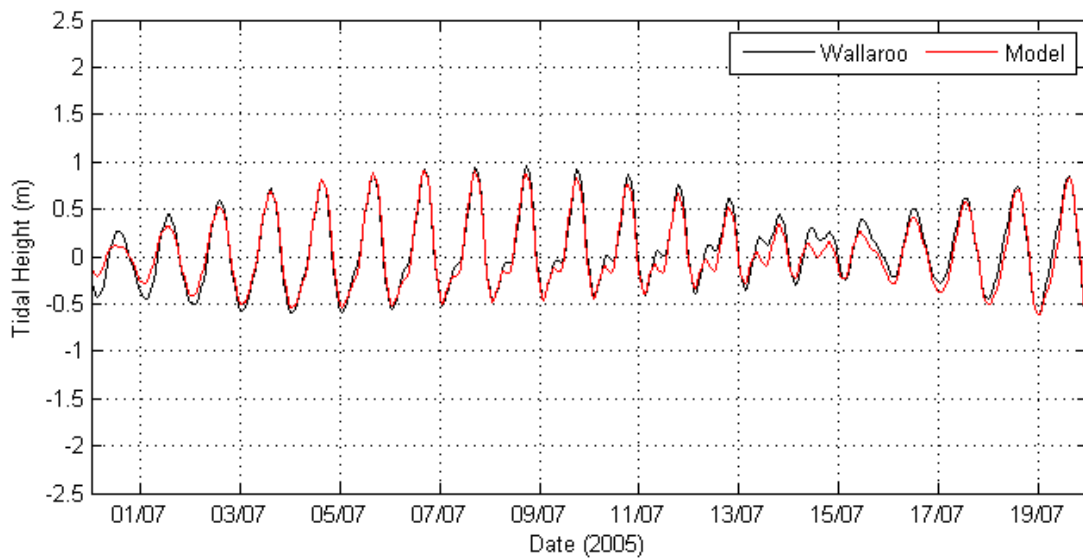
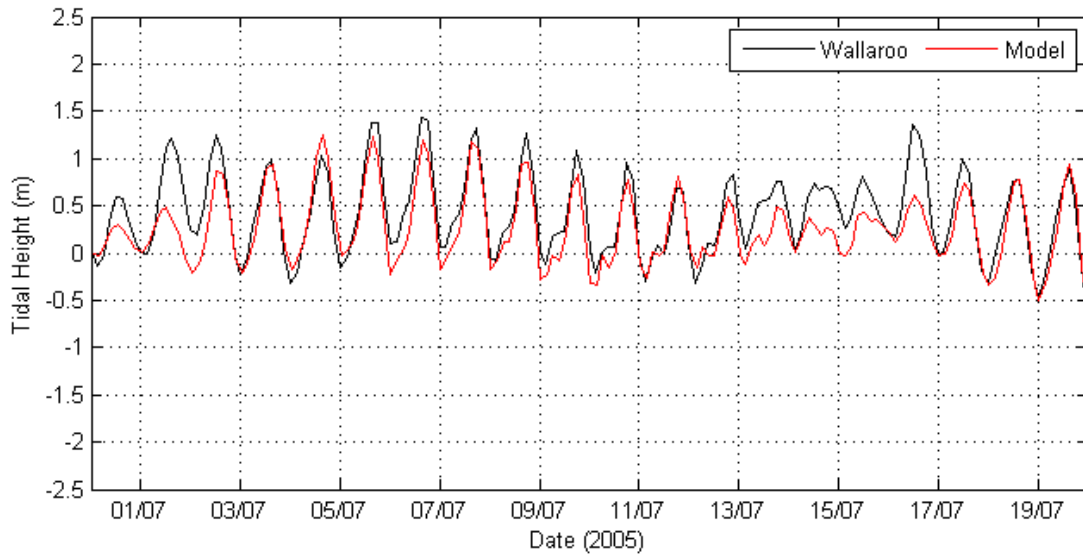


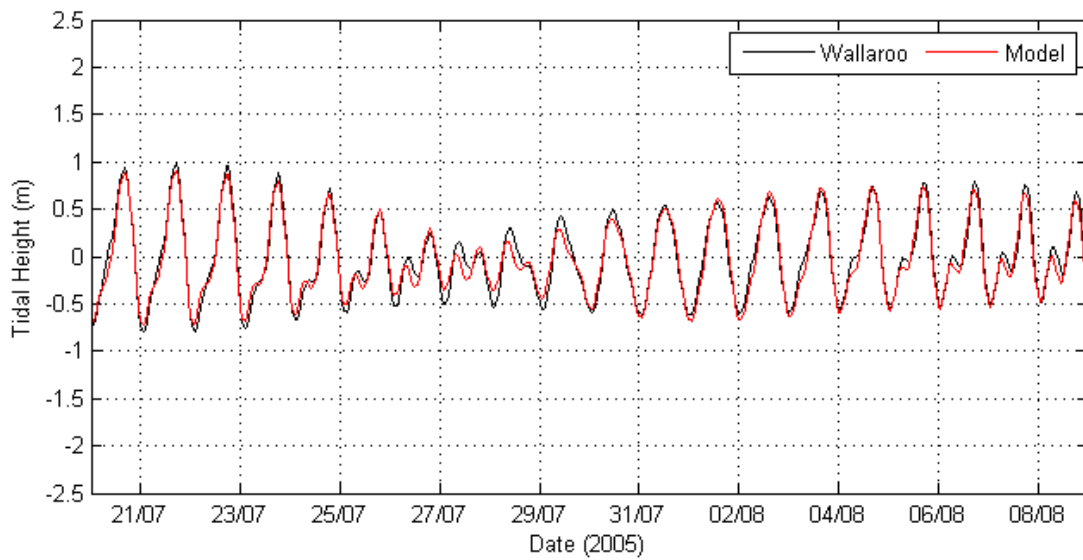
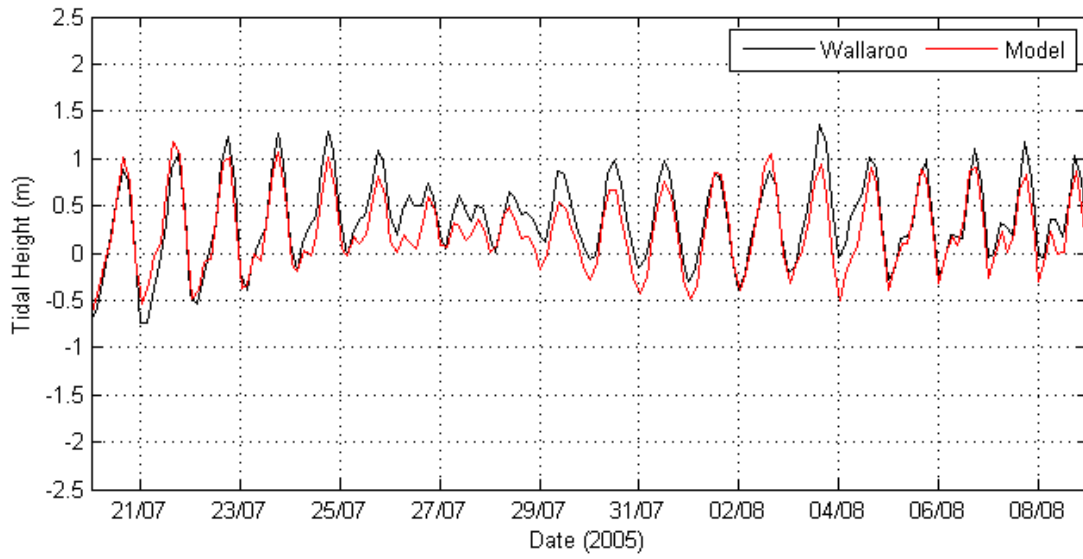




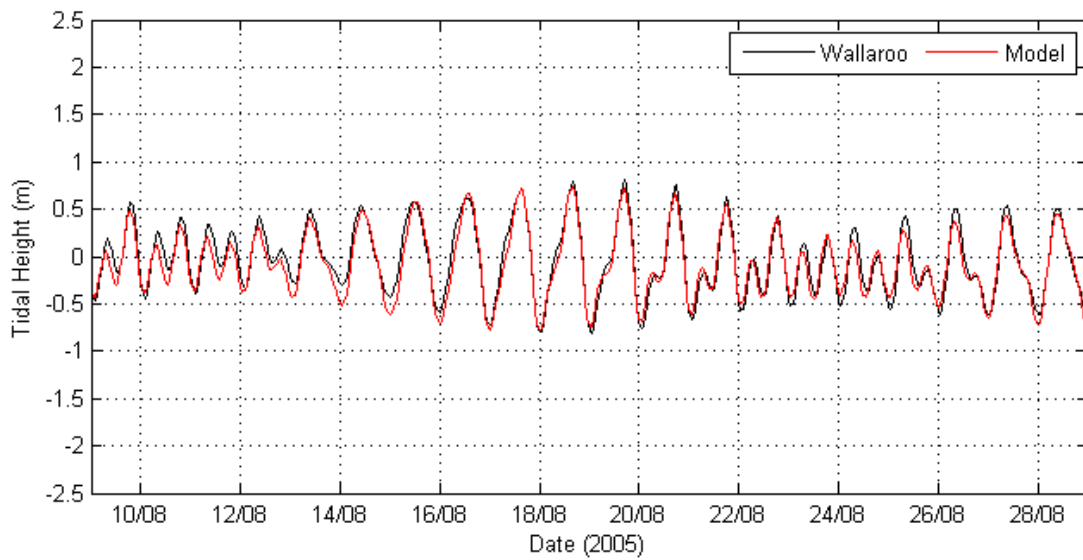
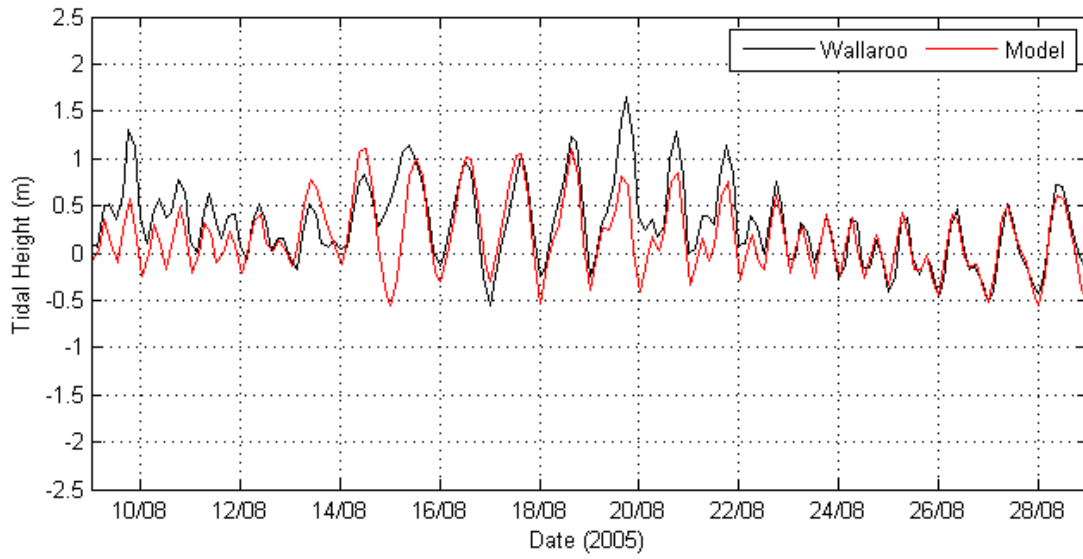


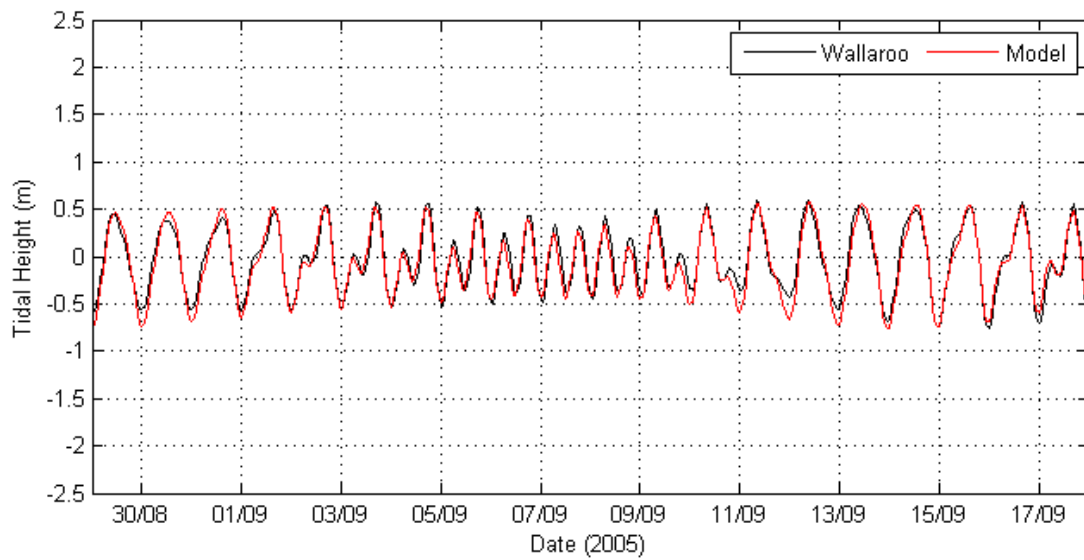
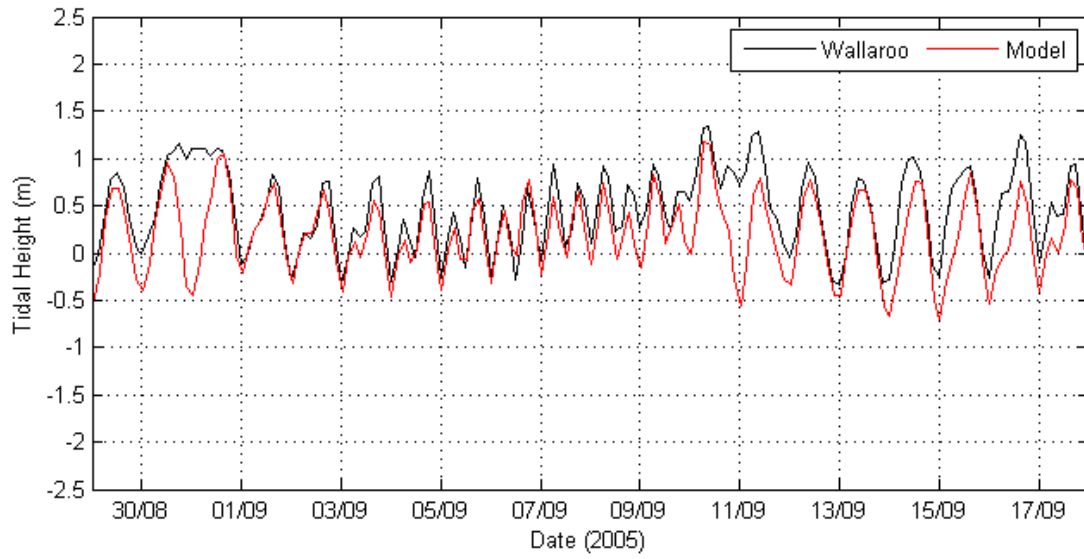


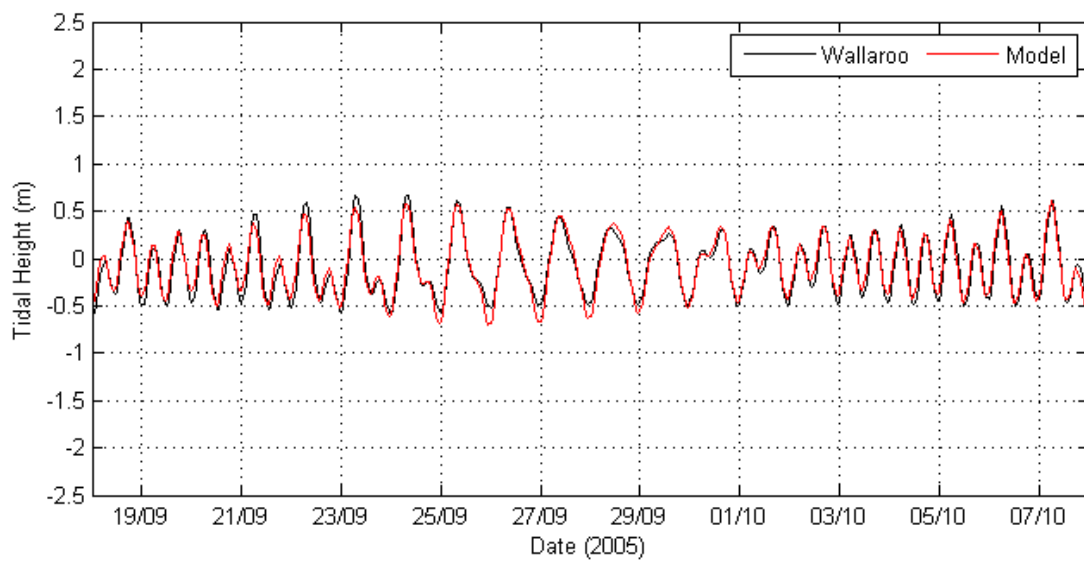
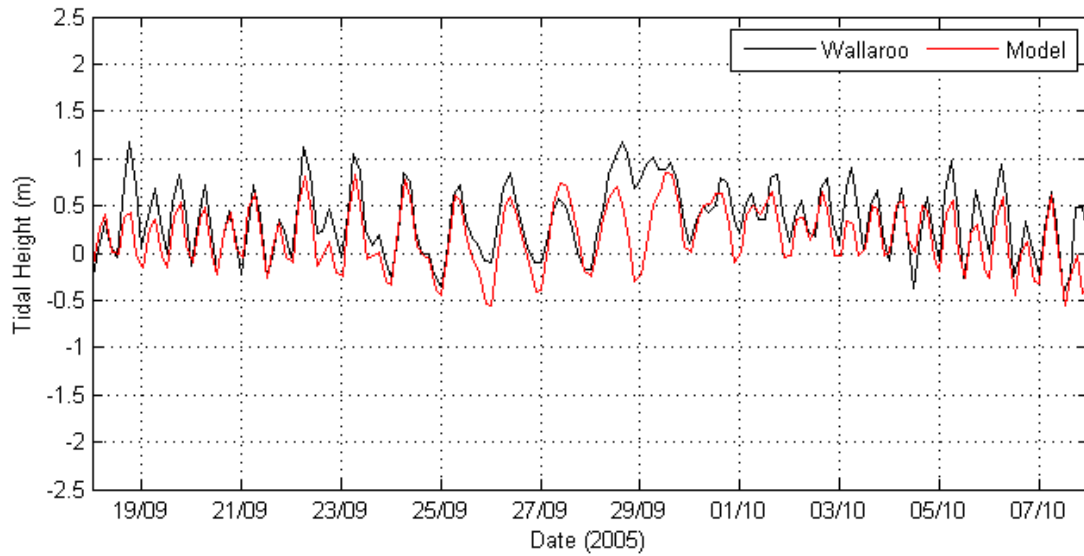


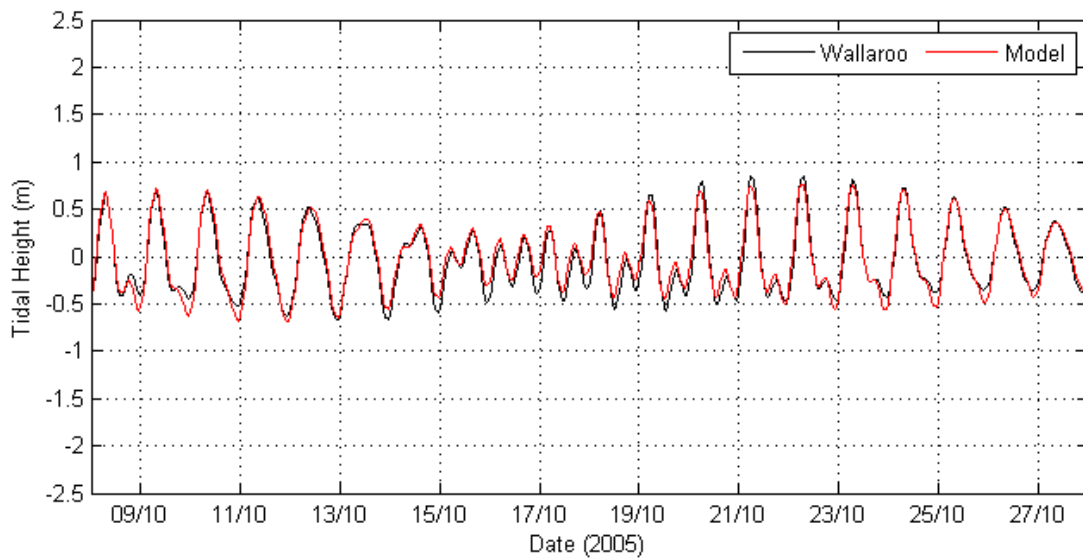
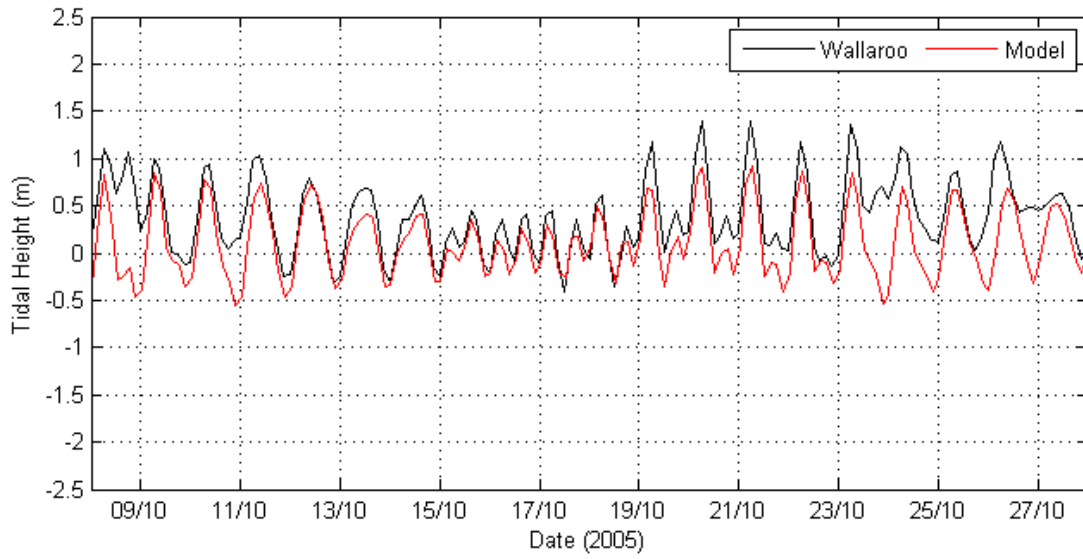


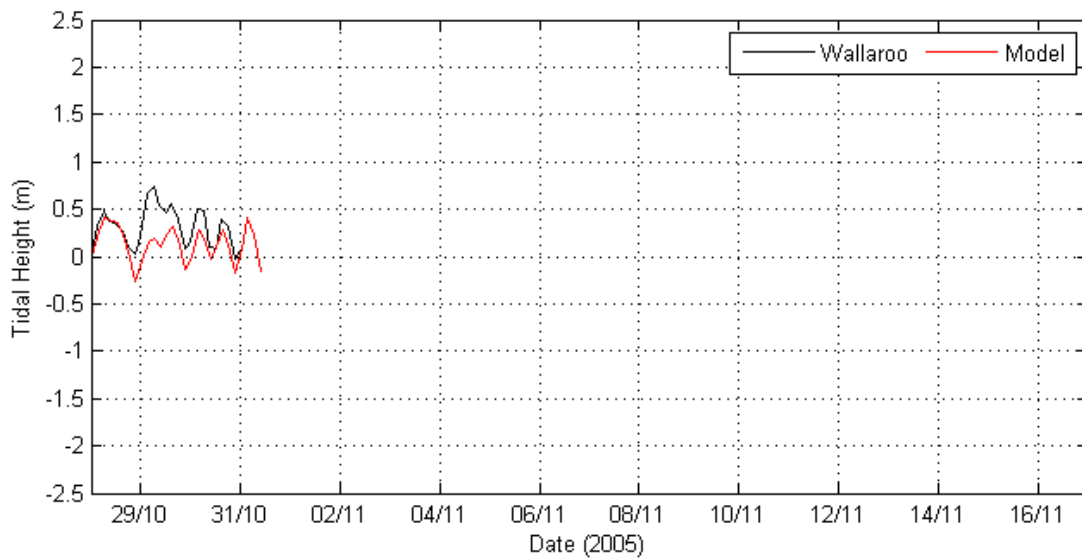
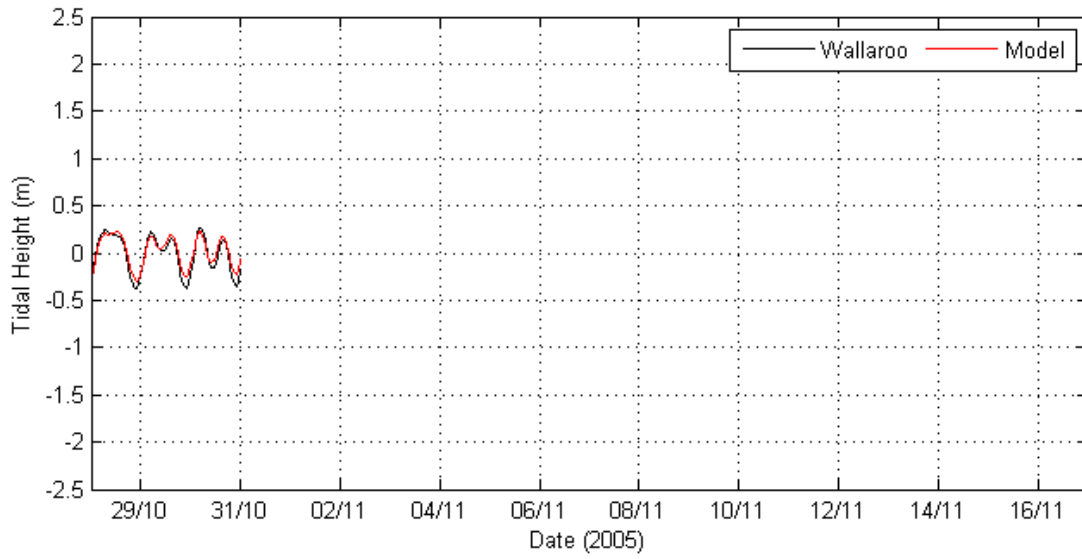




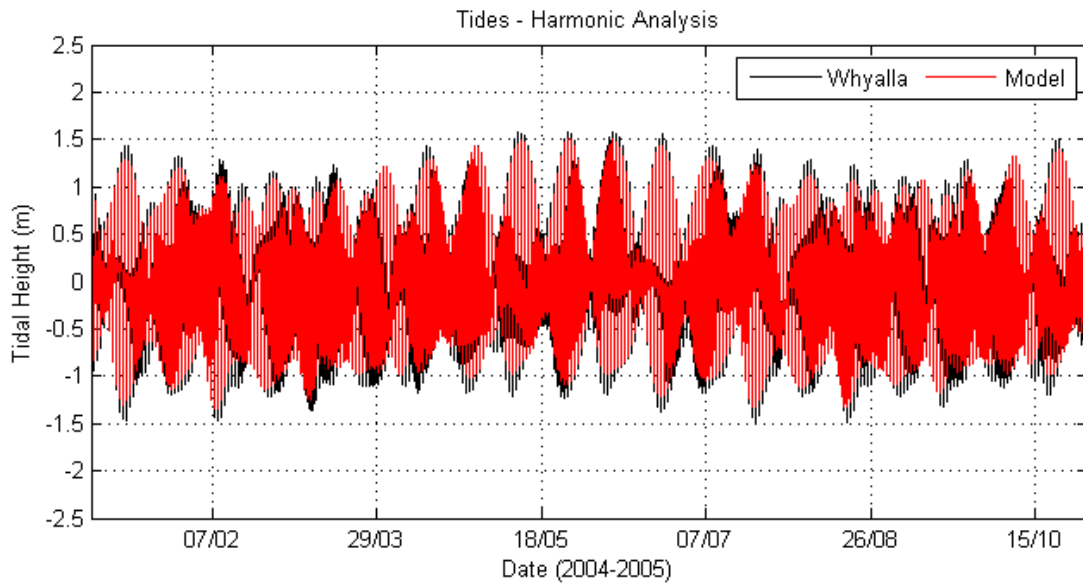
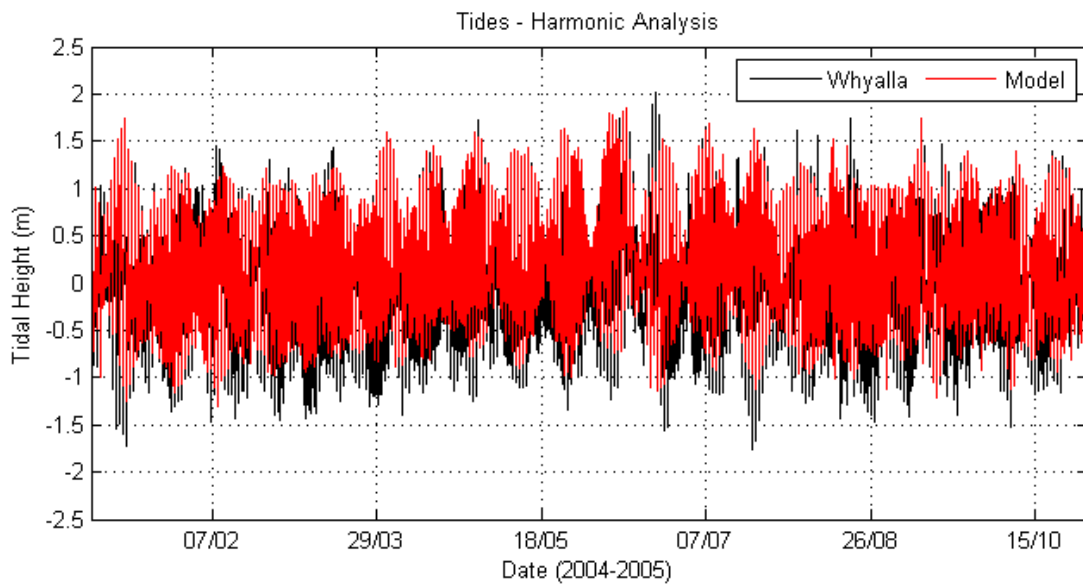


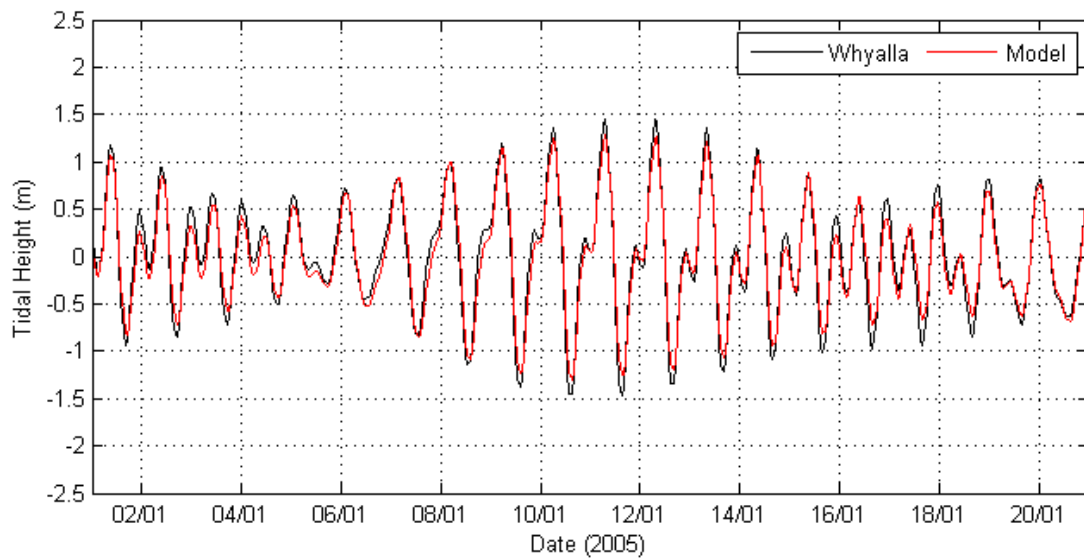
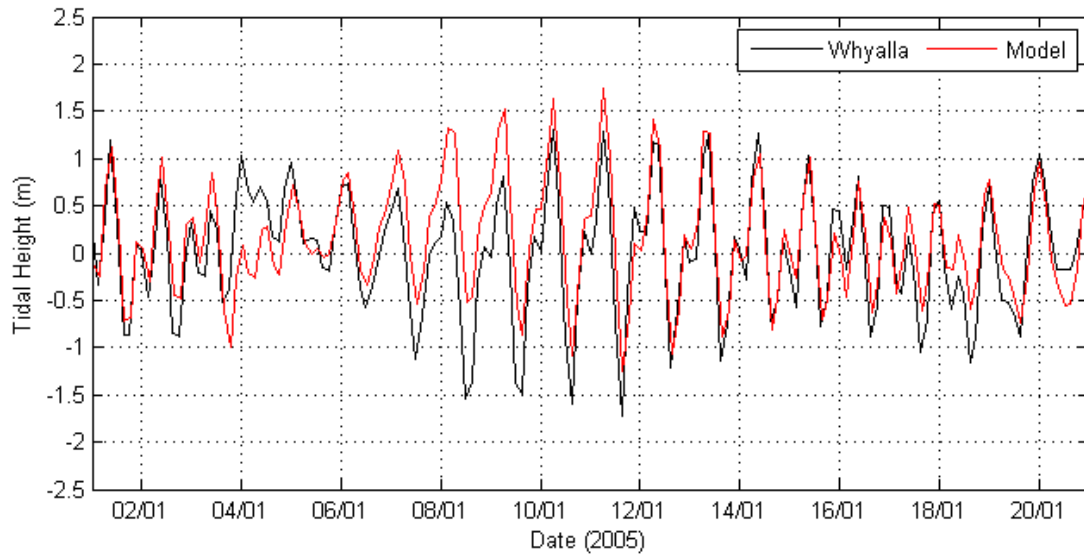


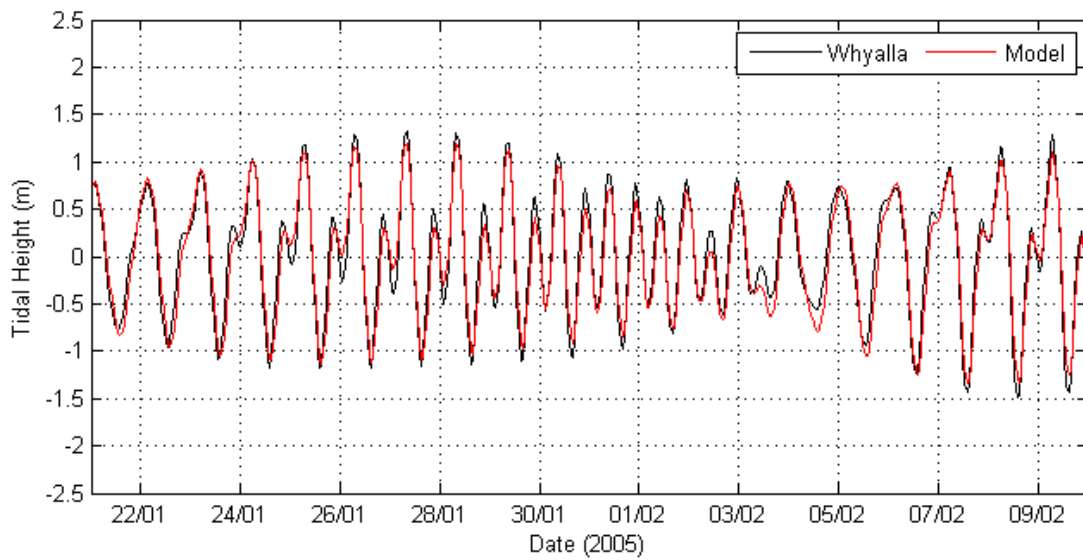
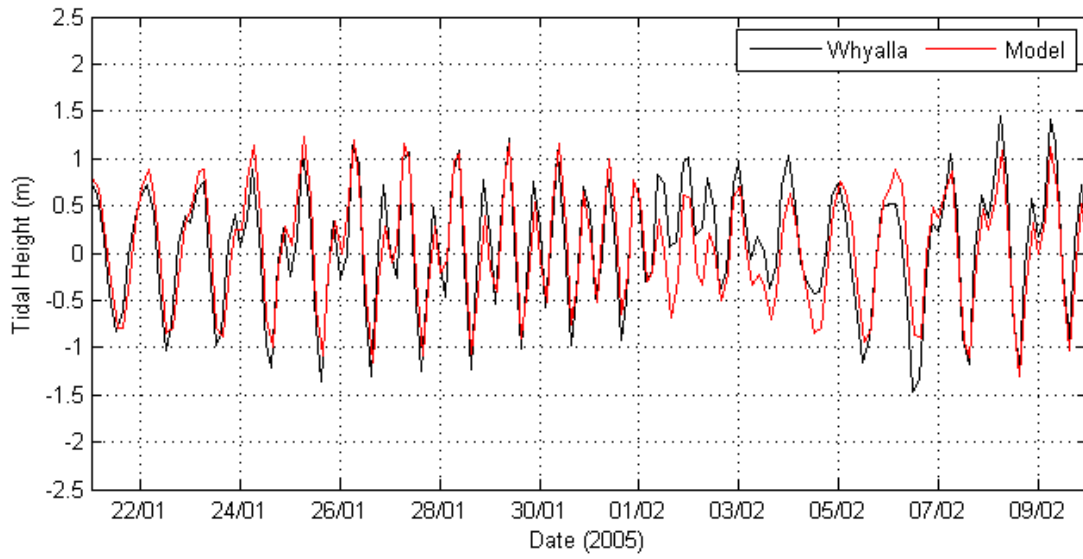




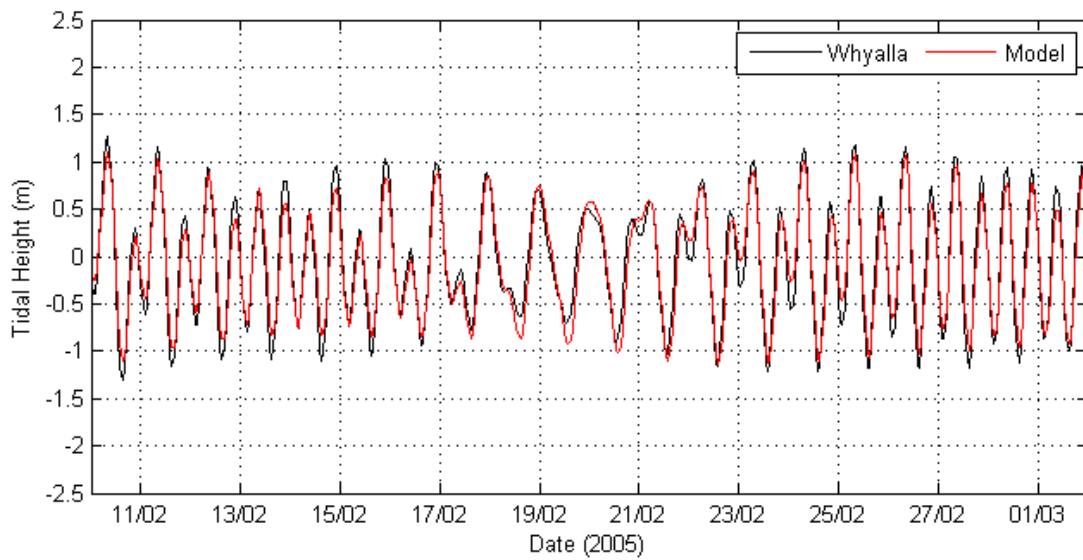
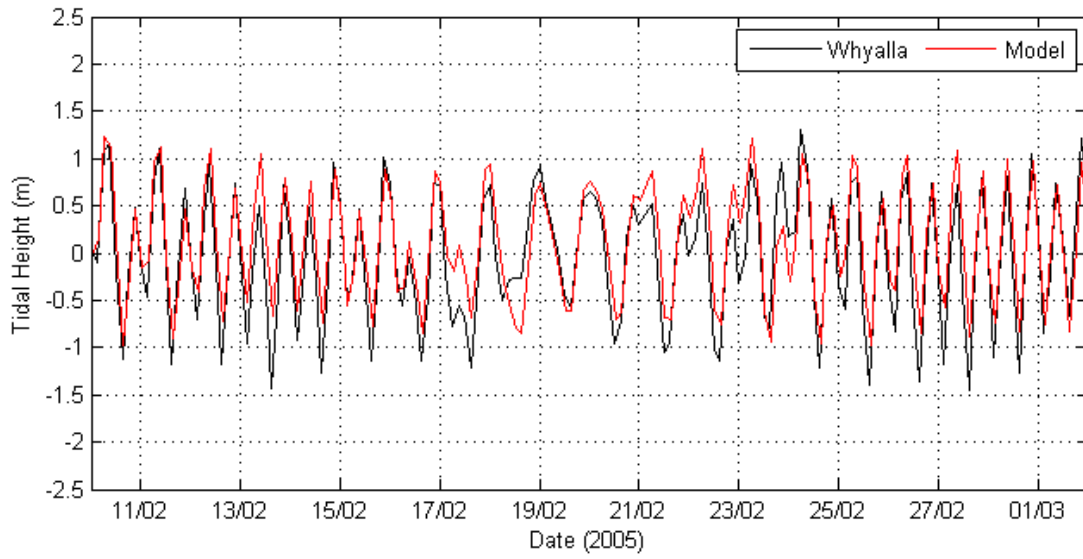
**Whyalla**

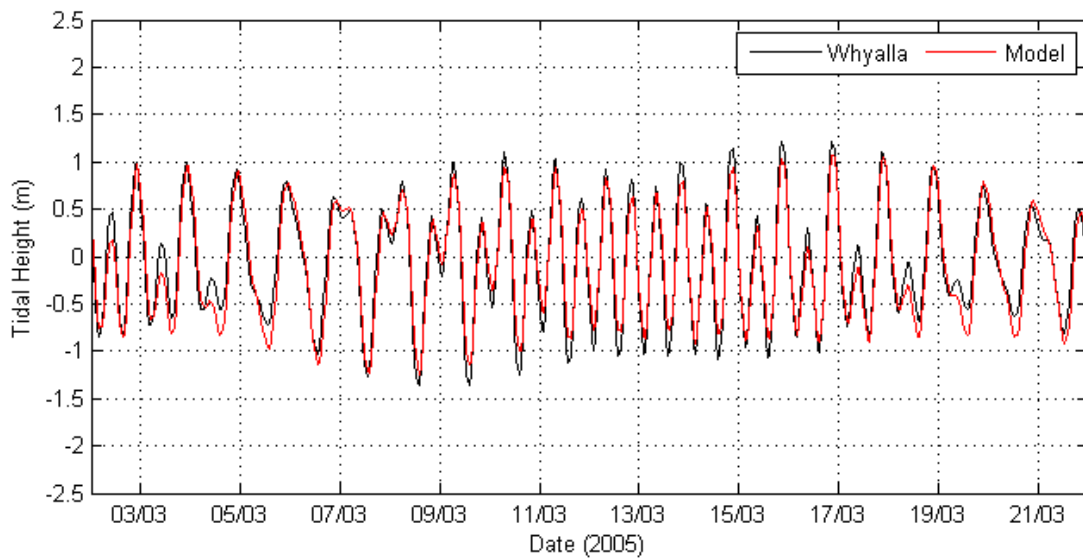
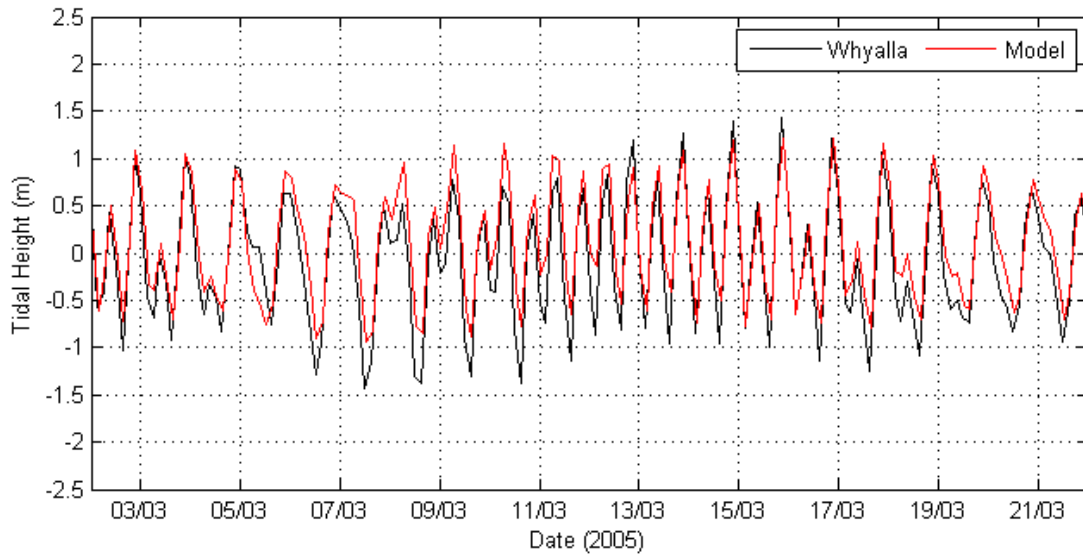


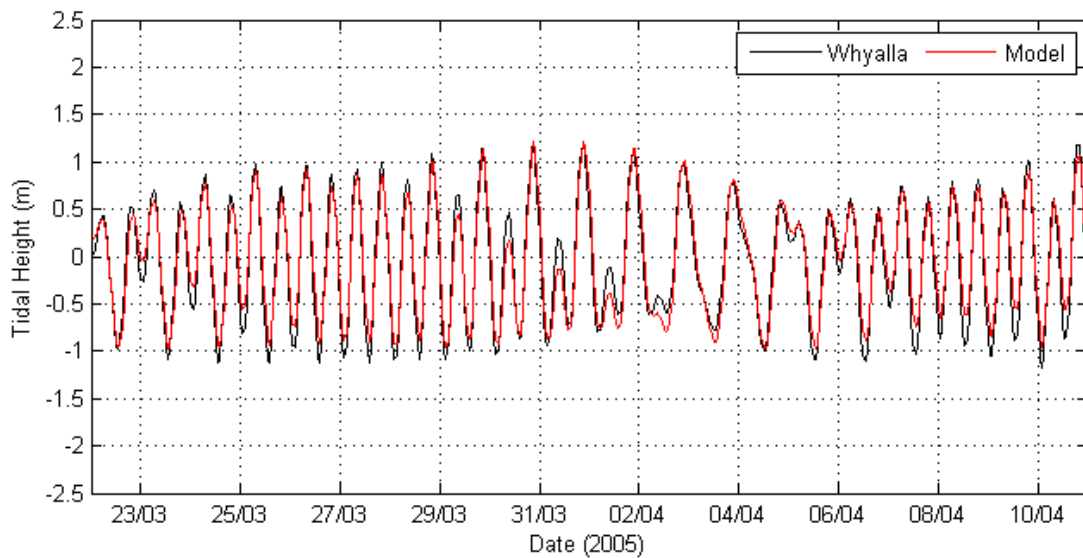
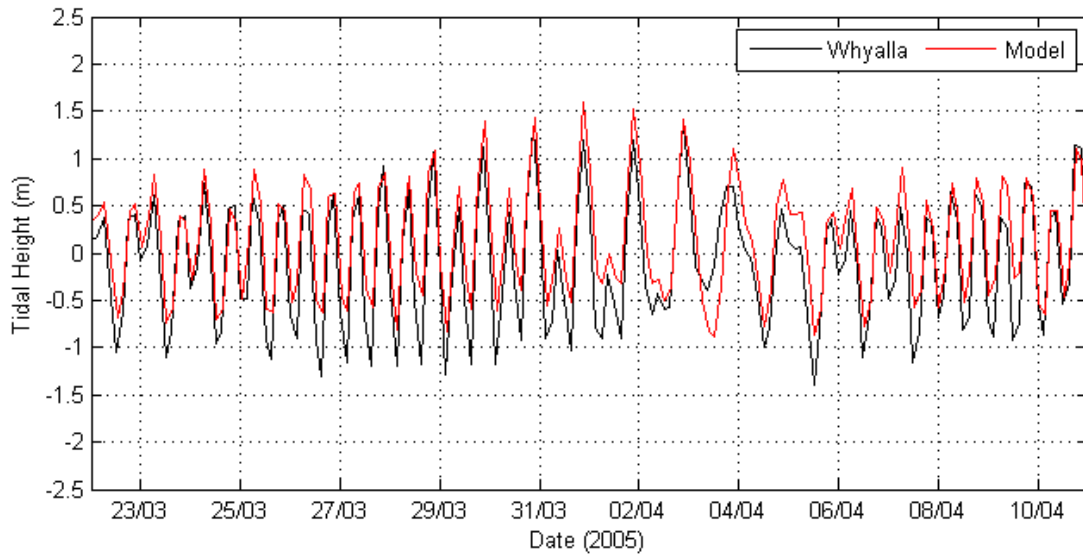


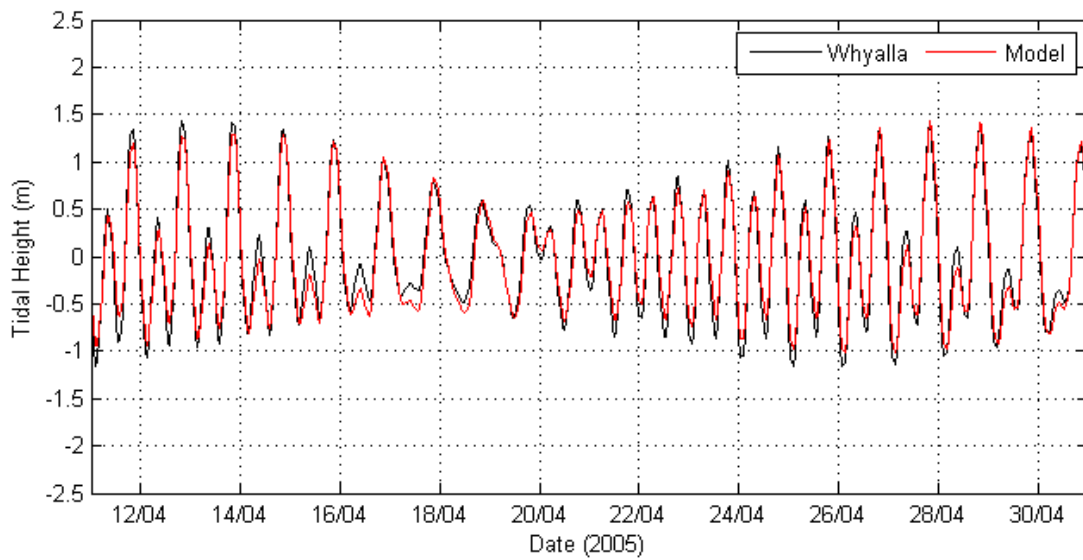
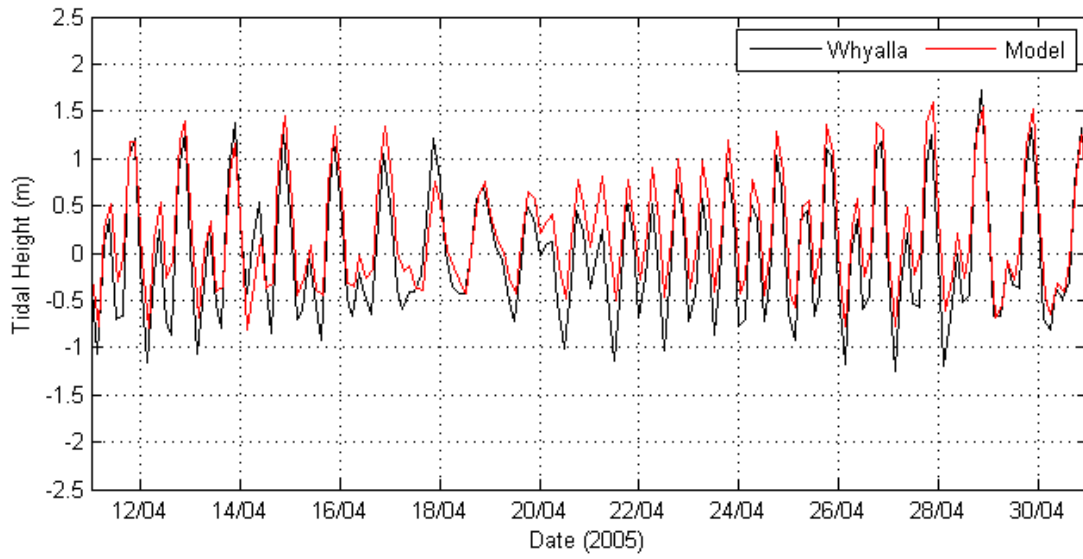


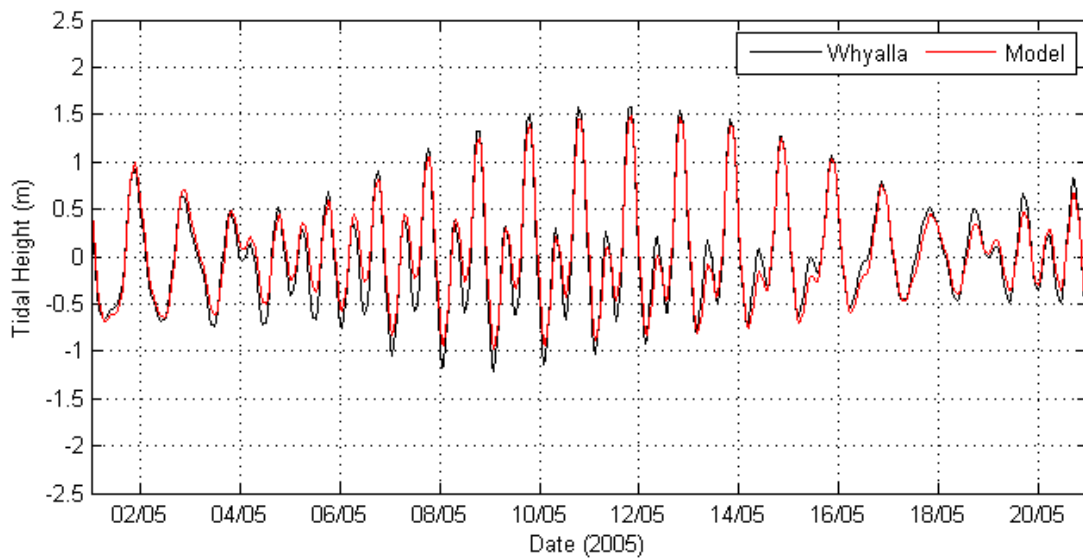
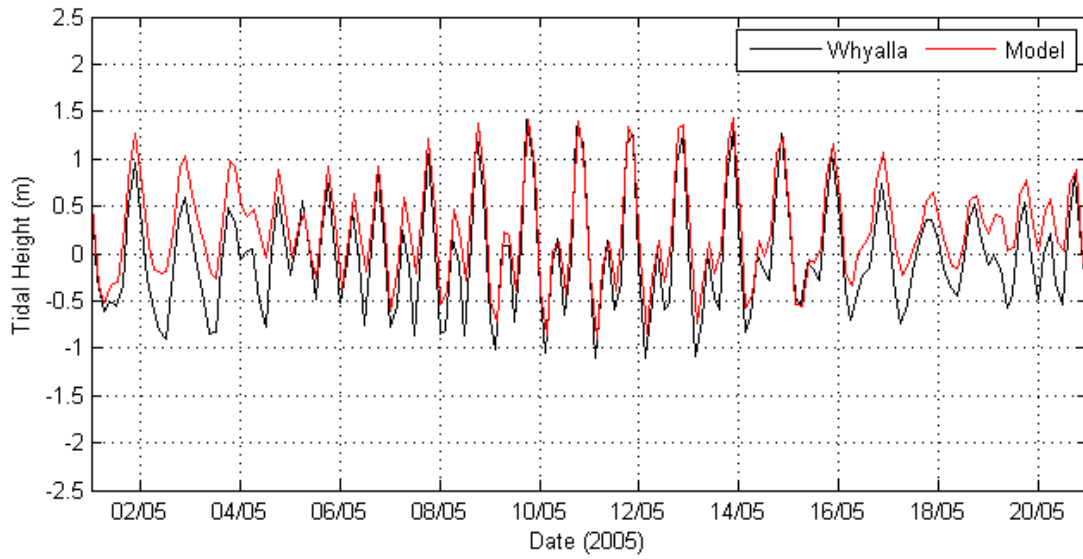


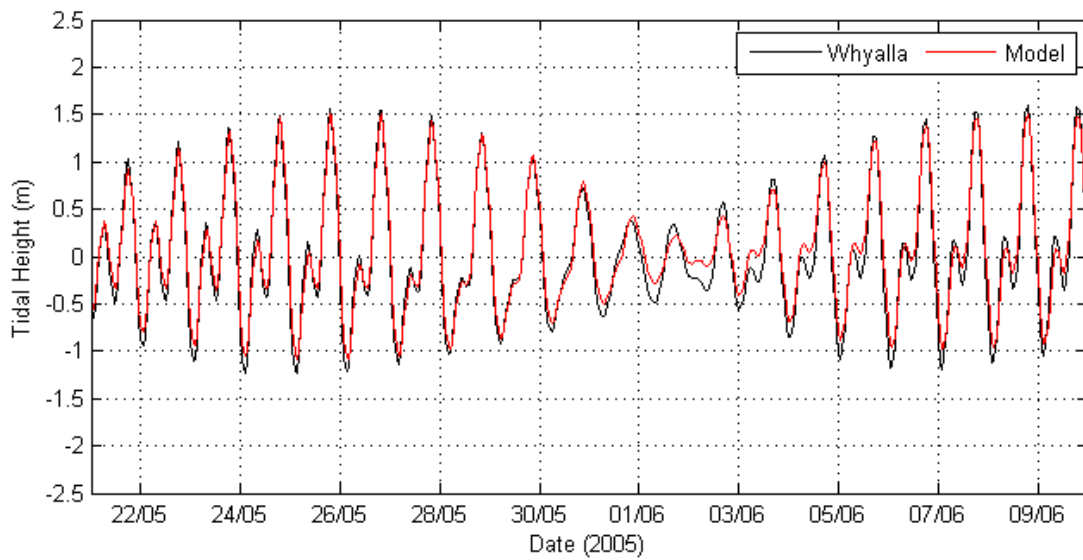
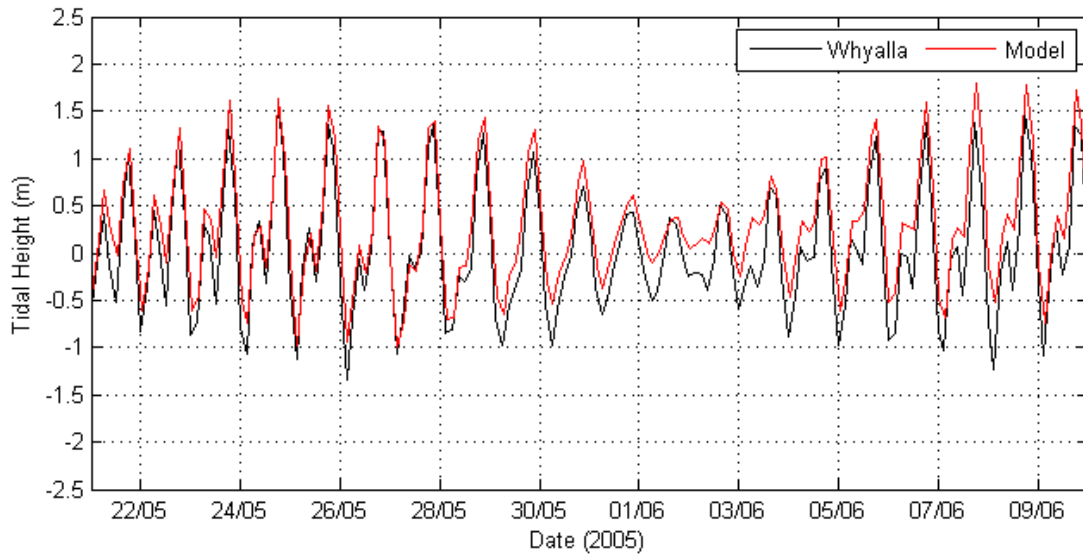


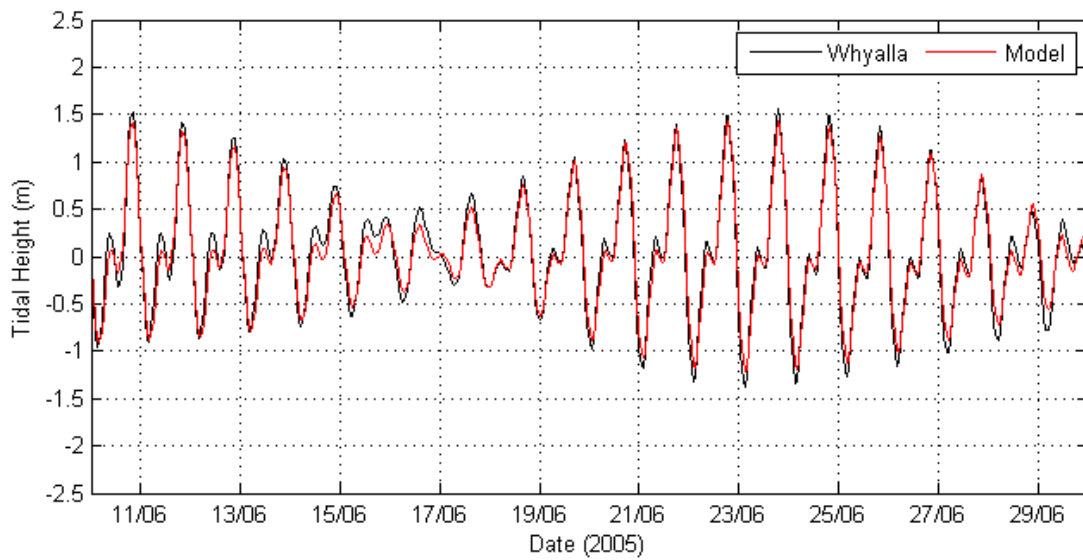
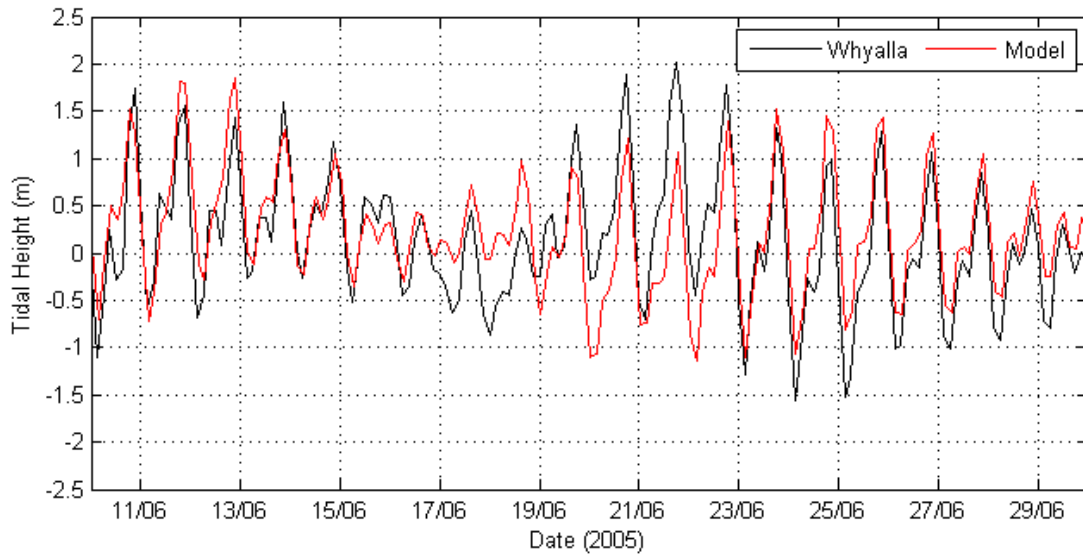


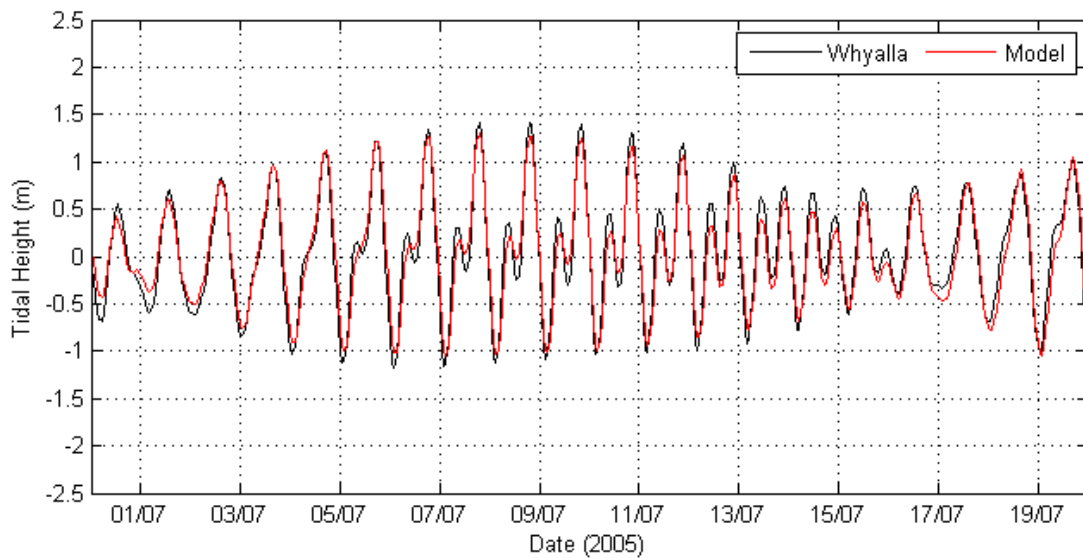
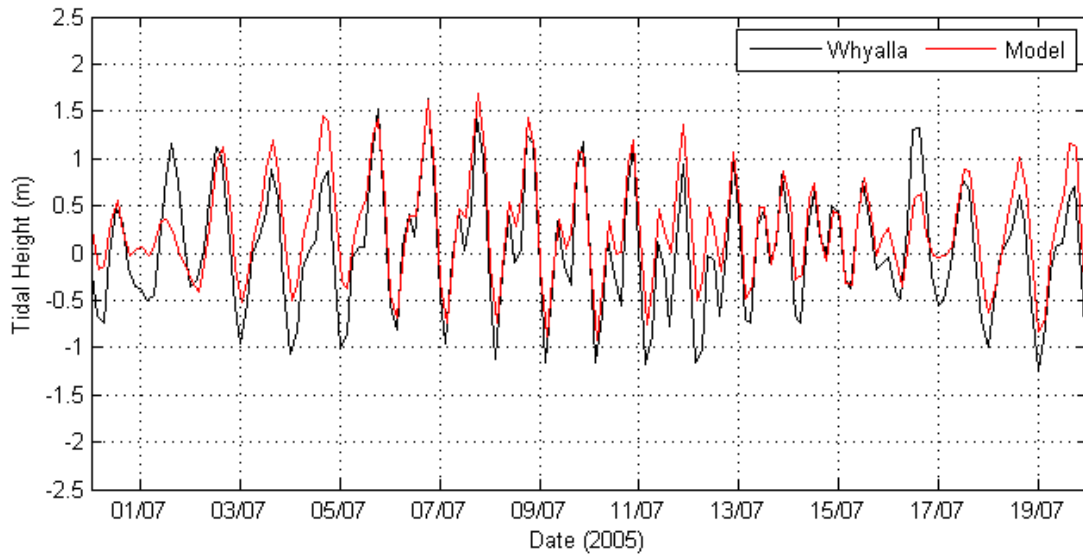




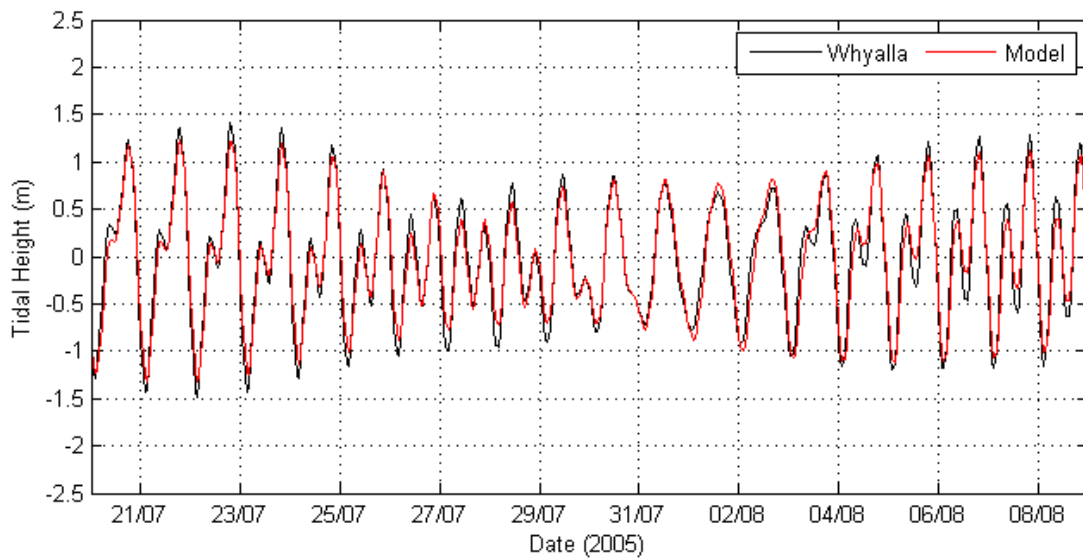
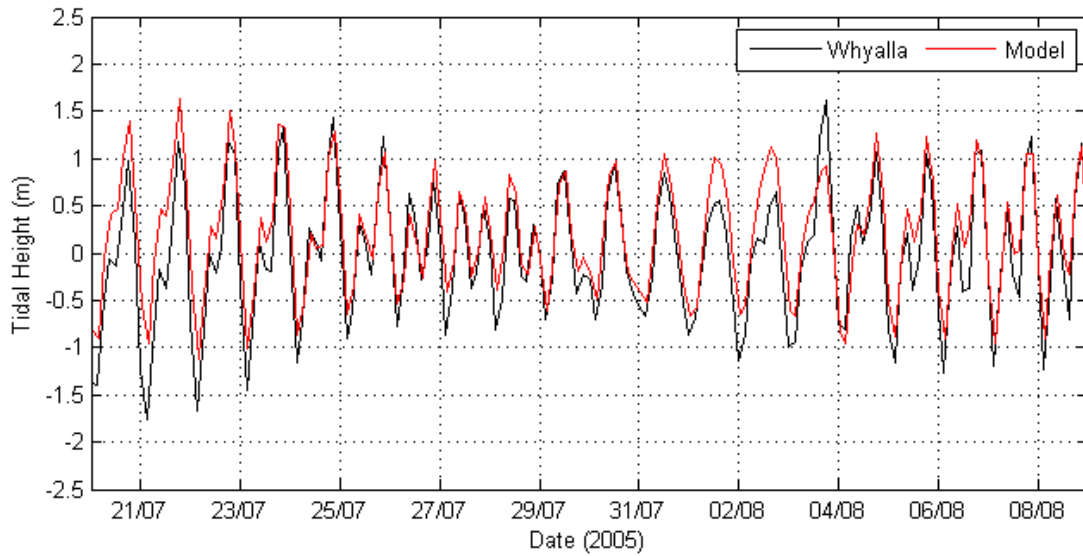


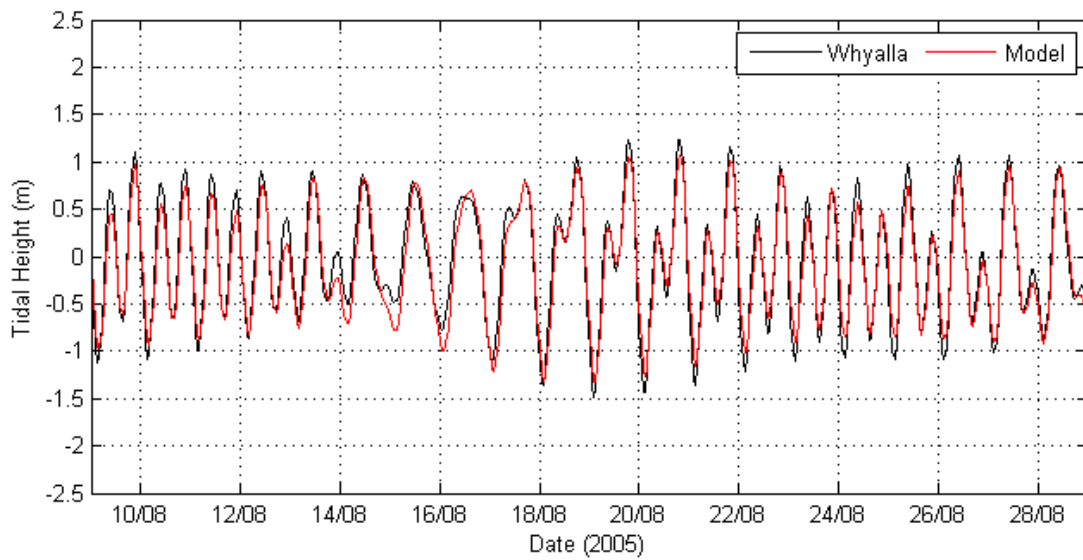
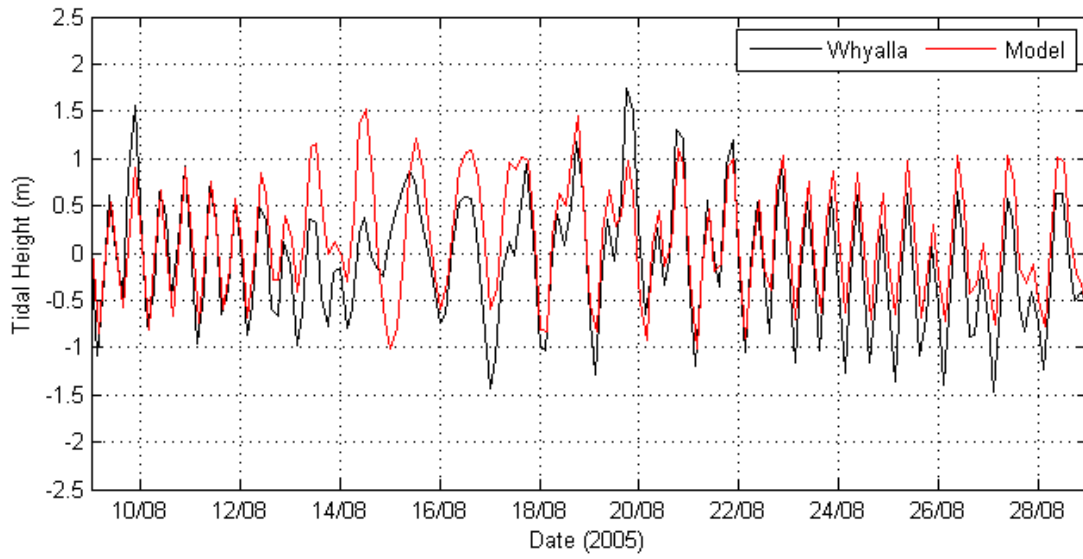


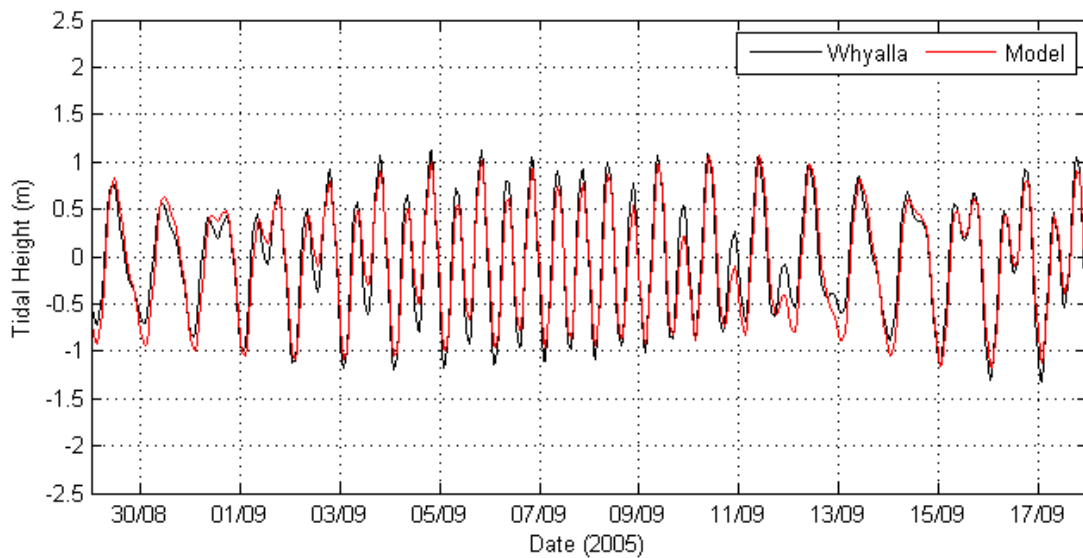
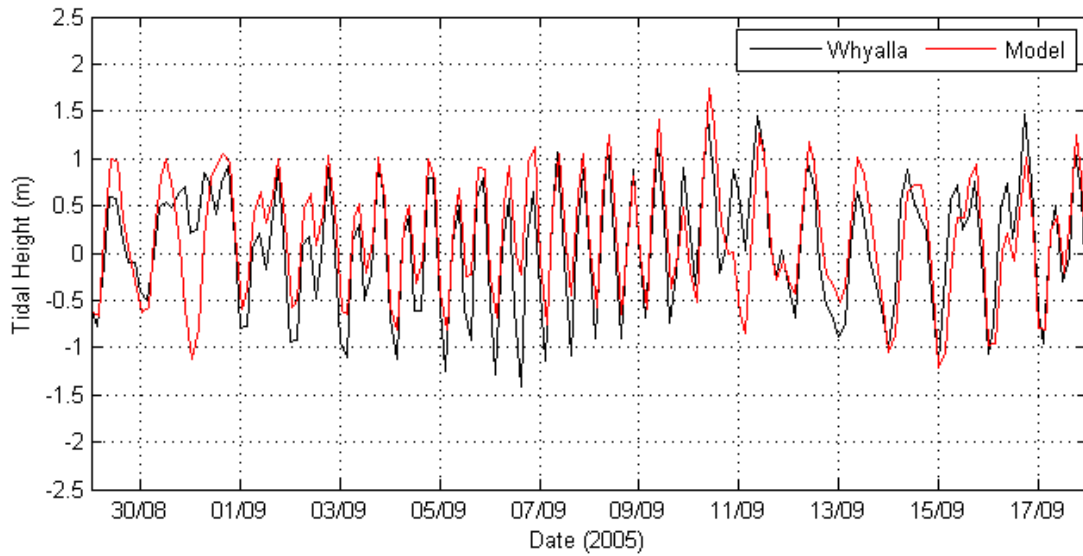


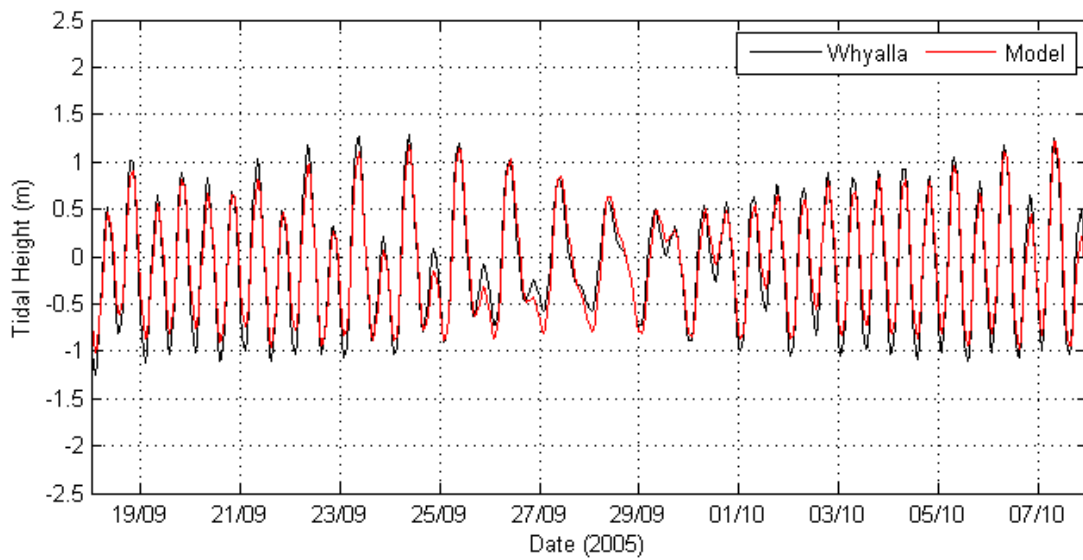
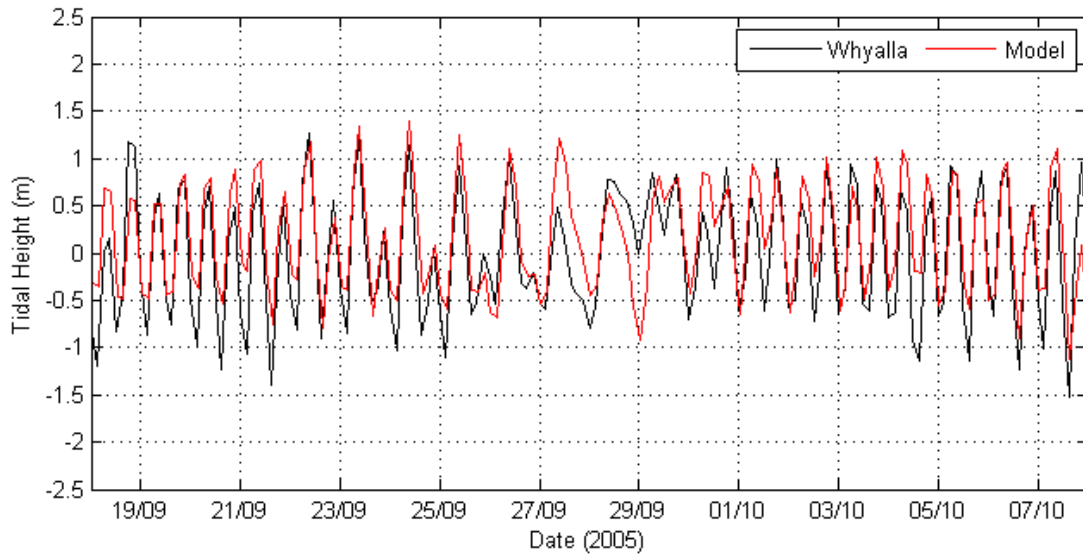


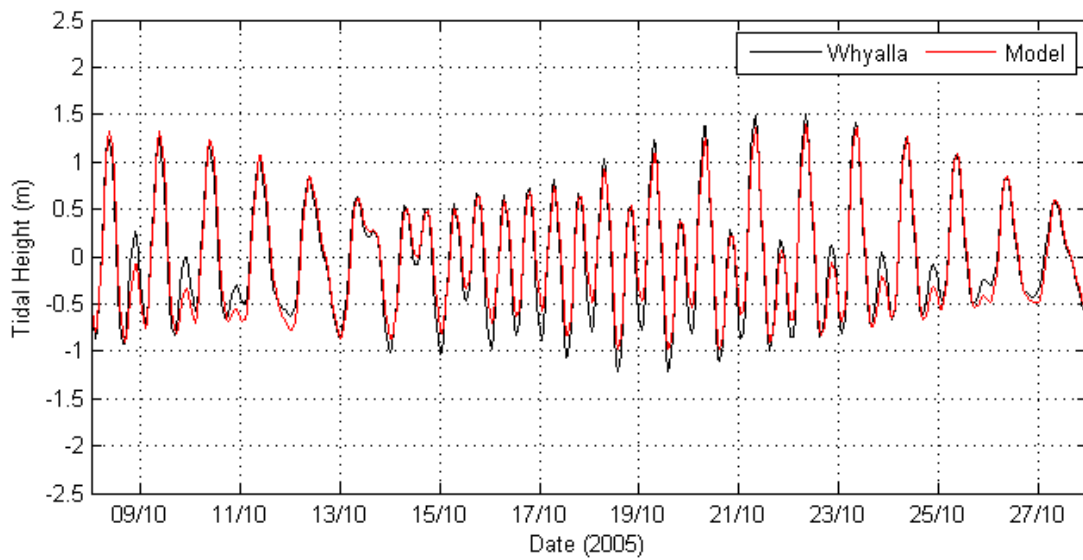
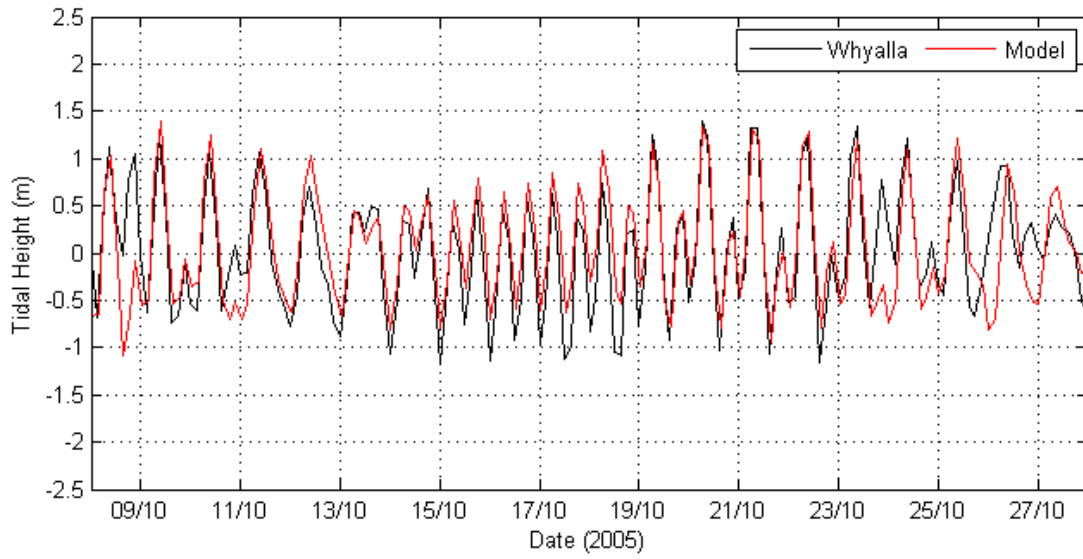


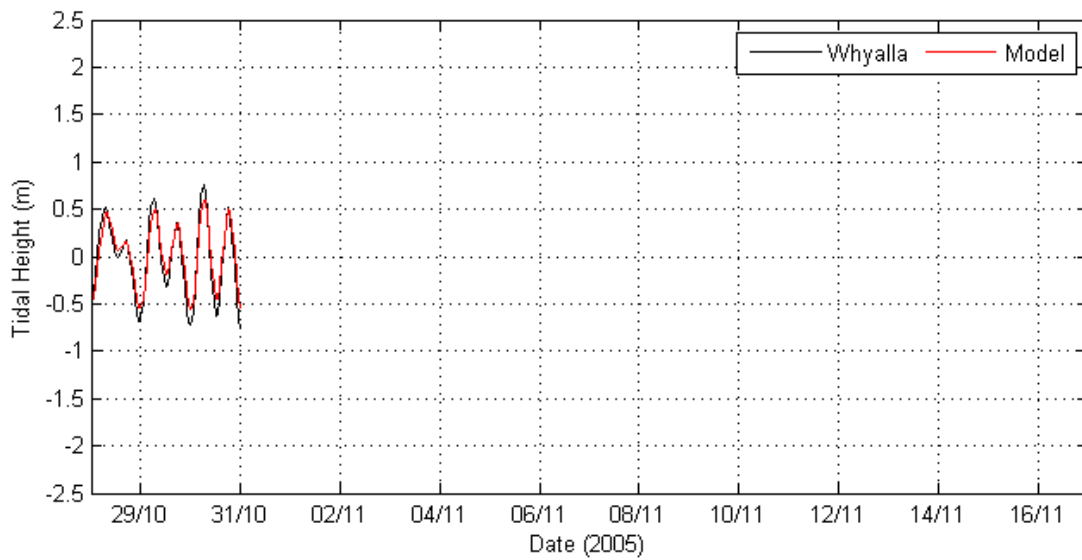
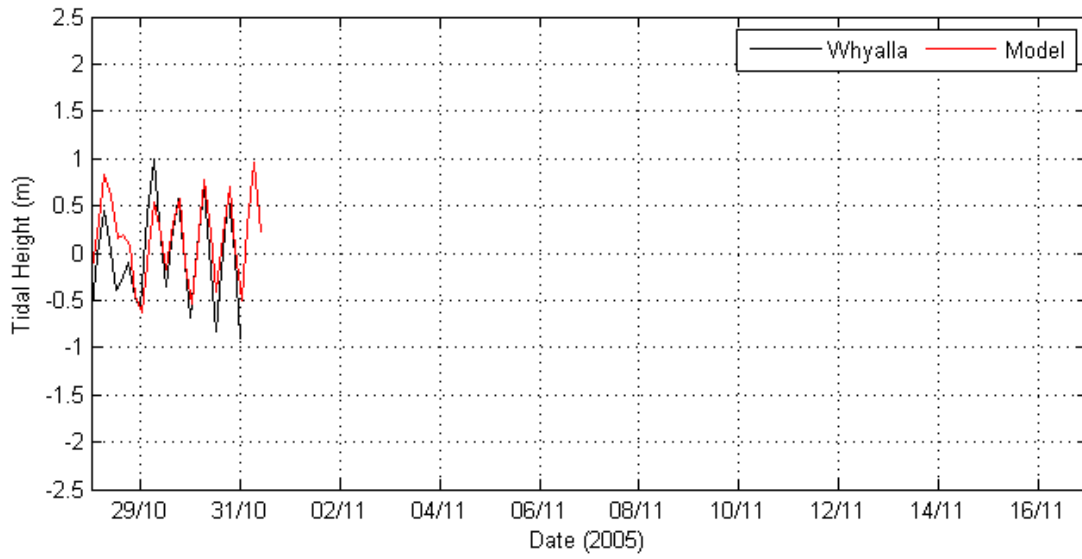






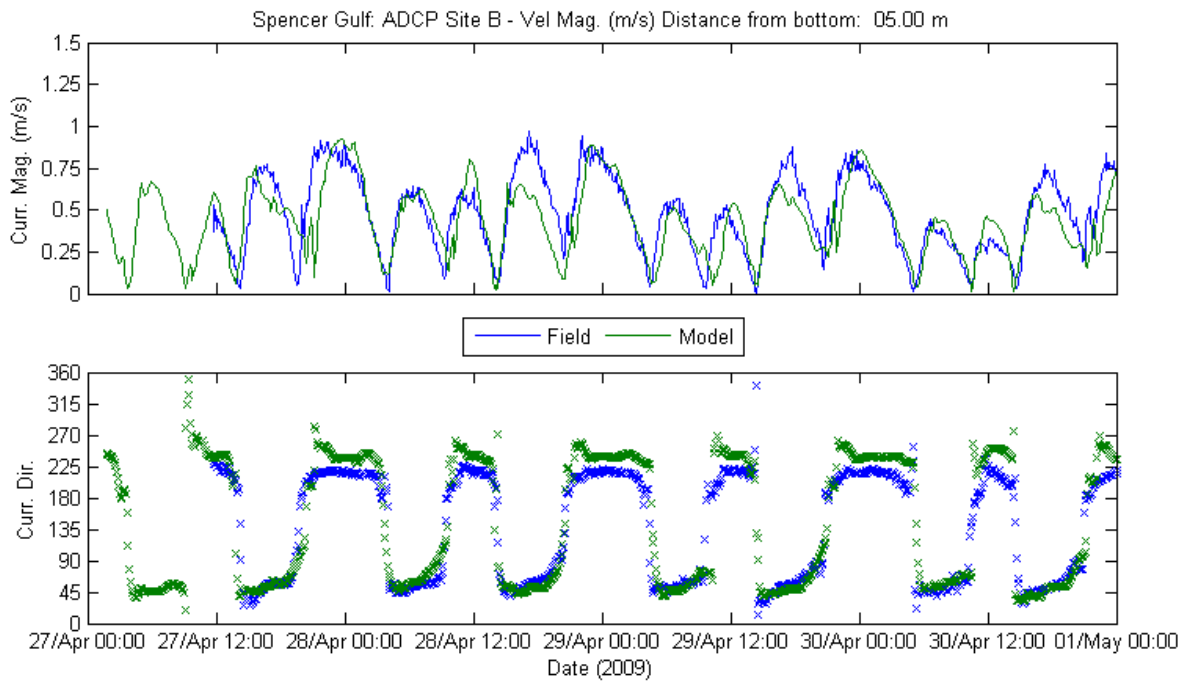
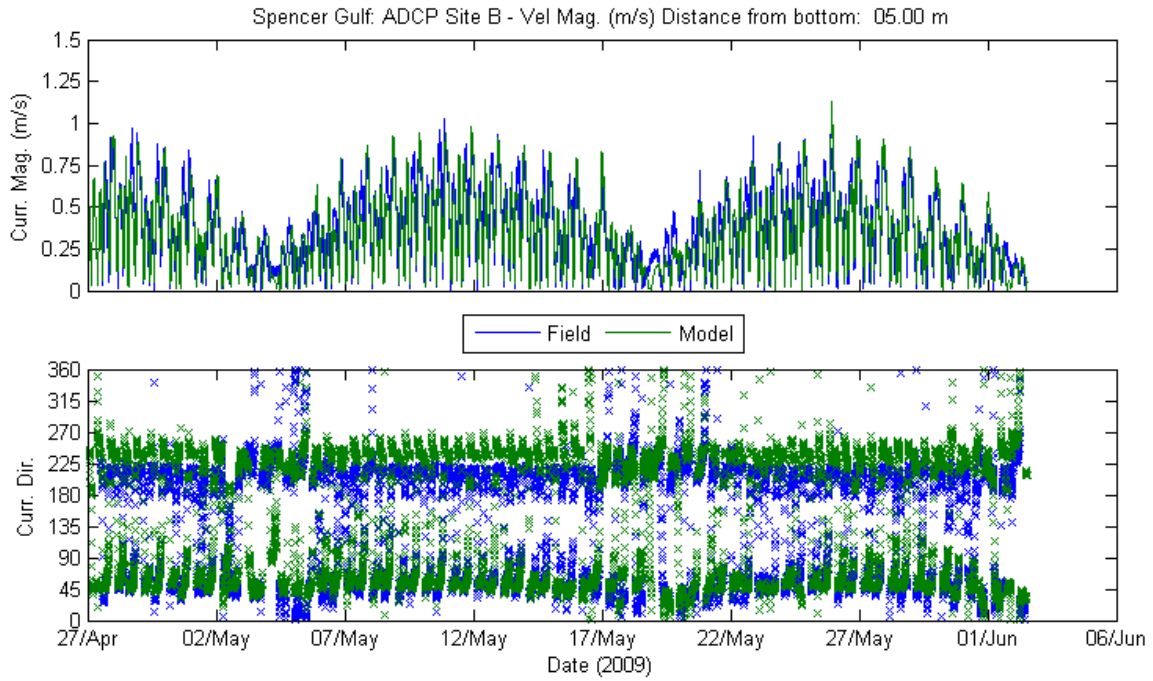


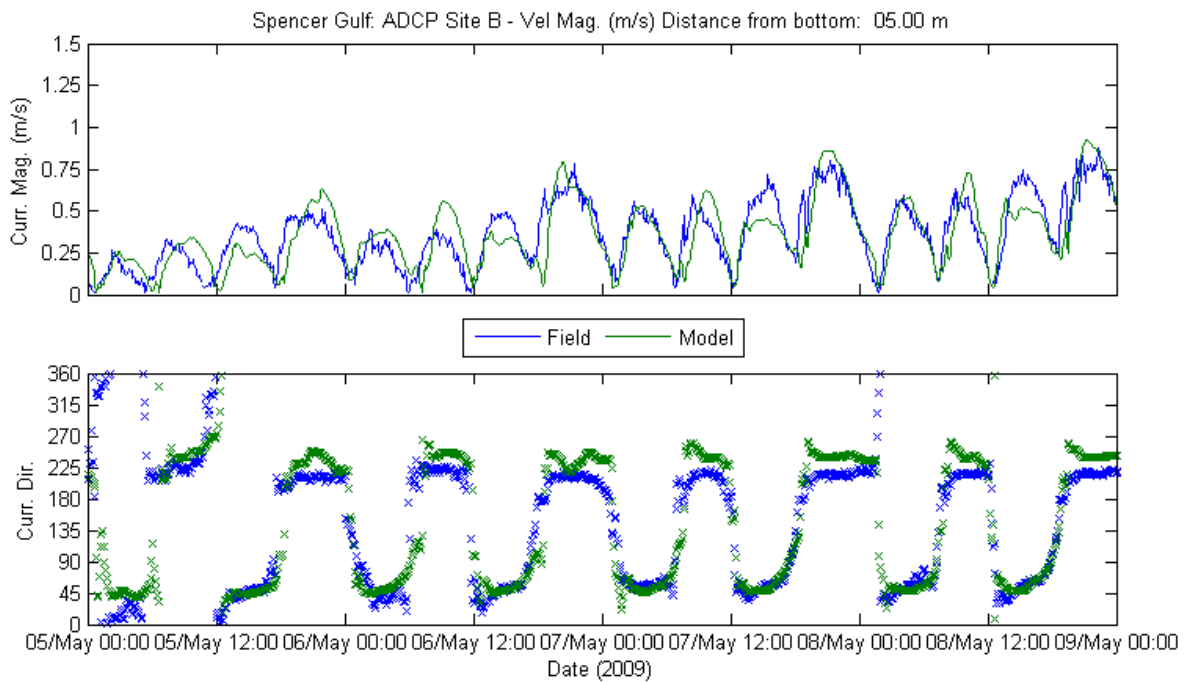
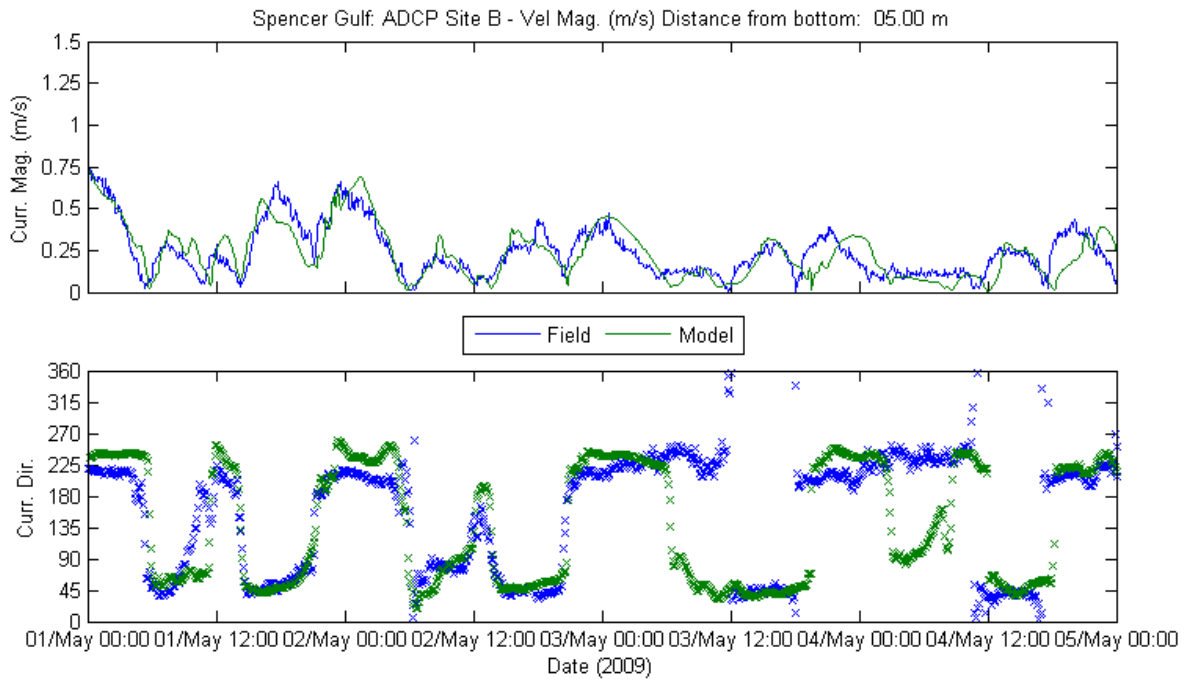




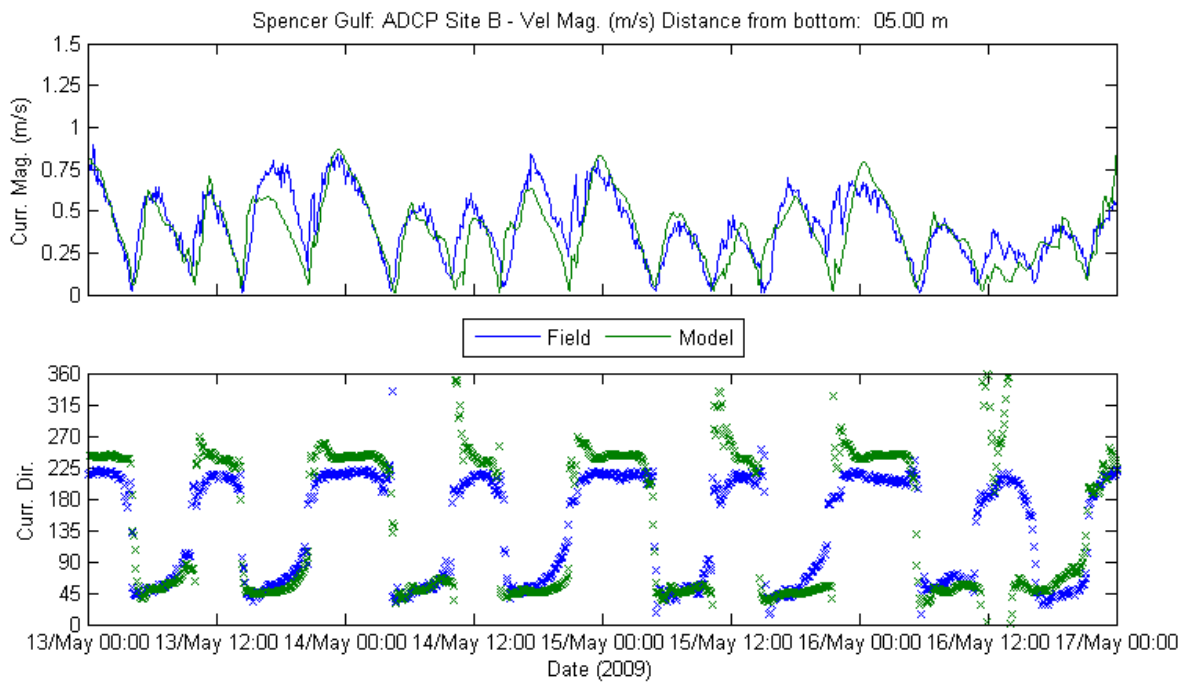
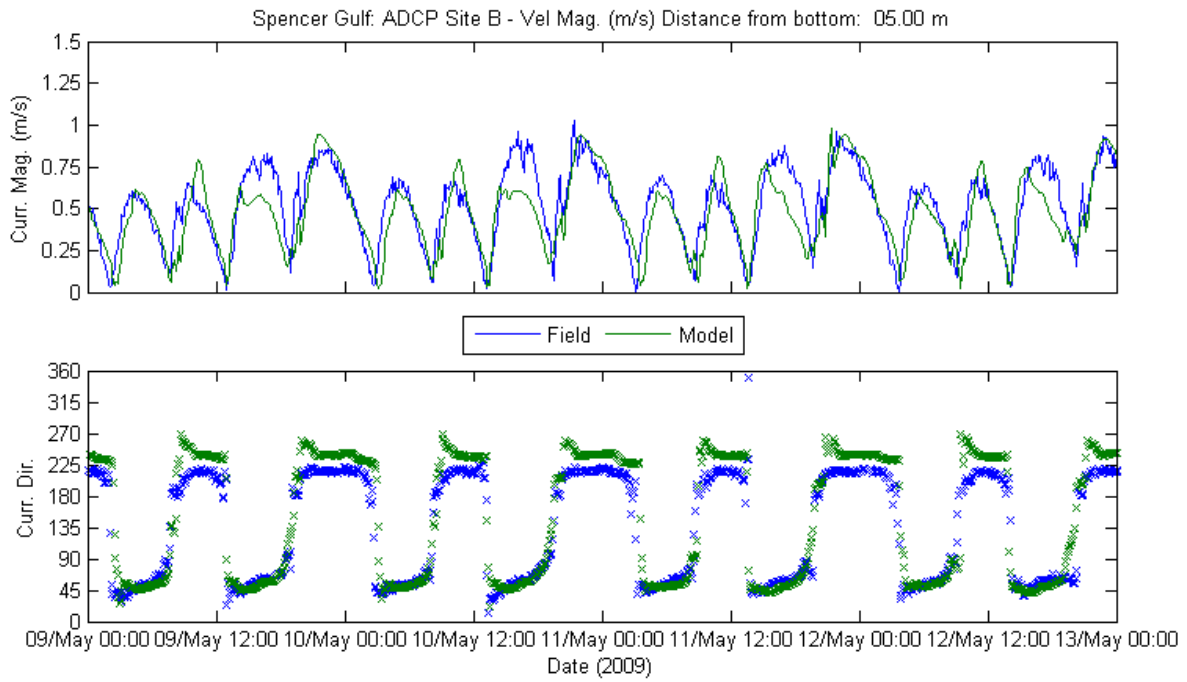
# APPENDIX E: FORTY DAYS VALIDATION PERIOD MOORED-ADCP COMPARISONS

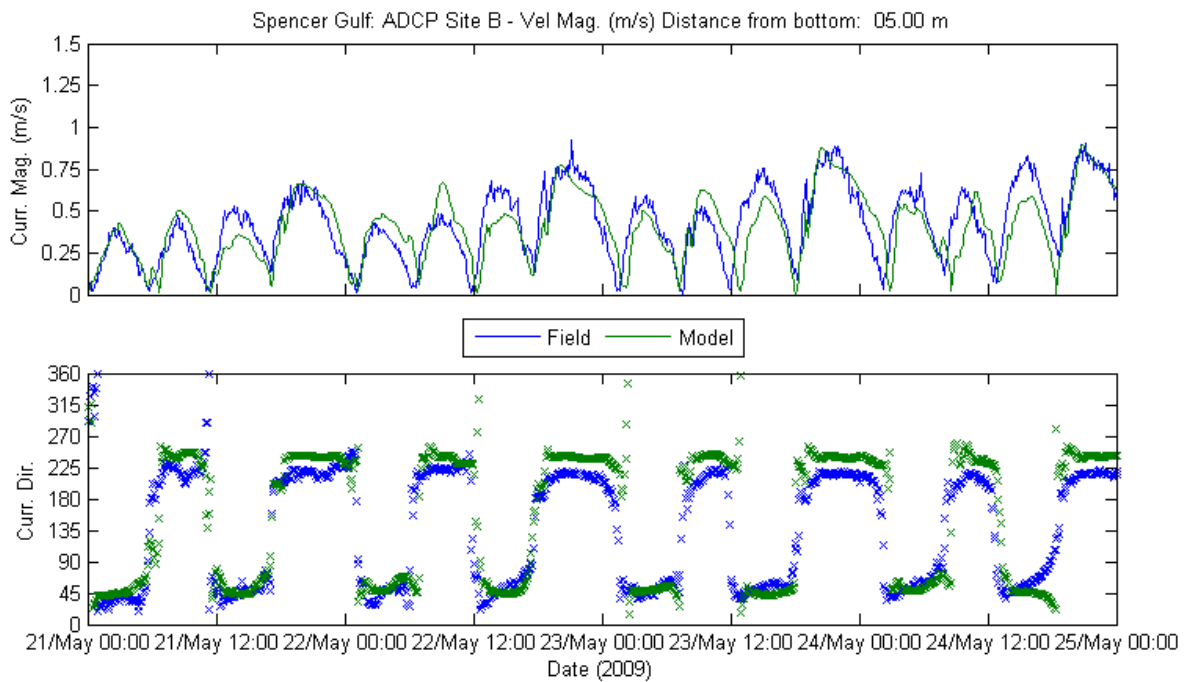
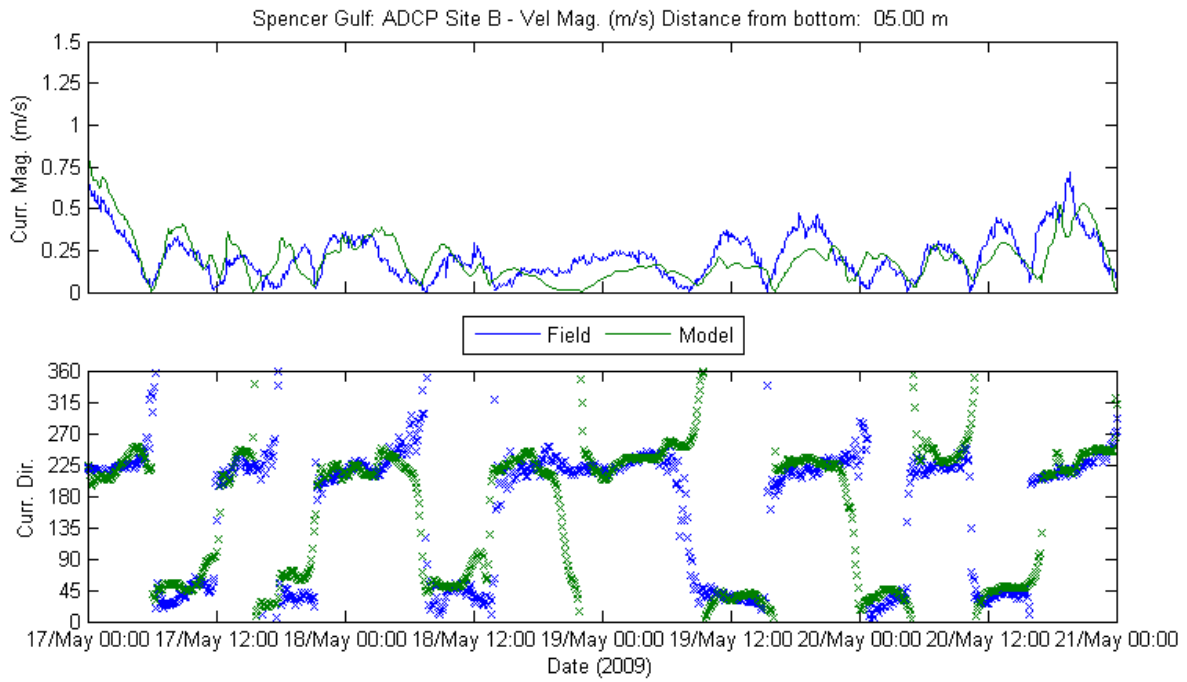
## Site B at 5.00m from Bottom

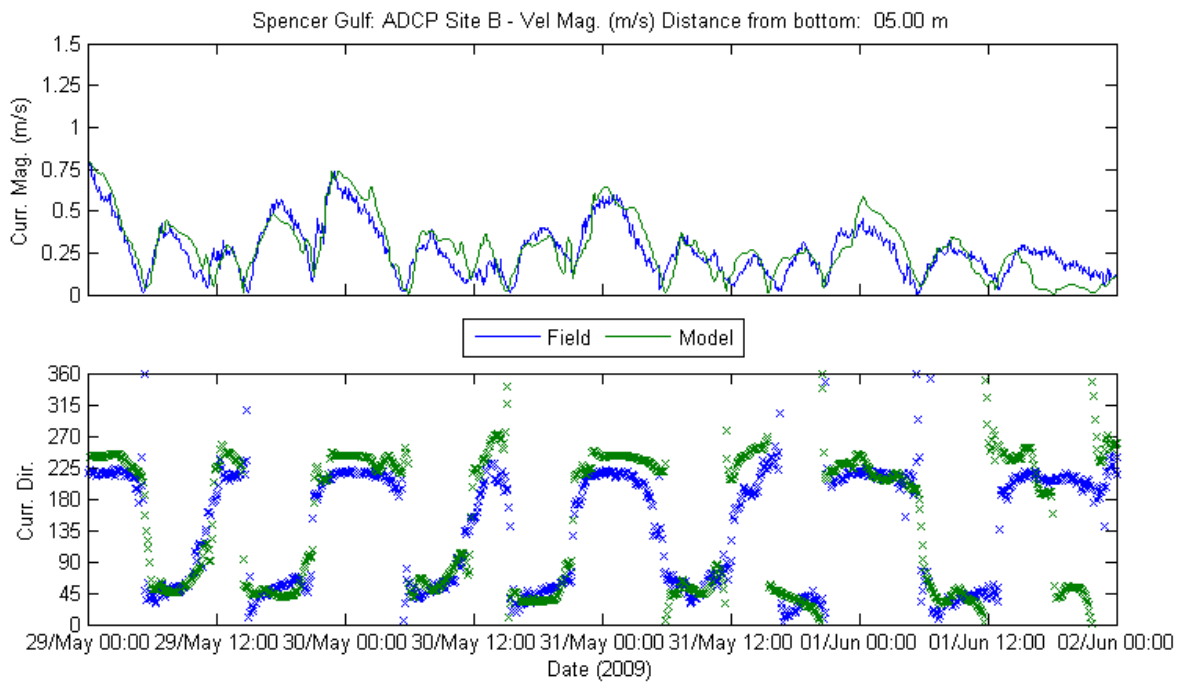
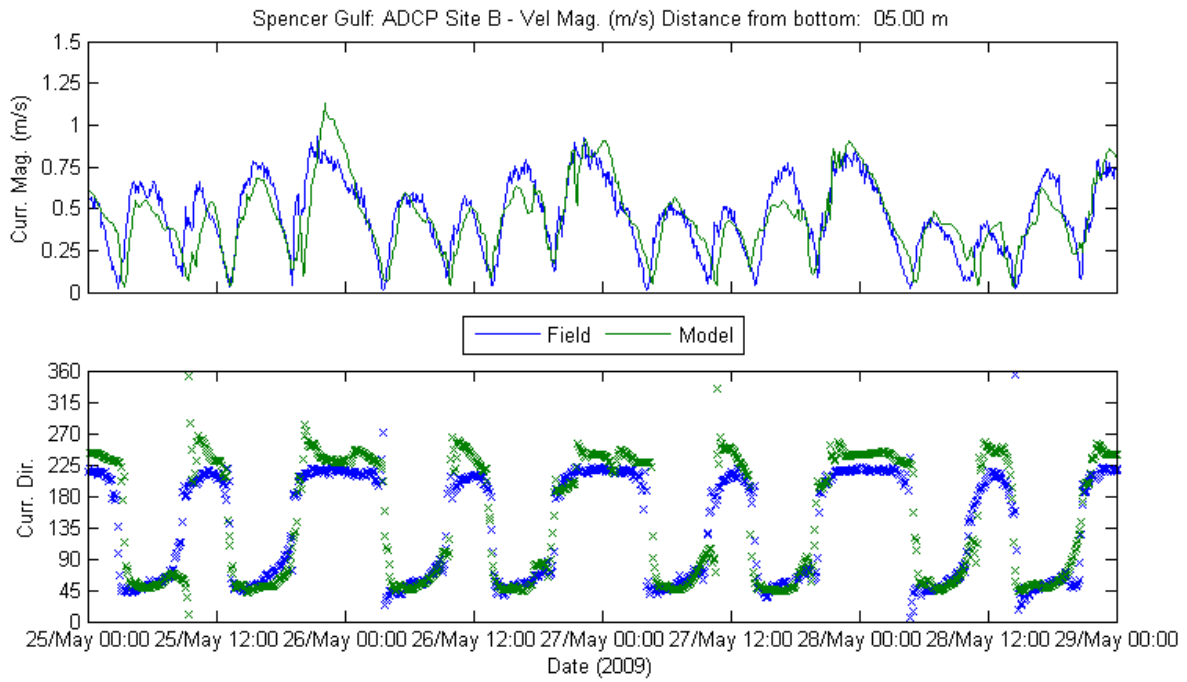


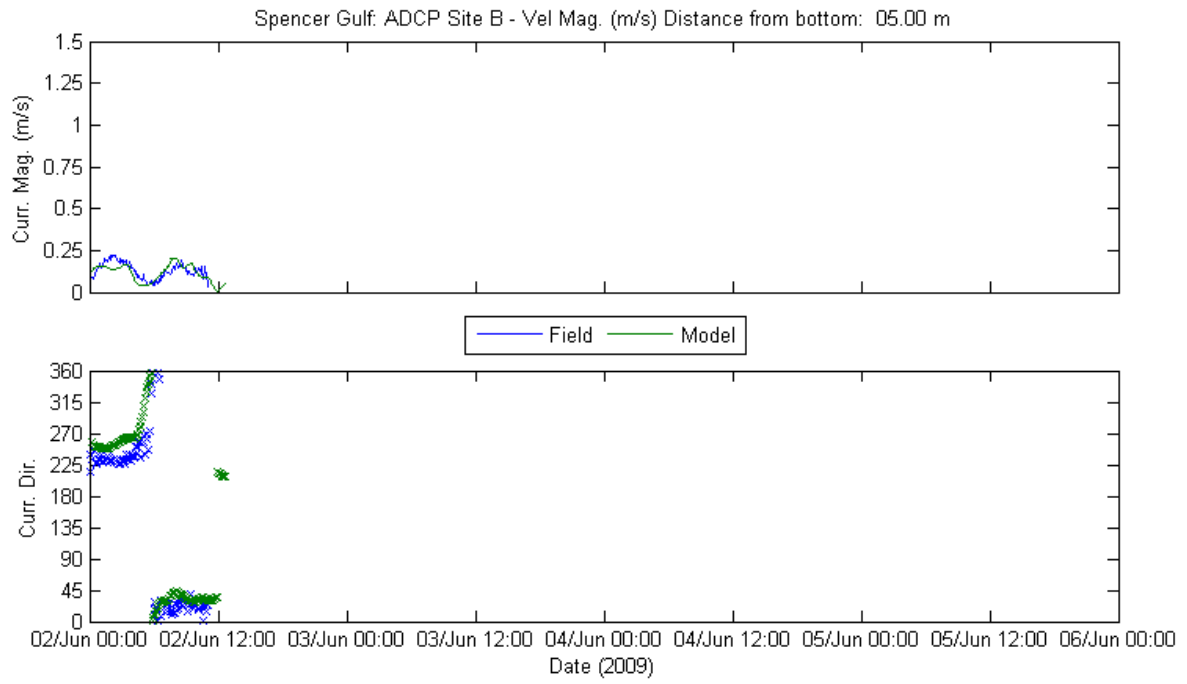




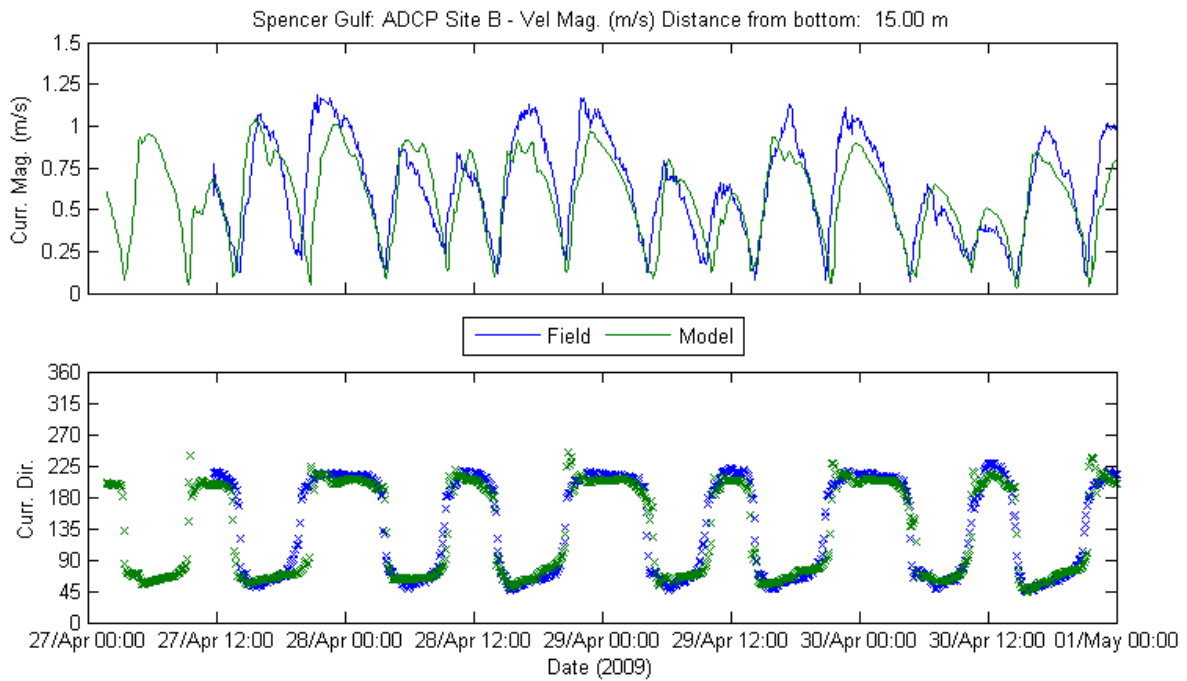
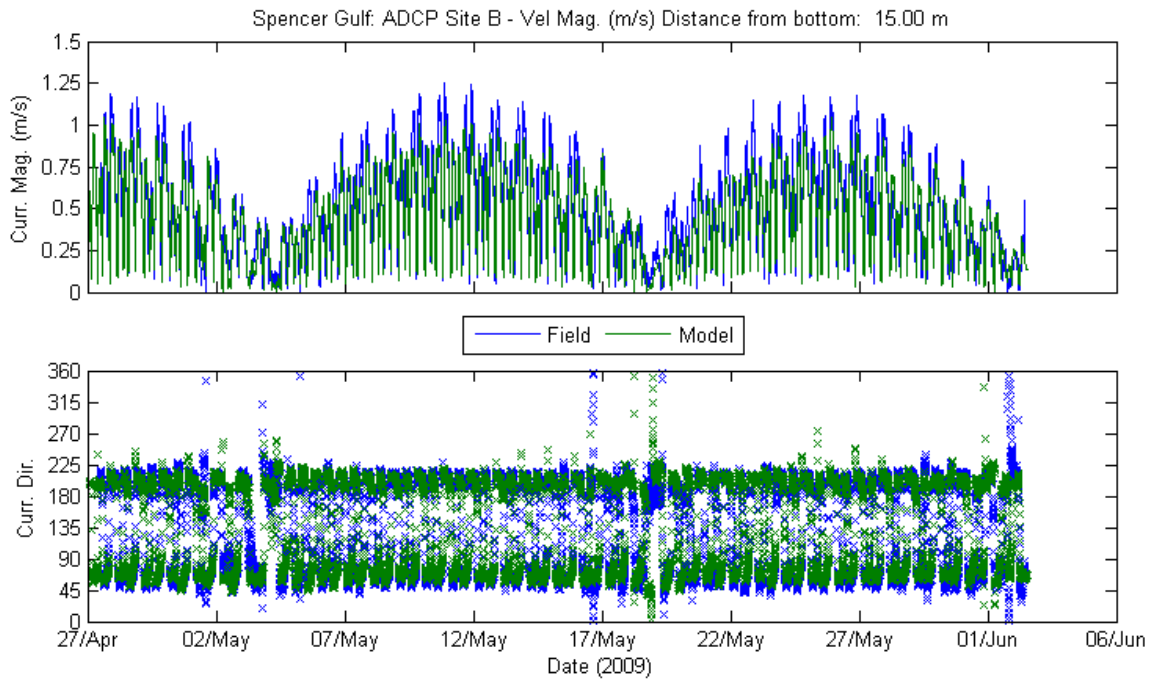


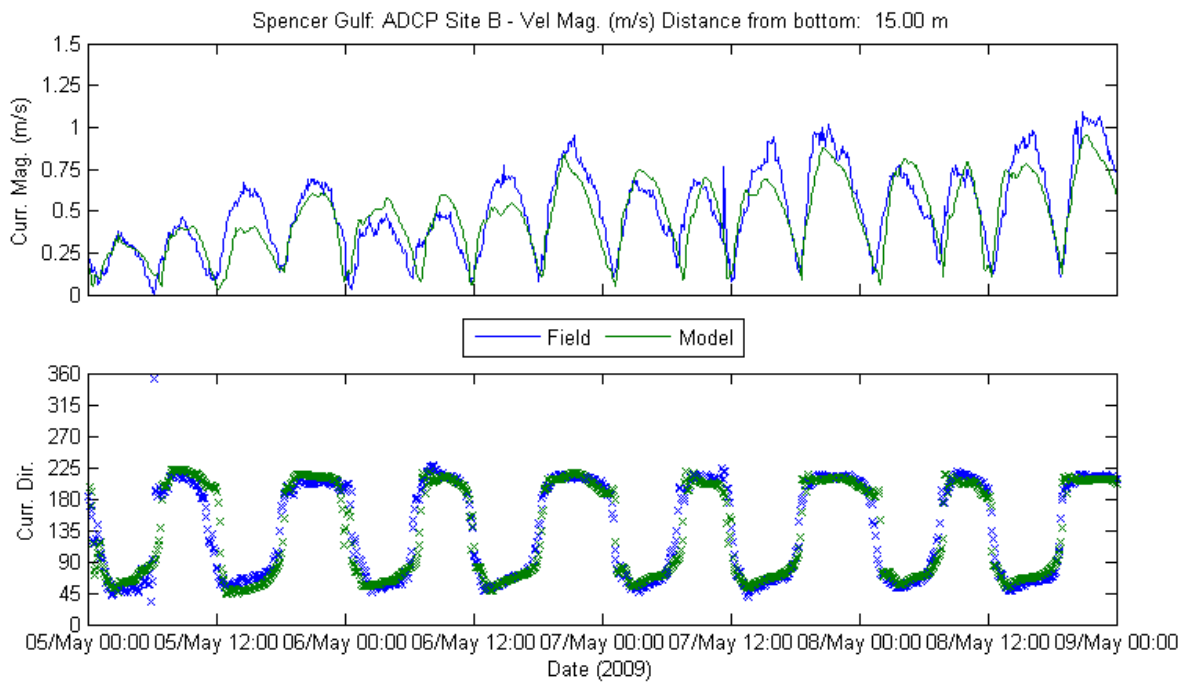
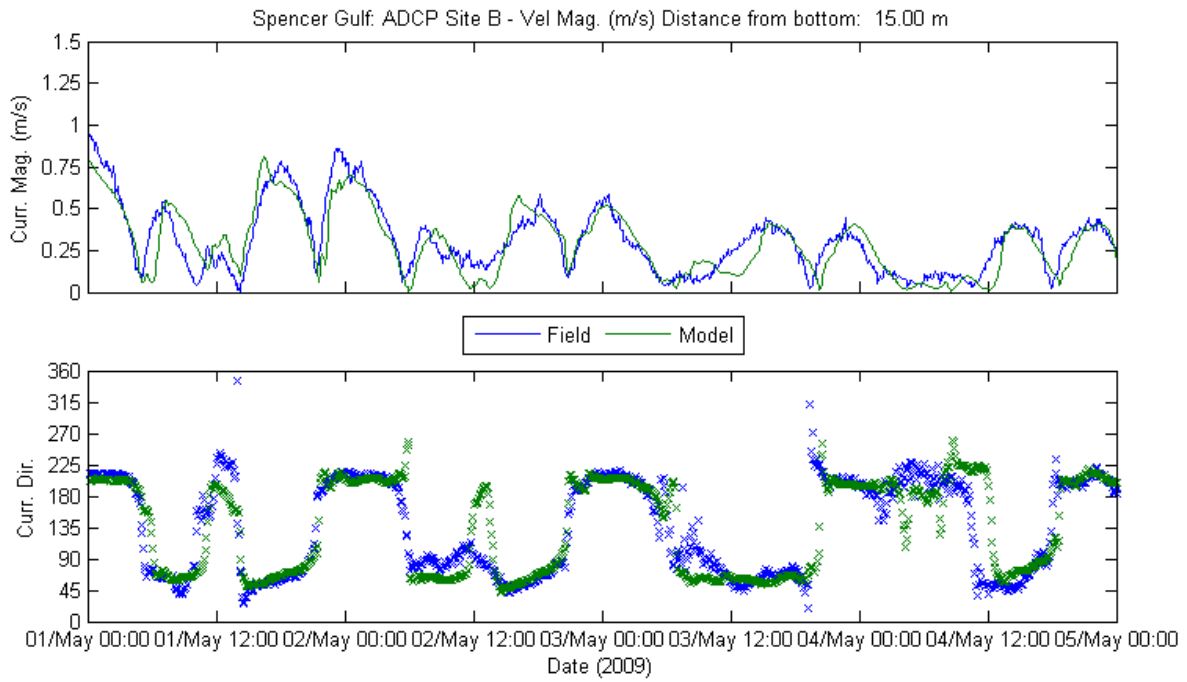


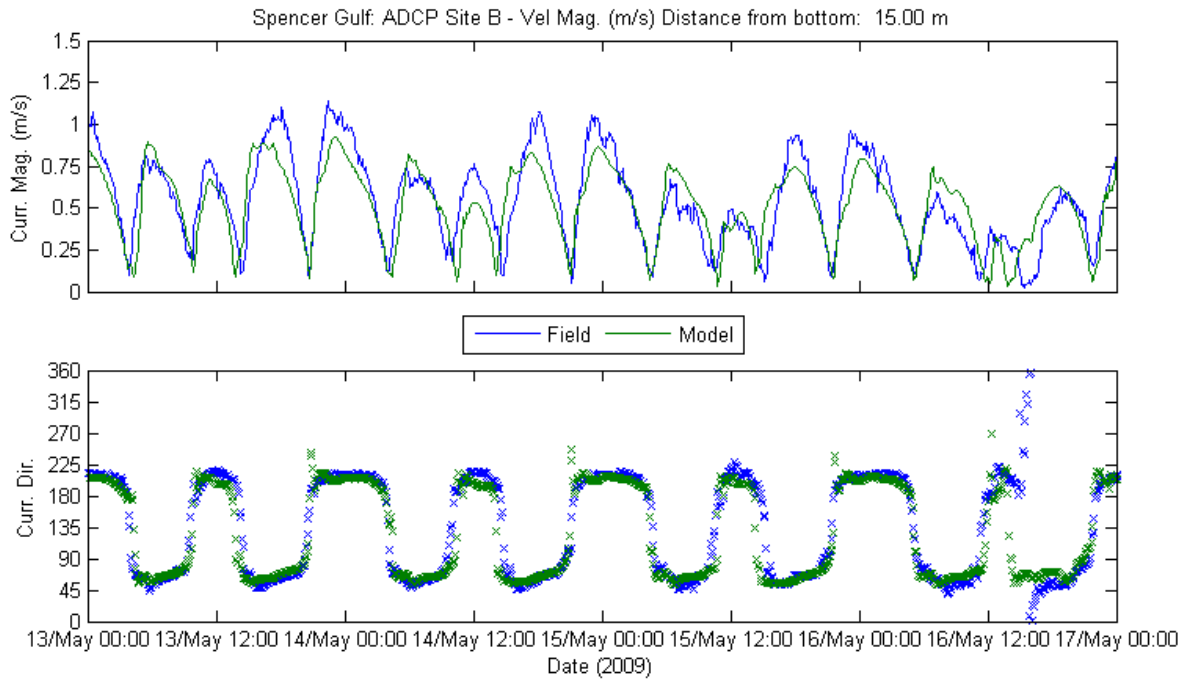
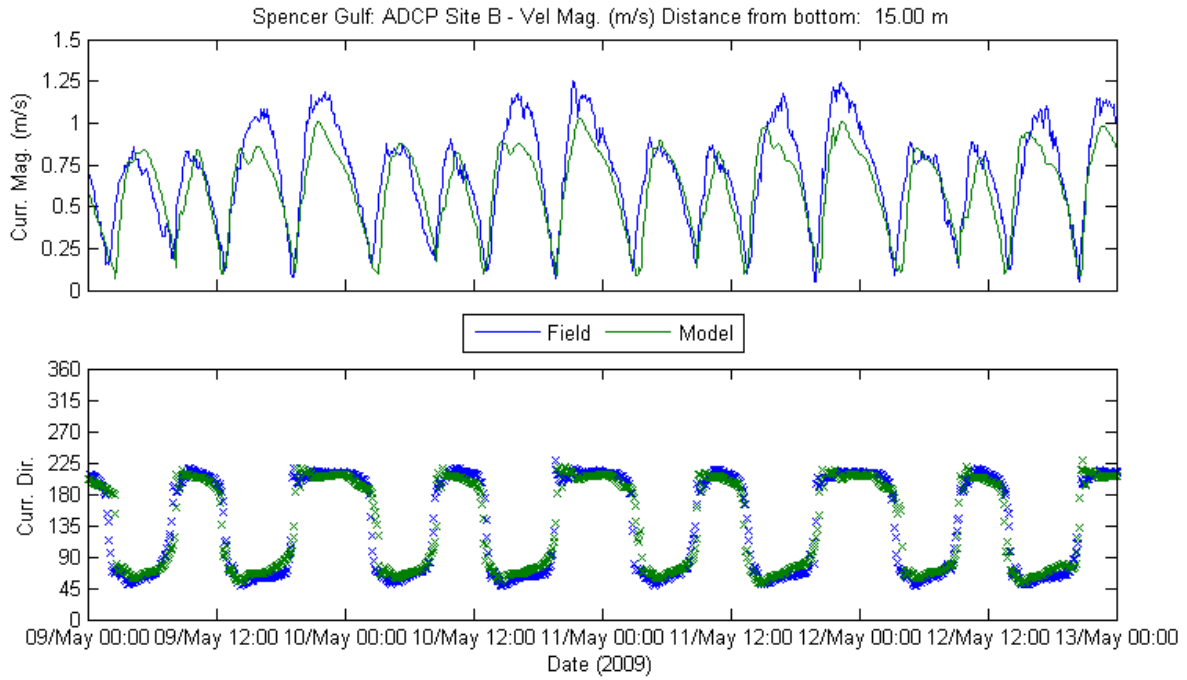


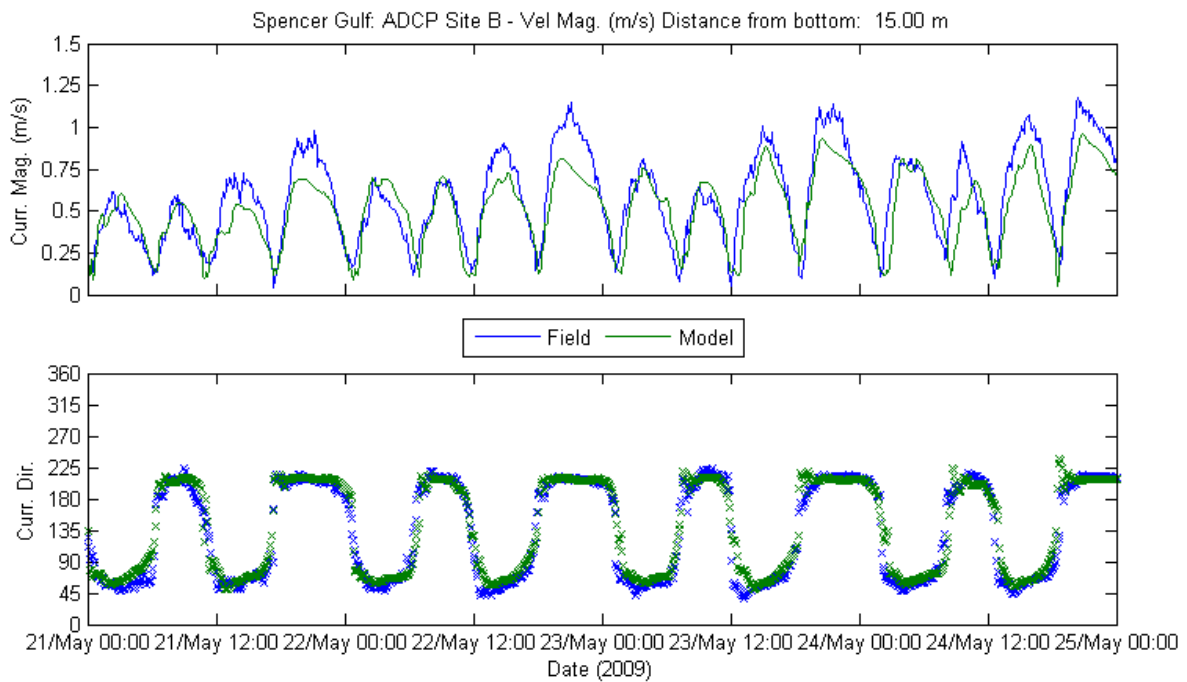
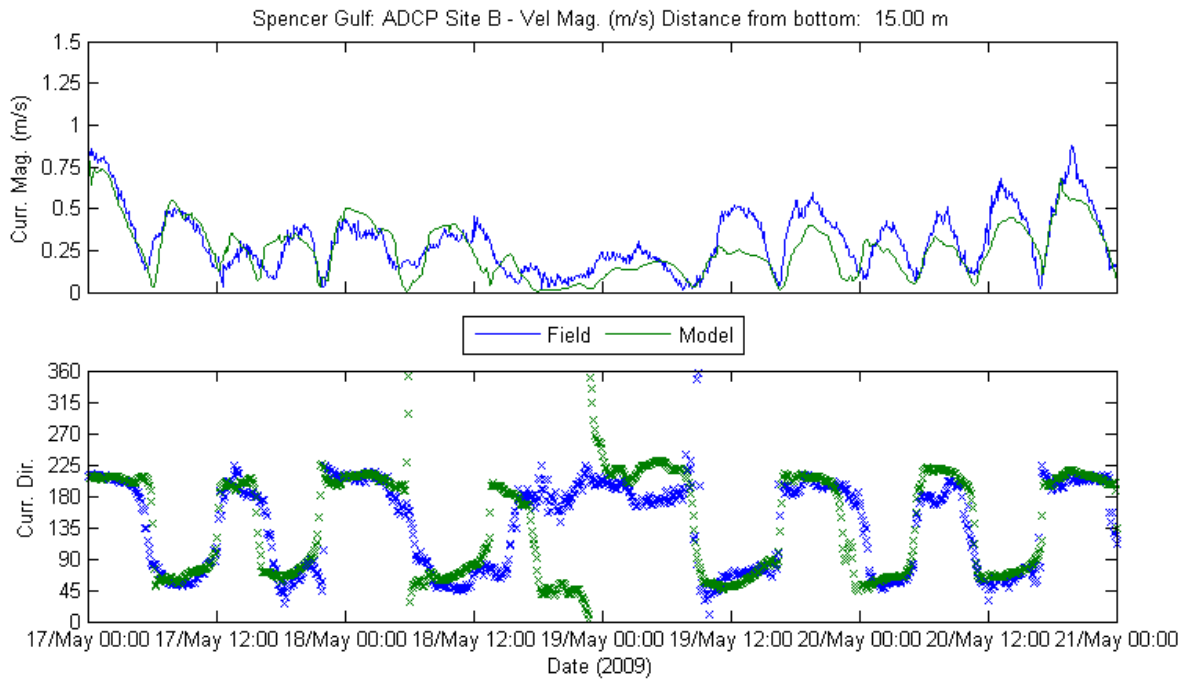


Site B at 15.00m from Bottom

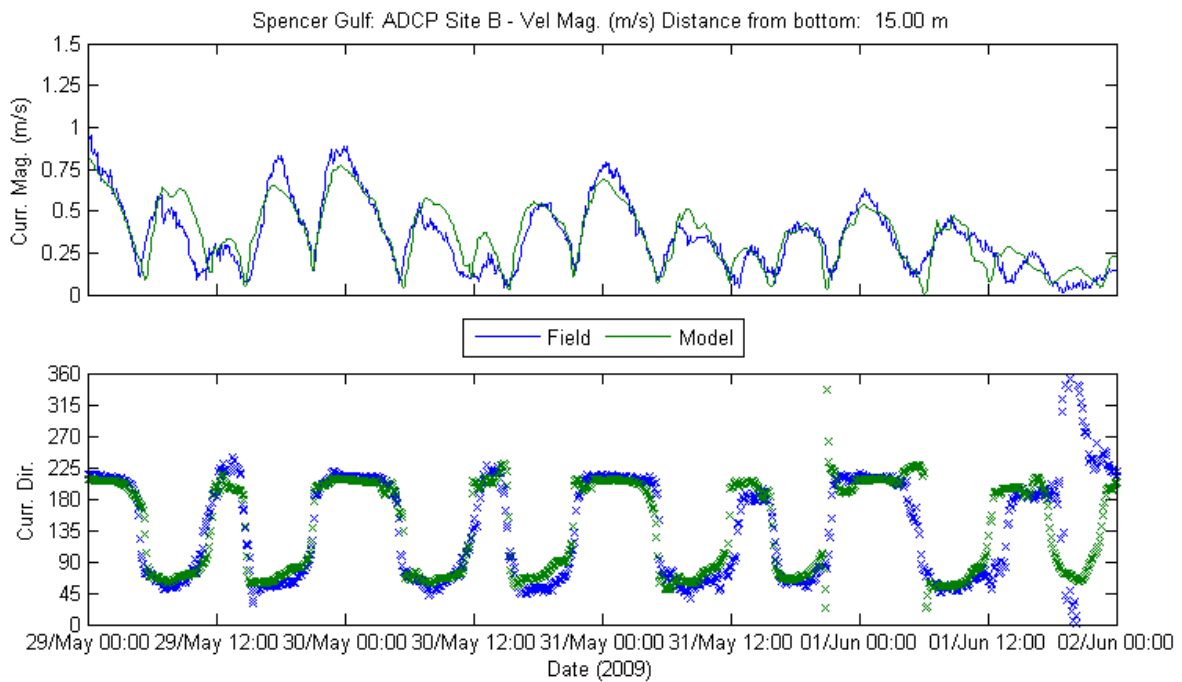
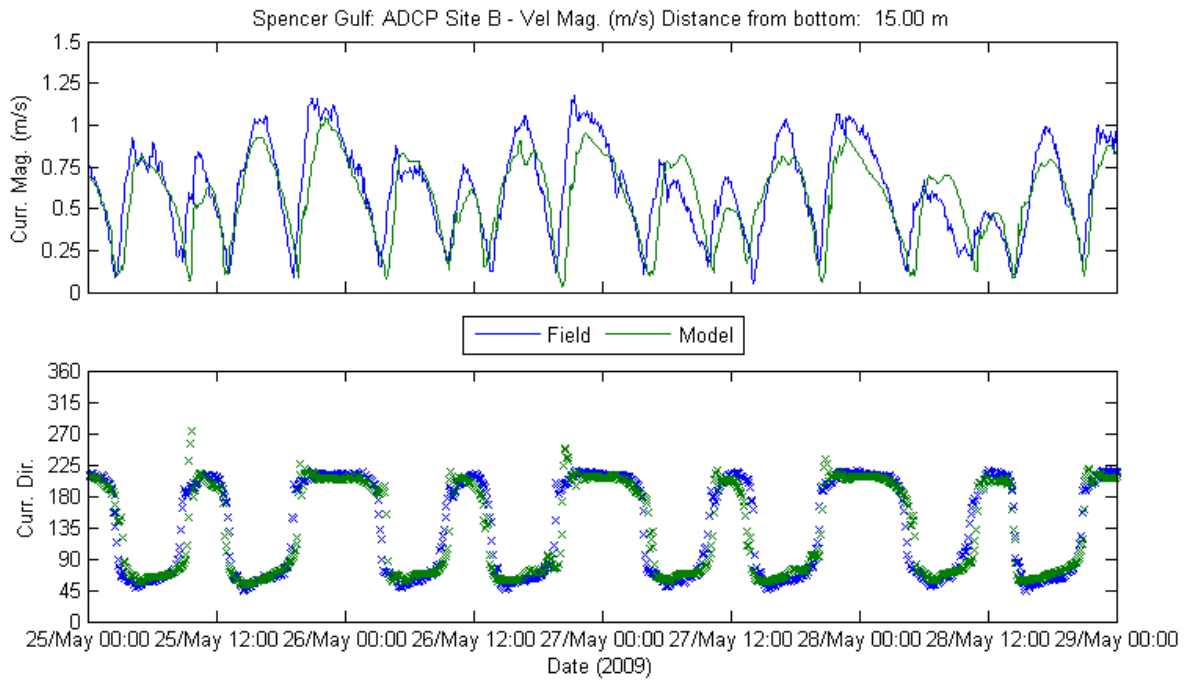


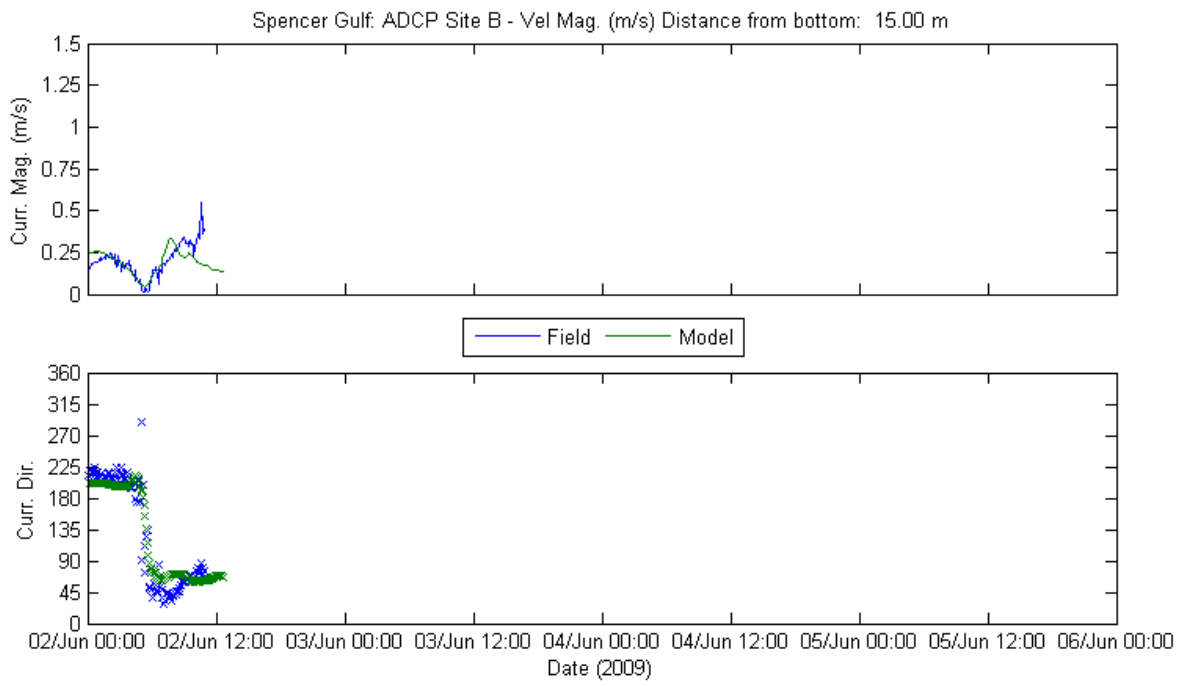




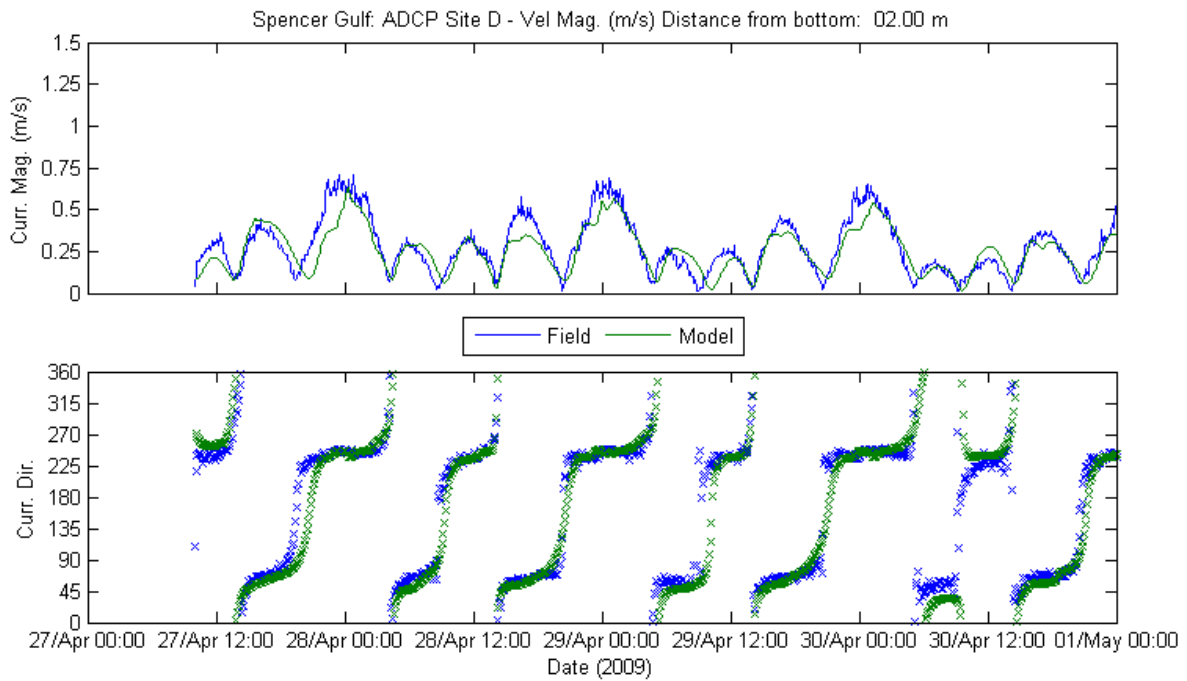
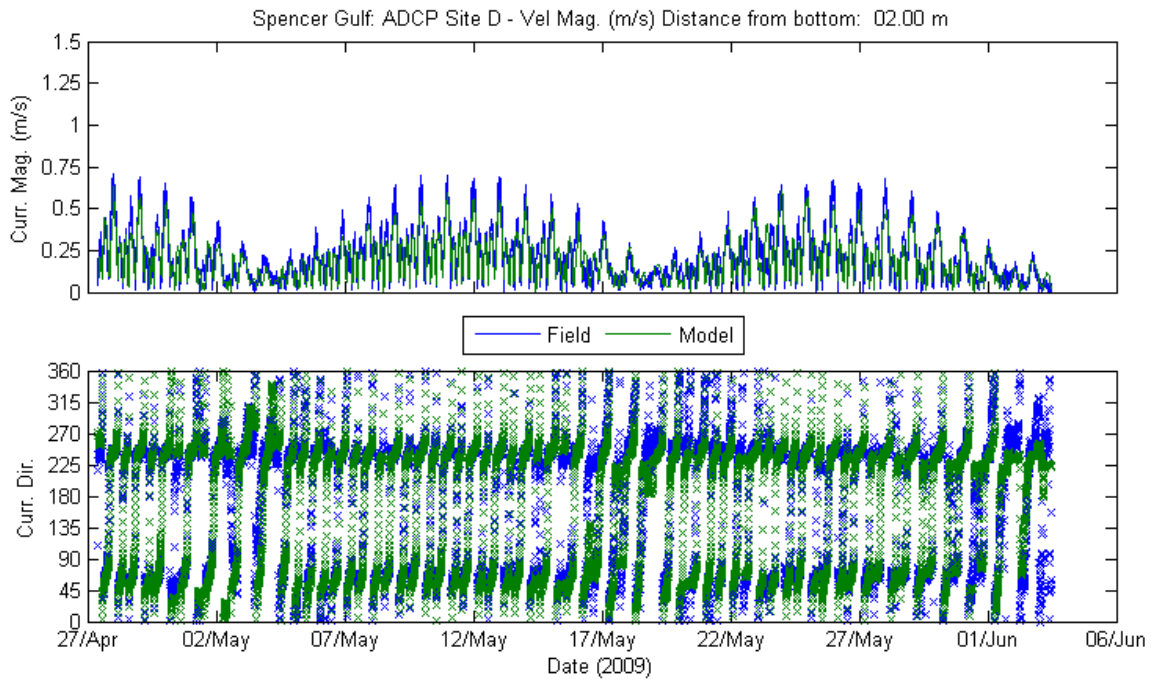


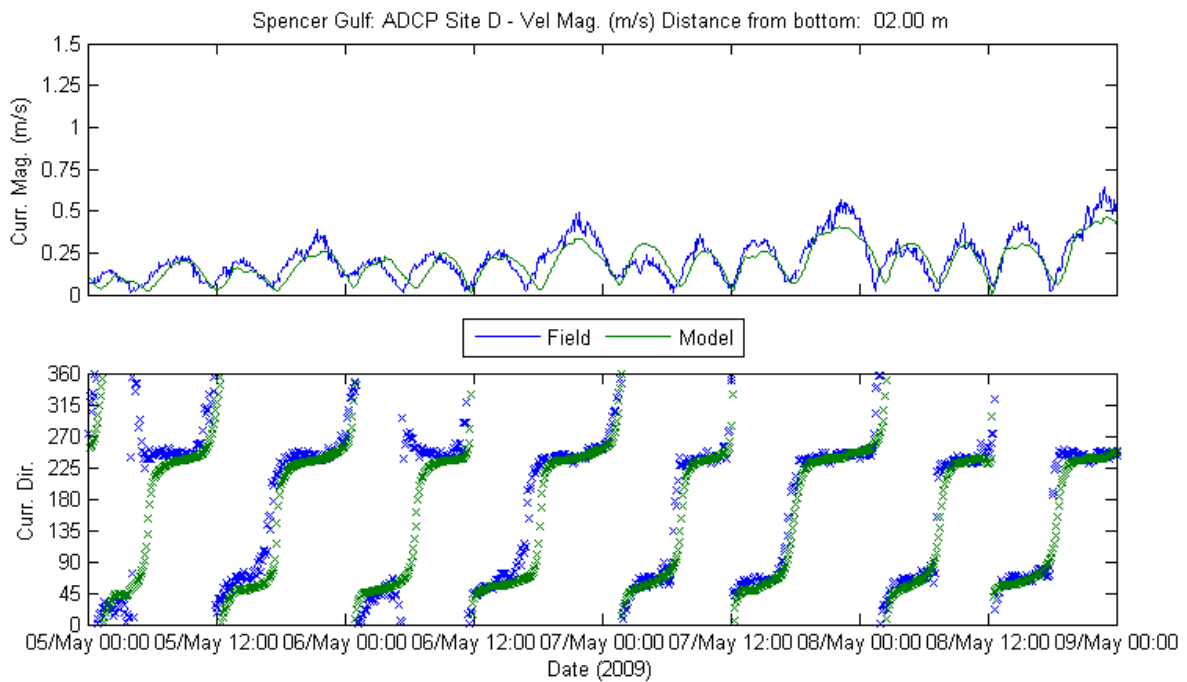
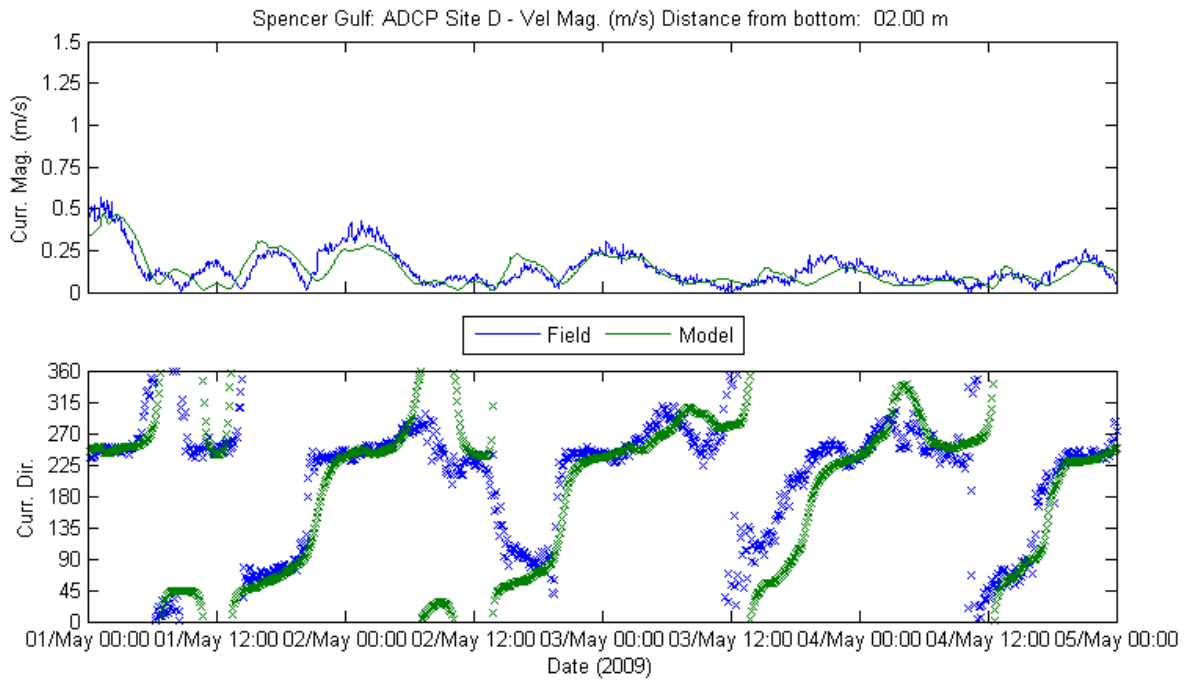


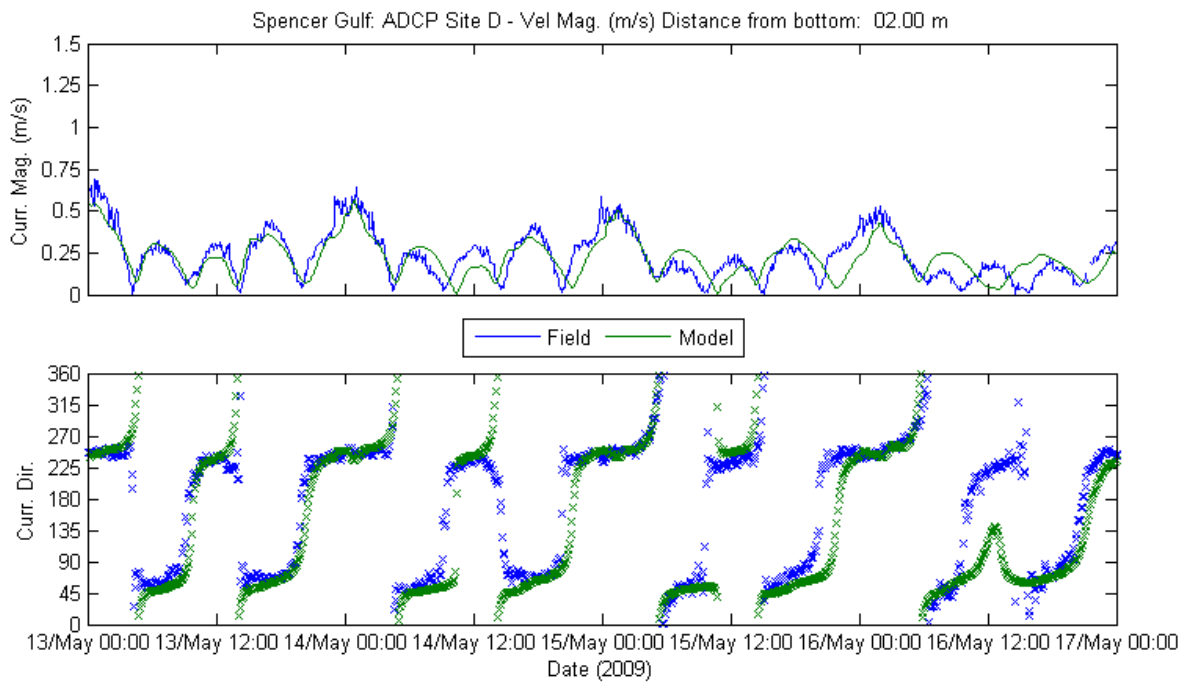
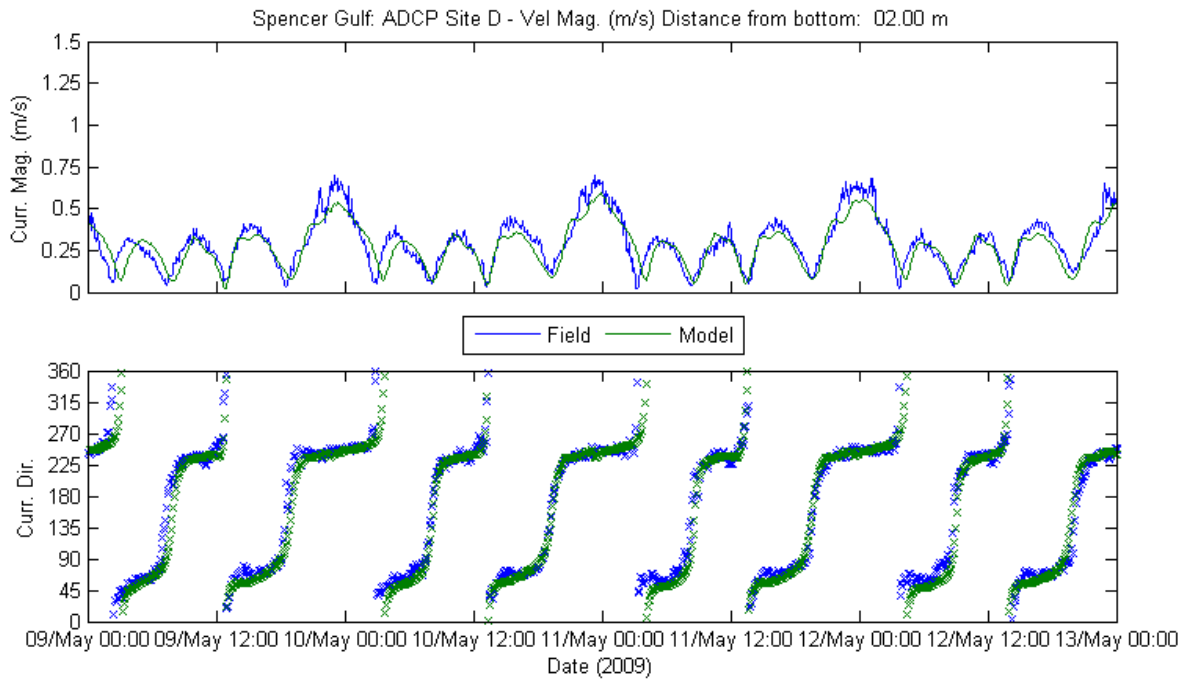


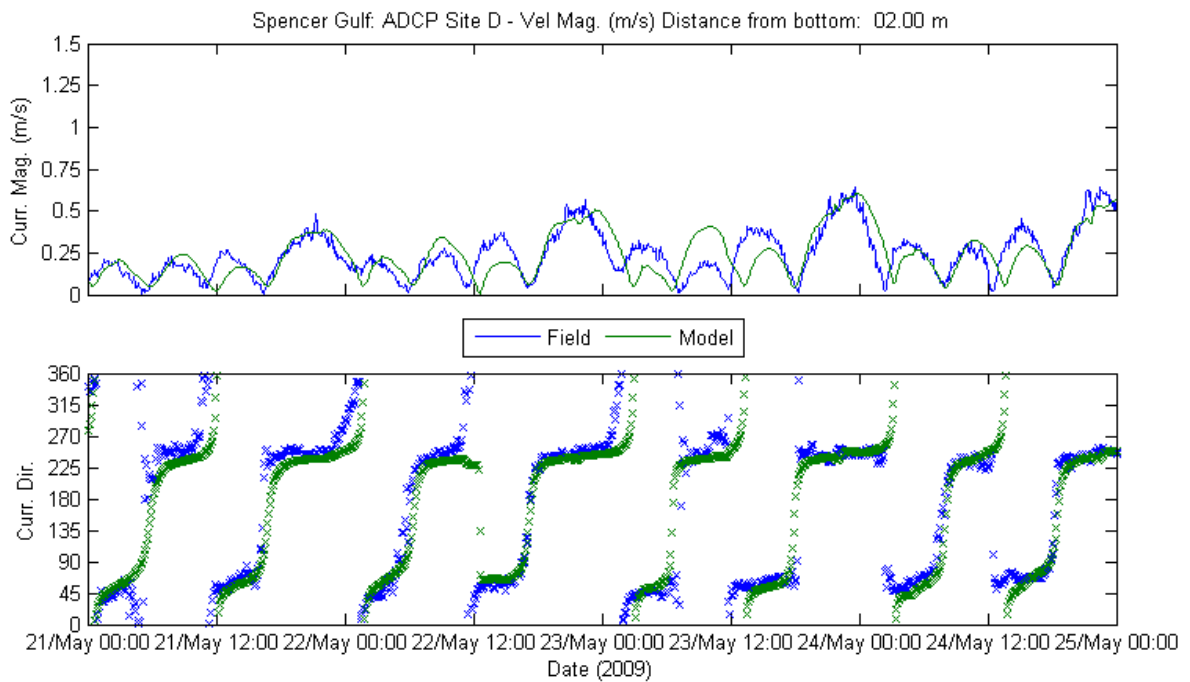
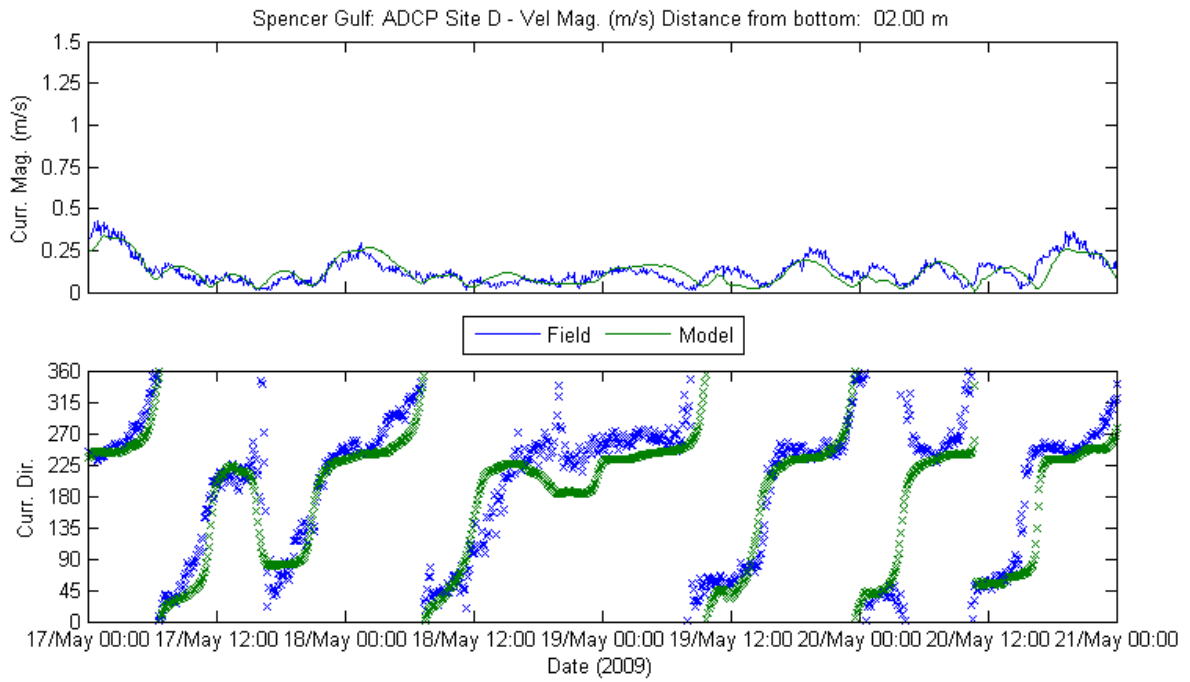


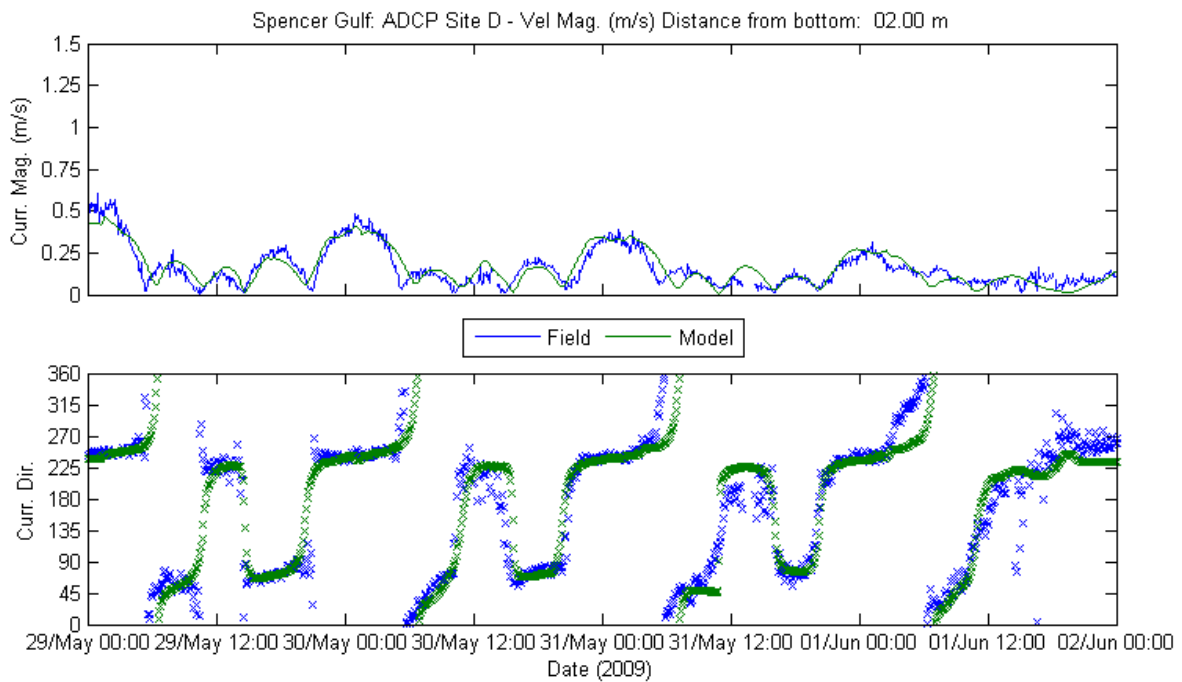
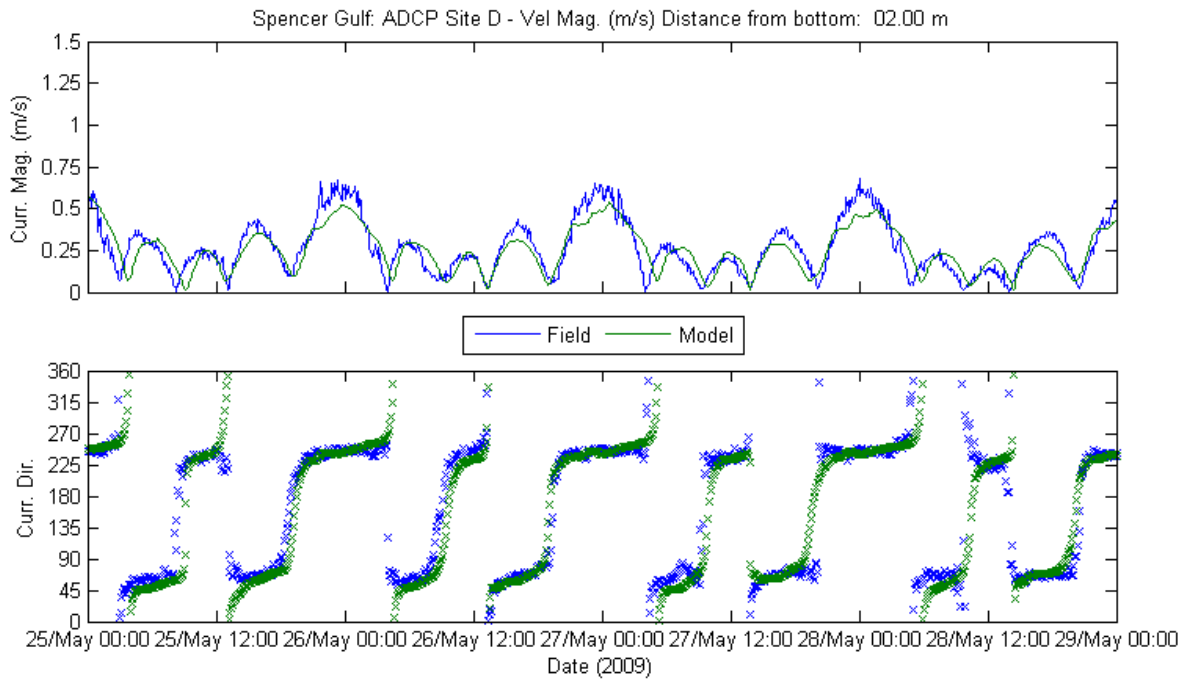
Site D at 2.00 m from Bottom

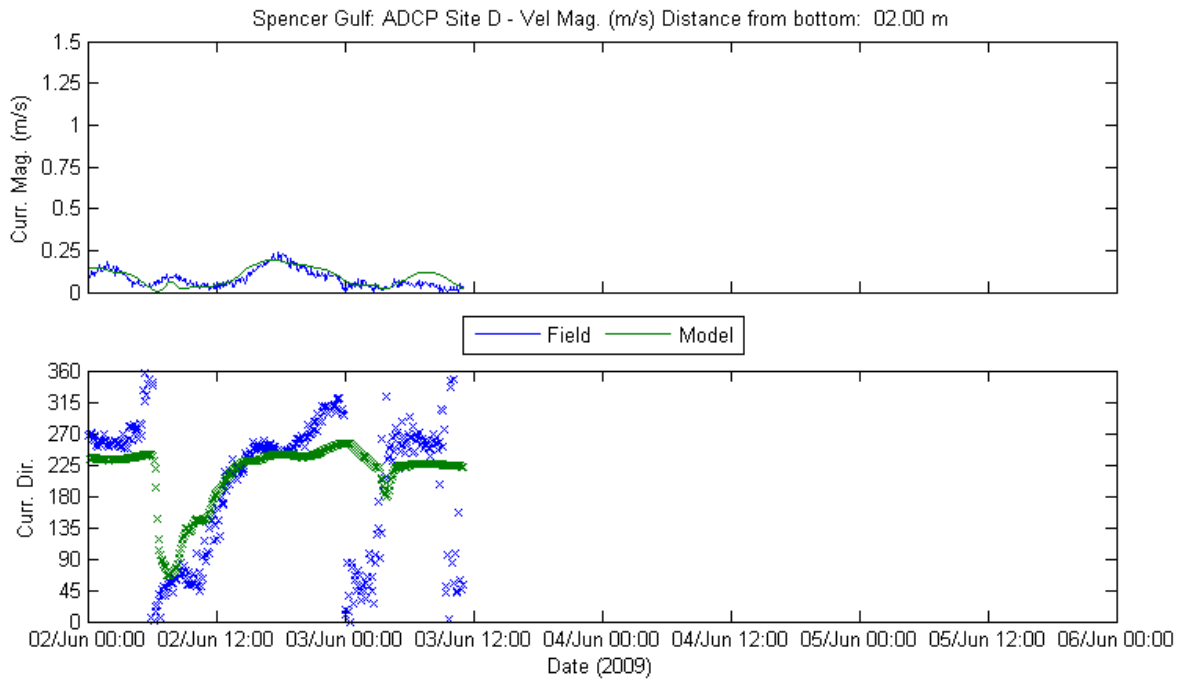






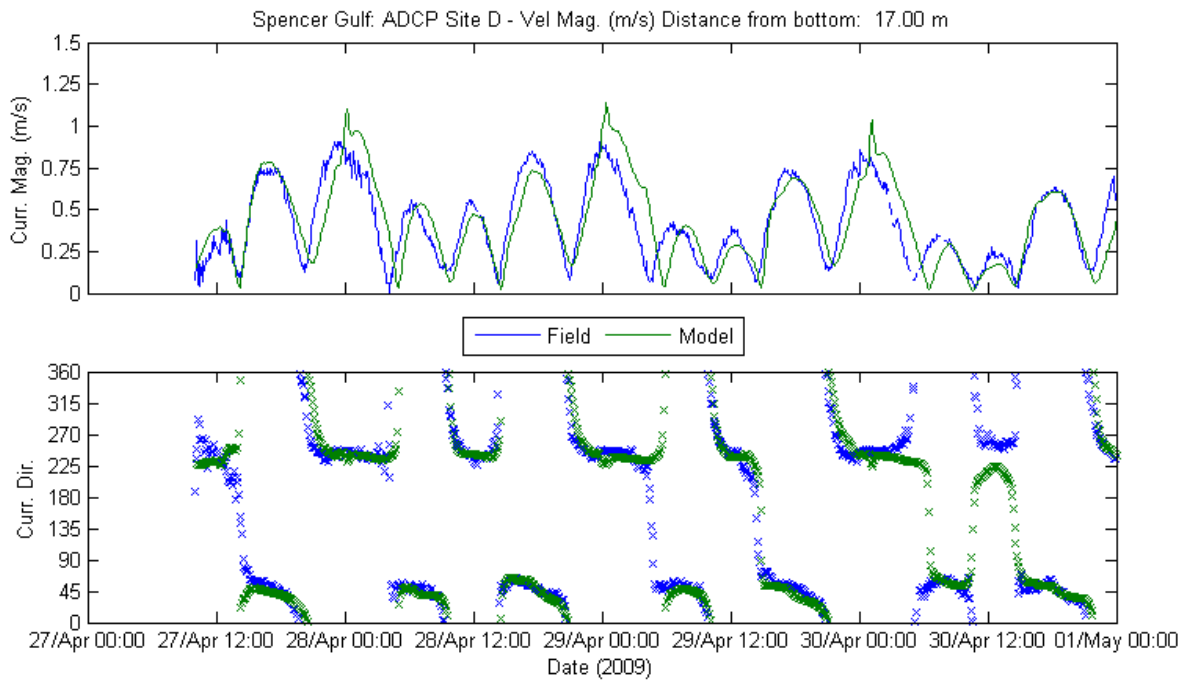
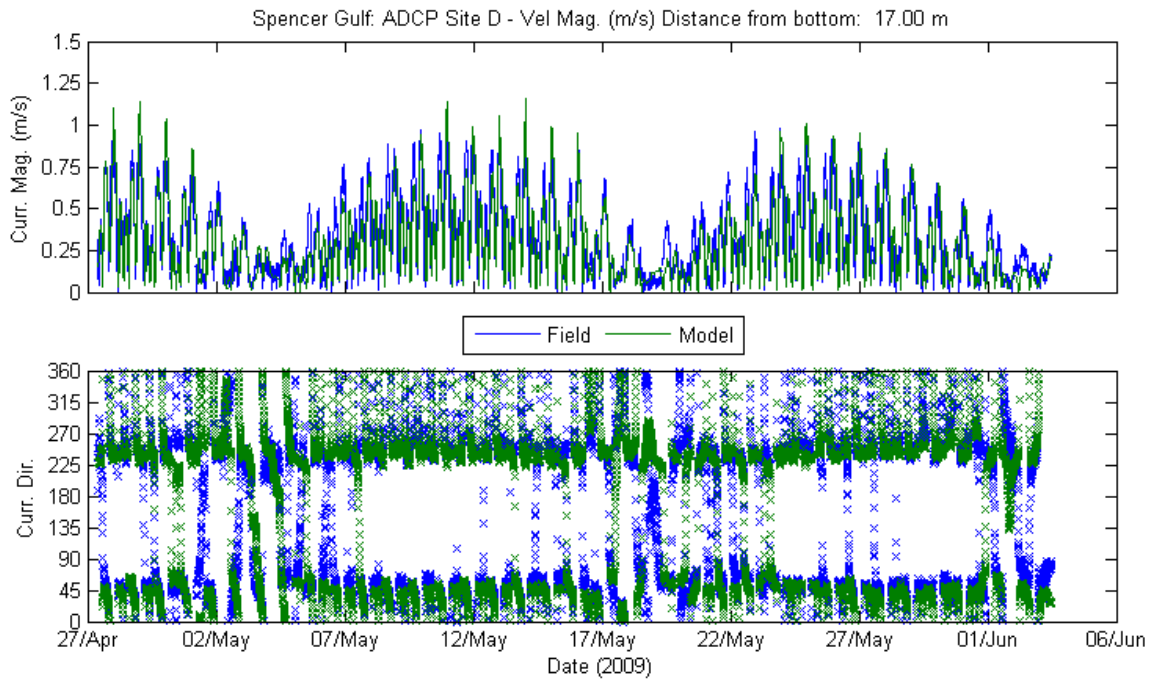


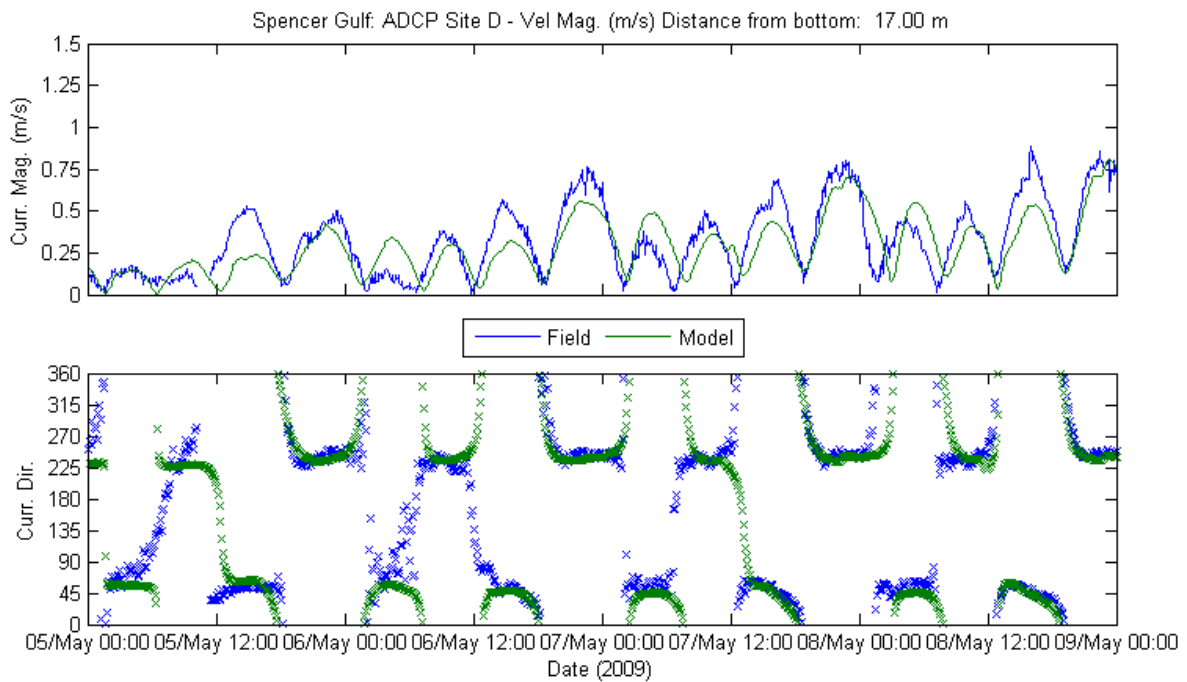
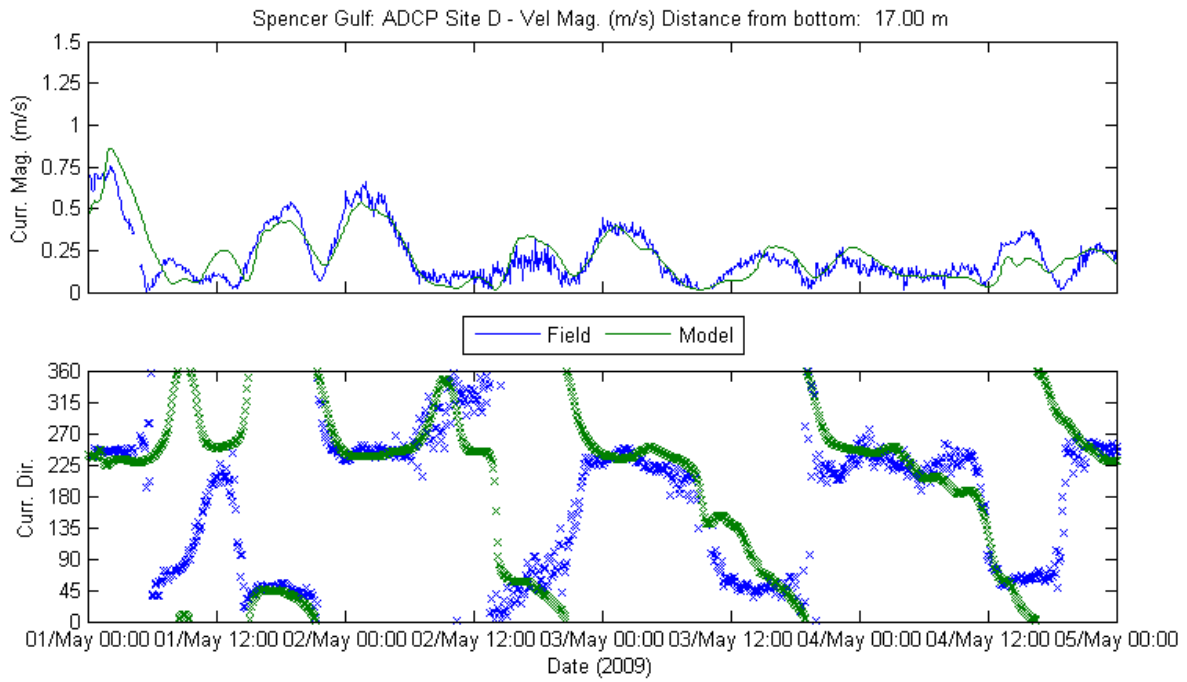


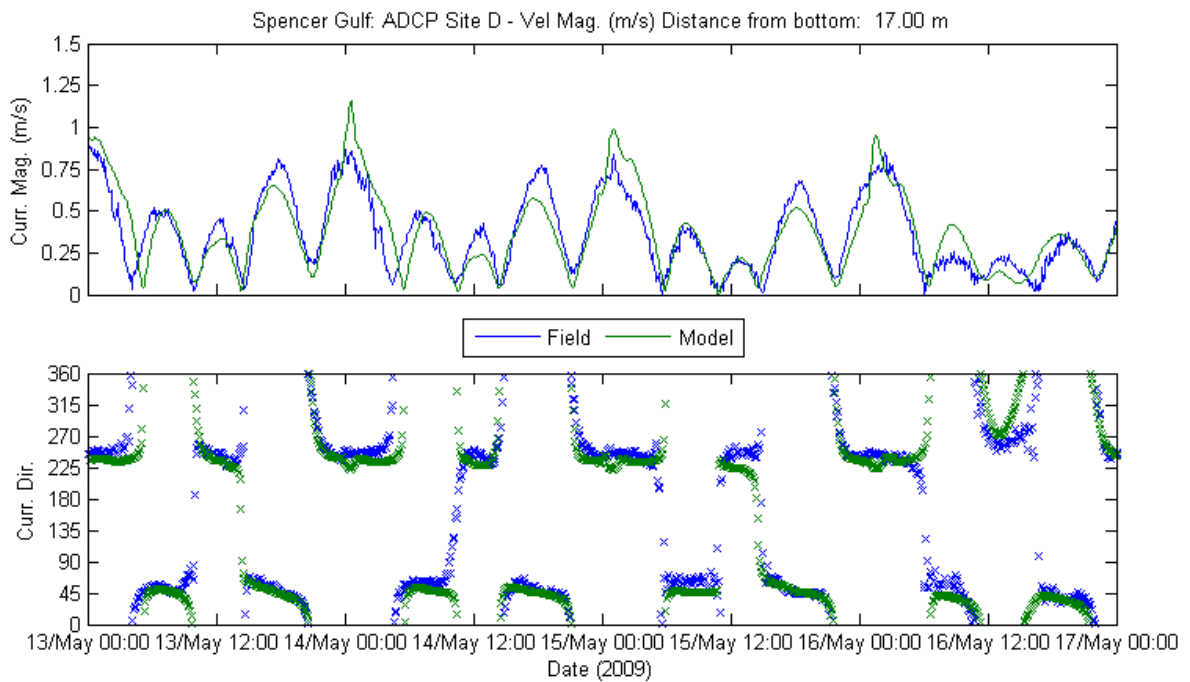
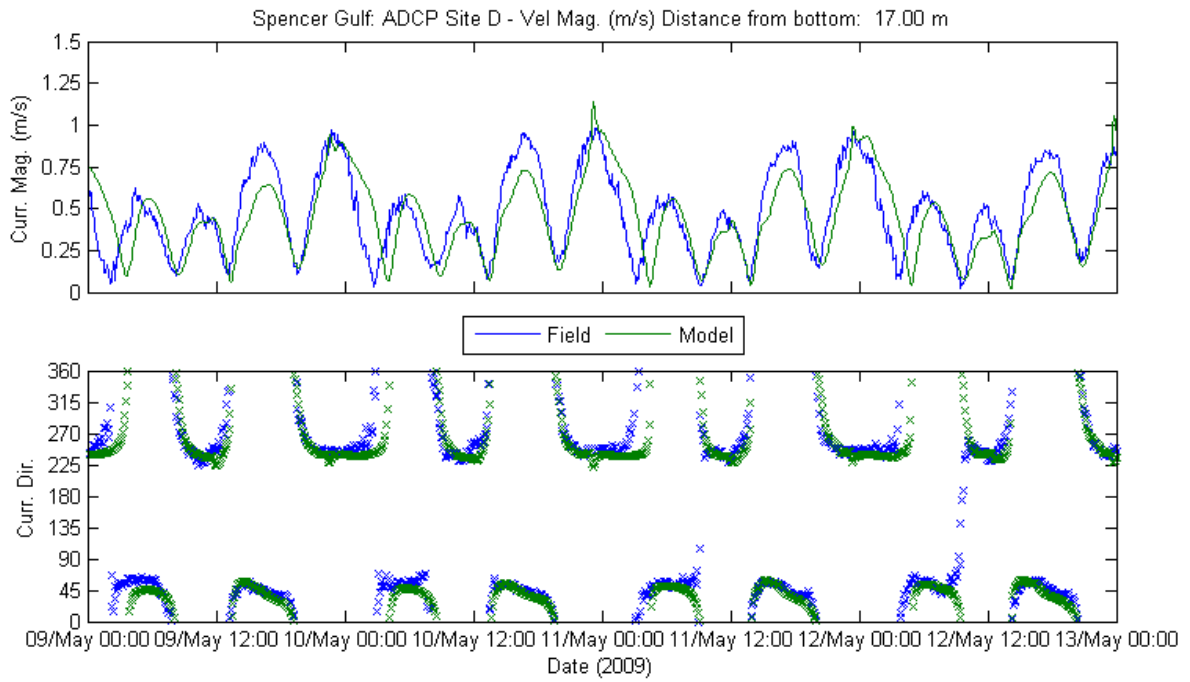


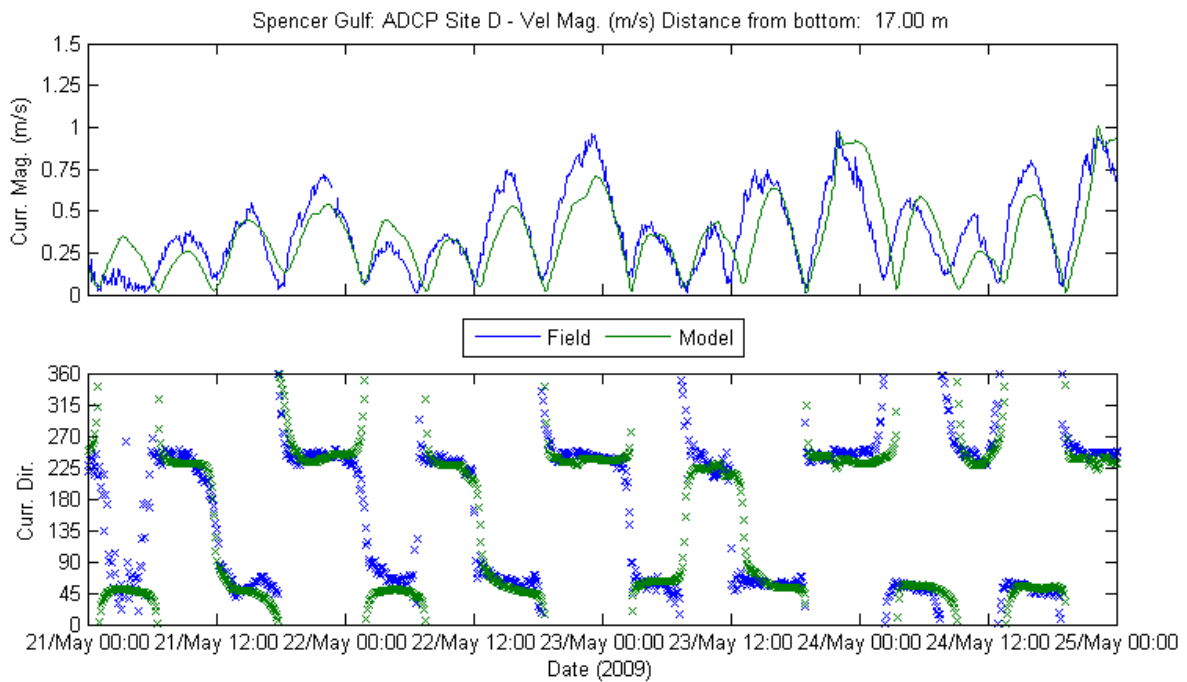
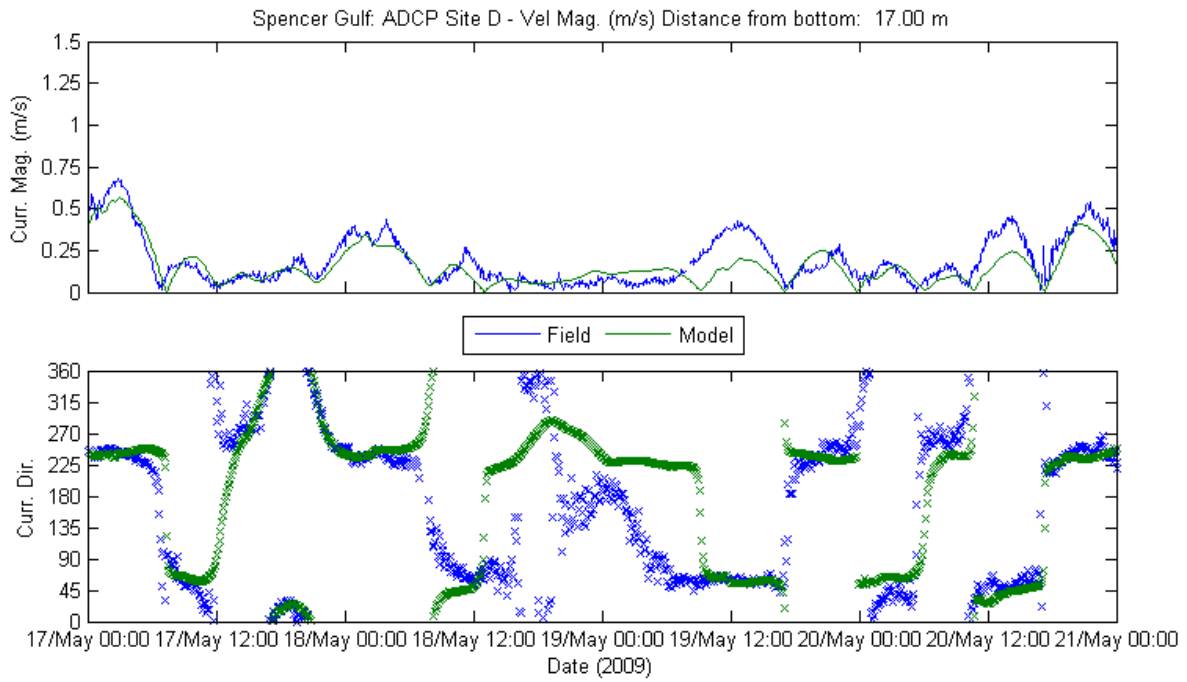


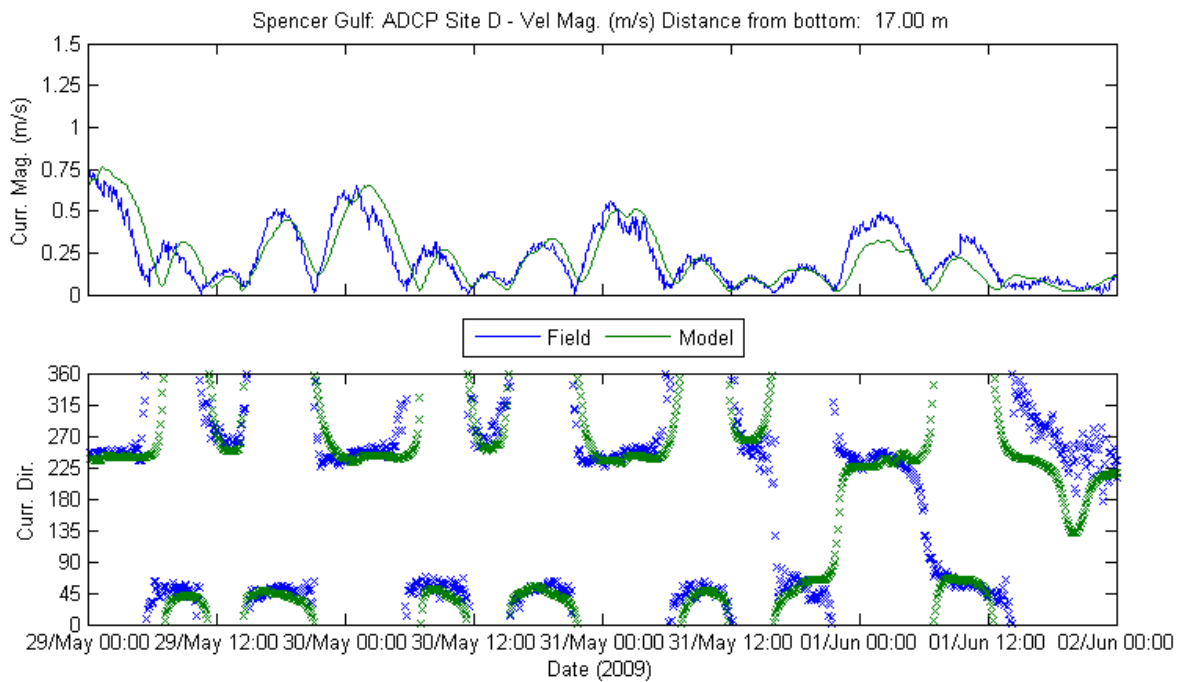
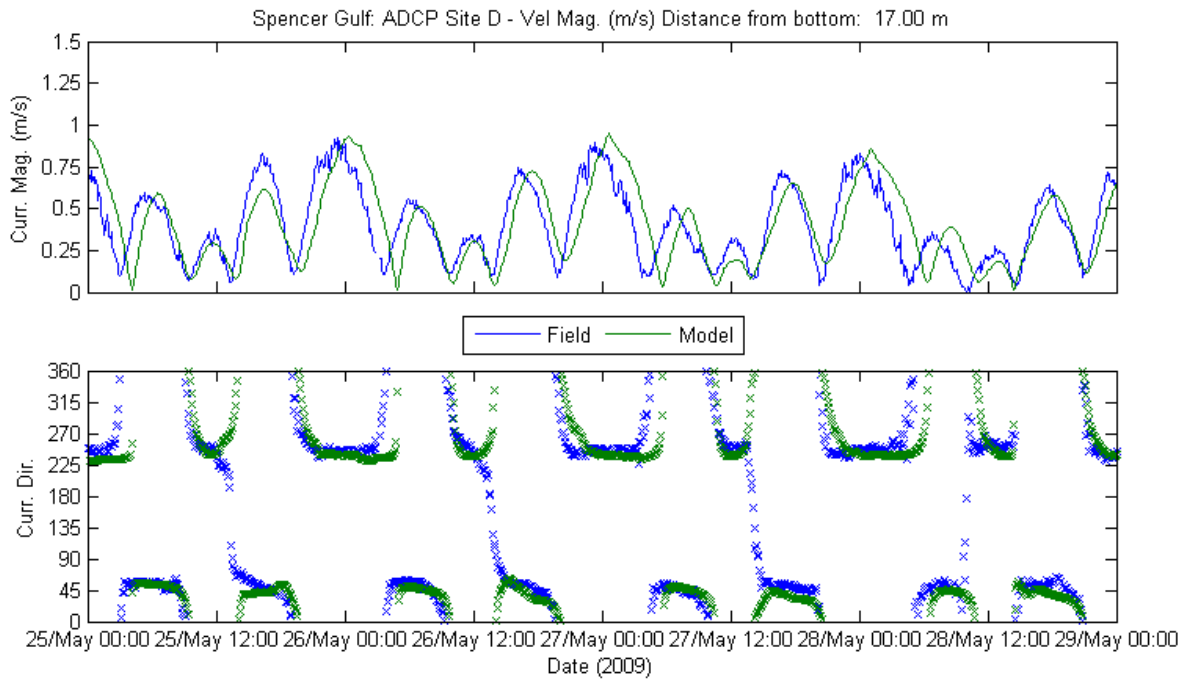
Site D at 17.00 m from Bottom

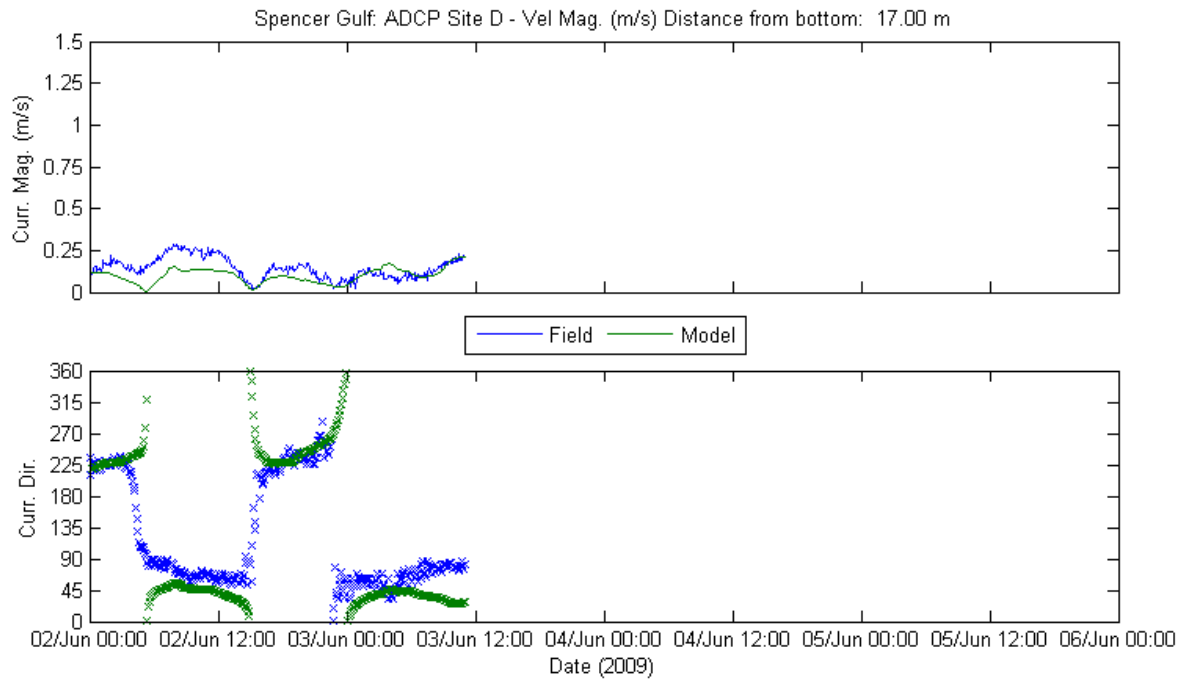




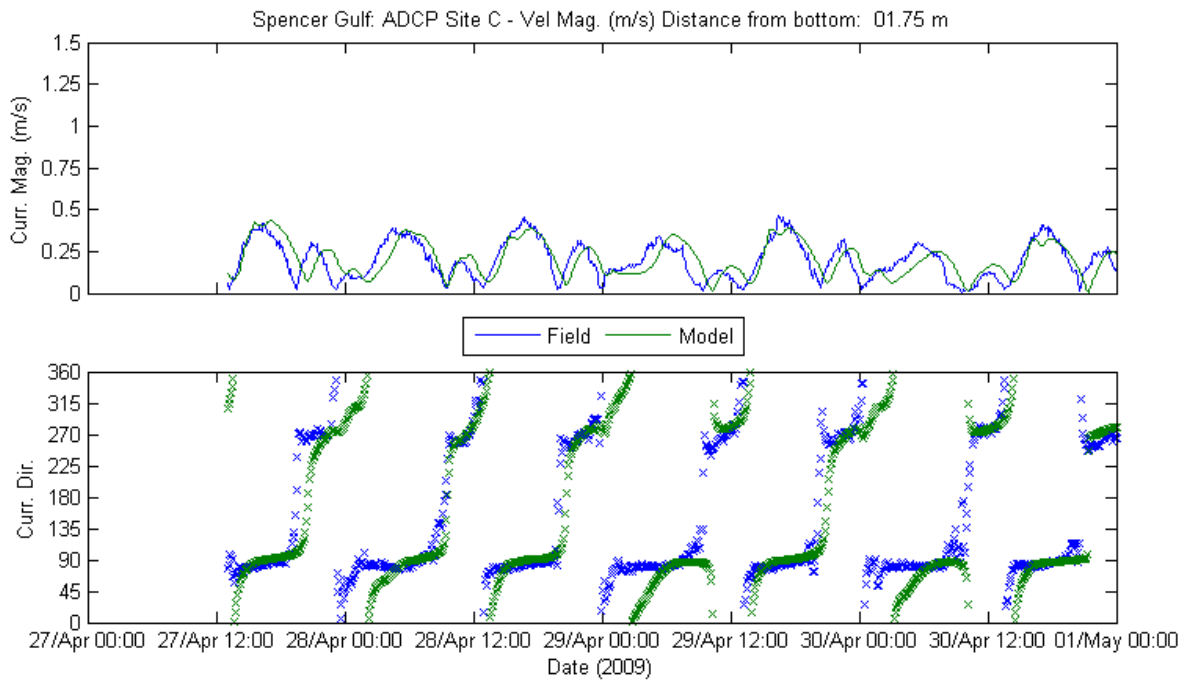
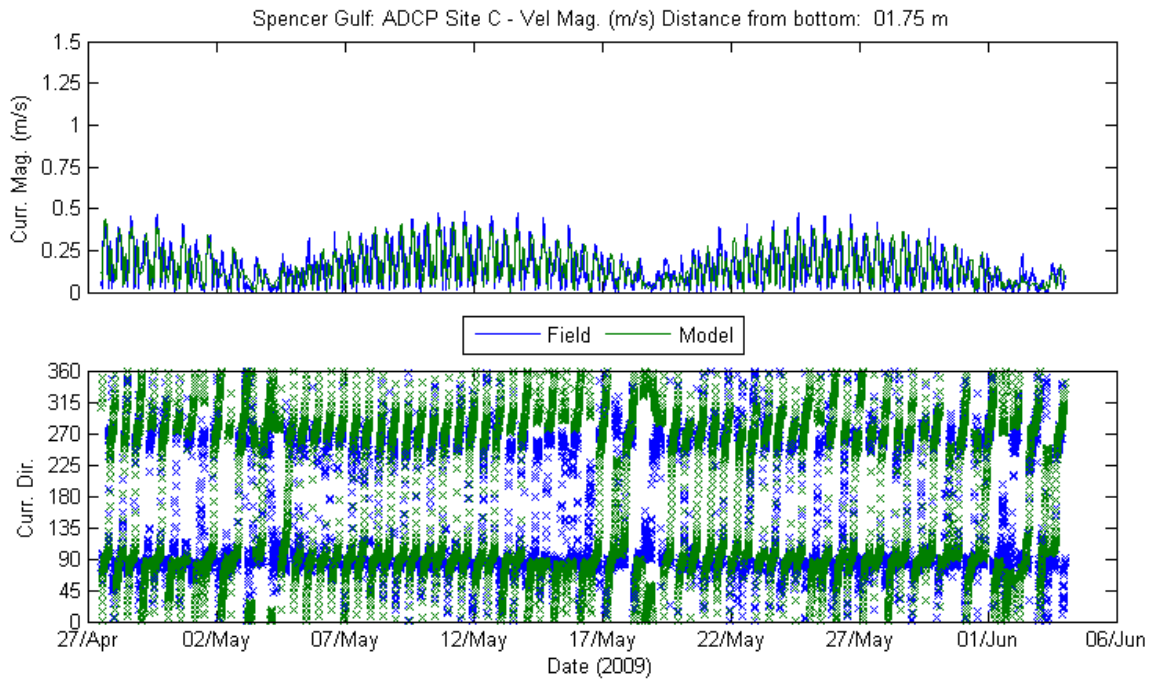


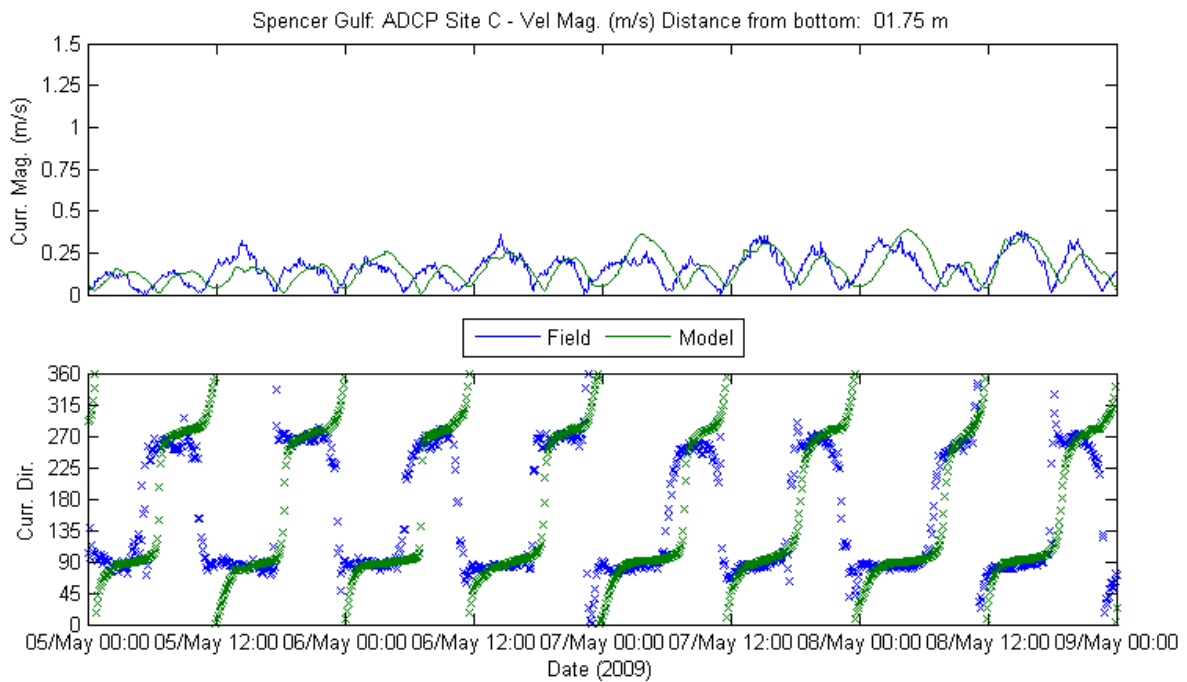
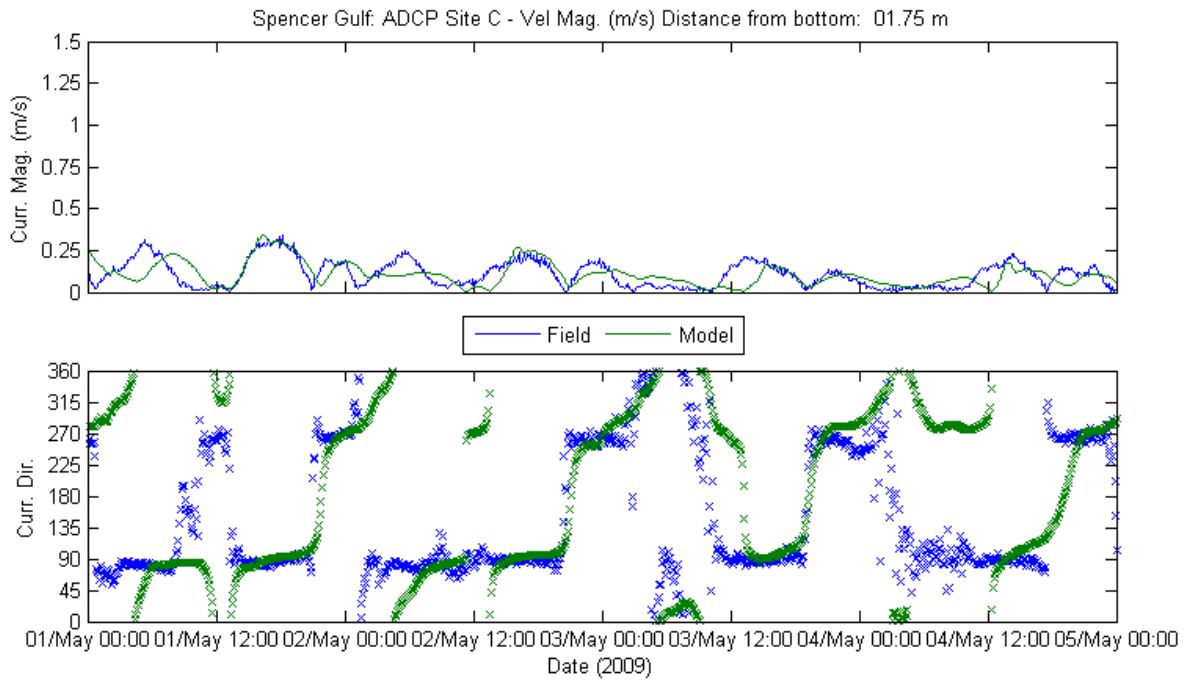




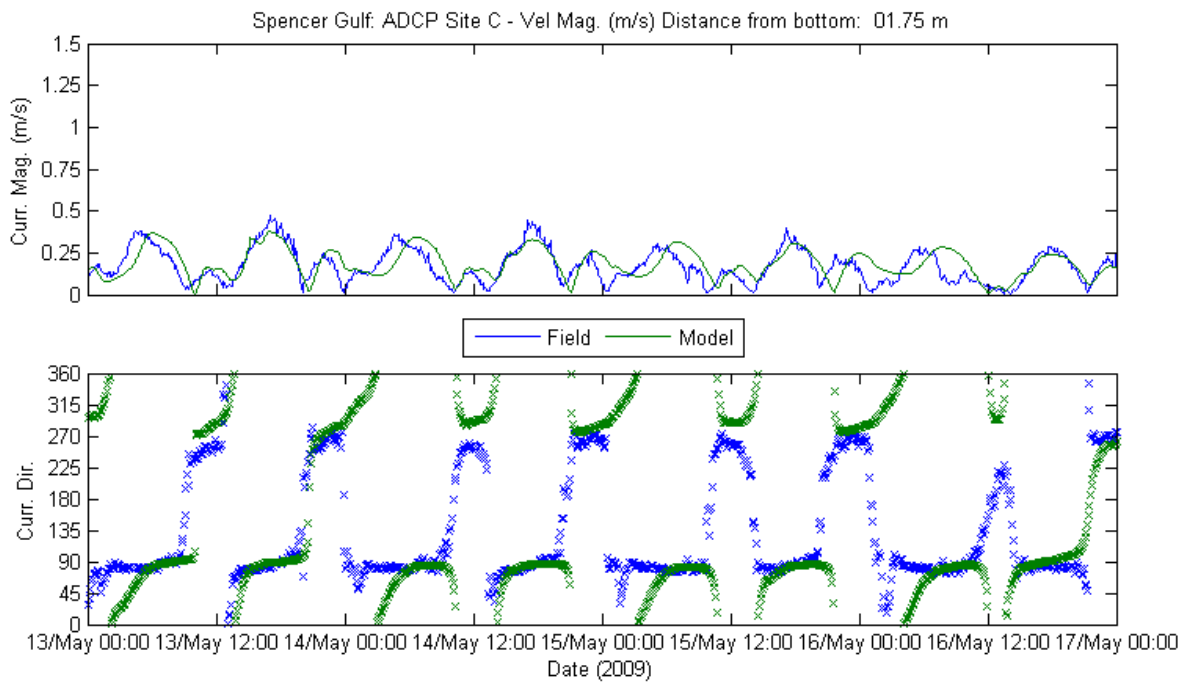
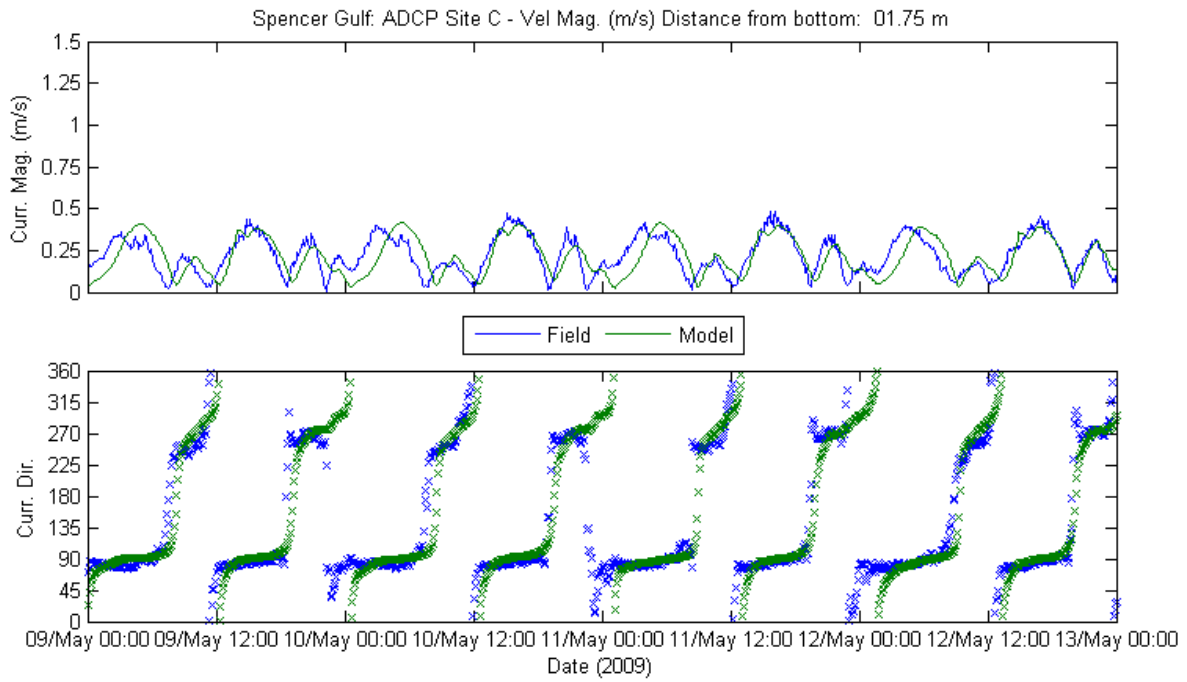


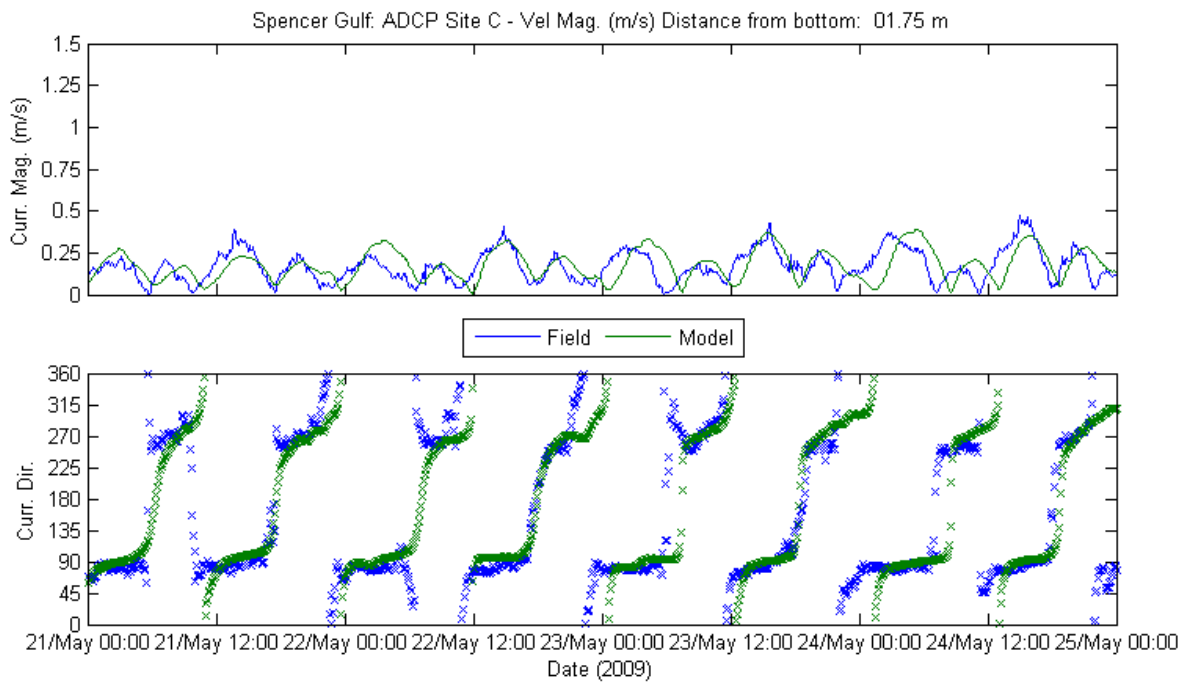
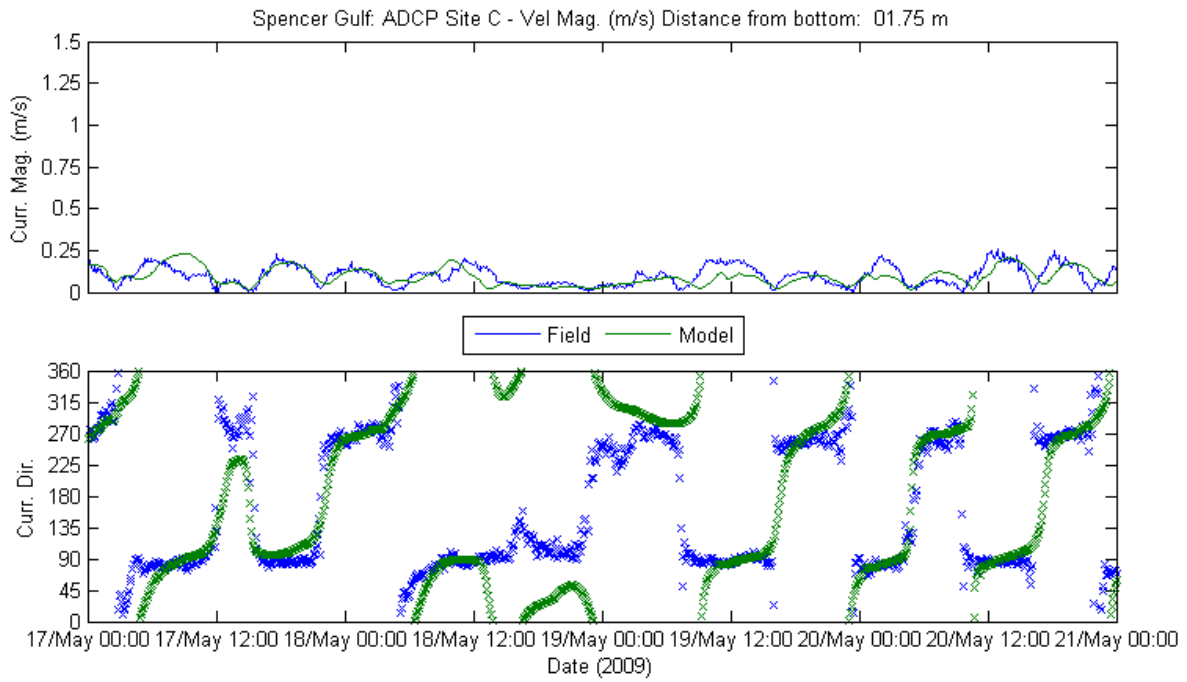
Site C at 1.75 m from Bottom

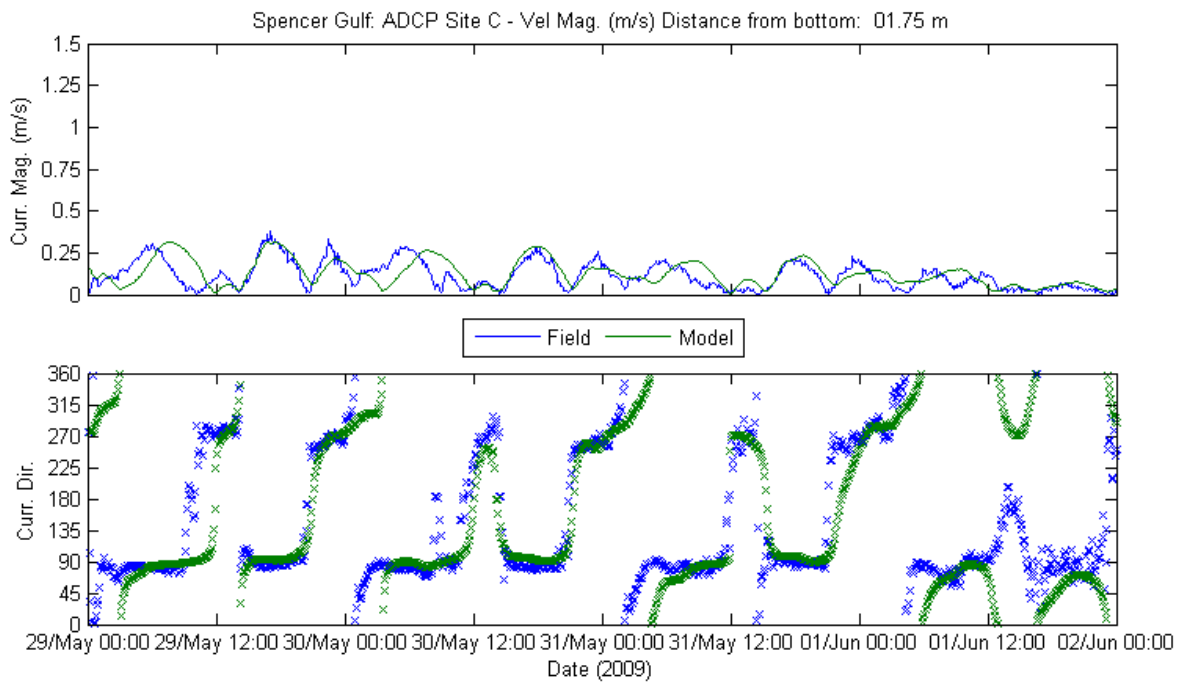
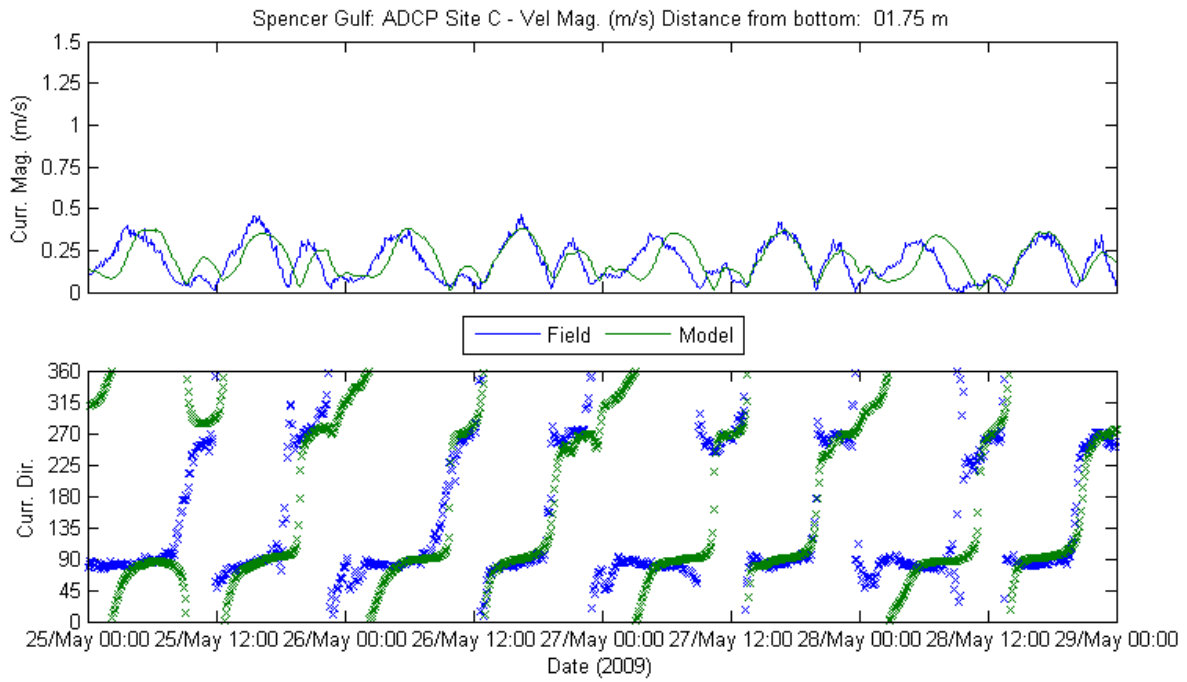


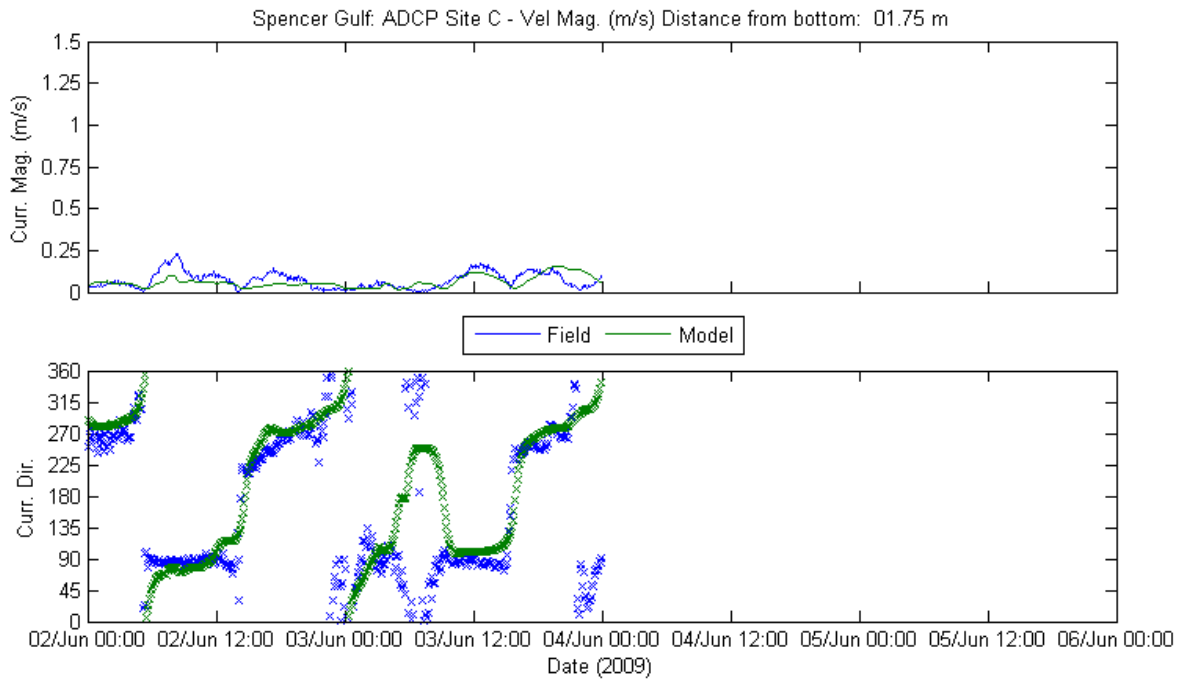




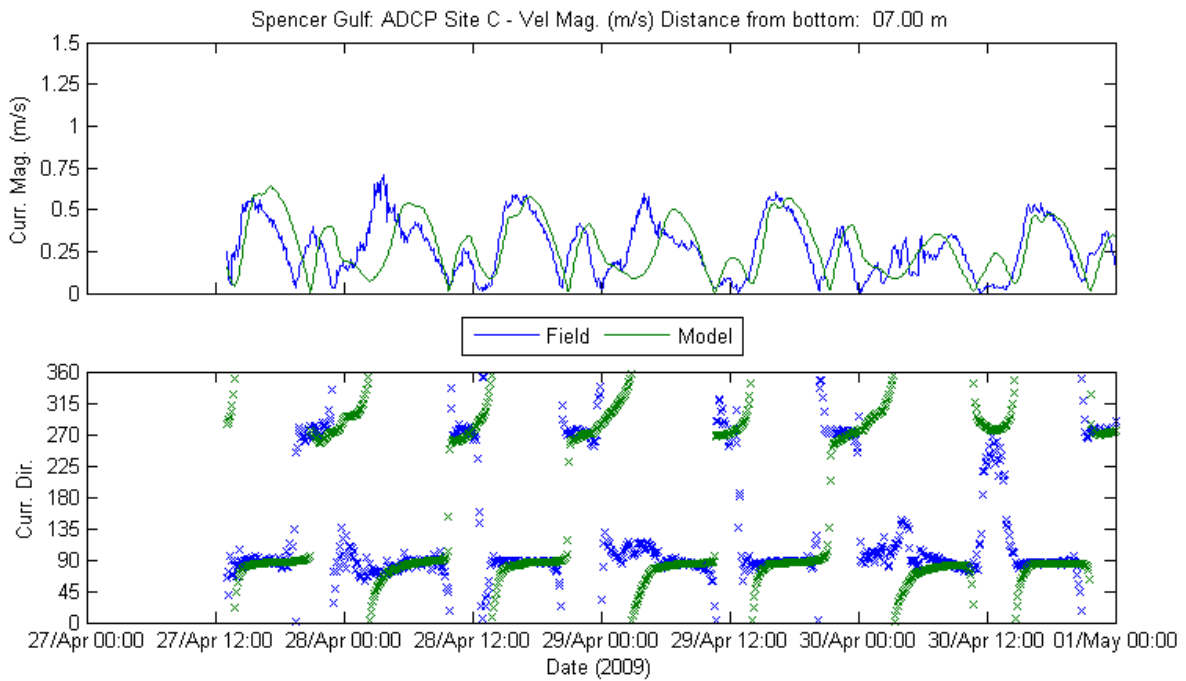
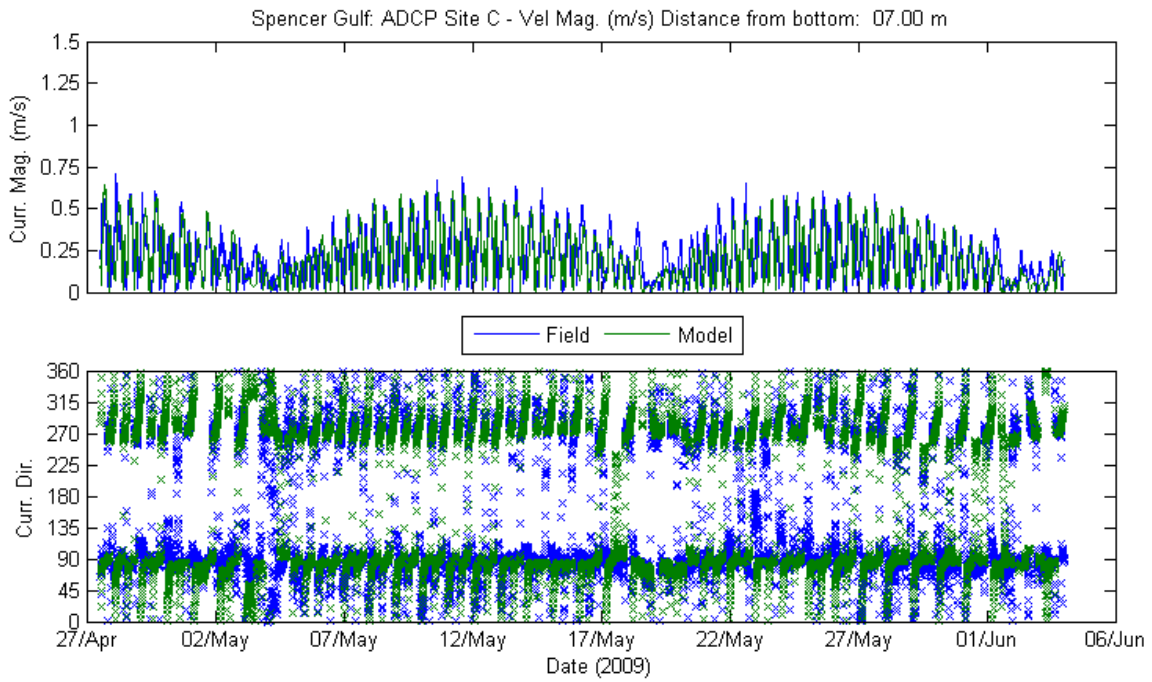


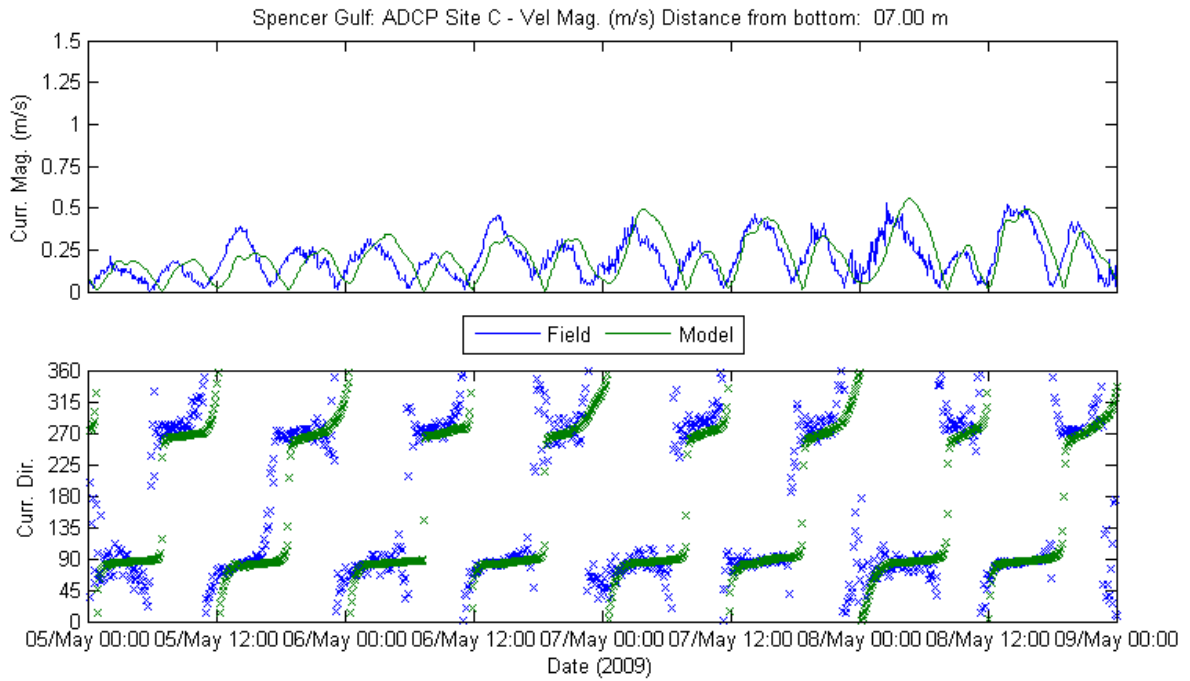
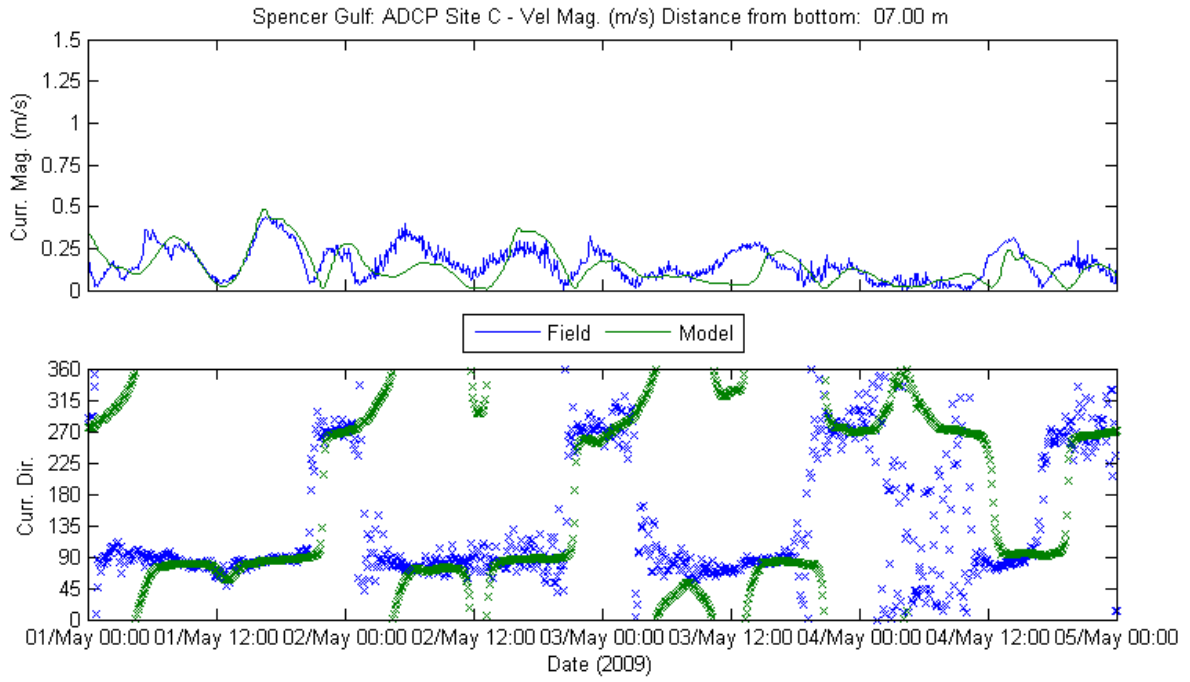


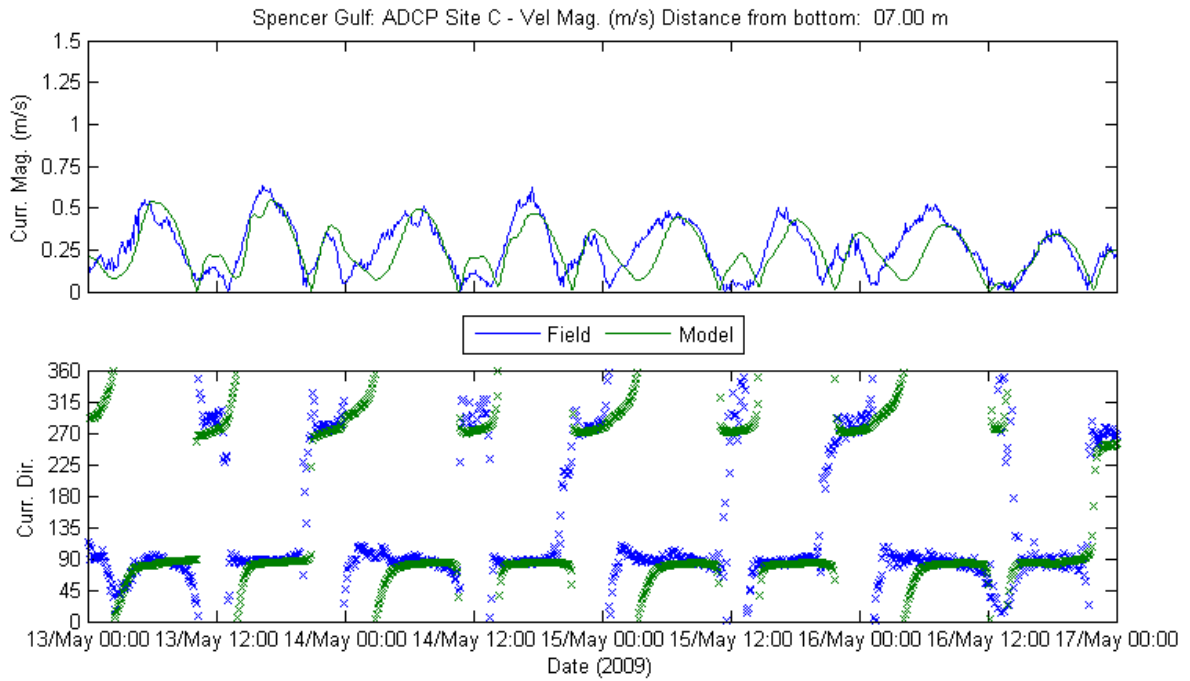
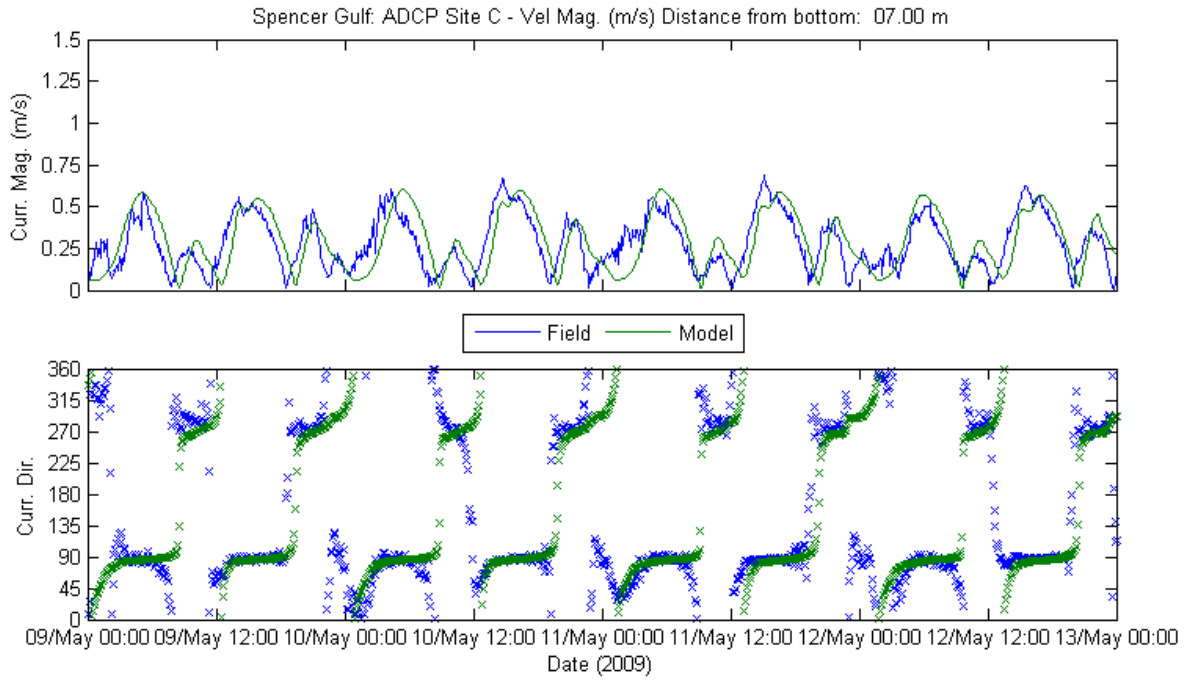


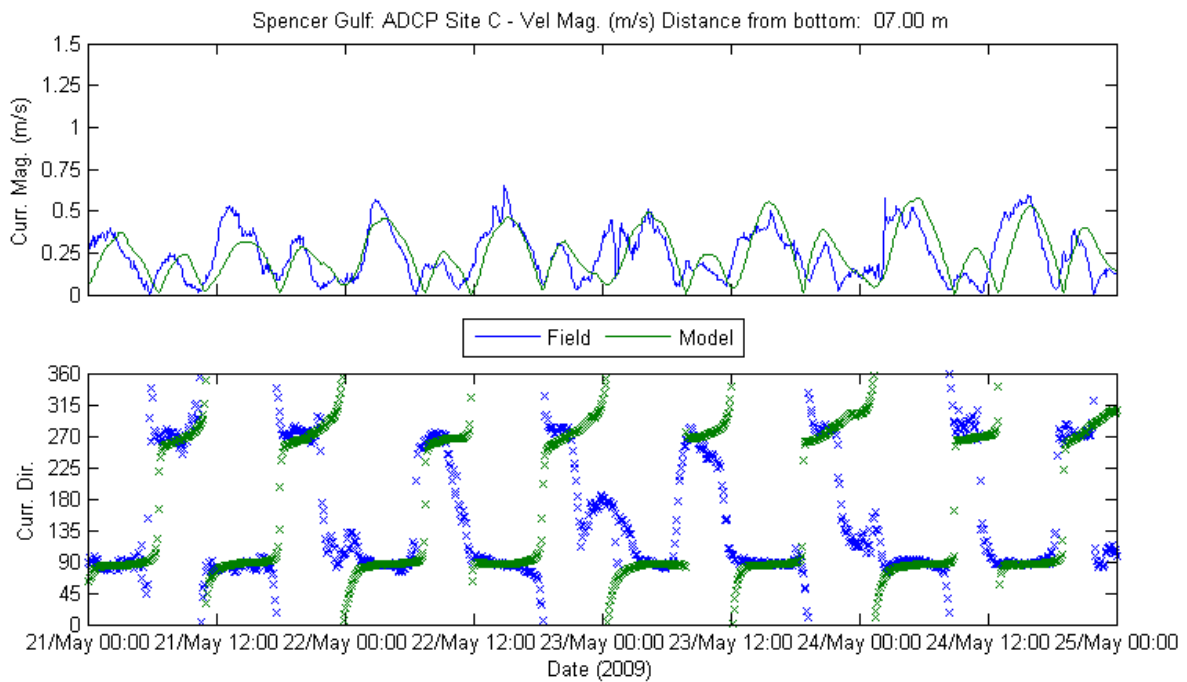
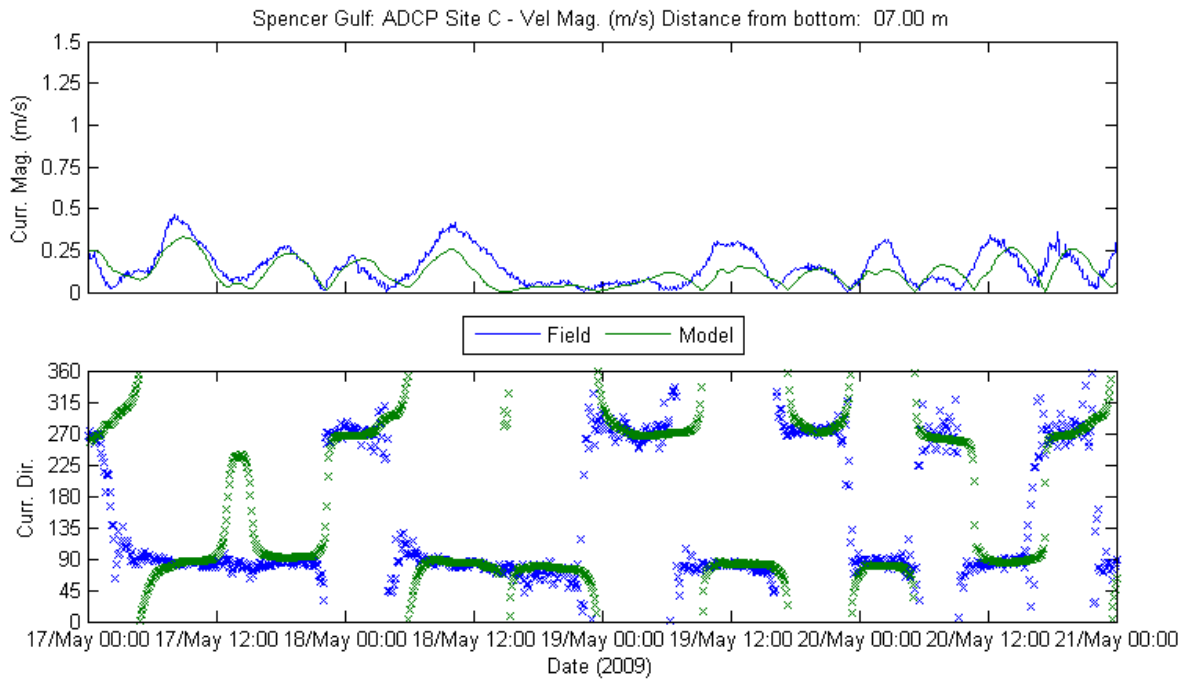


Site C at 7.00 m from Bottom

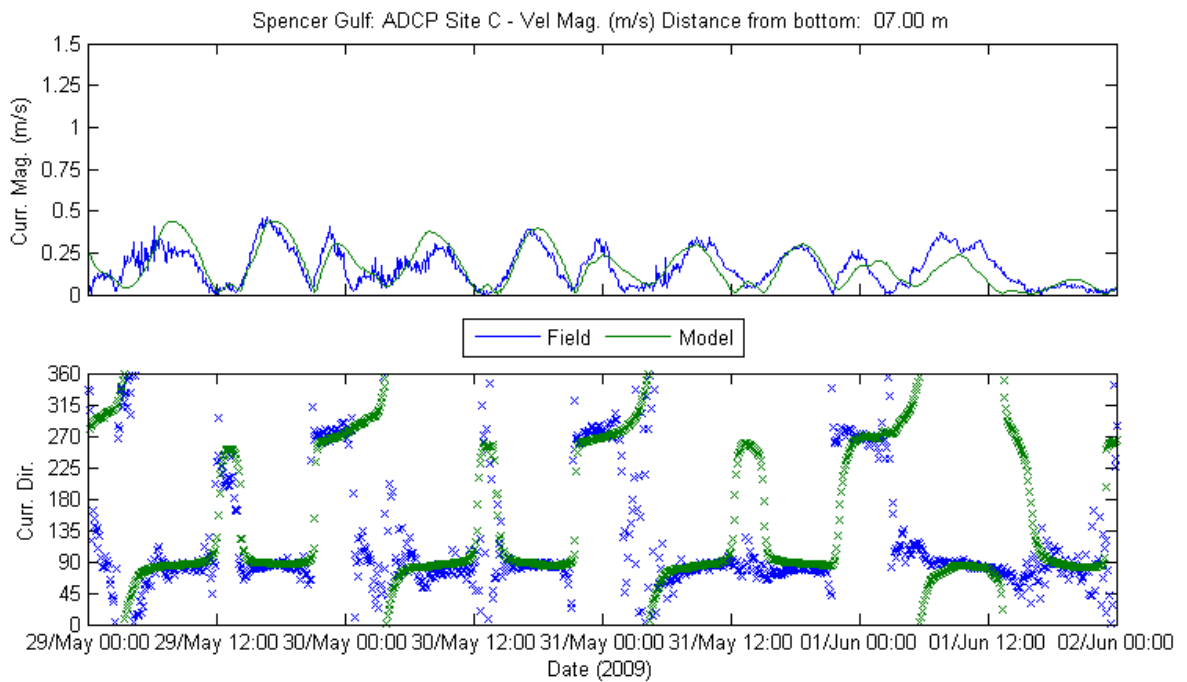
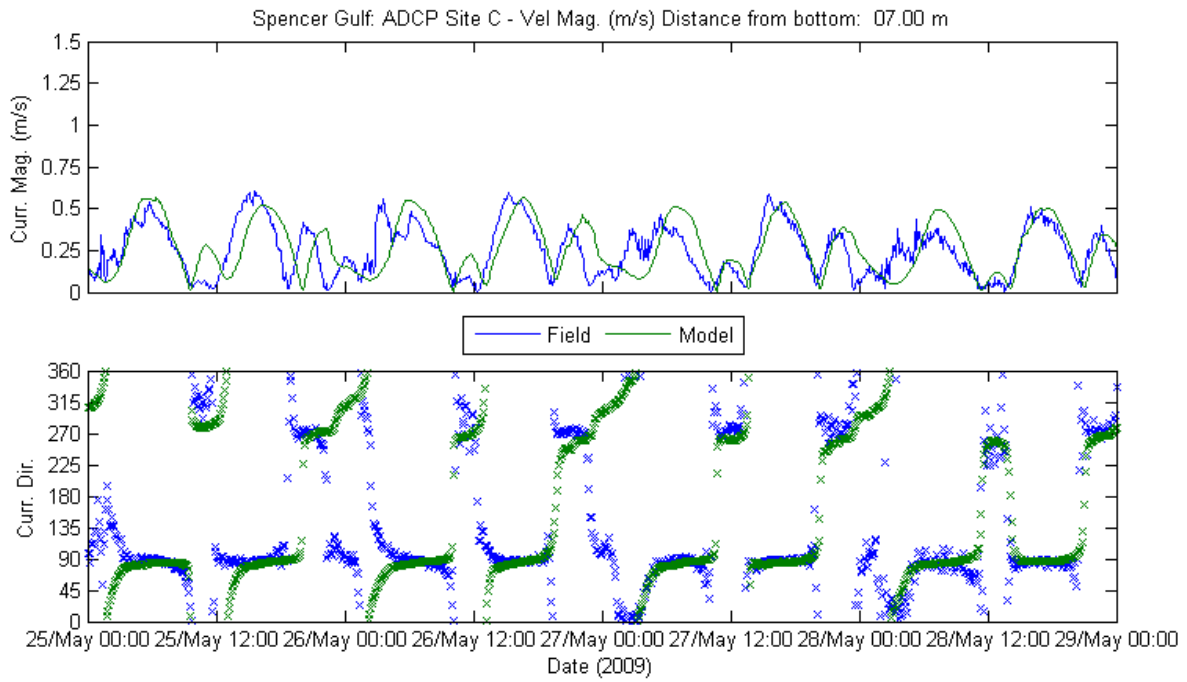


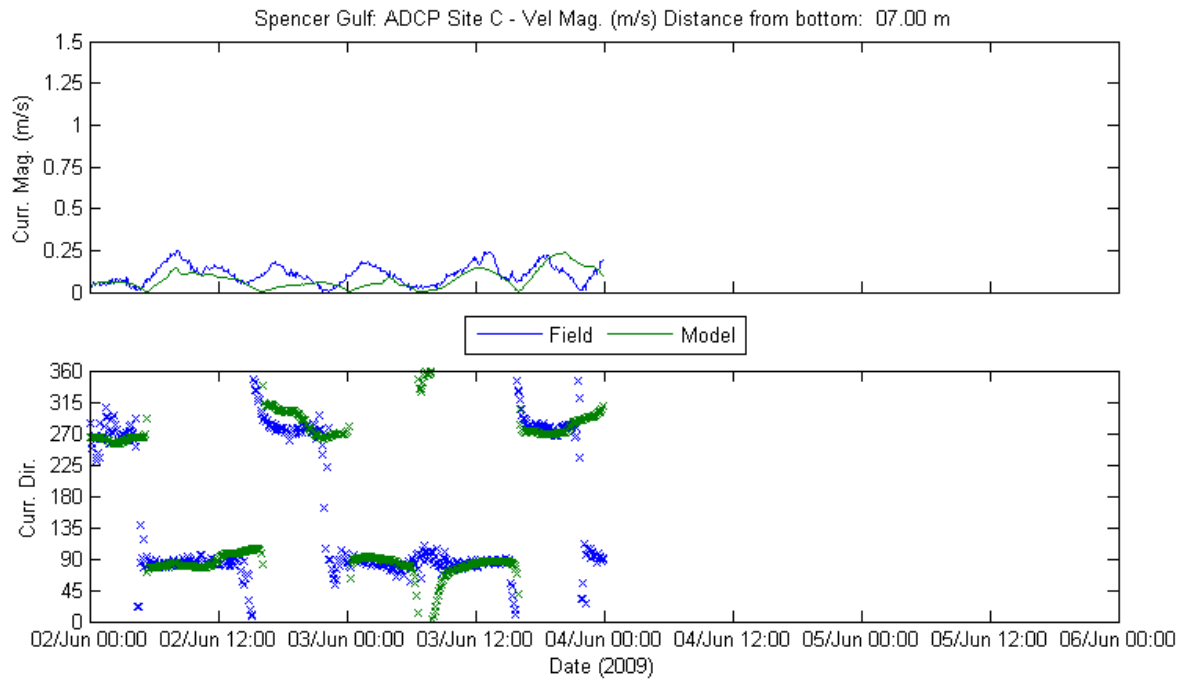




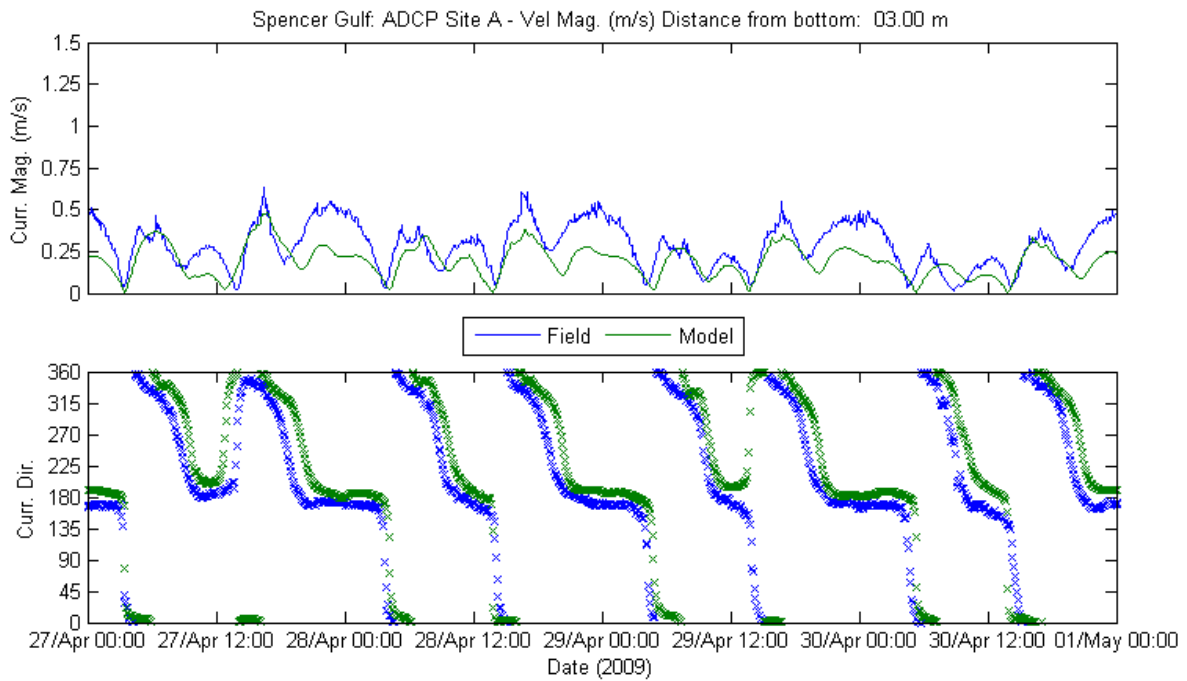
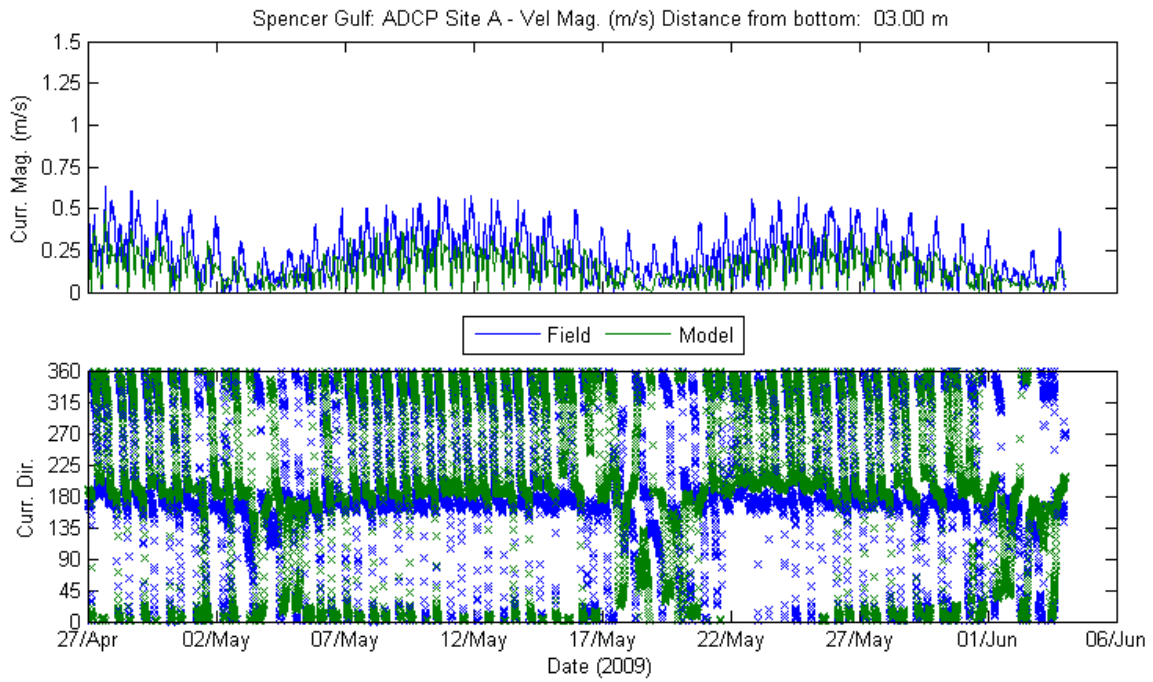


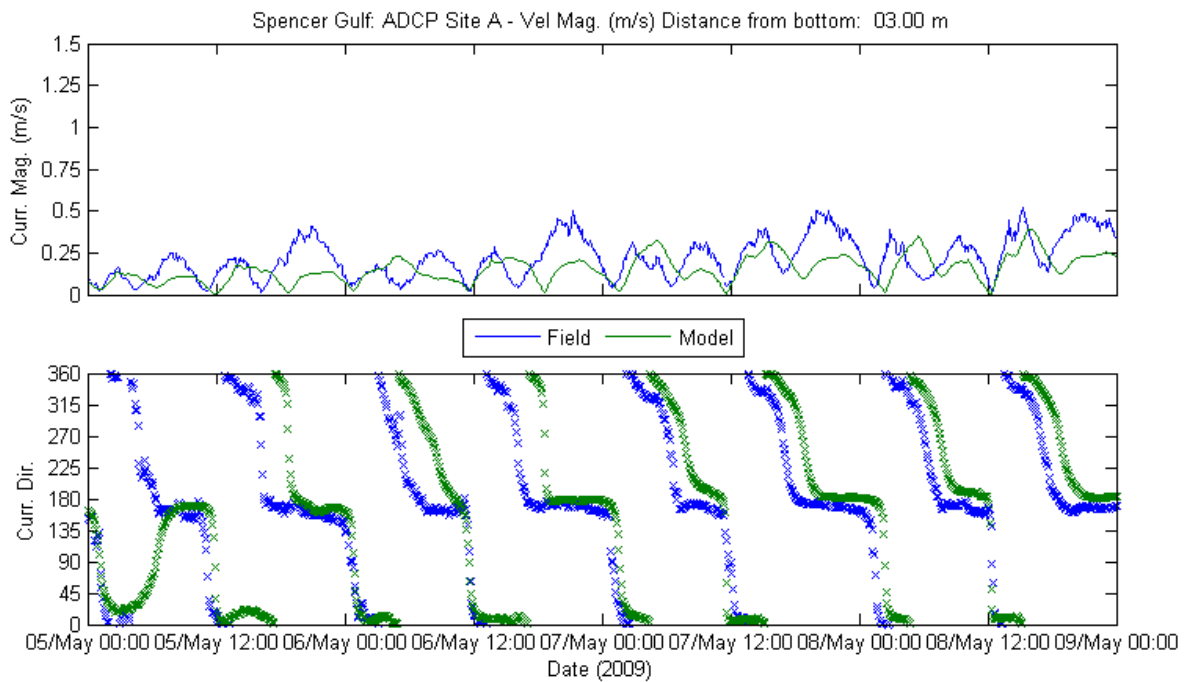
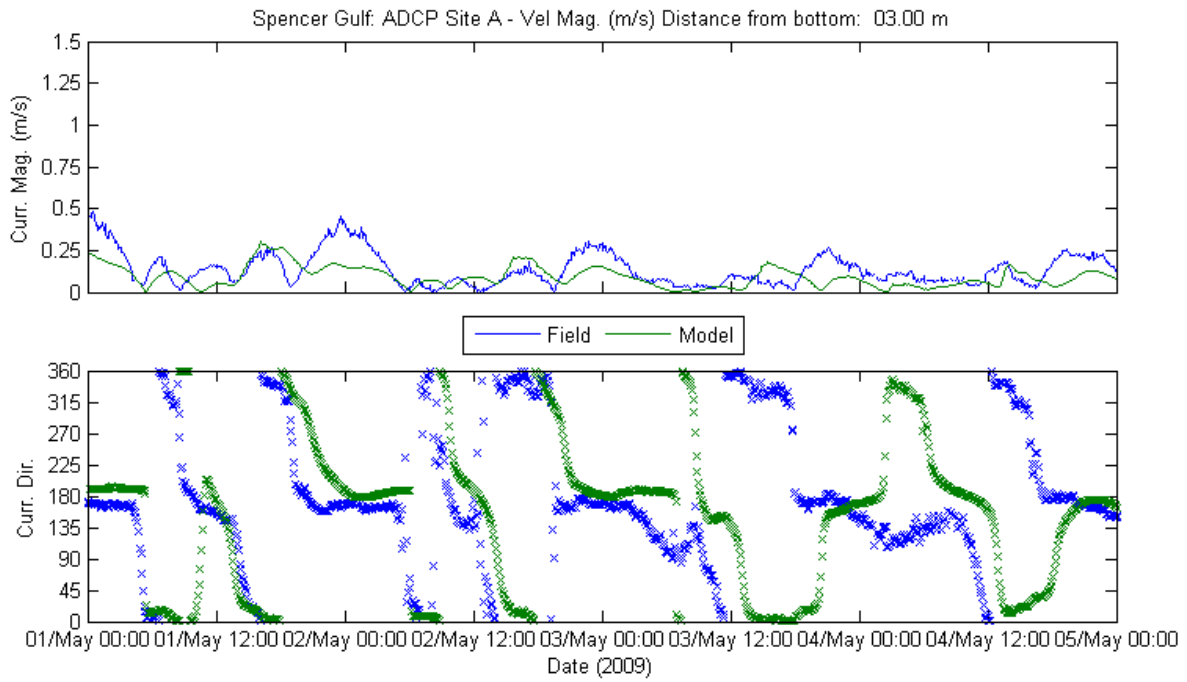


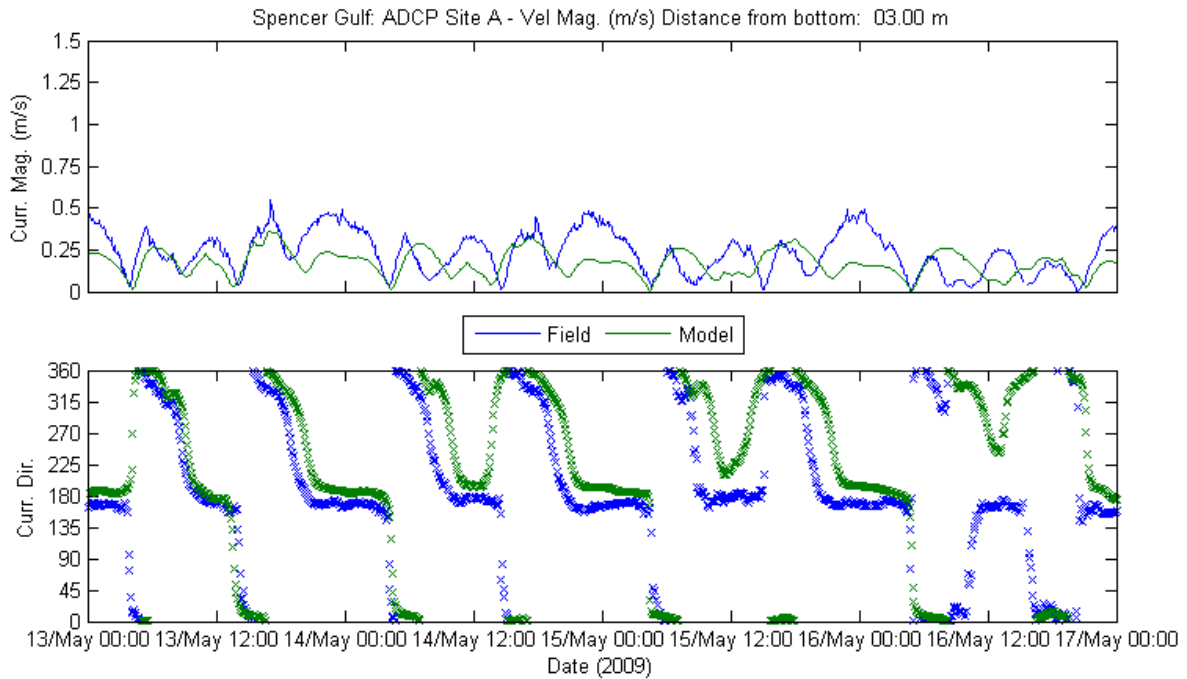
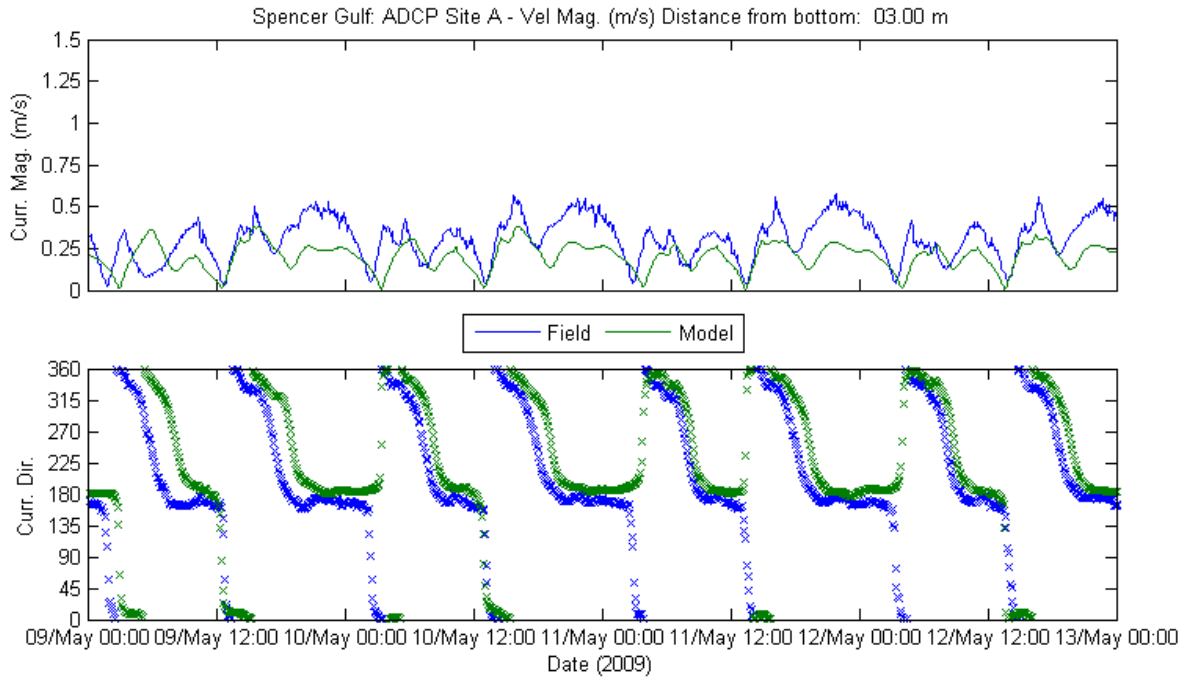


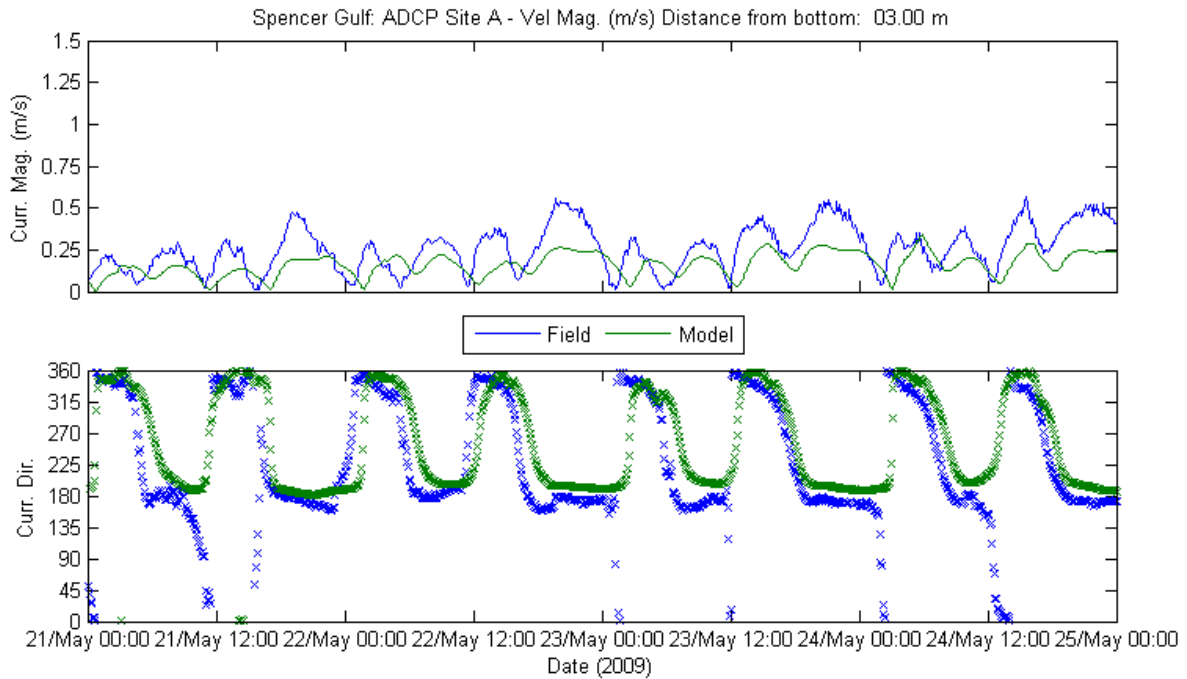
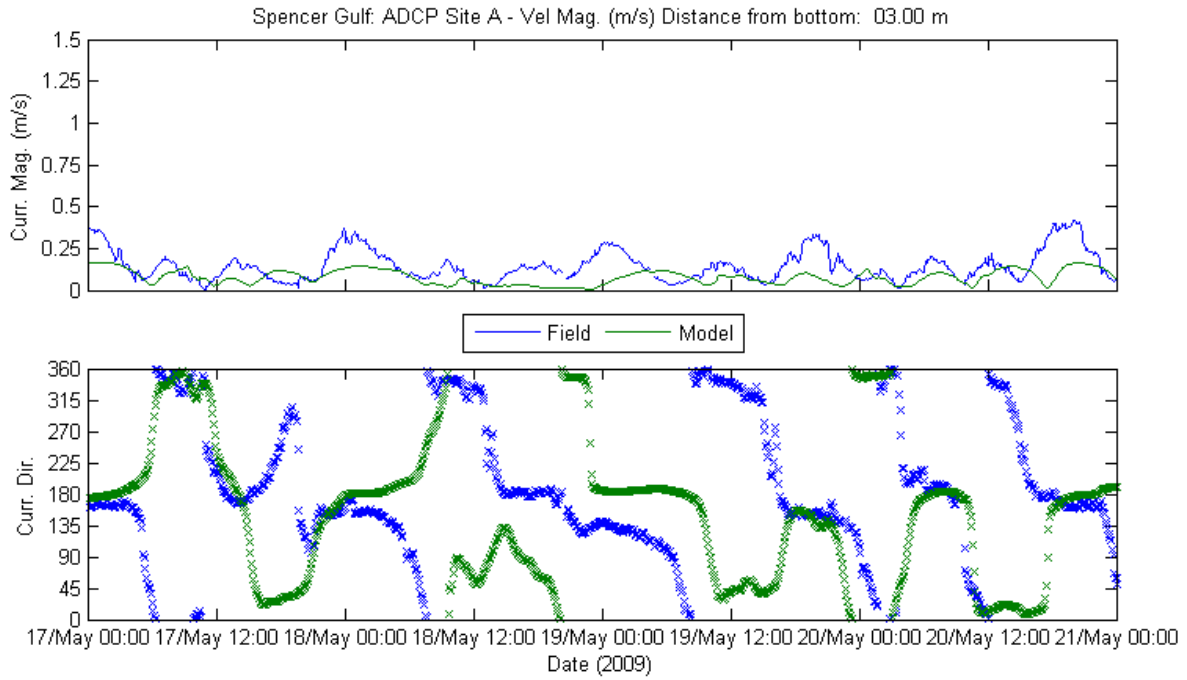


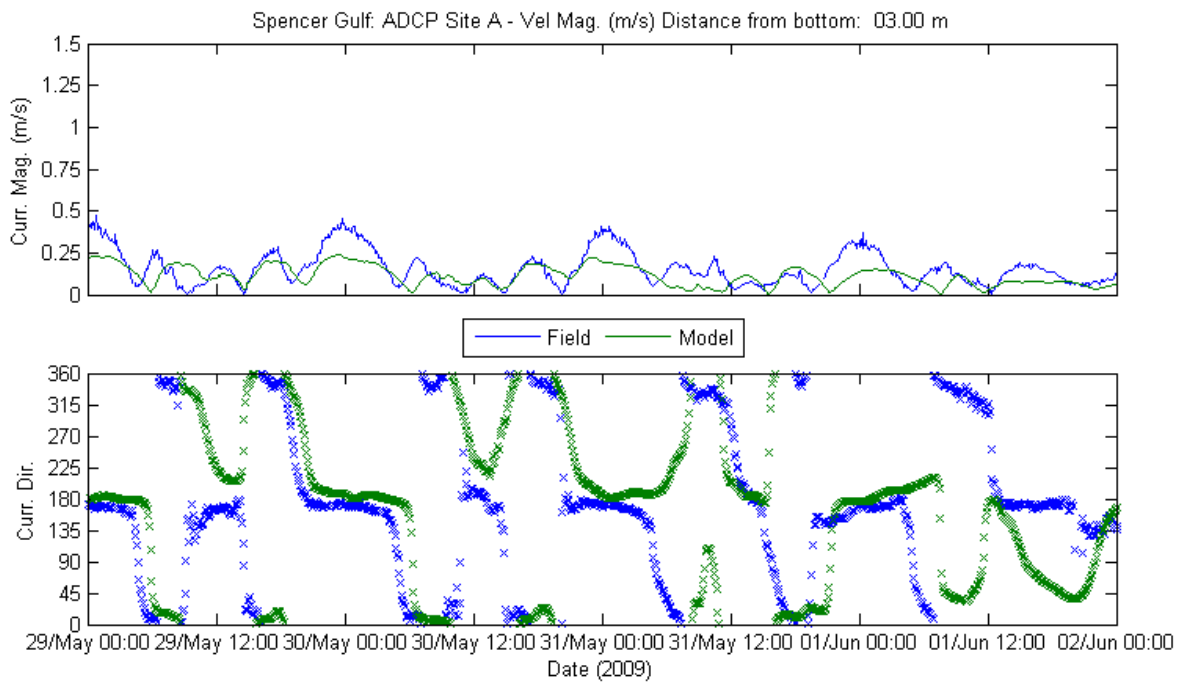
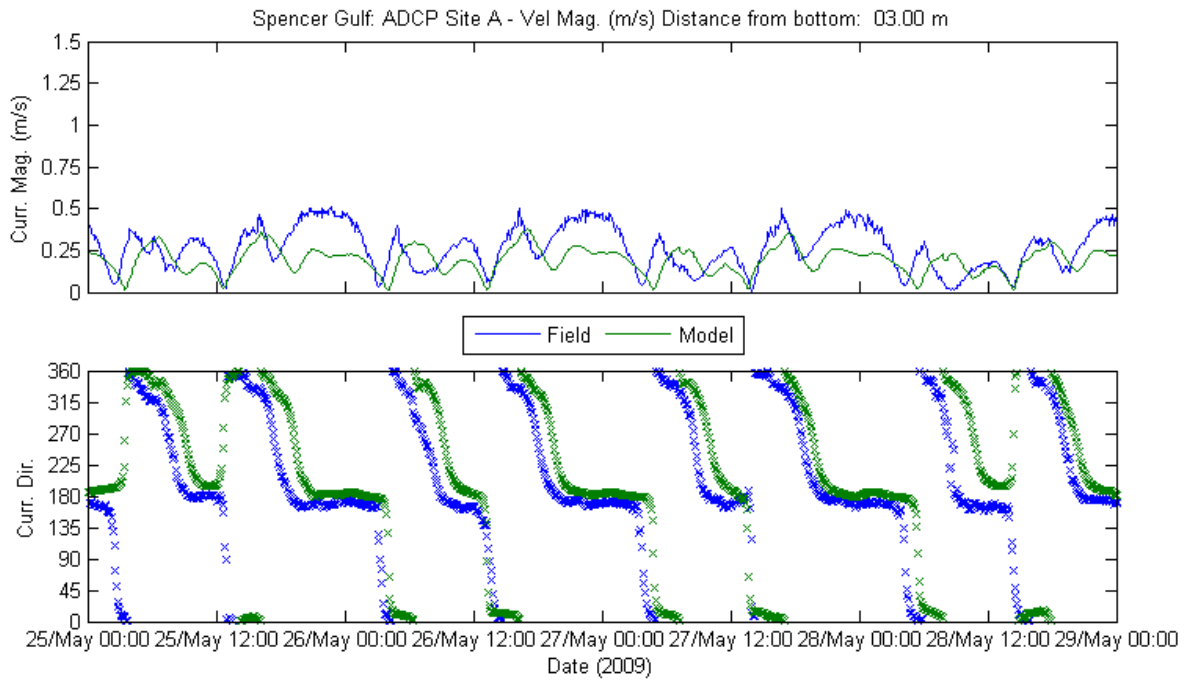
Site A at 3.00 m from Bottom

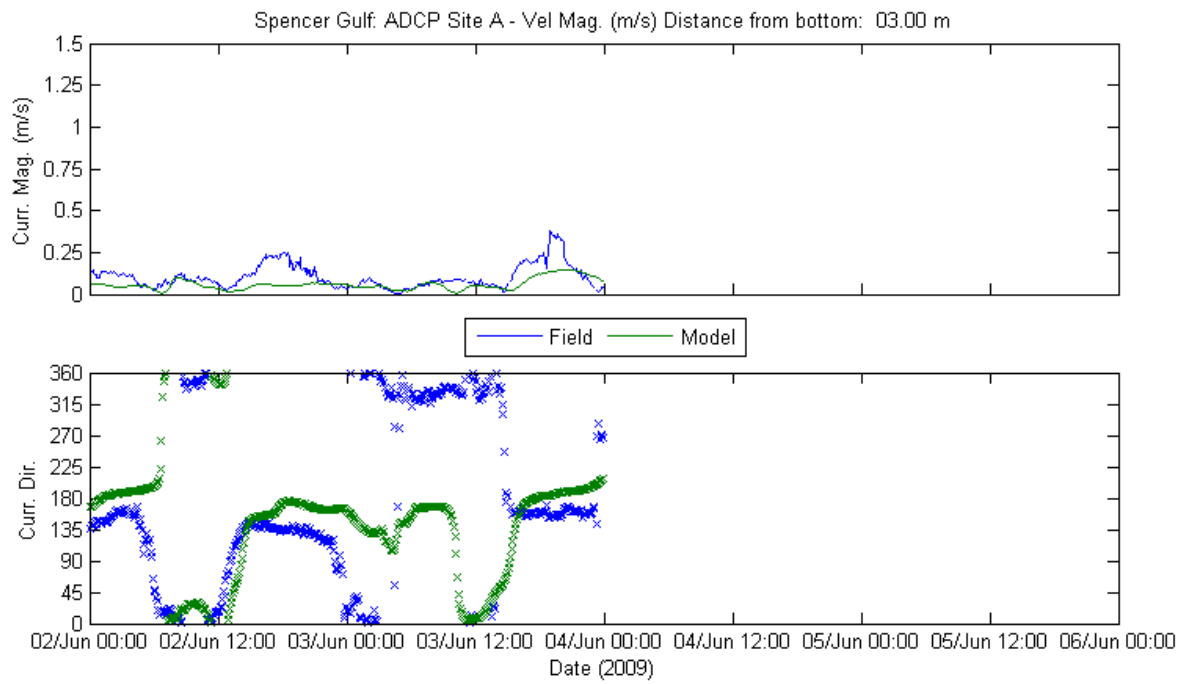






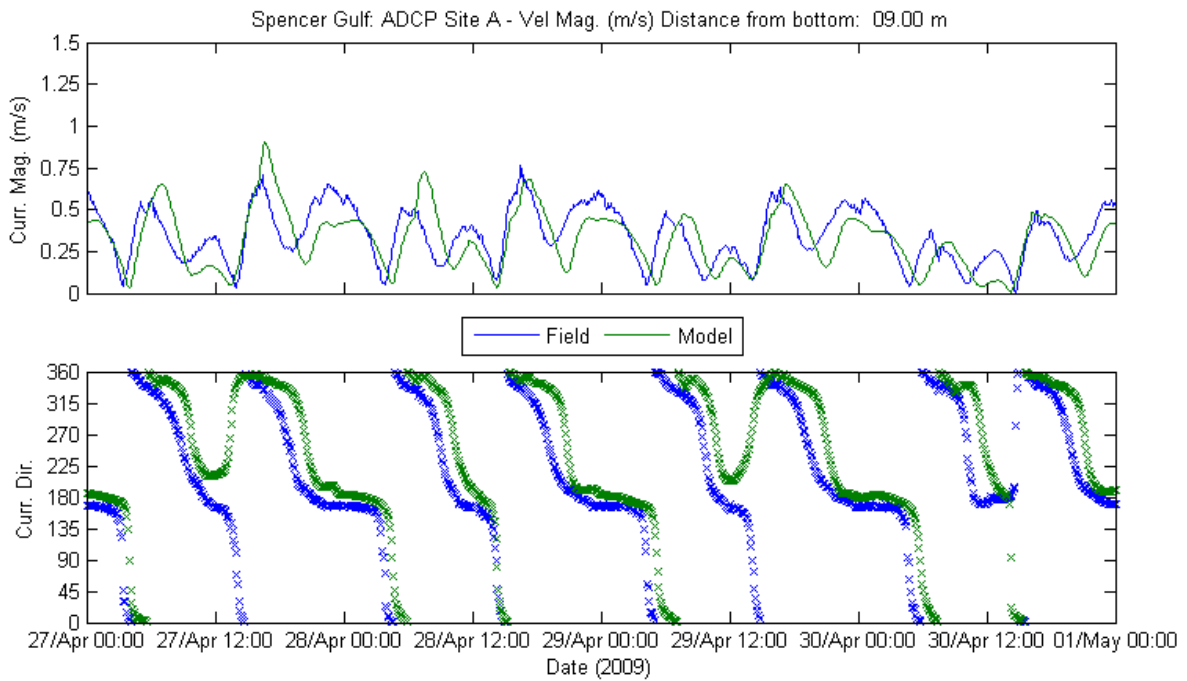
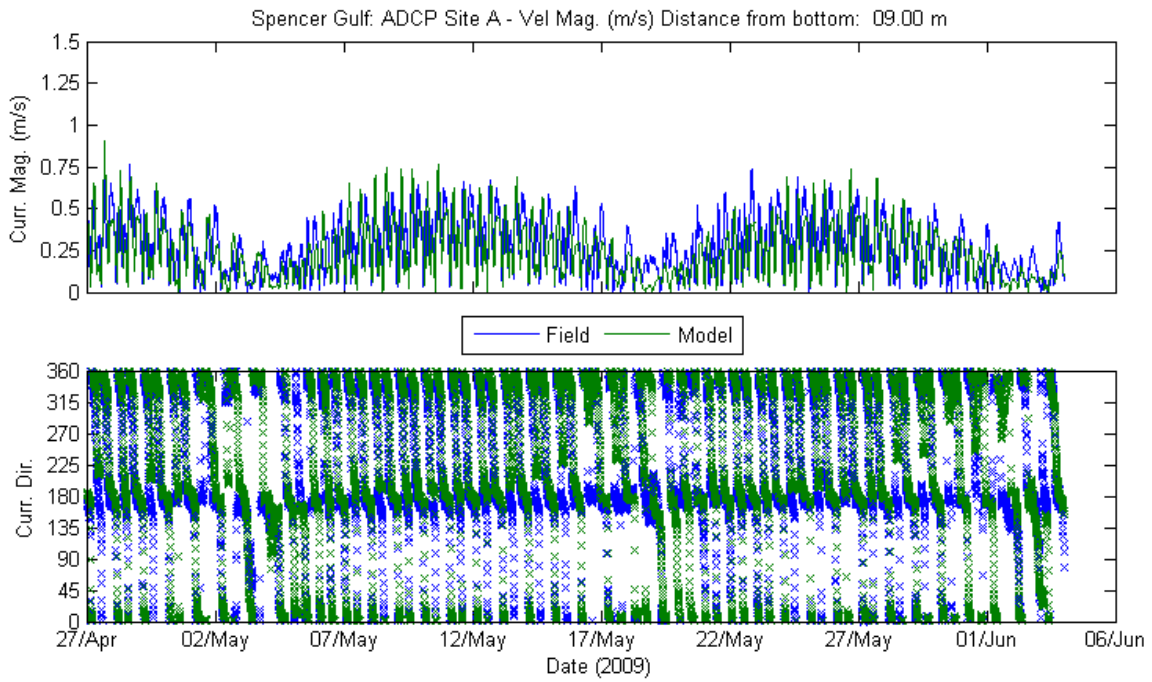


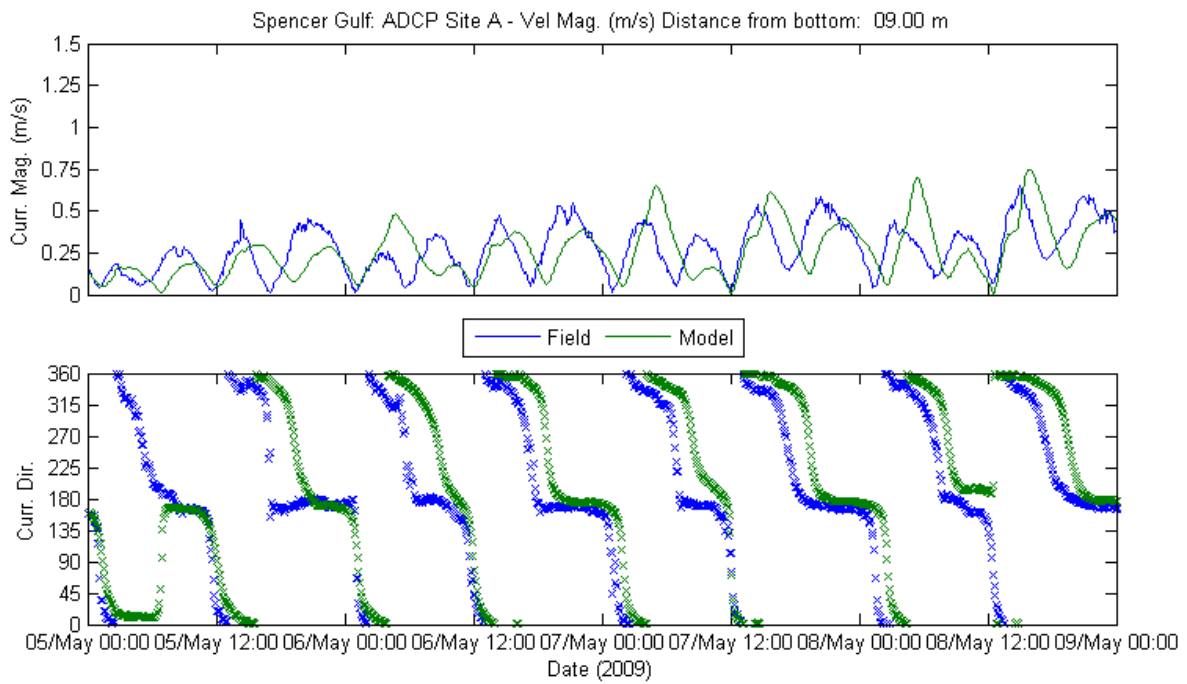
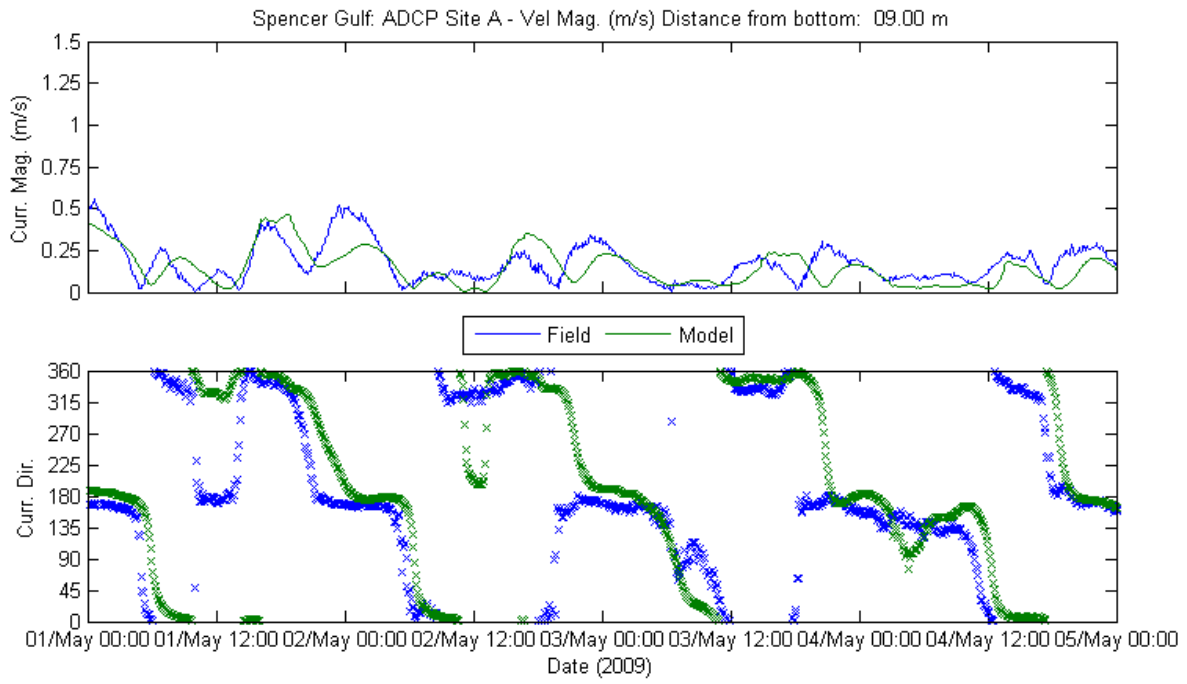


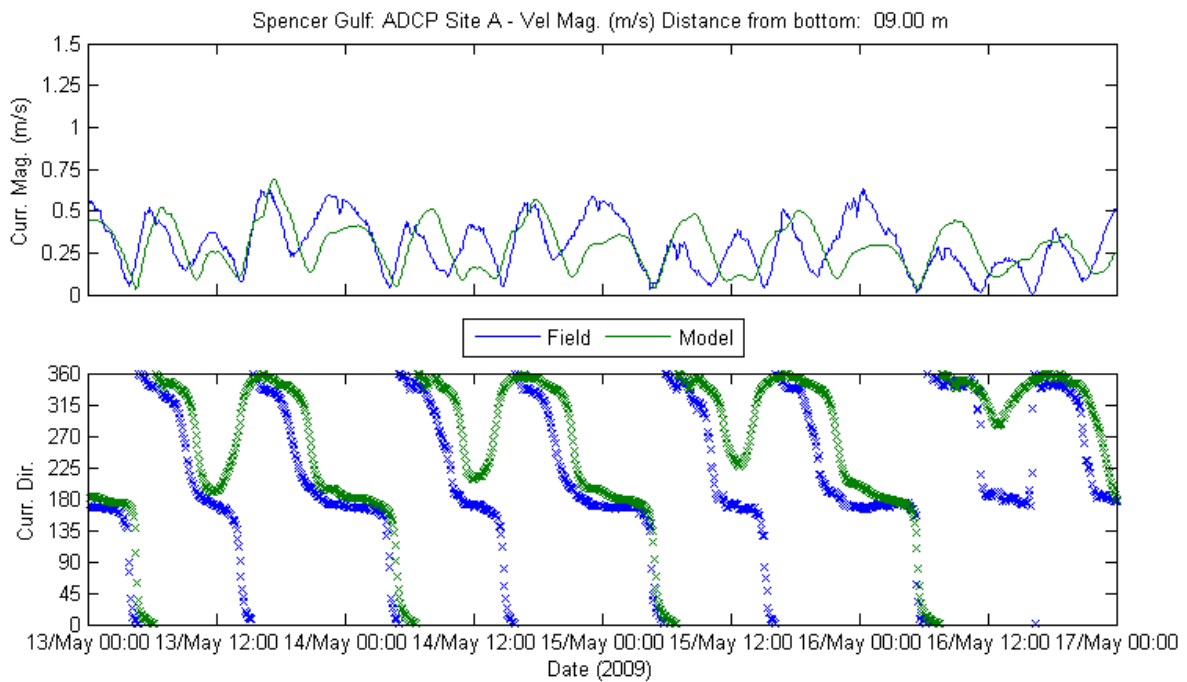
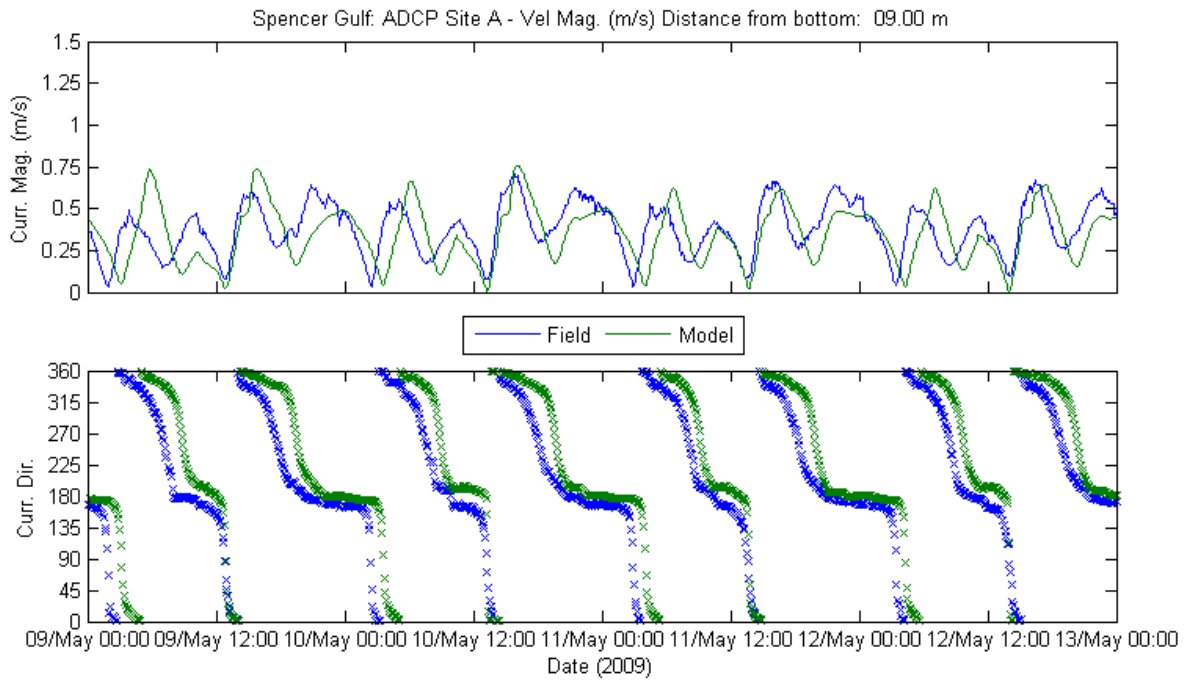


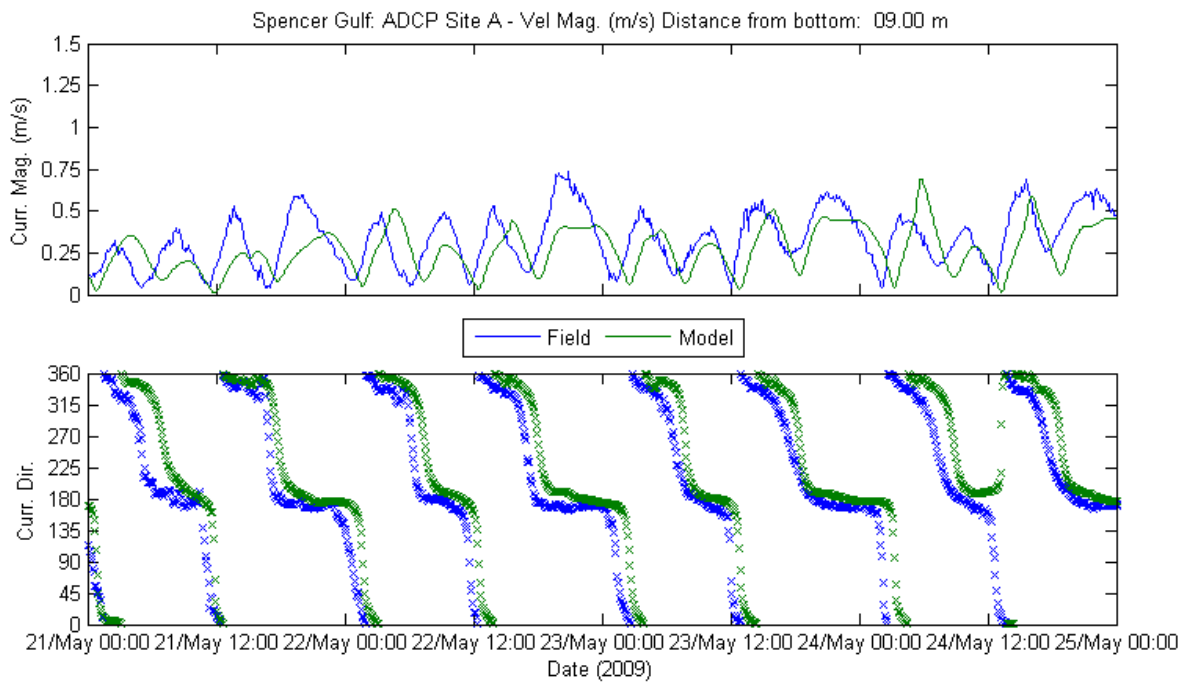
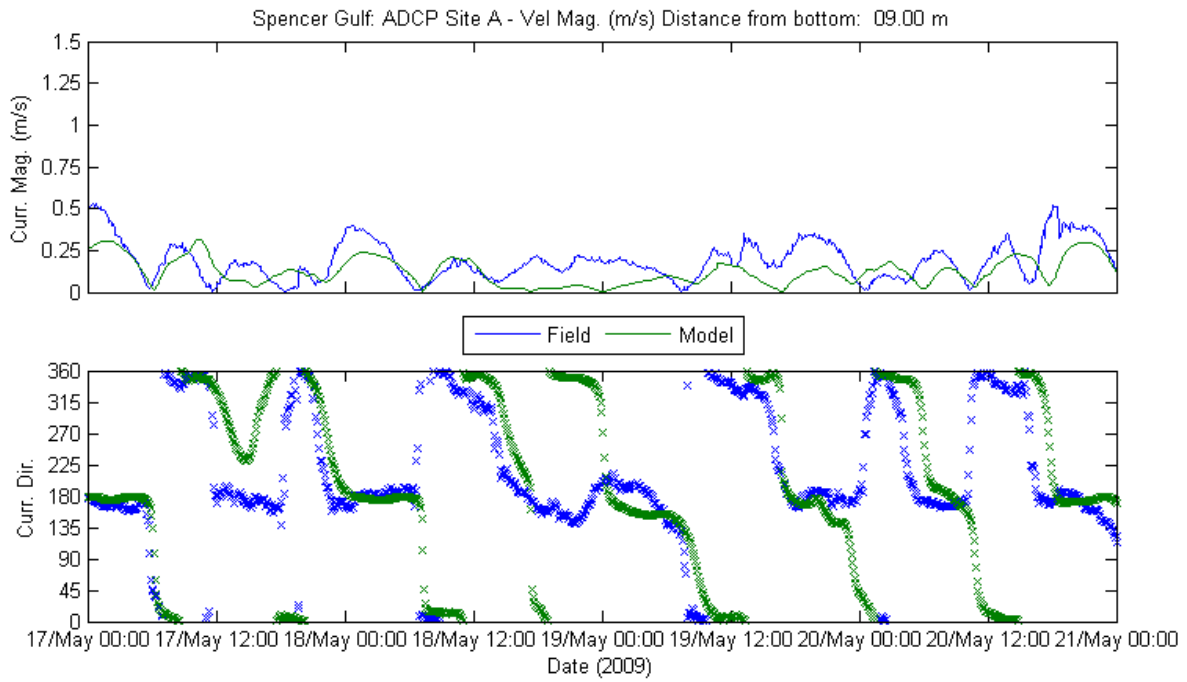


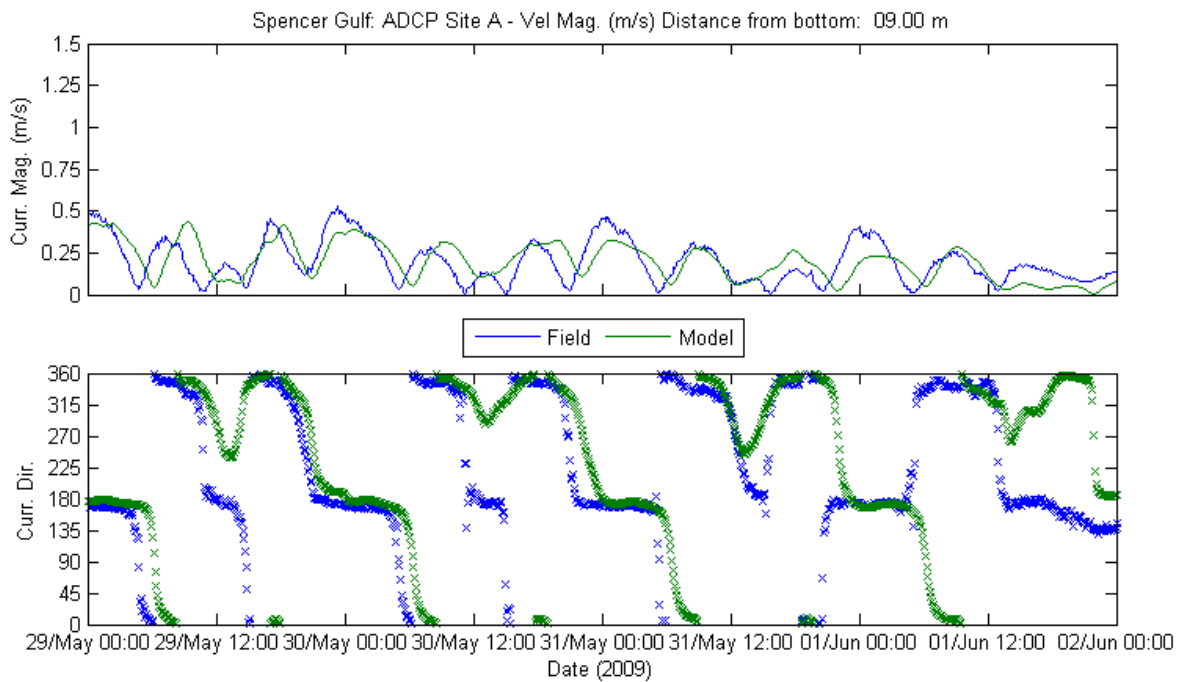
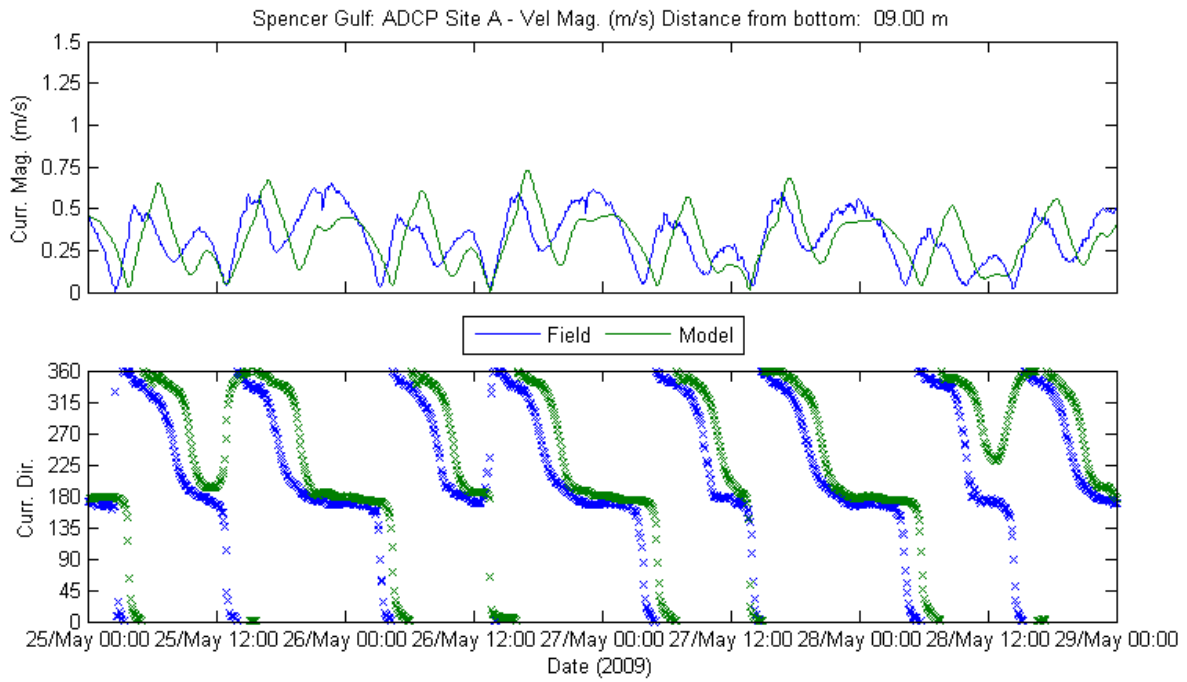
Site A at 9.00 m from Bottom

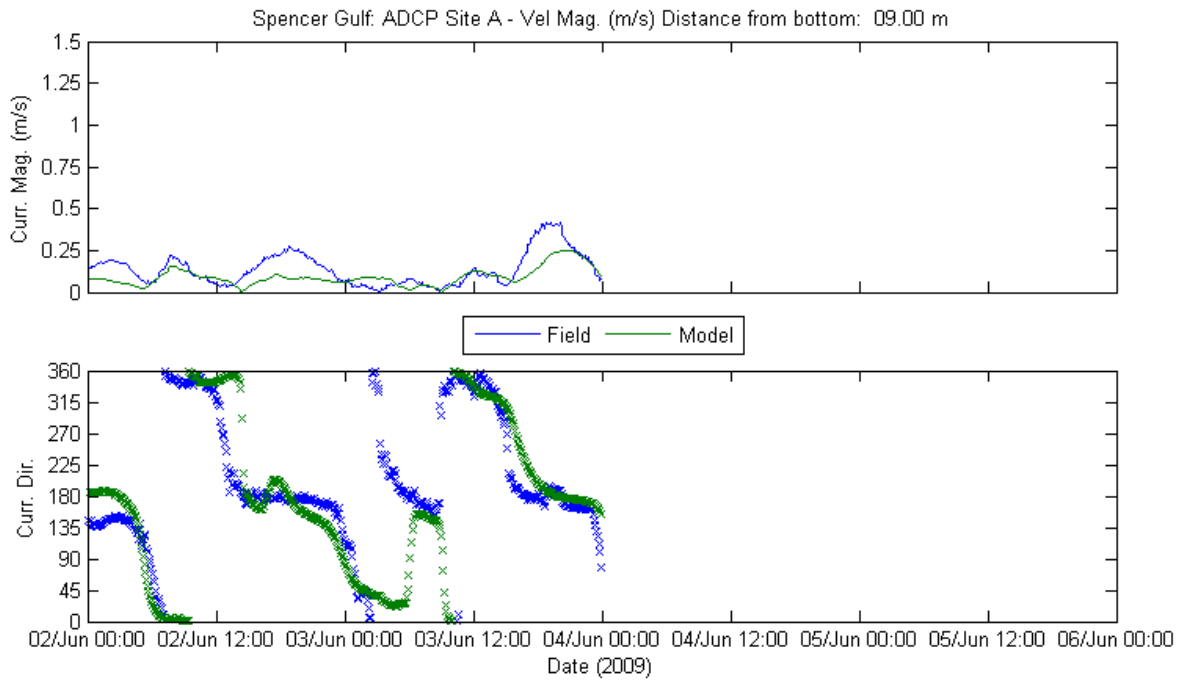






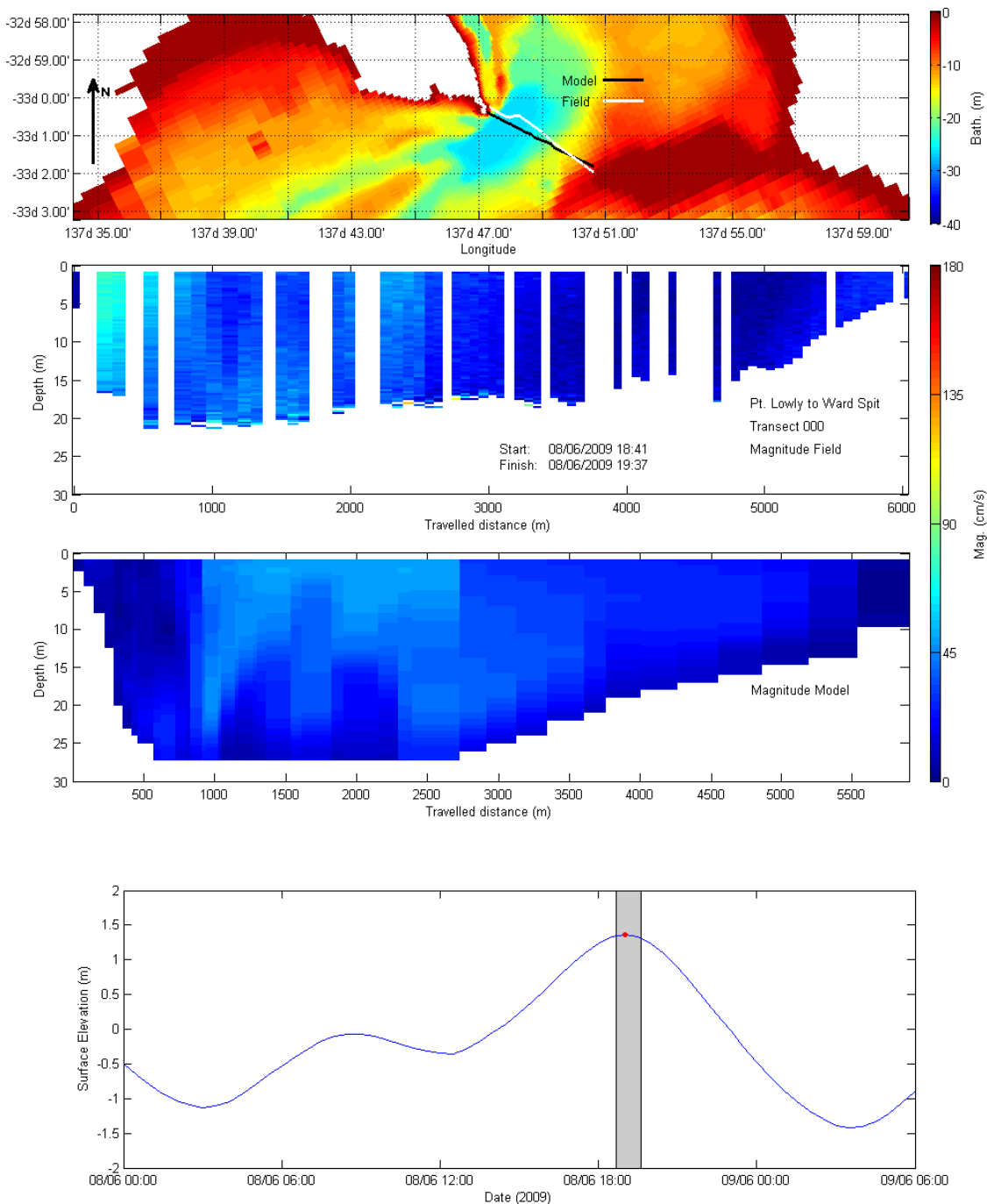


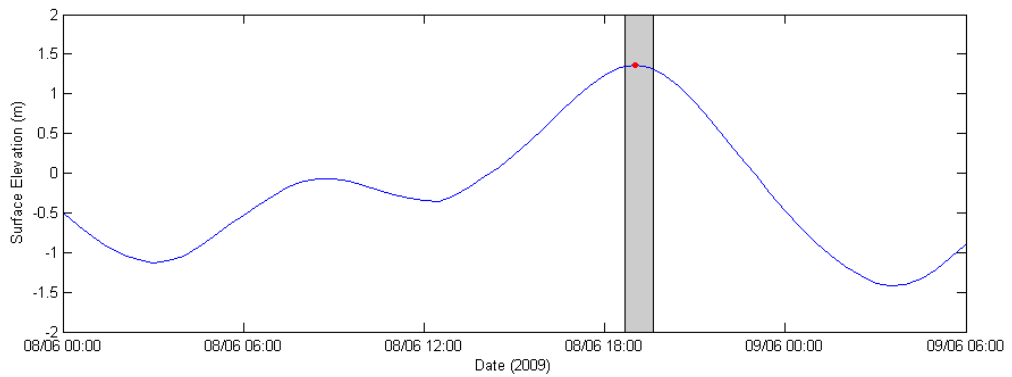
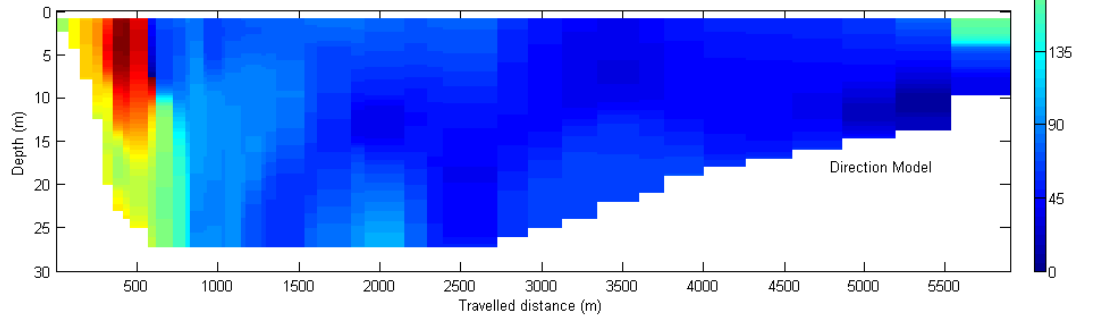
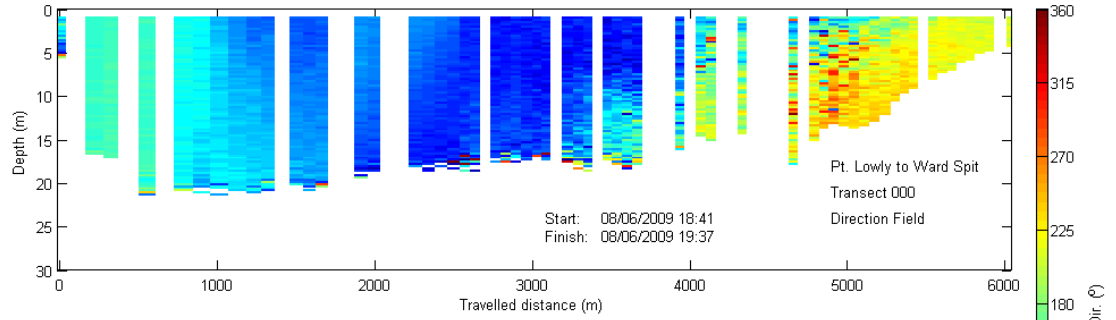
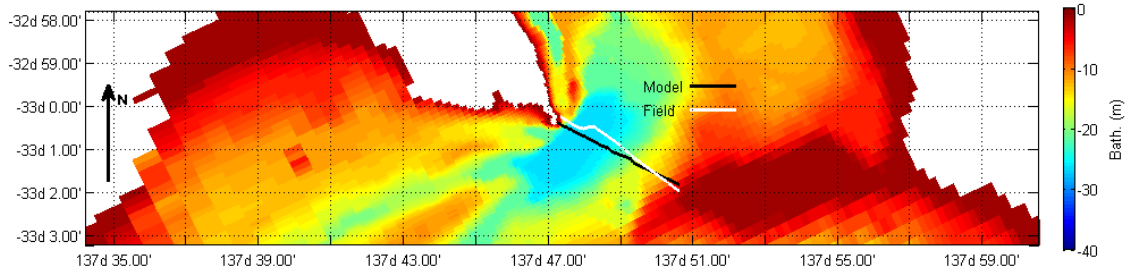




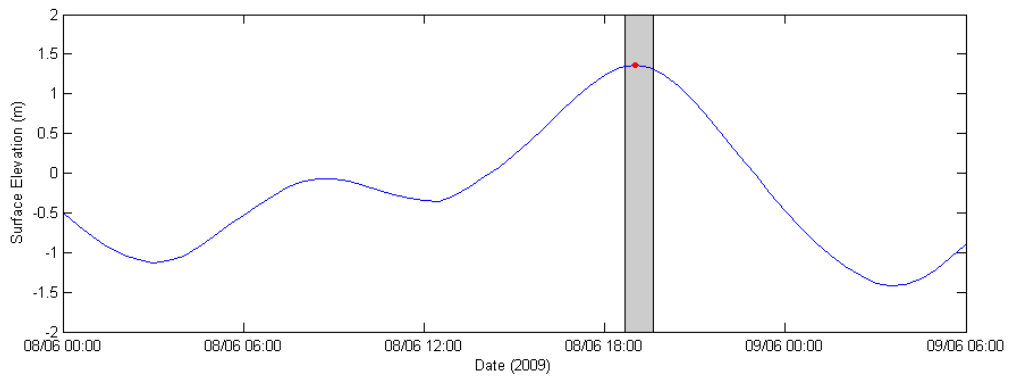
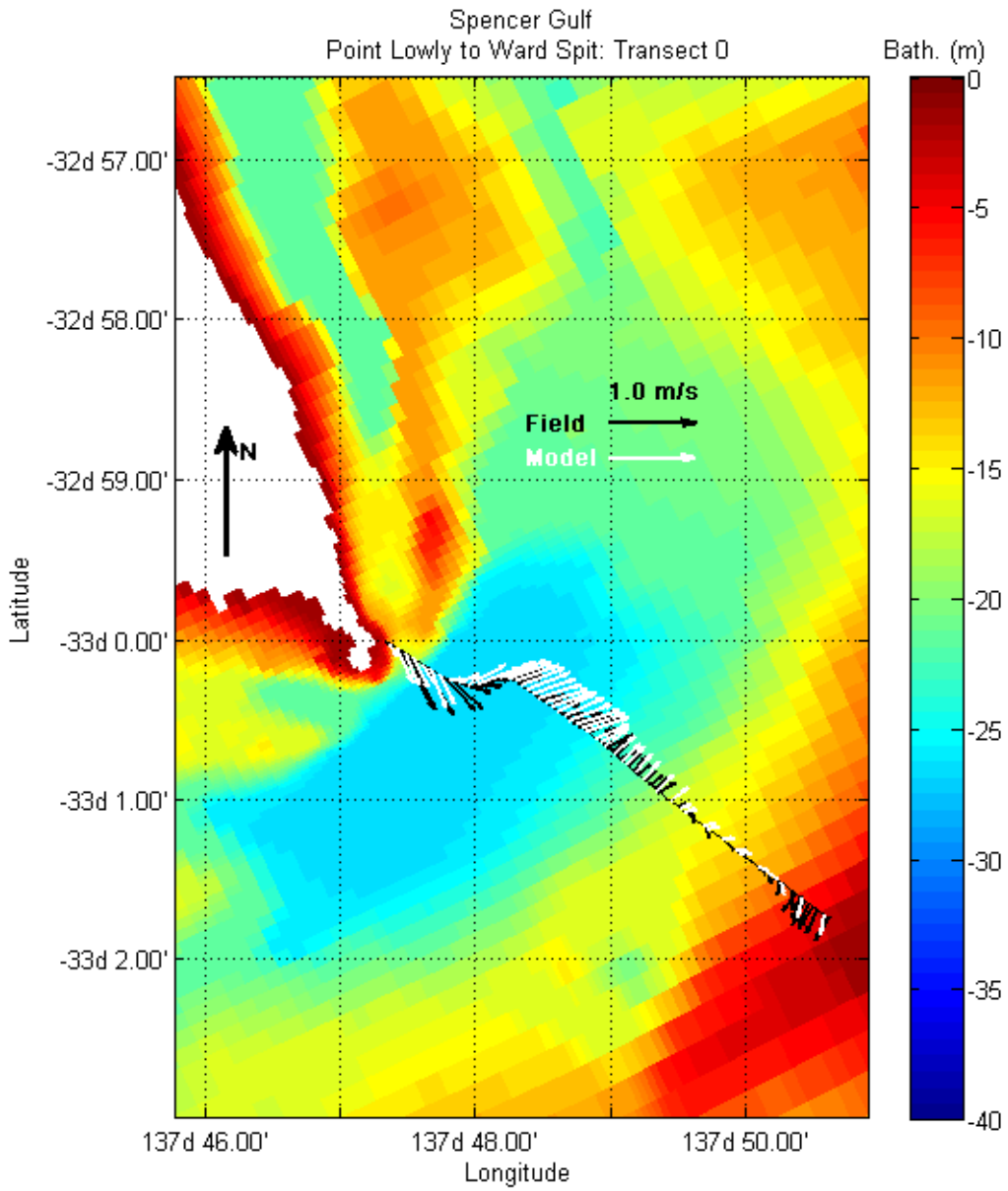
# APPENDIX F: FORTY-DAYS VALIDATION PERIOD ADCP TRANSECTS COMPARISONS

## Transect 000

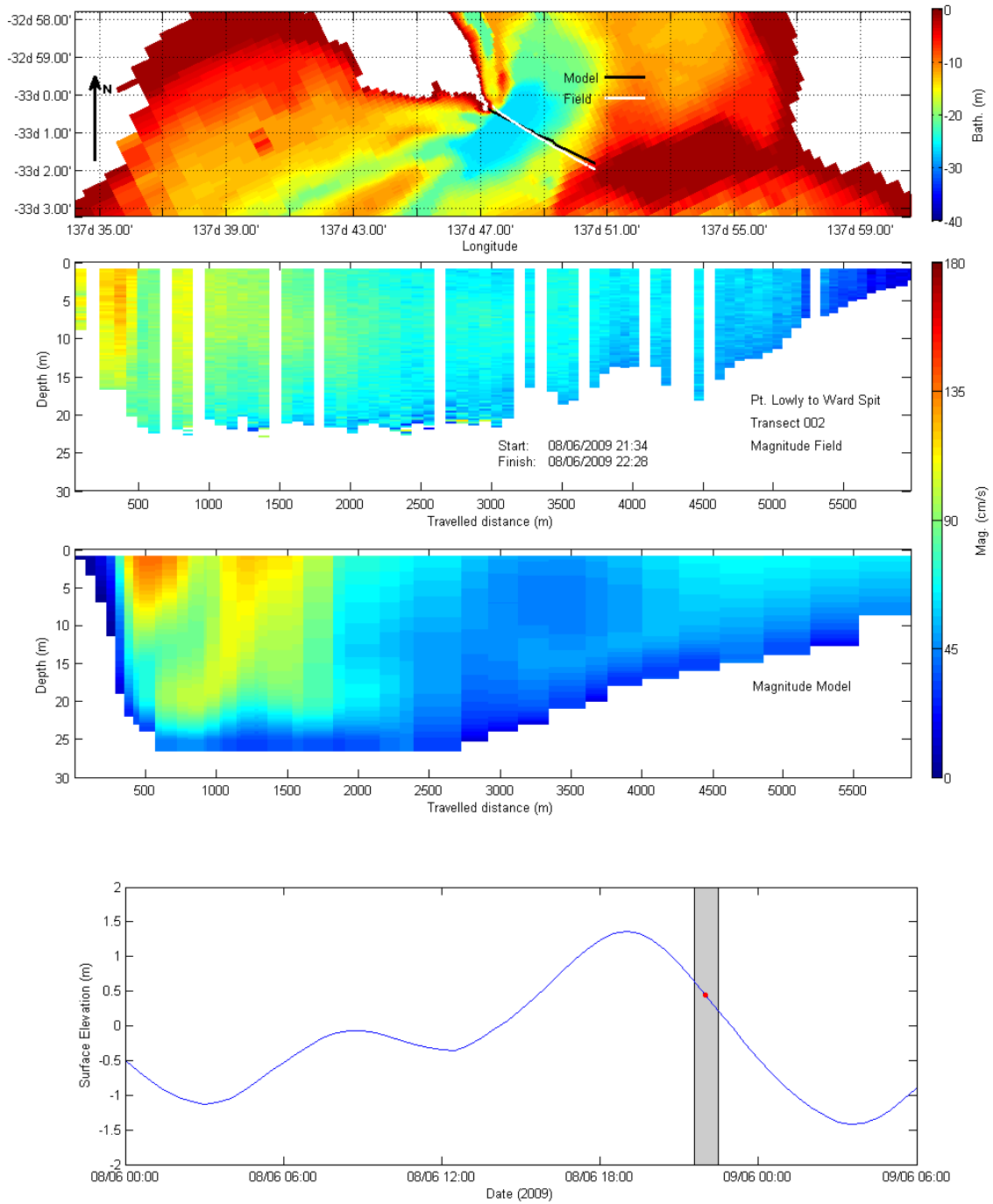


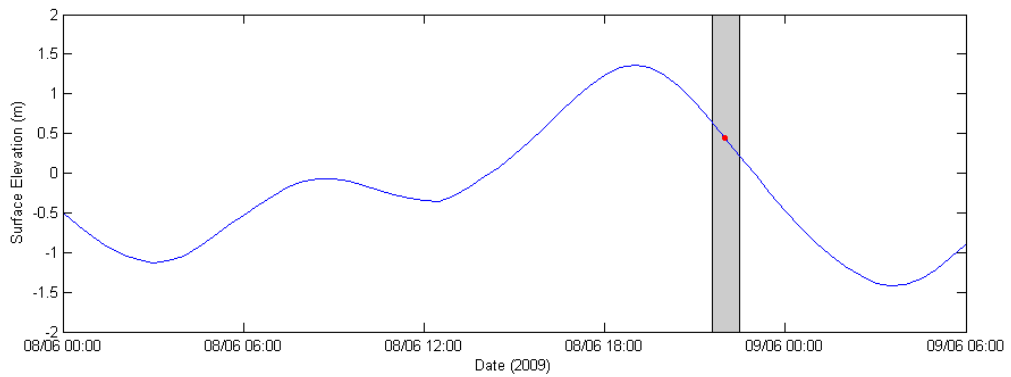
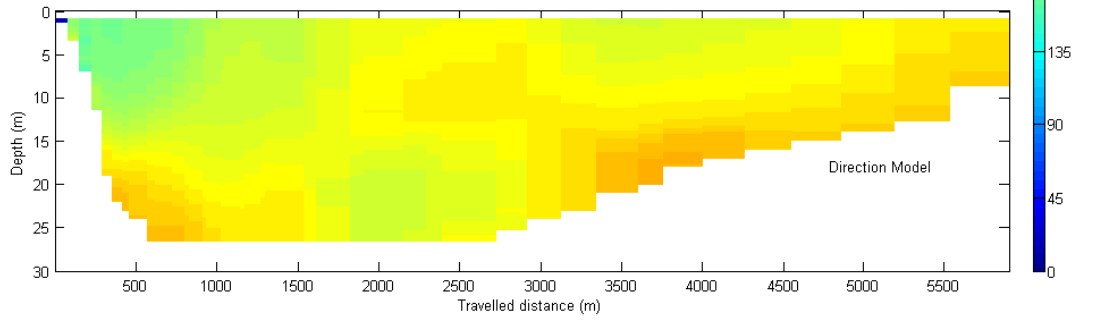
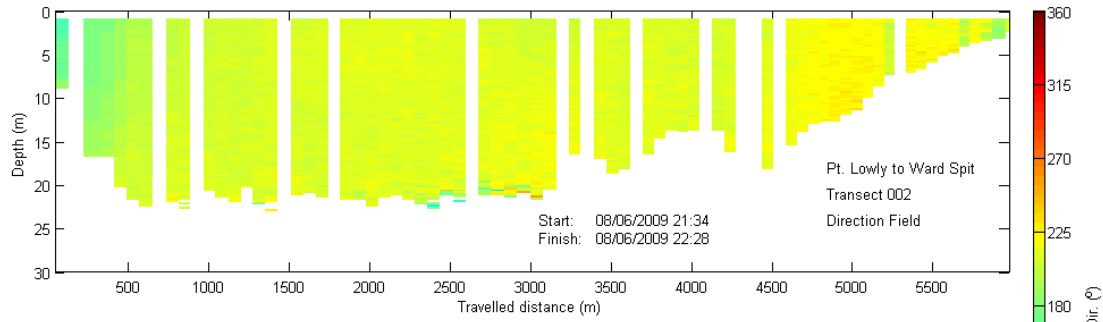
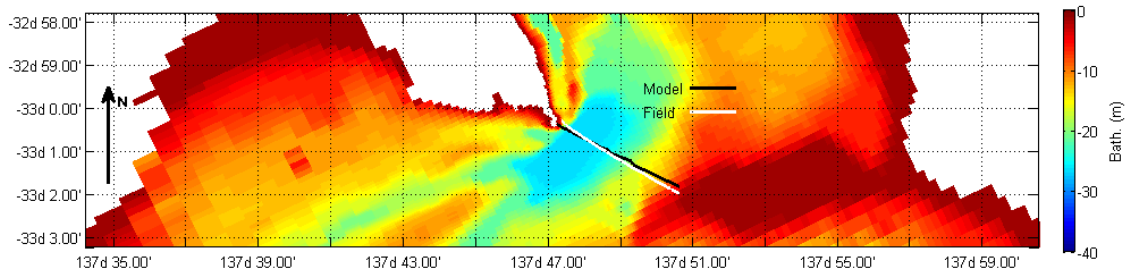


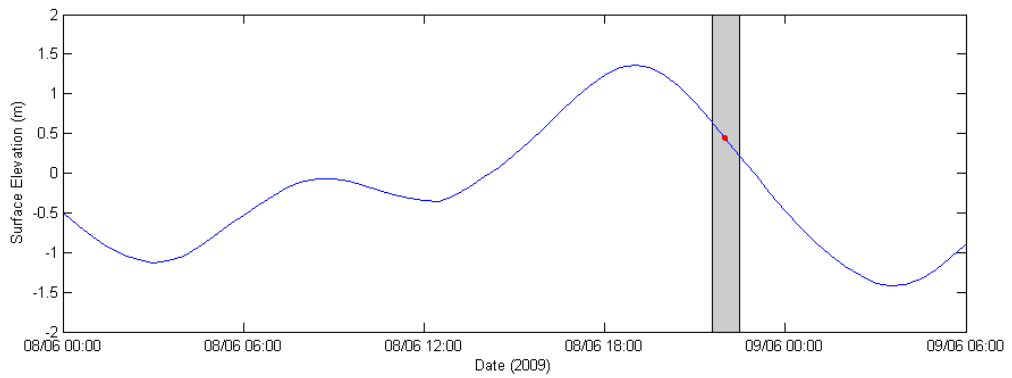
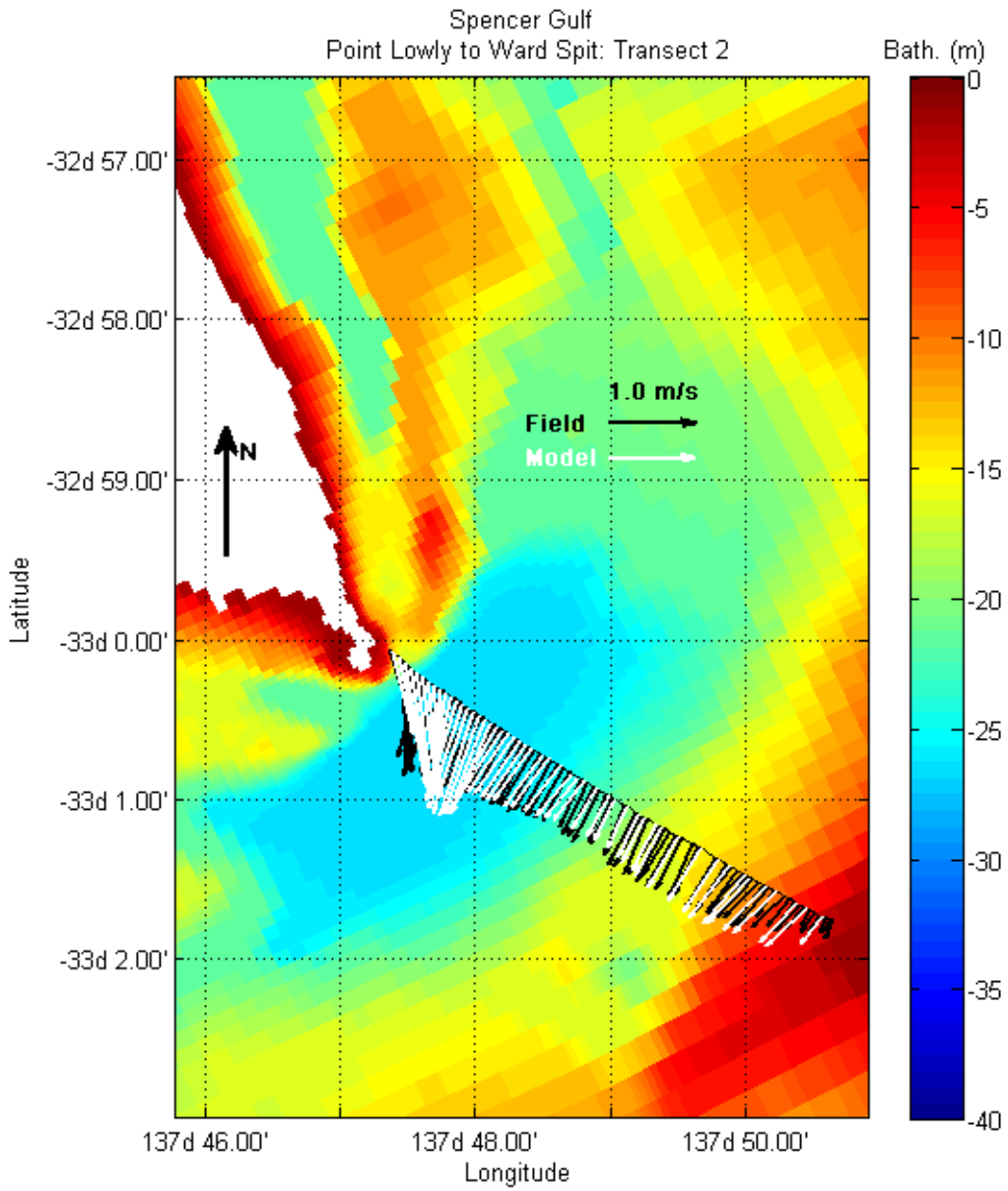




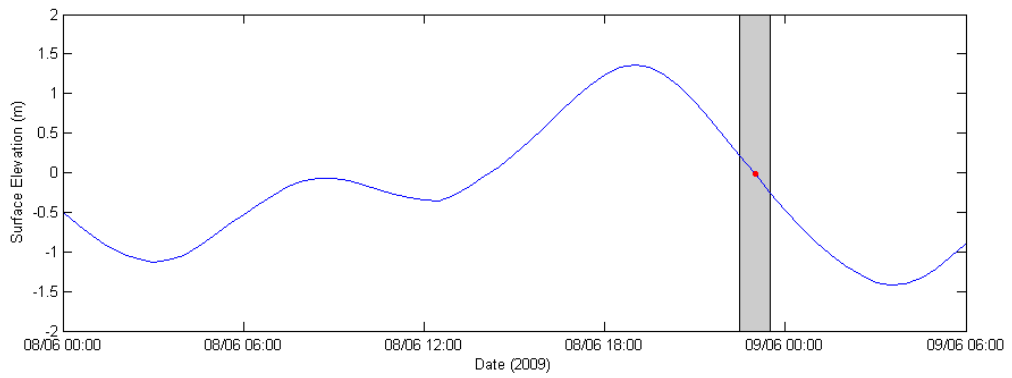
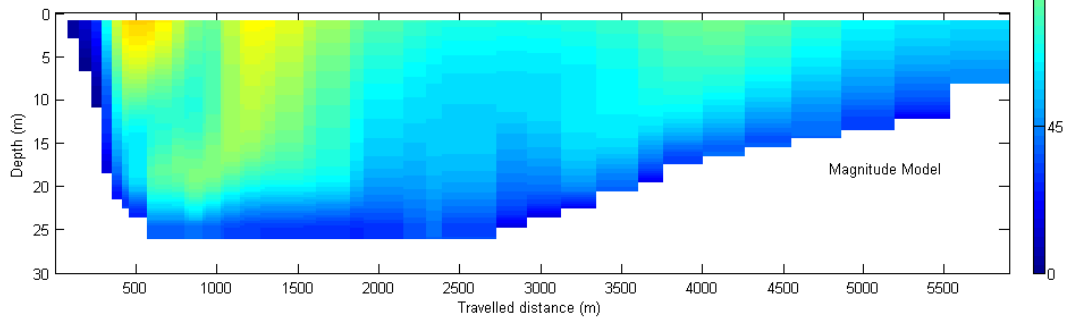
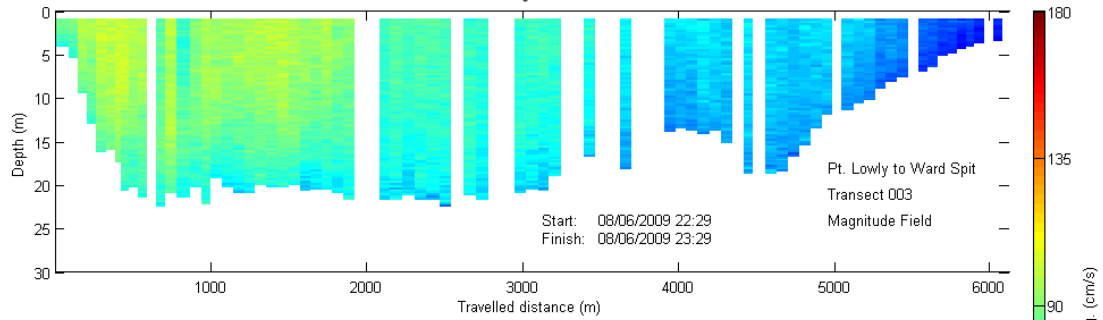
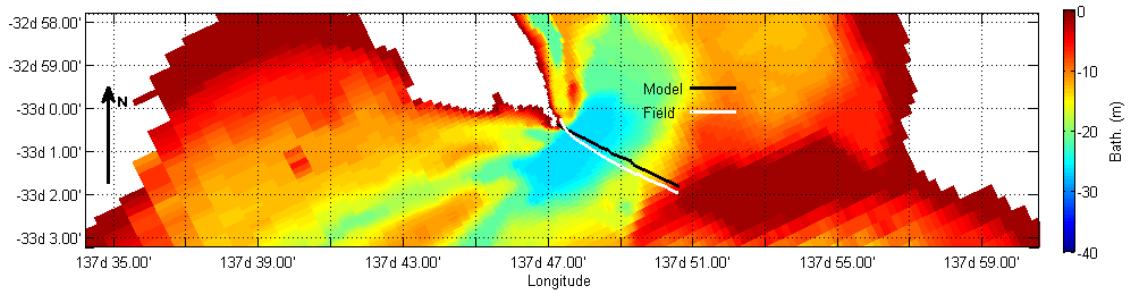
Transect 002

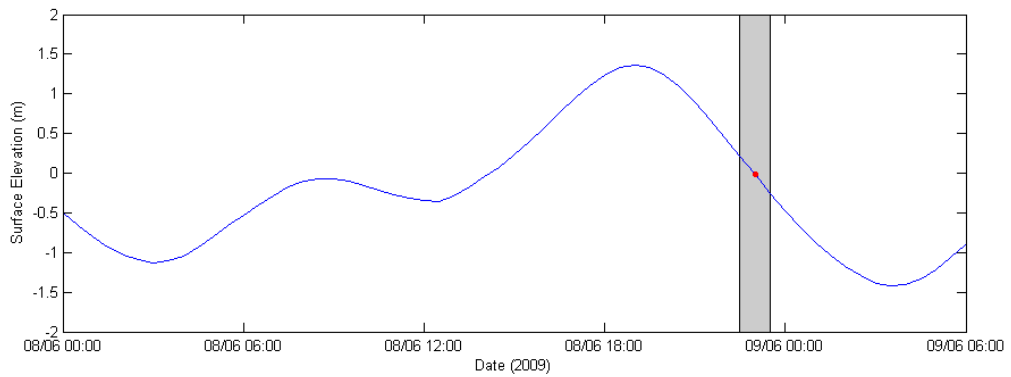
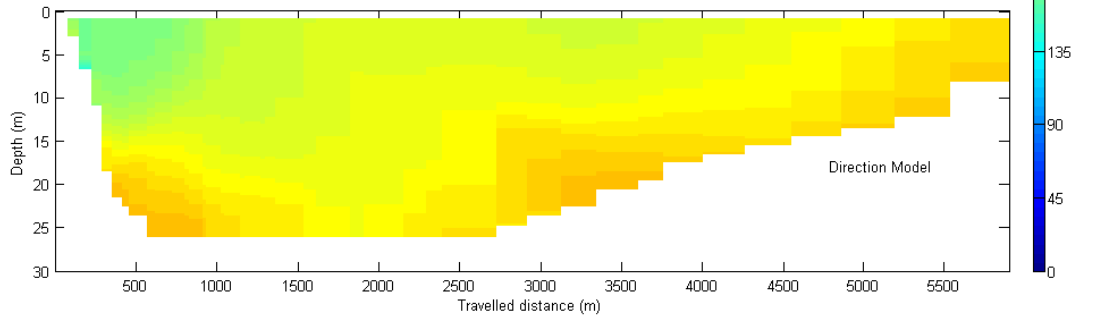
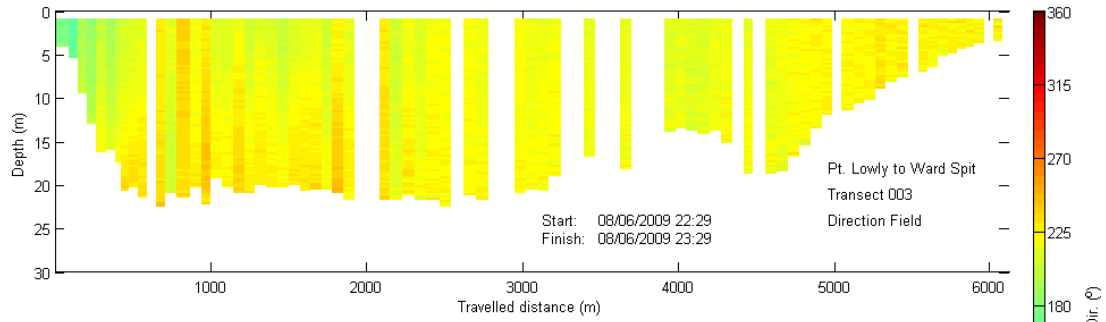
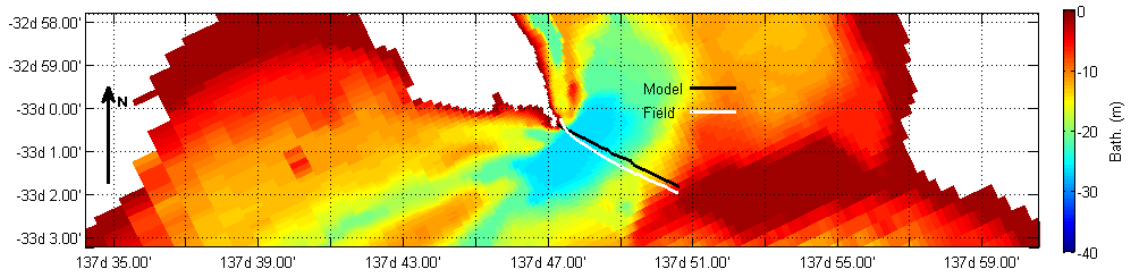


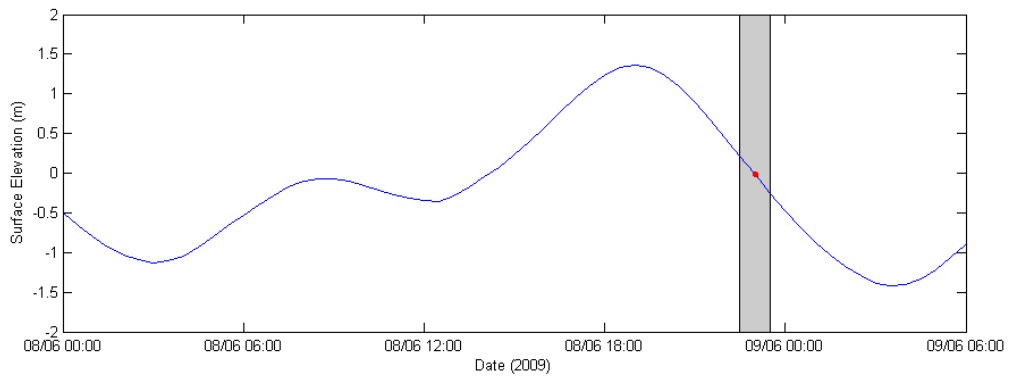
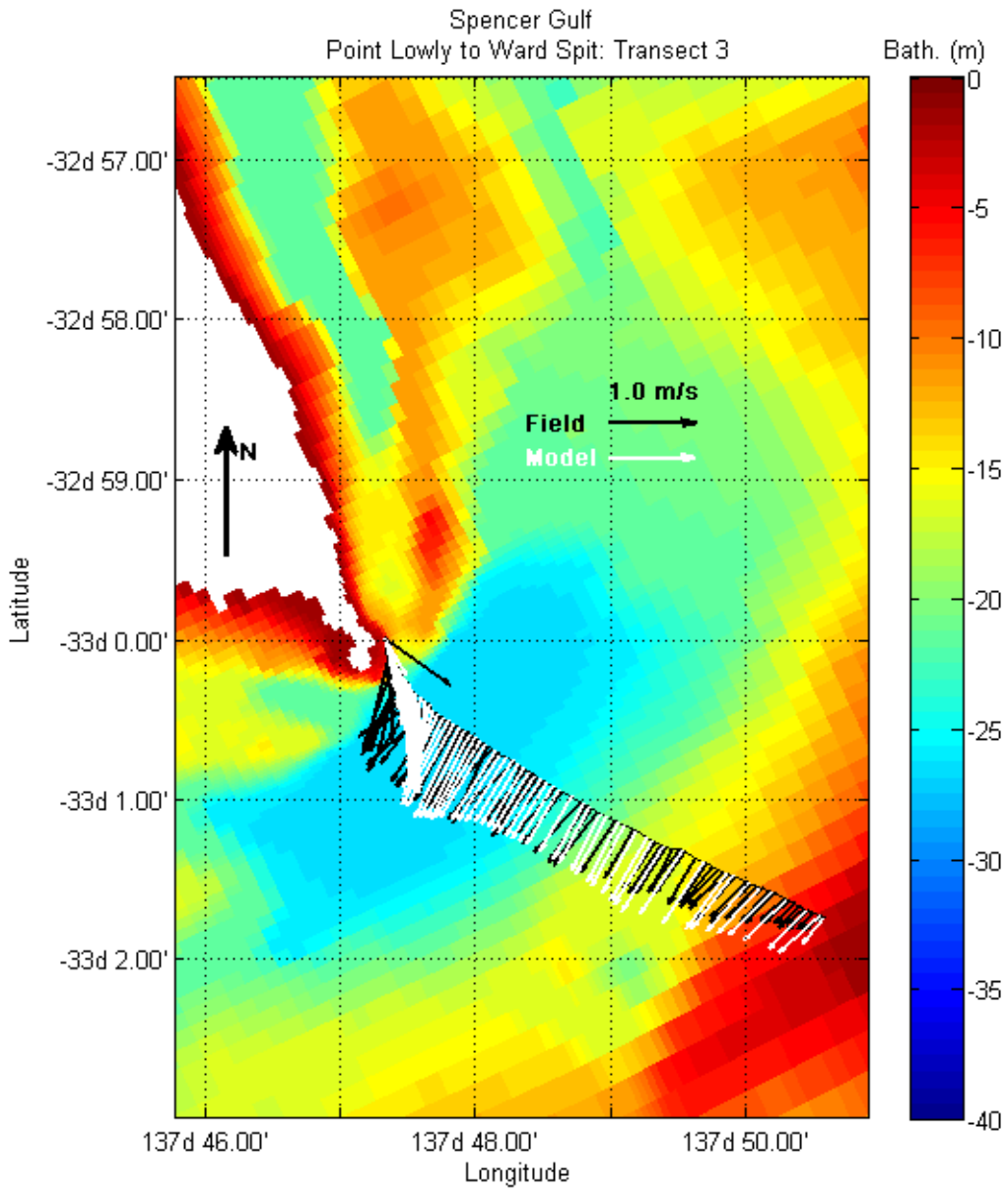




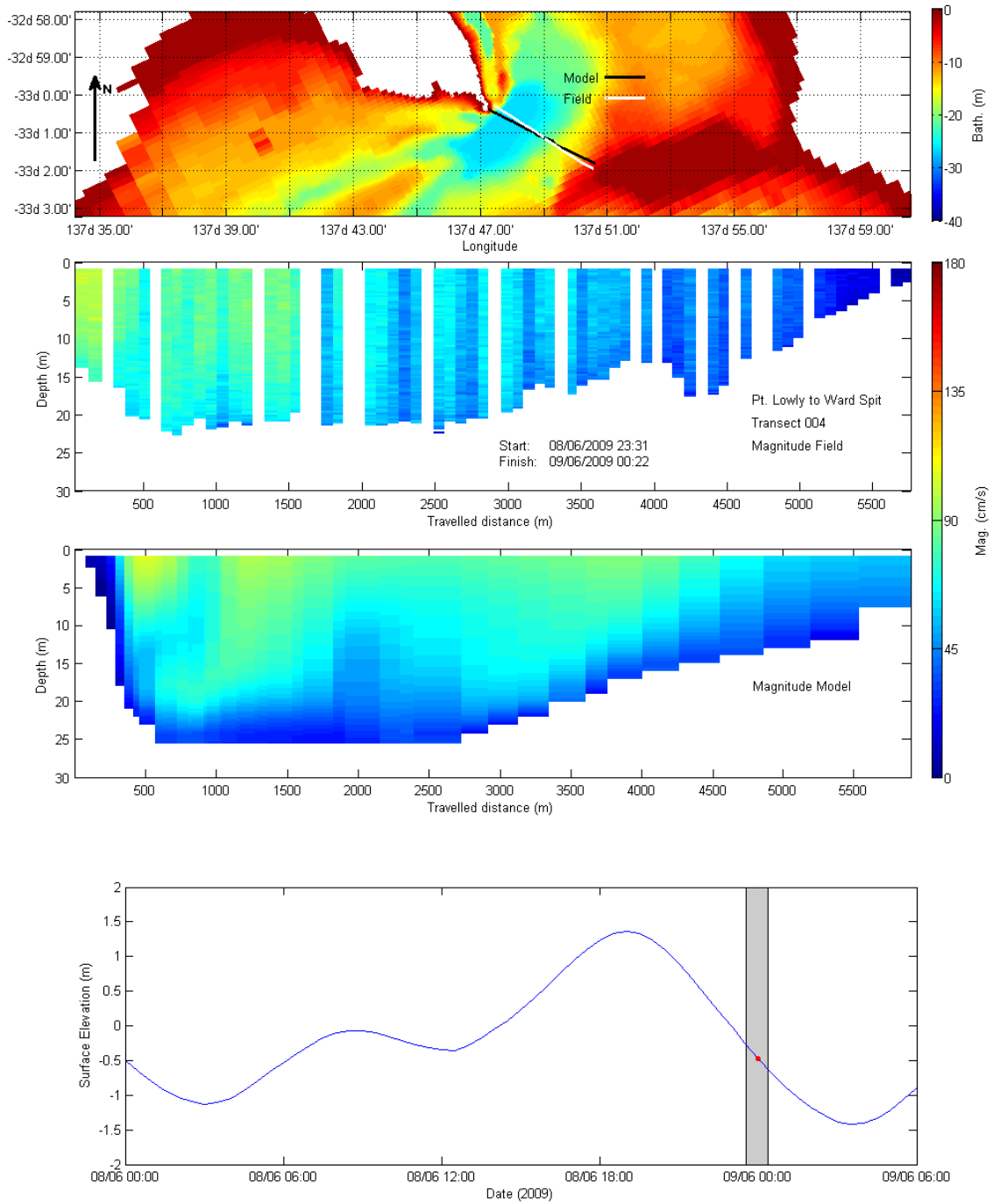
**Transect 003**



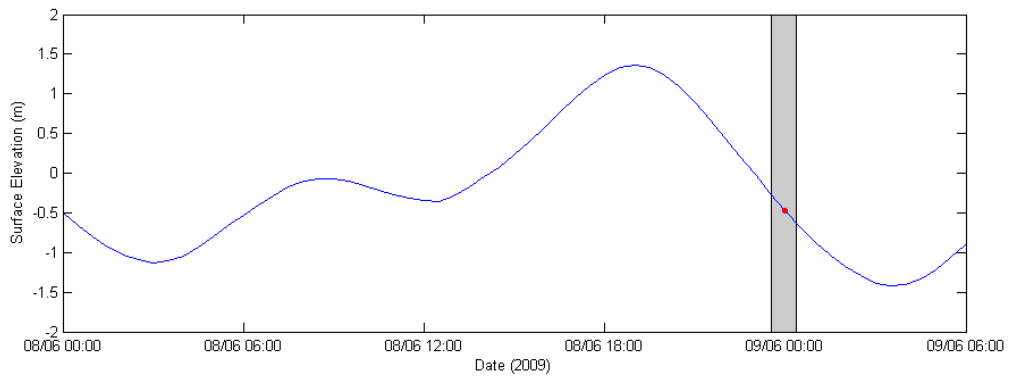
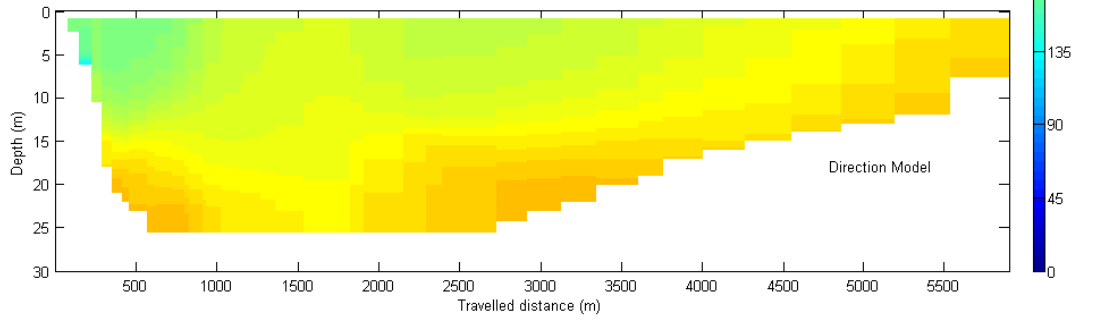
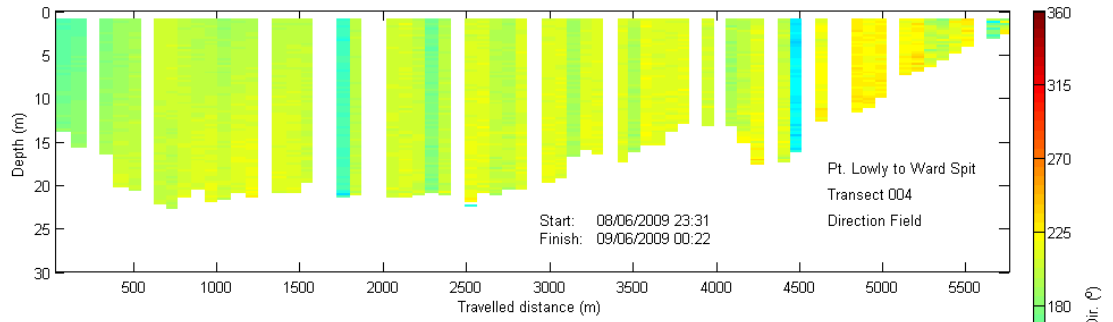
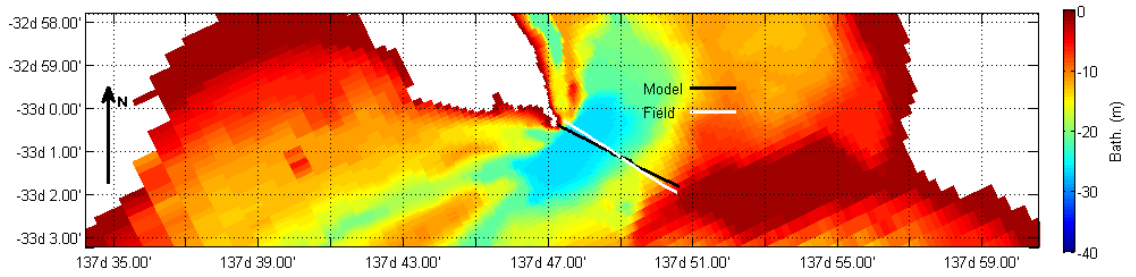


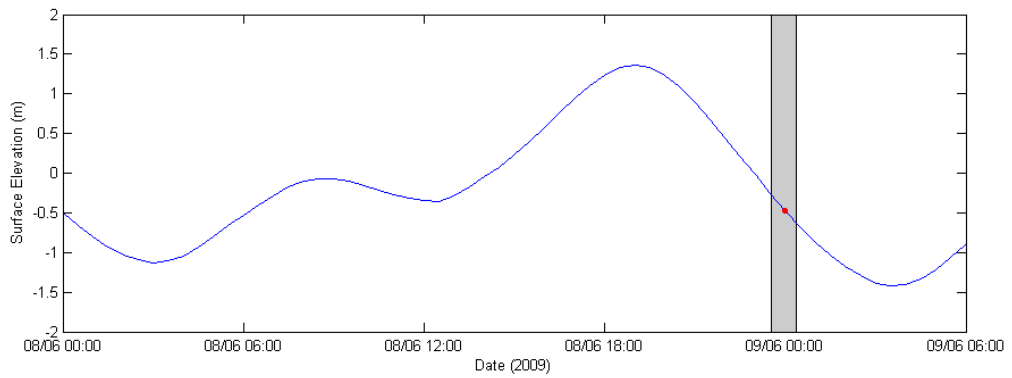
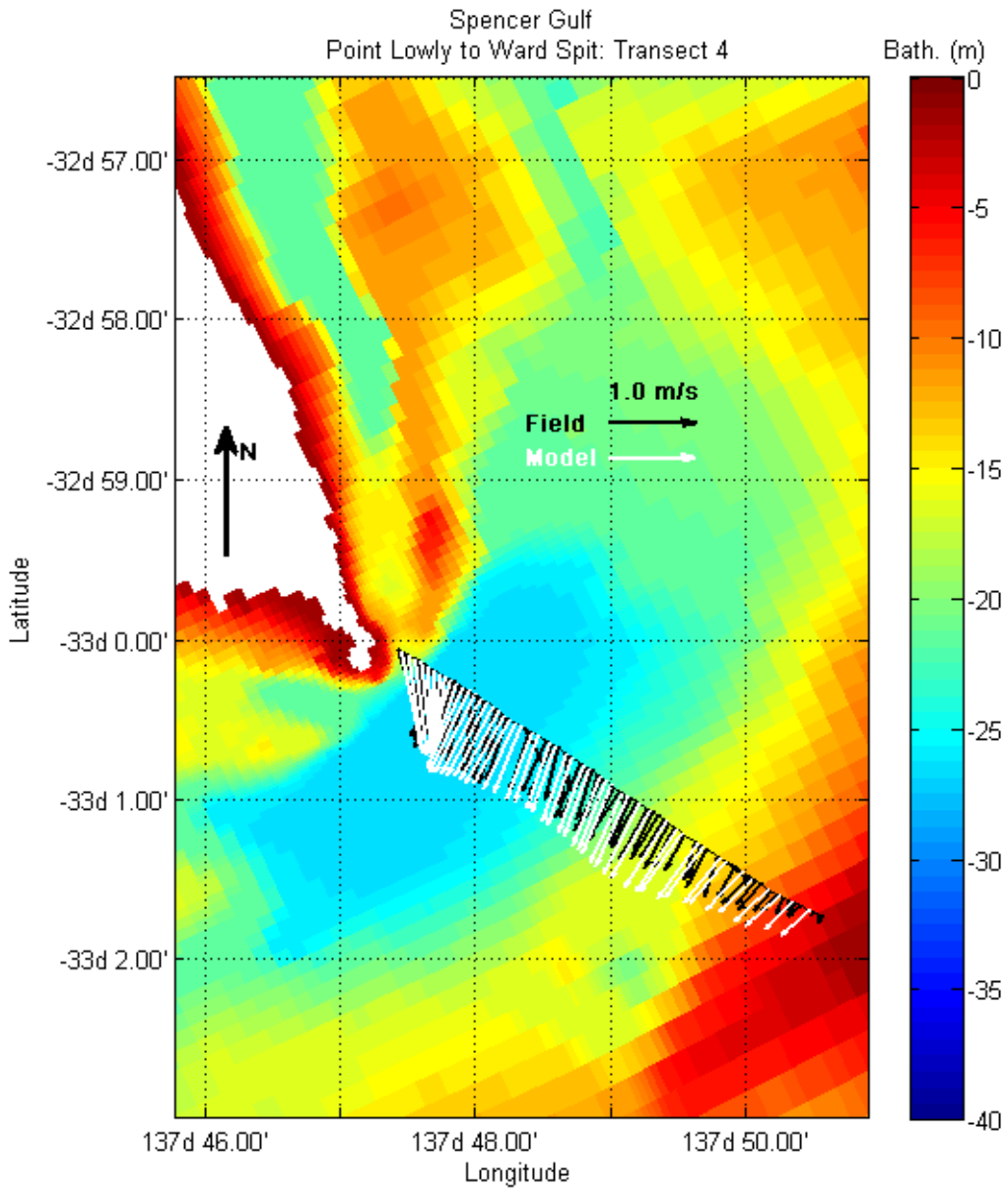


Transect 004

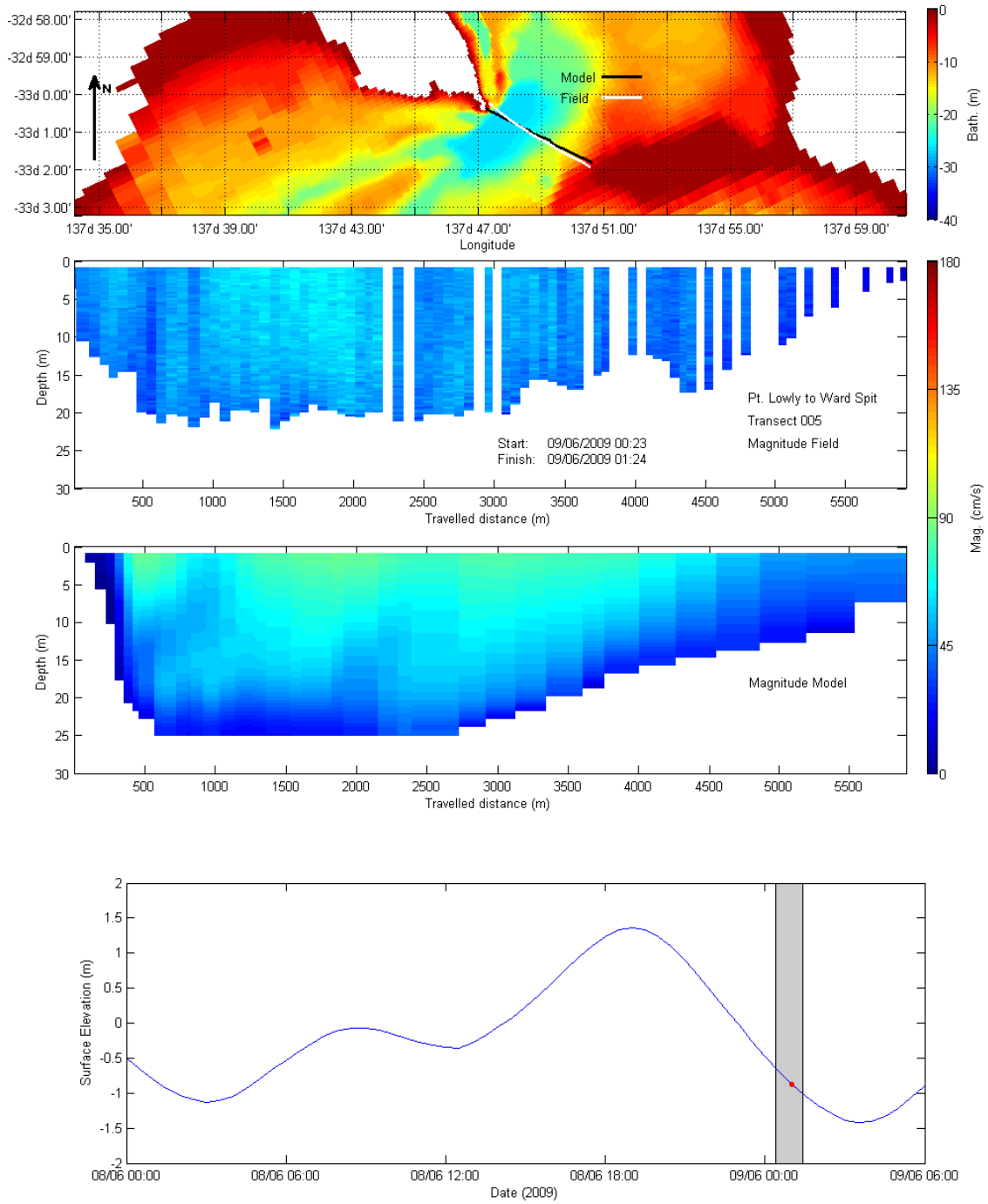


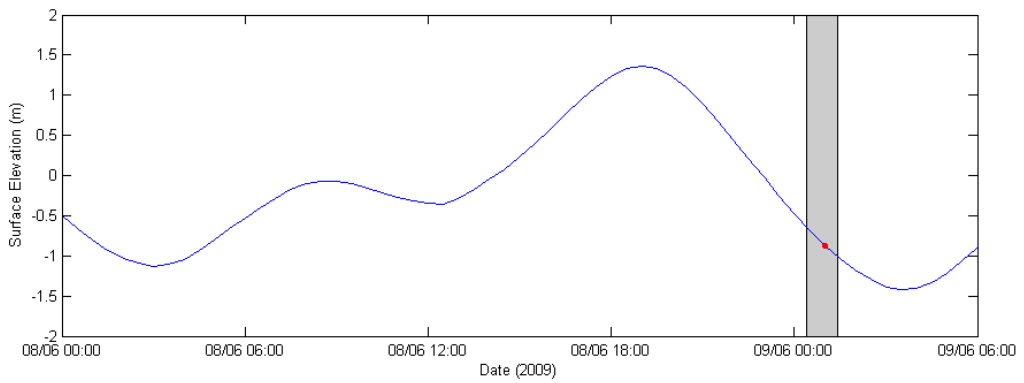
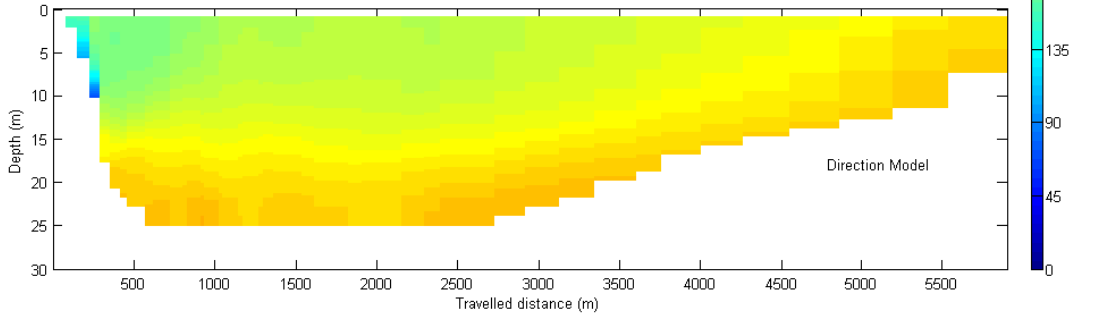
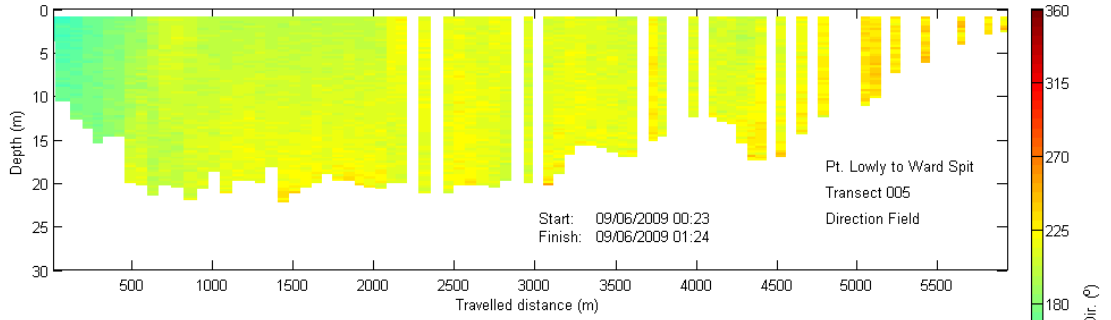
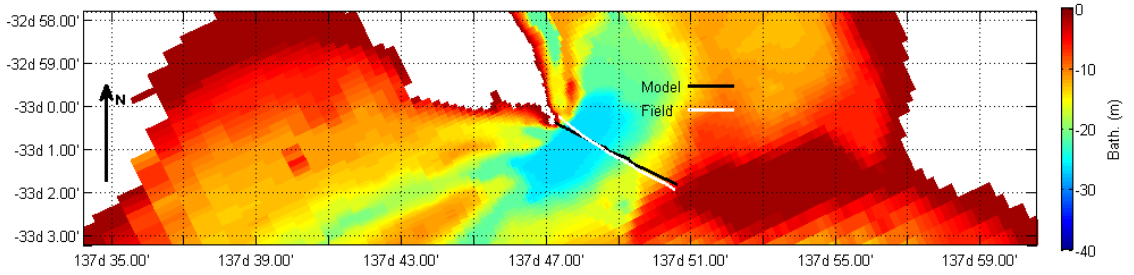


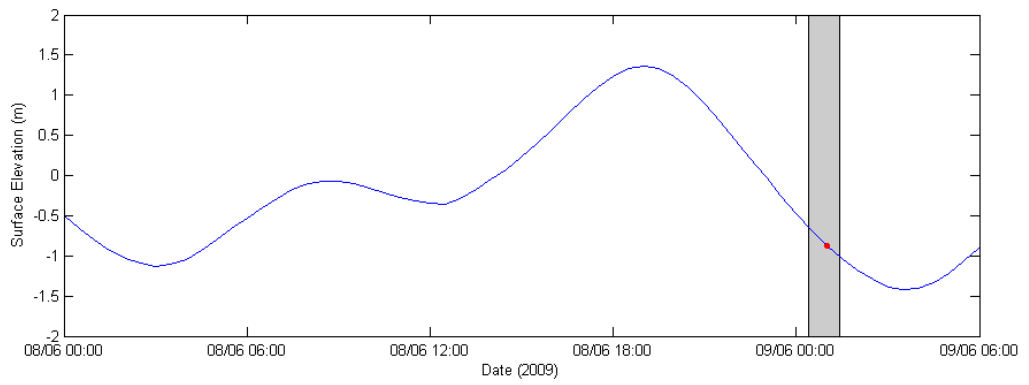
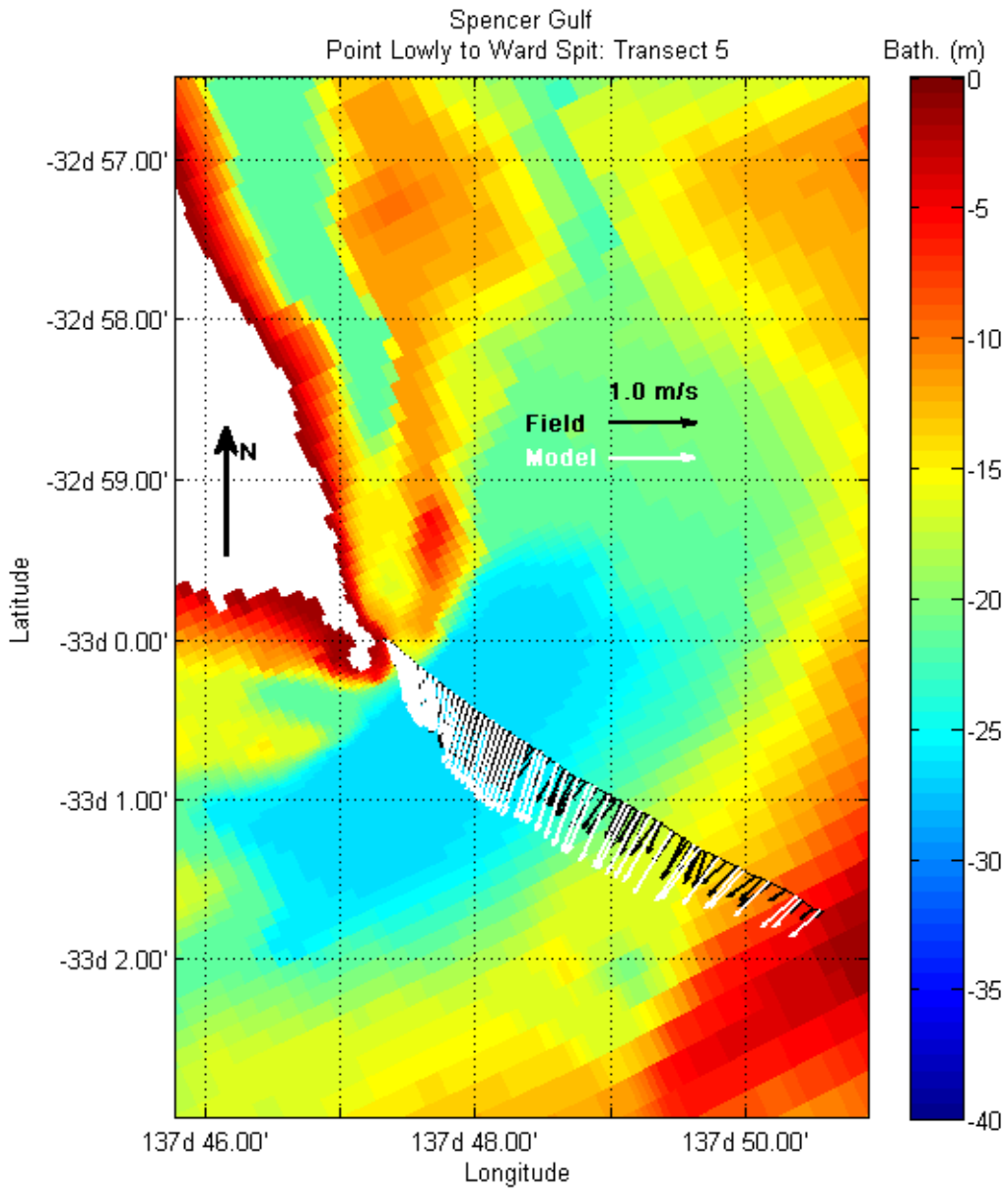




Transect 005

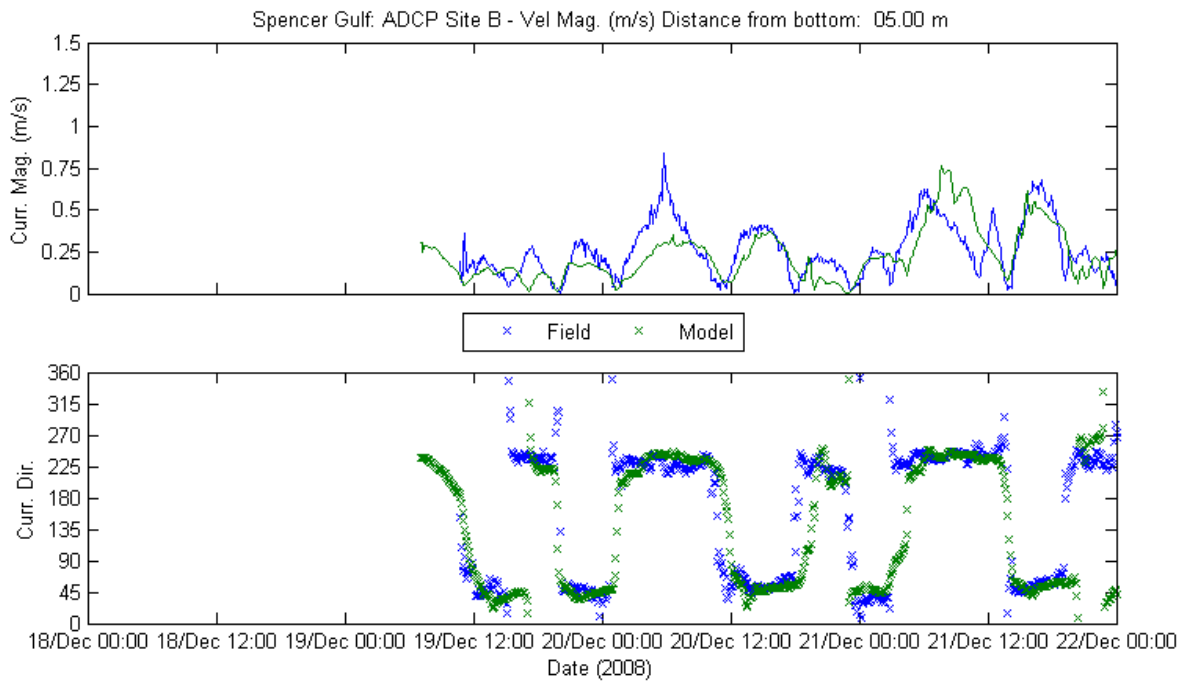
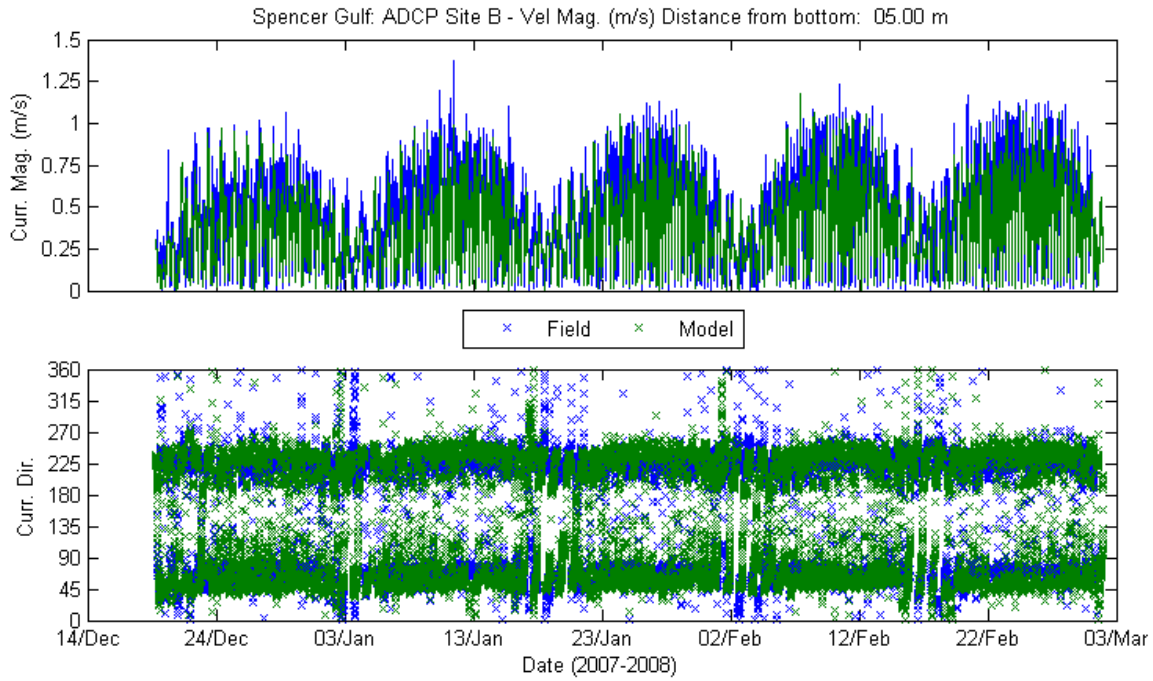


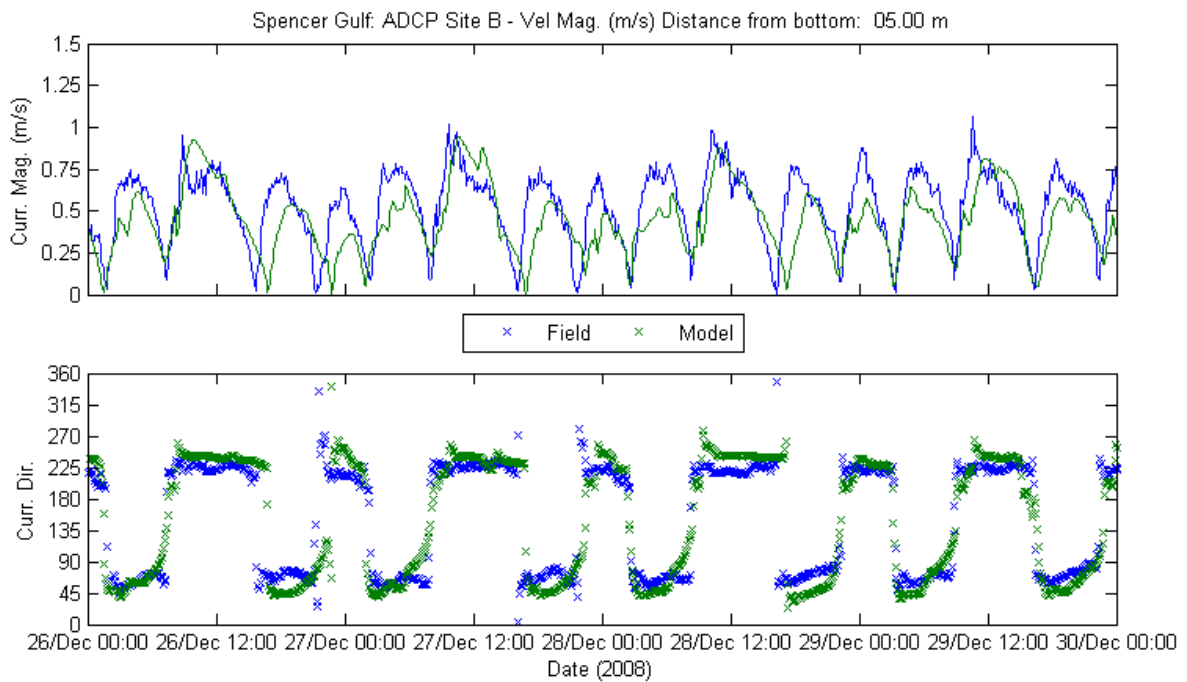
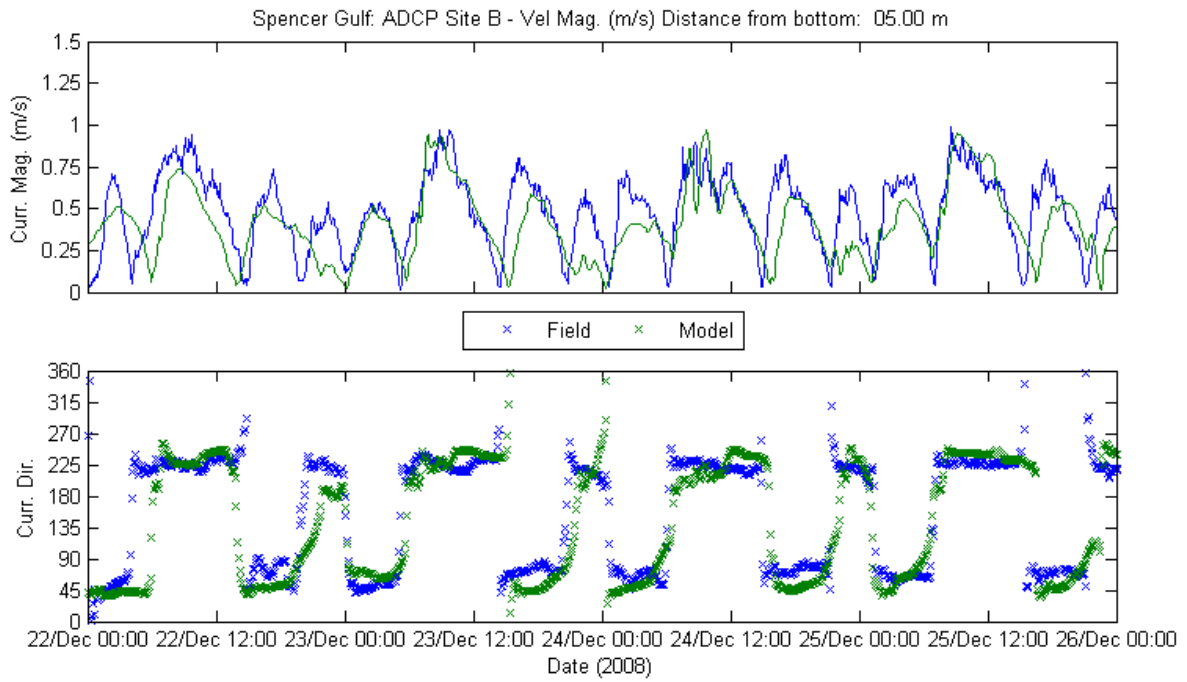


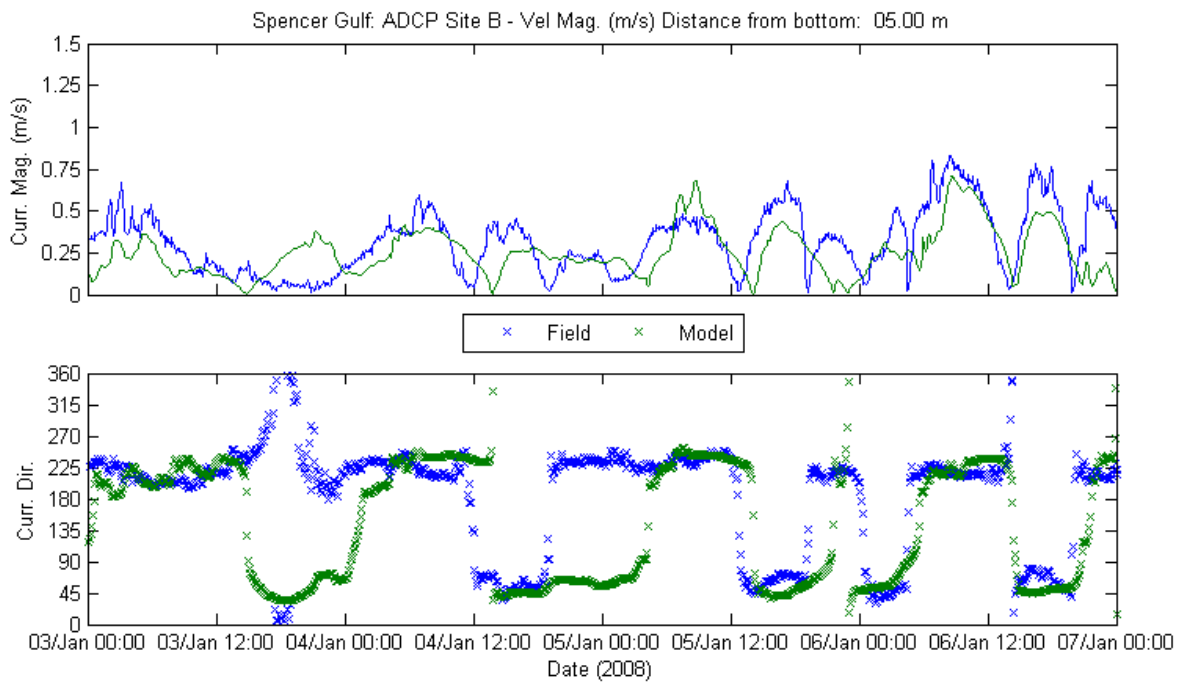
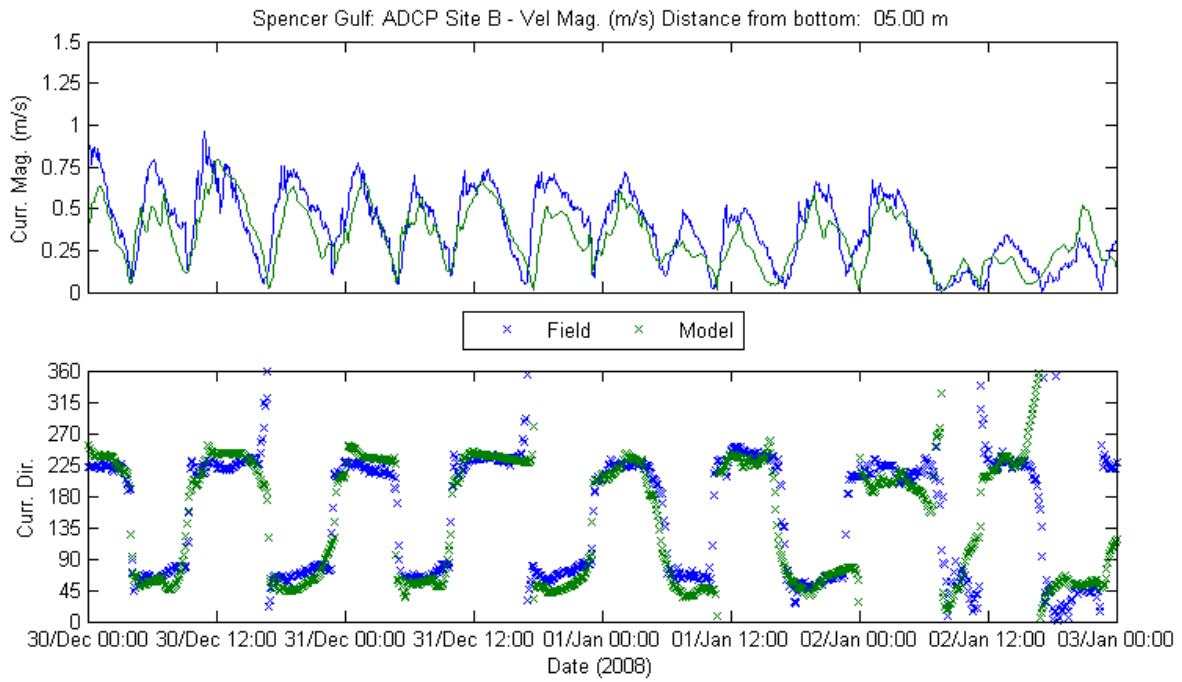


# APPENDIX G: THREE-MONTH VALIDATION PERIOD ADCP COMPARISONS

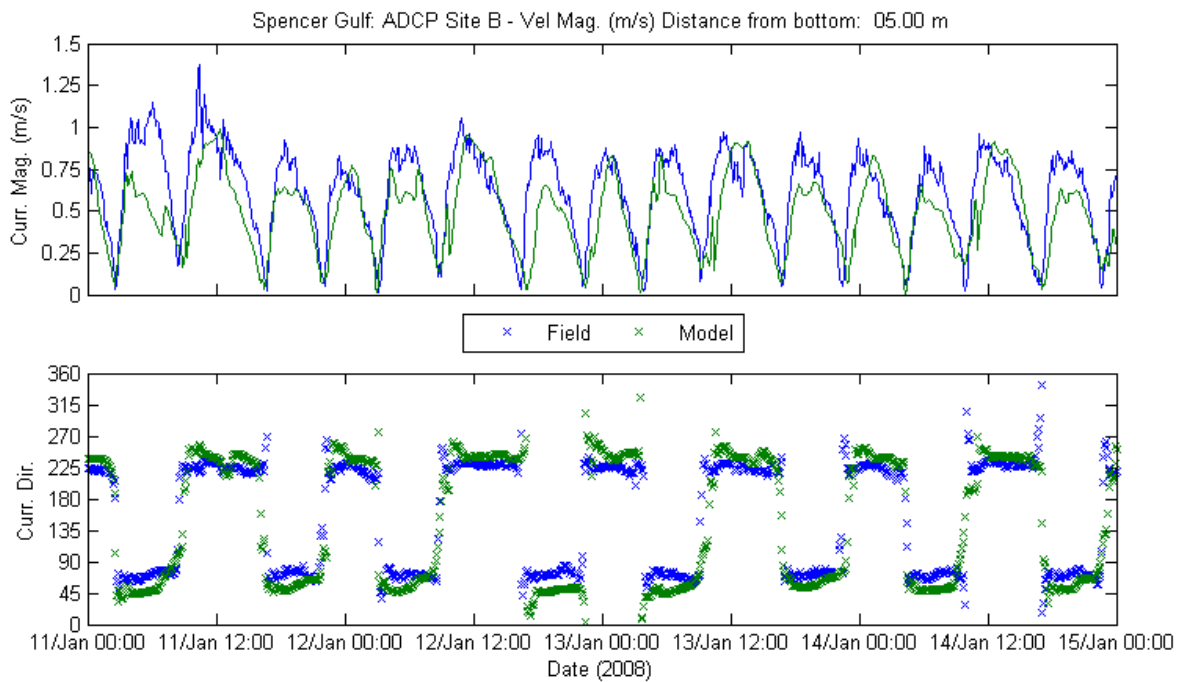
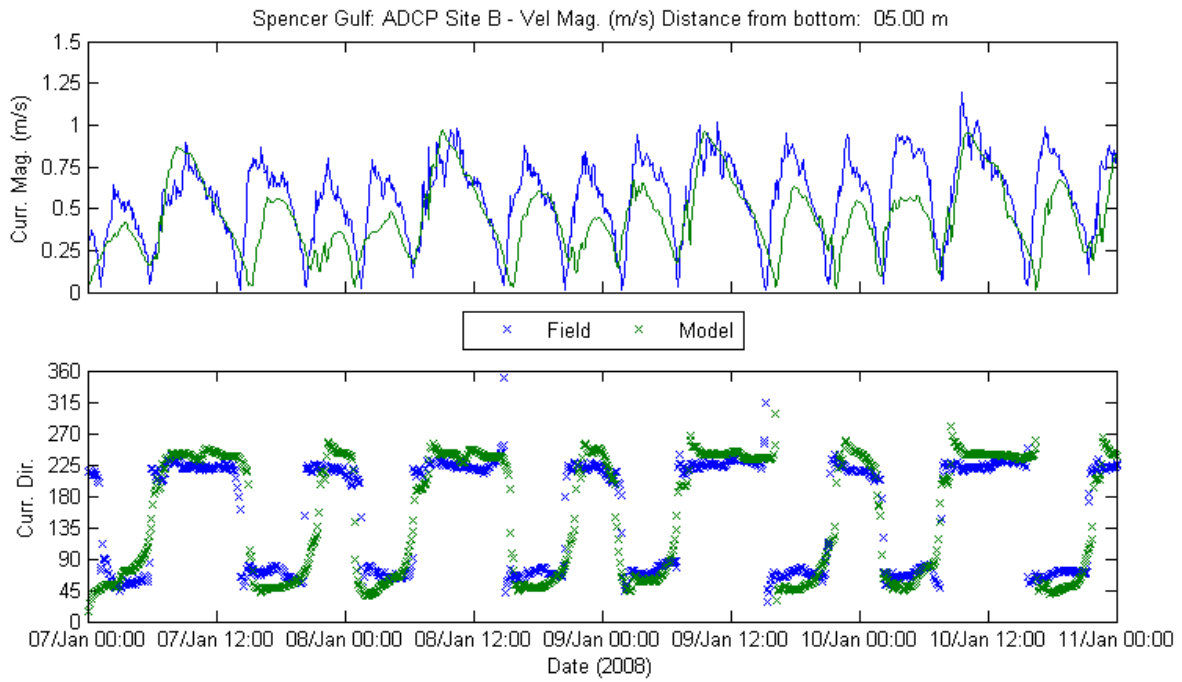
## Site B at 5.00 m from Bottom

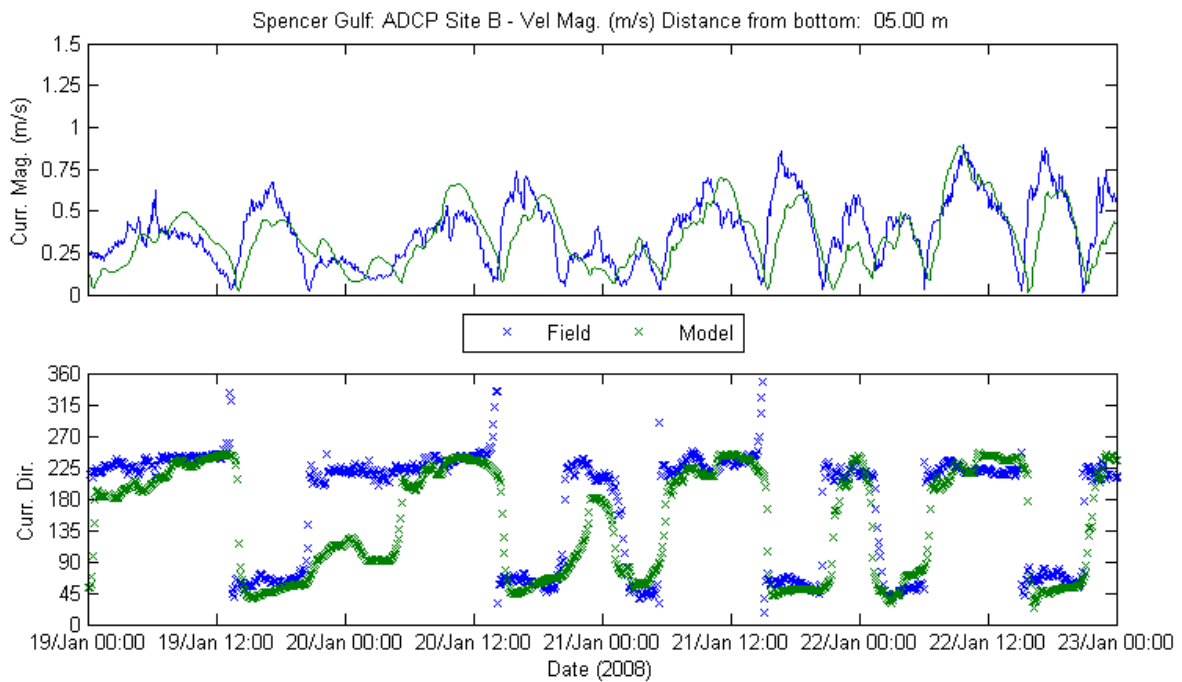
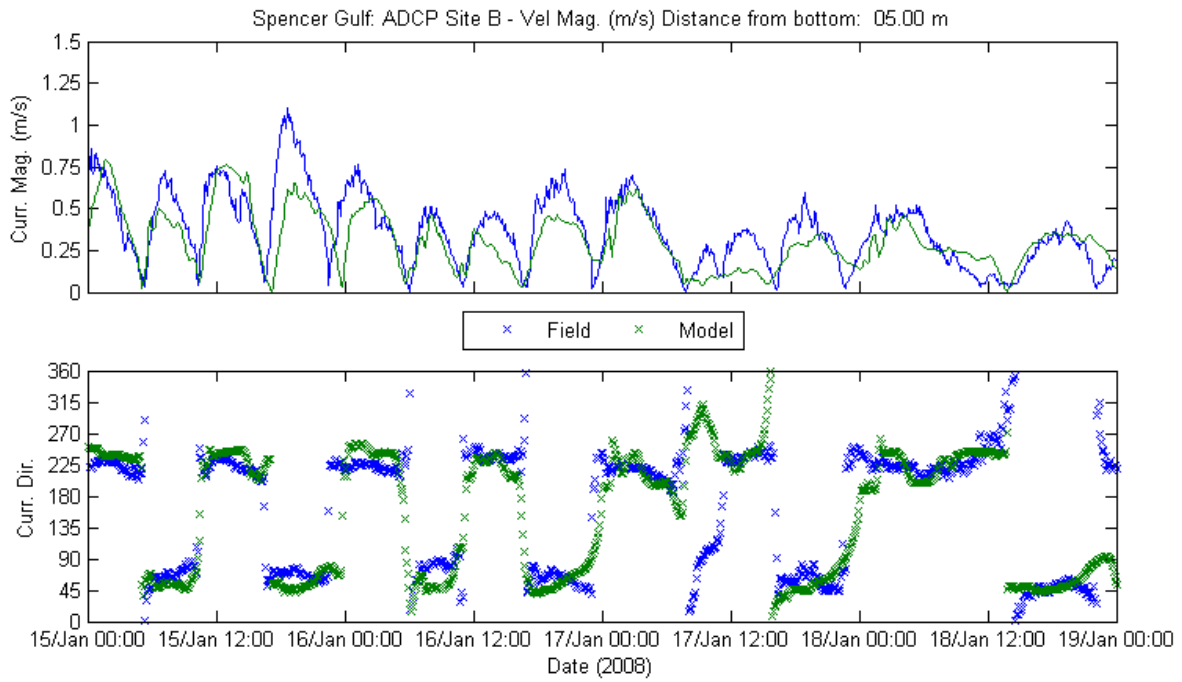


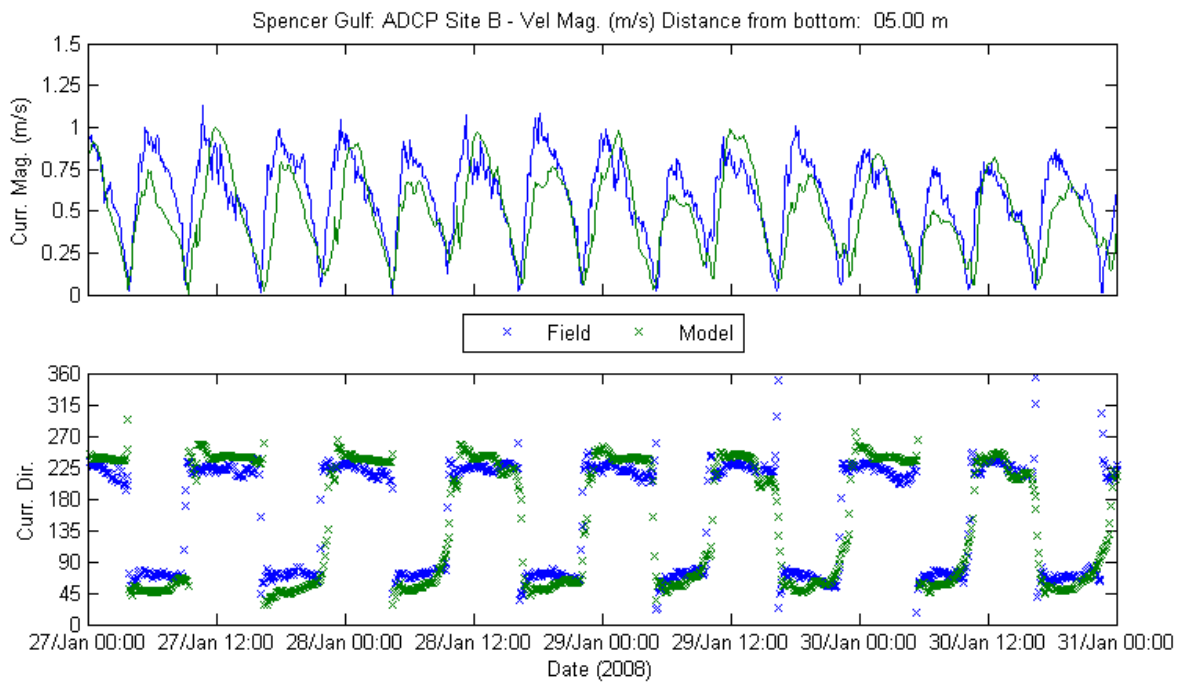
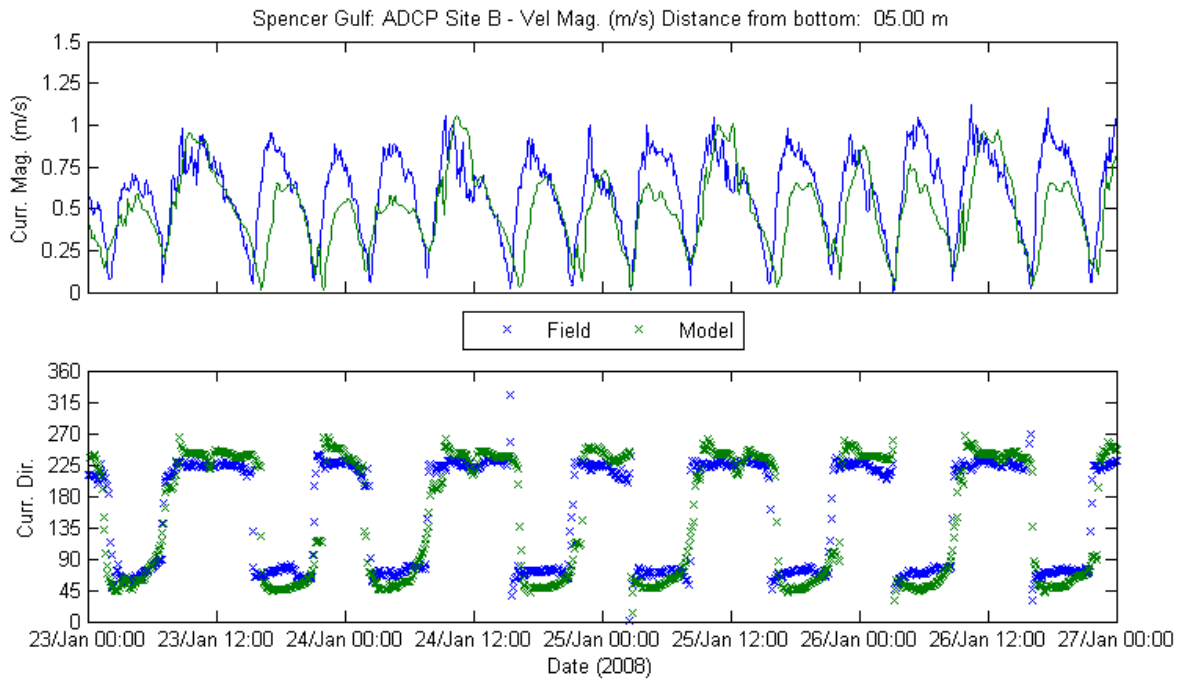


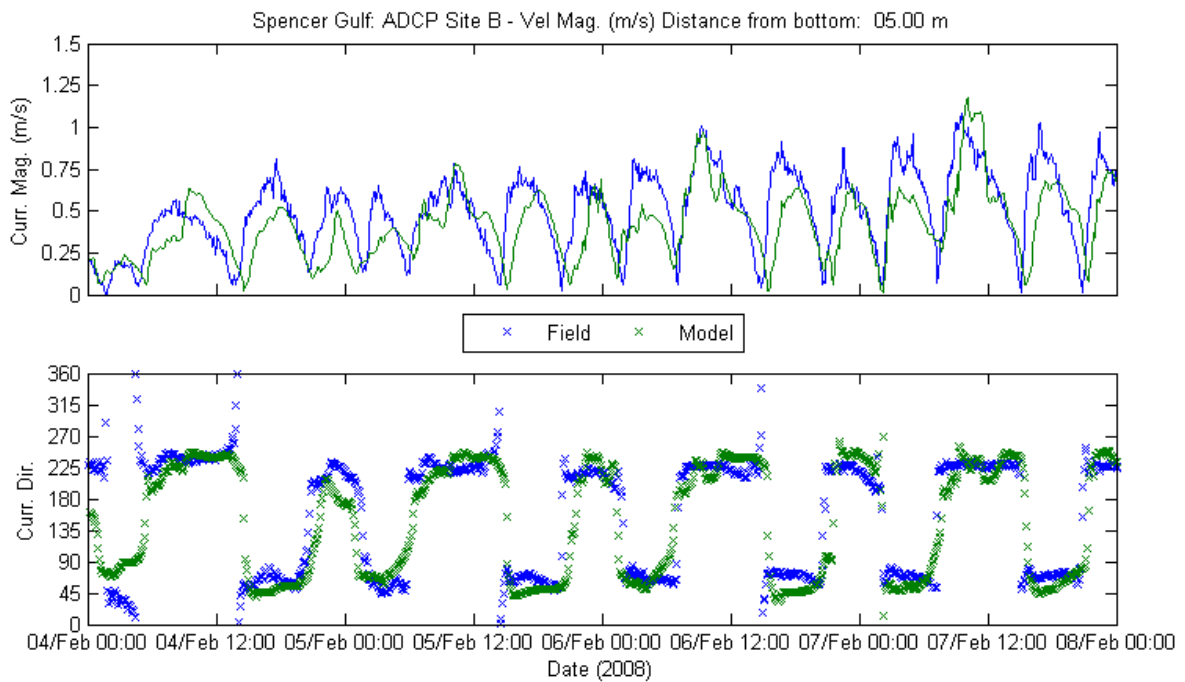
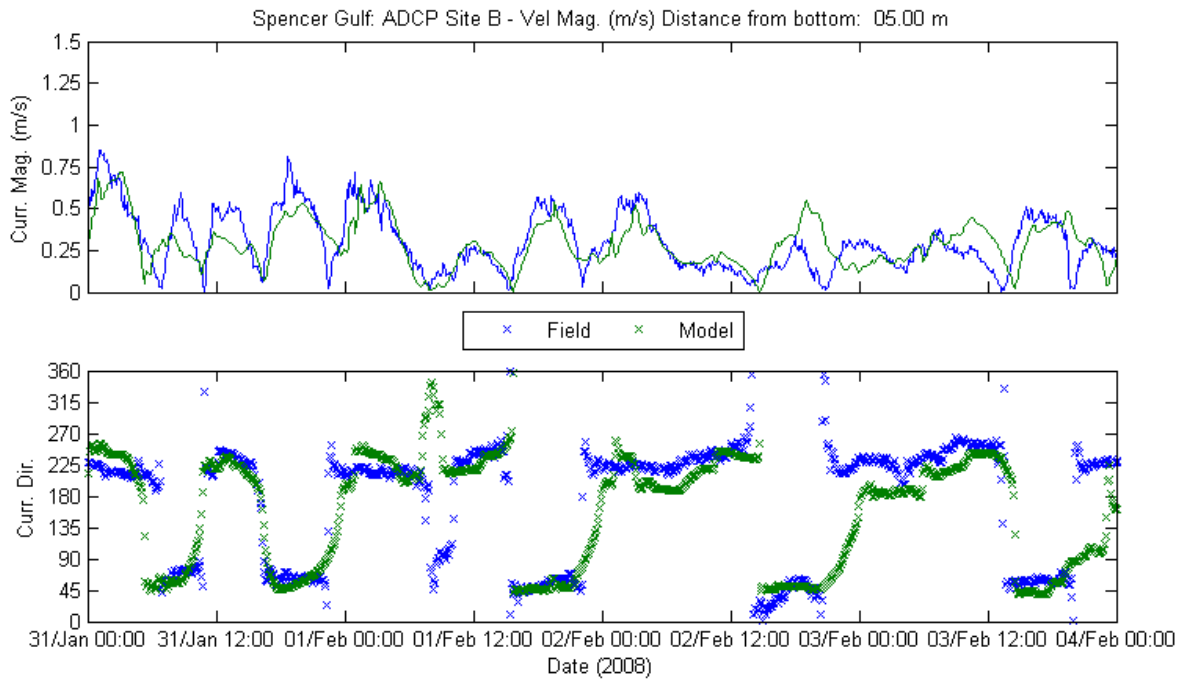


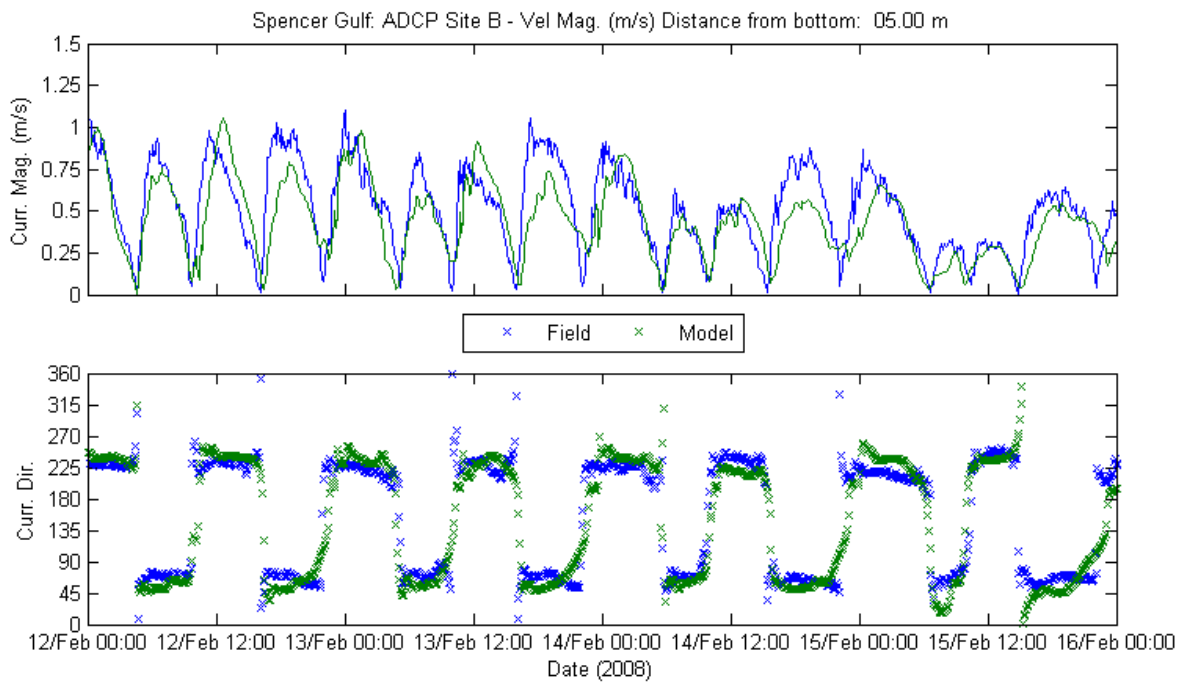
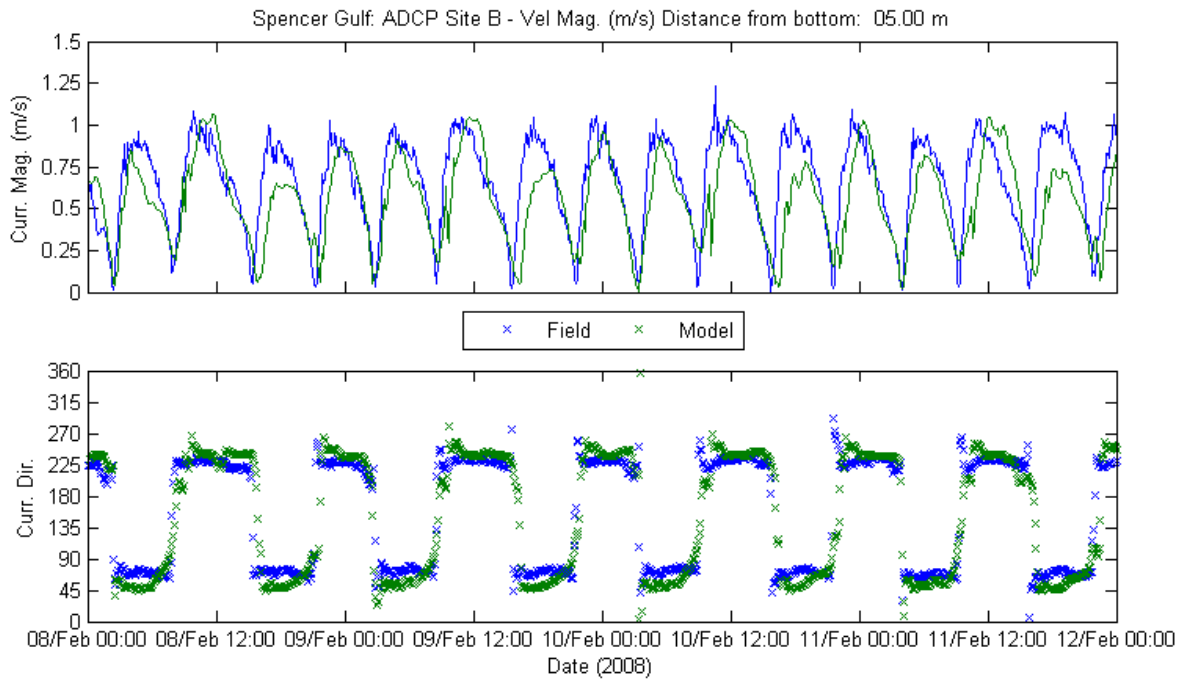


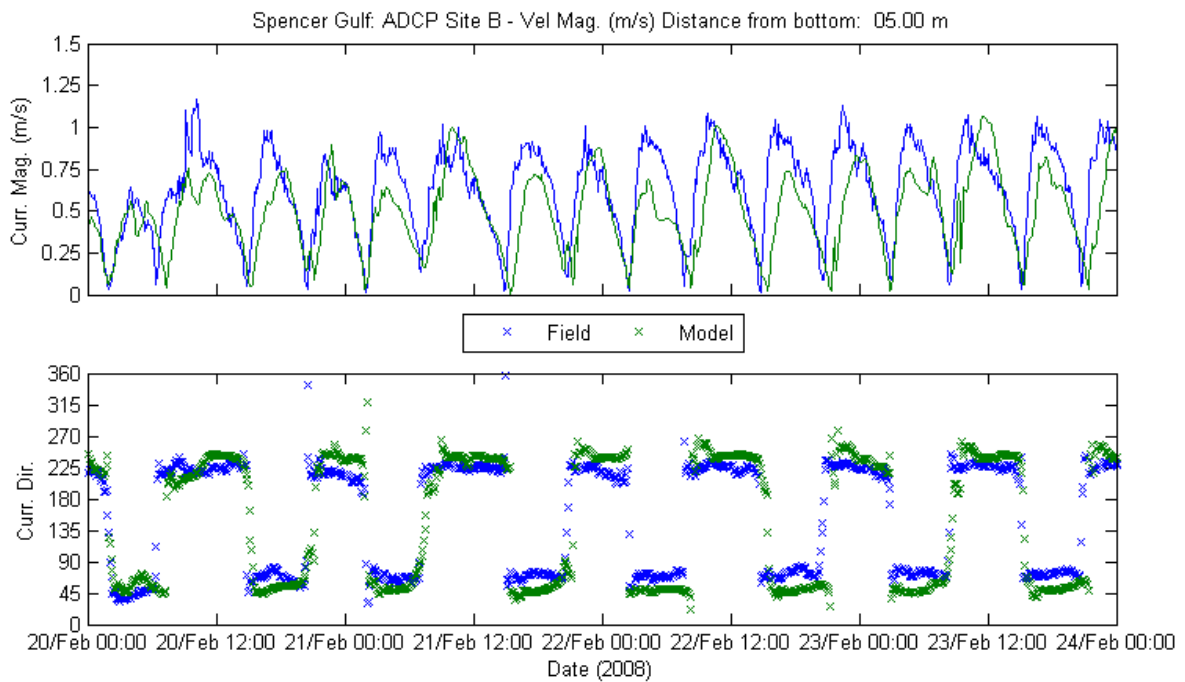
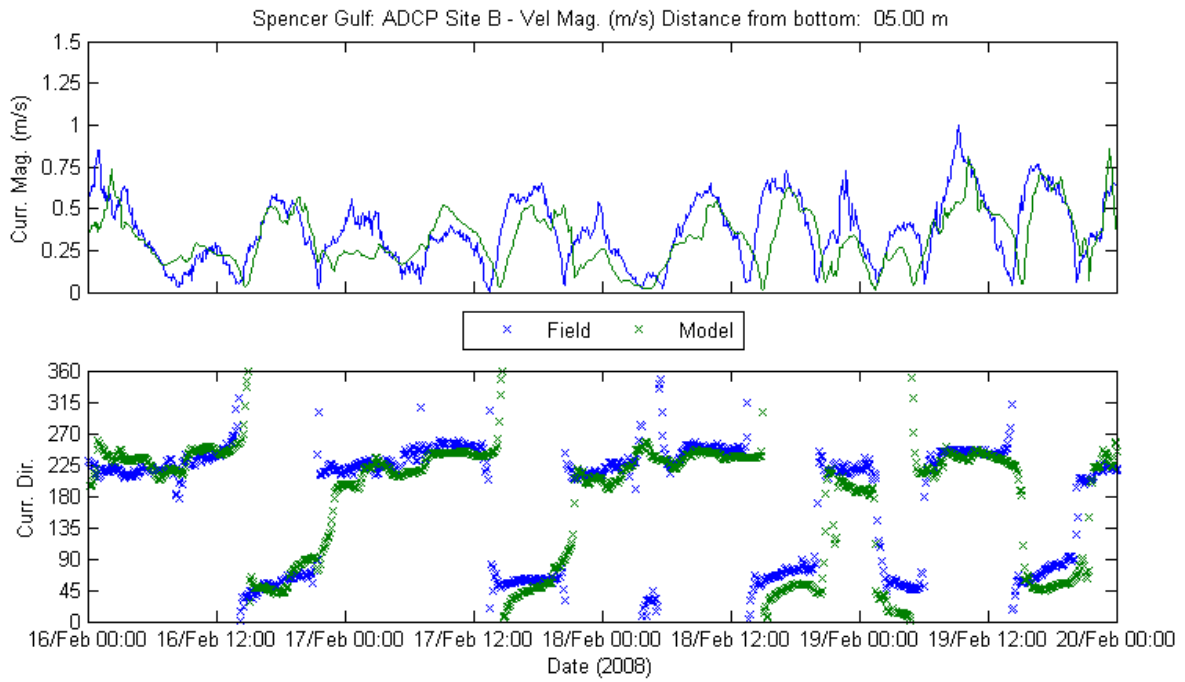


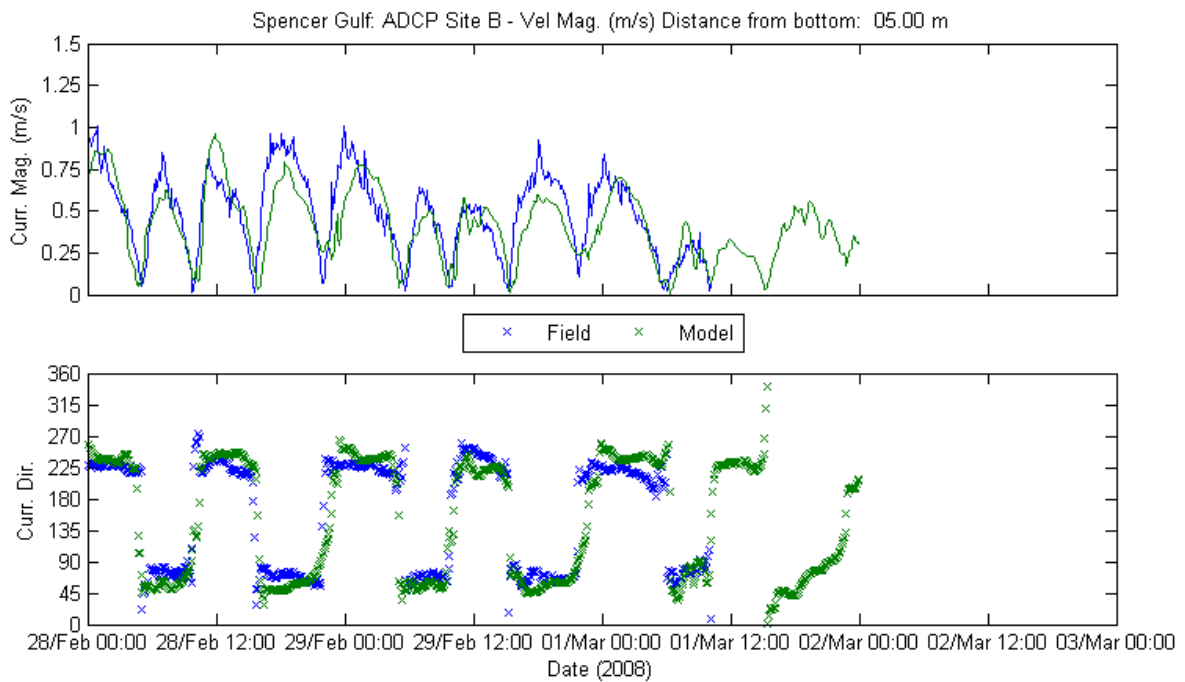
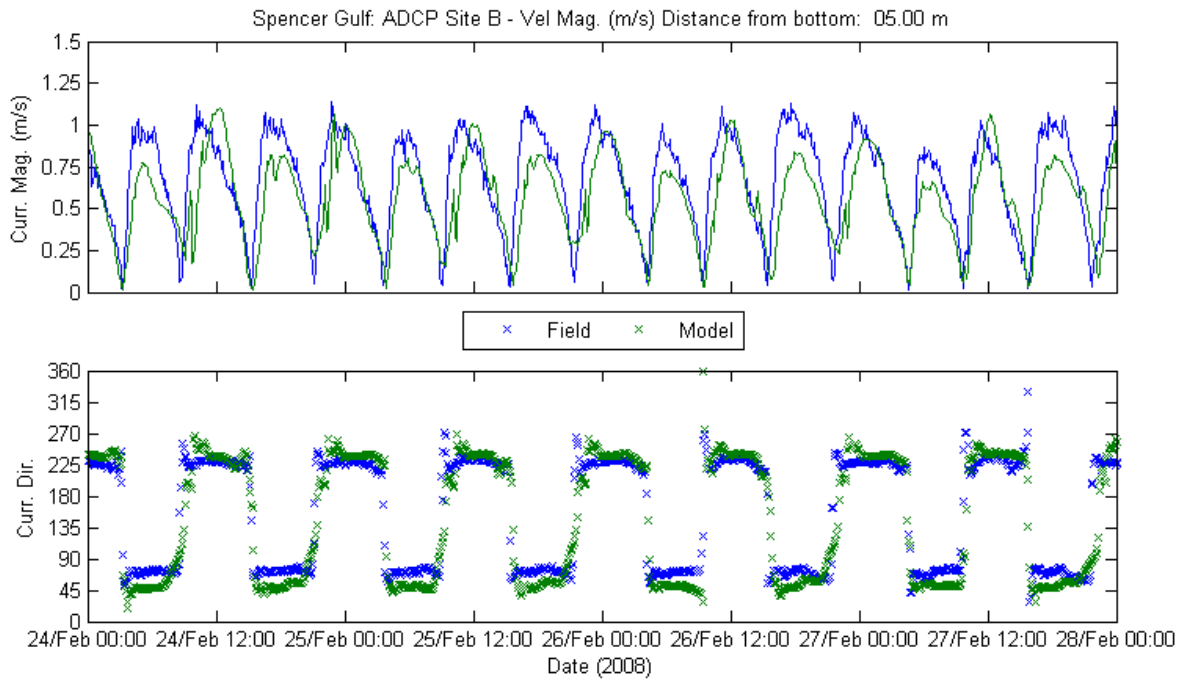




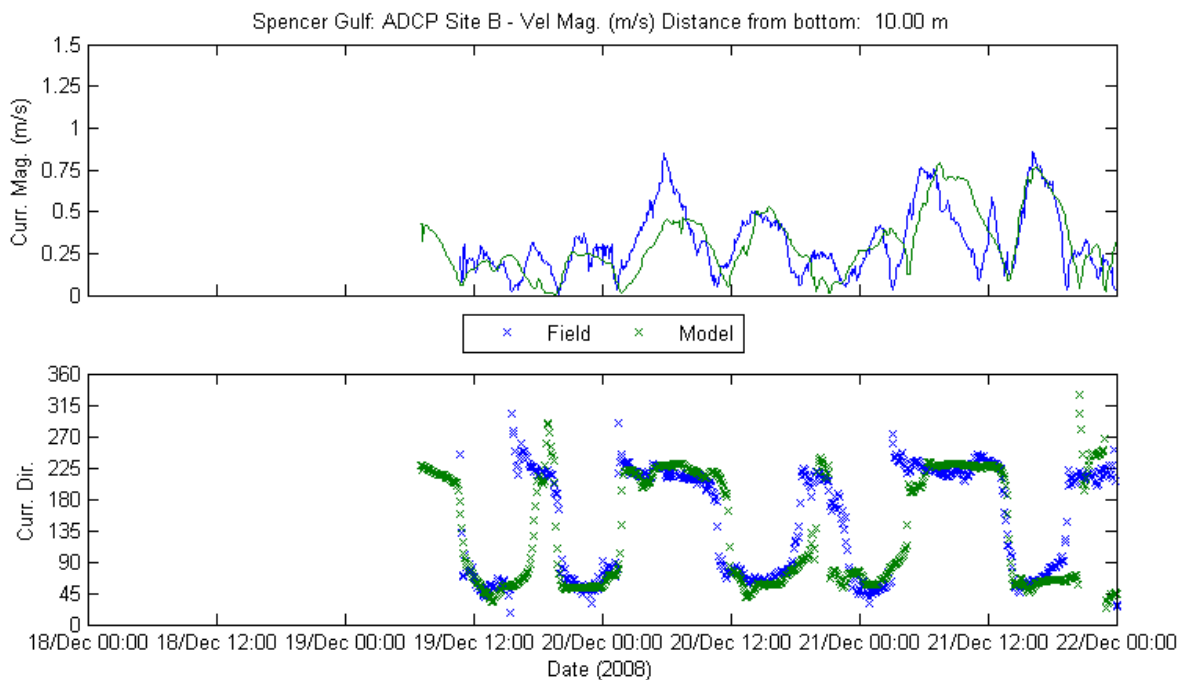
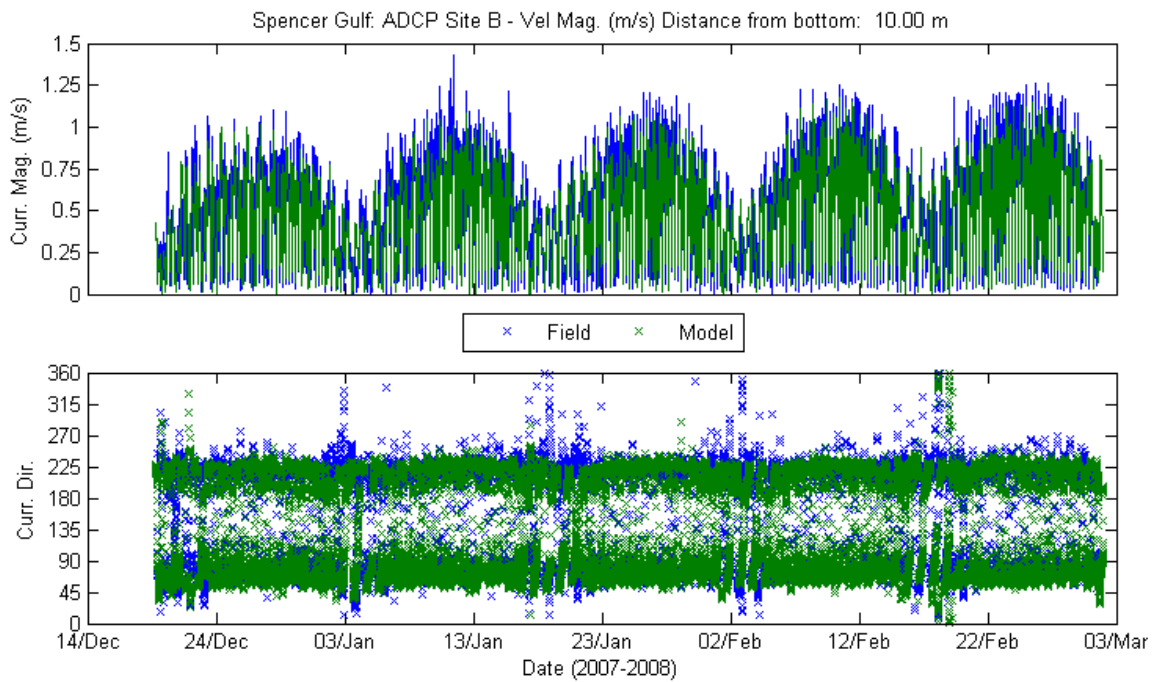




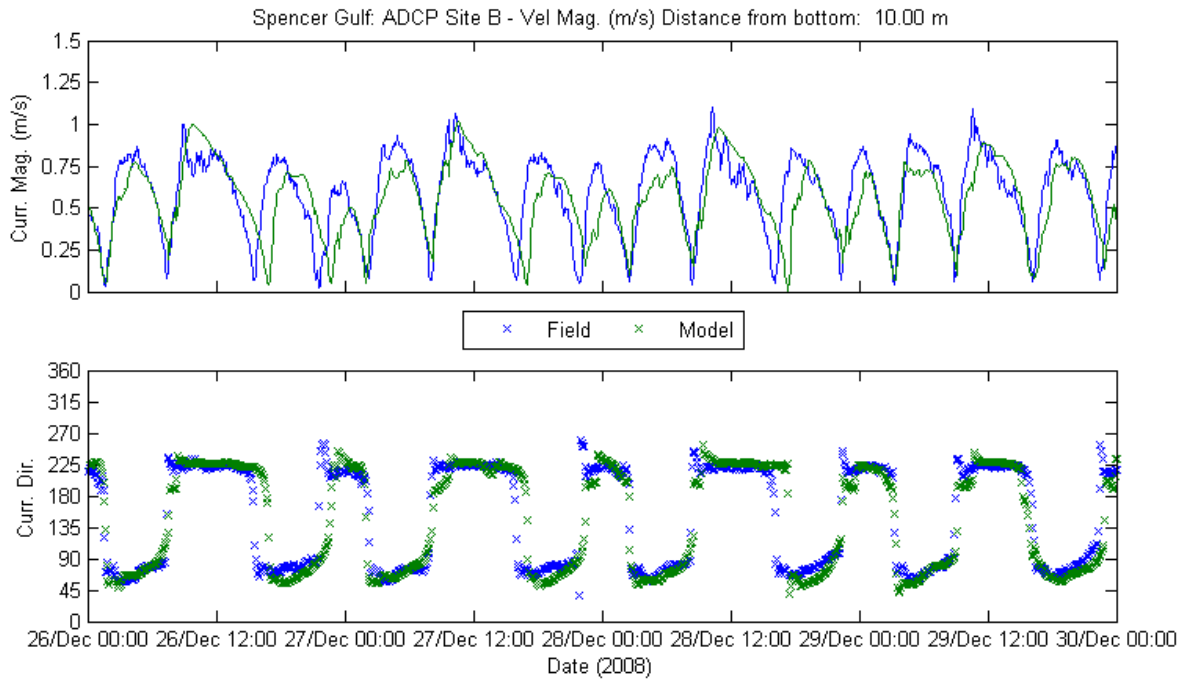
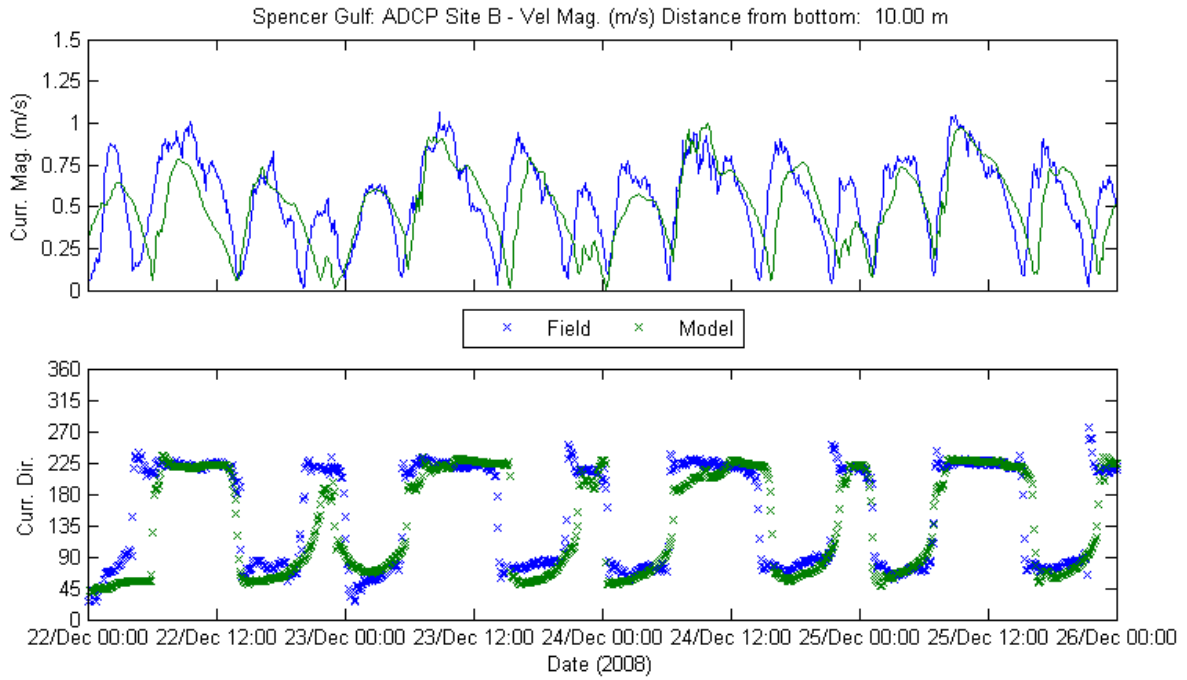


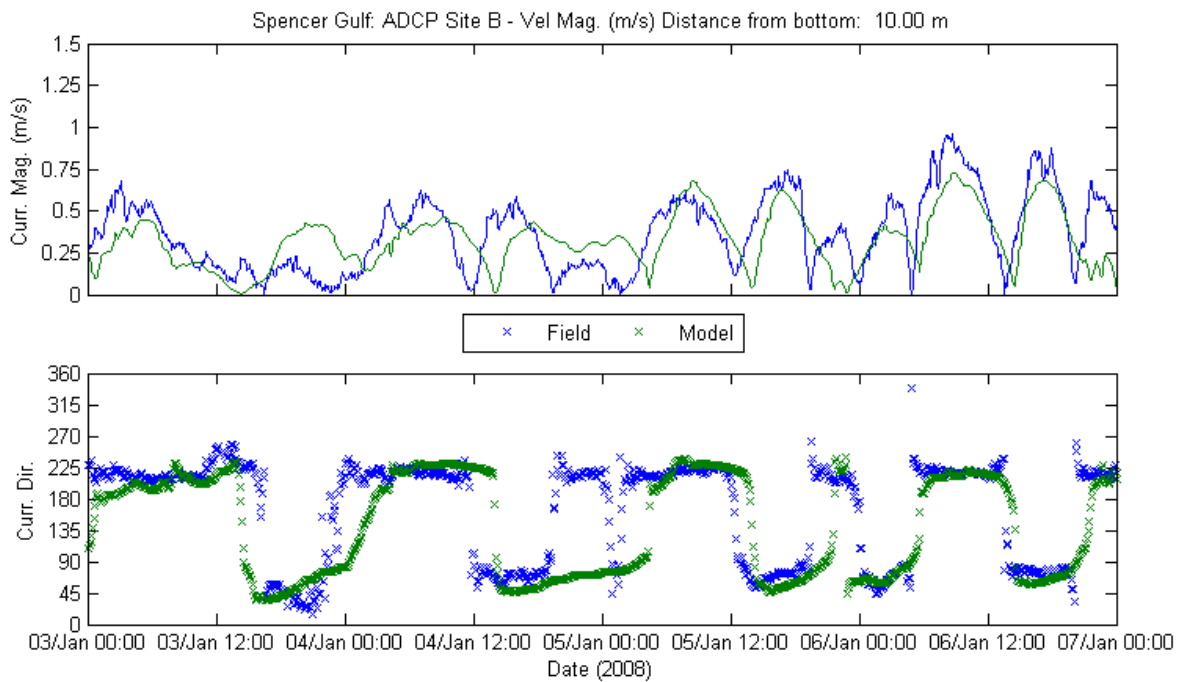
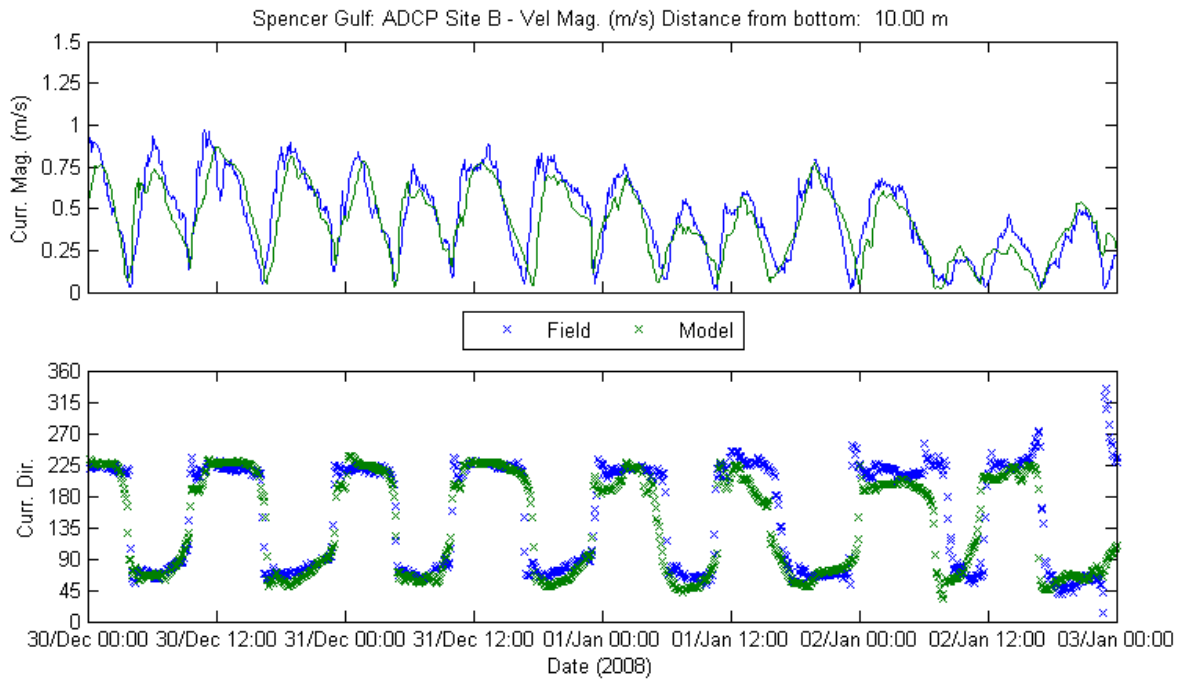


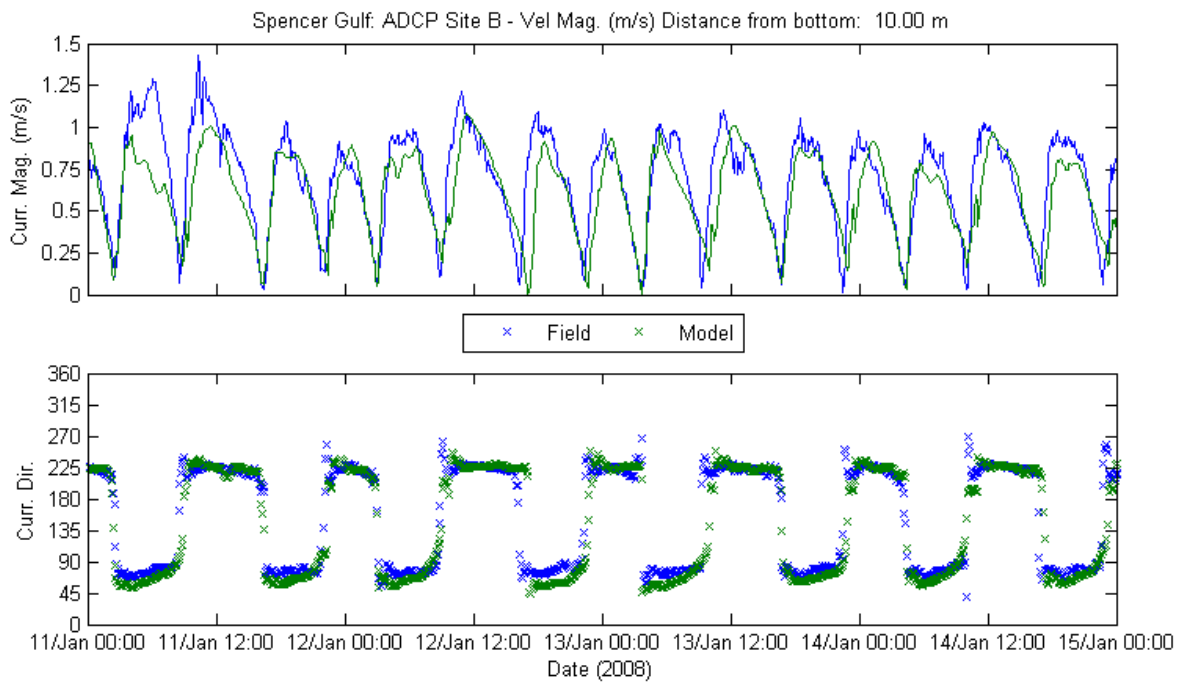
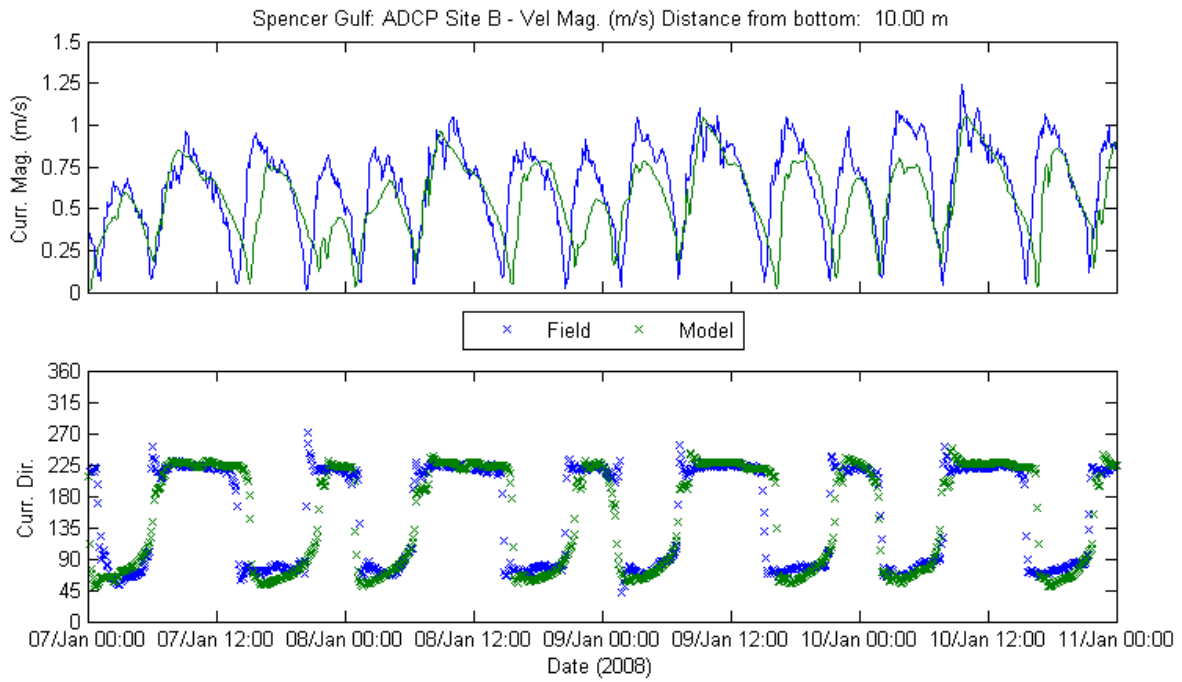
Site B at 10.00 m from Bottom

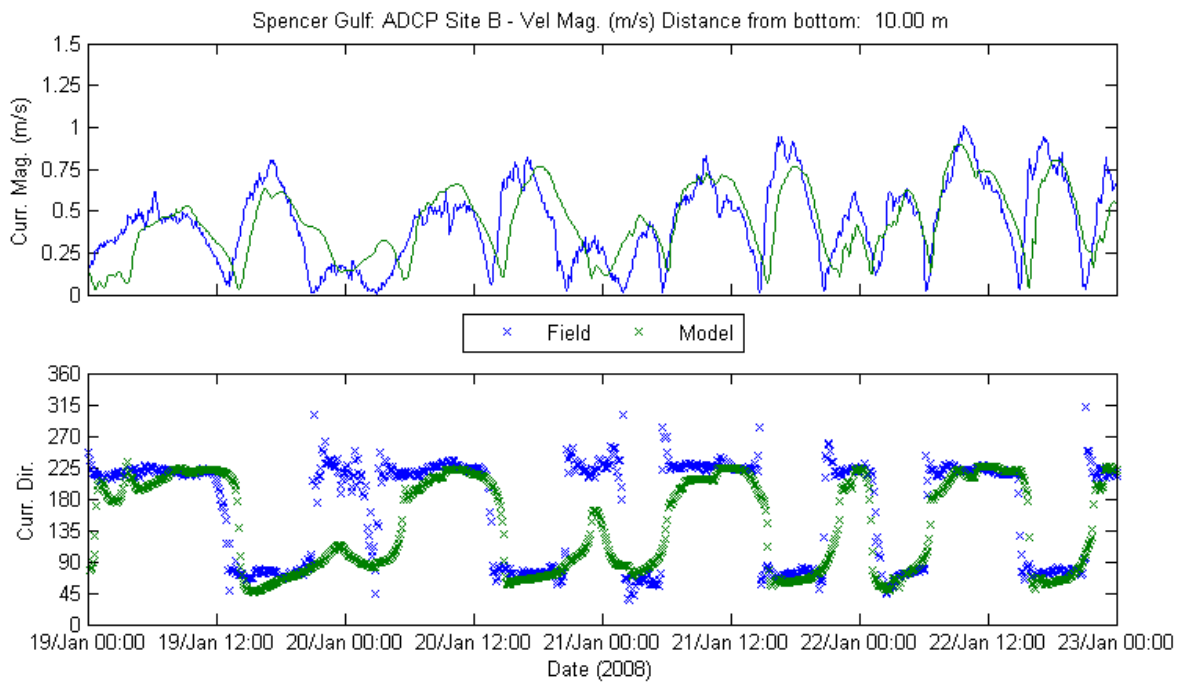
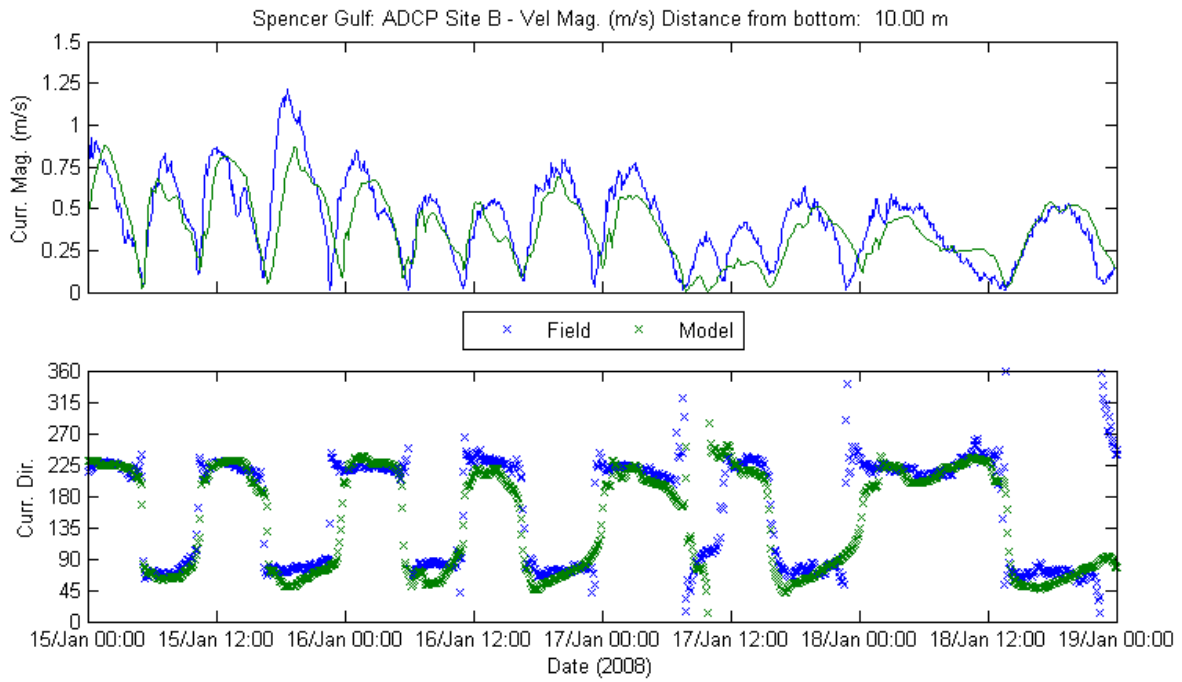


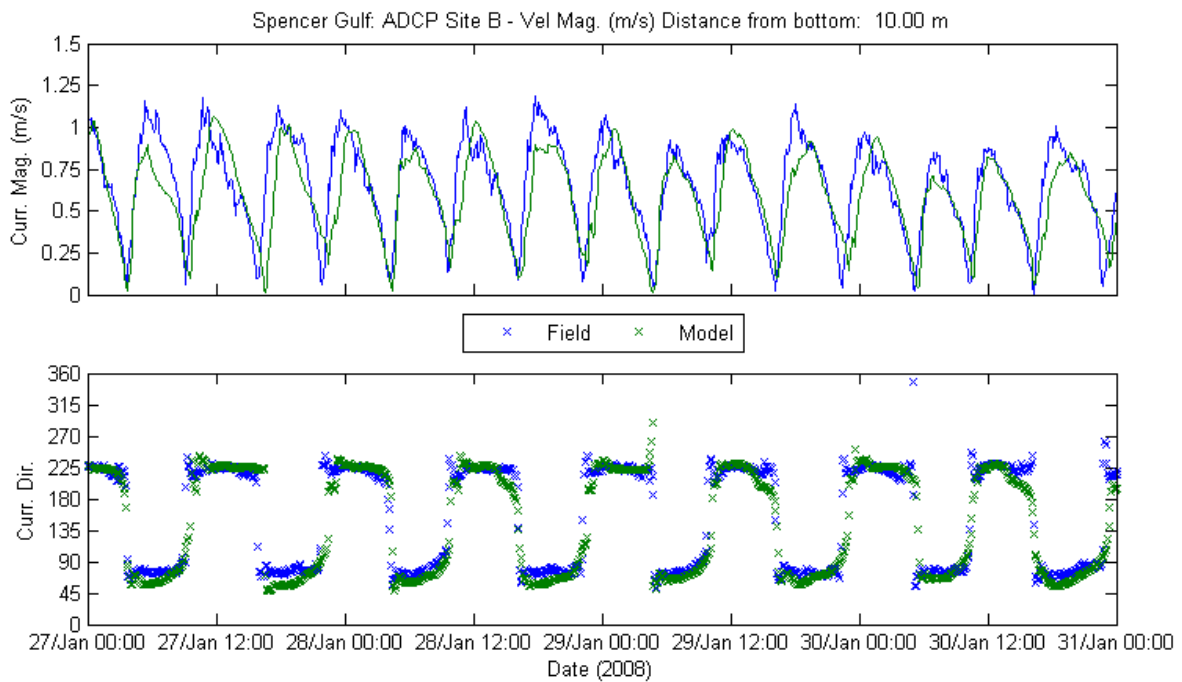
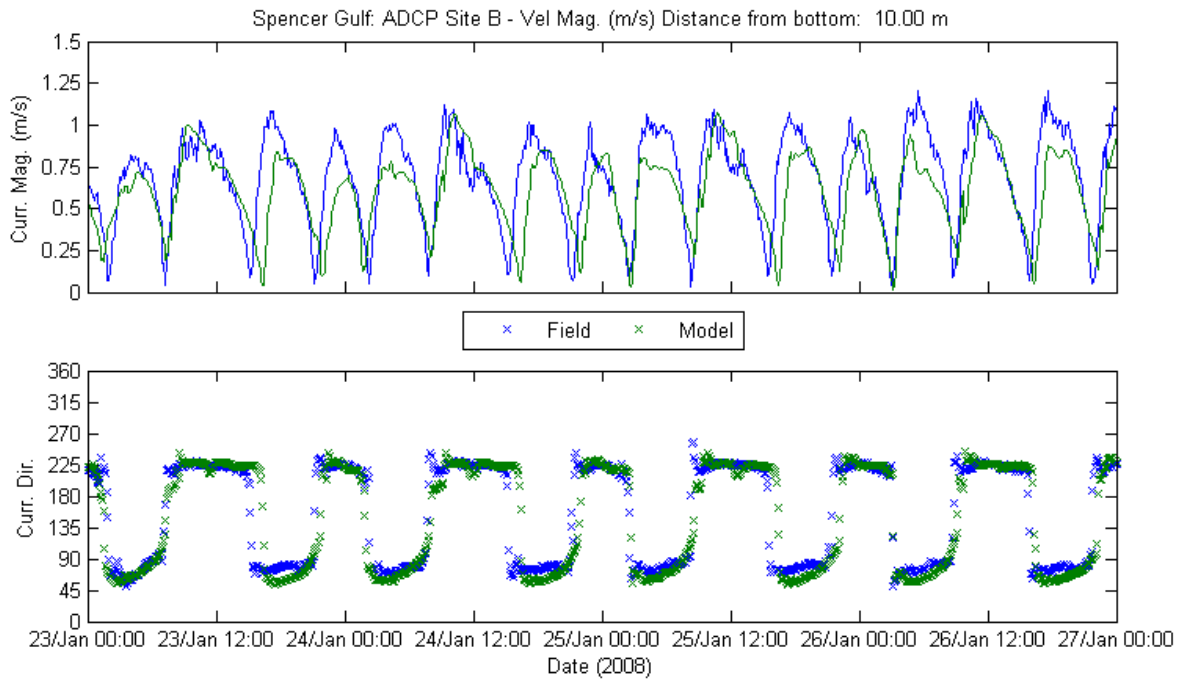


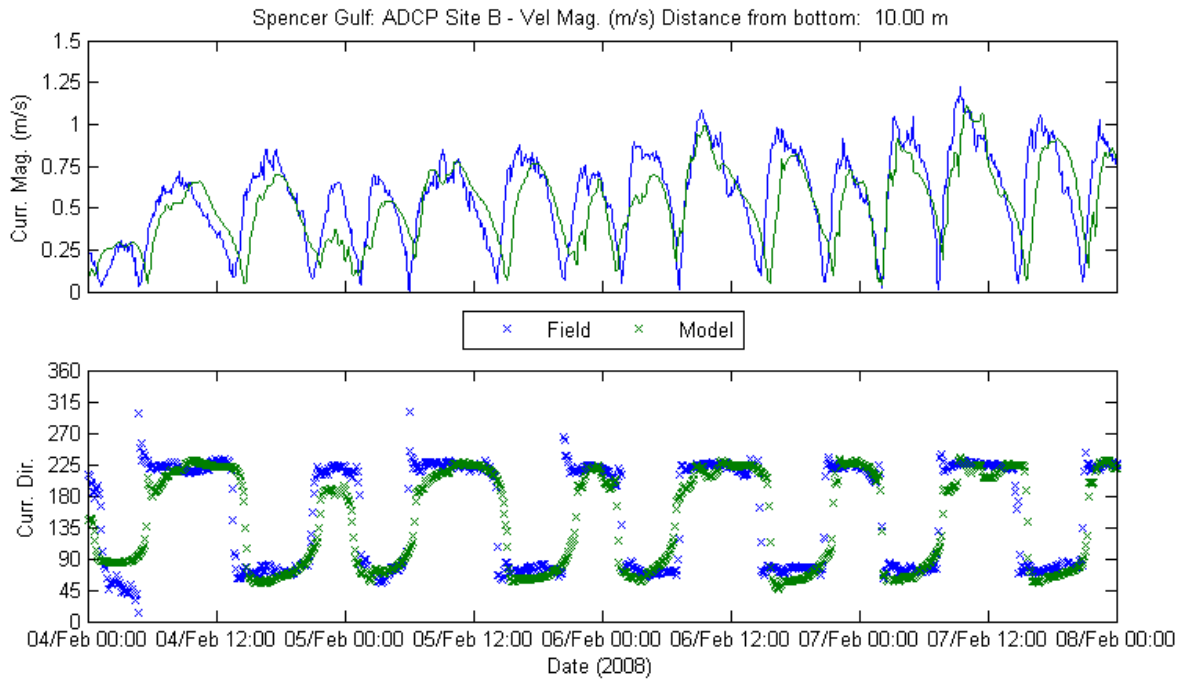
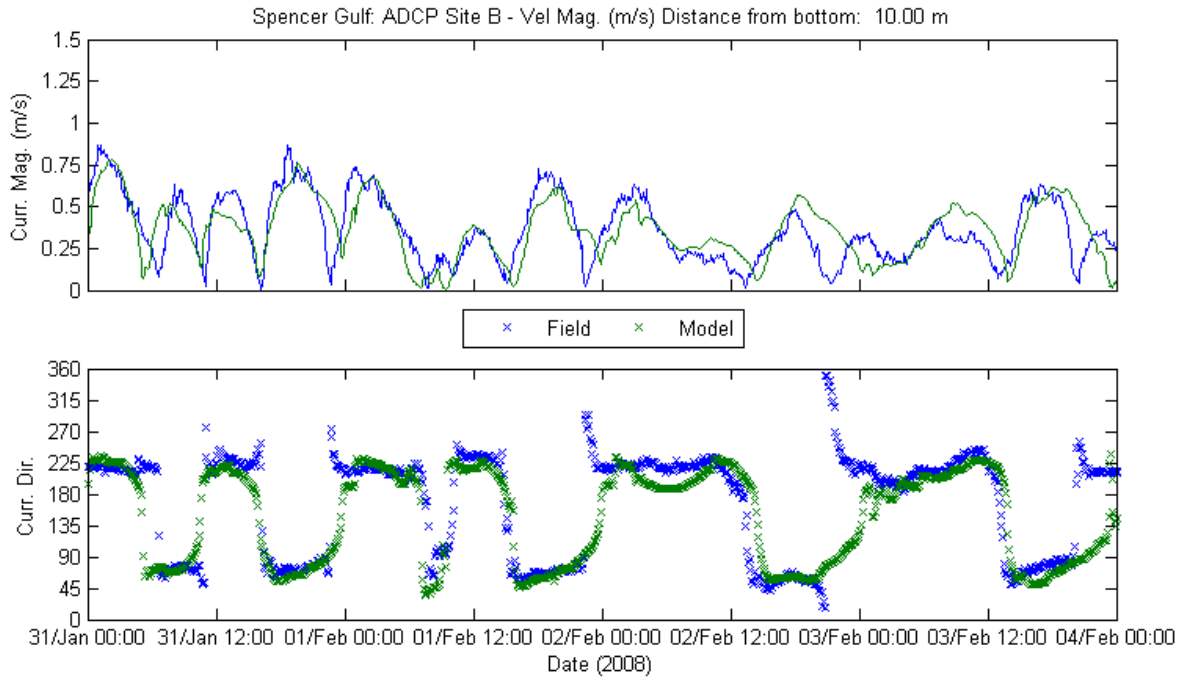


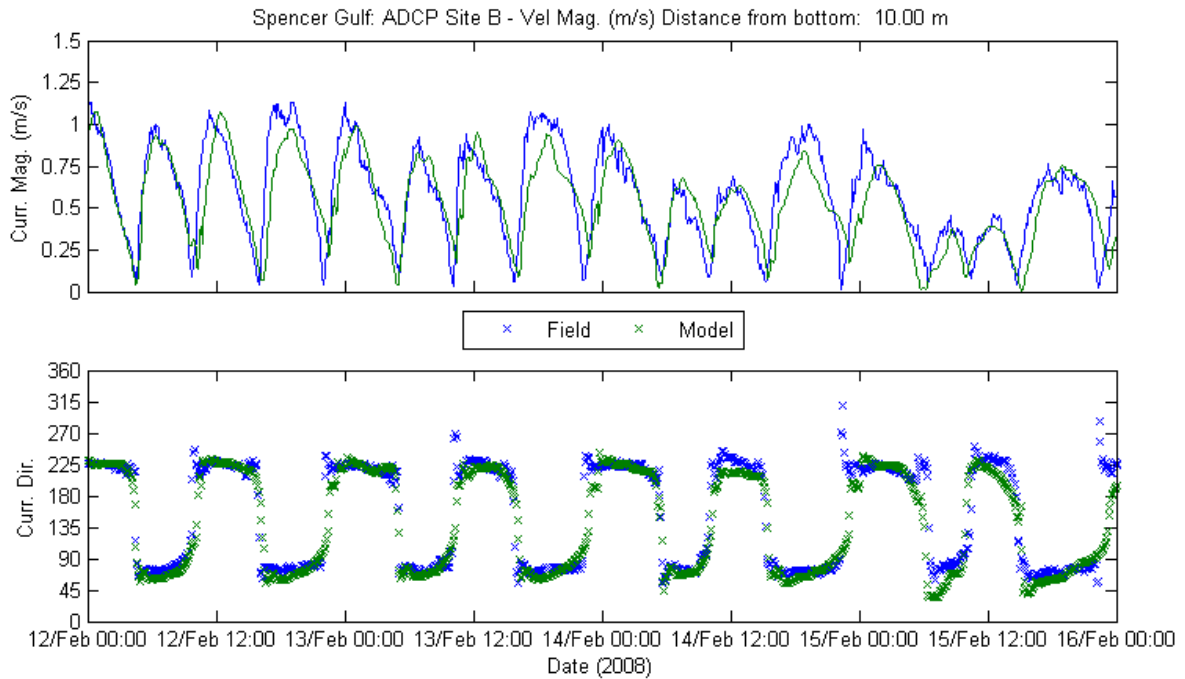
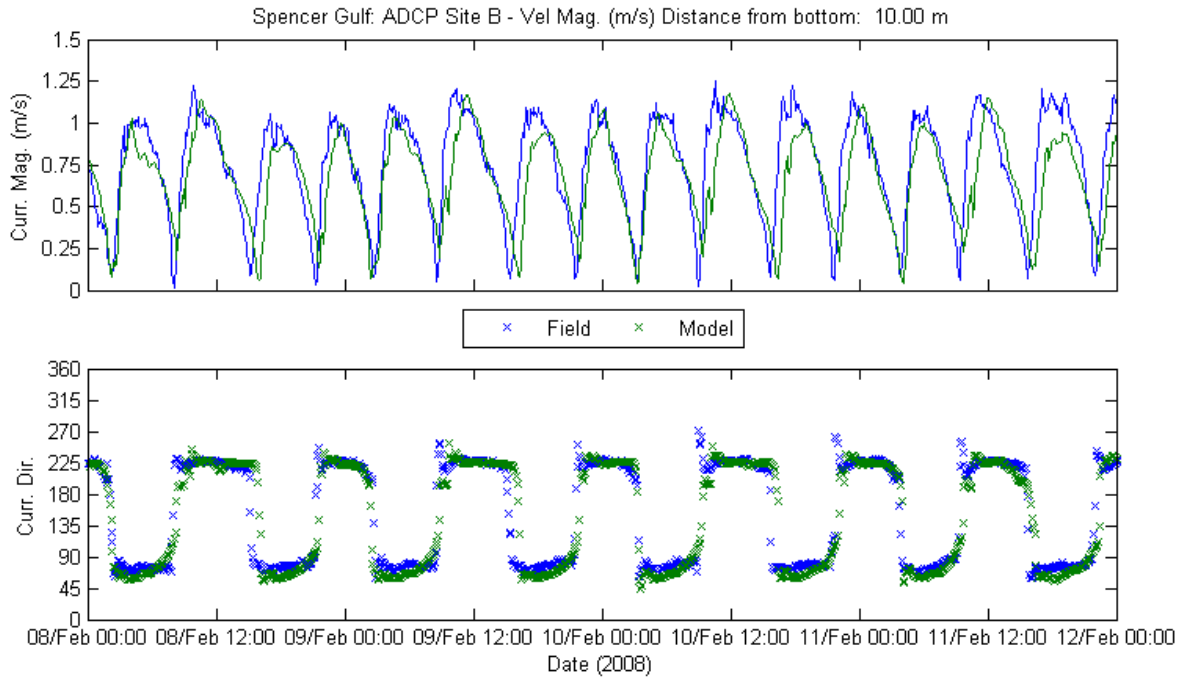


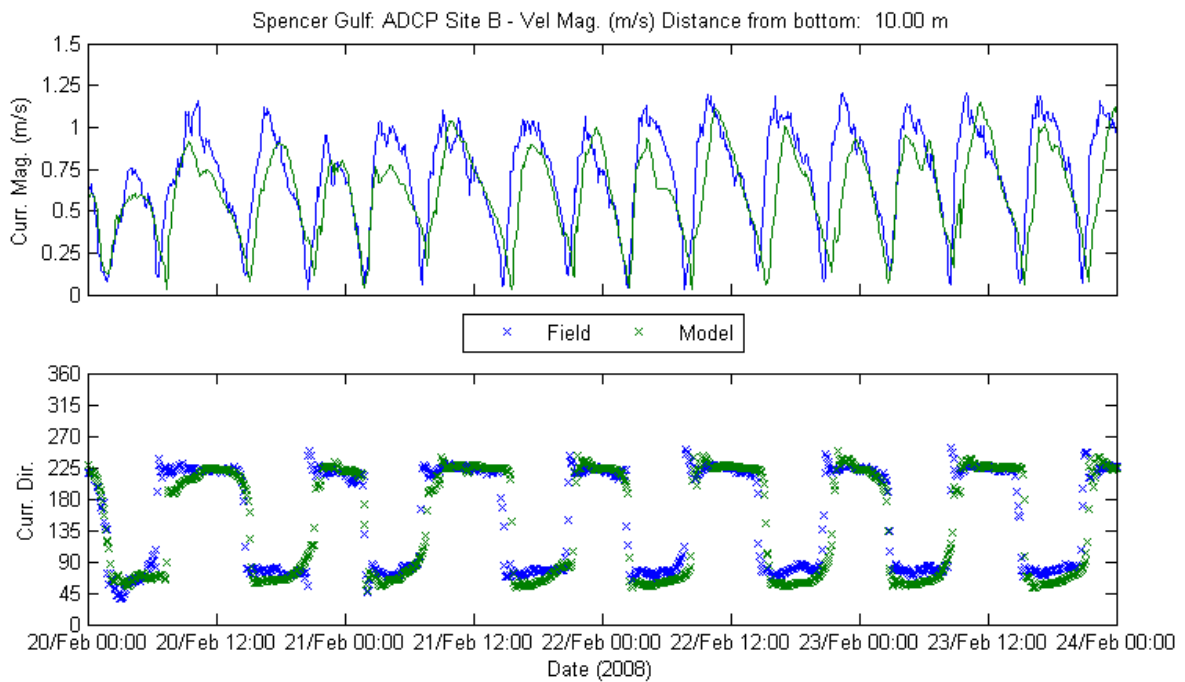
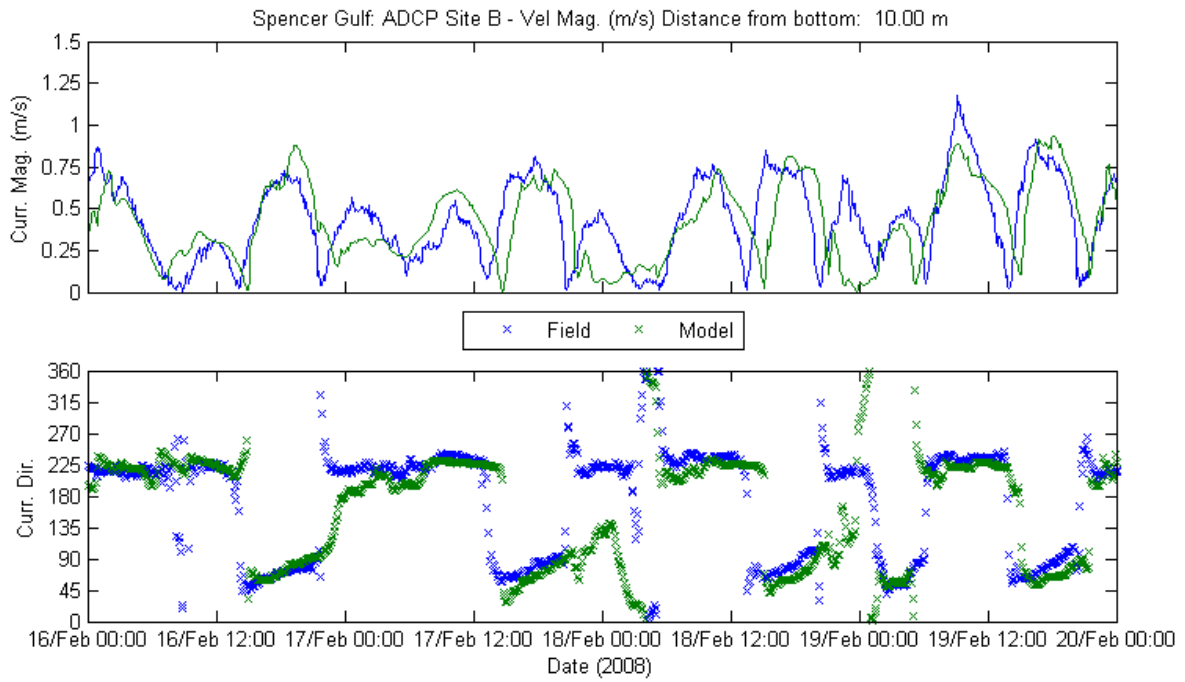




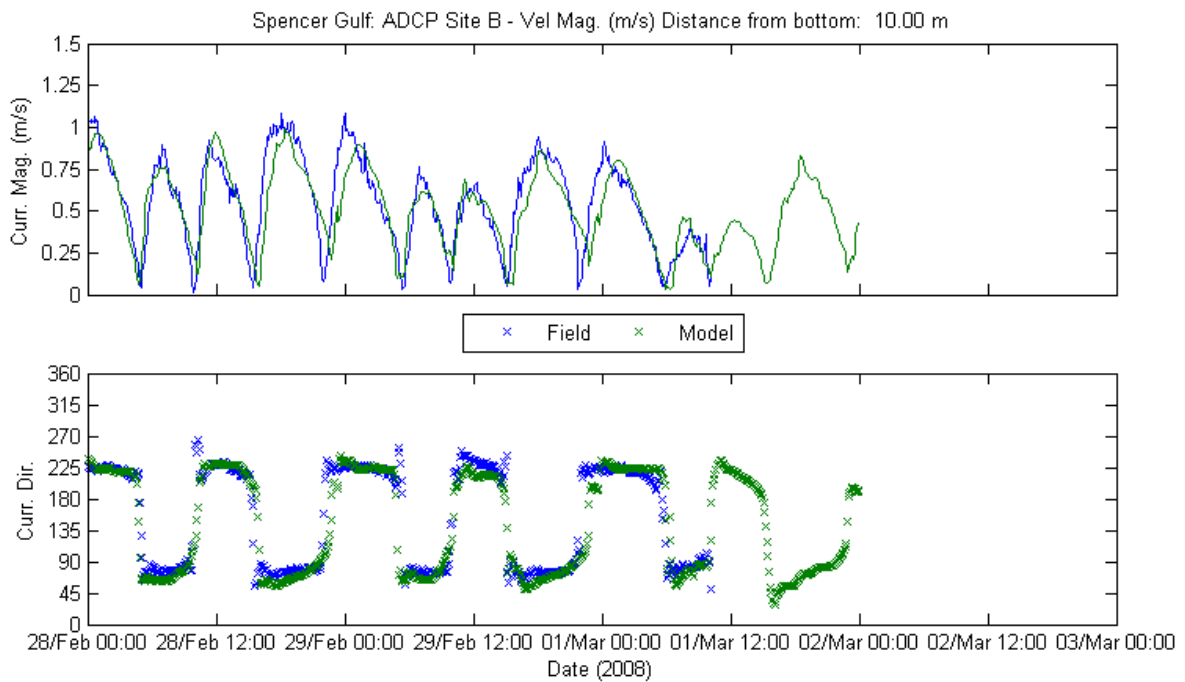
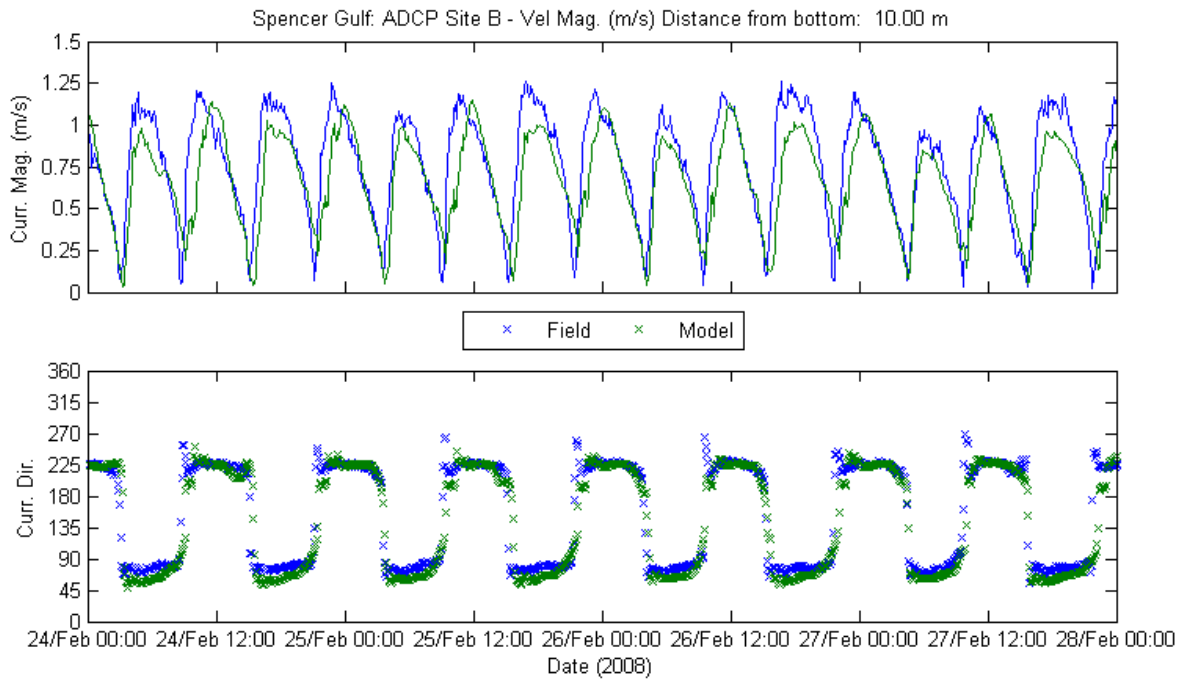




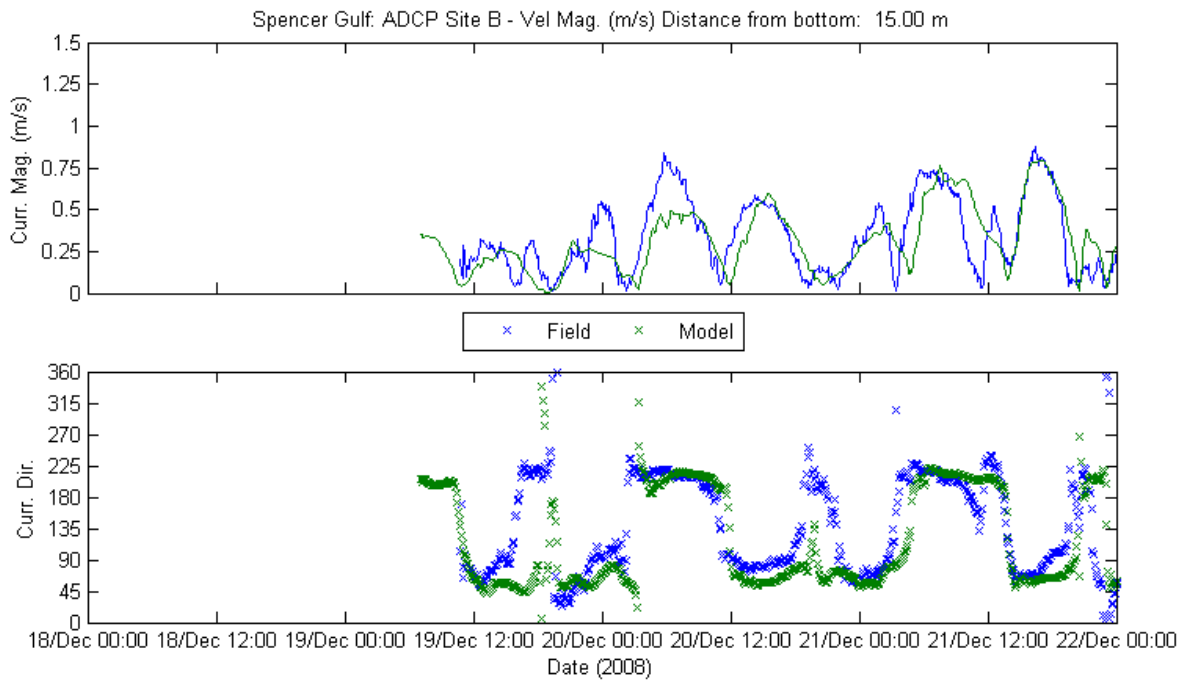
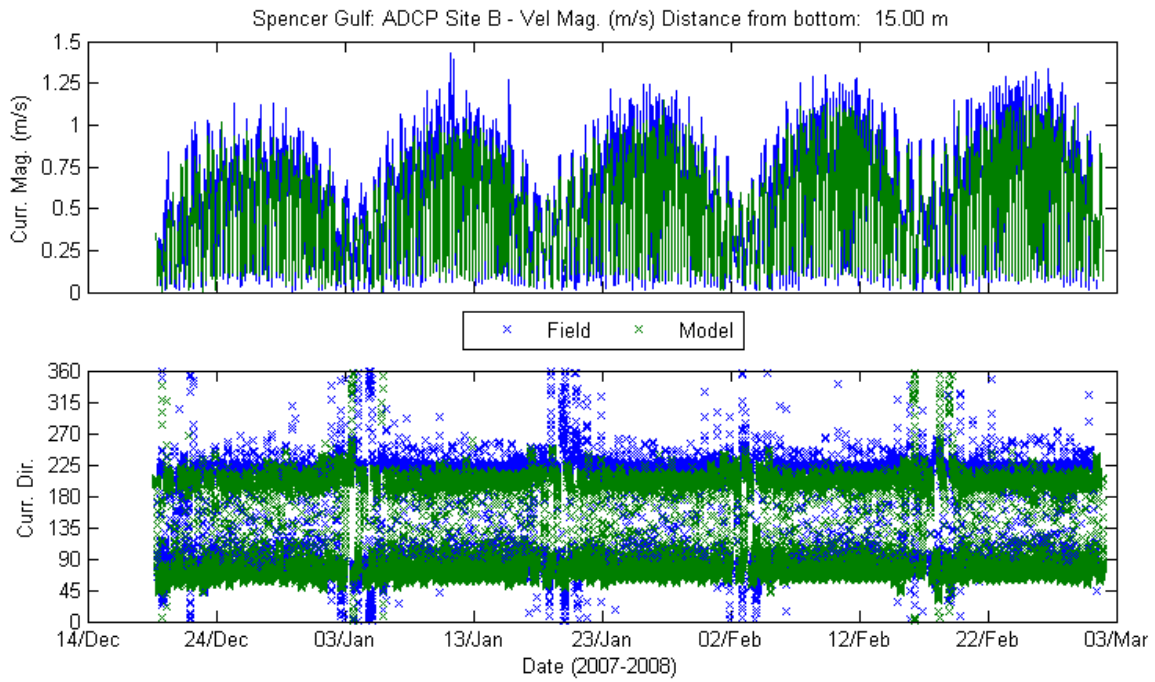


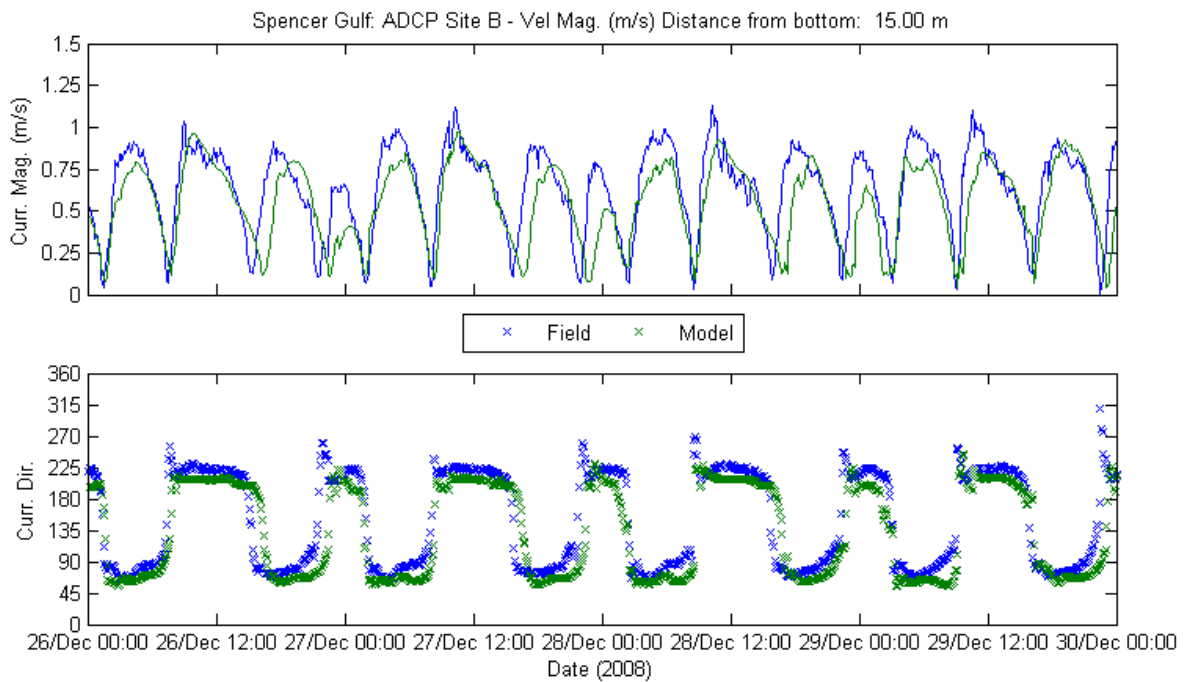
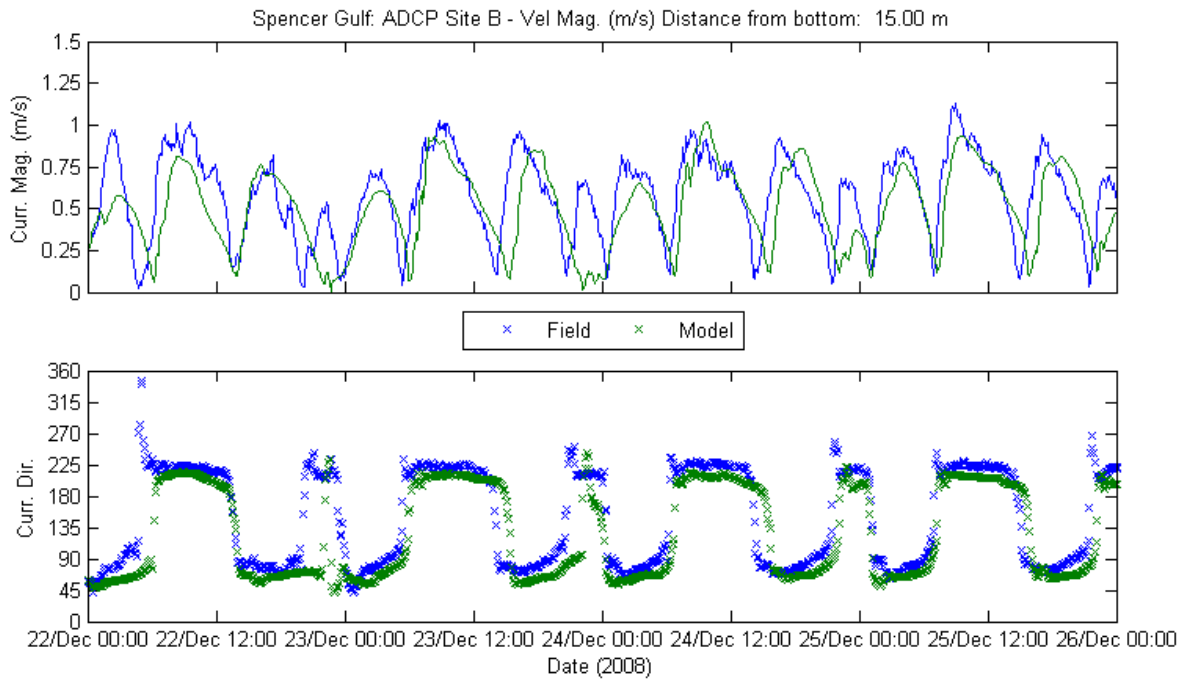


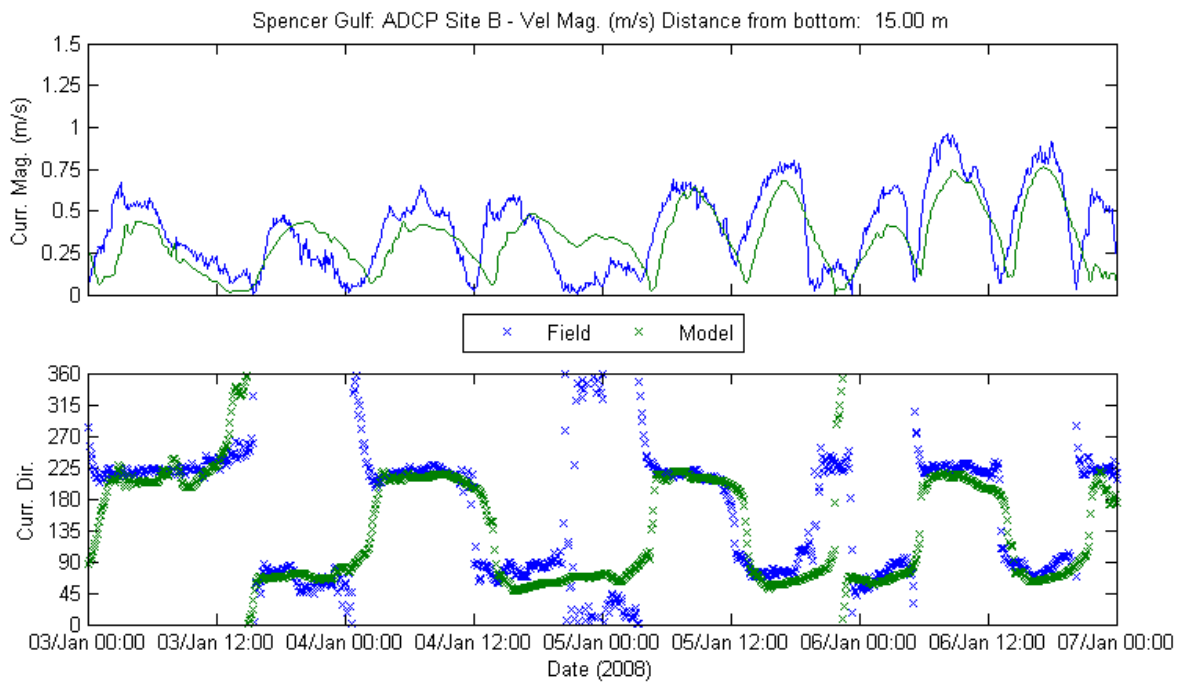
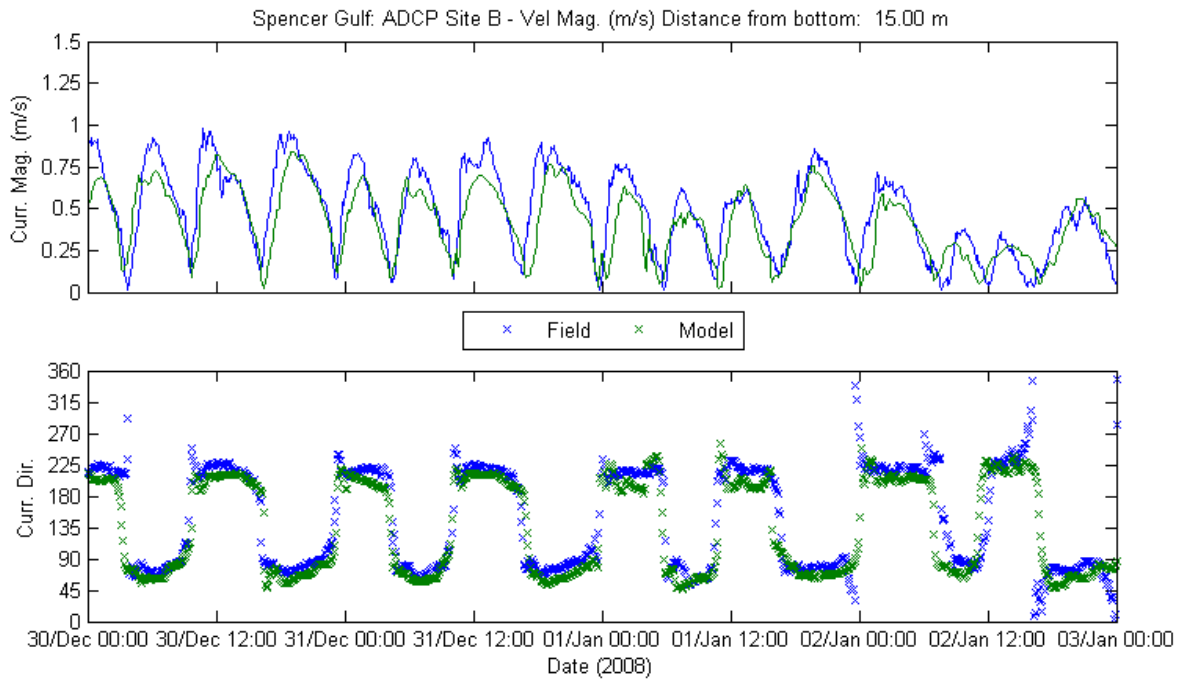


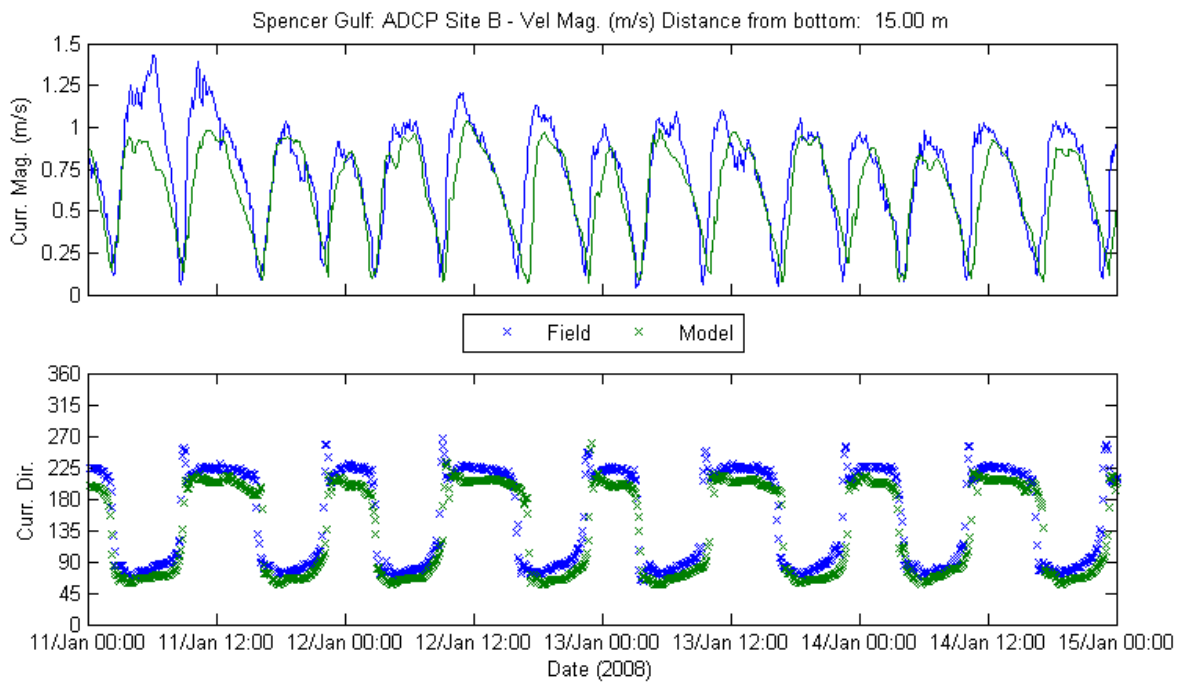
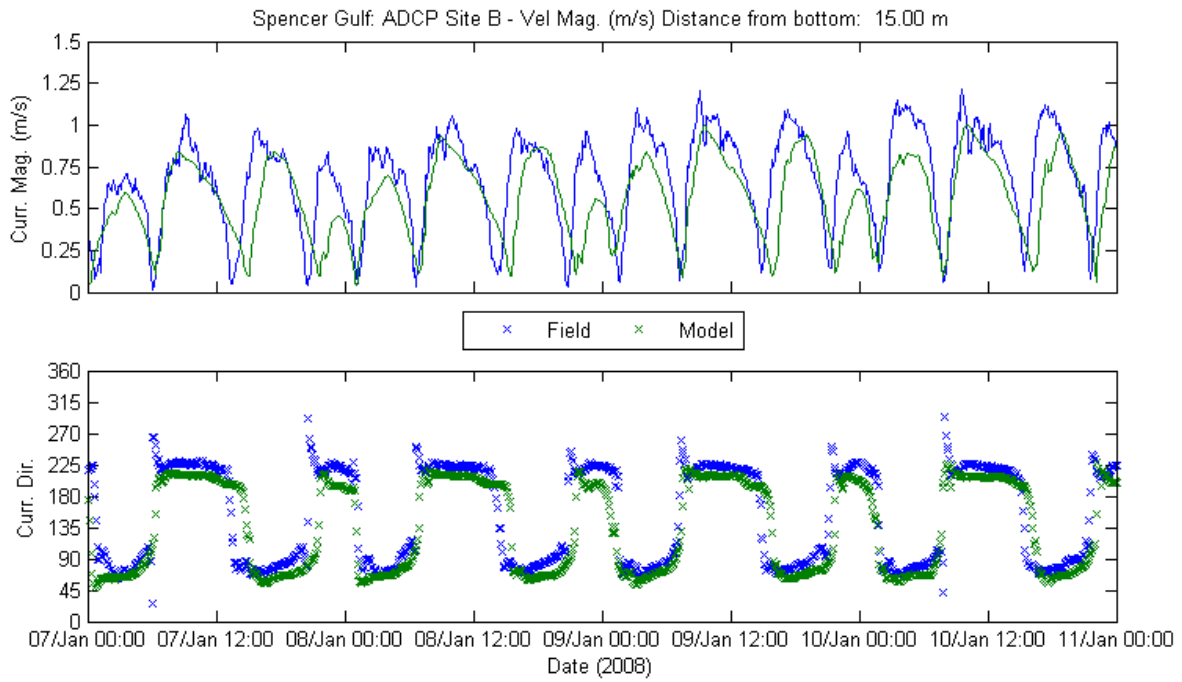


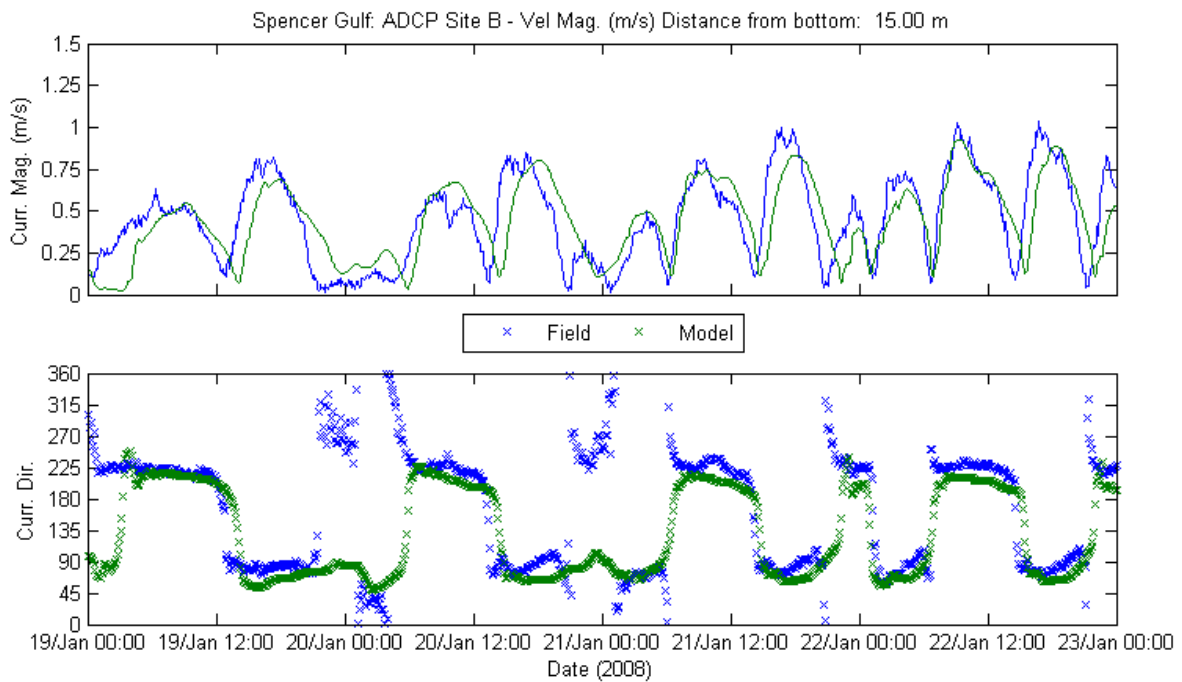
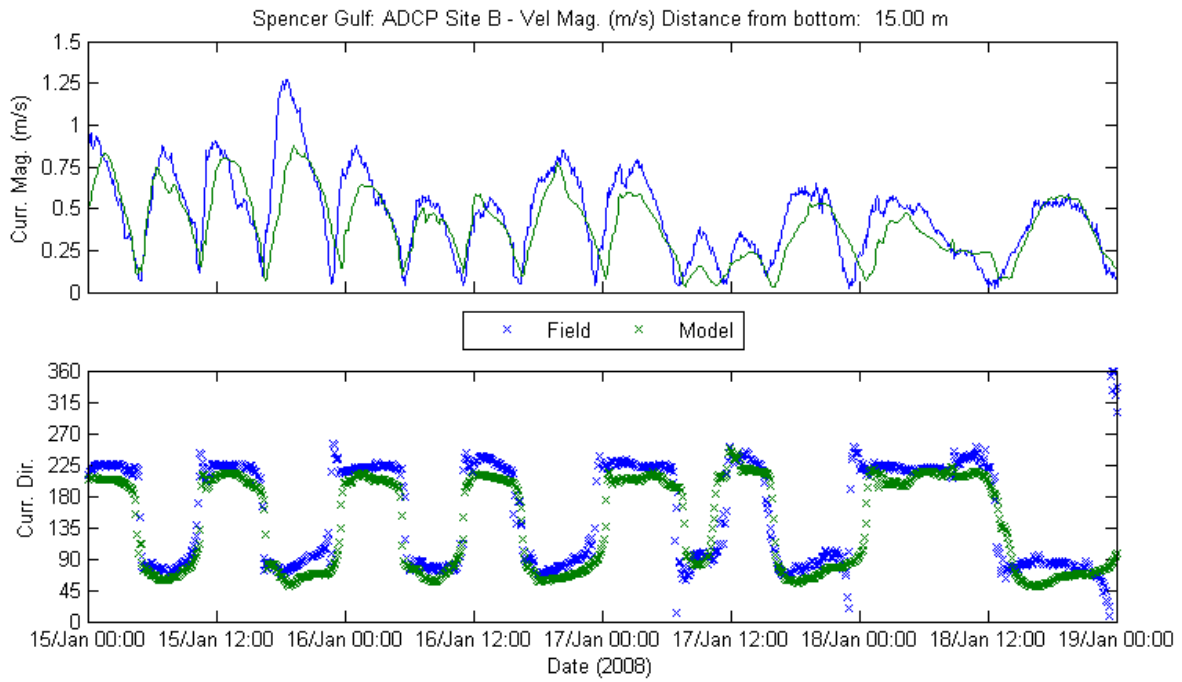
Site B at 15.00 m from Bottom

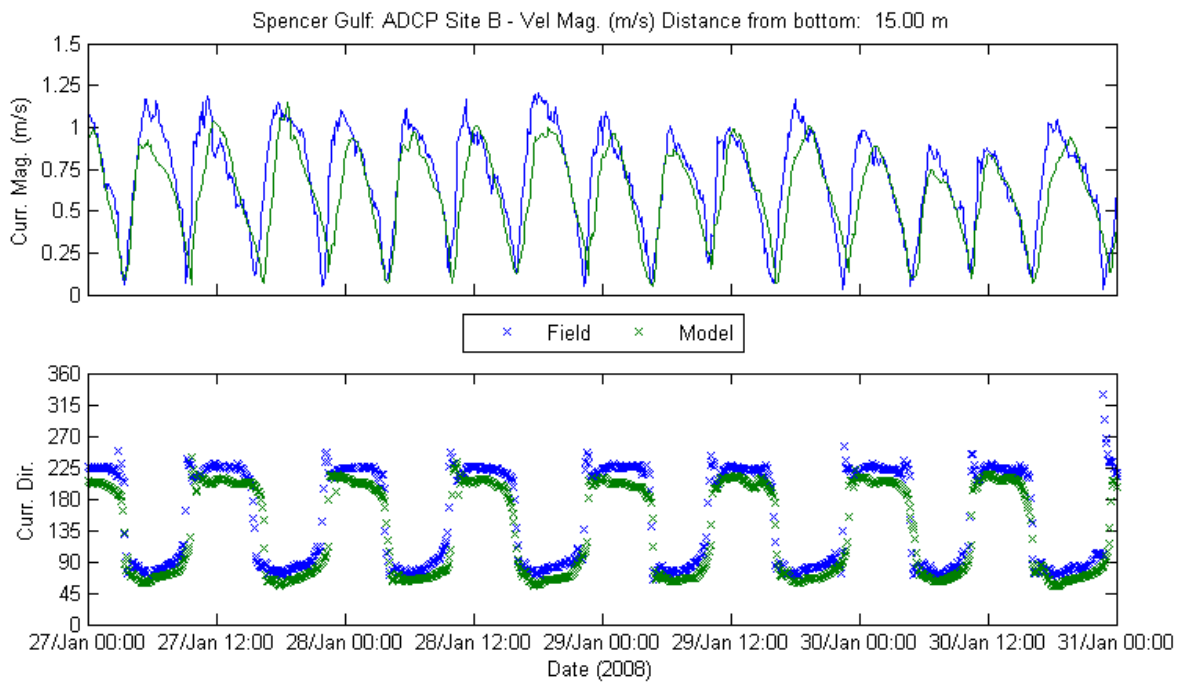
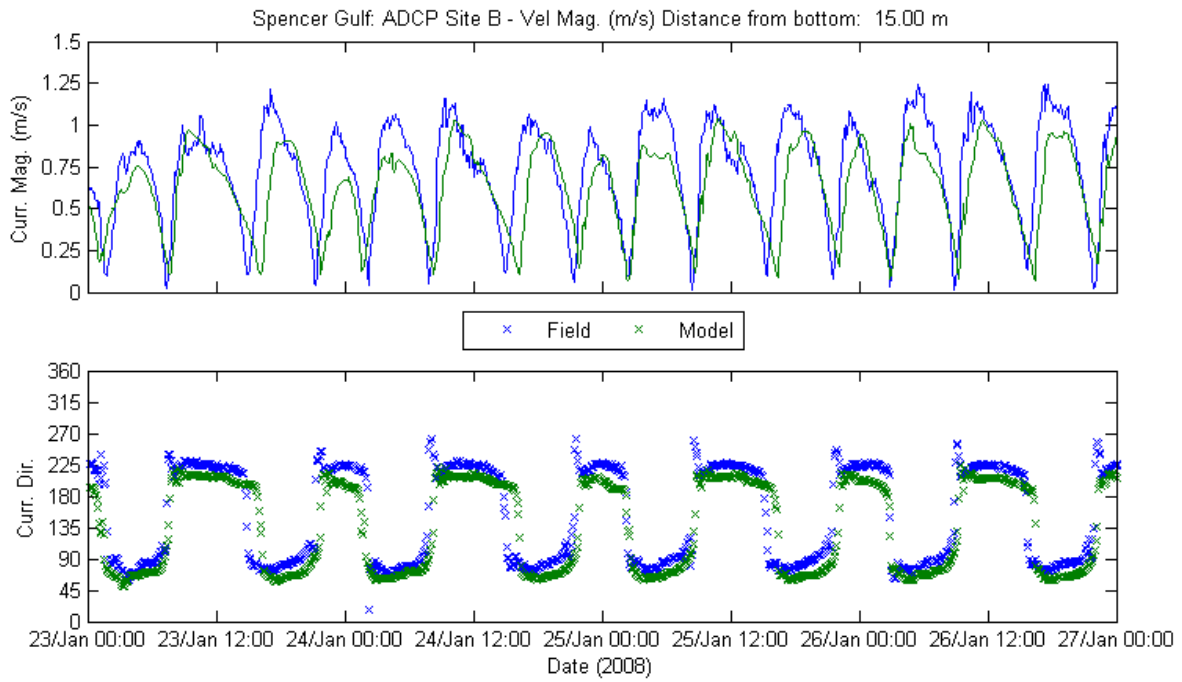


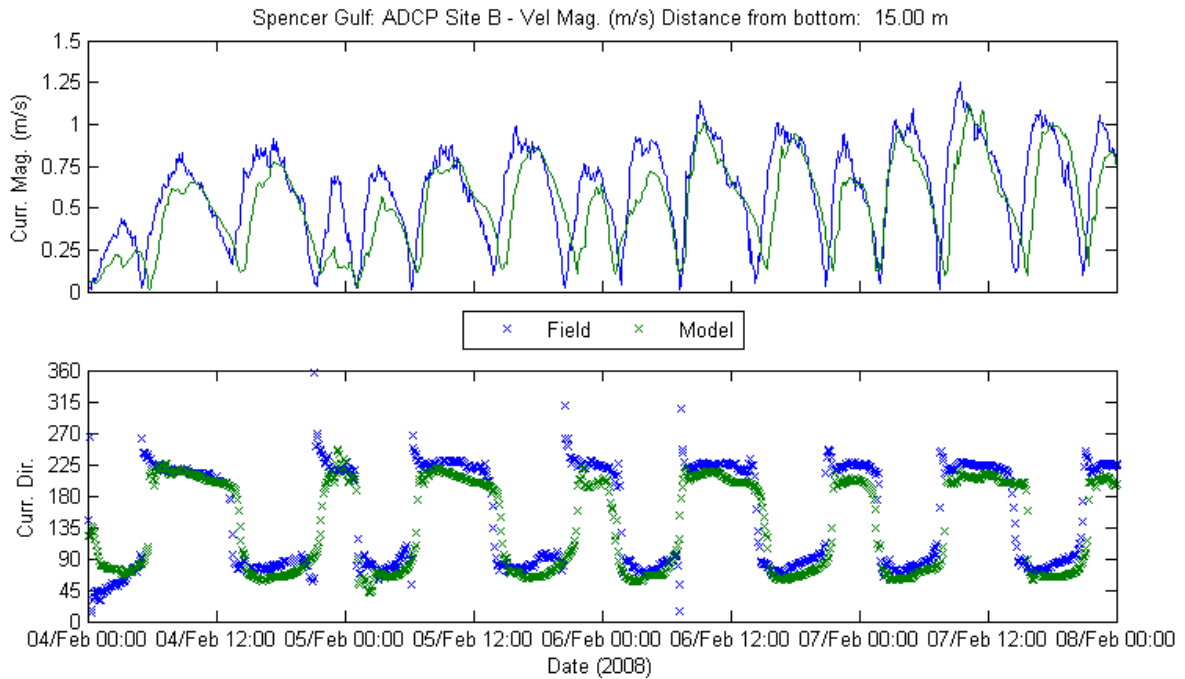
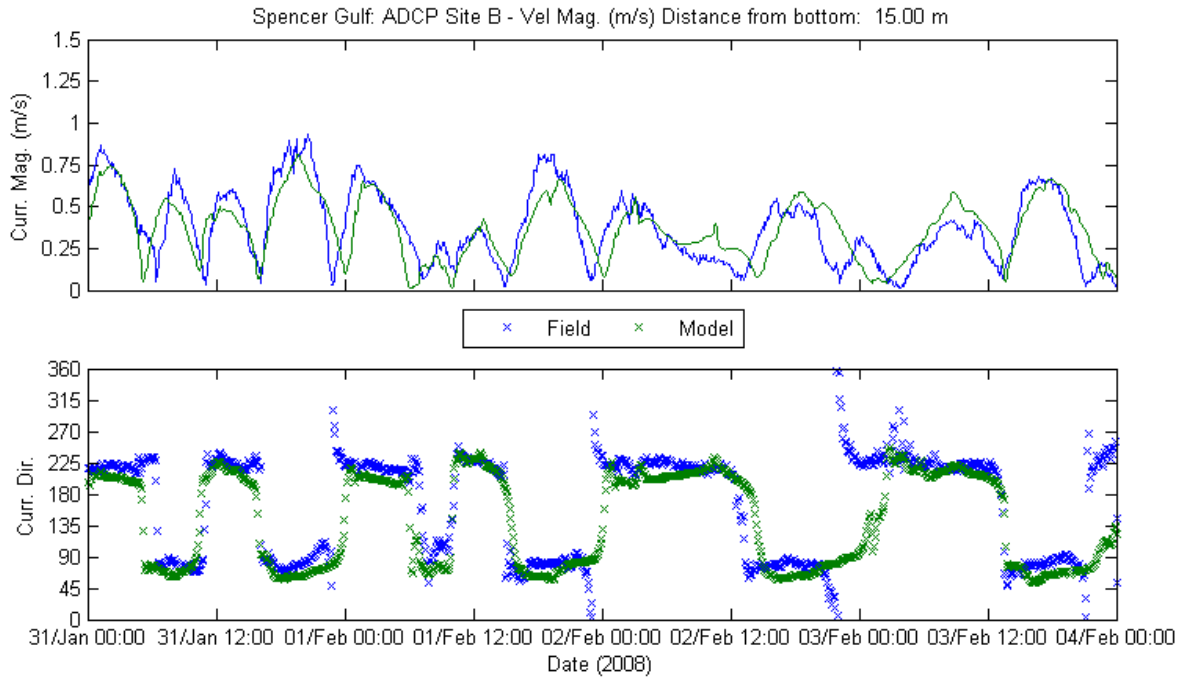




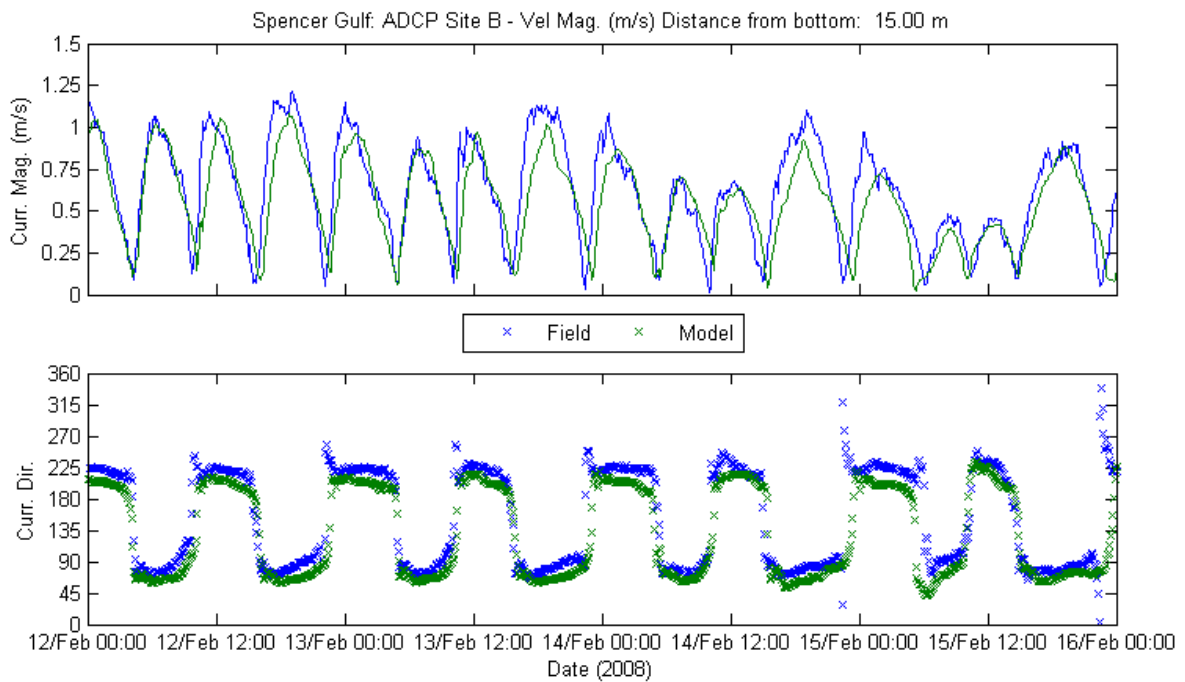
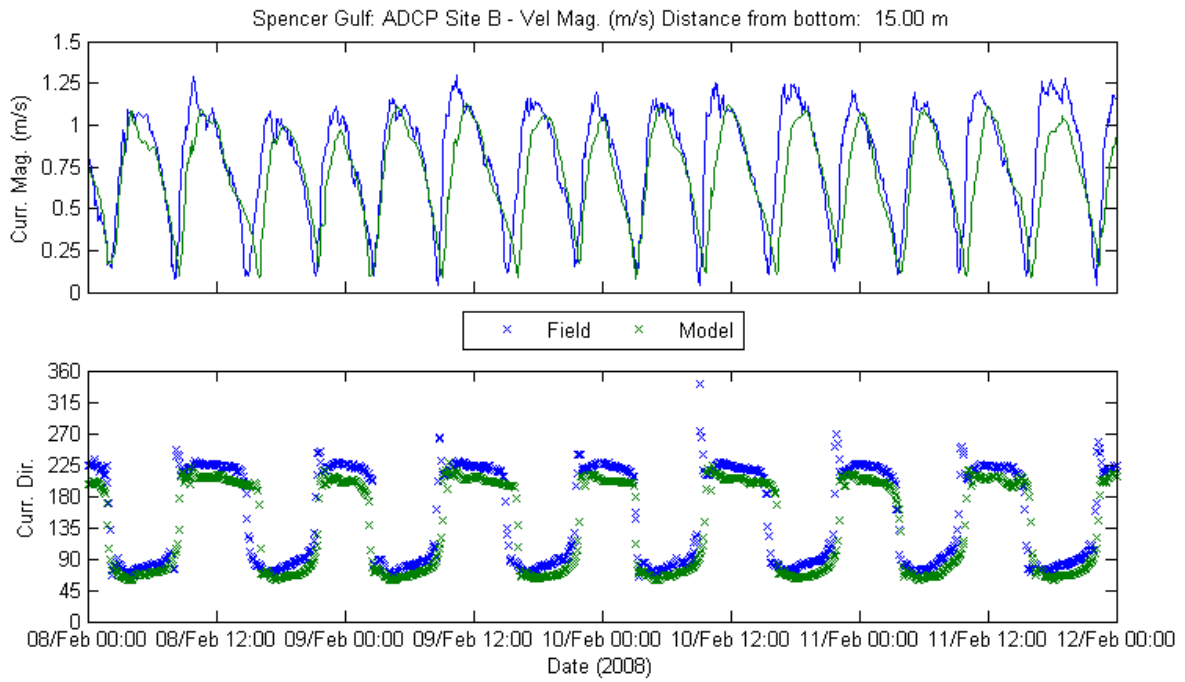


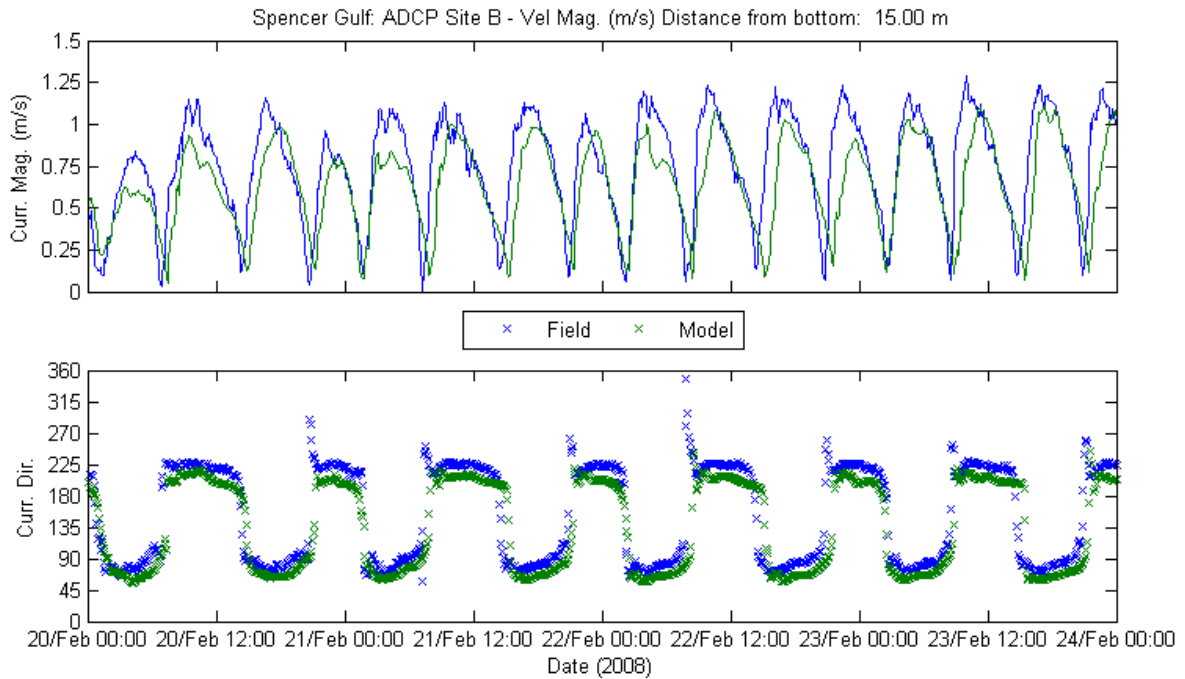
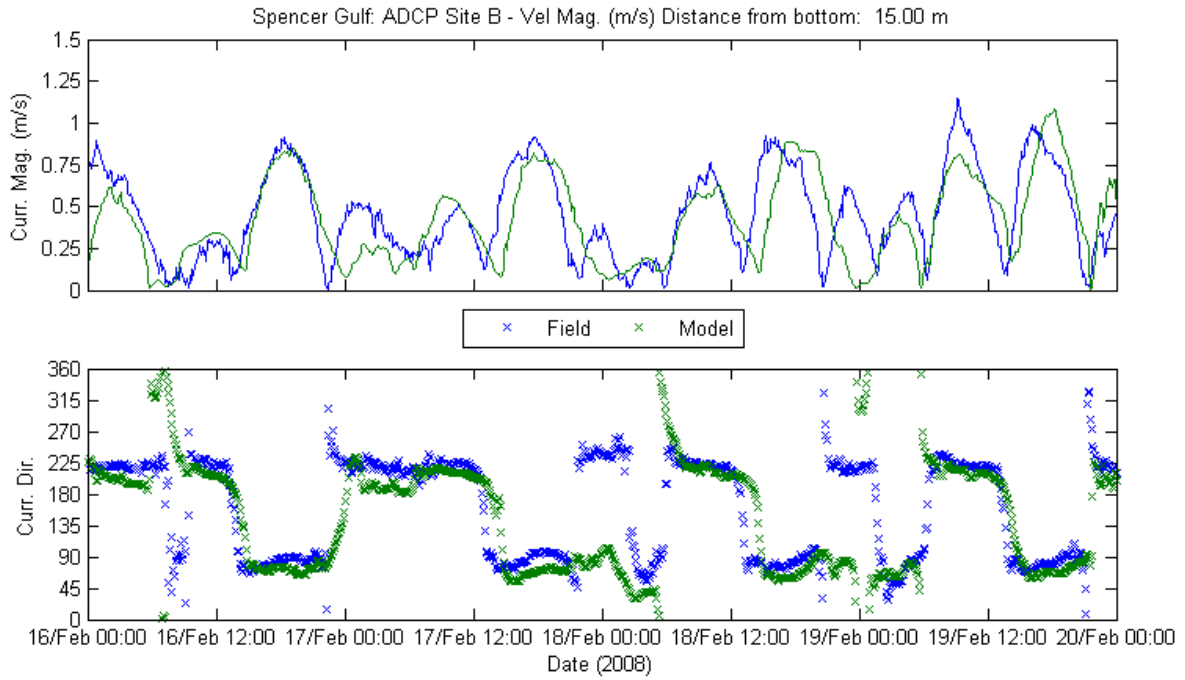


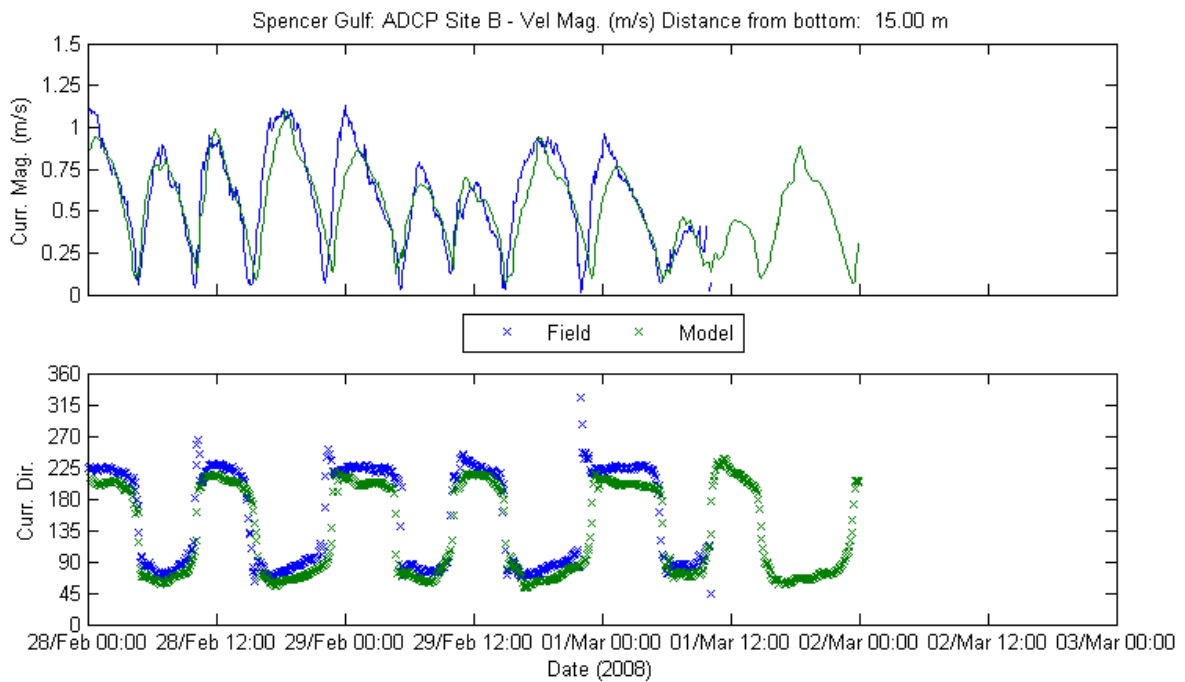
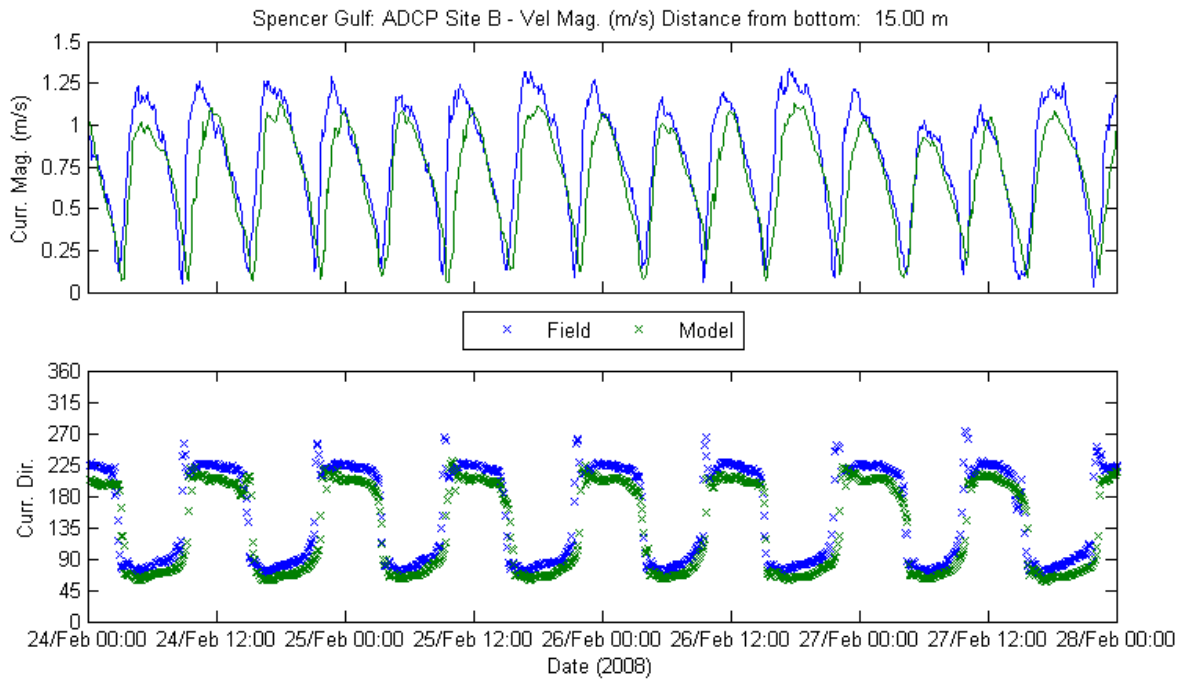




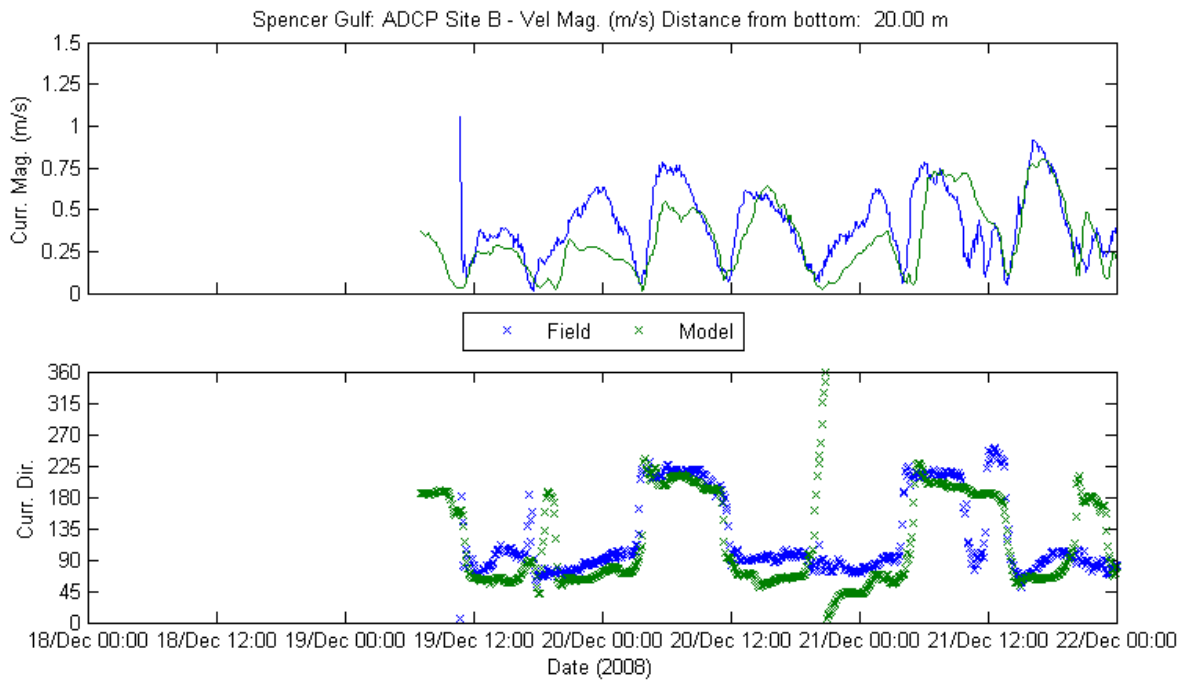
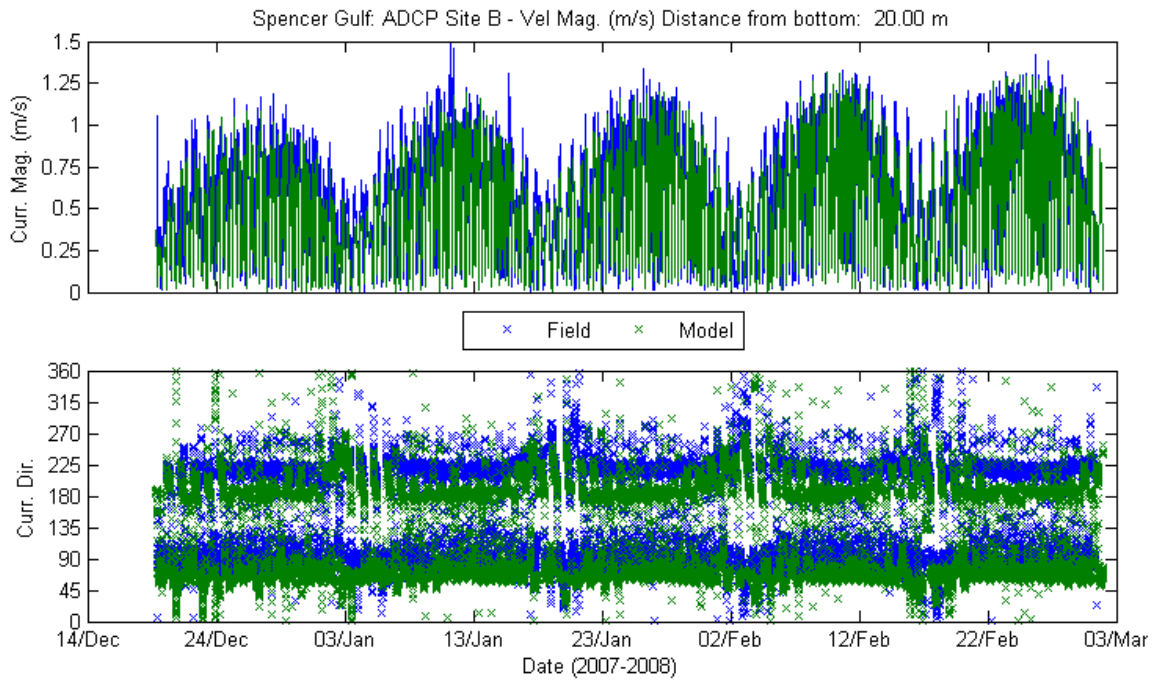


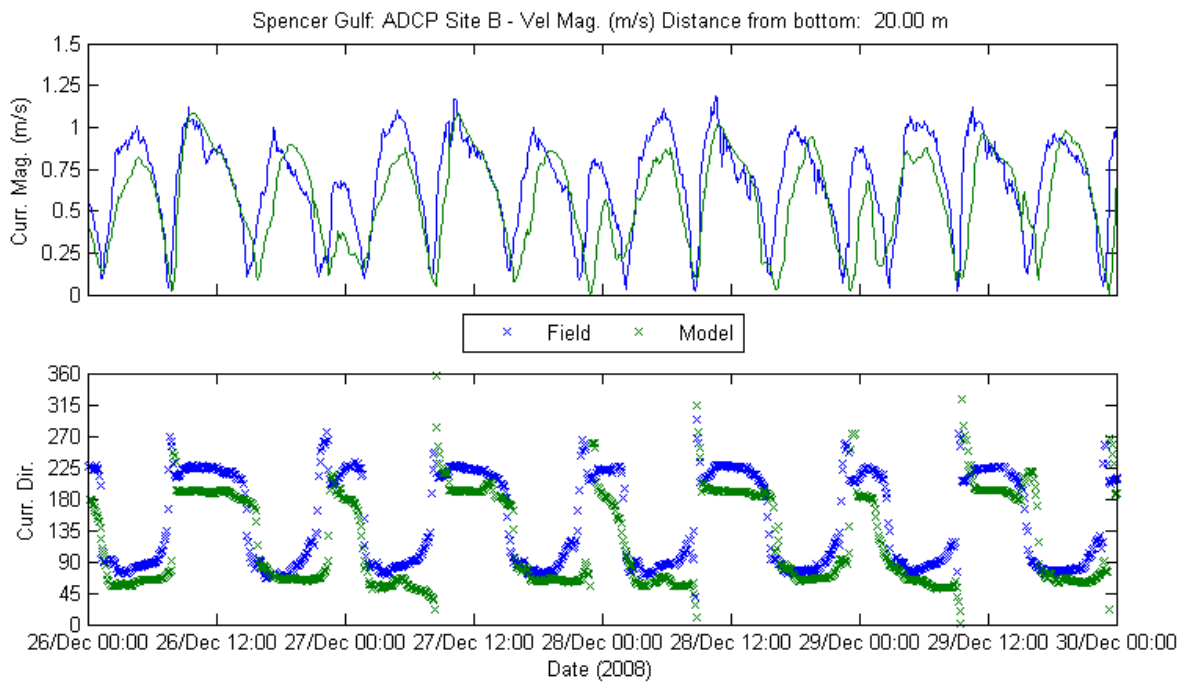
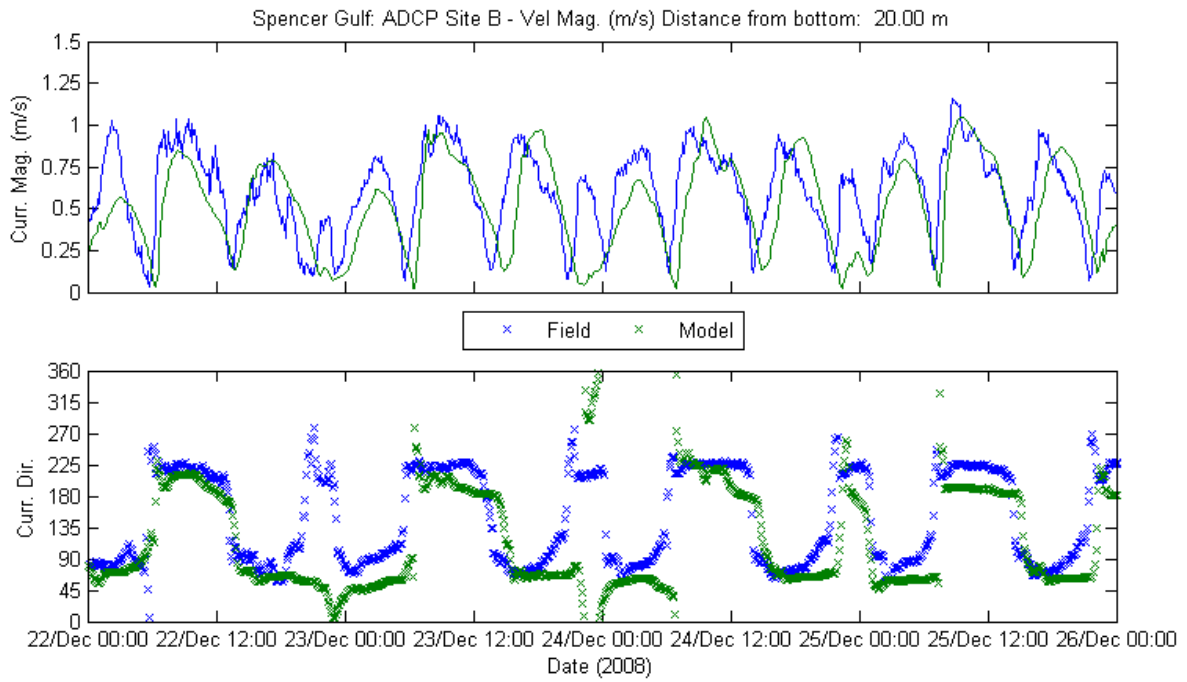


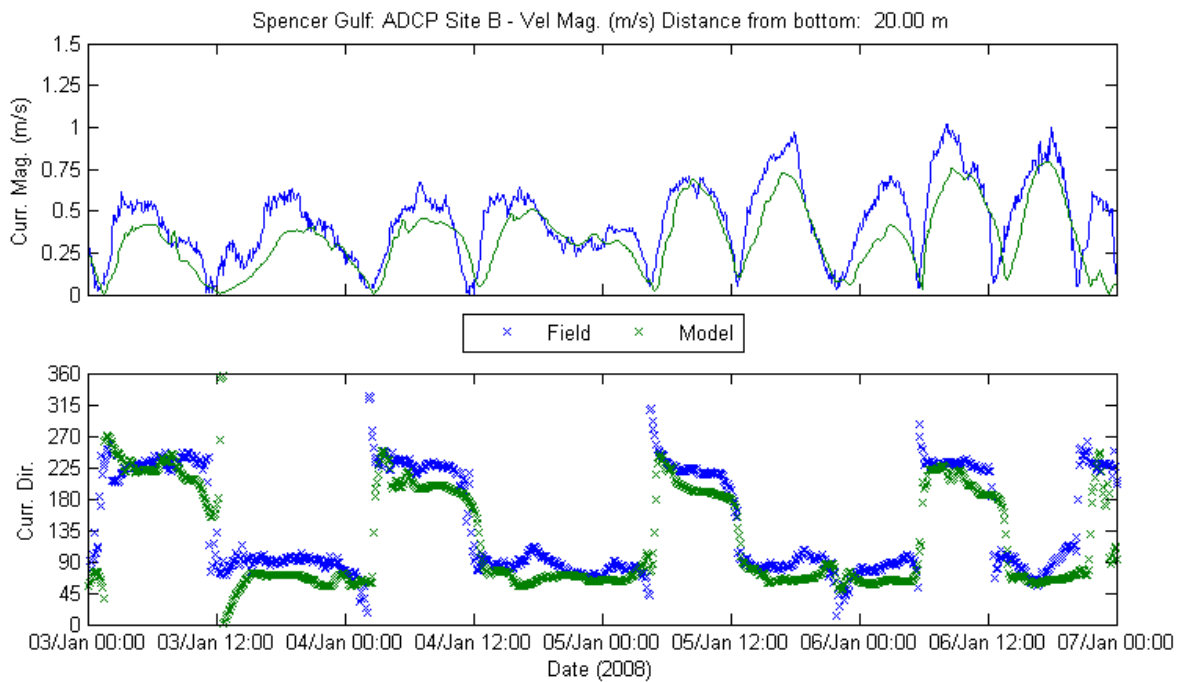
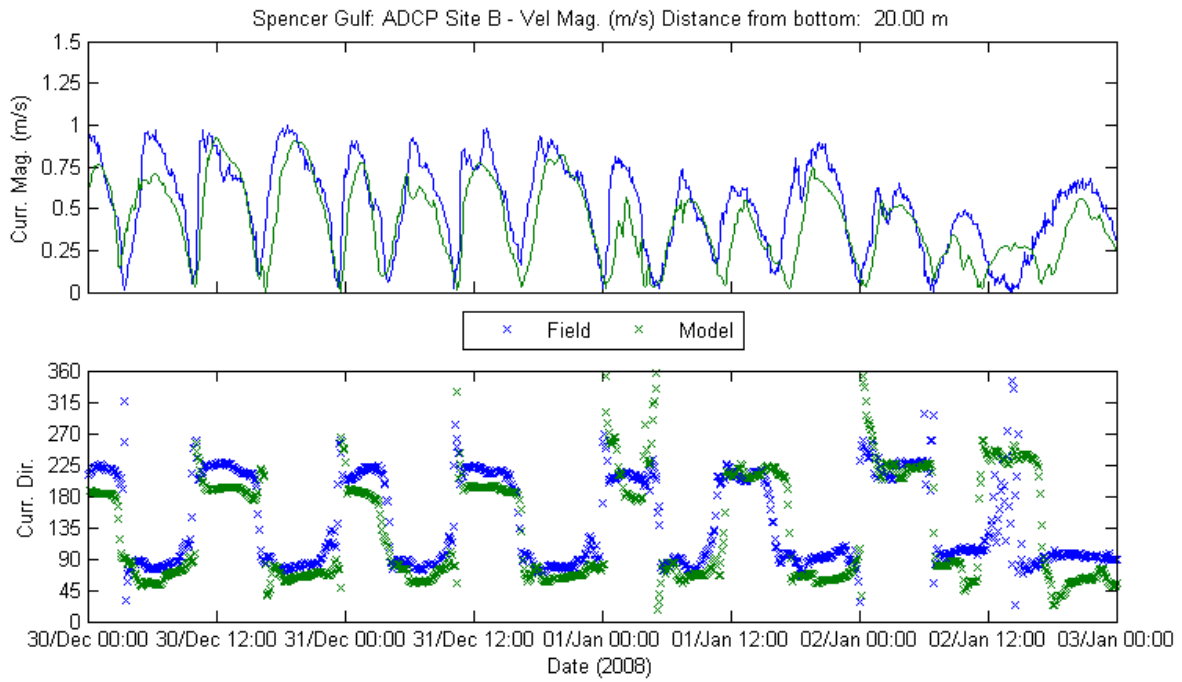


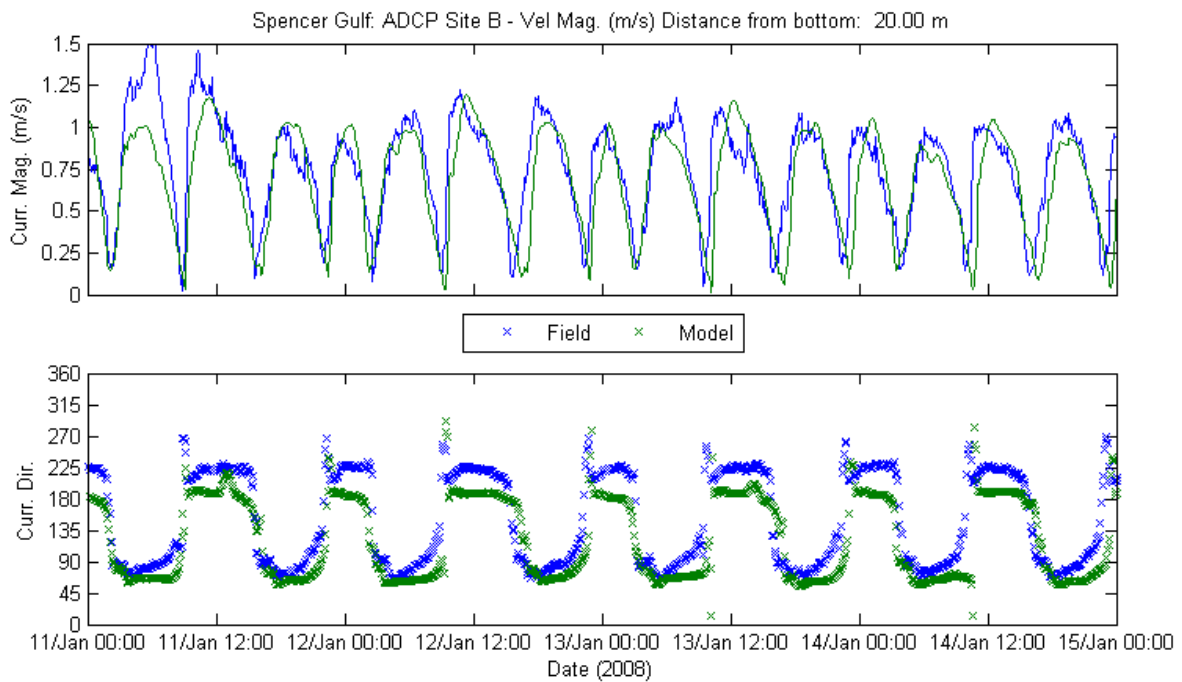
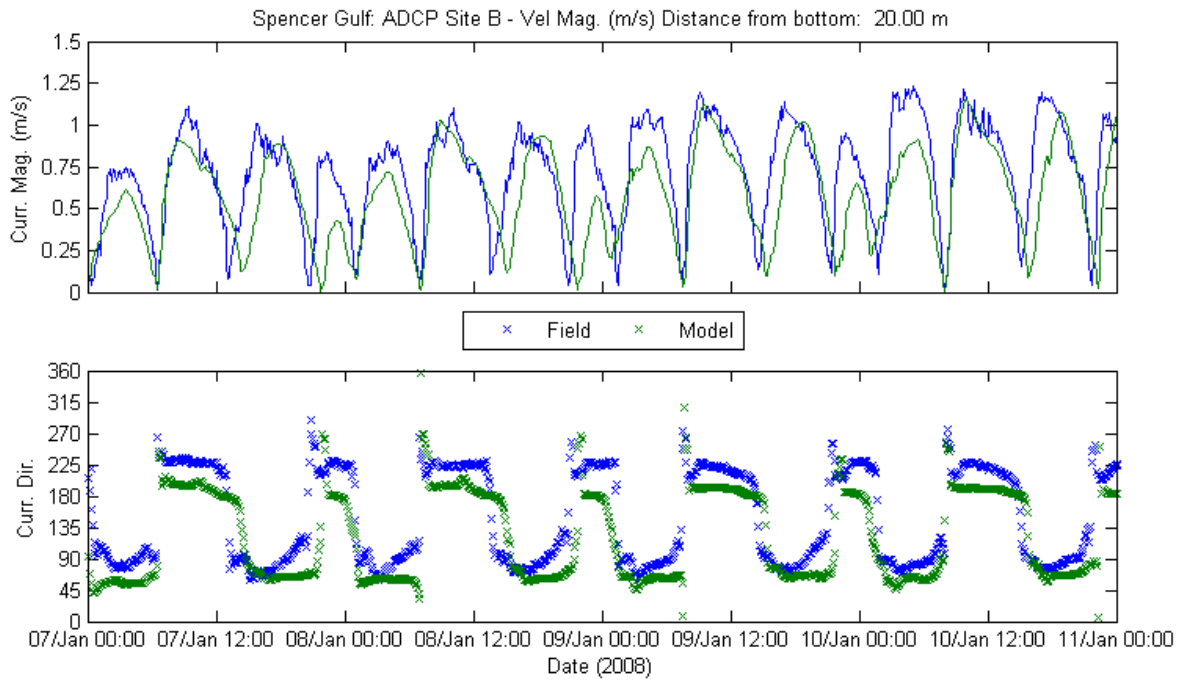


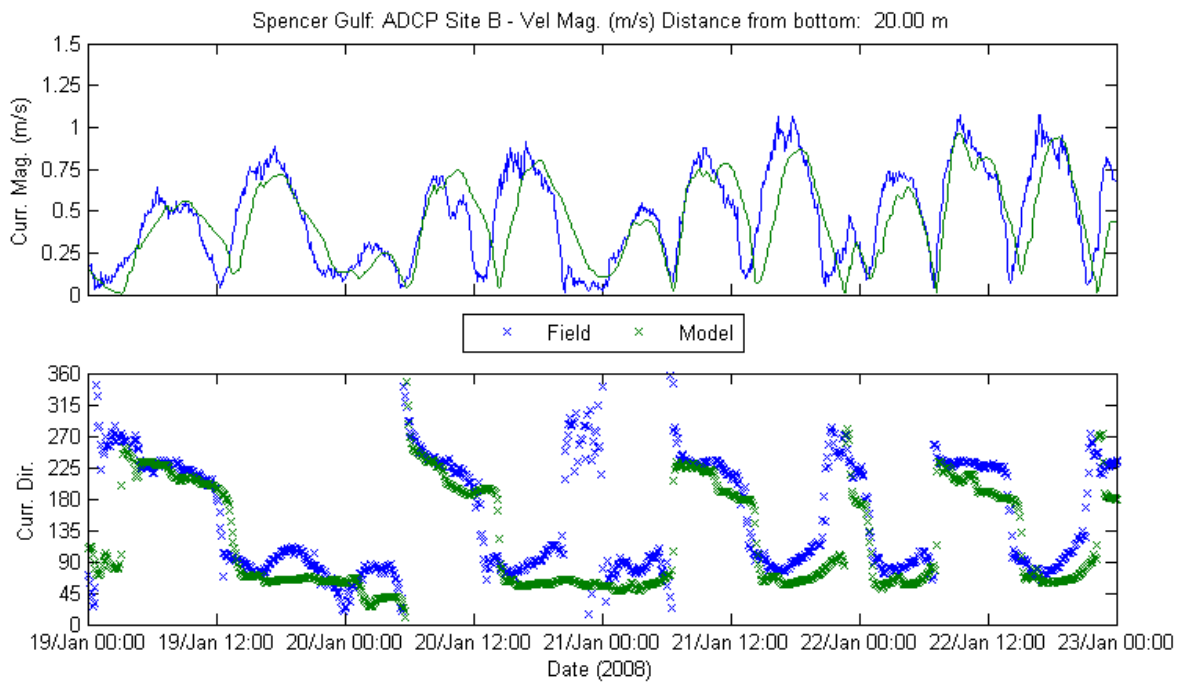
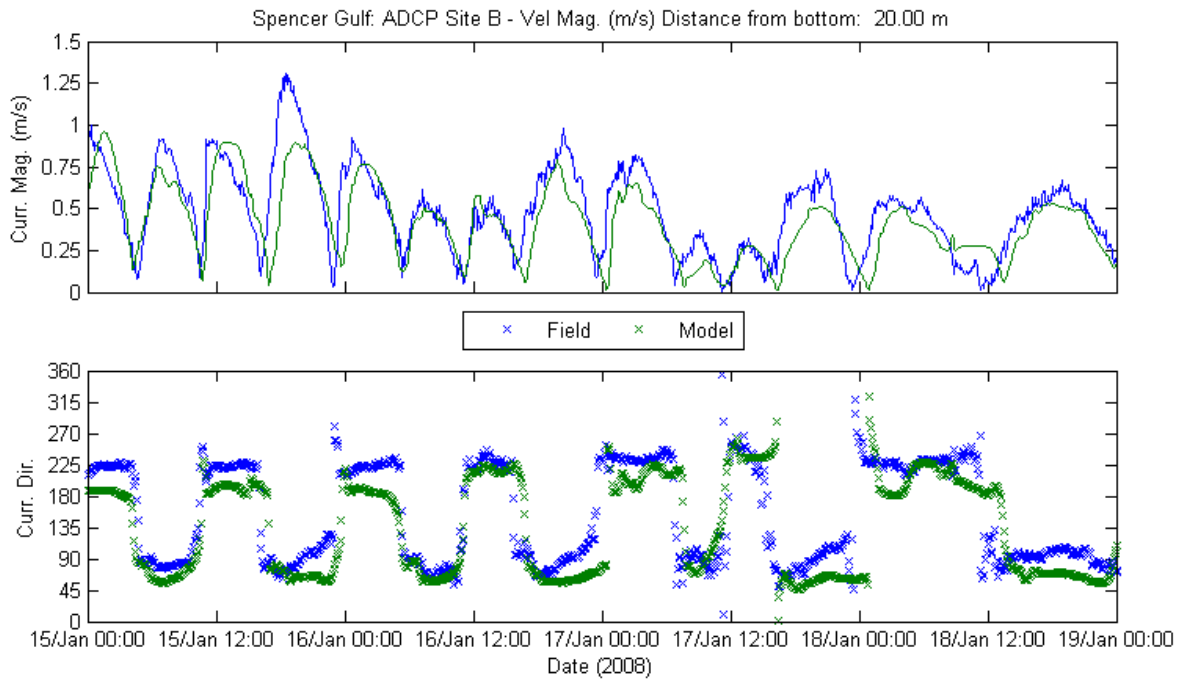
Site B at 20.00 m from Bottom



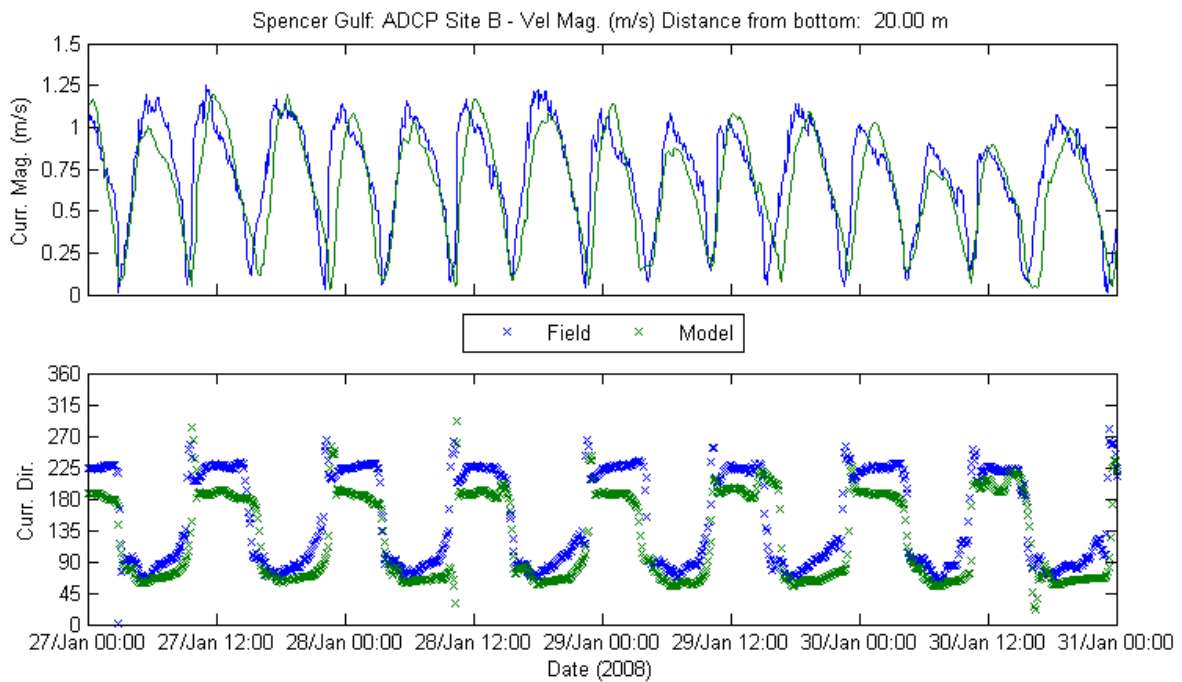
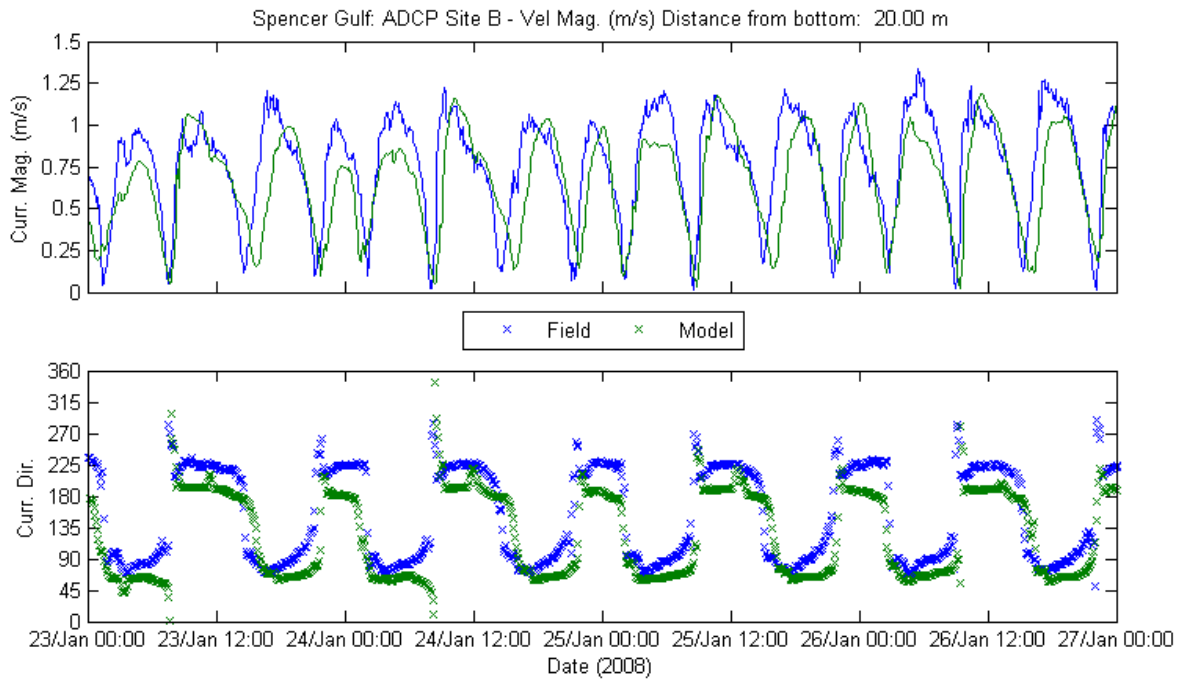


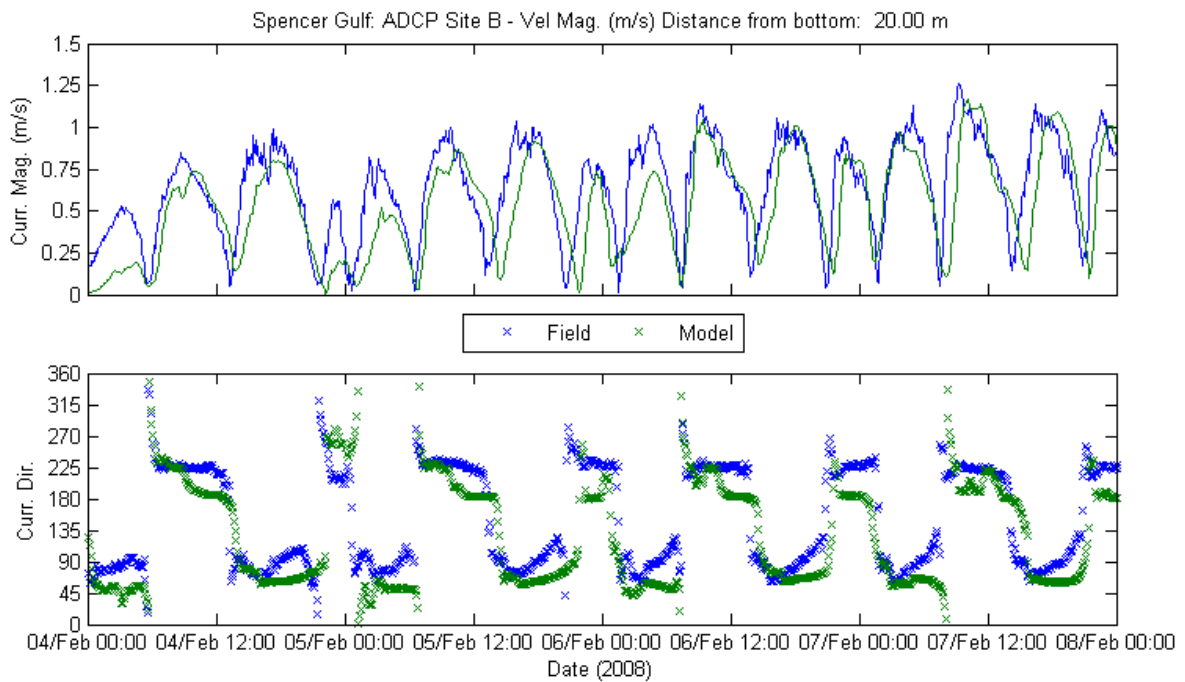
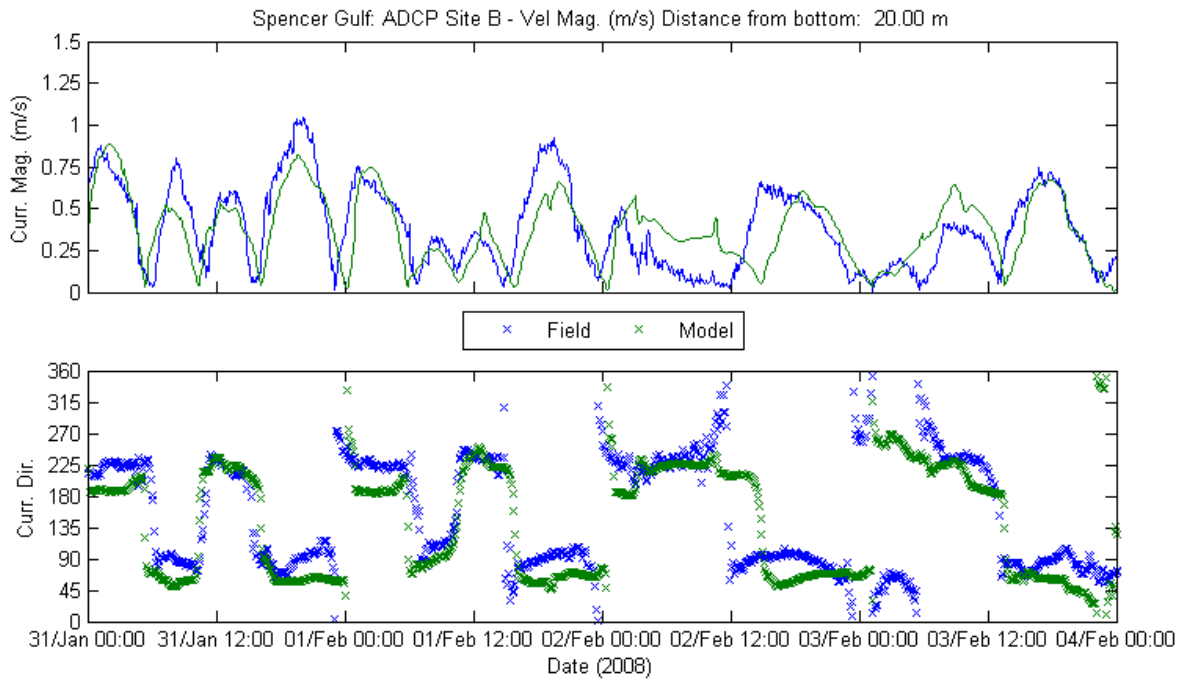


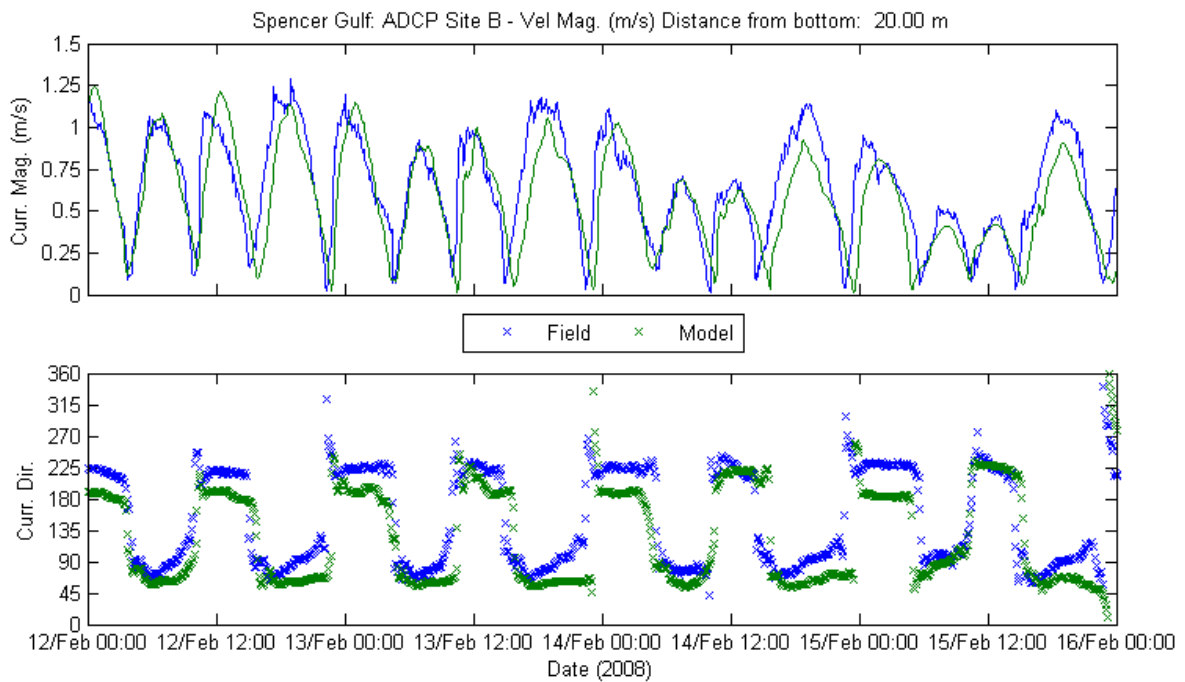
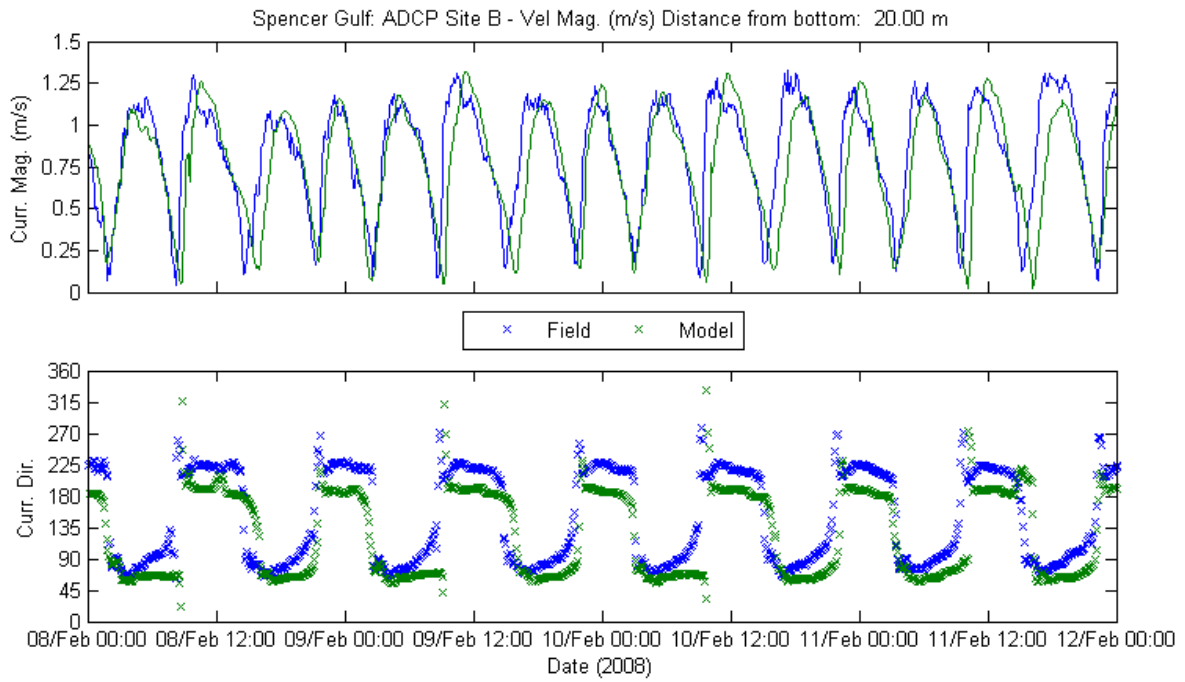


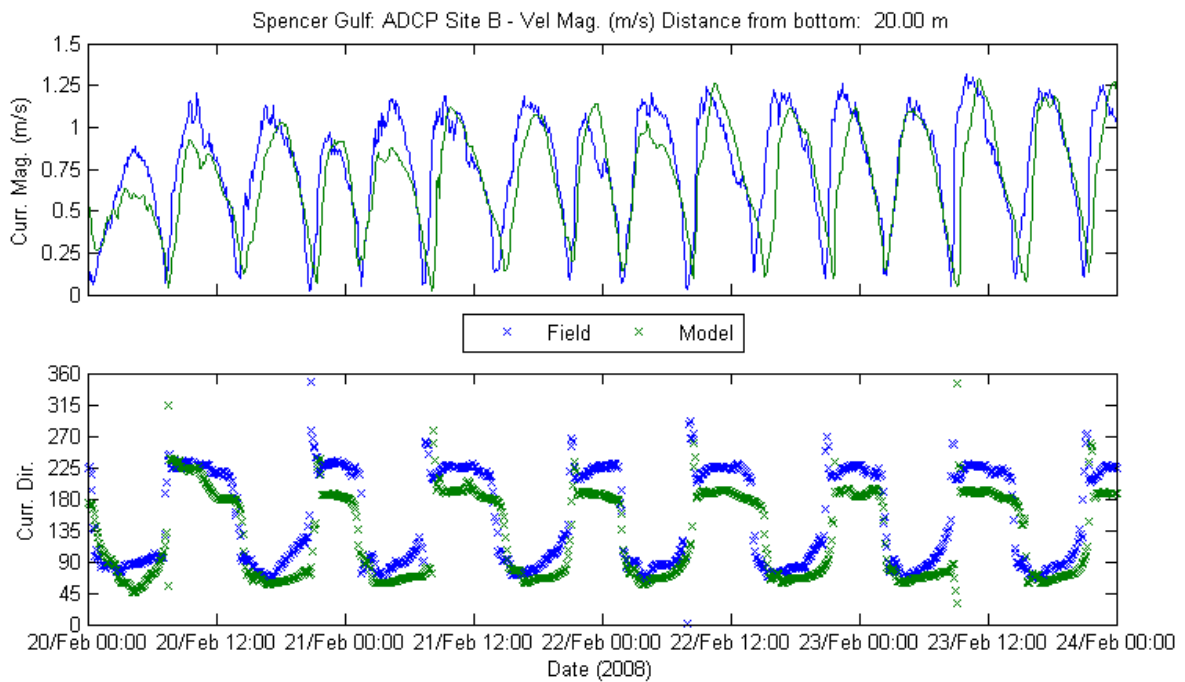
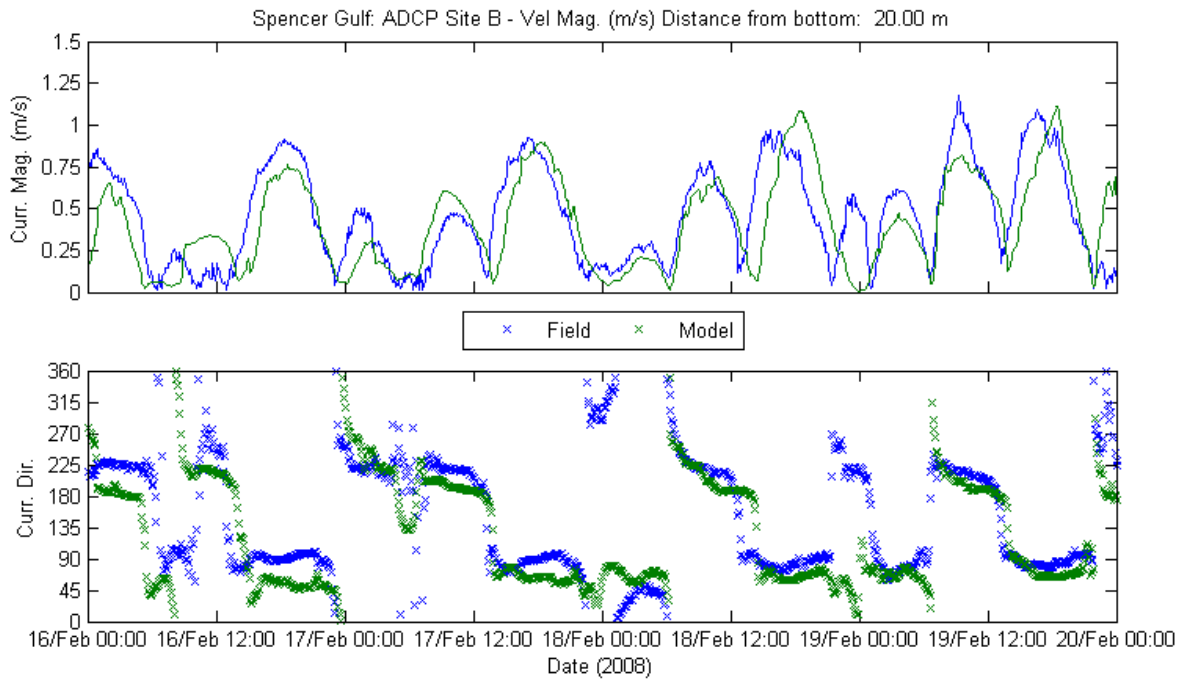


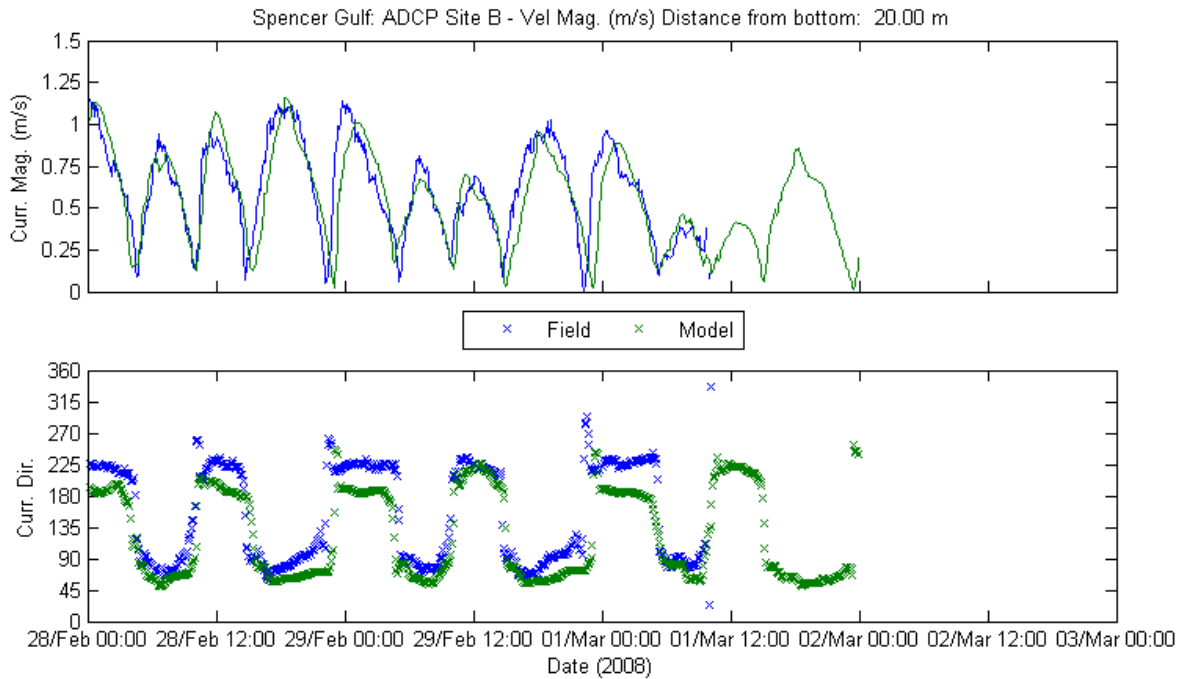
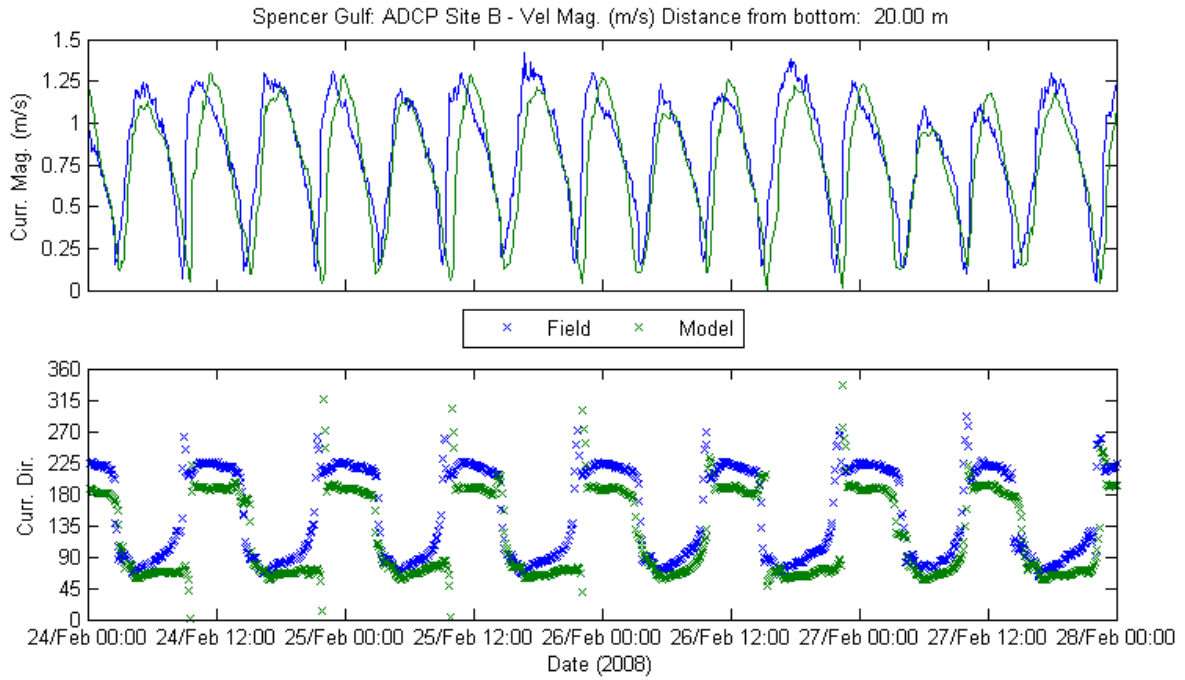












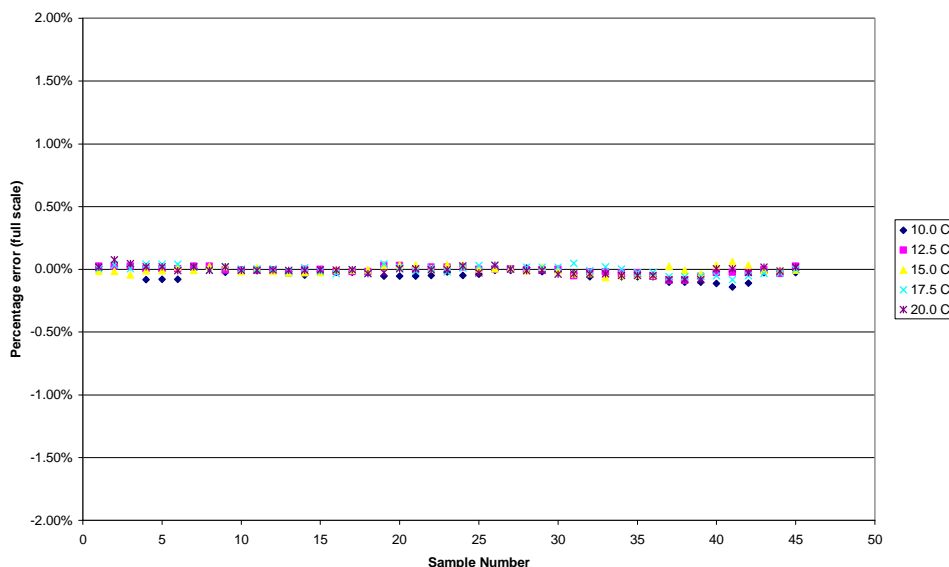
## APPENDIX H: ADDITIONAL FACTORY CTD CALIBRATION

In order to provide high quality measurements for the field deployment, all six (6) CTD sensors used were:

- Newly purchased from the manufacturer specifically for this deployment; and
- Subject to additional factory calibration with respect to conductivity prior to release to BMT WBM and subsequent deployment.

With regards to the second dot point, the manufacturer was involved in planning meetings and was well aware of the significance of the deployment. As such, the manufacturer noted (email correspondence 09/04/2009) that normal verification consists of taking 3 sensor readings at 5 temperatures (0.0, 12.5, 25.0, 37.5 and 50.0 deg C) with 9 EC points equally spaced between 0 and full scale, but that the sensors used in this study were put through extra testing to verify the calibration and sensor performance over the expected temperature and salinity range.

This extra testing consisted of 3 sensor readings at 5 temperatures (10.0, 12.5, 15.0, 17.5 and 20.0 deg C) with 14 EC points, with raw data and a calculated % full scale error assessed for each sensor. A representative conductivity timeseries plot corresponding to these additional tests (as supplied by the manufacturer) is provided below.



Sensor performance in this expanded testing was maintained well within specified tolerances, with the average error being 0.027% of full scale in this case. With assumed maximum temperature sensor error, this translates to a 0.2 to 0.3 g/L error in salinity measurements at most. This is of limited relevance for this study, however, as regular grab samples of seawater proximate to each sensor were collected and used to ground-truth and correct the CTD signals. These grab samples were sent to Flinders University for independent high accuracy salinity measurements. The maximum difference between sensor predictions and the Flinders University measurements was of this order.

---

## **APPENDIX I: THREE-MONTH VALIDATION PERIOD – LOW AND HIGH FREQUENCY ANALYSIS**



Following discussions in Adelaide (meeting between BMT WBM, SARDI, BHPB, and SA Govt.), additional analysis of model results was requested. The requested analysis included:

- 1 Production of a simulation with a longer spin-up time before the period of analysis;
- 2 Application of low-pass filter to both model and field data using a cut-off frequency lower than the tidal frequency (i.e. remove the tidal signal);
- 3 Computation of the mean correlation squared (i.e. coefficient of determination  $R^2$ ) between the low-pass filtered signals;
- 4 Subtraction of the low-frequency time series from the raw time series to obtain the high-frequency signal;
- 5 Computation of the mean correlation squared (i.e. coefficient of determination  $R^2$ ) between the high-frequency signals

Model simulations and analysis were performed as requested.

#### ***Simulations***

The simulation for which results are presented was set-up as follows:

- 1 Simulation period: 01 Nov 2008 to 09 June 2009. This is consistent with the simulation period adopted in report R.B17415.001.04 (i.e. Nov 2004 to 09 June 2005) that was used to show the model was able to reproduce the salinity high-frequency.
- 2 Initial conditions: data was specified with Dr. Rick Nunes-Vaz 1982-1983 data for the Northern Gulf and HYCOM profiles (BMT ARGOSS) for 01 Nov 2008 at the mouth of the Gulf. The data was then interpolated over the model domain. This is the same technique used throughout the model validation and assessments reports (R.B17415.001.04 and R.B17994.001.07, respectively).
- 3 Surface boundary conditions: Meteorological data (wind speed and direction, air temperature, relative humidity, solar radiation, and long wave radiation) obtained from BMT-ARGOSS WRF Model distributed over 108 boundary data sets.
- 4 Mouth boundary conditions:
  - (a) Surface elevations: combination of a BMT ARGOSS global tide model with HYCOM mean surface elevations;
  - (b) Temperature and salinity: HYCOM (BMT ARGOSS) profiles.
- 5 Other boundary conditions: Lower lakes in the head of the Gulf, and Port Augusta Power Station in the head of the Gulf.

Full details of these boundary conditions are given in the Hydrodynamic and Water Quality Modelling of Spencer Gulf: Model - Validation Report (report B17415.001.05).

Model results were output at the location of field deployments at a similar time resolution (6 minutes for both field and model) data. Locations of the instrument deployments are presented in Figure 1 below.



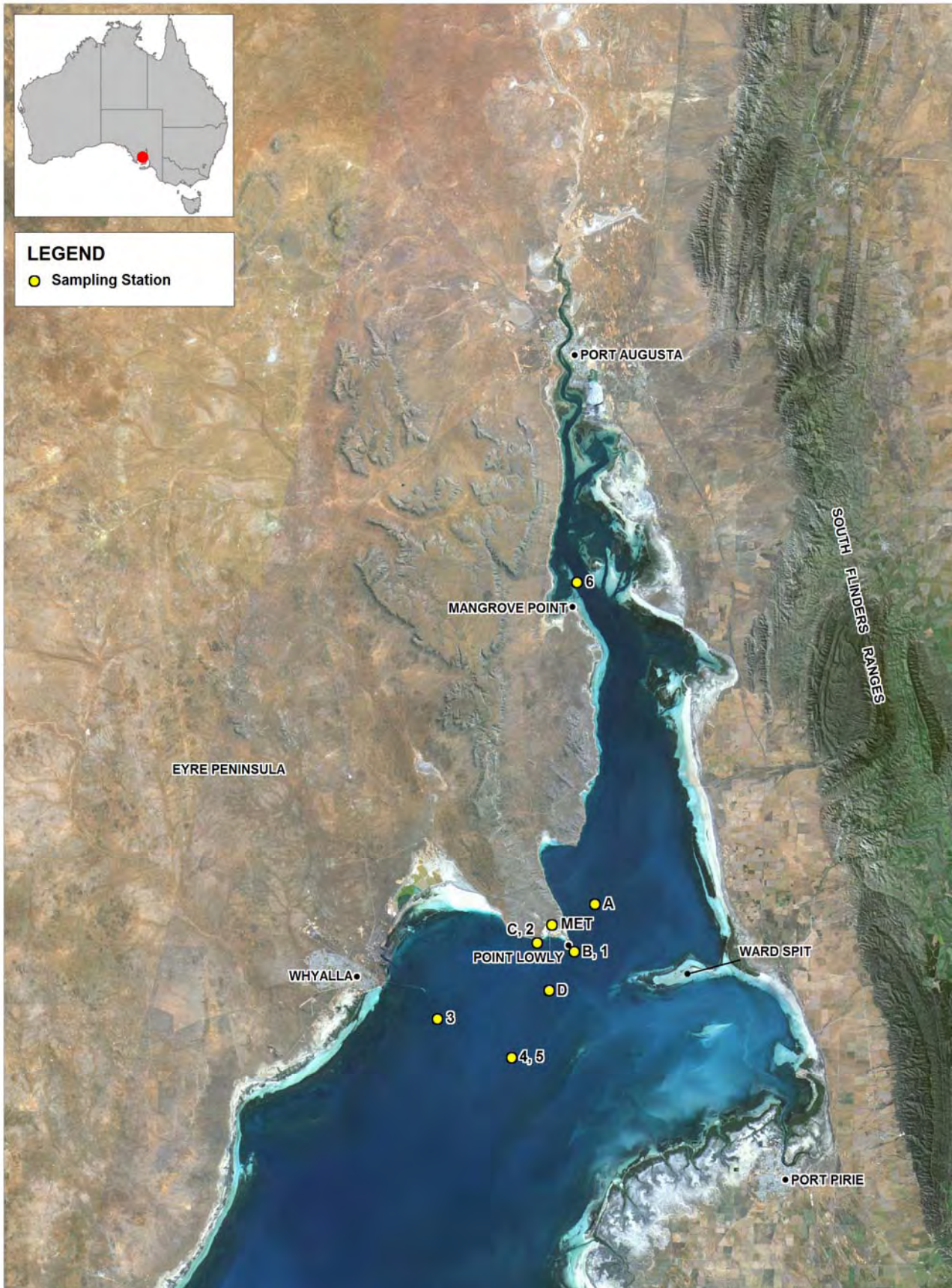


Figure 1 Location of the instrument deployments for which model comparisons are made. Numbers denote CTDs and letters denote ADCPs.

**A Note on R<sup>2</sup> as an Indicator of Model Skill****Definition**

Although R<sup>2</sup> is commonly used as an indicator of model skill, we are aware that its application to periodic signals can be misleading, as relatively small phase errors can attenuate R<sup>2</sup> significantly (see discussion in report R.B17415.001.05). Given this, we thought it would be instructive to further investigate the characteristics of R<sup>2</sup> prior to progression of comparative analyses. This investigation is summarised below.

R<sup>2</sup> is defined by the square of the covariance of a timeseries pair divided by the product of their own variances. The mathematical formula is as follows:

$$R^2 = \frac{E[(X - E(X))(Y - E(Y))]^2}{\sigma_x^2 \sigma_y^2} = \frac{E[(X - \bar{X})(Y - \bar{Y})]^2}{\sigma_x^2 \sigma_y^2} \approx \frac{\left( \sum_{i=1}^n (X_i - \bar{X})(Y_i - \bar{Y}) \right)^2}{\sum_{i=1}^n (X_i - \bar{X})^2 \sum_{i=1}^n (Y_i - \bar{Y})^2} \quad (1)$$

where E is the “expected” value (in this case the mean), X and Y are the time series, the bar indicates the time series means,  $\sigma^2$  is the variance of the time series, i is the sample number and n is the total number of samples.

Clearly R<sup>2</sup> varies between 0 and 1, with values closer to 1 representing a strong correlation, and values close to zero representing a weak correlation. R<sup>2</sup> is often defined as a determinant of what percentage of the X data variance can be explained by a linear relationship between X and Y.

**Test Cases**

To test and investigate the properties of this formulation of R<sup>2</sup> on a low pass filtered timeseries, we undertook some test case analyses, as described below.

In general terms, we can describe a time series as follows:

$$X = \bar{X} + X_n + x_n$$

where X<sub>n</sub> is a natural variation, and x<sub>n</sub> is some noise in the data, generally attributed to measurement/model errors. In order to use this formulation to derive example data sets similar in nature to the measured and modelled low passed salinity data shown below, we assumed two data sets X and Y, with:

- $\bar{X} = \bar{Y} = 42$ ;
- $X_n = Y_n = 0$ ; and
- x<sub>n</sub> and y<sub>n</sub> to be random normally distributed values with 0.0 mean and 0.07 standard deviation.

The distributions of x<sub>n</sub> and y<sub>n</sub> were selected to provide a small noise to signal ratio. This is analogous to considering two similar sensors measuring the same (unchanging) water sample over a given length of time. It is therefore clear that both instruments would be presenting the same measurement with a small standard deviation and thus, variance. The timeseries, the scatter plot of the timeseries and associated R<sup>2</sup> are presented in Figure 2.

Although the timeseries X and Y were statistically identical, the computed R<sup>2</sup> was very small (R<sup>2</sup> = 0.06). Critically, and by inspection of equation (1) it can be seen that the reason for this low R<sup>2</sup> was not because the data sets were statistically dissimilar, but because they have very small variations in mean signal over time (i.e.  $\bar{X} + \bar{Y}$  are unchanging). Importantly for this analysis, this small temporal variance is analogous to a low pass filtered timeseries of salinity at Point Lowly, over a comparatively short (40 day) period of time.

To provide a contrasting case,  $\bar{X}$ ,  $\bar{Y}$ ,  $x_n$  and  $y_n$  were defined in the exactly same way, but  $X_n$  and  $Y_n$  assigned values different from zero. For simplicity, linear relationships were chosen:

$$X_n = -10 + 20 \frac{i}{n}$$

$$Y_n = 6 - 12 \frac{i}{n}$$

These are shown in Figure 3. Despite the fact that  $X_n$  and  $Y_n$  have different slopes and offsets, the resulting correlation, as measured by  $R^2$  is very high. In fact, the same correlation would be obtained even if  $\bar{X}$ ,  $\bar{Y}$  were different from each other, which can be easily verified in any spreadsheet program (e.g., Microsoft Excel). This is because the noise is very small compared to the temporal variation of the mean signal of each data set. Importantly, this strong temporal variance is akin to the 40 day low passed temperature measurements at Point Lowly (see below), where a clearly decreasing trend is evident as Autumn progressed.

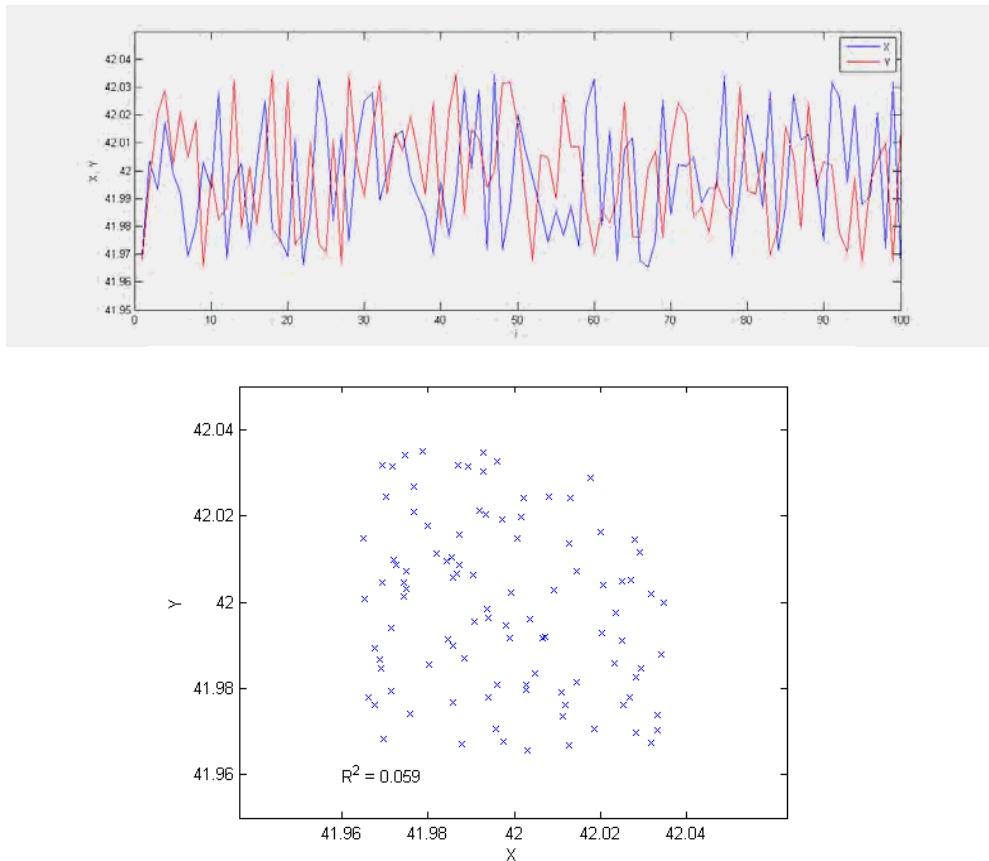


**Figure 2 Time series with same mean, null natural variability and small random sample deviations. Top: Time series X and Y. Bottom: Scatter plot of series.**

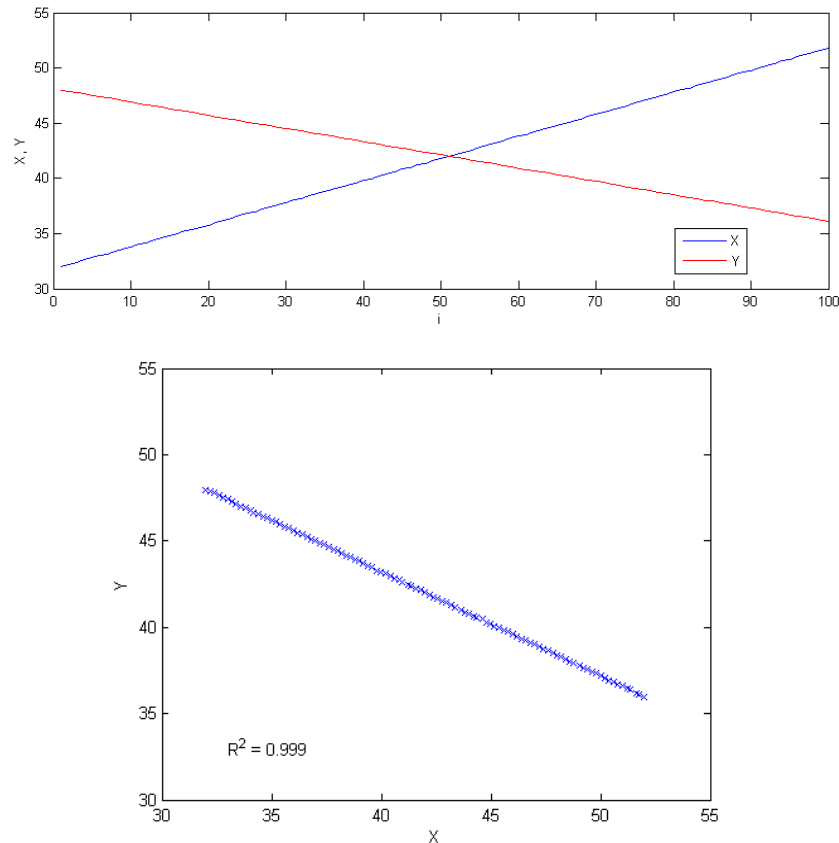


**Figure 3 Time series with same mean, linear natural variability and small random sample deviations. Top: Time series X and Y. Bottom: Scatter plot of series.**

In short, the analysis presented here shows that ‘low’ values of  $R^2$  do not necessarily imply poor model skill (if measured and modelled data are being compared), especially if the temporal variation in mean signal is small compared to noise. Similarly, it also shows that ‘high’ values of  $R^2$  do not necessarily imply good model skill in comparable data sets, again if measured and modelled data are being compared.

With this in mind, the filtering and  $R^2$  analyses requested have been undertaken and results are presented below.

#### **Low-Frequency Analysis - Scalars**

A low-frequency analysis was performed for temperature and salinity as follows:

- 1 The model data was linearly interpolated to the same time stamp as the field measurements;
- 2 Field and model data were filtered using a 2<sup>nd</sup> order Butterworth low-pass forward and reverse digital filter with a  $1/30 \text{ hour}^{-1}$  cut-off frequency;
- 3 The raw and filtered signals were plotted and the coefficient of determination  $R^2$  computed as per equation (1).

Figure 4 presents a comparison between field data and model results for temperature and salinity data at Site 1 (including low pass filtered timeseries). As can be seen,  $R^2$  was high for temperature but not for salinity. The lower  $R^2$  values for salinity are clearly an artefact of the low temporal variation of the low pass filtered (i.e. mean) data (over the majority of the 40 day period). In particular, the model presents better agreement with field data in the first two thirds of the record with differences rarely exceeding 0.2. This is borne out by simple

inspection of the timeseries data – the visual correspondence both in mean value and temporal variation between the two is generally very good during this period, although for reasons described above, this is not reflected in the  $R^2$  value. Specifically, if only the first two thirds of the record are taken into consideration, the corresponding  $R^2$  further decreases to 0.01, despite the excellent visual correspondence. This result further illustrates the relationship between  $R^2$  and the range of variation discussed above.

In contrast, temperature has a relatively strong mean (low pass) signal temporal variability, and correspondingly larger  $R^2$  value, despite the fact that inspection of data presented in Figure 4 reveals that deviations between the low pass filtered salinity and temperature signals are visually similar.

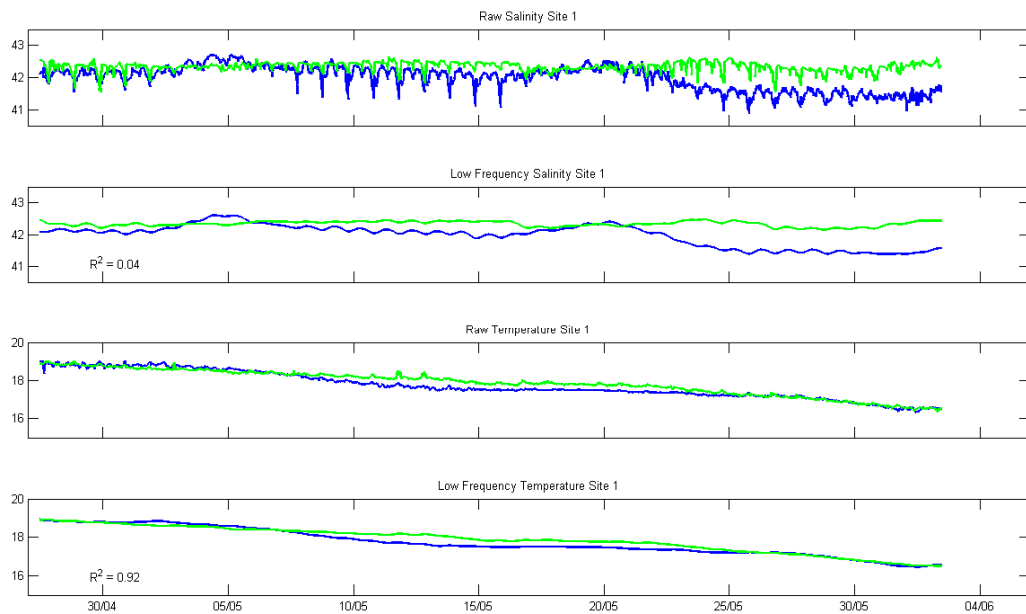


**Figure 4 Temperature and salinity comparisons at Site 2. Raw and filtered data. Blue lines are field data and green lines are model results.**

Table 1 presents  $R^2$  for all sites, showing the same pattern throughout. Site 6 is the only site that presents a slight improvement of  $R^2$  in relation to the other sites (Table 1). However, the improvement in  $R^2$  is due to the larger variance in the low passed field data, and not necessarily in better model skill at the site (Figure 5), as discussed above. The higher variance for Site 6 was imparted by the section of the signal that was considered questionable (see report R.B17415.001.05), so is of little meaning here.

**Table 1 Coefficient of Determination for Scalars**

Simulation: y010 (Nov 2008 to June 2009)		
Analysis: Low Frequency (30 hrs Cut-Off) $R^2$		
Site	Variable	
	Temperature	Salinity
1	0.92	0.04
2	0.90	0.03
3	0.86	N/A
4	0.94	0.06
5	0.95	0.09
6	0.89	0.20

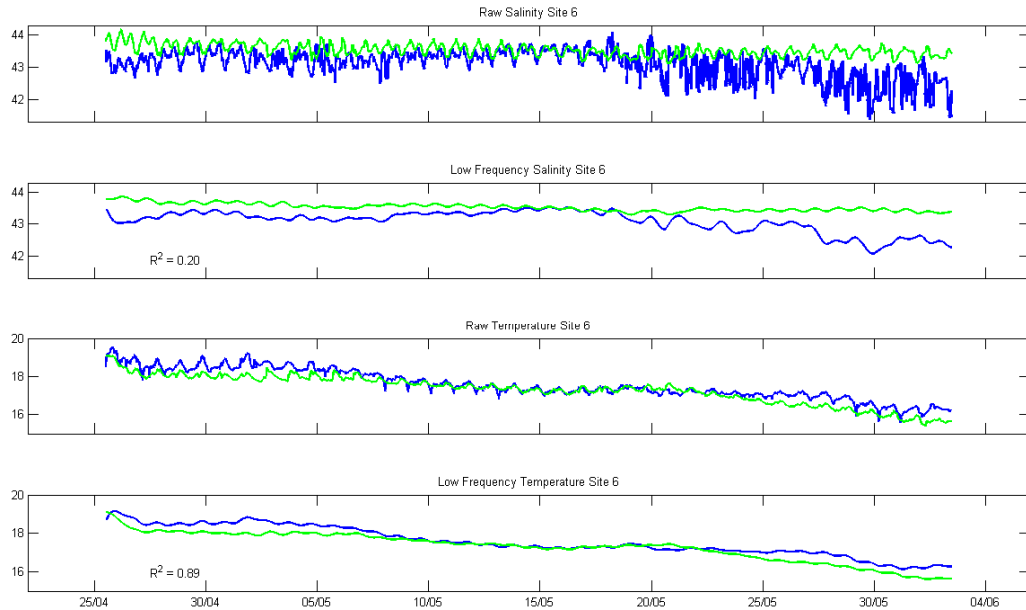


**Figure 5** Temperature and salinity comparisons at Site 6. Raw and filtered data. Blue lines are field data and green lines are model results.

#### *Low-Frequency Analysis - Velocities*

The data collected by the ADCPs at Sites 1 to 3 were depth-averaged and decomposed into N-S, and E-W direction components. The mean values over the measurement period were calculated and the velocities recalculated in terms of magnitude and direction. The mean or residual velocity obtained from this analysis is illustrated in Figure 6 below. The numerical results (including measurement error) are listed in Table 2. All results were within  $\pm 1.4$  cm/s in velocity magnitude and  $\pm 6^\circ$  in direction.

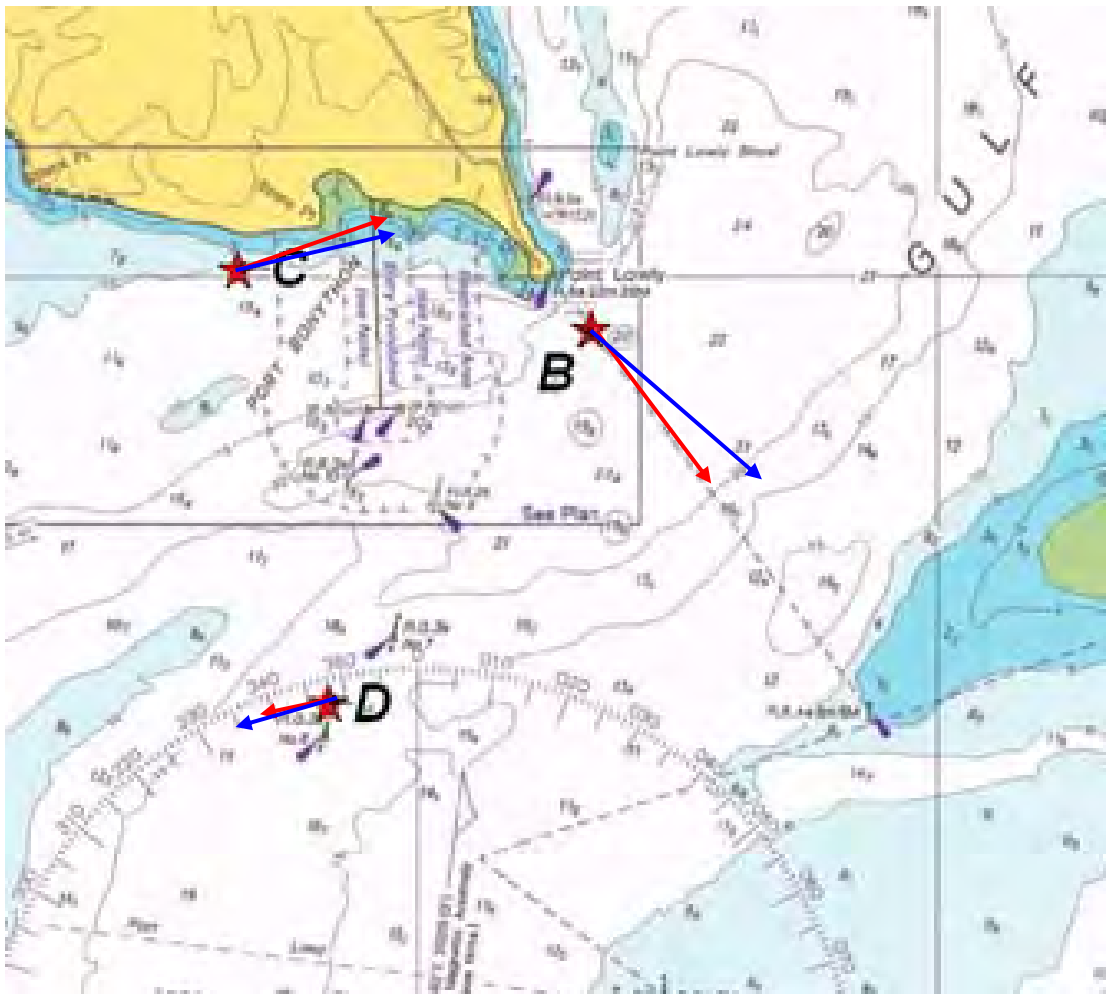


Figure 6 Residual depth-averaged velocities at Sites B, C, and D. Blue arrows are model results and Red arrows are measurements (no measurement errors taken into account).

Table 2 Residual Velocities. Range takes into account measurement error

Simulation: y010 (Nov 2008 to June 2009)				
Site	Velocity Magnitude (m/s)		Velocity Direction (°N)	
	Model	Measured	Model	Measured
B	0.124	0.090 – 0.110	131	137 – 148
C	0.087	0.079 – 0.090	77	69 – 74
D	0.057	0.027 – 0.045	254	245 - 267

### *High-Frequency Analysis – Scalars*

The model's skill in reproducing the high-frequency (tidal) motion with respect to scalars has already been presented in the report R.B17415.001.05. International peer review found that the results were considered adequate for the purposes of the desalination impact assessment. Here, we present results of spectral analysis to further illustrate the model's ability in reproducing the high-frequency Spencer Gulf dynamics.

The procedure for the spectral analysis was as follows:

- 1 The model data was linearly interpolated to the same time stamp as the field measurements;
- 2 Field and model data were filtered using a 2<sup>nd</sup> order Butterworth high-pass forward and reverse digital filter with a 1/30 hour<sup>-1</sup> cut-off frequency;
- 3 The raw and filtered signals were plotted;
- 4 The power spectral density (auto-spectrum) was computed for the measured and modelled filtered signals. Before the spectral estimates were obtained, the data was windowed using a "Hamming" window consisting of 3360 samples (14 days), adopting 50% overlap;
- 5 Similarly, the cross power spectral density between field and modelled filtered signals was computed;
- 6 The auto and cross-power spectral densities were used to obtain the magnitude-squared coherence between model and field signals;
- 7 The phase between signals was obtained from the argument of the (imaginary) cross power spectra.

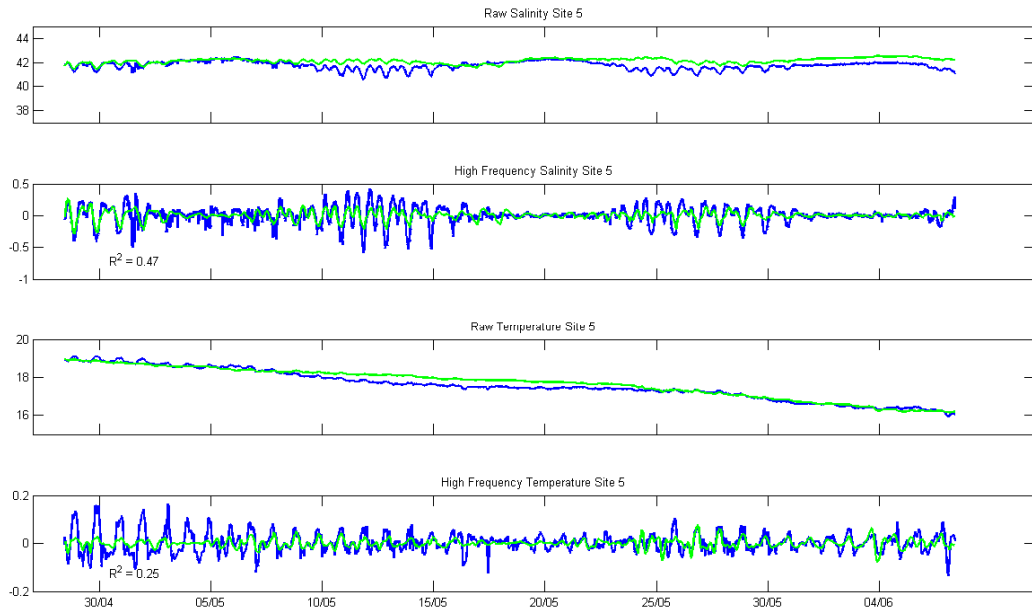
The data was analysed using both the Matlab "Signal Processing Toolbox" and Dr. Charles James "Spectral Analysis" Matlab script, giving similar results. Here, the "Matlab Signal Processing Toolbox" results are presented.

Figure 7 presents the raw and high-pass filtered measured and modelled data at Site 5. The associated spectral analyses are shown in Figure 8 and Figure 9 for salinity and temperature, respectively. The time series indicate that both measurements and model display increased signal amplitudes during spring tides and reduced amplitude during neap tides (as expected). The maximum salinity changes were the order of 0.4 and the temperature changes were the order of 0.15 °C. These changes indicated that for Site 5 the salinity change influences on density are 6 to 7 times stronger than the temperature.

For salinities, Figure 7 shows clear signatures of three spring tide cycles. The model reproduced similar amplitudes for the first cycle, but comparatively lower for the second and slightly lower for the third. Conversely, for temperature, the model did not reproduce the amplitudes at the early stages (first week) of the measurement period, and reproduced similar amplitudes at the end of the time series.

As expected, the measured and model power spectrum density peaks occurred at the same diurnal (1 per day) and semi-diurnal (2 per day) frequencies (Figure 7). The magnitude-squared coherence around these frequencies was above 0.8, and the phase differences near zero. The lower modelled spectral power densities were a reflection of the reduced amplitudes at the different stages of the cycle. Model results however, did reproduce the tidal dynamics of salinity with good skill.





**Figure 7** Temperature and salinity comparisons at Site 5. Raw and high-pass filtered data. Blue lines are field data, green lines are model results initialised in Nov 2008.

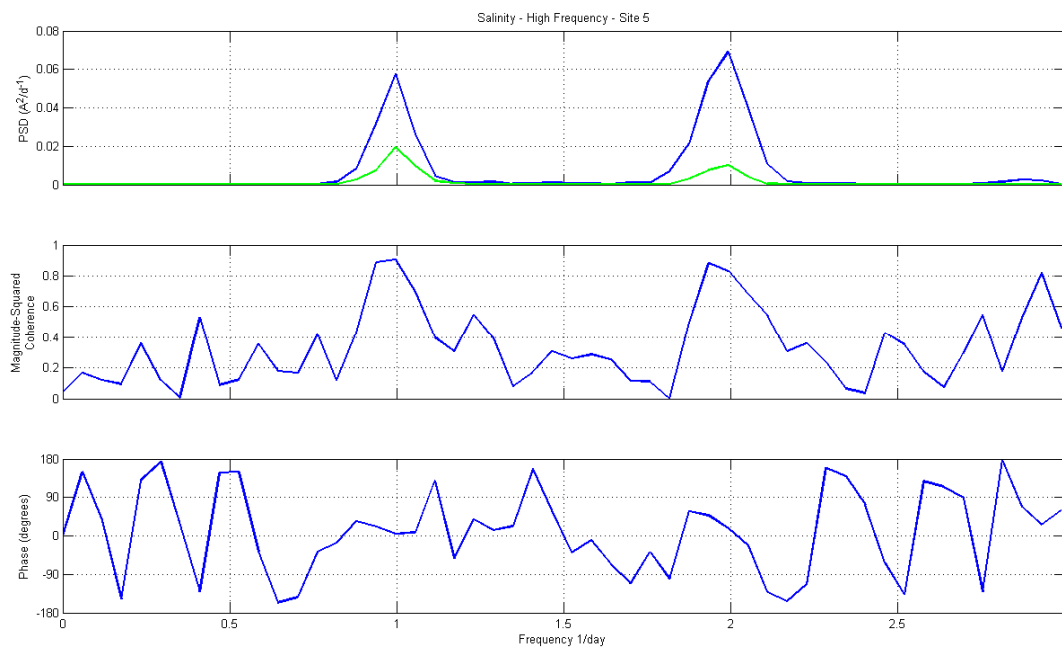


**Figure 8** Spectral analysis results for high-pass filtered salinity at Site 5. Top panel: Power spectral density. Blue lines are field data, green lines are model results initialised in Nov 2008. Middle panel: Magnitude squared coherence between the signals. Lower panel: Phase difference between the signals obtained from the cross spectral density.

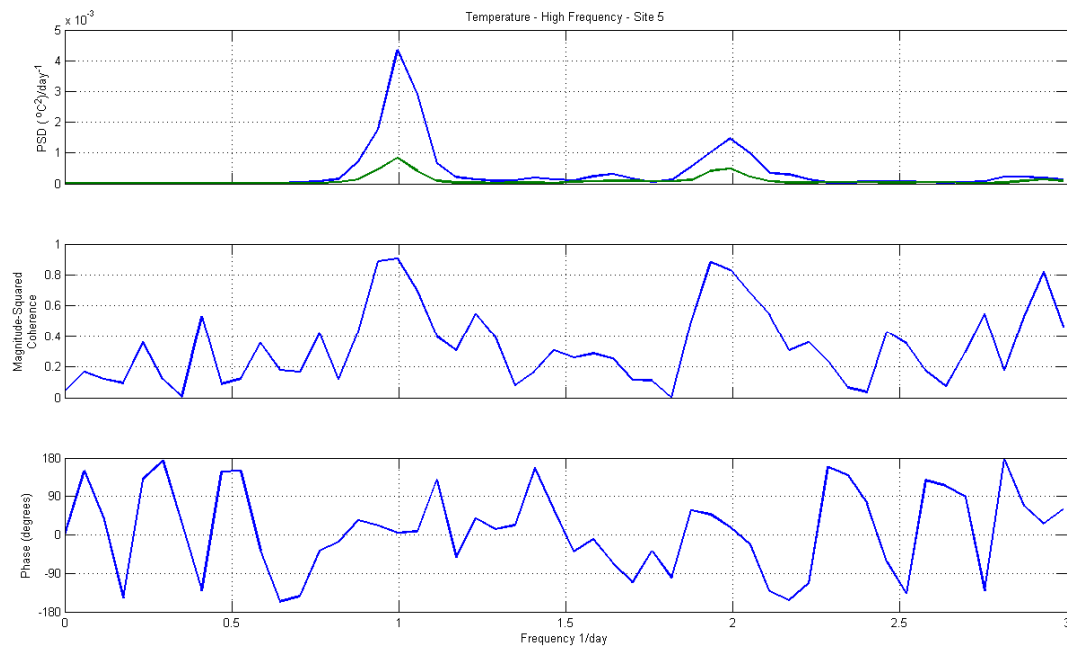


**Figure 9** Spectral analysis results for high-pass filtered temperature at Site 5. Top panel: Power spectral density. Blue lines are field data, green lines are model results initialised in Nov 2008. Middle panel: Magnitude squared coherence between the signals. Lower panel: Phase difference between the signals obtained from the cross spectral density.

#### *High-Frequency Analysis - Velocities*

Similarly to the preceding analysis for scalars, analysis of the high-frequency content in the velocity signals was undertaken. We note that a  $R^2$  values for velocities have already been presented in report R.B17415.001.05, and these were peer reviewed and found to be satisfactory. Here, we illustrate the results of the corresponding and supporting spectral analysis that parallel the previous work.

The time series at Site B and associated spectral analysis results for U and V-Velocity components are shown in Figure 10 to Figure 12, respectively. Site B is shown as it is the location of the proposed desalination discharge and therefore of more significance for model performance.

Given the model performs well in the time domain (as indicated by  $R^2$ ), it is no surprise that the model results were also in agreement with the field data in the frequency domain. In contrast to the scalar results, the modelled velocity amplitude fluctuations were about the same as the measurements. As a result, the power spectral densities were very similar.

The magnitude-squared coherence was very close to one for  $1/12 \text{ hr}^{-1}$  and  $1/24 \text{ hr}^{-1}$  frequencies. In other words, most of the field variability (in the dominant frequencies) is explained by the model – this confirms the model's ability to reproduce tidal motions that drive mixing and dispersion of brine, as was established in the validation report R.B17415.001.05.

For the U-velocity, only a small phase lag was obtained for the diurnal frequency ( $-4.5^\circ$ , about 18 minutes), and an extremely close match for the semi-diurnal frequency ( $3.2^\circ$ , about 6 minutes). Conversely, for the V-Velocity, close agreement was obtained for diurnal frequency and a small phase lag for the semi-diurnal frequency ( $+6^\circ$ , about 12 minutes). Although this result was achieved in a different way, it is consistent with what was established in the internationally peer reviewed validation report R.B17415.001.05.

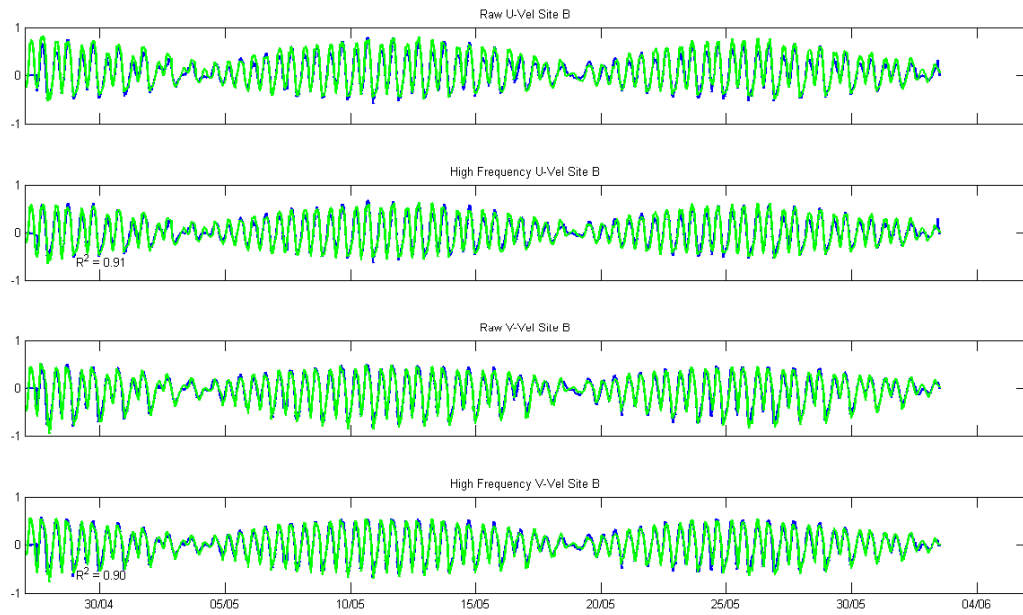


**Figure 10 Velocity comparisons at Site B. Raw and high-pass filtered data. Blue lines are field data, green lines are model results initialised in Nov 2008.**

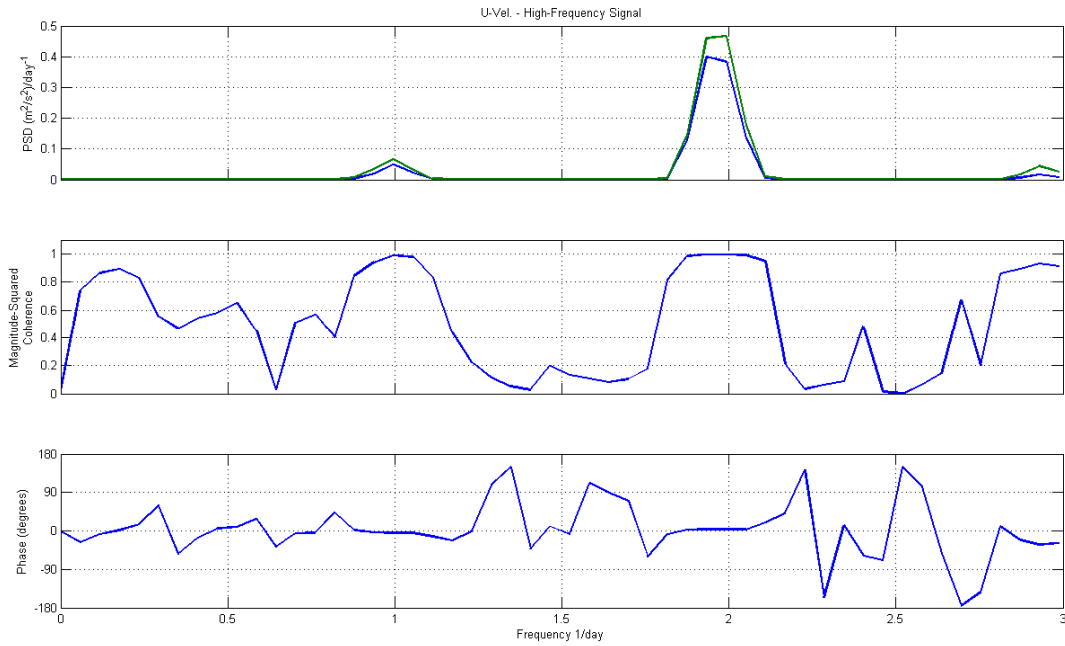


**Figure 11** Spectral analysis results for high-pass filtered (E-W) U-Velocity at Site B. Top panel: Power spectral density. Blue lines are field data, green lines are model results initialised in Nov 2008. Middle panel: Magnitude squared coherence between the signals. Lower panel: Phase difference between the signals obtained from the cross spectral density.

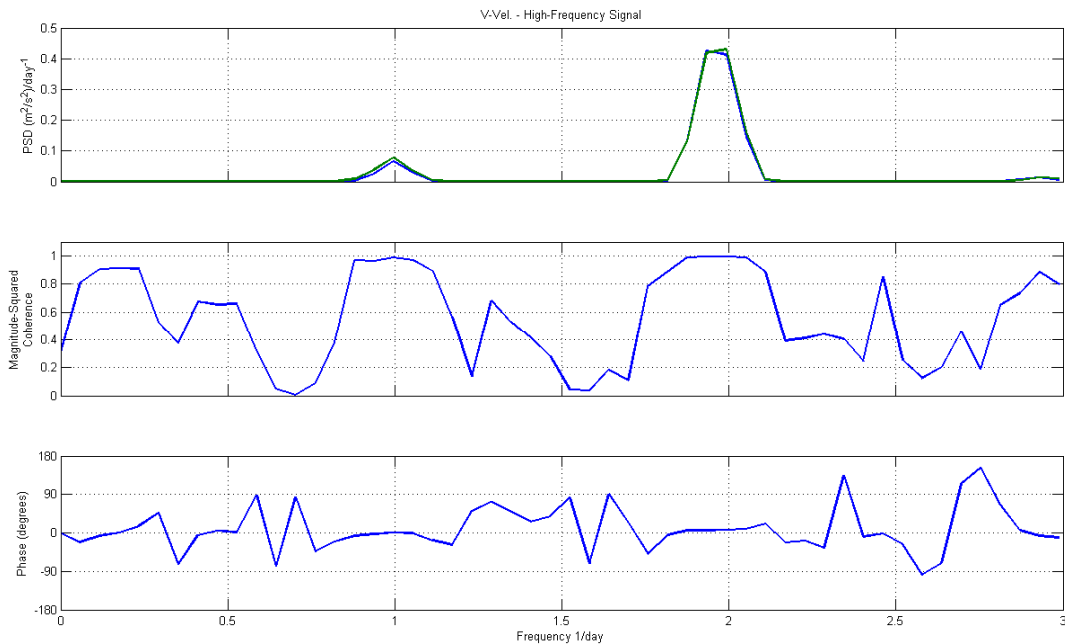


**Figure 12** Spectral analysis results for high-pass filtered (N-S) V-Velocity at Site B. Top panel: Power spectral density. Blue lines are field data, green lines are model results initialised in Nov 2008. Middle panel: Magnitude squared coherence between the signals. Lower panel: Phase difference between the signals obtained from the cross spectral density.

### *Discussion and Conclusions*

Modelled and measured temperature and velocity fields compared well overall, at least in part to their time varying mean signal. Filtering of the velocity signals showed that the model reproduced high-frequency motion exceptionally well in the location of the proposed discharge. Both temperature and salinity spectral analyses revealed phase agreement and squared-magnitude coherence between modelled and measured signals at the observed semi-diurnal and diurnal frequency peaks.

The field data available was not obtained over a long enough timeframe for the description of low-frequency (lower than the spring/neap cycle oscillation) salinity dynamics in the Northern Spencer Gulf, as salinity variation in the mean signal in time is very small. In this circumstance,  $R^2$  is a problematic indicator of model skill.

Site 5 was the only location where there is a clear indication of low-frequency (frequencies below  $1/30 \text{ hr}^{-1}$ ) response in salinity. In this case, the variability is not seasonal, but modulated by the spring/neap cycle (approximately 14 day period). In this location, the model reproduced the high-frequency signal with relatively good skill, particularly the diurnal component (Figure 7). The modelled signal had, however, smaller amplitudes on some of the spring cycles, leading to lower power spectral density in relation to the field measurements. Model spin-up over one summer season was sufficient to promote, at least partially, the salinity gradient North of Point Lowly. Given the temperature comparisons also presented similar (tidal) oscillations observed in the measured data, this further supports that the model properly reproduces the dispersion of the scalar fields near Point Lowly.

Notwithstanding this, the low-frequency baroclinic motion is controlled at larger scales (probably the order of 50 km or more, given the tidal excursions alone are the order of 20 km). Sometimes a lag could be observed between measured and modelled signals. The model also produced smaller low-frequency amplitude than the field.

ELCOM initialisation uses a global interpolation method, based on an inverse squared distance method in the horizontal. As a result, salinity gradient that drives the low-frequency (baroclinic) motion and high-frequency oscillations were smeared out, leading to slightly lower salinities in the northern Gulf and slightly higher in the southern parts of the Gulf.

The northern part of the gulf, where measurements were taken, responds more abruptly to changes imposed by the surface forcing (i.e. evaporation) as it is shallower. Thus, the high-frequency oscillations also readjust more quickly, such that the model was able to reproduce the dynamics with spin-up over one summer season.

Conversely, the generally deeper and wider southern portion of the Gulf adjusts more slowly.

The resulting modelled salinity gradients were likely to be weaker than the existing gradients in the field. As a result, the modelled low-frequency salinity variation amplitude was smaller than the field.

The actual (slowly adjusting) salinities are also likely to be different from the model initialisation, due to the non-coincidental (in time) data used to distribute the initial salinity field. As a result, the modelled low-frequency variation sometimes presents a lag in comparison to the field measurements. Despite these differences, the intricate details of this dynamic were accounted for in the model, although at somewhat different phase and amplitude.

In general, compared to the 40-day validation (and simulation) period presented in report B17415.001.04, the model was able to reproduce the measurements when provided with a longer spin-up time. A summary of the conclusions drawn from the analysis presented herein are presented in Table 3 below.

**Table 3 Summary of the Conclusions**

<b>Fields</b>	<b>Low frequency processes</b>	<b>High frequency processes</b>
Velocity	Model was in excellent agreement with measured data. Mean depth-averaged velocity magnitudes within $\pm 1.4$ cm/s and mean depth-averaged velocity directions within $\pm 6^\circ$	Model was in very close agreement to field data. Spectral analysis revealed the model was able to explain all variance in the measured signal. Very small phase lag for diurnal and semi-diurnal tidal components. Results are adequate for the purposes of the model.
Temperature	Model was able to reproduce the seasonal variation obtained in the signal.	Spectral analysis revealed the model reproduces the diurnal and semi-diurnal tidal oscillations, however the signal at times have relatively lower amplitude. Magnitude-squared coherence at peaks was above 0.8 and phase difference at the peaks was near $0^\circ$ . Results are adequate for the purposes of the model.
Salinity	<p>The 40-day data used in the analysis did not reveal required variation in the low frequency salinity field for meaningful <math>R^2</math> analysis.</p> <p>The only low-frequency motion revealed in the data set refers to the spring/neap tide cycle variations, which was relatively weak.</p> <p>The model reproduced this dynamics but at a slightly different magnitude and phase.</p> <p>Data used for initialisation, although based on the best available coverage of the Northern Spencer Gulf, was not coincident in time – collecting such data is not reasonable and has not been undertaken before. Additionally, salinity gradients that drive the baroclinic motion suffered from some smearing artefacts in the interpolation process used for initialisation.</p>	<p>Spectral analysis revealed the model reproduces the diurnal and semi-diurnal tidal oscillations, however the signal at times have relatively lower amplitude. Magnitude-squared coherence at peaks was above 0.8 and phase difference at the peaks was near <math>0^\circ</math>. Results are adequate for the purposes of the model intended use.</p>



- BMT WBM Brisbane**      Level 11, 490 Upper Edward Street Brisbane 4000  
PO Box 203 Spring Hill QLD 4004  
Tel +61 7 3831 6744 Fax +61 7 3832 3627  
Email [wbm@wbmpl.com.au](mailto:wbm@wbmpl.com.au)  
Web [www.wbmpl.com.au](http://www.wbmpl.com.au)
- BMT WBM Denver**      14 Inverness Drive East, #B132  
Englewood Denver Colorado 80112 USA  
Tel +1 303 792 9814 Fax +1 303 792 9742  
Email [wbm-denver@wbmpl.com.au](mailto:wbm-denver@wbmpl.com.au)  
Web [www.wbmpl.com.au](http://www.wbmpl.com.au)
- BMT WBM Mackay**      Suite 1, 138 Wood Street Mackay 4740  
PO Box 4447 Mackay QLD 4740  
Tel +61 7 4953 5144 Fax +61 7 4953 5132  
Email [wbm-mackay@wbmpl.com.au](mailto:wbm-mackay@wbmpl.com.au)  
Web [www.wbmpl.com.au](http://www.wbmpl.com.au)
- BMT WBM Melbourne**      Level 5, 99 King Street Melbourne 3000  
PO Box 604 Collins Street West VIC 8007  
Tel +61 3 8620 6100 Fax +61 3 8620 6105  
Email [wbm-melbourne@wbmpl.com.au](mailto:wbm-melbourne@wbmpl.com.au)  
Web [www.wbmpl.com.au](http://www.wbmpl.com.au)
- BMT WBM Newcastle**      126 Belford Street Broadmeadow 2292  
PO Box 266 Broadmeadow NSW 2292  
Tel +61 2 4940 8882 Fax +61 2 4940 8887  
Email [wbm-newcastle@wbmpl.com.au](mailto:wbm-newcastle@wbmpl.com.au)  
Web [www.wbmpl.com.au](http://www.wbmpl.com.au)
- BMT WBM Perth**      1 Brodie Hall Drive Technology Park Bentley 6102  
Tel +61 8 9328 2029 Fax +61 8 9486 7588  
Email [wbm-perth@wbmpl.com.au](mailto:wbm-perth@wbmpl.com.au)  
Web [www.wbmpl.com.au](http://www.wbmpl.com.au)
- BMT WBM Sydney**      Level 1, 256-258 Norton Street Leichhardt 2040  
PO Box 194 Leichhardt NSW 2040  
Tel +61 2 9713 4836 Fax +61 2 9713 4890  
Email [wbm-sydney@wbmpl.com.au](mailto:wbm-sydney@wbmpl.com.au)  
Web [www.wbmpl.com.au](http://www.wbmpl.com.au)
- BMT WBM Vancouver**      1190 Melville Street #700 Vancouver  
British Columbia V6E 3W1 Canada  
Tel +1 604 683 5777 Fax +1 604 608 3232  
Email [wbm-vancouver@wbmpl.com.au](mailto:wbm-vancouver@wbmpl.com.au)  
Web [www.wbmpl.com.au](http://www.wbmpl.com.au)